



HAL
open science

Analyses de lichens par spectrométrie de masse : déréplication et histolocalisation

Pierre Le Pogam-Alluard

► **To cite this version:**

Pierre Le Pogam-Alluard. Analyses de lichens par spectrométrie de masse : déréplication et histolocalisation. Chimie analytique. Université de Rennes, 2016. Français. NNT : 2016REN1S056 . tel-01439641

HAL Id: tel-01439641

<https://theses.hal.science/tel-01439641v1>

Submitted on 18 Jan 2017

HAL is a multi-disciplinary open access archive for the deposit and dissemination of scientific research documents, whether they are published or not. The documents may come from teaching and research institutions in France or abroad, or from public or private research centers.

L'archive ouverte pluridisciplinaire **HAL**, est destinée au dépôt et à la diffusion de documents scientifiques de niveau recherche, publiés ou non, émanant des établissements d'enseignement et de recherche français ou étrangers, des laboratoires publics ou privés.

THÈSE / UNIVERSITÉ DE RENNES 1

sous le sceau de l'Université Bretagne Loire

pour le grade de

DOCTEUR DE L'UNIVERSITÉ DE RENNES 1

Mention : Chimie

École doctorale Sciences De La Matière

présentée par

Pierre Le Pogam-Alluard

Préparée dans l'unité de recherche UMR CNRS 6226
Équipe PNSCM (Produits Naturels, Synthèses, Chimie Médicinale)
Faculté de Pharmacie, Université de Rennes 1

**Analyses de lichens
par spectrométrie de
masse : déréplication
et histolocalisation**

**Thèse soutenue à Rennes
le 09 Septembre 2016**

devant le jury composé de :

Martin GRUBE

Professeur à l'Université de Graz, Autriche /
rapporteur

Nicolas FABRE

Professeur à l'Université de Toulouse 3 / *rapporteur*

Yanyan LI

Chargée de Recherche au Muséum National
d'Histoire Naturelle (Paris 5) / *examineur*

David GUILLET

Professeur à l'Université d'Angers / *examineur*

David RONDEAU

Professeur à l'Université de Brest / *examineur*

Béatrice LEGOUIN

Maître de Conférences à l'Université de Rennes 1 /
co-directrice de thèse

Joël BOUSTIE

Professeur à l'Université de Rennes 1 / *directeur de
thèse*

The most beautiful thing one can experience is the mysterious. It is the source of all true art and science. He to whom the emotion is a stranger, who can no longer pause to wonder and stand wrapped in awe, is as good as dead - his eyes are closed

- Albert Einstein, Living Philosophies

Mal nommer un objet, c'est ajouter au malheur de ce monde

- Albert Camus, Poème 44

Remerciements

Je tiens tout d'abord à exprimer ma profonde reconnaissance aux différents membres du jury : à Messieurs **Nicolas Fabre** et **Martin Grube** pour m'avoir fait l'honneur d'être les rapporteurs de ce travail et à Madame **Yanyan Li** et Messieurs **David Guilet** et **David Rondeau** pour avoir accepté d'en être examinateurs.

Je ne saurais manquer de remercier **toute l'équipe du laboratoire de Pharmacognosie** où j'ai trouvé de vrais amis et où je suis convaincu d'avoir passé un des moments les plus heureux de ma vie.

En premier lieu, je remercie mon mentor, **Joël Boustie**, de m'avoir accueilli dans son laboratoire en Master 2 puis en Doctorat. Je vous remercie de m'avoir initié au fonctionnement de la recherche académique, accordé votre confiance en me faisant participer à des congrès nationaux et internationaux et guidé dans ce projet. En combinant la recherche en pharmacognosie/chimie analytique et les enseignements en mycologie, je n'aurais pas pu espérer de cadre qui me convienne davantage! Je le remercie également de ses remarquables et constantes qualités humaines qui ont créé une complicité que l'on pourrait qualifier de symbiotique, elle aussi. Sans doute fallait-il une rencontre comme la nôtre pour me convaincre de me lancer dans cette formidable aventure que je n'avais jamais envisagée auparavant. Aussi, avant même que la page de mon passage dans votre équipe ne se soit réellement tournée, je suis déjà en mesure de vous dire que cet environnement de travail me manque beaucoup. Rendre ce manuscrit, c'est perdre un des liens qui nous unit mais nul doute que cet épisode aura tissé une relation que le temps ne distendra jamais.

Je remercie également **Béatrice Legouin** d'avoir assuré la co-direction de cette thèse. Je te remercie de ton encadrement, de ton sens de l'organisation, de ta disponibilité sans faille et de ton aide au quotidien. Tes compétences en chimie analytique et ta rigueur dans l'approche expérimentale ont été précieuses.

Ce manuscrit ne serait pas ce qu'il est sans celle qui n'est autre que mon officieuse et supplémentaire co-directrice : **Anne-Cécile Le Lamer**. En dépit de mon insistance, tu as fait le choix de rester dans l'ombre aujourd'hui en ne siégeant pas dans le jury mais tu n'en demeures pas moins l'un des acteurs phares de cette thèse. Quel timing parfait pour ton nouveau séjour à Rennes qui suivait exactement les contours de mon Master 2 puis de ma thèse ! Je te dois une très grande partie des compétences opérationnelles que j'ai acquises durant ces trois années. Ton allant et ton enthousiasme ont porté à peu près tous les volets de ce travail et m'ont redonné confiance durant les (nombreuses) phases où j'y croyais (beaucoup) moins. Difficile également de ne pas louer le zèle dont tu as fait preuve lorsqu'il s'agissait de relire mes propositions de manuscrit et la pertinence de tes remarques pour les améliorer. Merci d'avoir toujours été là, aussi bien scientifiquement qu'humainement.

Je tiens également à citer les membres du laboratoire non directement impliqués dans la direction de ma thèse mais qui ont contribué de façon considérable à certains volets de ce manuscrit avec beaucoup de sympathie et de disponibilité. En ce sens, je remercie beaucoup **Françoise Lohézic-Le Dévéhat** qui a été d'un apport incontournable pour les analyses en lien avec l'imagerie et la CCM-MS et **Marylène Chollet-Krugler** pour toutes les problématiques associées aux mycosporines mais également pour m'avoir initié aux techniques de base du laboratoire à mon arrivée en Master 2. Pour ce second volet, j'associe à ces remerciements **Thi Thu Tram Nguyen** qui m'a beaucoup appris concernant les gestes de base en laboratoire de Pharmacognosie lors de cette même période.

Si nous n'avons pas eu l'occasion de collaborer directement en recherche, je remercie **Sophie Tomasi** de son intérêt pour mes travaux ainsi que pour les Travaux Pratiques de Pharmacognosie et de Mycologie que nous avons eu le plaisir de réaliser ensemble. À ce titre, je remercie une nouvelle fois **Françoise Lohézic-Le Dévéhat** ainsi que **David Delmail** pour ces excellentes expériences d'enseignements.

Pour m'avoir constamment guidé et accompagné dans mes manipulations avec une bonne humeur et une disponibilité exemplaires, je remercie chaleureusement les techniciennes de l'unité. Merci à **Aurélie Sauvager** d'avoir toujours guidé avec beaucoup de maîtrise mes analyses HPLC. Un grand merci à **Isabelle Rouaud** pour sa rigueur et de sa méticulosité concernant les essais de cytotoxicité qui ont été providentiels pour valoriser nos nouvelles molécules. Enfin, tous mes remerciements vont également à **Solenn Ferron**, particulièrement pour son aide lors de la réalisation des spectres RMN sur les spectromètres de la plate-forme PRISM, mais également pour ses cadeaux végétaux et pour avoir été une voisine de bureau d'une remarquable qualité.

L'équipe PNSCM, c'est également le département de chimie organique dont je remercie les différents membres pour leur accueil toujours excellent et leur intérêt constant pour mes travaux. Parmi eux, je remercie en particulier **Philippe Uriac** de ses conseils avisés, toujours prodigués avec beaucoup de pertinence et de pédagogie. C'est sans doute aussi l'occasion de te dire que si je suis aujourd'hui aussi sensible à la beauté des molécules, c'est en grande partie grâce aux enseignements passionnés que tu dispensais en pharmacie. De la même façon, je remercie **Michèle David**, également enseignante emblématique de mon cursus de pharmacien, dont le constant soutien m'a été précieux et qui s'est toujours montrée disponible et enthousiaste pour venir écouter mes diverses répétitions orales.

Je remercie également beaucoup **Maryse Demay**, secrétaire de notre unité de ses nombreux services et de sa gentillesse.

Je n'oublie pas non plus le soutien dont j'avais bénéficié de la part de **Maryvonne Charrier** lors des recherches de financement pour effectuer une thèse. Je la remercie ici de nos échanges de qualité et suis très heureux que ce projet se concrétise aujourd'hui par la thèse d'**Alice Gadéa**. Aussi, j'espère vivement que les approches développées dans le cadre de ce mémoire vous seront utiles à l'avenir.

Au cours de cette expérience, j'ai aussi eu la possibilité d'encadrer **Aline Pillot** et **Tiffanie Ziajko**, stagiaires de Master de Chimie Moléculaire 1^{ère} année et de troisième année de licence en Chimie à qui je sais gré de leur travail et de leur motivation. De la même façon, s'est également présentée l'opportunité d'encadrer la Thèse de Pharmacie de **Carole Pilorget** dont je loue ici la qualité et le sérieux.

Pour avoir rendu ces années aussi productives qu'épanouissantes, je tiens à exprimer ma gratitude à tous les membres – anciens ou présents – du laboratoire: **Marie-Laurence Abasq-Paofaï**, **Gilles Argouarch**, **Jean-Charles Corbel**, **Patricia Courtel**, **Jean-François Cupif**, **Corentin Daugan**, **Alice Gadéa**, **Nicolas Gouault**, **René Grée**, **Jean-Pierre Hurvois**, **Mickaël Jean**, **Mathilde Jégo**, **Sarah Komaty**, **Claudia Lalli**, **Nathalie Legrave**, **Myriam Le Roch**, **Thi Thu Tram Nguyen**, **Alba Noël**, **Delphine Parrot**, **Jacques Renault**, **Pierre van de Weghe**, **Thi Huyen Vu**...

Ce travail est riche des différentes collaborations extérieures qui y ont été nouées, points de départ de partenariats fructueux qui ont considérablement enrichi la trame de ces travaux et par la même étoffé mes connaissances dans de nombreuses disciplines. Aussi, je tiens à remercier les personnes de ces différentes équipes de leurs expertises variées et inspirantes, de leurs nombreux conseils et de leur gentillesse.

Je remercie chaleureusement **David Rondeau** avec qui nous avons eu la plaisir de mener à bien le volet DART-MS de ce manuscrit. Si ce point représente à lui seul un développement tout à fait crucial de ce manuscrit, je vous remercie de m'avoir initié de façon plus générale à la spectrométrie de masse avec une pédagogie et une passion toujours très marquées. Merci d'avoir toujours pris le temps de préparer le spectromètre de masse en amont de mes nombreuses visites au bâtiment 24 malgré des calibrations souvent chronophages et éprouvantes. Cette thèse, comme le Master 2 qui avait précédé, vous doit beaucoup.

Un autre grand tournant de cette thèse a été le succès des analyses en LDI réalisées à Angers avec **Andreas Schinkovitz** et **Pascal Richomme**. Cela a été pour moi un plaisir de retourner en Anjou

pour retrouver ponctuellement les enseignants du Master 2 P²AON qui m'avaient passionné et donné l'envie de poursuivre par ce Doctorat. Si nous avons fait de ces résultats une publication dans *Analytical Chemistry* plutôt que dans un autre journal, je n'oublie pas que c'est grâce à ta suggestion Andreas. En plus d'avoir permis de mener ces travaux, je remercie également Pascal Richomme d'avoir été présent à mon comité de thèse à mi-parcours et de s'être initialement libéré pour faire partie de ce jury de thèse bien que les changements de date opérés depuis aient finalement compromis sa participation.

Un troisième temps fort de ce manuscrit a été l'étude phytochimique des apothécies d'*Ophioparma ventosa*. Cet axe de travail a largement bénéficié des compétences de **Bandi Siva**, doctorant à l'IICT d'Hyderabad, concernant aussi bien la phytochimie que l'élucidation structurale et je remercie à ce titre le LIA franco-indien initié par **René Grée** d'avoir permis son accueil en France. L'élucidation structurale de ces pigments n'aurait été possible sans les spectromètres RMN de la plate-forme PRISM et les connaissances d'**Arnaud Bondon** dont les expertises pour le choix des séquences à réaliser et l'interprétation des spectres ont été décisives. La détermination de la stéréochimie des composés a reposé sur l'expertise de **Jérôme Gratton** et de **Denis Jacquemin** que je remercie de leur efficacité et de leur disponibilité pour répondre à mes questions. Enfin, il m'importe d'associer à ces remerciements **Walter Obermayer** pour nous avoir fourni à deux reprises des échantillons d'*Ophioparma ventosa* mais aussi pour ses précieuses lumières de lichénologue dans l'interprétation des clichés d'imagerie.

Mes remerciements vont également à **Thierry Bataille** et **Laurent Le Pollès** pour les études de diffraction des rayons X par les poudres de lichens. Merci d'avoir accepté de m'initier à ces techniques originales pour un pharmacogyste avec pédagogie et efficacité ainsi que des relectures attentives des parties correspondantes de ce manuscrit.

J'ai également une reconnaissance toute particulière pour **Audrey Geairon** et **Hélène Rogniaux** de la plate-forme BIBS de l'INRA de Nantes pour les analyses menées en LDI-imagerie. Je les remercie ici de leur zèle et de leur constante réactivité qui ont permis à cet axe de travail d'être à la fois fructueux et toujours très agréable. De façon similaire, je remercie **Jean-François Muller**, **Gabriel Krier** et **Lionel Vernex-Loiset** (Université de Metz) pour les analyses de LDI imagerie à 266 nm.

À de nombreuses reprises, les travaux décrits dans ce manuscrit ont reposé sur le parc d'équipements de la plate-forme H2P2 et sur la mise à contribution d'**Alain Fautrel** dont l'aide consentie a grandement contribué à de multiples volets de ce mémoire (coupes au cryostat, micro-dissection capture laser, premiers pas en spectromicroscopie Raman)... Je le remercie vivement de sa gentillesse, de sa disponibilité et de son efficacité.

J'exprime toute ma gratitude à **Yanyan Li** qui m'a reçu très chaleureusement dans son laboratoire, au Muséum National d'Histoire Naturelle. Mes remerciements les plus sincères pour avoir accepté de m'initier aux techniques de biologie moléculaire mises en œuvre dans le cadre de ce manuscrit lors desquelles j'ai pu apprécier sa haute compétence et son efficacité. J'ai également bénéficié au cours de la rédaction de ce mémoire de ses conseils judicieux, toujours accompagnés de beaucoup de gentillesse. Avec elle, je remercie les différents membres de son équipe pour leur gentillesse et leur aide au quotidien, en particulier **Victor Sayous**, **Jimmy Mevaere**, **Zhilai Hong** et **Andrea Diaz**. Je n'oublie pas que nos premiers pas dans ce volet biologie moléculaire ont été initiés par **Annie Guiller** que je remercie de ses conseils avisés et de ses encouragements bienveillants qui ont véritablement amorcé ce projet.

Je remercie très sincèrement le CRMPO pour les nombreuses analyses en spectrométrie de masse haute résolution réalisées pour moi. Je remercie plus particulièrement **Nicolas Le Yondre** de ses nombreuses lumières par rapport à mes projets mais également pour avoir accepté d'accueillir Tiffanie pour une bonne partie de son stage. J'adresse toute ma gratitude à **Philippe Jehan** de sa disponibilité constante pour échanger de mes résultats avec une expertise que j'ai hautement appréciée tout au long de mes travaux au laboratoire.

Au-delà de leur étude chimique, la découverte des lichens à l'occasion de cette thèse m'a ouvert les portes d'un monde fascinant. Je remercie en ce sens l'**AFL** de m'avoir permis de découvrir ces organismes et en particulier **Chantal Van Haluwyn** ainsi que **Danièle** et **Olivier Gonnet**. De la même façon, j'ai eu le privilège de bénéficier d'une semaine de formation en taxonomie au NHM de Londres et j'exprime toute ma gratitude à **Holger Thües** et à **Pat Wolseley** de leur sympathie et de la très grande qualité de leurs enseignements en lichénologie. Pour rester dans les remerciements naturalistes, je tiens à saluer ma chère association mycologique, l'**AMPM**, et ses éminents membres qui me permettent chaque saison de progresser dans la connaissance des champignons. J'en remercie les présidents et vice-présidents, **Pascal Hériveau** et **Patrick Dorval** ainsi que l'ensemble des habitués que j'ai plaisir à retrouver chaque automne.

Ces dernières années ont également été constellées de rencontres très marquantes, au premier rang desquelles figure celle d'une très grande Chercheuse qui me fait l'immense honneur de sa présence aujourd'hui : **Françoise Guéritte**. Je l'en remercie très respectueusement et l'assure de ma profonde reconnaissance.

Je n'aurais garde d'oublier tous mes collègues et amis qui m'ont soutenu tout au long de ce travail et sans lesquels cette thèse n'aurait définitivement pas été la même. À commencer par mes amis historiques de l'Année Internationale de la Cristallographie : les indissociables **Benoît Boichard** et **Nicolas Brisset** dont la passion pour les sciences au sens très large et l'éclectisme débordant m'ont rappelé à chacune de nos nombreuses rencontres combien cette situation de doctorant était un défi intellectuel exaltant. De la même façon, je remercie chaleureusement tous mes amis que j'ai toujours eu plaisir à retrouver périodiquement en dehors des murs du laboratoire, avec en particulier **Grichka Biver**, **Bruna Casanova**, **Vianney Durel**, **Benjamin** et **Emmanuelle Guieu**, **Lorène Héraud**, **Isabelle Mazerie**, **Valentin Renesme** et **Nicolas Touraine**. D'autres amis de longue date ont été d'un apport crucial pour moi : je pense tout d'abord à **Youna** et **Tom Audouard**. Les trois dernières années ont été l'occasion de confirmer ton rôle stratégique de *spin doctor* pour moi, Youna, et je tiens beaucoup à nos conversations téléphoniques fleuves qui, bien que trop rares, me donnent chaque fois l'impression que l'on s'est quittés la veille. Je remercie également **Sabine Boustie**, **Cathy Dhaleine**, **Karine Mov** et **Karine Péron** d'avoir gardé un contact amical avec moi à l'issue de mon stage de 6^{ème} année de Pharmacie en 2012 que ce soit pour les dîners annuels ou à d'autres occasions. Merci d'avoir été présents et votre amitié à tous m'honore, reste désormais à garder le contact malgré notre prévisible éloignement. Le panorama de mes précieuses relations de pharmacie ne saurait être complet sans évoquer **Cécile Le Normand** que je remercie de sa présence et de sa gentillesse au cours de cette thèse.

J'ai enfin l'immense plaisir de remercier ma famille de son exceptionnelle présence au cours des trois dernières années en dépit de l'éloignement lié à l'exaltante vie de thésard qui m'a souvent amené à me livrer corps et âme dans la passion de l'instant, sans véritablement se soucier de son impermanence.

Je remercie d'abord ma **grand-mère** de ses constantes attentions pour moi et d'avoir été toujours présente. Je me souviens très bien t'entendre dire lorsque j'étais à l'école primaire que tu m'accompagnerais jusqu'à la fin de l'Université. Sans doute ne mesurais-tu pas pleinement la portée de cet engagement mais tu as effectivement toujours été là et je t'en suis reconnaissant bien au-delà des mots. Mon **grand-père** également a été d'une importance cruciale dans ma vie en général mais également lors de mon Master 2 et de cette thèse. Si tu n'avais pas été présent, il apparaît clairement que je n'aurais pas poursuivi les études au-delà de mon cursus initial de pharmacie. Sois en remercié ici.

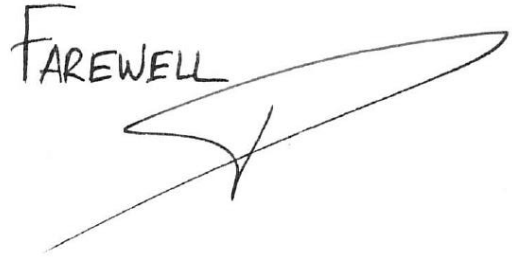
Je terminerai en remerciant mes parents pour m'avoir donné le privilège d'étudier. J'exprime toute ma gratitude à mon **père** de s'être toujours inquiété de me fournir les meilleures conditions de travail possibles et de m'avoir soutenu dans les tous choix d'orientation que j'ai pu faire. Je remercie très chaleureusement ma **mère** d'avoir été présente du début à la fin de cette thèse et de m'avoir soutenu dans les bons mais aussi et surtout dans les mauvais moments. Tu as toujours été prête à tout pour

moi et je ne saurais jamais t'en remercier suffisamment tant rien de cela n'aurait été concevable sans ton écoute assidue et tes paroles positives... Et je suis très sensible au fait que tu me retrouves lorsque tu écoutes *Ton Héritage* de Benjamin Biolay...

Merci à vous et je vous aime.

Le mot de la fin sera pour les assez nombreuses personnes qui ont été intriguées de cette poursuite d'études. Je répondrai simplement ici que toutes les initiatives entreprises ces dernières années, quelque variées qu'elles furent, avaient pour seul but de s'imprégner de l'éther des choses. Le reste n'est que détail.

FAREWELL



Sommaire

Remerciements	II
Sommaire	VII
Production scientifique	X
Liste des abréviations	XIII
Table des figures.....	XV
Introduction	1
PARTIE 1 : LES LICHENS : DE SINGULIERS CHAMPIGNONS	4
I. Position systématique des lichens au travers des siècles	4
II. Généralités sur les champignons.....	5
III. Présentation des lichens	8
A. Bases métaboliques, caractéristiques physiologiques et rôles écologiques.....	8
B. Morphologie des lichens	12
C. Reproduction des lichens	14
D. La phytochimie singulière des lichens.....	16
a. Diversité structurale et voies de biosynthèse	16
b. Bioactivités des métabolites secondaires lichéniques: de l'écologie chimique aux perspectives thérapeutiques.....	18
i. Contraintes abiotiques	18
ii. Stress biotiques	19
c. Approches analytiques pour le profilage chimique de lichens	20
E. Conclusion	54
PARTIE 2 : APPROCHES DÉRÉPLICATIVES INNOVANTES EN LICHÉNOLOGIE	56
I. Analyses de lichens par CCM-ESI-MS	57
II. Nouvelles techniques pour l'analyse de lichens <i>in situ</i>	72
A. Apport déréplicatif du DART-MS.....	72
a. Profilage chimique de <i>Lichina pygmaea</i>	73
b. Profilage chimique d' <i>Ophioparma ventosa</i> et études phytochimiques associées.....	84
c. Profilage chimique de lichen divers pour la détection d'autres classes structurales	104
B. Déréplication par diffraction par poudres des rayons X : application à quelques lichens appartenant au genre <i>Cladonia</i>	105
III. Apport du LDI-MS pour la déréplication de lichens	111
PARTIE 3 : HISTOLOCALISATION DE COMPOSÉS LICHÉNIQUES	132
I. État de l'art.....	132
II. Distribution tissulaire des composés produits par <i>Ophioparma ventosa</i> par LDI-MSI : écologie chimique.....	134
III. Étude de la contribution des symbiontes dans la biosynthèse de composés : application à la biosynthèse de la mycosporine sérinol de <i>Lichina pygmaea</i> par une approche alliant imagerie par spectrométrie de masse et génétique	144
A. Mycosporines : données structurales et connaissances sur leur biosynthèse	144
B. Investigation moléculaire (LDI-MSI) et génétique de <i>Lichina pygmaea</i>	151
a. Stratégie générale	151
b. Approches retenues pour histolocaliser les mycosporines.....	151
i. Spectromicroscopie Raman.....	151
ii. Imagerie par spectrométrie de masse LDI à 266 nm.....	154
iii. Profilage chimique de cellules pures micro-disséquées.....	154
c. Recherche des gènes du cluster de biosynthèse des mycosporines.....	154

i.	Procédures expérimentales.....	154
1.	Matériel lichénique	154
2.	Recueil isolé des partenaires de la symbiose	155
3.	Extraction de l'ADN génomique de <i>Lichina pygmaea</i> (lichen total ou champignon microdisséqué) et de <i>Rivularia sp.</i> (cyanobactérie microdisséquée).....	156
4.	Recherche des gènes par PCR dégénérée et purification des amplicons	156
a.	Désignation des amorces cyanobactériennes	156
b.	Désignation des amorces fongiques.....	157
c.	Conditions de PCR	157
5.	Sous-clonage des produits PCR	157
6.	Transformation des cellules et sélection des clones recombinants.....	158
7.	Purification de l'ADN plasmidique.....	158
8.	Séquençage	158
ii.	Premiers résultats sur l'équipement génétique des symbiontes.....	158
	CONCLUSION GÉNÉRALE/PERSPECTIVES	165
	BIBLIOGRAPHIE	171
	Annexe 1 : Biosynthèse des métabolites secondaires lichéniques	187
A.	Voie des polyacétates/polymalonates	187
a.	Polyacétates aromatiques	187
1.	Depsides	189
2.	Depsidones	189
3.	Depsones	190
4.	Dibenzofuranes et acide usnique	191
5.	Diphényléthers	193
6.	Quinones, xanthones et chromones	193
b.	Polyacétates non aromatiques.....	197
B.	Voie de l'acide mévalonique	197
C.	Voie de l'acide shikimique.....	198
	Annexe 2 : Généralités sur la diffraction des rayons X par la matière cristallisée	200
A.	Concepts cristallographiques de base	200
B.	Rappels généraux sur la diffraction.....	203
C.	Conditions de diffraction des rayons X par la matière cristallisée	205
D.	Techniques de diffraction de rayons X	207
a.	Diffraction de monocristal.....	207
b.	Diffraction sur poudres.....	207
	Annexe 3 : Supporting Material TLC-MS draft	210
	Annexe 4 : Supporting Material Phytochem. Anal. 2016; 27: 354-363	214
	Annexe 5 : Supporting Material J. Nat. Prod. 2016 ; 79(4) : 1005-1011	234
	Annexe 6 : Molecules 2016 ; 21(3) : 294	257
	Annexe 7 : Supporting Material Anal. Chem. 2015; 87(10): 10421-10428	288
	Annexe 8 : Supporting Material LDI-imaging <i>Ophioparma ventosa</i>, Sci. Rep. 2016; 6: 37807	323
	Annexe 9 : Données complémentaires de biologie moléculaire	327
A.	Extraction de l'ADN génomique.	327
a.	Principe.....	327
b.	Protocole	327
B.	Alignement de séquences pour la désignation des amorces.....	328
C.	Principe du sous-clonage par Topo-cloning	335

D. Transformation des cellules électro-compétentes et principe de la transformation par électroporation.....	335
E. Sélection des cellules recombinantes	337
F. Protocole de purification de l'ADN plasmidique par lyse alcaline	339
a. Principe.....	339
b. Protocole	339
G. Fragments de gènes séquencés	340

Production scientifique

Publications

Pierre Le Pogam, Béatrice Legouin, Anne-Cécile Le Lamer, Joël Boustie, David Rondeau
Analysis of the cyanolichen *Lichina pygmaea* metabolites using *in situ* DART-MS: from detection to thermochemistry of mycosporine serinol, *Journal of Mass Spectrometry* **2015**, 50, 454-462.

Pierre Le Pogam, Andreas Schinkovitz, Béatrice Legouin, Anne-Cécile Le Lamer, Joël Boustie, Pascal Richomme
Matrix-free Laser Desorption and Ionization Mass Spectrometry as a versatile approach for accelerating dereplication studies on lichens, *Analytical Chemistry* **2015**, 87, 10421-10428.

Pierre Le Pogam and Joël Boustie
Xanthones of lichen source : a 2016 update, *Molecules* **2016**, 21, 294.

Pierre Le Pogam, Anne-Cécile Le Lamer, Bandi Siva, Béatrice Legouin, Arnaud Bondon, Jérôme Graton, Denis Jacquemin, Isabelle Rouaud, Solenn Ferron, Walter Obermayer, K. Suresh Babu, Joël Boustie
Minor pyranonaphthoquinones from the apothecia of the lichen *Ophioparma ventosa*, *Journal of Natural Products* **2016**, 79, 1005-1011.

Pierre Le Pogam, Anne-Cécile Le Lamer, Béatrice Legouin, Joël Boustie, David Rondeau
In situ DART-MS as a versatile and rapid dereplication tool in lichenology: chemical fingerprinting of *Ophioparma ventosa*, *Phytochemical Analysis* **2016**, 27, 354-363.

Pierre Le Pogam, Béatrice Legouin, Audrey Geairon, Hélène Rogniaux, Walter Obermayer, Joël Boustie, Anne-Cécile Le Lamer
Laser Desorption Ionization Mass Spectrometry Imaging to delineate the role of lichen compounds through spatial mapping: application to *Ophioparma ventosa*, *Scientific Reports* **2016**, 6, 37807.

Thuc-Huy Duong, Bui Linh Chi Huynh, Warinthorn Chavasiri, Marylène Chollet-Krugler, Kieu Nguyen Van, Thu Nguyen Thi Hoai, Poul Erik Hansen, Pierre Le Pogam, Holger Thüs, Joël Boustie, Kim Phi Phung Nguyen
New erythritol derivatives from the fertile form of *Rocella montagnei*, *Phytochemistry* (**under revision**)

Pierre Le Pogam, Aline Pillot, Françoise Le Dévéhat, Anne-Cécile Le Lamer, Béatrice Legouin, Alice Gadea, Aurélie Sauvager, Damien Ertz, Joël Boustie
Mass spectrometry as a versatile ancillary technique for the rapid *in situ* identification of lichen metabolites directly from TLC plates, *The Lichenologist* (**submitted**)

Béatrice Legouin, Françoise Lohézic-Le Dévéhat, Solenn Ferron, Isabelle Rouaud, Pierre Le Pogam, Laurence Cornevin, Michel Bertrand, Joël Boustie
Specialized metabolites of *Vulpicida pinastri* (Scop.) Gray act as photoprotective agents, *Fitoterapia* (**submitted**)

Alice Gadea, Pierre Le Pogam, Grichka Biver, Anne-Cécile Le Lamer, Joël Boustie, Françoise Le Dévéhat, Maryvonne Charrier
Which secondary metabolites does the native subantarctic gastropod *Notodiscus hookeri* extract from the consumption of the lichens *Usnea taylorii* and *Pseudocyphellaria crocata*?, *Molecules* (**in preparation**)

Thuc-Huy Duong, Pierre Le Pogam, Xuan-Phong Ha, Warinthorn Chavasiri, Joël Boustie, Marylène Chollet-Krugler, Thapond Teerawatananond, Nongnuj Muangsin, Bohari Mohd Yahmin, Bui Linh Chi Huynh, Kim Phi Phung Nguyen

New 12H-6,12-methanodibenzo[d,g][1,3]dioxocine derivatives isolated from the lichen *Parmotrema sancti-angelii* (Lynge) Hale, *Tetrahedron* (in preparation)

Chapitres d'ouvrage

Pierre Le Pogam, Gaëtan Herbette, Joël Boustie.

Analysis of lichen metabolites: a variety of approaches. In: Recent advances in Lichenology. **2015**, 229-261.

Communications orales

Chemical profiling of the lichen Ophioparma ventosa using DART-MS

XXII^{ème} rencontre du Groupement des Pharmacochimistes de l'Arc Atlantique, Nantes, France, 28-29 Août 2014.

LDI-MSI : distribution of metabolites within Ophioparma ventosa

2^{ème} symposium international AFERP-STOLON – Biodiversité et Substances Naturelles, Lyon, France, 15-17 Juillet 2015.

Innovative mass spectrometry tools in lichenology to screen for new molecules and delineate their bioactivities through spatial mapping

6^{ème} journée Pharmacie Recherche, Rennes, France, 20 janvier 2016.

Dereplication and histolocalization for lichen metabolites

Indo-French Joint Laboratory for Natural Products and Synthesis towards Affordable Health, 2016 symposium, Rennes, France, 17-18 mars 2016.

Mass spectrometry for high-throughput chemical profiling and chemical ecology studies on lichens

Séminaire d'équipe MDCEM (Molécules de Défense et de Communication dans les Ecosystèmes Microbiens), Muséum National d'Histoire Naturelle, Paris 5, France, 22 avril 2016.

Histolocalisation de métabolites secondaires par spectrométrie de masse: application au thalle du lichen Ophioparma ventosa

- Journée d'animation scientifique de l'axe Analyse Structurale et Métabolomique (Biogenouest), Phénotypages, chémotypages, analyses structurales : caractérisation multi-échelles, Angers, France, 16 juin 2016.
- Demie Journée Interface du programme Biology and Chemistry (BiChe), Rennes, France, 17 juin 2016.

Communications affichées

Pierre Le Pogam, Béatrice Legouin, Joël Boustie, David Rondeau

Detection and chemical reactivity of lichen secondary metabolites using in situ DART-MS.

The European Proteomics Association (EuPA) Scientific Meeting, Saint-Malo, France, 17 octobre 2013.

Pierre Le Pogam, Anne-Cécile Le Lamer, Béatrice Legouin, Joël Boustie, David Rondeau

In situ DART-MS : a promising dereplicative approach in lichenology

5^{ème} journée Pharmacie Recherche, Rennes, France, 21 janvier 2015.

Pierre Le Pogam, Andreas Schinkovitz, Béatrice Legouin, Anne-Cécile Le Lamer, Joël Boustie, Pascal Richomme

LDI-MS as a versatile and accelerated dereplicative approach for lichens

2^{ème} symposium international AFERP-STOLON – Biodiversité et Substances Naturelles, Lyon, France, 15-17 Juillet 2015.

Pierre Le Pogam, Anne-Cécile Le Lamer, Béatrice Legouin, Audrey Geairon, David Rondeau, Alain Fautrel, Joël Boustie

*Innovative mass spectrometry approaches to delineate the role of lichen compounds through spatial mapping : chemical ecology of *Ophioparma ventosa**

9th Joint Natural Products Conference, Copenhagen, Danemark, 24-27 Juillet 2016.

Andreas Schinkovitz, Thomas Guillemette, N. Blond, Pierre Le Pogam, Nathalie Jaozara, Katia Kerdja, Joël Boustie, Philippe Simoneau, Pascal Richomme

*Antifungal activity of lichen extracts and compounds against *Alternaria brassicola**

9th Joint Natural Products Conference, Copenhagen, Danemark, 24-27 Juillet 2016.

Alice Gadéa, Françoise Le Dévéhat, Anne-Cécile Le Lamer, Pierre Le Pogam, Damien Ertz, Maryvonne Charrier, Joël Boustie

*Sectorial land snail damage to the lichen *Argopsis friesiana* could be explained by metabolites profiles*

- 9th Joint Natural Products Conference, Copenhagen, Danemark, 24-27 Juillet 2016.
- 8th International Association of Lichenology Symposium, Helsinki, Finland, 1-5 August 2016.

Liste des abréviations

3-DQ : 3-DehydroQuinate
aDHQS : amino DeHydroQuinate Synthase
ADN : Acide DésoxyriboNucléique
ADNg : Acide DésoxyriboNucléique génomique
Amu : Atomic Mass Unit
APCI : Atmospheric Pressure Chemical Ionization
ARNm : Acide RiboNucléique messenger
ATP : Adénosine TriPhosphate
BLAST : Basic Local Alignment Sequence Tool
CCM : Chromatographie Couche Mince
CDA : Chiral Derivatizing Agent
CID : Collision Induced Dissociation
CoA : Coenzyme A
COSY : Correlation Spectroscopy
Da : Dalton
DAD : Diode Array Detector
DART : Direct Analysis in Real Time
DCM : DiChloroMethane
Deg. : Degenerate
DESI : Desorption ElectroSpray Ionization
DHGO : DeHydroGeodine Oxidase
DHQS : DeHydroQuinate Synthase
DMSO : DiMethylSulfOxide
dNTP : désoxy Nucléotides Tri Phosphate
DO : Densité Optique
DOS : 2-deoxy-scylo-inosose synthase
DPPH : DiPhenylPicrylHydrazine
ECD : Electronic Circular Dichroism
EDTA : Ethyle Diamine Tetra Acetic acid
ESI : ElectroSpray Ionization
EVS : 2-*epi*-5-*epi*-Valiolone Synthase
FAB : Fast Atom Bombardment
FISH : Fluorescent In Situ Hybridization
FPA : Focal Plane Array
FTIR : Fourier Transform Infra Red
GAW : Glycérol – Alcool – Eau (1-1-1)
GC : Gas Chromatography
GE : Glycérol – Acide acétique glacial (E pour Essigsäure) (3-1)
HMBC : Heteronuclear Multiple Bond Correlation
HMQC : Heteronuclear Multiple Quantum Coherence spectroscopy
HPTLC : High Performance Thin Layer Chromatography
HRESIMS : High Resolution ElectroSpray Ionization
HRMS : High Resolution Mass Spectrometry
HSQC : Heteronuclear Single Quantum Coherence spectroscopy
IC₅₀ : Concentration Inhibitrice à 50%
IM-MS : Ion Mobility – Mass Spectrometry
IMS : Imaging Mass Spectrometry
INC : Ion-Neutral Complex
IPTG : IsoPropyl β-D-1-ThioGalactopyranoside
IR : Infra Rouge
K : Potasse

LAESI : Laser Ablation Electrospray Ionization
Laser : Light amplification by stimulated emission of ray
LB : Lysogeny Broth
LCM : Laser Capture Microdissection
LDI : Laser Desorption Ionization
LMMS : Laser Microprobe Mass Spectrometry
MAA : Mycosporine-like Amino Acids
MALDI : Matrix-Assisted Laser Desorption Ionization
MEB : Microscopie Electronique à Balayage
MS : Mass Spectrometry
MSI : Mass Spectrometry Imaging
MTBE : Methyl-*tert*-Butyl Ether
MTPA : MethoxyTrifluoromethylPhenylAcetic acid
NBT : NitroBlue Tetrazolium
Nd:YAG : Neodymium-doped Yttrium Aluminium Grenat
NI : Negative Ionization
NIMS : NanoStructure Initiator Mass Spectrometry
NMR : Nuclear Magnetic Resonance
NOESY : Nuclear Overhauser Effect Spectroscopy
NRPS : Non-Ribosomal Protein Synthase
O-MT : O-MethylTransferase
OCT : Optimal Cutting Temperature
ORD : Optical Rotatory Dispersion
ORF : Open Reading Frame
P : Para-phénylène diamine
Pb : Paires de Bases
PCB : Poly Chlorinated Biphenyl
PCR : Polymerase Chain Reaction
PDA : Photo Diode Array
PI : Positive Ionization
PKS : PolyKetide Synthase
PNSCM : Produits Naturels, Synthèses, Chimie Médicinale
Ppm : partie par million
Rf : Rapport frontal
RIC : Reconstructed Ion Chromatogram
ROESY : Rotating Frame nuclear Overhauser Effect Spectroscopy
ROS : Reactive Oxygen Species
rpm : Rotations par minute
SCF : SuperCritic Fluid
SFE : Supercritic Fluid Extraction
SIMS : Secondary Ions Mass Spectrometry
SY : Survival Yield
TDDFT : Time-Dependent Density Functional Theory
TIC : Total Ion Chromatogram
TLC : Thin Layer Chromatography
TMEM : Transient MicroEnvironment Mechanism
TOCSY : Total Correlation Spectroscopy
TOF : Time Of Flight
UV/Vis : UltraViolet/Visible

Table des figures

Figure 1 : Trois exemples de champignons saprotrophes : A - <i>Oudemansiella mucida</i> se développant généralement sur des branches de hêtre tombées à terre ; B - <i>Agaricus xanthoderma</i> , champignon rencontré dans des prairies ; C – <i>Mitruha paludosa</i> , espèce s'établissant sur des débris végétaux immergés.....	6
Figure 2: Champignons parasites à l'égard d'hôtes divers. A – <i>Armillaria solidipes</i> est un virulent parasite des racines d'arbre ; B – <i>Beauveria bassiana</i> est un champignon entomopathogène ; C – Un exemple de mycoparasite : <i>Asterophora parasitica</i> poussant sur une russule noircissante (<i>Russula nigricans</i>).	6
Figure 3 : Deux types de mycorhizes très répandus : A – les mycorhizes à vésicules et arbuscules et B – les ectomycorhizes.	7
Figure 4 : Trois lichens représentant les associations symbiotiques lichéniques dans leur diversité. A – <i>Ophioparma ventosa</i> est dans le cas de figure majoritaire en associant un ascomycète à une algue verte du genre <i>Trebouxia</i> ; B – <i>Lichina pygmaea</i> réunit un ascomycète et une cyanobactérie (genre <i>Calothrix</i>) ; C – <i>Dictyonema glabratum</i> entre dans les deux cas de figure minoritaires en contenant un basidiomycète et une cyanobactérie (<i>Chroococcus</i>).....	8
Figure 5 : Deux exemples de lichens à céphalodies externes. A – <i>Peltigera aptosa</i> et ses céphalodies noires ponctiformes; B – <i>Placopsis gelida</i> présente des céphalodies orangées.....	9
Figure 6 : Les deux phototypes de <i>Sticta canariensis</i> . A – Thalle à algue verte et B – Thalle à cyanobactérie prédominante présentant une couleur bleue/noire en environnement plus humide et/ou sombre, quelques parties éparses de thalles à algue verte restent visibles.....	9
Figure 7 : Contribution du photobionte dans la structuration du thalle lichénique. A – Photobionte uniquement localisé sous le cortex supérieur (Microscopie Électronique à Balayage du thalle de <i>Parmelia sulcata</i>) et B – Photographie de <i>Coenogonium lepreurii</i> dont le thalle est structuré par une algue filamenteuse du genre <i>Trentepohlia</i>	10
Figure 8: a) Localisation des bactéries sur une coupe transversale de thalle de <i>Lobaria pulmonaria</i> , modélisation tridimensionnelle à partir d'imagerie FISH. Les Eubactéries (visualisées en rouge) et les Alphaprotéobactéries (représentées en jaune) montrent une localisation ubiquiste sur les deux faces du lichen, à l'inverse, les Bétaprotéobactéries (roses) sont moins abondantes et confinées à des régions précises du thalle. b) Vue moderne de la symbiose lichénique incorporant le bactériobionte et les rôles présumés de chaque participant de cet écosystème (Figure extraite de (Grube et al., 2015)).	11
Figure 9 : Illustration des variétés de biotopes colonisés par les lichens. A – <i>Lichina pygmaea</i> est un cyanolichen se développant sur l'estran, notamment le long des côtes bretonnes (Roullier et al., 2011), B – Les lichens appartenant au genre <i>Dermatocarpon</i> sont amphibies et se développent sur des roches siliceuses bordant les cours d'eau, à mi-ombre (Fontaine et al., 2012) C – <i>Flavocetraria nivalis</i> réalise la photosynthèse à des températures descendant à -20°C (Kallio and Heinonen, 1971), D – <i>Xanthoria elegans</i> est un lichen cosmopolite pouvant être rencontré jusqu'à 7.000 mètres d'altitude dans l'Himalaya (Øvstedal and Smith, 2001) et pouvant survivre à une atmosphère martienne (Brandt et al., 2015), E – D'importantes étendues du désert de Namib recouvertes par les thalles fruticuleux de <i>Teloschistes capensis</i> (Lange et al., 2006).	12
Figure 10 : Illustration des principaux types morphologiques de lichens. A – Thalle crustacé de <i>Diploicia canescens</i> ; B – Thalle foliacé de <i>Vulpicida pinastri</i> ; C – Thalle fruticuleux de <i>Flavocetraria nivalis</i> ; D – Thalle squamuleux de <i>Normandina pulchella</i> ; E – Thalle lépreux de <i>Lepraria membranacea</i> ; F – Thalle gélatineux d' <i>Enchylium tenax</i> ; G – Thalle complexe de <i>Stereocaulon evolutum</i>	13

Figure 11: Principales structures histologiques rencontrées chez les lichens. De gauche à droite : thalle hétéromère, thalle homéomère et thalle radié. 14

Figure 12: Propagules de dissémination symbiotique rencontrées chez les lichens. A et B – Schémas représentant les sorédies et les isidies. C – Soralies jaunes de *Pseudocyphellaria crocata* et D – Isidies coralloïdes (noires) de *Lasallia pustulata*. 15

Figure 13: Organes de reproduction sexuée chez les ascolichens. A – Apothécies de *Teloschistes chrysophthalmus* ; B – Lirelles de *Graphis scripta* ; C – Périthèces de *Pyrenula laevigata*. 16

Figure 14: Basidiomes de *Lichenomphalia meridionalis*. 16

Figure 15: Voies de biosynthèse rencontrées chez les lichens et motifs structuraux associés. 17

Figure 16 : Principales techniques de spectrométrie de masse à ionisation ambiante et quelques possibles applications (tiré de (Li et al., 2013))..... 72

Figure 17: Photographies de *Lichina pygmaea* et structure de ses métabolites secondaires détectés en DART-MS..... 73

Figure 18 : Photographie d'*Ophioparma ventosa* et métabolites secondaires isolés au cours de l'étude phytochimique associée 85

Figure 19: Naphtoquinones isolées au cours de l'étude phytochimique menée sur les apothécies d'*Ophioparma ventosa* 96

Figure 20 : *Cladonia* utilisés lors des analyses dérégulatives par diffraction de rayons X : photographies et métabolites secondaires majoritaires. 106

Figure 21: Diffractogrammes rayons X sur poudres relatifs à *Cladonia portentosa* et à ses métabolites secondaires. Noir, poudre totale de lichen sans tamisage (après soustraction du fond continu) ; rouge, acide perlatolique ; bleu, acide usnique. 107

Figure 22: Diffractogrammes rayons X sur poudres relatifs à *Cladonia portentosa* : noir, non tamisé ; rouge, fraction supérieure à 125 µm ; bleu, grains compris entre 80 et 125 µm et vert, grains inférieurs à 80 µm. 107

Figure 23: Formations cristallines à la surface du cortex supérieur de *Cladonia portentosa* observées en Microscopie Électronique à Balayage (x 5000) 108

Figure 24 : Diffractogrammes rayons X sur poudres relatifs à *Cladonia rangiferina* et à ses métabolites secondaires. Noir, poudre totale de lichen sans tamisage (après soustraction du fond continu) ; bleu, acide fumarprotocétrarique ; rouge, atranorine. Les pics marqués en vert sont associés à la présence de quartz dans l'échantillon. 109

Figure 25 : Diffractogrammes rayons X sur poudres relatifs à *Cladonia rangiferina* : noir, non tamisé ; rouge, fraction supérieure à 125 µm ; bleu, grains compris entre 80 et 125 µm et vert, grains inférieurs à 80 µm. 109

Figure 26: Diffractogrammes rayons X sur poudres relatifs à *Cladonia ciliata* et à l'acide usnique. Noir, poudre totale de lichen sans tamisage (après soustraction du fond continu) ; rouge, acide usnique. Les pics marqués en vert sont associés à la présence de quartz dans l'échantillon et celui en bleu correspond à la présence de NaCl..... 110

Figure 27: Diffractogrammes rayons X sur poudres relatifs à *Cladonia ciliata* : noir, non tamisé ; rouge, fraction supérieure à 125 µm ; bleu, grains compris entre 80 et 125 µm et vert, grains inférieurs à 80 µm. 110

Figure 28 : Principe de l'ionisation MALDI et homologues structurales entre le DiHydroxyBenzoate (matrice commerciale) et l'acide usnique 111

Figure 29: Principe de l'acquisition des données en imagerie par spectrométrie de masse LDI 133

Figure 30: Noyaux des oxo- et des iminomycosporines et données spectrales associées. 144

Figure 31 : Produits issus des voies métaboliques initiées par DHQS et les enzymes DHQS-like. DOS = 2-deoxy-scyllo-inosose synthase, EVS = 2-epi-5-epi-valiolone synthase, DHQS = DeHydroQuinateSynthase, aDHQS= amino DeHydroQuinate Synthase (Wu et al., 2007). 146

Figure 32: Motifs structuraux obtenus sous l'action de différentes enzymes DHQS-like. Le 4-désoxygadusol est obtenu directement et non par l'intermédiaire de 3-DQ.....	146
Figure 33: Biosynthèse de la shinorine chez <i>Anabaena variabilis</i> d'après Balskus et Walsh : structures chimiques des différents intermédiaires et enzymes impliquées.....	148
Figure 34: Hypothèse de Shick concernant la biosynthèse des mycosorines chez les coraux hermatypiques, adapté de (Shick et al., 1999). Ce scénario biogénétique est inspiré par la séquence de biosynthèse des mycosporines chez les coraux. La récente découverte du cluster de 4 gènes chez le cnidaire anthozoaire <i>Acropora digitata</i> semble aller à l'encontre de cette hypothèse (Shinzato et al., 2011).....	149
Figure 35 : Structures chimiques des mycosporines isolées de lichens indiquant le nom du lichen produisant ce composé et les références de la publication décrivant leur isolement. Les noms de lichens indiqués en bleu correspondent aux cyanolichens tandis que ceux écrits en vert sont des chlorolichens. Références : (Büdel et al., 1997; Torres et al., 2004; De la Coba et al., 2009; Roullier et al., 2009, 2011; Nguyen et al., 2015).....	150
Figure 36 : Approches retenues pour étudier la contribution des symbiontes dans la biosynthèse des mycosporines chez <i>Lichina pygmaea</i> (Photographie : Pierre Le Pogam et Alain Fautrel).....	151
Figure 37: Diffusion Rayleigh et Diffusion Raman http://www.ifremer.fr/rd_technologiques/Moyens/Laboratoires/Spectroscopies-Techniques-de-mesures-in-situ/Spectroscopie-Raman	152
Figure 38: Bases quantiques des différentes techniques de spectroscopie vibrationnelle https://www.surfgroup.be/raman	153
Figure 39: Spectre Raman : Raies Stokes et Anti-Stokes http://www.raman.de/htmlEN/basics/intensityEng.html	153
Figure 40: Illustration du processus de micro-dissection capture laser A- Différentes étapes permettant la capture des cellules dans un film de polymère fondu sous l'action d'une irradiation UV (adapté de (Espina et al., 2006)) et B – Le bouchon portant les cellules capturées s'adapte sur un tube Eppendorf et des tampons de lyse permettent d'extraire le type de biomolécules d'intérêt (tiré de (Simone et al., 1998)).	155
Figure 41 : Recherche des gènes DHQS-like et ATP-grasp (amorces cyanobactériennes dans les deux cas) au sein de la cyanobactérie microdisséquée (<i>Rivularia</i>).....	159
Figure 42 : Cluster de gènes associé à la biosynthèse des mycosporines chez <i>Rivularia sp.</i> PCC 7116.....	159
Figure 43 : Recherche des gènes DHQS-like et ATP-grasp (amorces fongiques dans les deux cas) au sein du lichen total.	159
Figure 44 : Résumé des amplifications de gènes ATP-grasp	160
Figure 45 : Recherche des séquences homologues (BLASTx) des fragments de gène amplifiés par les amorces ATP-like cyanobactériennes sur le lichen total mais pas sur <i>Rivularia sp</i>	161
Figure 46 : Résumé des amplifications de gènes DHQS-like	161
Figure 47: Principe de la spectrométrie de mobilité ionique couplée à la spectrométrie de masse..	167
Figure 48 : Résultats et perspectives associés au DART-MS et au LDI-MS à l'issue de ces travaux....	168
Figure 49 : Méthodologies envisageables pour établir la distribution tissulaire de métabolites lichéniques et problématiques dans lesquelles ces analyses peuvent s'inscrire.....	170
Figure 50 : Familles structurales de métabolites lichéniques obtenues par condensations d'unités monoaromatiques.	188
Figure 51 : Voies de biosynthèse des depsidones.....	190
Figure 52 : Biosynthèse proposée pour les depsones et filiations biogénétiques possibles avec quelques depsides, depsidones et diphényléthers qui leur sont structurellement apparentées	191
Figure 53 : Biosynthèse de l'acide usnique (adapté de (Ingolfssdottir, 2002)).....	192

Figure 54 : Biosynthèse de dibenzofuranes <i>sensu stricto</i> (adapté de (Chooi, 2008))	192
Figure 55 : Possible transformation de la diploïcine en buelline	193
Figure 56: Biosynthèse des quinones à partir de l'intermédiaire poly- β -cétoester.....	193
Figure 57: Biosynthèse des xanthones ayant un pattern d'oxygénation de type lichéxanthone	194
Figure 58: Biosynthèse des xanthones affiliées à la thioméline et aux bisxanthones de type acide sécalonique et eumitrine (Le Pogam and Boustie, 2016).	195
Figure 59: Biosynthèse des chromones.....	196
Figure 60: Biosynthèse de diphényléthers <i>via</i> un intermédiaire anthraquinone	196
Figure 61 : Formules chimiques de quelques acides aliphatiques lichéniques.....	197
Figure 62: Familles structurales issues de la voie du mévalonate	198
Figure 63: Biosynthèse des dérivés de l'acide pulvinique (Gill and Steglich, 1987).....	199
Figure 64: Les sept systèmes cristallins.....	200
Figure 65 : Notions de base en cristallographie : nœuds, réseau et motif.	200
Figure 66 : Les 14 réseaux de Bravais.....	202
Figure 67: Montage expérimental dérivé des fentes de Young caractérisant les notions d'interférence et de diffraction lumineuses.....	204
Figure 68 : Géométrie illustrant les conditions de diffraction par les rayons X (loi de Bragg).....	205
Figure 69: Schéma illustrant les conditions de diffraction de Laue	206
Figure 70: Détermination du rayon de la sphère d'Ewald	206
Figure 71 : Formation des tâches de diffraction lors de la rotation du monocristal.....	207
Figure 72: Diffractogramme sur poudre d'échantillons microcristallins.....	208
Figure 73: Diffractogramme de poudres aux rayons X de sels de table et de la spécialité Excedrin°. Les diffractogrammes de référence associés aux produits cristallins purs sont fournis sur le diffractogramme total. Les ordonnées présentent l'intensité du signal de diffraction, normalisé sur le signal le plus intense (Hulien et al., 2015).....	209
Figure 74 : Alignement de séquences ATP-grasp extraites de cyanobactéries d'intérêt. Les séquences ciblées pour la désignation des amorces dégénérées sont surlignées en gris. Ava_3856 de <i>A. variabilis</i> ATCC 24913 ; WP_019491246.1 de <i>Calothrix</i> sp. PCC 7103 ; WP_039715341 de <i>Scytonema millei</i> ; WP_015199130.1 de <i>Calothrix parietina</i> ; KIJ85250.1 de <i>Scytonema tolypothrichoides</i> VB-61278 ; WP_017743130.1 de <i>Scytonema hofmanni</i>	329
Figure 75 : Alignement de séquences DHQS-like extraites de cyanobactéries d'intérêt. Les séquences ciblées pour la désignation des amorces dégénérées sont surlignées en gris. Ava_3858 de <i>A. variabilis</i> ATCC 24913 ; WP_019491244.1 de <i>Calothrix</i> sp. PCC 7103 ; WP_039715343.1 de <i>Scytonema millei</i> ; AFZ02505.1 de <i>Calothrix</i> sp. PCC 6303 ; KIJ85256.1 de <i>Scytonema tolypothrichoides</i> VB-61278 ; WP_026134319.1 de <i>Scytonema hofmanni</i>	329
Figure 76 : Alignement de séquences ATP-grasp extraites de champignons d'intérêt. Les séquences ciblées pour la désignation des amorces dégénérées sont surlignées en gris. KUJ16163.1* de <i>Phialocephala scopiformis</i> ; XP_007805993.1 d' <i>Endocarpon pusillum</i> Z07020 ; XP_007681459.1 de <i>Baudoinia panamericana</i> UAMH 10762 ; XP_013283808.1* de <i>Fonsecaea pedrosoi</i> CBS 271.37 ; XP_008713719.1* de <i>Cyphellophora europaea</i> CBS 101466 ; XP_007756893.1* de <i>Cladophialophora yegresii</i> CBS 114405 ; KIW 13571.1 d' <i>Exophiala spinifera</i> ; KKY35075.1 de <i>Diaporthe ampelina</i> ; KUI55508.1 de <i>Valsa mali</i> var. <i>pyri</i> ; XP_003719130.1 de <i>Magnaporthe oryzae</i> 70-15; KXJ90766.1 de <i>Microdochium bolleyi</i> ; XP_007839533.1 de <i>Pestalotiopsis fici</i> w106-1.* les protéines marquées d'une étoile sont dotées d'une réductase à leur extrémité n-terminale qui n'a pas été utilisée pour les alignements.....	332
Figure 77 : Alignement de séquences DHQS-like extraites de champignons d'intérêt. Les séquences ciblées pour la désignation des amorces dégénérées sont surlignées en gris. XP_007681536.1 de <i>Baudoinia panamericana</i> UAMH 10762 ; XP_008713717.1 de <i>Cyphellophora europaea</i> CBS 101466 ;	

KIW 13573.1 d'*Exophiala spinifera* ; XP_007756891.1 de *Cladophialophora yegresii* CBS 114405 ; XP_013283806.1 de *Fonsecaea pedrosoi* CBS 271.37 ; KUJ21542.1 de *Phialocephala scopiformis* ; XP_007805994.1 de *Endocarpon pusillum* Z07020 ; XP_007839531.1 de *Pestalotiopsis fici* w106-1 ; KKY35074.1 de *Diaporthe ampelina* ; KUI55509.1 de *Valsa mali* var. *pyri* ; XP_003719131.1 de *Magnaporthe oryzae* 70-15; KXJ90767.1 de *Microdochium bolleyi*..... 334

Figure 78 : Vecteur Pcr2.1-TOPO TA et régions d'intérêt 335

Figure 79 : Métabolisation de X-Gal par la β -galactosidase..... 337

Figure 80: Sélection des clones transformés recombinants par le système LacZ. Figure adaptée de http://ol.saulnier.free.fr/espace_travail/blanc_bleu.html..... 338

Figure 81 : Séquence du fragment de gène amplifié par les amorces DHQS-like cyanobactériennes sur *Rivularia sp.* microdisséqué..... 340

Figure 82 : Séquences des fragments de gène amplifiés par les amorces ATP-grasp cyanobactériennes sur le lichen total mais pas sur *Rivularia sp* 340

INTRODUCTION



Introduction

Les lichens représentent l'association symbiotique entre un champignon (*Ascomycota* dans 98% des cas) et un partenaire réalisant la photosynthèse (algue verte le plus souvent, parfois remplacée ou accompagnée par une cyanobactérie). Ce mode de vie singulier, représenté par plus de 18.500 espèces, confère à cet éco-système une autonomie énergétique permettant de coloniser de nombreux biotopes mais également une remarquable résilience à l'égard de stress environnementaux variés. Cette résilience tient pour partie à la constitution d'un arsenal de défense chimique recelant de nombreux métabolites secondaires uniques dans le vivant. Cette chimiodiversité, essentiellement façonnée au travers de trois voies de biosynthèse, compte aujourd'hui plus de 1.000 molécules correspondant en fait à une vingtaine de structures de base hautement modulées par des réarrangements et des ornementsations chimiques. En marge de leur rôle écologique, ces molécules sont également dotées de bioactivités variées et souvent significatives, faisant des lichens des candidats attractifs et atypiques dans la recherche de nouvelles molécules d'intérêt thérapeutique. La valorisation de cette ressource privilégiée doit toutefois s'adosser à des outils de dérégulation précoces et performants pour pouvoir cerner l'originalité structurale en amont d'études phytochimiques.

C'est dans ce contexte que l'équipe PNSCM (Produits Naturels, Synthèse, Chimie Médicinale) de l'UMR CNRS 6226 (Institut des Sciences Chimiques de Rennes) s'appuie sur cette chimiodiversité originale pour obtenir de nouvelles molécules valorisables à des fins thérapeutiques ou cosmétiques. Les recherches s'y articulent autour de trois approches complémentaires :

- l'extraction, l'isolement et l'élucidation structurale de molécules à partir de sources naturelles, les lichens, mais aussi plus récemment des cohortes bactériennes qui leur sont associées ;
- la synthèse de composés organiques, y compris de la synthèse totale de produits naturels ;
- les tests permettant la découverte et l'optimisation des composés bioactifs selon des approches de chimie médicinale.

Les enjeux de ce travail, entrepris dans le cadre de la première thématique mentionnée ci-dessus était double :

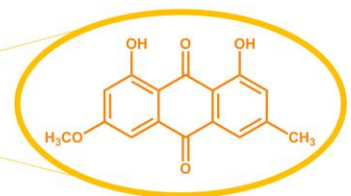
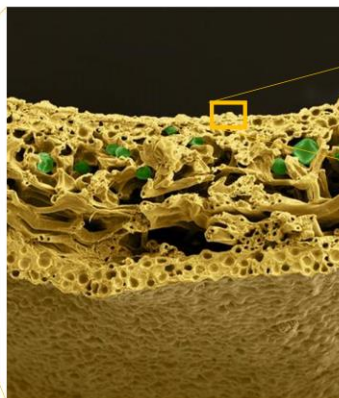
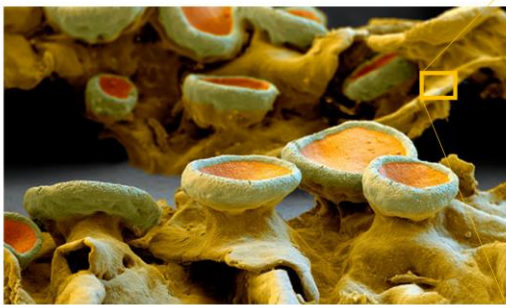
- connaître aussi rapidement que possible et de manière fiable les métabolites secondaires d'un lichen (dérégulation, chimiotaxonomie...) ;
- cartographier la distribution des métabolites secondaires au sein de thalles lichéniques. L'accès à cette donnée spatiale est d'un intérêt majeur pour comprendre le rôle écologique des métabolites secondaires lichéniques.

De succinctes présentations de ce que sont les lichens, leurs métabolites secondaires et les méthodes analytiques employées jusqu'à présent pour en réaliser le profilage chimique seront abordées au titre d'une première partie de ce mémoire.

Un premier volet de ce travail a donc consisté à développer de nouvelles stratégies analytiques pour cerner, en un minimum de temps et de préparation, le profil chimique de lichens. Le second chapitre de ce mémoire décrira ainsi l'apport dérégulatif de deux techniques de spectrométrie de masse ici appliquées de façon pionnière aux lichens : le DART-MS (*Direct Analysis in Real Time*) et le LDI-MS (*Laser Desorption and Ionization*). En parallèle de ces développements analytiques, il est apparu que les apothécies de l'un de nos organismes modèles, *Ophioparma ventosa*, contenaient de nouvelles molécules. L'étude phytochimique ayant permis d'y caractériser 4 nouveaux composés est décrite au titre de cette seconde partie.

Dans un second temps, ce projet s'est penché sur la localisation des métabolites secondaires au sein de thalles lichéniques par imagerie LDI. Sur la base de profils chimiques différents entre les faces supérieure et inférieure d'*Ophioparma ventosa* fournis par analyses DART, des analyses d'imagerie LDI ont été menées sur ce lichen pour pouvoir préciser la distribution de tous les métabolites secondaires qu'il contient avec une résolution spatiale de 50 μm . Les images acquises ainsi que les données d'écologie chimique qui en découlent seront présentées au cours du troisième chapitre de ce manuscrit. Les travaux d'histolocalisation entrepris dans le cadre de cette thèse se sont également penchés sur les mycosporines lichéniques dans l'idée de mieux comprendre l'implication des partenaires de la symbiose lichénique dans la biosynthèse de ces composés, qui sont aussi décrits à partir de champignons, d'algues et de cyanobactéries vivant à l'état libre. Cette étude s'est doublée d'une analyse du matériel génétique des symbiontes dans l'idée de préciser le(s)quel(s) détien(nen)t l'arsenal biosynthétique permettant de former ces composés.

LES LICHENS : DE SINGULIERS CHAMPIGNONS



PARTIE 1 : LES LICHENS : DE SINGULIERS CHAMPIGNONS

I. Position systématique des lichens au travers des siècles

Les lichens ont longtemps été des organismes en errance taxonomique à l'instar des champignons dont la position systématique est restée erronée pendant des siècles. Jusqu'en 1969, les biologistes divisent le Vivant en deux règnes extrêmement simples : les animaux, entités mobiles qui se nourrissent en ingérant des proies et les végétaux dont le métabolisme est alimenté par le dioxyde de carbone et les nutriments du sol.

Cette classification traditionnelle du Vivant place l'Homme au sommet de ce qui est en fait une hiérarchie des organismes. Les autres organismes s'éloignent de ce sommet selon les caractères qui leur font défaut. Cette perception du Vivant aboutit à définir des groupes négativement et sont ainsi rencontrés chez les végétaux les Cryptogames, dépourvus de fleurs, mais également les Thallophytes qui n'ont ni tiges, ni feuilles, ni racines. De la même façon, les champignons sont alors identifiés comme des végétaux dépourvus de chlorophylle.

Concernant les lichens, les naturalistes de la renaissance les associent aux mousses et Tournefort a été le premier à distinguer ces deux types d'organismes en 1694. Il est toutefois à noter que les lichens tels que définis par Tournefort incluent quelques hépatiques, mousses et fougères. Une première classification basée sur la morphologie des thalles de ce groupe erroné est proposée par l'allemand Dillenius en 1741. Une douzaine d'années plus tard, Carl Von Linné (1707-1778) applique la nomenclature binomiale qu'il a créée à de nombreux lichens. Linné et ses disciples rattachent les lichens aux algues (Gavériaux, 2006).

Le botaniste suédois Erik Acharius (1757-1819) distingue le premier les lichens des autres Cryptogames et référence les organes présents à la surface du thalle avec les notions d'apothécies, de sorédies... Cette nouvelle branche de la Cryptogamie pose les bases de la classification des lichens et introduit des genres et des espèces dont beaucoup sont toujours d'usage (Gavériaux, 2006).

Ce n'est qu'en 1867 que la véritable nature symbiotique du lichen, unissant une micro-algue verte et/ou une cyanobactérie à un champignon est décrite pour la première fois par Schwendener et De Bary (Honegger, 2000). D'emblée, cette conception révolutionnaire du lichen est reçue avec un accueil controversé attirant notamment les foudres du botaniste Wilhelm Nylander (1822-1899) qui qualifie cette théorie symbiotique « d'assertion de pure fantaisie » et de « calomnie ». Nylander réaffirme en 1896 que les lichens « constituent une noble et vénérable classe autonome de végétaux n'ayant rien de sérieusement commun avec les champignons et les algues ». Et ce dernier de conclure sur l'idée « que subordonner les lichens aux champignons est encore plus absurde que de réunir les Characées aux algues ». Il s'avèrera par la suite que les Characées sont des algues.

Tandis que la dichotomie animal/végétal apparaît vaguement satisfaisante pour différencier des organismes visibles à l'œil nu, les limitations associées à cette classification pour le moins simpliste deviennent évidentes lorsqu'il s'agit de classer les organismes unicellulaires. Une nouvelle dichotomie est alors introduite par le biologiste français Edouard Chatton pour palier à cette insuffisance en différenciant les organismes constitués de cellules sans noyaux (qu'il nomme procaryotes) et les organismes dotés de cellules à noyaux (les eucaryotes) (Soyer-Gobillard, 1985).

Cette importante découverte restructure la conception du Vivant et posera les premières bases vers l'actuelle classification distinguant cinq règnes :

- les procaryotes, organismes unicellulaires dépourvus de noyaux ;
- les protistes, eucaryotes très généralement unicellulaires ;
- les végétaux, eucaryotes très généralement pluricellulaires autotrophes, réalisant la photosynthèse ;
- les animaux, eucaryotes pluricellulaires hétérotrophes qui ingèrent ;
- les champignons, organismes hétérotrophes qui absorbent.

II. Généralités sur les champignons

Il est donc aujourd'hui admis que les champignons constituent un règne autonome, défini par sept caractéristiques fondamentales (Whittaker, 1969) :

- ce sont des organismes eucaryotes ;
- ils sont hétérotrophes vis-à-vis du carbone ;
- ils sont absorbotrophes c'est-à-dire qu'ils absorbent au travers de leur paroi cellulaire les nutriments issus d'une digestion extracellulaire qu'ils opèrent grâce à leur arsenal enzymatique ;
- ils sont filamenteux, diffus et tubulaires. L'organisme fongique est très discret dans son état végétatif car il est constitué de filaments microscopiques enfouis dans le substrat colonisé (= le mycélium). Ce feutrage mycélien permet d'explorer le sol avec une grande finesse et donc d'y optimiser le prélèvement d'eau et de sels minéraux. L'agrégation de ces réseaux peut parfois rendre le mycélium visible à l'œil nu soit sous la forme de fines toiles soit plus rarement sous la forme de structures plus conséquentes évoquant des racines (les rhizomorphes) ;
- ils se reproduisent par des spores ;
- les spores ne sont pas flagellées (exceptionnellement un seul flagelle) ;
- leur paroi cellulaire contient de la chitine et jamais de cellulose.

L'un des points fondamentaux de cette ségrégation est donc l'absence de photosynthèse qui rend ces organismes hétérotrophes vis-à-vis du carbone, d'où le besoin pour les champignons de se procurer dans leur environnement des sources de carbone organique.

Cette contrainte métabolique peut être assumée par trois stratégies différentes, selon la provenance des sources de carbone organique (Lewis, 1973) :

- le **saprophytisme** qui consiste à prélever les nutriments à partir d'un substrat organique mort (Figure 1). Ces champignons détiennent un rôle écologique majeur en favorisant la décomposition des feuilles et du bois pour réintégrer leurs éléments constitutifs dans la chaîne trophique (Grinhut et al., 2007). Ces espèces peuvent être cultivées artificiellement pour peu qu'une combinaison adéquate de nutriments leur soit fournie ;



FIGURE 1 : TROIS EXEMPLES DE CHAMPIGNONS SAPROTROPHES : A - *OUDEMANSIELLA MUCIDA* SE DÉVELOPPANT GÉNÉRALEMENT SUR DES BRANCHES DE HÊTRE TOMBÉES A TERRE ; B - *AGARICUS XANTHODERMA*, CHAMPIGNON RENCONTRÉ DANS DES PRAIRIES ; C – *MITRULA PALUDOSA*, ESPÈCE S’ÉTABLISSANT SUR DES DÉBRIS VEGETAUX IMMERGÉS.

- le **parasitisme**, où le prélèvement de matière organique est réalisé au détriment d’un autre organisme vivant en lui portant préjudice (parfois jusqu’à le tuer). Des organismes de différents règnes peuvent être affectés : plantes (agents de maladies cryptogamiques, syndromes racinaires des Armillaires...) mais également parfois des insectes ou encore d’autres champignons (c’est dans ce dernier cas de l’hyperparasitisme) (Desprez-Loustau et al., 2007) (Figure 2). De tels organismes peuvent également poser de sérieux problèmes pour les écosystèmes. Ainsi, une colonie d’*Armillaria solidipes* détient le titre de plus grand organisme vivant puisqu’un individu s’étalant sur près de 9 km² pour un âge estimé à 2.200 ans a été décrit dans la forêt nationale de Malheur dans l’Orégon où elle décime d’importantes populations de conifères (Ferguson et al., 2003) ;



FIGURE 2: CHAMPIGNONS PARASITES À L’ÉGARD D’HÔTES DIVERS. A – *ARMILLARIA SOLIDIPES* EST UN VIRULENT PARASITE DES RACINES D’ARBRE ; B – *BEAUVERIA BASSIANA* EST UN CHAMPIGNON ENTOMOPATHOGENÈ ; C – UN EXEMPLE DE MYCOPARASITE : *ASTEROPHORA PARASITICA* POUSSANT SUR UNE RUSSULE NOIRCISANTE (*RUSSULA NIGRICANS*).

- enfin, la **ymbiose** désigne l’association durable et mutuellement bénéfique du champignon avec un partenaire qui va lui fournir sa matière organique obtenue par autotrophie. Les champignons engagés dans des relations symbiotiques incluent les champignons mycorhiziens et les lichens.

Dans le cadre des champignons mycorhiziens, le partenaire symbiotique est un végétal et les échanges vont se produire au niveau d’une structure mixte : les mycorhizes (du grec « mukês » pour champignon et « rhiza » pour racines) (Figure 3). Le feutrage mycélien du champignon entoure ou envahit partiellement les racines de la plante pour y prélever les sucres. En contrepartie, le champignon offre de l’eau et des sels minéraux prélevés dans les minuscules espaces poreux du sol à l’aide de ses fines hyphes, remplissant ainsi le rôle absorbant normalement dévolu aux poils absorbants des racines (Selosse et al., 2006). Près de 90 % des plantes terrestres sont ainsi mycorhizées et histologiquement, diverses organisations mycorhiziennes peuvent être distinguées (Figure 3). Les arbres forestiers des régions tempérées s’associent à des champignons (Bolets,

Amanites...) en des mycorhizes sans pénétration cellulaire, où le feutrage mycélien développe un manteau autour de la racine (Brundrett, 2009; Malloch et al., 1980). Chez les Orchidées en revanche, le champignon est peu abondant autour de la racine, mais pénètre les cellules où il forme des accumulations de filaments appelés pelotons (Selosse et al., 2011). 74% des plantes développent des associations mycorhiziennes avec des *Glomeromycota* qui ne donnent jamais de fructifications visibles, c'est notamment le cas de la plupart des herbes mais également des arbres tropicaux et des mousses (Ligrone et al., 2007; van der Heijden et al., 2015). Enfin, certaines familles botaniques ne sont jamais mycorhizées, c'est notamment le cas des Brassicacées, des Crassulacées et des Protéacées parmi d'autres (Lambers and Teste, 2013).

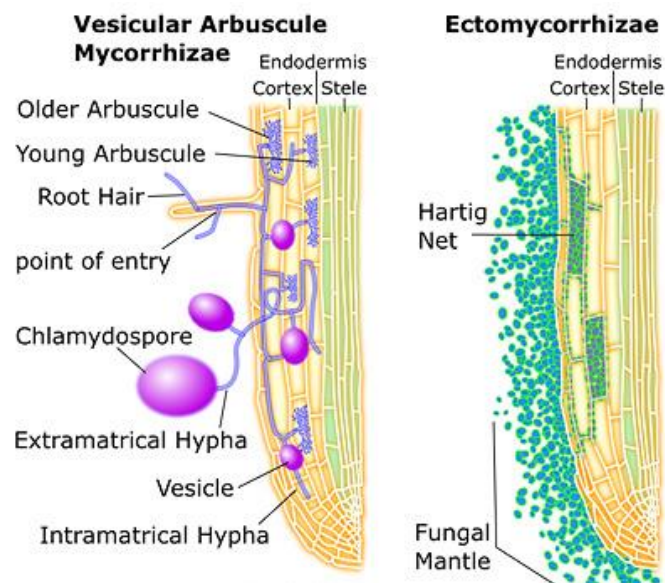


FIGURE 3 : DEUX TYPES DE MYCORHIZES TRÈS RÉPANDUS : A – LES MYCORHIZES À VÉSICULES ET ARBUSCULES ET B – LES ECTOMYCORHIZES.

L'endosymbiose est un mode de vie découvert plus récemment. Le mycélium se développe alors dans les tissus d'une plante sans y provoquer de lésions. Ce partenariat endosymbiotique est bénéfique pour le végétal en augmentant sa tolérance à certains stress environnementaux mais également la résistance à divers pathogènes *via* la production de toxines (pour revue, consulter (Rodriguez et al., 2009)).

Les lichens, notre objet d'étude, résultent de la symbiose entre un champignon qualifié de mycobionte (du grec mykês : champignon, et bios : vie) et d'un partenaire réalisant la photosynthèse qualifié de photobionte (du grec photo : lumière et bios : vie) qui correspond soit à une algue verte soit à une cyanobactérie, parfois les deux. Dans ce cas, le partenaire photosynthétique est généralement représenté minoritairement et une communication étroite entre les filaments de champignons et les algues peut être observée au microscope : l'on parle d'haustorium (Honegger, 1986a).

La lichénisation représente donc une stratégie nutritionnelle parmi d'autres pour assumer l'hétérotrophie des champignons. À ce titre, les lichens ne relèvent d'aucun statut particulier dans le règne des champignons. Il s'agit de champignons à part entière. De récentes études démontrent d'ailleurs que le processus de lichénisation s'est produit à plusieurs reprises au cours de l'évolution des champignons (Gargas et al., 1995). De façon symétrique, le mode de vie lichénisé s'est perdu à plusieurs reprises de telle sorte que de nombreux champignons non lichénisés dérivent d'ancêtres lichénisants (Lutzoni et al., 2001).

Si les lichens sont des champignons à part entière, le champignon lichénisé acquiert de nouvelles propriétés qui vont être brièvement passées en revue.

III. Présentation des lichens

A. Bases métaboliques, caractéristiques physiologiques et rôles écologiques

La symbiose lichénique structure un appareil végétatif rudimentaire, le thalle, organisme parfaitement autotrophe où la synthèse de matière organique est assurée par l'algue se développant au sein du mycélium aérien (Figure 4). L'algue est en contrepartie protégée de la déshydratation par le champignon. Ce dernier apparaît clairement comme le partenaire dominant de la symbiose dont il assure la reproduction sexuée. L'algue semble à l'inverse détenir des droits limités au sein de cette symbiose en étant cantonnée à certaines régions du thalle et en ne se reproduisant pas sexuellement. De telles considérations font que la symbiose lichénique est parfois considérée comme un élevage d'algues par des champignons plutôt que comme une authentique symbiose. Complètement intégrés à la classification des champignons, les lichens (ou formellement, champignons lichénisants) sont très majoritairement des Ascomycètes (donnant naissance aux ascolichens dans 98% des cas), les quelques 2% restants correspondant à des Basidiomycètes (Lutzoni and Miadlikowska, 2009). Le nom du lichen correspond en fait au nom du champignon lichénisant, et avec plus de 18.500 espèces décrites (Feuerer and Hawksworth, 2007), il est estimé qu'ils représentent environ 2/5 de tous les Ascomycètes connus (Lutzoni and Miadlikowska, 2009) et 1/5 de tous les champignons identifiés à ce jour (Honegger, 1998, 1995). 40 genres de photobiontes (25 pour les algues vertes et 15 chez les cyanobactéries (Ainsworth, 2008)) ont été décrits dans le cadre de la symbiose lichénique, il s'agit dans 90% des cas de photobiontes de type algue verte, essentiellement représentés par le genre unicellulaire *Trebouxia* et le genre filamenteux *Trentepohlia*. Les cyanobactéries (anciennement algues bleues) sont retrouvées chez environ 10% des lichens et appartiennent le plus souvent aux genres *Nostoc* et *Scytonema* (Friedl and Büdel, 1996).



FIGURE 4 : TROIS LICHENS REPRÉSENTANT LES ASSOCIATIONS SYMBIOTIQUES LICHÉNIQUES DANS LEUR DIVERSITÉ. A – *OPHIOPARMA VENTOSA* EST DANS LE CAS DE FIGURE MAJORITAIRE EN ASSOCIANT UN ASCOMYCÈTE À UNE ALGUE VERTE DU GENRE *TREBOUXIA* ; B – *LICHINA PYGMAEA* RÉUNIT UN ASCOMYCÈTE ET UNE CYANOBACTÉRIE (GENRE *CALOTHRIX*) ; C – *DICTYONEMA GLABRATUM* ENTRE DANS LES DEUX CAS DE FIGURE MINORITAIRES EN CONTENANT UN BASIDIOMYCÈTE ET UNE CYANOBACTÉRIE (*CHROOCOCCUS*).

Quelques lichens (3-4%) associent un champignon à deux photobiontes donnant lieu à des symbioses dites tripartites (Rai and Bergman, 2002). L'intérêt de telles associations triples réside dans le fait que les cyanobactéries sont plus efficaces pour fixer l'azote atmosphérique (Millbank and Kershaw, 1970; Palmqvist et al., 1998; Rai and Bergman, 2002). Le photobionte principal est alors l'algue verte, et la cyanobactérie est généralement confinée dans des compartiments fongiques appelés céphalodies. Ces céphalodies peuvent être externes pour apparaître sous des présentations variables à la surface du thalle (e.g *Placopsis*, *Peltigera*...) (Figure 5) ou être internes et se développer alors dans l'épaisseur de la médulle (e.g *Lobaria* et *Sticta* notamment) (Jordan, 1970; Honegger, 2012a). Chez

certains lichens toutefois, les cyanobactéries ne sont pas cantonnées à certaines portions du lichen mais sont retrouvées sur l'ensemble du thalle. C'est notamment le cas chez *Solorina crocea*, où la couche de cyanobactéries (*Nostoc*) s'établit juste en dessous de celle occupée par les algues vertes (*Coccomyxa*) (Hawksworth, 1988).

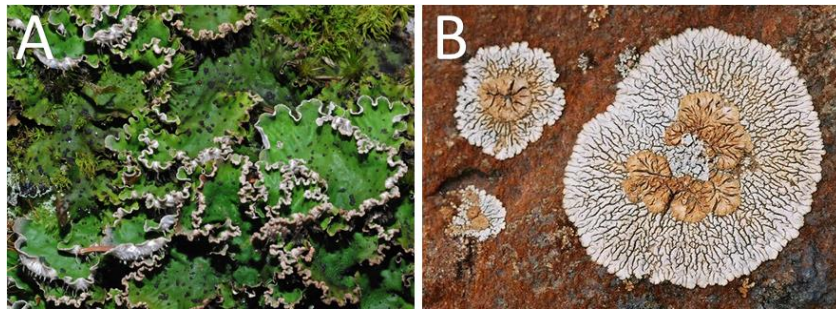


FIGURE 5 : DEUX EXEMPLES DE LICHENS À CÉPHALODIES EXTERNES. A – *PELTIGERA APHTOSA* ET SES CÉPHALODIES NOIRES PONCTIFORMES; B – *PLACOPSIS GELIDA* PRÉSENTE DES CÉPHALODIES ORANGÉES.

Selon les conditions environnementales, il peut arriver que le mycobionte change de partenaire photobionte, ce qui est à l'origine de modifications plus ou moins marquées de la morphologie du thalle (on parle alors de phototypes ou de photomorphes) (Tønnsberg and Holtan–Hartwig, 1983) (Figure 6). Tandis que les lichens à algue verte (ou chlorolichens) peuvent utiliser la vapeur d'eau, les lichens à cyanobactéries (ou cyanolichens) ont besoin d'eau liquide (Büdel and Lange, 1991; Taylor et al., 1997). De façon générale, les chlorolichens sont associés à des environnements plus secs que les cyanolichens. Aussi, ces derniers représentent plus de la moitié des lichens rencontrés en milieu tropical humide (Richardson, 2002).



FIGURE 6 : LES DEUX PHOTOTYPES DE *STICTA CANARIENSIS*. A – THALLE À ALGUE VERTE ET B – THALLE À CYANOBACTÉRIE PRÉDOMINANTE PRÉSENTANT UNE COULEUR BLEUE/NOIRE EN ENVIRONNEMENT PLUS HUMIDE ET/OU SOMBRE, QUELQUES PARTIES ÉPARSES DE THALLES À ALGUE VERTE RESTENT VISIBLES.

Le champignon, biomasse dominante du lichen, est responsable de la structuration du thalle. Chez de rares lichens, le thalle est façonné par le partenaire algal, comme c'est notamment le cas d'espèces du genre *Coenogonium* où les algues filamenteuses (*Trentepohlia*) confèrent à ces espèces un aspect de dentelle (Figure 7). Macroscopiquement, ces lichens ne diffèrent de *Trentepohlia* libres que par la présence d'apothécies éparées, les hyphes myceliennes étant apprimées le long des filaments d'algue (Meier and Chapman, 1983).

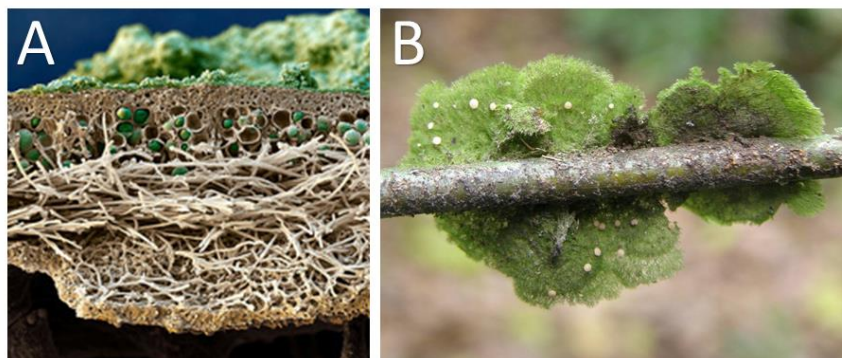


FIGURE 7 : CONTRIBUTION DU PHOTOBIONTE DANS LA STRUCTURATION DU THALLE LICHÉNIQUE. A – PHOTOBIONTE UNIQUEMENT LOCALISÉ SOUS LE CORTEX SUPÉRIEUR (MICROSCOPIE ÉLECTRONIQUE À BALAYAGE DU THALLE DE *PARMELIA SULCATA*) ET B – PHOTOGRAPHIE DE *COENOGONIUM LEPRIEURII* DONT LE THALLE EST STRUCTURÉ PAR UNE ALGUE FILAMENTEUSE DU GENRE *TRENTEPOHLIA*

Les lichens sont également associés à d'importantes cohortes de champignons épiphytiques et endophytiques, dont plus de 1.500 espèces sont actuellement décrites (Hoffman and Arnold, 2010; Honegger et al., 2013; Lawrey and Diederich, 2003; Muggia et al., 2013). Cette biodiversité, dont l'étude est en plein essor, est à l'origine de molécules originales appartenant à des séries structurales variées (Chen et al., 2013; Li et al., 2012; Zhang et al., 2012, 2009). Depuis quelques années, il est également établi que les lichens présentent d'importantes communautés bactériennes aussi bien à leur surface qu'à l'intérieur de leur thalle, développant des biofilms au niveau de certaines portions de thalles (Cardinale et al., 2008, 2006). Ces bactéries contribuent à la symbiose par des fonctions multiples à un tel point qu'on parle désormais de bactériobionte. Certaines de ces fonctions incluent la nutrition des lichens et certaines souches bactériennes pourraient être d'une importance cruciale pour l'approvisionnement en azote, notamment chez les lichens à algue verte (Grube and Berg, 2009), mais également en phosphore et en soufre. Le bactériobionte intervient également dans la défense contre les agents pathogènes via la sécrétion de puissants antibiotiques (Davies et al., 2005) et dans la résistance vis-à-vis de diverses contraintes abiotiques (Grube et al., 2015). Certaines souches bactériennes peuvent dégrader les parties sénescentes du thalle au profit de plus jeunes parties du lichen (Grube and Berg, 2009). Enfin, la synthèse d'acide indole acétique par les bactéries pourrait être d'importance pour structurer le développement du thalle dans son ensemble (Grube et al., 2009; Liba et al., 2006). Il est également suggéré que le microbiome puisse favoriser le processus de photosynthèse en approvisionnant l'algue en vitamine B12 (Grube et al., 2015).

Les lichens représenteraient ainsi un véritable écosystème où les différents partenaires interagissent à des degrés plus ou moins bien établis (Figure 8).

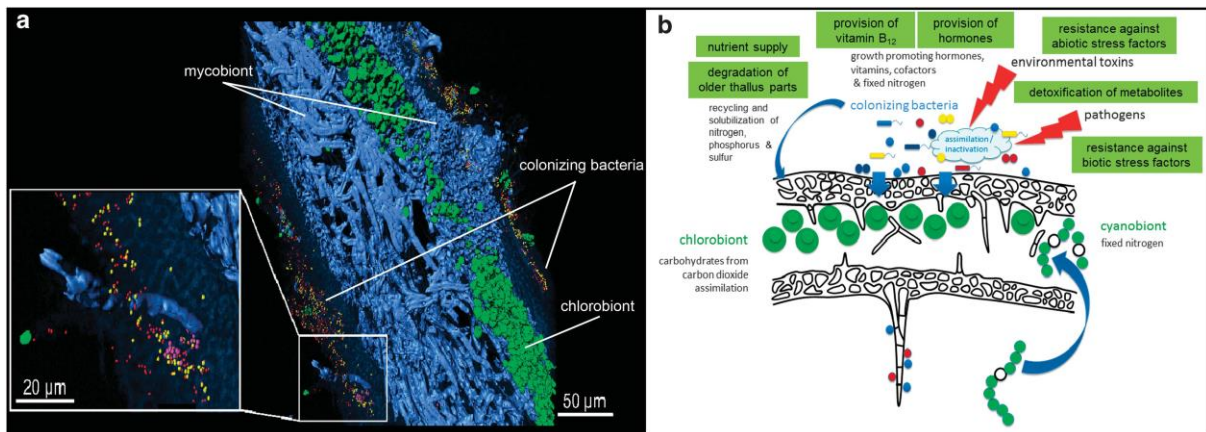


FIGURE 8: A) LOCALISATION DES BACTÉRIES SUR UNE COUPE TRANSVERSALE DE THALLE DE *LOBARIA PULMONARIA*, MODÉLISATION TRIDIMENSIONNELLE À PARTIR D'IMAGERIE FISH. LES EUBACTÉRIES (VISUALISÉES EN ROUGE) ET LES ALPHAPROTÉOBACTÉRIES (REPRÉSENTÉES EN JAUNE) MONTRENT UNE LOCALISATION UBIQUISTE SUR LES DEUX FACES DU LICHEN, À L'INVERSE, LES BÉTAPROTEOBACTÉRIES (ROSES) SONT MOINS ABONDANTES ET CONFINÉES À DES RÉGIONS PRÉCISES DU THALLE. B) VUE MODERNE DE LA SYMBOSE LICHÉNIQUE INCORPORANT LE BACTÉRIOBIONTE ET LES RÔLES PRÉSUMÉS DE CHAQUE PARTICIPANT DE CET ÉCOSYSTÈME (FIGURE EXTRAITE DE (GRUBE ET AL., 2015)).

Les lichens jouent un rôle écologique majeur d'organismes pionniers. Du fait de leur autotrophie, ils s'installent sur n'importe quel support où ils constituent souvent la première matière organique à s'établir, initiant ainsi les premiers jalons de la chaîne alimentaire (Lipnicki, 2015). Les lichens sont de fait répandus à travers toutes les régions du monde et ils représentent environ 8% de la couverture terrestre (Larson, 1987), s'installant dans des cours d'eau, au niveau de l'estran, dans des déserts arides mais également dans des régions polaires (où certaines espèces peuvent résister à des températures extrêmes de -40°C) (Figure 9). La photosynthèse des lichens antarctiques est toujours effectuée à des températures avoisinant -20°C avec un record de -24°C atteint chez *Cladonia alpicornis* (Kappen et al., 1996; Lange, 1966; Lange and Kappen, 1972). Divers lichens antarctiques hydratés ont pu supporter 12 heures passées dans l'azote liquide sans dommages (Kappen, 1993). Des *Umbilicaria* ont survécu à 10 années de conservation à -20°C sans que cela n'affecte leurs performances photosynthétiques et respiratoires pour certains d'entre eux (e.g *Umbilicaria deusta*) (Larson, 1989). L'entreposage pendant 3 années et demie du lichen fruticuleux *Alectoria ochroleuca* à -60°C a permis à ce lichen d'y survivre tout en préservant ses comportements de photosynthèse et de respiration (Larson, 1978). Cette extrême résilience fait des lichens des organismes modèles de choix pour la recherche en astrobiologie (Sancho et al., 2008). Diverses équipes ont en effet pu démontrer la survie de divers lichens exposés à des conditions spatiales (Raggio et al., 2011; Sancho et al., 2007) ou à une atmosphère martienne (Brandt et al., 2015; de Vera et al., 2014).



FIGURE 9 : ILLUSTRATION DES VARIÉTÉS DE BIOTOPES COLONISÉS PAR LES LICHENS. A – *LICHINA PYGMAEA* EST UN CYANOLICHEN SE DÉVELOPPANT SUR L’ESTRAN, NOTAMMENT LE LONG DES CÔTES BRETONNES (ROULLIER ET AL., 2011), B – LES LICHENS APPARTENANT AU GENRE *DERMATOCARPON* SONT AMPHIBIES ET SE DÉVELOPPENT SUR DES ROCHES SILICEUSES BORDANT LES COURS D’EAU, À MI-OMBRE (FONTAINE ET AL., 2012) C – *FLAVOCETRARIA NIVALIS* RÉALISE LA PHOTOSYNTHÈSE A DES TEMPÉRATURES DESCENDANT A -20°C (KALLIO AND HEINONEN, 1971), D – *XANTHORIA ELEGANS* EST UN LICHEN COSMOPOLITE POUVANT ÊTRE RENCONTRÉ JUSQU’À 7.000 MÈTRES D’ALTITUDE DANS L’HIMALAYA (ØVSTEDAL AND SMITH, 2001) ET POUVANT SURVIVRE À UNE ATMOSPHÈRE MARTIENNE (BRANDT ET AL., 2015), E – D’IMPORTANTES ÉTENDUES DU DÉSERT DE NAMIB RECOUVERTES PAR LES THALLES FRUTICULEUX DE *TELOSCHISTES CAPENSIS* (LANGE ET AL., 2006).

Cette résilience est notamment permise par le phénomène dit de reviviscence qui permet au lichen de passer de manière rapide et réversible d’un état sec à un état hydraté (Aubert et al., 2007). Lors d’épisodes de précipitations intenses, les lichens à algue verte peuvent se gorger d’eau à hauteur de 200 à 300% de leur poids sec. Les lichens à cyanobactéries peuvent quant à eux atteindre jusqu’à 2.000% de leur poids sec (Kranmer et al., 2008). À l’échelle cellulaire, de tels cycles de déshydratation/réhydratation modifient le pH intracellulaire et la force ionique du cytoplasme en favorisant la production de ROS (Mittler, 2002) (pour *Reactive Oxygen Species* ou espèces activées de l’oxygène) à l’origine de stress oxydants pouvant endommager un large panel de biomolécules : ADN (génotoxicité), les lipides (peroxydation lipidique) mais également les protéines (e.g oxydation de ponts disulfures en radicaux thiyl entraînant des pontages intra- ou intermoléculaires). La colonisation de biotopes hostiles expose également les lichens à d’intenses irradiations UV dont les effets délétères sont notamment contrés par la présence de pigments corticaux (Nguyen et al., 2013).

B. Morphologie des lichens

Le mycobionte, qui représente plus de 90% de la biomasse lichénique, est la plupart du temps responsable de la morphologie et de la structuration du lichen qui se décline en sept présentations principales (Van Haluwyn et al., 2009) (Figure 10) :

- les thalles **crustacés** sont les plus communs et sont encroûtants au niveau de leur substrat, dans lequel ils pénètrent plus ou moins profondément pour en être difficilement dissociables ;
- les thalles **foliacés** ont la forme de feuilles plus ou moins lobées ou découpées et se détachent facilement du substrat ;
- les thalles **fruticuleux** ont un port buissonnant et vont présenter des lanières plus ou moins

- ramifiées, dressées ou pendantes. Ils s'ancrent à leur substrat par une surface réduite ;
- les thalles **squamuleux** forment de petites écailles qui vont se chevaucher plus ou moins partiellement ;
- les thalles **lépreux** sont pulvérulents et se détachent aisément de leur substrat ;
- les thalles **gélatineux**, très essentiellement des cyanolichens, sont noirs et cassants à l'état sec et ont une consistance gélatineuse lorsqu'ils sont hydratés. La morphologie du thalle peut être crustacée, foliacée, fruticuleuse ou squamuleuse ;
- enfin, les thalles **complexes** ou composites comportent un thalle primaire foliacé adhérent au substrat à partir duquel se dresse un thalle secondaire plus ou moins ramifié ou en trompette (le podétion).

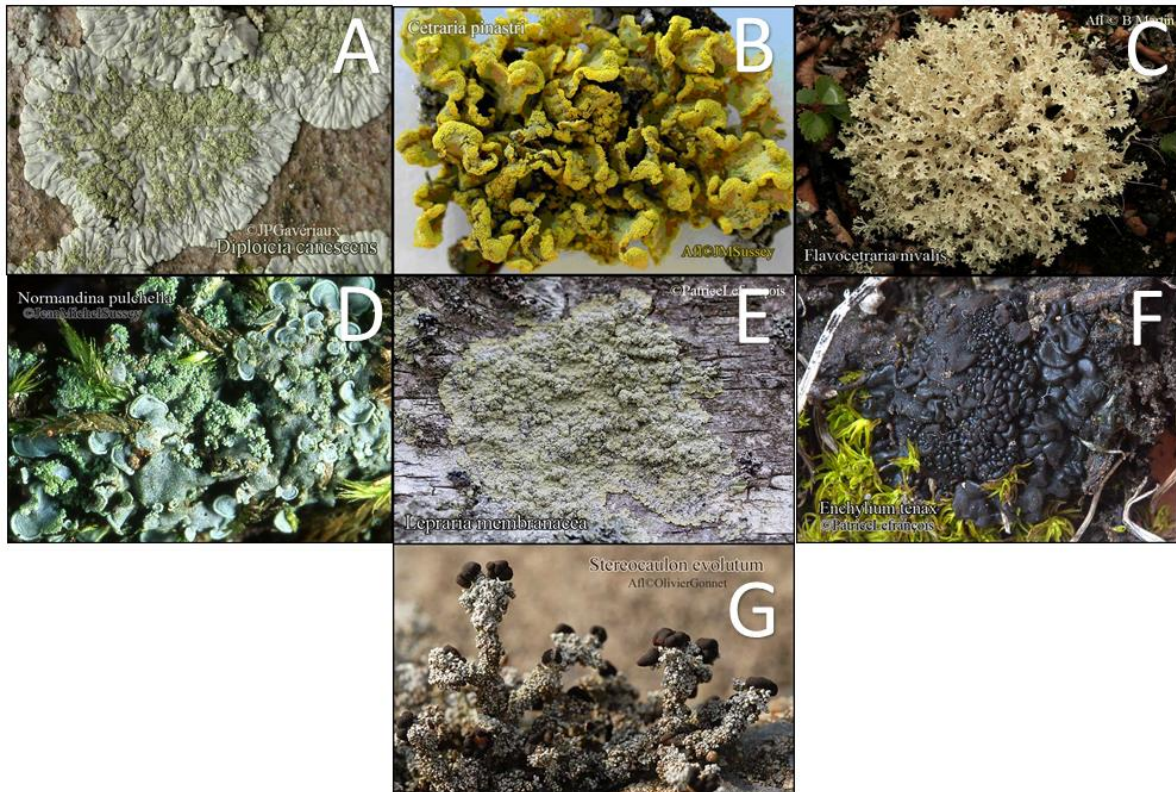


FIGURE 10 : ILLUSTRATION DES PRINCIPAUX TYPES MORPHOLOGIQUES DE LICHENS. A – THALLE CRUSTACÉ DE *DIPLOICIA CANESCENS* ; B – THALLE FOLIACÉ DE *VULPICIDA PINASTRI* ; C – THALLE FRUTICULEUX DE *FLAVOCETRARIA NIVALIS* ; D – THALLE SQUAMULEUX DE *NORMANDINA PULCHELLA* ; E – THALLE LÉPREUX DE *LEPRARIA MEMBRANACEA* ; F – THALLE GÉLATINEUX D'*ENCHYLIUM TENAX* ; G – THALLE COMPLEXE DE *STEREOCAULON EVOLUTUM*.

Histologiquement, en dépit de ces morphologies remarquablement différentes, les lichens présentent une certaine unité mais deux types de structures doivent être distingués (Figure 11) :

- les lichens à structure **homéomère** ont des cellules algales réparties uniformément parmi les filaments mycéliens ;
- la grande majorité des lichens adopte une organisation dite **hétéromère** qui correspond à une structure stratifiée comprenant les tissus suivants, de la surface vers la profondeur du lichen :
 - o un **cortex supérieur** formé de filaments mycéliens soudés, à parois plus ou moins épaissies ;
 - o une **couche gonidiale** formée par des algues entourées de filaments mycéliens ;
 - o une couche d'hyphes plus ou moins densément entrecroisées ou parallèles constituant la **médulle** ;

- la face inférieure se termine tantôt par des hyphes s'enfonçant dans le substrat tantôt par un **cortex inférieur** éventuellement muni de rhizines pour s'ancrer au substrat.

Certains lichens hétéromères présentent une symétrie centrale. De telles structures, qualifiées de **radiées**, possèdent la même trame histologique mais ne contiennent pas de cortex inférieur.

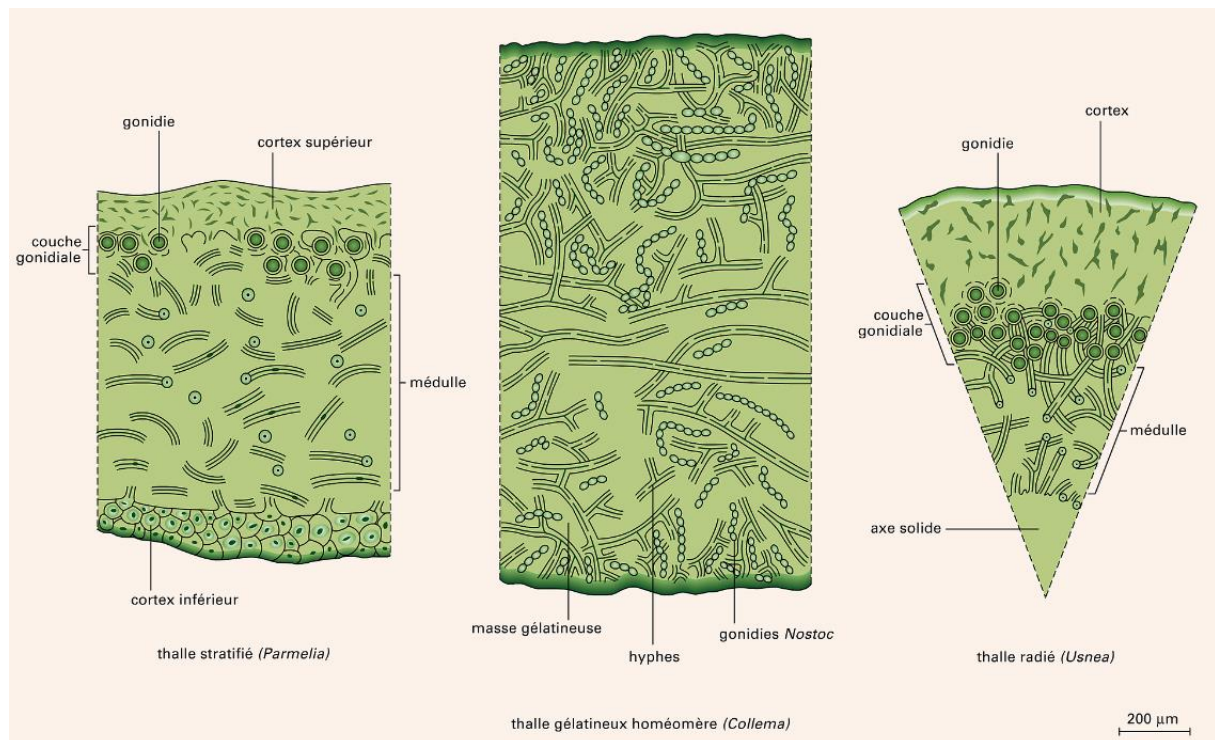


FIGURE 11: PRINCIPALES STRUCTURES HISTOLOGIQUES RENCONTRÉES CHEZ LES LICHENS. DE GAUCHE À DROITE : THALLE HÉTÉROMÈRE, THALLE HOMÉOMÈRE ET THALLE RADIÉ.

C. Reproduction des lichens

Les lichens peuvent adopter deux modes de reproduction : soit végétative, soit sexuée. Cette dernière modalité implique que les spores fongiques rencontrent par la suite un photobionte pour pouvoir reformer la symbiose. De manière générale chez les lichens, la reproduction sexuée est nettement prédominante par rapport à la reproduction végétative. Ainsi, 90% des lichens d'Irlande et de Grande-Bretagne adoptent une reproduction sexuée, tandis que seuls 29% d'entre eux connaissent une reproduction asexuée (Murtagh et al., 2000).

La reproduction asexuée ou végétative est assurée par des propagules de dissémination symbiotique essayant simultanément les deux partenaires de la symbiose. Elles sont principalement de deux types (Bowler and Rundel, 1975) (Figure 12) :

- les **soralies** correspondent à des interruptions du cortex qui laissent échapper de petits amas, les **sorédies**, formés d'algues enchevêtrées dans des filaments mycéliens ;
- les **isidies** à l'inverse sont des petites excroissances cortiquées formées d'algues et de champignons.

L'aspect de ces formations et leur implantation sont souvent des critères importants pour l'identification des lichens.

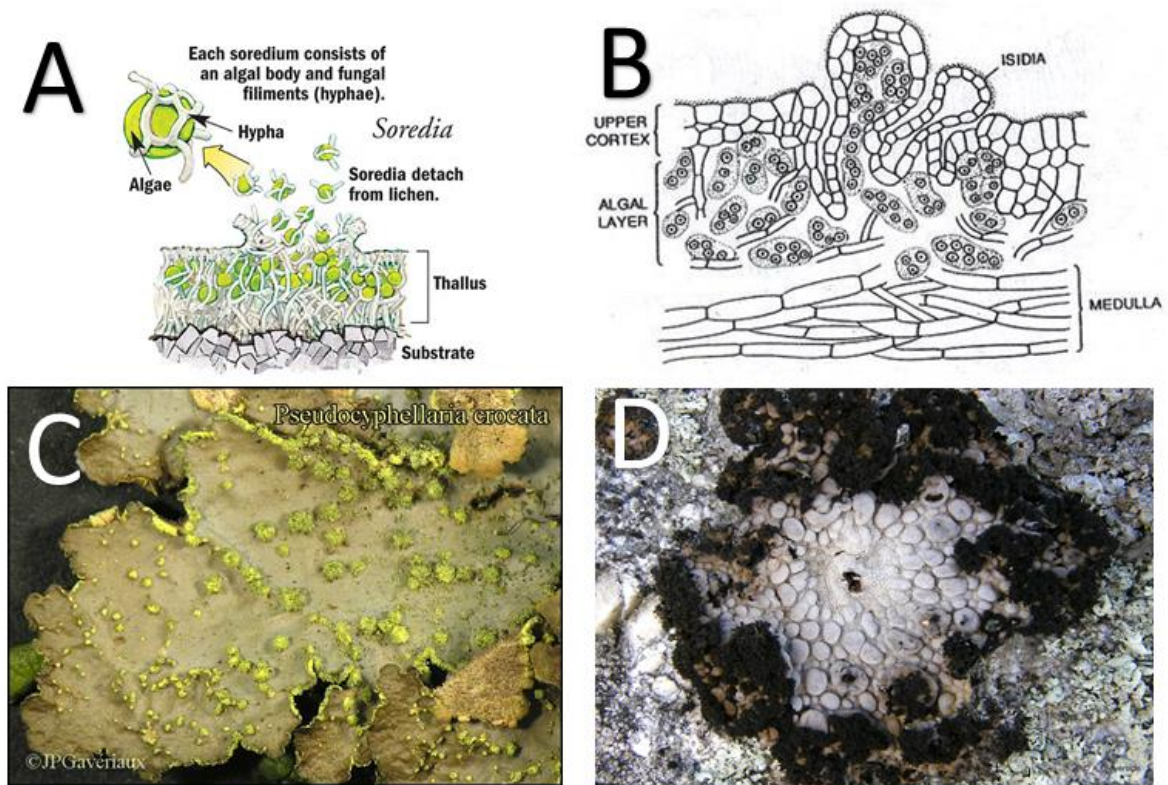


FIGURE 12: PROPAGULES DE DISSÉMINATION SYMBIOTIQUE RENCONTRÉES CHEZ LES LICHENS. A ET B – SCHÉMAS REPRÉSENTANT LES SORÉDIES ET LES ISIDIAS. C – SORALIES JAUNES DE *PSEUDOCYPHELLARIA CROCATA* ET D – ISIDIAS CORALLOÏDES (NOIRES) DE *LASALLIA PUSTULATA*.

L'algue ne se divisant que par mitoses, le champignon est le seul à former des organes reproducteurs qui vont donc correspondre à des ascomes le plus souvent et parfois à des basidiomes (Bowler and Rundel, 1975).

Les Ascomycètes tirent leur nom des asques qui contiennent les spores. Ces dernières sont libérées par rupture du sommet de l'asque ou désintégration de leur paroi. Les Ascolichens développent le plus souvent des organes reproducteurs sous la forme de disques plus ou moins saillants appelés **apothécies** et dont la structure évoque la fructification d'Ascomycètes non lichénisants comme les pézizes (Letrouit-Galinou, 1968). La forme des apothécies est un critère de grande importance pour l'identification des lichens. Des critères d'intérêt pour orienter les déterminations sont l'éventuelle présence d'algues sur le pourtour de l'apothécie (présence = apothécies lécanorines ; absence = apothécies lécidéines), de pédicelles, de cristaux visibles en lumière polarisée (Letrouit-Galinou, 1968)... Les apothécies dont la longueur excède le double de leur largeur prennent le nom de **lirelles**. Les **périthèces** désignent quant à eux des ascomes globuleux, qui débouchent à l'air libre par un pore apical (Figure 13).



FIGURE 13: ORGANES DE REPRODUCTION SEXUÉE CHEZ LES ASCOLICHENS. A – APOTHÉCIÉS DE *TELOSCHISTES CHRYSOPHTALMUS* ; B – LIRELLES DE *GRAPHIS SCRIPTA* ; C – PÉRITHÈCES DE *PYRENULA LAEVIGATA*.

Les Basidiomycètes forment des spores à l'extérieur de cellules fertiles, les basides. Les **basidiomes** sont généralement de petits champignons à lames d'un aspect tout à fait semblable à celui de Basidiomycètes non lichénisés (Figure 14).



FIGURE 14: BASIDIOMES DE *LICHENOMPHALIA MERIDIONALIS*.

D. La phytochimie singulière des lichens

a. Diversité structurale et voies de biosynthèse

L'exceptionnelle résilience des lichens tient pour partie à la constitution d'un arsenal de défense chimique unique dans le vivant. Le nombre de métabolites secondaires isolés de cette symbiose ne cesse de croître. En 2008, 1.050 métabolites secondaires avaient été décrits à partir de lichens (Stöcker-Worgotter, 2008). Parmi ces composés, une très grande majorité est propre aux lichens avec seulement 5 à 10% d'entre eux décrits chez d'autres organismes (plantes, champignons non lichénisés).

Il est communément admis que les métabolites secondaires caractéristiques des lichens sont d'origine fongique. De très récentes études ont effectivement pu relier la biosynthèse des différents polyacétates à un cluster de gènes fongiques (Abdel-Hameed et al., 2016a, 2016b). Ces résultats vont dans le sens d'études plus anciennes qui avaient constaté que la plupart de ces composés peut être obtenue par culture du seul mycobionte dans des conditions adéquates. Cependant, certains métabolites secondaires ne parviennent pas à être synthétisés par le seul mycobionte ce qui suggère de possibles coopérations métaboliques pour réaliser la biosynthèse de ces composés (e.g arthothéline) (Brunauer et al., 2006). À l'inverse, Takahashi a décrit la présence de xanthones qui ne sont synthétisées que par le mycobionte isolé et ne le sont plus lorsque la symbiose lichénique est reconstituée (Takenaka et al., 2000; Tanahashi et al., 1999). La symbiose lichénique rassemble également des partenaires dont chacun est connu pour pouvoir isolément les biosynthétiser. C'est notamment le cas des mycosporines qui sont synthétisées aussi bien par des cyanobactéries, des champignons et des algues vertes. Si le fait d'avoir constamment isolé les mycosporines de

cyanolichens jusqu'en 2015 pouvait laisser penser que leur biosynthèse dans le cadre de la symbiose lichénique était dévolu aux cyanobactéries, l'isolement de mycosporines à partir du chlorolichen *Dermatocarpon miniatum* doit amener à reconsidérer la question (Nguyen et al., 2015).

La diversité des métabolites secondaires lichéniques est façonnée au travers de trois voies de biosynthèse qui sont des plus aux moins représentées (Figure 15) :

- La voie des **polyacétates-polymalonates**
- La voie de l'**acide mévalonique**
- La voie de l'**acide shikimique**

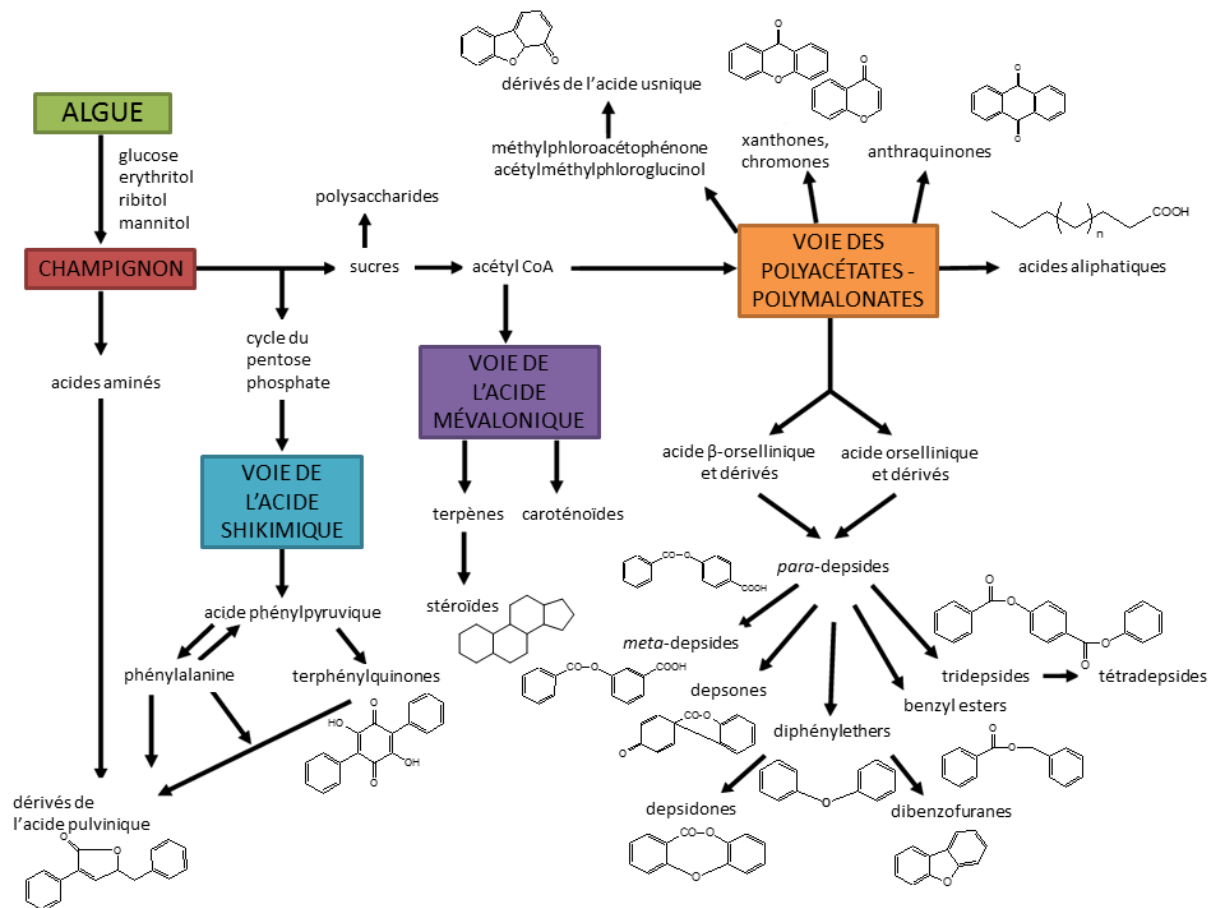


FIGURE 15: VOIES DE BIOSYNTÈSE RENCONTRÉES CHEZ LES LICHENS ET MOTIFS STRUCTURAUX ASSOCIÉS.

D'un lichen à l'autre, telle ou telle autre voie de biosynthèse va être préférentiellement activée pour retrouver chez un même lichen des molécules structurellement apparentées (chémosyndrome). Le métabolisme secondaire des lichens est hautement modulable. Aussi est-il fréquent de constater que des lichens de la même espèce mais de localisations géographiques différentes et/ou confrontés à des contraintes écologiques diverses présentent des profils chimiques différents (Bialońska and Dayan, 2005). La culture *in vitro* de mycobiontes de *Xanthoparmelia flavecentireagens* démontre que la synthèse de métabolites secondaires intervient dans des conditions environnementales défavorables (appauvrissement du milieu de culture, période de sécheresse, changements de température) (Stocker-Wörgötter, 2015). En soumettant ce mycobionte à divers stress environnementaux, Stocker-Wörgötter parvient à déclencher la biosynthèse de différents métabolites secondaires, soulignant la plasticité dont les lichens peuvent faire preuve pour s'accomoder des contraintes écologiques qu'ils subissent. Les connaissances actuelles concernant les voies de biosynthèse de ces composés sont rassemblées en Annexe 1 (p. 187).

b. Bioactivités des métabolites secondaires lichéniques: de l'écologie chimique aux perspectives thérapeutiques

Le rôle écologique assuré par les métabolites secondaires lichéniques reste souvent peu connu mais il apparaît clairement qu'ils aident le lichen à se protéger d'environnements hostiles (Stocker-Wörgötter, 2015).

i. Contraintes abiotiques

Les métabolites secondaires lichéniques sont souvent secrétés à la surface des hyphes fongiques où ils sont présents sous forme amorphe ou cristalline (Stocker-Wörgötter, 2008). Les capacités d'**absorption dans l'UV** des principales familles structurales énoncées ci-dessus ainsi que la distribution corticale de nombreux composés lichéniques indiquent leur rôle dans la photoprotection du lichen (Nguyen et al., 2013). En ce sens, il a été constaté que l'irradiation UV induit la biosynthèse de nombreux composés lichéniques : acide usnique (Bjerke et al., 2002; McEvoy et al., 2006; Nybakken and Julkunen-Tiitto, 2006), pariétine (Nybakken et al., 2004; Solhaug and Gauslaa, 1996), dérivés de l'acide pulvinique (Holder et al., 2000; Rubio et al., 2002; Wynn-Williams et al., 1999)... Ces caractéristiques font des métabolites secondaires lichéniques des molécules intéressantes à des fins cosmétiques (photoprotection) (Lohézic-Le Dévéhat et al., 2013). De façon intéressante, les émissions fluorescentes de l'atranorine ont une longueur d'onde située dans la gamme d'absorption des chlorophylles algales suggérant leur possible utilisation dans la photosynthèse (Rao and LeBlanc, 1965).

Les intenses irradiations UV subies par les lichens mais également les cycles de déshydratation/réhydratation génèrent d'importants stress oxydants qui sont combattus par les activités **antioxydantes** de nombreux métabolites lichéniques. Pour l'heure, une soixantaine de molécules lichéniques a été étudiée pour leurs propriétés anti-oxydantes. Une revue compilant ces travaux est parue en 2014 (Le Dévéhat et al., 2014).

Les métabolites secondaires lichéniques peuvent intervenir dans la **tolérance aux pollutions** notamment liées aux métaux lourds. Différentes substances lichéniques peuvent en effet chélater de tels atomes comme les acides psoromique (Purvis et al., 1990), norstictique (Purvis et al., 1987) et usnique (Hauck et al., 2008; Takani et al., 2002) notamment. L'acide fumarprotocétrarique de *Lecanora conizaeoides* réduit ainsi l'absorption de manganèse, augmentant la tolérance du lichen à des biotopes pollués par ce métal (Hauck and Huneck, 2007a). De la même façon, les métabolites secondaires d'*Hypogymnia physodes* limitent l'influx de Cu^{++} et de Mn^{++} au sein du thalle, par comparaison à des spécimens débarrassés de leurs polyphénols par rinçage à l'acétone. Les teneurs élevées en métaux au niveau des écorces où s'établit ce lichen pourraient être létales au lichen sans de telles régulations (Hauck, 2008). Le profil chimique de ce lichen montre une certaine plasticité et il est constaté une importante élévation de la production d'acide physodalique lorsque des thalles d'*H. physodes* sont transplantés de sites non pollués vers des sites pollués, suggérant l'implication de cette depsidone dans la gestion de ce stress (Hauck and Huneck, 2007b). Il a ensuite pu être établi que l'acide physodalique peut lier les métaux lourds pour prévenir leur entrée dans la cellule (Hauck and Huneck, 2007a). À l'inverse, les acides divaricatique et usnique favorisent l'absorption de micronutriments disponibles en très faible quantité dans l'environnement des lichens (Hauck et al., 2009b). L'aptitude des métabolites lichéniques à chélater des métaux peut aussi permettre d'effriter le support rocheux sur lequel les lichens se développent. Ainsi, l'excrétion d'acide divaricatique au contact de la roche est invoquée pour expliquer l'inhabituelle profondeur à laquelle se développent les hyphes mycéliennes d'*Ophioparma ventosa* dans leur substrat (Bjelland and Thorseth, 2002).

Il est aussi constaté que des lichens de compositions chimiques proches s'établissent sur des substrats de pH voisins (Wirth, 1985). Ainsi, les lichens producteurs d'acide usnique ont un pH de prédilection compris entre 4,0 et 4,5 (Hauck and Jürgens, 2008). La présence d'acides forts à la surface des hyphes mycéliennes et les propriétés acides de nombreux composés lichéniques laissent présager de la possible implication des métabolites secondaires dans la **tolérance des lichens à l'acidité** de leur environnement. En effet, les protons seuls ne peuvent pas franchir les membranes cellulaires lipophiles et doivent donc s'associer aux acides présents à la surface des cellules pour traverser sous une forme neutre. Une fois cette forme internalisée, la molécule se dissocie dans le cytosol pour générer des protons pouvant gravement endommager la cellule. La présence d'espèces fortement dissociées peut alors être perçue comme un mécanisme cytoprotecteur et la présence d'acides ayant de faibles pKa comme les acides fumarprotocétrarique, perlatoïque et thamnolique est récurrente chez les lichens rencontrés en milieux acides (Hauck et al., 2009a)

Outre les rôles écologiques précis pouvant être assurés par les métabolites lichéniques, il est également envisagé que le tapissage de ces composés renforce l'hydrophobicité des parois cellulaires (Honegger, 2012b).

ii. Stress biotiques

Un nombre conséquent de métabolites lichéniques impacte également les interactions que développe le lichen avec des organismes compétiteurs.

Une trentaine d'études s'est ainsi intéressée aux **activités antibiotiques** de métabolites lichéniques (Shrestha and St. Clair, 2013).

Les lichens sont aussi susceptibles d'être consommés par de nombreux **herbivores** allant des gastéropodes aux vertébrés (Lawrey, 1983). L'herbivorie de lichens reste rare en raison de leur pauvre qualité nutritionnelle (Lawrey, 1986), de leur présentation (e.g texture gélatineuse de cyanolichens comme les *Collema* (Rundel, 1978)) mais également de la production de composés de défense (Lawrey, 2009). L'allocation de ces métabolites défensifs est souvent asymétrique chez les lichens qui vont tendre à les concentrer au niveau des organes reproducteurs (Asplund et al., 2010; Hyvärinen et al., 2000) ou des parties juvéniles du thalle (Golojuch and Lawrey, 1988). Des observations de terrain et de laboratoire ont permis d'objectiver que les comportements alimentaires de nombreux animaux sont guidés par la chimie des lichens et les choix nutritionnels des herbivores se portent généralement sur les espèces ne synthétisant pas de métabolites secondaires notamment chez des limaces (Lawrey, 1980), des escargots (Gauslaa, 2004), des larves de papillons de nuit (Pöykkö et al., 2005; Pöykkö and Hyvärinen, 2003) et des coléoptères (Nimis and Skert, 2006), notamment. L'élimination par l'acétone des composés phénoliques des lichens (*acetone rinsing*) annule dans de nombreux cas ces évitements alimentaires, démontrant la défense qu'ils procurent (Gauslaa, 2004; Nybakken et al., 2010; Pöykkö et al., 2005). Il est généralement admis que ces défenses sont constitutives et ne peuvent pas être induites par broutage du thalle lichénique (Asplund et al., 2009; Lawrey, 2009). Une seule publication fait état d'une possible induction par des dommages au thalle en décrivant la biosynthèse d'acide rhodocladonique chez *Cladonia bacilliformis* et *C. norvegica* en réponse aux attaques d'une mite lichénicole (Timdal, 1989). La consommation de denrées supplémentées en métabolites secondaires lichéniques peut ralentir la croissance des organismes consommateurs (Emmerich et al., 1993; Giez et al., 1994; Slansky, 1979) voire être à l'origine d'intoxications aiguës (Cetin et al., 2008; Emmerich et al., 1993; Giez et al., 1994; Slansky, 1979).

La toxicité des métabolites lichéniques s'exerce parfois sur des organismes bien plus conséquents et la mort de 400 à 500 élans en hiver 2004 dans l'Etat du Wyoming a été imputée à la consommation de *Xanthoparmelia chlorochroa* et reliée plus précisément à l'acide usnique qu'il contient (Cook et al., 2007; Dailey et al., 2008). À l'inverse, pour les rennes habitant dans la toundra, les lichens restent souvent la seule ressource trophique à disposition et il semble que la tolérance de ces derniers à l'égard de la toxicité de l'acide usnique soit notamment médiée par la présence de souches bactériennes capables de le métaboliser et de le détoxifier dans leur rumen (Sundset et al., 2008). Il est d'ailleurs à noter que l'acide usnique présente une forte hépatotoxicité chez l'Homme et sa consommation dans des formules à visée amincissante a entraîné plusieurs décès (Durazo et al., 2004; Neff et al., 2004).

Nombre de substances lichéniques affectent le **développement et la croissance d'organismes compétiteurs**: mousses, plantes vasculaires et autres lichens. Concernant ce dernier volet, il est ainsi constaté qu'un *Lepraria* lichénicole se distribue de façon non aléatoire à la surface de deux *Xanthoparmelia* morphologiquement similaires mais chimiquement différents, préférant coloniser les thalles de *X. verruculifera* et de *X. loxodes* (Culberson et al., 1977). Les acides évernique et vulpinique s'opposent à la germination des spores de *Graphis scripta*, de *Caloplaca citrina* (Whiton and Lawrey, 1984) et également de *Cladonia cristatella* (Whiton and Lawrey, 1982). De telles compétitions chimiques régissent vraisemblablement les équilibres et les dynamiques au sein de communautés de lichens (Armstrong and Welch, 2007). Les acides évernique et squamatique inhibent la germination de spores de mousses ainsi que la croissance de leurs protonèmes (Lawrey, 1977). *Cladonia stellaris* et *Cladonia rangiferina*, deux lichens fréquemment rencontrés dans les forêts boréales, exercent une action allélopathique sur le pin gris (*Pinus banksiana*) et l'épinette blanche (*Picea glauca*) (Fisher, 1979). Les composés phénoliques extraits de *Lethariella canariensis* s'opposent à la germination de graines de chou, de laitue, de poivre et de tomate (Marante et al., 2003). L'acide usnique exerce également une phytotoxicité marquée à l'égard de végétaux divers. Cette toxicité est notamment médiée par une diminution de la fluorescence de la chlorophylle a, une baisse des taux de chlorophylle et de caroténoïdes et une baisse de la viabilité cellulaire (Bud'ova et al., 2006; Cardarelli et al., 1997; Endo et al., 1998). De façon intéressante, l'acide usnique a tendance à se localiser à la surface des cellules de photobionte, les exposant à la toxicité de ce métabolite (Avalos and Vicente, 1987; Herrero-Yudego et al., 1989; Liao et al., 2010). Il est toutefois constaté que les algues intégrées dans la symbiose lichénique sont moins sensibles à la phytotoxicité de cette molécule que des algues vivant librement ce qui suggère une longue co-évolution des algues lichénisées (Bačkor et al., 2010). Une hypothèse pour justifier l'accumulation d'acide usnique au contact des algues est que cette molécule sert à ralentir le métabolisme de ces dernières pour permettre au champignon de maîtriser une croissance harmonieuse du thalle et de maintenir un ratio mycobionte/photobionte optimal (Bačkor et al., 2010).

c. Approches analytiques pour le profilage chimique de lichens

Cette thématique a fait l'objet d'un chapitre d'ouvrage paru en 2015 (Le Pogam et al., 2015a) (*Analysis of Lichen Metabolites : A Variety of Approaches In Recent Advances in Lichenology*). Le texte intégral de cette revue est fourni ci-dessous.

Analysis of Lichen Metabolites, a Variety of Approaches

11

Pierre Le Pogam, Gaëtan Herbette and Joël Boustie

Contents

11.1	Introduction.....	230	11.5	Deciphering Metabolic Networks and Partners' Cooperation at the Very Heart of Symbiotic Systems.....	252
11.2	Oldest Analytical Methods.....	233	11.6	Conclusion	254
11.2.1	Spot Test (Reagents Directly Applied on the Lichen Thallus)	233	References	255	
11.2.2	Crystal Tests	235			
11.2.3	Melting Point	235			
11.3	Structure-elucidating Methods	237			
11.3.1	NMR Spectroscopy (NMR, MAS-NMR, Innovative Methods).....	237			
11.3.2	Mass Spectrometry	239			
11.3.3	Infrared Spectroscopy.....	241			
11.3.4	UV Spectroscopy.....	241			
11.3.5	Stereochemistry Determination	243			
11.4	Dereplicative Tools	244			
11.4.1	Thin-layer Chromatography (TLC).....	244			
11.4.2	High-performance Liquid Chromatography	247			
11.4.3	Gas Chromatography.....	249			
11.4.4	In Situ Detection.....	250			

Abstract

Lichens produce secondary metabolites which have been first considered as a chemical support fully involved in lichen taxonomy. As a consequence, analytical methods were developed and applied to these organisms from a long time, some of them being standardized. Then, lichen analysis benefitted from new developments and techniques applied for isolation and identification of secondary metabolites which are exposed and discussed herein. Some ancient techniques for lichen taxonomy are still used as spot tests, which involve application of specific reagents directly on the lichen thallus. TLC is also still extensively used with standardized protocols affording more accurate information on lichens' metabolic profiles. Identification of lichen compounds from the shape of crystals observed under microscope was facilitated as some major lichen metabolites are extracted in high yields. X-rays are now used in some cases where classical spectroscopic, UV, IR, MS, and NMR techniques do not allow unambiguous assignments. Using such techniques for isolated lichen compounds, some characteristic identification patterns of these substances are

P. Le Pogam · J. Boustie (✉)
Faculté des Sciences Pharmaceutiques et
Biologiques, Institut des Sciences Chimiques de
Rennes, PNSCM-UMR 6226, Université
Européenne de Bretagne, Univ. Rennes 1, 2 Av. Du
Pr Léon Bernard, 35043 Rennes Cedex, France
e-mail: joel.boustie@univ-rennes1.fr

P. Le Pogam
e-mail: pierre.lepogam-alluard@univ-rennes1.fr

G. Herbette
Spectropole, Aix-Marseille Université, Campus
Scientifique de Saint Jérôme, Service, 511, 13397
Marseille Cedex 20, France
e-mail: gaetan.herbette@univ-amu.fr

© Springer India 2015
D.K. Upreti et al. (eds.), *Recent Advances in Lichenology*,
DOI 10.1007/978-81-322-2181-4_11

229

presented here. Hyphenated techniques, coupling separation and identification, are more and more used and broaden the analysis facilities of lichen compounds. They enable early dereplication and subsequent focusing on bioactive or original compounds. Other trends in lichenology involve in situ analyses thanks to specific and innovative NMR or MS techniques that yield valuable information directly from the natural complex matrix. Several advantages can be expected from those approaches: no extraction steps, qualitative and quantitative information in a few minutes or hours, and direct analysis of genuine compounds, avoiding chemical artefacts associated with extraction and purification processes (Table 11.2). Moreover, some of these methods pave the way for the development of imaging techniques that might help correlating metabolites to their specific ecological environment. Altogether, such enhancements might enable harnessing of lichens' unique chemo-diversity.

Keywords

Secondary metabolites · Characterization · Identification · Spectroscopic analysis · Phytochemistry · Natural structure

11.1 Introduction

The lichenous lifestyle is maintained by approximately 18,900 known species (Feurerer and Hawksworth 2007) resulting from the association between a fungus and an alga (chlorolichens). For 10 % of lichens, green alga is replaced or accompanied by a cyanobacterium, which can absorb atmospheric nitrogen due to specific structures named heterocysts. The fungus plays a role in water and mineral supply and in mechanical protection of the whole organism. Algal or cyanobacterial partners realize photosynthesis and provide their fungal associate organic compounds to be metabolized.

Irrespective of the shape and the size of the lichen thallus, the symbiotic thallus yields unique metabolites among all life forms (Fig. 11.1). Most lichen substances are phenolic orcinol and β -orcinol derivatives: dibenzofurans and usnic

acids (pannaric acid and usnic acid), depsides (thamnolic acid and atranorin), depsidones (norstictic acid), depsones (picrolichenic acid), diphenylethers (leprolomin), benzyl esters (alecatorialic acid), and tridepsides (gyrophoric acid). Other than specific and unique lichen metabolites, various other structural families can be recognized: aliphatic acids (roccellic acid) and related lactones, xanthenes (lichexanthone), chromones (siphulin), pulvinic acid derivatives (pulvinic acid dilactone), quinones (haemoventosin, parietin), terpenes (zeorin), steroids (ergosterol peroxide), and carotenoids (astaxanthin). Cyanolichens mostly contain sugars and amino acid derivatives although original compounds such as mycosporines were detected recently (Torres et al. 2004; Roullier et al. 2011).

Unusual compound families can also be encountered as polypropionates, cyclic depsipeptides, brominated depsidones, and brominated acetylenic fatty acids, along with some glycosides (Boustie and Grube 2005). One should find a recent update of lichenic chemodiversity in the catalogue established by Elix (2014) (<http://www.anbg.gov.au/abrs/lichenlist/Chem%20Cat%203.pdf>). This diversity is also extended through the increasing number of metabolites isolated from the cultivated fungi and microflora associated with the lichen thallus (Grube et al. 2012).

Lichen metabolites considered in this chapter are mainly produced by the fungal partner and often released into the extracellular space to subsequently crystallize on or near the hyphal surface (Honegger 1986; Ozenda and Clauzade 1970; Hale 1983). Thus, large amounts of secondary metabolites can be detected in a lichen thallus. Extraction yields can rate from 1 to 25 % of dried lichen material, and composition is frequently characterized by one to three metabolites accumulated in high yields (over 80 % ratio) (Boustie et al. 2011).

Lichen secondary compounds are mainly arising from four pathways of biosynthesis: polyketide path, mevalonic acid path, shikimic acid path, and photosynthetic products of the phycobionts as presented in Fig. 11.2.

Phenols are the most frequently produced lichen metabolites and generally found accumulated in high yields as extrolites, crystallized

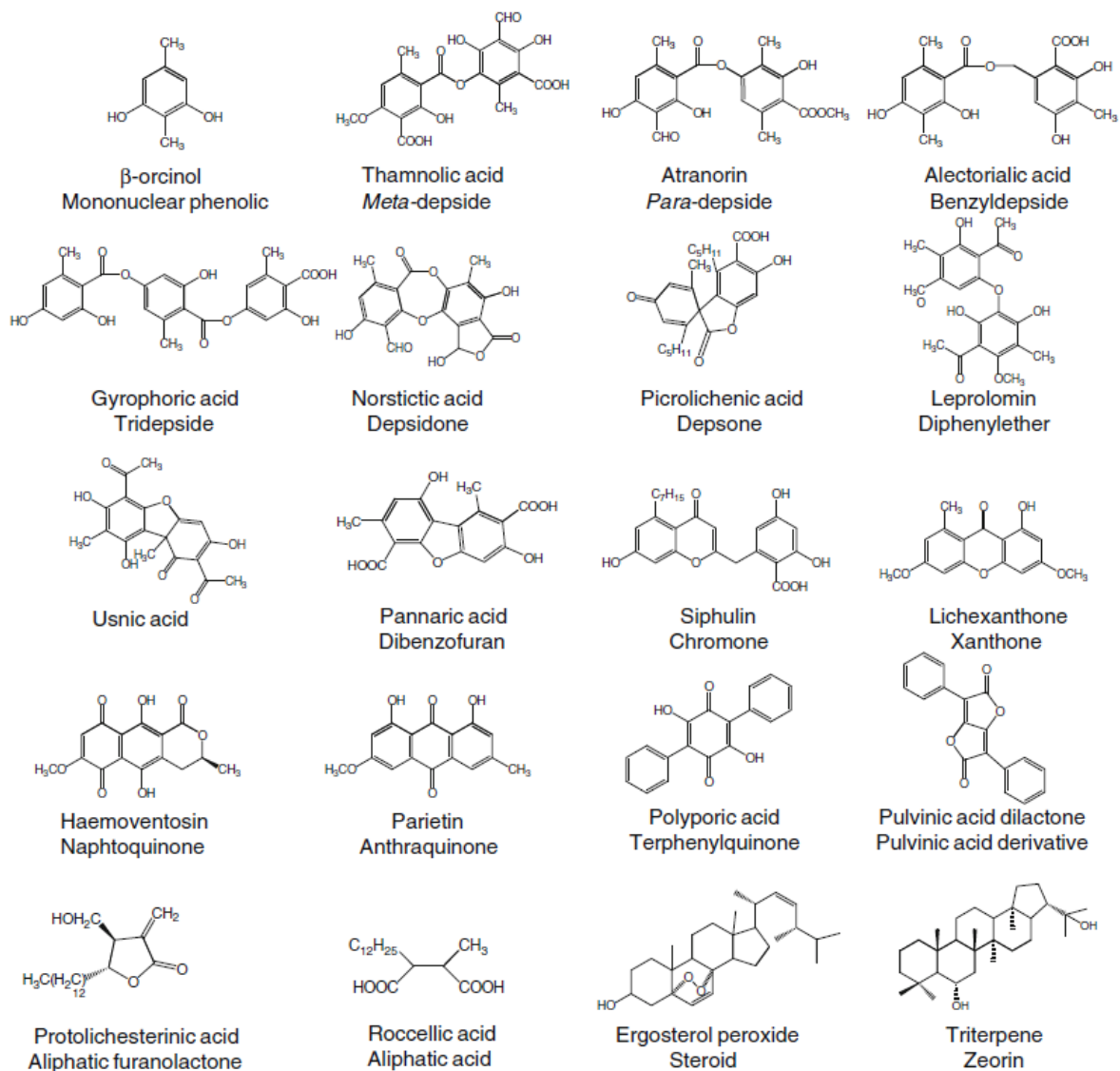


Fig. 11.1 Some typical secondary lichen metabolites illustrating a variety of structural classes

outside of the fungal hyphae. Oxidative coupling of orcinol and beta-orcinol derivatives result in the most typical lichen metabolites corresponding to depsides, depsidones, and dibenzofurane derivatives (Fig. 11.3). These lichen substances have indeed several possible biological roles that may impact biotic and abiotic interactions of lichens with their environment (Rikkinen 1995; Molnár and Farkas 2010).

Lichen secondary metabolites can act as allelochemicals, affecting the development and growth of lichens (Culberson et al. 1977; Whitton and Lawrey 1984), mosses (Heilman and Sharp

1963; Lawrey 1977), vascular plants (Pyatt 1967; Fisher 1979; Marante et al. 2003), and microorganisms that compete for space and light on a variety of substrates (Ranković et al. 2008; Schmeda-Hirschmann et al. 2008; Halama and Van Haluwin 2004). Strong experimental data support protection of lichens from herbivores grazing granted by lichen secondary metabolites (Asplund and Gauslaa 2008; Nimis and Skert 2006; Pöykkö et al. 2005; Dailey et al. 2008).

Ertl (1951) first observed that cortical accumulation of lichen compounds increased opacity of the upper cortex, restraining solar irradiance

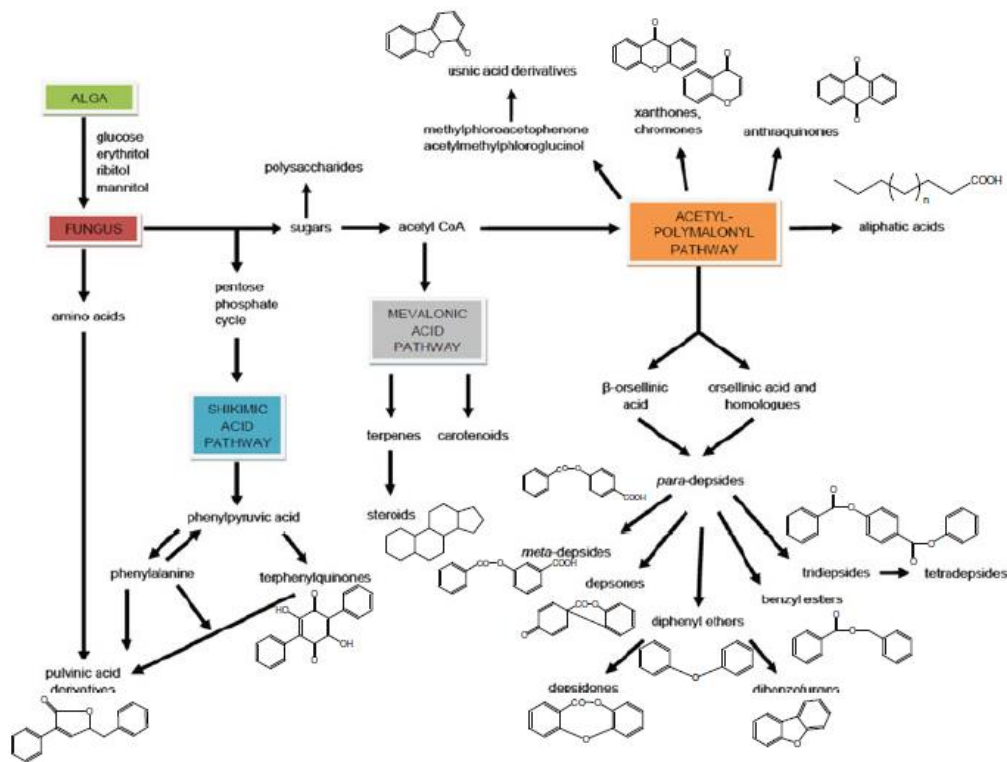


Fig. 11.2 Main metabolic pathways recognized in lichens [adapted from Elix (1996) and Stocker-Wörgötter (2008)]

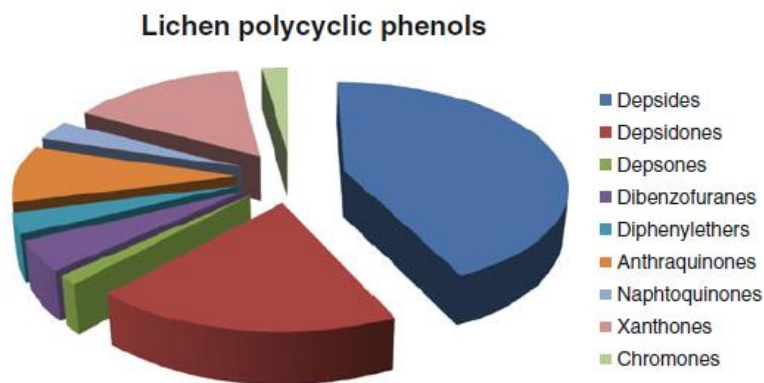


Fig. 11.3 Distribution of the main polycyclic lichen phenols arising from the acetyl-polymalonyl pathway (based on the 600 lichen polycyclic phenols compiled by Huneck and Yoshimura 1996)

reaching the light-sensitive algal layer. Various light-screening pigments display strong UV absorption abilities and might function as filters in order to prevent excessive UV-B irradiation (Nguyen et al. 2013). Some lichen phenolics have high ability to scavenge toxic free radicals generated by UV light (Russo et al. 2008;

Odabasoglu et al. 2006; Karakus et al. 2009). Some other metabolites step in metal homeostasis and pollution tolerance (Hauck and Huneck 2007a, b; Hauck et al. 2009). Secondary metabolites quantification revealed tremendous changes in the concentrations of secondary metabolites from *Hypogymnia physodes* when

thalli were transplanted to areas polluted with heavy metals and acidic inorganic sulfur compounds (Bialonska and Dayan 2005). As a result, the value of lichen metabolites in chemotaxonomy and systematics is questionable, but their isolation and identification is mandatory to recognize new active compounds and/or original physicochemical properties.

Most common biological activities deal with cytotoxicity and antibiotic activities (for a review see Shukla et al. 2010; Shrestha and St. Clair 2013). Additionally, miscellaneous other properties were described within several families of lichen products including antiviral or antiretroviral (Yamamoto et al. 1995; Pengsuparp et al. 1995), anti-inflammatory (Vijayakumar et al. 2000; Freysdottir et al. 2008), and analgesic activities (Okuyama et al. 1995). As natural plant-derived products have a less detrimental impact on the environment than synthetic chemicals, lichen metabolites also represent good candidates for new pesticides (Cetin et al. 2008) (Dayan and Romagni 2001). However, although studies carried on lichens to value their secondary metabolites are increasing, difficulties encountered in identification of the species, collection of bulk quantities, and the isolation of pure substances limit the number of tested compounds. Moreover, detection and isolation of minor compounds is generally complicated by the high abundance of redundant lichen compounds and techniques designed to bypass such a difficulty should allow findings of more specific and interesting compounds.

This chapter aims at presenting successive analytic methods developed during the history of lichens' secondary metabolites analysis. Arising from spot tests used in the first lichen taxonomy approaches, thin-layer chromatography (TLC) is still extensively used and standardized protocols have been established. Crystallography from crystal shapes to X-rays accurate measurements has been developed with lichen metabolites. The main classical spectroscopic techniques, UV, IR, MS, NMR used to identify isolated lichen compounds, are presented herein with a focus on

some characteristic identification patterns of these substances. Early and refined dereplication approaches to eliminate already known compounds and to focus on species containing original or bioactive compounds have now to be used first. Accumulated spectroscopic data and hyphenated techniques, coupling separation and identification, are more and more used and broaden the analysis facilities of lichen compounds. Subsequent trends in lichenology involve in situ analyses due to more specific and innovative NMR or MS techniques that yield valuable information directly from the natural complex matrix.

Some of these methods are described in a second part as well as expected results they should yield. A special insight is given to some imaging techniques with high potential to dramatically improve our understanding of the metabolic activities revealed at the very root of the lichen symbiosis.

11.2 Oldest Analytical Methods

11.2.1 Spot Test (Reagents Directly Applied on the Lichen Thallus)

Color reactions should be considered as useful hints for the presence of functional groups or elements within lichen molecules and thus remain rather limited compared with classical spectroscopic analysis methods. Nevertheless, spot tests, involving application of tiny amounts of specific reagents directly to the lichen thallus or parts of this thallus (i.e., cortex, medulla, apothecia), have been applied since the nineteenth century (Nylander 1866) and can lead to distinguish varieties and even sometimes species according to any associated color change or not. This is particularly useful to distinguish some closely shaped species which could not be unambiguously discriminated on the basis of morphological characters. For instance, species of the *Ramalina siliquosa* complex are tricky to be separated and display a remarkable chemical plasticity, leading

to six different chemotypes according to different thallus reactions related to the main compound as assessed with LC-DAD-MS analysis (Parrot et al. 2013). So, such colors obtained with given reagents are found in herbarium specimens since the method has been standardized.

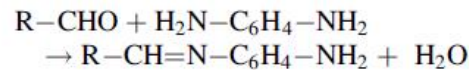
Nowadays, spot tests remain either helpful or necessary to confidently discriminate between some lichens and are still met as a very important criterion in determination keys. However, color intensities which are to be interpreted are not easy to standardize, attribution to a given major compound is often hazardous, and this technique is poorly informative in analysis of pure compounds. Noteworthy, because different compounds are present in specific parts of the lichen, reference tests usually describe parts of the thallus which should be tested, which corresponds to a first attempt toward histo-localization (Fig. 11.4). Three main reagents used in color reactions are potassium hydroxide (commonly called K), sodium hypochlorite (abbreviated C), and paraphenylenediamine (mainly known as P or PD).

K (consisting of 10 % potassium hydroxide in water) is a useful reagent to differentiate between quinones and pulvinic acid derivatives as it turns quinones into a bright red to deep purple color. It also turns yellow and then red with most *ortho*-hydroxy aromatic aldehydes.

C (saturated aqueous $\text{Ca}(\text{OCl})_2$ or commercial laundry bleach) is a reagent for *meta*-dihydroxy phenols, except for those substituted between the hydroxy groups with a $-\text{CHO}$ or $-\text{COOH}$. This explains why arthothelin and thiophanic acid are C+, whereas lichexanthone does not react with C (Fig. 11.5). Different colors can be obtained ranging from light yellow to blood red. C turns green with dihydroxy dibenzofurans (Nash 2008).

In some cases, successive reagent application is required, and KC+ is pretreatment by KOH before having a coloration with C reagent. KC turns red with C- depsides and depsidones which undergo rapid hydrolysis to yield a *meta*-dihydroxy phenolic moiety. Blue color is obtained with dihydroxy dibenzofurans, whereas a yellow reaction appears with usnic acid (Nash 2008).

Although highly toxic, last routinely used macrochemical reagent is ethanolic solution of para-phenylenediamine (2–5 %) that gives yellow to orange colors with aldehyde-containing depsides and depsidones turned into a Schiff base according to the following reaction:



Various other reagents can be found in literature, but their use is not common compared with those previously described. FeCl_3 can be used to

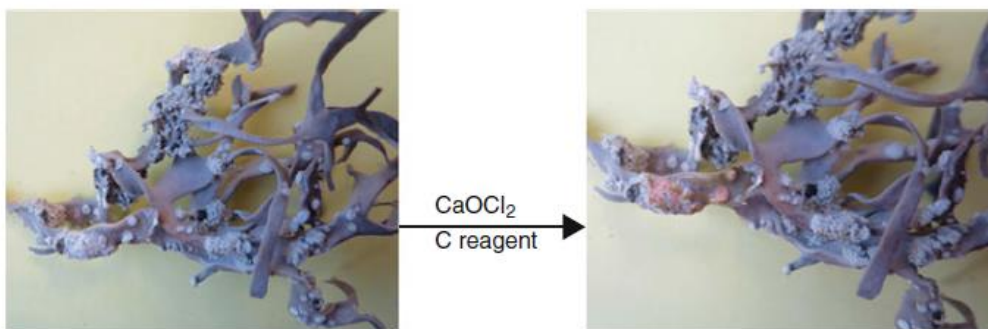


Fig. 11.4 Spot test with $\text{Ca}(\text{OCl})_2=\text{C}$ reagent drop on a thallus of the fruticose *Roccella fuciformis*. On the right picture, the C+ bright red reaction is limited to soralia (= white parts, corresponding to medulla as the gray

thallus cortex is disrupted). This test is also confirming the distinction with the related species *Roccella phycopsis* where only the gray cortex is turning rose red C+

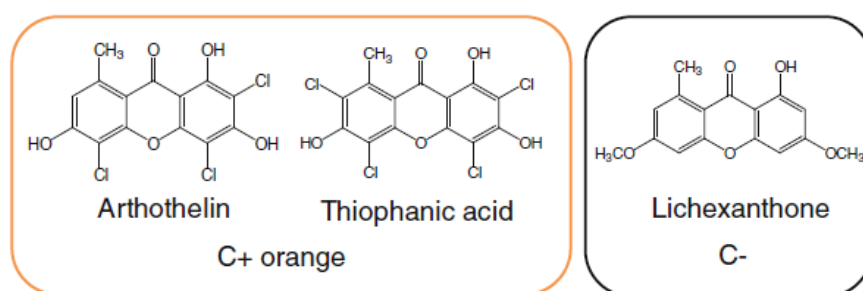


Fig. 11.5 Structures of chromones exemplifying the marked *orange* color obtained with $\text{Ca}(\text{OCl})_2$ reagent =C spot test, indicating the presence of *m*-dihydroxyphenols in arthothelin and thiophanic acid compared to lichexanthone

detect phenolic groups (leading to red to violet coloration), quinones having free hydroxyl group in β -position are revealed with both 2 % magnesium acetate ethanolic solution (red or violet) and Dimroth's reagent, e.g., boric acid solved in acetic anhydride giving red to violine colors. Chlorinated metabolites can be detected thanks to Beilstein test which consists of bringing one milligram of the molecule on the tip of a glowing copper wire introduced into the flame of a Bunsen burner, halogenated compounds then transiently turn the flame into a deep green color (Huneck and Yoshimura 1996). Spot tests corresponding to a set of typical lichen products can be found below (Table 11.1). Chromones, xanthones, anthraquinones, and pulvinic acids are naturally colored compounds.

11.2.2 Crystal Tests

Microcrystallization was once a very if not the most important way to identify lichen metabolites in times without TLC and high-performance liquid chromatography (HPLC). Microcrystallization of lichen substances was mainly developed by Asahina and Shibata since 1950 (Shibata 2000). This approach was based on the formation of distinctive crystals from lichen extracts (Fig. 11.6).

The general procedure can be summarized as follows: the extract of a small piece of lichen is first filtered before being evaporated. Acetone is the most used solvent as it extracts compounds with a wide range of polarity. Dried residue is then transferred to a microscope slide, and a drop

of proper microcrystallization reagent is added on it before capping with a cover glass. Different microcrystallization solutions were described, the most commonly used being GAW and GE, corresponding to H_2O /glycerol/ethanol 1:1:1 (v/v/v) and to acetic acid/glycerol 1:3, respectively. Slides using GE or GAW are further gently heated over microflame (other solvents do not need this heating step) and then let aside for progressive cooling, enabling the crystallization process to occur. Once formed, crystals are best observed under polarized light with a 200–1,000-fold magnification and present incredible diversity in both shapes and colors that was used to recognize the major metabolite in a given specimen. Although now outstod by modern analysis methods, this concept is still used nowadays after compound purification with great performances thanks to modern X-ray crystallography (Deschamps 2010).

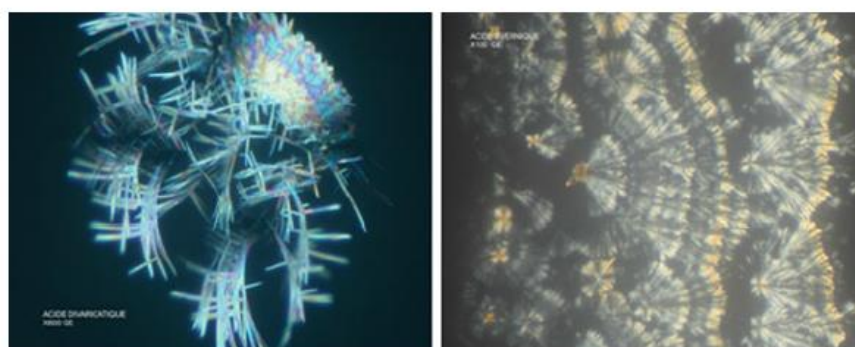
This simple and rapid technique allowed to characterize the major metabolites in hundreds of lichen species but was obviously useless to detect minor substances and to analyze too complex mixtures of lichen substances.

11.2.3 Melting Point

Melting point was once an important criterion for identification of a pure lichen substance. It can be determined with a few crystals under a glass capillary or with a Köfler device. It should be noted that some compounds do not have a sharp melting point but decompose over a wide range

Table 11.1 Thalline reactions corresponding to a set of common lichen metabolites (Brodo et al. 2001)

Compound	K	C	KC	PD
<i>Depsidones</i>				
Psoromic acid	–	–	–	Light yellow
Salazinic acid	Dark red	–	–	Orange
Stictic acid	Yellow	–	–	Orange
Virensic acid	–	–	–	Orange/red
<i>Benzyldepsides</i>				
Alectorialic acid	Pale yellow	Red	Red	Dark yellow
Barbatolic acid	Yellow	–	–	Yellow
<i>Dibenzofurans and related</i>				
Didymic acid	–	Green	Green	–
Pannaric acid	–	Olive green	Olive green	–
Strepsilisins	–	Green	Green	–
Usnic acid	–	–	Yellow	–
<i>Chromones</i>				
Siphulin	Yellow brown	Violet	–	–
<i>Xanthones</i>				
Arthothelin	–	Orange	Orange	–
Lichexanthone	–	–	–	–
Thiophanic acid	–	Orange	Orange	–
<i>Anthraquinones</i>				
Nephromin	Red purple	–	–	–
Parietin	Red purple	–	–	–
Skyrin	Red purple	–	–	–
<i>Triterpenoids</i>				
Zeorin	–	–	–	–
<i>Pulvinic acid derivatives</i>				
Calycin	–	–	–	–
Rhizocarpic acid	–	–	–	–
Vulpinic acid	–	–	–	–


Fig. 11.6 Microcrystallizations of secondary lichen metabolites: divaricatic acid and evermic acid (both crystallized in GE from an acetone lichen extract then magnified 100-fold and observed through polarized light) (pictures from Jacques Lagabrielle)

of temperature. Decomposition of lichen substances may be accompanied with characteristic odors that can differ between aliphatic molecules, phenolic compounds, or triterpenes. Obviously, melting points can only serve as a hint to further confirm structural elucidation granted by other means. One could find a list of lichen substances' melting points in Hüneck and Yoshimura's reference book (Hüneck and Yoshimura 1996).

11.3 Structure-elucidating Methods

General chemical procedure to study secondary metabolites is done from lichen extracts in organic solvent and further purification through crystallization or chromatography separation. Isolated compounds are then analyzed in most cases by NMR, MS, IR, and UV spectroscopy plus stereochemistry studies, if required.

11.3.1 NMR Spectroscopy (NMR, MAS-NMR, Innovative Methods)

As for any organic compound, NMR is an essential method for the structural determination of lichen secondary metabolites. Structural determinations for lower milligram samples could be made with data obtained in proton and carbon NMR. The assignments of signals can be achieved via crosspeak correlation observed in homonuclear 2D spectra of scalar couplings (COSY, TOCSY ...) or dipolar couplings (NOESY, ROESY) and heteronuclear 1J type (HSQC/HMQC ...) and $^{2,3}J$ type (H2BC, HMBC ...), 2D or 3D sequences to detect heteronuclear scalar couplings as HSQC-TOCSY, and HSQC-NOESY generally for complex structures.

However, most secondary lichen metabolites isolated so far belong to a limited variety of structural families as illustrated in Fig. 11.1. Some dedicated NMR studies related to several structural families were published: depsides (Cheng et al. 2013), tridepsides (Narui et al. 1998), depsidones and depsones (Sundholm and Hüneck 1980, 1981), xanthonones (Sundholm 1978, 1979),

and triterpenes (Wenkert et al. 1978; Wilkins et al. 1990). A compilation of the published NMR data of lichen compounds is reported in the Hüneck and Yoshimura (1996).

Solubilization of pure lichen compounds is often a challenge, but most of the NMR spectra are recorded after dissolution in $CDCl_3$ or $DMSO-d_6$. Some characteristic NMR features commonly found in NMR spectra of lichen compounds are selected here for monoaromatic or rearranged phenols corresponding to depsides, depsidones, depsones, or dibenzofuranes along with some NMR landmarks for aliphatic and related paraconic acids.

11.3.1.1 Phenolic Compounds

Chemical shifts are greatly influenced by inductive and mesomeric effects originating from other substituents that depend on their respective position. Some publications reported on the effect of substituents nature and respective position to predict corresponding chemical shift with the reference being the benzene chemical shift of 128.5 ppm (Ewing 1979). For orcinol, phenol-bearing carbons are deshielded (140–160 ppm) as well as the carbon that has two *meta*-hydroxy moieties (140 ppm), whereas *ortho*-hydroxy-located carbons are shielded (100–110 ppm). Aromatic methyls are usually found around 20 ppm. Noteworthy, for the closely related β -orcinol, the second aromatic methyl can be easily distinguished since it is strongly shielded due to two *ortho*-hydroxy groups (8 ppm). Side chains are evidenced through a variable number of signals arising in the 10–40 ppm range (divarinol, olivetol). Carbonyl functions are easily observable in ^{13}C NMR where shifts around 170–200 ppm have to be distinguished between a methyl ester from an acid function, e.g., methyl orsellinate at 170.3 ppm compared to orsellinic acid at 173.3 ppm, while shifts of aldehyde function are found around 194 ppm as of haematommic acid.

Depending on the substitution on the aromatic ring, 1H NMR spectrum shows sometimes only one aromatic signal (singlet) due to the symmetry

of the molecules with a signal at 6.09 ppm in ^1H NMR and at 106.7 ppm in ^{13}C NMR (β -orcinol). According to moieties present on the aromatic ring, other signals are methyl groups at 2.14 ppm (orcinol), 2.08 and 1.89 ppm (β -orcinol), 2.47 and 2.00 ppm (orsellinic acid), variable hydroxyl and acid shifts, or alkyl chains between 0.85 and 2.47 ppm as the pentyl moiety of the olivetol. Signals can also be found at 3.82 ppm indicating a *O*-methyl group (4-*O*-methylolivetolcarboxylic) or at 3.92 ppm for acid or ester (methyl- β -orcinolcarboxylate). A signal around 10.3 ppm is indicative for an aldehyde function (haematommic acid).

11.3.1.2 Dibenzofuranes

Most true dibenzofuranes exhibit two aromatic protons (6.6 and 6.9 ppm) while related compounds such as the commonly found and related usnic acid display a shielded aromatic signal at 5.92 ppm. Additional ^1H NMR signals correspond to the substitution of the dibenzofuran skeleton by a variety of substituents such as methyl, alkyl chain, hydroxyl, acid, ester, or ketone. The ^{13}C NMR of the aromatic ring signals is observed between 98.3 and 179.4 ppm, and those corresponding to the ketone function are at around 200 ppm and to methyl groups between 7.7 and 32.0 ppm (usnic acid).

A fourth cycle from a gamma-lactone (e.g., strepsilin) or a delta-lactone (e.g., haemophaein) may also occur with a ^{13}C NMR chemical shift around 170 ppm. Such an additional ring, which may be substituted by methyl (e.g., alectosarmentin), hydroxyl groups, and/or alkyl chains (e.g. haemophaein), is also found for some depsides and depsidones.

11.3.1.3 Depsides, Depsidones, and Depsones

Depsides are phenolic compounds bounded by ester linkage of two units (didepside), three units (tridepside), or four units (tetradepside). Barbatic acid, a didepside, shows two signals in ^{13}C NMR at 171.4 and 174.8 ppm for ester and acid function, respectively. Aromatic rings may be substituted

by different groups: hydroxyl, aldehyde, methoxy, methyl, saturated or unsaturated alkyl chain with a ketone function, and halide (chlorine or bromine). Aromatic methyl groups' chemical shifts range from 7 to 30 ppm according to the neighboring substituents as previously discussed. Methoxyl groups can be easily recognized with chemical shifts ranging from 50 to 60 ppm, methylenic groups of alkyl chains have a chemical shift between 26 and 40 ppm, and methyls are encountered around 15 ppm. Noteworthy, one may recognize patterns of signals corresponding to the constitutive monomers within some depsides (e.g., isolecanoric acid and orsellinic acid, divaricatic acid and divaricatinic acid). Tri- and tetra-depsides obviously contain more carbon signals and can thus be easily distinguished from classical didepsides.

Benzyldepsides have an additional characteristic chemical shift at 5.60 ppm in ^1H NMR and 66.0 ppm in ^{13}C NMR of the methylenic group (alectorialic acid) due to a strong deshielding of the ester function and the aromatic ring in *alpha* position.

Depsidones are characterized by an ether linkage bridging the two aromatics moieties through a third ring including the C_7 carbonyl of the ether linkage which is shielded around 161 ppm while found around 169 ppm in depsides. The number of aromatic protons and substituents is consecutively reduced with regard to depsides, but substitutive patterns are often similar.

Depsones are usually picrolichenic acid derivatives which are cyclized depsides by a C_1 - C_5 bond thereby forming a gamma-lactone with a signal at 170 ppm in ^{13}C NMR. A quaternary C_1 at 59 ppm and a cyclic ketone at 188 ppm are in most cases accompanied with signals of two alkyl chains.

11.3.1.4 Aliphatic Acids and Paraconic Acids

Aliphatic acids contain a long carbon chain whose chemical shifts are comprised between 10 and 40 ppm in ^{13}C NMR, and a variable number of carboxylic acid moieties located around 180 ppm. Identification of carbons

belonging to the carbon chain is tricky since most of them are very close to one another. Double bond-containing compounds display a distinct chemical shift around 130–140 ppm (lichesterylic acid, fumaric acid), whereas molecules containing hydroxyl or methoxyl groups possess chemical shifts in the 60–80 and 50 ppm range, respectively.

Such aliphatic acids can cyclize, thus forming a gamma-lactone ring. The carbon bearing the lactone function displays a typical ^{13}C NMR chemical shift located between 174 and 178 ppm, whereas the carbon linked to the oxygen of the cycle is slightly deshielded at around 50 ppm. NMR is useful to characterize the length of the alkyl chain in C_{11} (nephrosterinic acid), C_{13} (lichesterinic acid), or C_{15} (muronic acid) as well as the substitution by a ketone (220.3 ppm in ^{13}C NMR, muronic acid), hydroxyl function (68.4 ppm in ^{13}C NMR, neuropogolic acid), a terminal acid group (168 ppm in ^{13}C NMR, protopraesorediosic acid), or acetoxy group (174.7 ppm in ^{13}C NMR, 19-acetoxylichesterinic acid). α , β -unsaturated- γ -lactones (e.g., neuropogolic acid) give signals in the range of ethylenic carbons (120–160 ppm) and deshields neighboring carbon (commonly found at 80 ppm). γ -lactones displaying an exocyclic methylenic function (e.g., protolichesterinic acid) are more shielded (125 ppm) than those comprising the double bond inside the lactone ring (135–145 ppm) with two characteristic signals in ^1H NMR at 6.39 and 6.03 ppm as doublets (J 3 Hz).

The gamma-lactone cycle may be substituted by a methyl group and an acid function as respectively observed at 14.4 and 177.3 ppm for (–)-dihydropertusaric acid. Structure of unsaturated lactones like isomuronic acid with two ethylenic carbons at 139.0 and 146.6 ppm in ^{13}C NMR or of lactones with an exocyclic ethylenic group can be resolved with NMR ^1H NMR characteristic signals (6.03 and 6.39 ppm as two doublets (J 3 Hz) in ^1H NMR and signals at 125.9 and 132.6 ppm in ^{13}C NMR).

Solid-state MAS-NMR (magic angle spinning) techniques enable monitoring the chemical

composition in the solid state of intact biological samples (Miglietta and Lamanna 2006).

Identification of molecules from 5 *Cladonia* lichens, hardly differentiated on the basis of botanical characters, could be achieved by comparison of the ^{13}C CP-MAS-NMR (CP: Cross Polarization) spectrum of solid crushed lichens with the reference powder spectra of the three major secondary metabolites (fumarprotocetraric acid, perlatolic acid, and usnic acid) that enabled attributing the chemical content to different unambiguous NMR signals (Chollet-Krugler et al. 2008).

Likewise, ^1H HR-MAS-NMR (HR standing for high resolution) provided specific fingerprints that could be reliably assigned to different carbohydrates detected from several intact lichens (Alcantara et al. 2007).

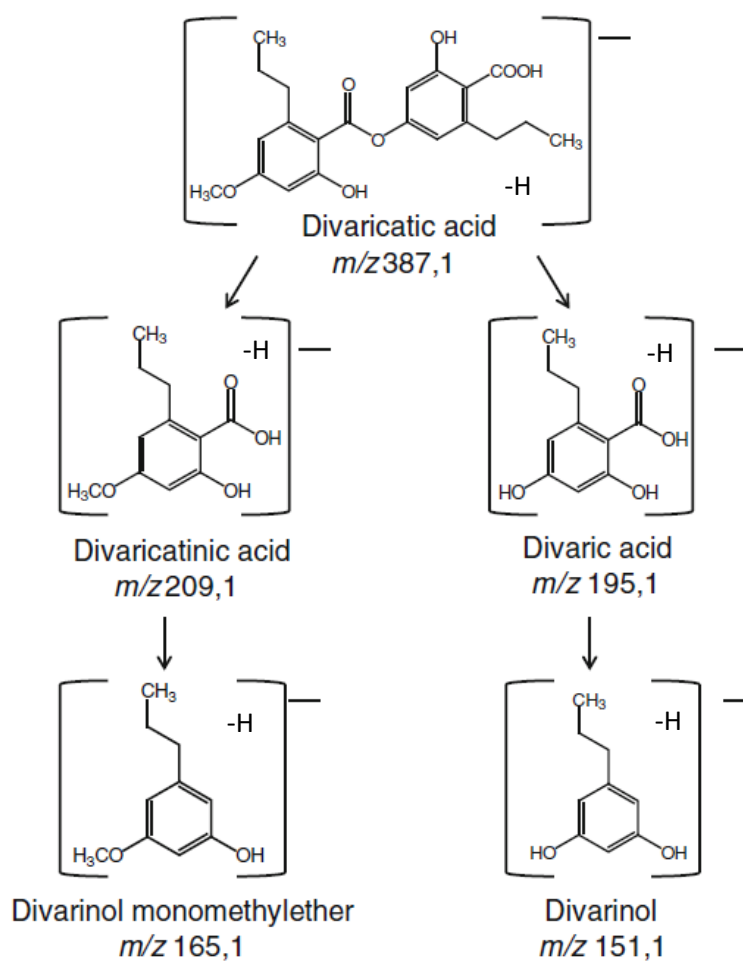
Recent NMR studies describe ^1H NMR spectra to achieve analysis under metabolomic conditions. Overall spectra from complete extract, with no further workup, display specific fingerprints enabling direct characterization of major compounds. Eisenreich et al. (2011) submitted methanol-D₄ extract of chlorolichen *Xanthoria parietina* and cyanolichen *Peltigera horizontalis* to ^1H NMR. Those spectra comprise lichen-specific features as well as strong signals standing for mannitol, while those corresponding to sucrose are missing. Such methods seem interesting for both comparative studies (developing fingerprinting for given lichen species) or to assess metabolite modulations in response to environment changes (see Sect. 11.4).

11.3.2 Mass Spectrometry

The formula of an organic compound can be calculated from HR mass spectrometry data. Fractionations and skeletal rearrangements are also of particular significance in the application of mass spectrometry to structure elucidation. As an example, the fractionation of divaricatic acid is given below (Fig. 11.7).

Mass spectrometry also provides characteristic peaks regarding signature elements or specific

Fig. 11.7 Fractionation of divaricatic acid in negative-mode electrospray mass analysis



organic moiety, which hints regarding chemical structure of analyzed compounds. For instance, substances containing chloride give characteristic isotope pattern in their mass spectrum, indicating the number of chlorine atoms per molecule.

Huneck et al. (1968) first reported on mass spectra in both positive and negative mode corresponding to numerous depsides, depsidones, depsones, dibenzofuranes, and diphenylbutadienes. This paper described for the first time the main fragmentation route of depsides, consisting in the cleavage of its ester bond, enabling structural assignments to the carboxylic acid or phenolic parts of the molecule (Huneck et al. 1968). The specific cleavage of the ester bond as a typical process of didepsides can be followed by loss of water as the result of *ortho* interaction of the 2-hydroxybenzoic acid residue (Elix and Norfolk 1975; Addison 1985; Dmitrenok et al. 1987;

Holzmann and Leuckert 1990). The classical fragmentation patterns of depsidones include neutral loss of CO_2 on their central ring to yield a dibenzofurane moiety alongside different elimination processes depending on the nature of the substituents (Parrot et al. 2013). Mass spectrum behavior of dibenzofuran and usnic acid derivatives was thoroughly discussed (Kutney et al. 1974; Schmidt et al. 1981). Hüneck and Schmidt (1980) described the fragmentation behavior of 16 usnic acid derivatives and established elimination mechanisms using deuterated analogues in both positive and negative modes. Characteristic rearrangements were also reported with some pulvinic acid derivatives (Letcher and Eggers 1967), polyporic acid derivatives (Grigsby et al. 1974), di- and tri-oxygenated stictane triterpenoids, and their trimethylsilyl derivatives (Holland and Wilkins 1979).

Non-hyphenated mass spectrometry was also applied to the screening of lichen compounds. Santesson developed a special technique, the so-called lichen mass spectrometry by introducing small lichen samples (sometimes less than 50 ng) into the direct inlet system of a mass spectrometer aiming to study xanthone pigments. The xanthenes sublime as the temperature is increased (150 °C) under very low pressure, and the mass spectrum is recorded. Xanthenes generally give prominent molecular ions, and the spectrum of the mixtures is often seen as additive of the individual components. However, this method remained limited to lichens containing only a few compound, otherwise giving spectra that are too complex to be interpreted (Santesson 1969).

Other mass spectrometry techniques relied on combination of soft-ionization negative-mode fast atom bombardment yielding intense $[M-H]^-$ ions that were subsequently analyzed by MS/MS. This enabled investigation of individual $[M-H]^-$ ions originating from crude extracts of lichen material and the selective study of the structure of components (Holzmann and Leuckert 1990). Tabacchi et al. (1991) also directly analyzed *Pseudevernia furfuracea* and *Lobaria pulmonaria* by tandem MS.

Recently, NMR and HRMS are the most commonly used structure-elucidating methods. Hyphenations of mass spectrometry with chromatographic techniques will be developed in Sect. 11.3 on dereplicative tools as well as recent innovations in the field of ambient and imaging mass spectrometry.

11.3.3 Infrared Spectroscopy

Like Raman spectroscopy, infrared spectroscopy is a technique based on the vibrations of the atoms of a molecule. The infrared spectrum is obtained by passing infrared radiation through a sample, in virtually any physical state, and further determining what fraction of the incident radiation is absorbed at a particular energy. Thus, infrared spectroscopy gives ability to associate

patterns of absorption peaks with their corresponding functional groups (Stuart 2004). For example, carboxylic acid might be identified by a broad peak centered around $3,000\text{ cm}^{-1}$, a strong peak around $1,720\text{ cm}^{-1}$, and a broad medium intensity band around 920 cm^{-1} (Woodruff and Munk 1977). One might find pattern of absorption peaks corresponding to a wide variety of functional groups in Silverstein et al. (1998).

Infrared spectrometry is part of the classical set of structure-elucidating methods and IR data are thus most of the time available in Huneck and Yoshimura (1996).

Further enhancements in infrared spectroscopy now enable collecting space-resolved information, which has been discussed in detail in the Sect. 11.3.

11.3.4 UV Spectroscopy

As previously described, lichens are miniature ecosystems that can survive under very harsh conditions. Therefore, these stress-resistant organisms developed adaptive mechanisms to cope with such high light exposure including synthesis of UV-protectant metabolites (Nguyen et al. 2013). As most lichen compounds have chromophores, UV is useful for their detection and identification but remains most of the time associated with TLC or HPLC (see further).

Yoshimura et al. (1994) first divided lichen secondary metabolites into three groups according to their UV spectral pattern.

- depsides and monocyclic compounds
- depsidones
- dibenzofurans, pulvinates, xanthenes, and anthraquinones exhibit typical UV spectra and are therefore easy to distinguish.

Then, mycosporines, more recently reported in lichens (Torres et al. 2004), are characterized through their UV spectrum absorbing in the 310–365 nm range with a strong molar extinction coefficient and a symmetrical shape. Detection through analytical techniques hyphenated with a PDA spectrophotometer offers a simple and easy method to screen them from lichen extracts

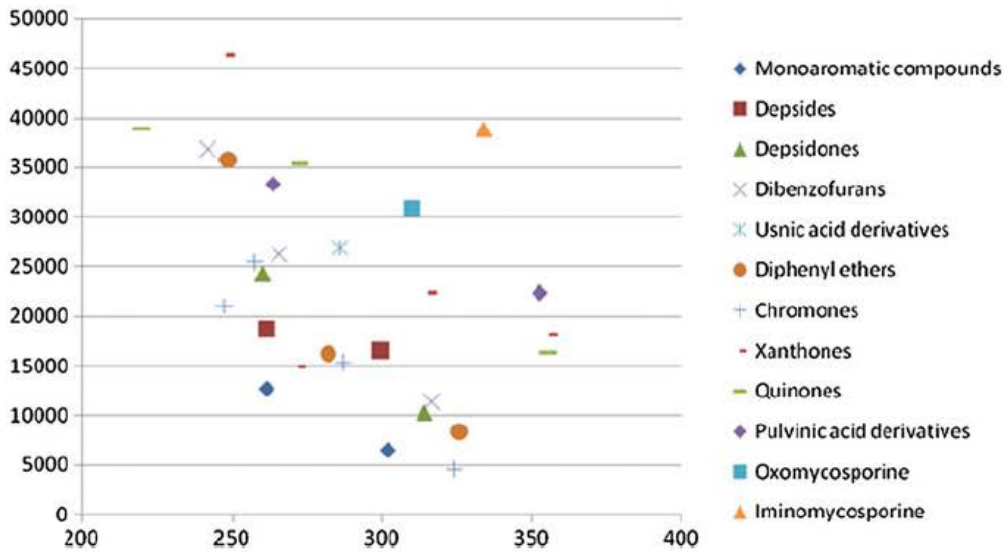


Fig. 11.8 UV properties of main structural families met within lichens (for quinones, additional absorptions are observed in visible range with medium λ_{max} of 458 and 529 nm) [adapted from Huneck and Yoshimura (1996)]

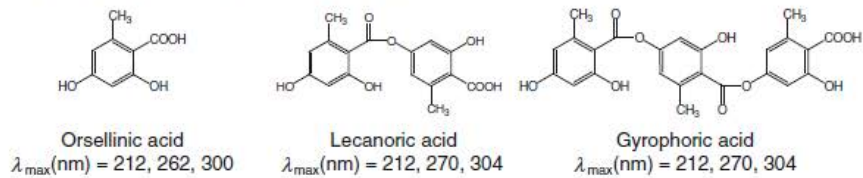
(Roullier et al. 2011). As an attempt, UV data of most lichen structural families are visualized in the Fig. 11.8:

Some relationships between chemical structures and UV spectra of depsides have been considered (Fig. 11.9) (Yoshimura et al. 1994).

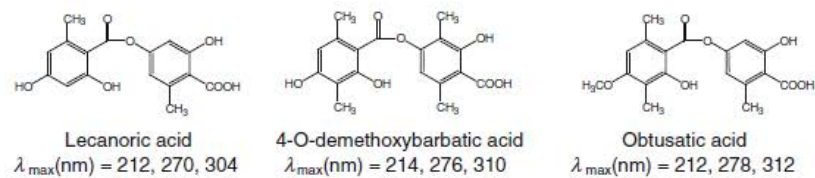
First, it was noted that molecular weight affects UV spectra. For instance, comparison of orsellinic acid with lecanoric and gyrophoric acids, containing two and three orsellinic acid units, respectively, showed quite a similar spectrum, but both lecanoric and gyrophoric acids

Fig. 11.9 Some relationships between chemical structure and UV features of depsides [adapted from Yoshimura et al. (1994)]

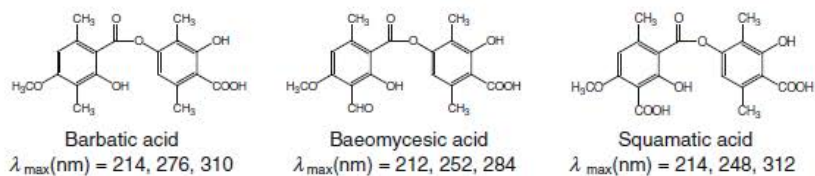
Effect of depside molecular weight



Effect of depside type



Effect of substituent on β -orcinol depsides



displayed bathochromic shifts of long wavelength bands and lower absorbance. Moreover, monocyclic compounds (except 2-*O*-methyl derivatives) have broader UV second bands ($\lambda_{\max} \sim 260$ nm).

Spectral differences were also linked to the depside type. Indeed, depsides are classically divided into three groups: orcinol type (e.g., lecanoric acid), β -orcinol type (having C₁ unit at 3 position of benzene ring, e.g., 4-*O*-demethylbarbatic), and mixed β -orcinol/orcinol type (e.g., obtusatic acid). Attachment of the methyl moiety has an influence on UV spectra as the second band of 4-*O*-demethylbarbatic acid and obtusatic acid is bathochromically shifted (+10 and +20 nm in comparison with lecanoric acid, respectively).

Influence of substitutions of β -orcinol depsides has also been studied. β -orcinol depsides may have CH₃, CH₂OH, CHO, or a COOH substituent at the 3 position of a benzene ring. Using barbatic acid (CH₃), baeomycesis acid (CHO), and squamatic acid (COOH), it was demonstrated that changing from CH₃ to CHO or COOH allows conjugation with the other ring and thus complicates the corresponding UV spectrum.

Hydroxyl group at the 2 position of depsides and monocyclic compounds is seldom methylated. Such 2-*O*-methylated compounds have shorter wavelength and lower intensity for their second band in comparison with their 4-*O*-methylated derivatives.

Methylation and alkyl chain length modifications of depsides do not affect their UV spectrum.

11.3.5 Stereochemistry Determination

Interests in determining the absolute stereochemistry of a chiral organic molecule originate from the widely admitted fact that stereochemistry determines important features regarding both chemical, biological, and physical properties.

X-ray crystallography remains the primary method to determine the absolute configuration of a molecule and originates from crystallographic studies that grant unambiguous, accurate, and reliable three-dimensional structural parameters (Deschamps 2010).

In a number of aromatic lichen substances, fully unsaturated structures do not justify the measurement of molecular optical activity. However, numerous lichen substances are optically active. Most associated optical rotations could be found in reference books (Huneck and Yoshimura 1996) and generally expressed through $[\alpha]^{DT}$ values according to the Biot formula. Nevertheless, accurate measurements require full solubilization and solutions in g/100 mL which are sometimes difficult to achieve.

Alternatively, optical rotatory dispersion (ORD) corresponding to the variation of circular birefringence as a function of wavelength (Brittain 1998) has been determined for lichen products, including different classes of compounds: macrolactone glycosides (Rezanka and Guschina 2001a), aliphatic acid derivatives (Rezanka and Guschina 2001b), aliphatic lactones (Aberhart et al. 1970; David et al. 1990), triterpenoids (Huneck 1976), quinones (Ejiri et al. 1975), and carotenoids (Czygan 1976).

Circular dichroism is another option when experimental circular dichroism of the molecule can be compared to either (i) a set of experimental spectra from related compounds, (ii) data from literature or (iii) calculated theoretical curves (Berova et al. 2007). Circular dichroism can also grant information regarding conformational features and was applied to a wide array of lichen compounds including aliphatic acids (Bodo and Molho 1980), cycloaliphatic compounds (Huneck and Himmelreich 1995; Polborn et al. 1995; Aberhart et al. 1970; Huneck and Höfle 1980; Huneck et al. 1986; Huneck and Takeda 1992), quinones (Mathey et al. 1980), chromones (Huneck 1972), carotenoids (Czczuga et al. 1988), and dibenzofuran-related compounds (Millot et al. 2013).

Assignment of absolute configuration by NMR represents another approach. Most of such NMR techniques rely on previous derivatization of the substrate prior to its analysis into two different species. This is performed with enantiomeric substances known as chiral derivatizing agents (CDA). Most used CDA is Mosher reagent (also known as methoxy trifluoromethyl phenyl acetic acid—MTPA) (Seco et al. 2004).

Some reports stand with application of Mosher derivatization to elucidate stereochemistry of lichen metabolites (Rezanka and Dembitsky 1999a; Rezanka and Guschina 2001a, b).

11.4 Dereplicative Tools

Over the last three decades, considerable attention has been paid to the development of hyphenated techniques, which combine different separation techniques (TLC, LC, GC) with structure-elucidating methods (mass spectrometry, NMR, UV/Vis spectroscopy).

11.4.1 Thin-layer Chromatography (TLC)

Study of lichen metabolites moved one step forward with the advent of commercially available TLC at the end of the 60s leading to a marked decrease of Asahina's crystal tests.

In 1952, Wachtmeister first introduced paper chromatography for the separation and characterization of lichen substances (Wachtmeister 1952, 1956). A few relationship between chemical structure and chromatographic behavior has been studied (Mitsuno 1953).

Ramaut (1963a, b) applied TLC in the field of lichenology to separate depsides and depsidones. Then, because different authors used different solvent systems and chromatographic conditions (Bendz et al. 1967; Santesson 1967a), procedures methods for routine identification of lichen products by TLC were first attempted by Santesson who reported R_f values of 80 lichen

metabolites (Santesson 1967b). Culberson and Kristinsson (1970) first described a TLC-based method to cope with R_f variations ensuring higher reproducibility and associating other identification methods to curtail identification possibilities. Indeed, to overcome R_f varying problems, internal standards atranorin and norstictic acid were chromatographed alongside samples of interest, and 8 R_f classes were defined according to the relative positions of each spot compared with atranorin and norstictic acid. TLC was developed in three solvent systems ("A": benzene/dioxane/acetic acid 90/25/4; "B": hexane/ethyl ether/formic acid 5/4/1; "C": toluene/acetic acid 85/15). Further identification possibilities among compounds that share same R_f classes for both 3 solvents were further narrowed according to (i) reaction after spraying H_2SO_4 and heating (ii) color reactions (as previously described), (iii) appearance of the spot under visible light, short- and long-wave UV light, and (iv) any other pertinent data available as solubility in different solvents. One hundred and four compounds were listed into R_f classes according to this approach (Culberson and Kristinsson 1970) Table 11.2. Due to diethyl ether fast evaporation, it was later replaced in solvent system B by a higher boiling ether with nearly identical chromatographic properties: Methyl tertiary butyl ether (MTBE) and corresponding changes in R_f of lichen metabolites were also published (Culberson and Johnson 1982). Another solvent system (referred to as solvent G: toluene/ethyl acetate/formic acid 139/83/8) was later introduced to separate polar compounds such as β -orcinol depsidones (Culberson et al. 1981).

Further enhancements of this previous method were later published. In particular, it was reported that acidic hydrolysis (with concentrated sulfuric acid) of a number of compounds difficult to distinguish under their intact form might yield fragments that chromatograph very well in standard solvent systems and thus enable identification of the unhydrolyzed fragments (Culberson 1972). Another simple derivatization step

Table 11.2 Various reagents used to detect the lichen substance

Reagent	After treatment	Identified compounds	References
UV light (254, 365 nm)	None	Most lichen substances Specific set of wavelengthes can enable detection of compounds with characteristic UV profiles, e.g., mycosporines 310 nm	
Iodine vapor	Place the chromatogram into a chamber in which some crystals of iodine have been placed. Iodine vapor is more quickly generated by gently warming the chamber	General detection reagent All lichen compounds, brown spots	Brante (1949) Munier and Macheboeuf (1949)
Sulfuric acid A: Mix equal parts of 95 % sulfuric acid and methanol with cooling B: 5 % ethanolic solution of 95 % sulfuric acid C: 5 % solution of 95 % sulfuric acid in acetic anhydride D: Mix equal parts of 95 % sulfuric acid and glacial acetic acid	Spray the chromatogram with one of these reagents. Allow to dry for 15 min in the air and heat to 110 °C until maximal visualization of the spots	All lichen compounds, gray, brown or blue spots	Jones et al. (1963) Metz (1961)
Chlorosulfonic acid dissolve 5 ml chlorosulfonic acid in 10 ml glacial acetic acid with cooling	Heat 5–10 min at 130 °C	All lichen compounds, wide array of colors, terpenoids violet	Tschesche et al. (1961) Tschesche and Wulff (1961) Takeda et al. (1963)
Sulfuric anisaldehyde A: anisaldehyde + 1 mL sulfuric Acid + 8.5 mL methanol or B: 0.5 ml anisaldehyde in 50 ml glacial acetic acid and 1 ml 97 % sulfuric acid 5 % p-phenylene diamine	Heat to 100–105 °C until maximum visualization of the spots	Deposides, depsidones, diphenylethers, monophenolic compounds, pink, red, blue-violet Aromatic aldehydes, yellow to red	Stahl and Kaltenbach (1961) Lisboa and Diczfalusy (1963) Huneck and Yoshimura (1996)
Ninhydrin 0.2 % ninhydrin in ethanol or 0.3 mg ninhydrin in 100 mL 1-butanol and add 3 mL glacial acetic acid	Heat at 110 °C until maximal visualization of the spots	Aminoacids, peptides, proteins, yellow (secondary aminoacids) to purple (primary aminoacids)	Patton and Chism (1951) Fahmy et al. (1961) Friedman (2004)

(continued)

Table 11.2 (continued)

Reagent	After treatment	Identified compounds	References
0.5 % magnesium acetate in methanol	Heat 5 min at 90 °C	Anthraquinones glycosides and related aglycones (pink to violet)	Shibata et al. (1950)
0.2 % primulin solution	Dip and wait for 30 min	Lipids, aliphatic compounds. White fluorescent spots at 366 nm	
Sulfuric thymol Dissolve 0.5 g thymol in 95 ml ethanol and add 5 ml 97 % sulfuric acid with caution	Heat 15 min at 120 °C	Sugars. Pink spots	Adachi (1965)
Diazotized benzidine + NaOH (solution A: 2.5 g benzidine + 7 mL conc.HCl in 500 ml H ₂ O; solution B: 50 g NaNO ₂ in 500 mL H ₂ O; equal volumes of A and B are mixed immediately before the application of the reagent)	The reagent is stable for a few hours Colors can appear quickly or develop long after depending on the nature of the phenol	Depsidic, depsidones, monophenolic compounds, red	Sherma and Hood (1965)

described is *O*-methylation using diazomethane that can be used as another identification hint. Eventually, acidic hydrolysis of *O*-methyl derivatives can provide further evidence for structure identification and to establish the order of linkage of phenolic acid units in simple depsides. As a consequence, R_f of hydrolyzed and *O*-methyl derivatives began being compiled, while an increasing number of lichen metabolites was also referenced (Culberson 1972). A useful tool for separation of complex mixtures is two-dimensional TLC as successfully applied for the separation of β -orcinol depsides from *Parmelia loxodes* and *P. verruculifera* (Culberson and Johnson 1976). TLC separation of (+) and (–) usnic acid was enabled by reaction with brucine as performed by Bendz et al. (1967).

Later, the use of high-performance thin-layer chromatography (HPTLC) in screening lichen substances was developed. HPTLC is more sensitive, allows the running of more samples in a shorter period of time, and requires smaller amounts of solvent (Arup et al. 1993).

As similar R_f value does not mean single compound, therefore, reliability to only R_f value remains a challenging and risky task. However, standardized methods listed above enable

collecting valuable clues regarding chemical structures and might curtain identification possibilities.

Image-giving format of open, stationary phase of TLC can lead to numerous hyphenations. In particular, TLC can grant valuable information dealing with bioactivity and thus guide fractionation to focus on biologically active compound. For instance, bioautography is a microbial detection method developed on a planar chromatography plate and designed to recognize compounds with antibacterial and antifungal properties (Choma and Grzelak 2011). Thus, TLC bioautography was used to assess antibiotic properties of metabolites from *Ramalina farinacea* (Tay et al. 2004), anti-*Helicobacter* activity from various species of lichens (Luo et al. 2011) as well as fungitoxic compounds from *Lobaria kurokawae* (Wang et al. 2009). Biochemical detection can also be used, and for instance, screening of radical scavenging molecules can be evaluated using TLC by spraying stable free radical DPPH, which has already been performed on several lichen extracts (Bhattarai et al. 2008).

To sum up, TLC was one of the way to perform multiple detection in situ for (i) physical detection, (ii) microchemical detection, and

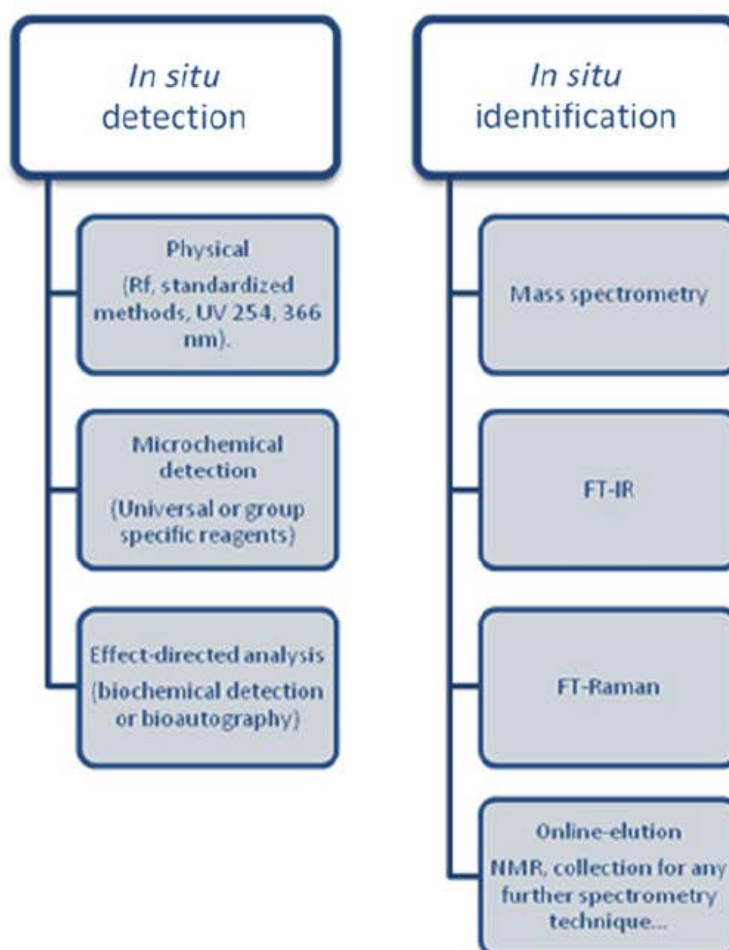
(iii) effect-directed analysis (either biochemically or microbiologically). Recent innovations in TLC allow successful hyphenations with different kinds of spectroscopic tools enabling proper *in situ* identification. Without any doubt, most developed hyphenated techniques are those combining TLC with mass spectrometry either online (Morlock and Schwack 2010) or off-line (Cheng et al. 2011). However, associating TLC with Fourier transform infra-red (FTIR) or Raman spectroscopy remain possible approaches. Furthermore, development of zone-collecting techniques (Luftmann et al. 2007) permits selective desorption and collection of molecules from a single TLC spot and further achievement of any structure elucidation technique as NMR (Morlock and Schwack 2010) (Fig. 11.10).

11.4.2 High-performance Liquid Chromatography

HPLC has become an important and efficient tool for the separation and identification of lichen substances, especially for compounds that cannot be studied by gas chromatography (GC) either because they are not volatile enough or are too unstable at high temperatures. First attempts were undertaken for chemotaxonomy with reversed-phase columns using methanol–water–acetic acid solvent system (Culberson and Culberson 1978).

Although such isocratic methods gave excellent results, gradient elution methods were later developed that better fit with complex lichen extracts containing a wide range of hydrophobic compounds (Culberson and Elix 1989). Gradient

Fig. 11.10 Possible hyphenations with thin-layer chromatography [modified from Morlock and Schwack (2010)]



elution in lichenology was introduced by Strack et al. (1979) that separated 13 different lichen products (depsides, depsidones, dibenzofurans, and pulvinic acids) using a reversed-phase column with a linear gradient based on a water/methanol system. A first standardized method for separation of lichen aromatic products was described using different kinds of reversed-phase column on the basis of a methanol/orthophosphoric acid gradient system and including two internal standards: benzoic acid (low retention time) and bis-(2-ethyl-hexyl)phtalate (high retention time) (Huovinen 1987) according to which retention indices are defined ensuring better reliability. However, the latter standard was further replaced by solorinic acid (more hydrophobic) making the method suitable for the identification of lichen extracts containing chloroxanthenes or long chain depsides as well. This second standardized reversed-phase HPLC method for identification of aromatic secondary metabolites from lichens was published by Feige et al. (1993) and is based on a retention index I calculated from the elution time of the appropriate peak compared with the standards benzoic and solorinic acids.

Such a relative index corresponding to 331 lichen compounds was determined by Feige et al. (1993), and this protocol was successfully applied to several genera of lichens (Lumbsch et al. 1993). Mietzsch et al. (1994) developed a computer program dedicated to lichen metabolites identification named Wintabolites. This software made use of HPLC- R_f values, TLC- R_f values, UV/visible colors of TLC spots, and lichen spot tests to identify molecules. The program database included 550 lichen compounds.

Derivatization techniques were further published to enable detection of aliphatic lichen acids (e.g., roccellic, rangiformic acids, licheterinic acids) using the same method. Such metabolites are previously transformed into their phenacyl, para-nitrophenyl, or benzyl esters that display strong absorption in the UV (λ_{\max} ca. 240 nm) (Huneck et al. 1994).

Later, hyphenation with photodiode array spectrophotometers (DAD), leading to complete UV-Vis spectra of corresponding peaks, greatly

helped for the identification of molecules. Yoshimura et al. described detection of lichen metabolites according to their UV spectra features and relative retention time. HPLC was achieved using a reversed phase with an isocratic method (MeOH/H₂O/H₃PO₄). Retention times were expressed according to 2 standards: acetone and 1-phenyl-1-dodecanone.

However, relying on retention times only (even normalized with internal standard) and UV spectrum is not always sufficient to unambiguously identify a given compound. Nowadays, most liquid chromatography strategies rely on LC-DAD-ESI-MS that enable both (i) collection of UV-Vis spectrum and (ii) determination of the molecular weight associated with each peak of the chromatogram.

Hyphenated techniques are now commonly used as powerful tools of dereplication to focus on original or biologically relevant metabolites.

As an example, screening of mycosporines within different lichens was first based on their characteristic UV symmetrical shape while parallel ESI-MS helped focusing on undescribed molecules according to their molecular weight. Therefore, purification of a new molecule mycosporine hydroxyglutamicol from *Nephroma laevigatum* was achieved from 8 g of dried lichen material (Roullier et al. 2011). However, since the last standardized method described by Feige et al. and Yoshimura et al. in the nineties, no further publication updated extensively the behavior of lichen metabolites with hyphenated techniques such as LC-DAD-ESI/MS. Such a standardized method of reversed-phase LC-DAD-ESI/MS is described for the conspicuous reign of microfungi in which are described retention time, UV/Vis spectrum, and monoisotopic mass for 474 fungal metabolites (Nielsen and Smedsgaard 2003). Noteworthy, this database includes some fungal metabolites that can also be met within lichens (e.g., emodin, lichexanthone, skyrin ...).

As previously discussed, NMR is arguably the most versatile analytical platform for complex mixture analysis (Corcoran and Spraul 2003). Indeed, successful interfacing of high-pressure liquid chromatography with parallel NMR and mass spectrometry were reported, yielding

extensive structural data on each chromatographed compound (Exarchou et al. 2005). Wolfender et al. (2001) stated that coupling of HPLC with NMR is the one of the most powerful methods for the separation and structural elucidation of unknown compounds in mixture. However, to the best of our knowledge, no LC-NMR analysis was reported yet in the field of lichenology.

11.4.3 Gas Chromatography

GC found some limited applications in lichenology, since most lichen substances are polar and present low volatility. To cope with this problem, prior derivatization is usually required in order to yield volatile enough compounds to be analyzed by GC, most of the time as their trimethylsilyl, acetyl, methyl, or trifluoroacetyl derivatives. Derivatization procedures have been described by Nishikawa et al. (1973).

Using this method, Ikekawa et al. (1965) separated trimethylsilyltriterpene derivatives belonging to ursane, oleanane, and lupane groups (including compounds found within lichens as friedelin, taraxerol, taraxerone, and zeorin among others). Different C₂₇, C₂₈, and C₂₉ sterols from the moss tree lichen *Pseudevernia furfuracea* were also characterized and quantified by GC-MS (Wojciechowski et al. 1973) after acylation from low polar organic solvent extractions. A few studies described GC analyses carried out on other structural families among which Furuya et al. (1966) demonstrated that retention time increases with the number of hydroxyl on the anthraquinone skeleton.

Low molecular weight carbohydrates from eight species of lichens were analyzed and quantified by GC as their acetyl, trifluoroacetyl, and trimethylsilyl derivatives in comparison with standard specimens. Arabitol, fructose, glucose, glycerol, erythritol, mannitol, sucrose, and trehalose were commonly found within tested

samples alongside more specific sugars (as umbilicin, among others) (Nishikawa et al. 1973). Later publications reported on GC-MS characterization of *Ramalina celastri*'s mono and polysaccharides as their acetate derivatives (Stuelp et al. 1999). In the same way, acetylated saccharides from *Sticta* sp. were analyzed by GC-MS (Corradi da Silva et al. 1993) as well as carbohydrates from *H. physodes* and *Platismatia glauca* (Dahlman et al. 2003).

Fatty acid compositions of different *Parmelia* species were examined by capillary GC-MS. This enabled detection of 68 fatty acids as their methyl ester, trimethylsilyl, or oxazoline ethers (Dembitsky et al. 1992c). Fatty acid and phospholipid compositions were also reported within lichens growing in the Volga river basin using GC-MS (Dembitsky et al. 1992a), in the Tian Shan Mountains (Rezanka and Dembitsky 1999b), with different species of *Cladonia* (Dembitsky et al. 1991) or different lichens belonging to Lecanorales (Dembitsky et al. 1992b). More recently, fatty acid components—either free or combined—of the tropical lichen *Teloschistes flavicans* were analyzed by GC-MS of derived methyl esters and compared to those of separately cultivated symbionts. It was evidenced that the fatty acid compositions of the whole lichen strikingly differ from those of isolated symbionts. Moreover, changes were also observed according to the temperature. Likewise, capillary GC-MS demonstrated that seasonal changes also occurred in the fatty acid composition of two species of *Physcia* as well as in *Xanthoria parietina* (Bychuk 1993; Dembitsky et al. 1994).

In some cases, GC-MS analyses were performed for biomonitoring purposes as lichens are known to accumulate some given pollutants in their tissues (especially epiphytic lichens). Therefore, GC-MS air pollution assessment techniques were applied to detect polycyclic aromatic hydrocarbons within different Pyrenean lichens (Blasco et al. 2008) or within Italian alps-dwelling lichens (Nascimbene et al. 2014).

11.4.4 In Situ Detection

As discussed earlier, having access to the distribution of secondary metabolites could help understanding both fundamental facts about the symbiosis itself and enlightening relationships existing between the lichen and its environment. In many lichens, some metabolites are only present or occur in higher concentration in reproductive compared to somatic structures, giving support for optimal defense theory in lichens (Hyvärinen et al. 2000). Accordingly, it was shown that grazing pattern of snails inversely reflects the partitioning of the secondary compounds that have a documented deterring effect, avoiding reproductive parts of the lichen due to internal defense allocation (Asplund et al. 2010). Moreover, in situ characterization of compounds has always been considered as a very interesting approach since it eliminates complications and artifacts caused by time-consuming isolation procedures that are still required when structural analysis is achieved using conventional spectroscopic methods (Mathey et al. 1987).

11.4.4.1 Histochemical Reactions

First attempts of mapping metabolites' distribution within lichens used spot tests as described above. Indeed, specific pattern of distribution of some metabolites make thalline reactions organ specific (Kirschbaum and Wirth 1997). Honegger (1986) described ultrastructural studies of various *Parmeliaceae* using enhanced scanning electron microscopy sample preparation techniques to avoid dissolution of lichen substances. SEM images showed varying amounts of crystals covering the surface of both fungal and algal cells within different parts of the lichen thallus. Moreover, histochemical reactions (K, C, KC, PD) performed with thallus fragments or cryostats allowed localizing different secondary metabolites within the different layers of the thallus. The presence of mycobiont-derived crystalline lichen products on the surface of algae raises questions. One possible reason may be that such substances might slow down the metabolism of the photobiont to keep an harmonious

growth pattern with a mycobiont whose growth abilities are limited (Kinraide and Ahmadjian 1970; Honegger 1986).

11.4.4.2 Laser Microprobe Mass Spectrometry

Along with thalline reactions, the first general method used to in situ analyze lichen substances on a microscale was laser microprobe mass spectrometry (LMMS also known as LAMMA) (Mathey 1981). Physical principle of this mass spectrometry method relies upon the irradiation of inorganic or organic samples with pulsed power UV laser under vacuum. Resulting ions are further analyzed using a time of flight or Fourier transform mass spectrometer (Van Roy et al. 1996). Microscale detection is enabled thanks to a concomitant light microscopic observation of thin cryosection that allows to focus laser beam on any sample detail (Wink et al. 1984). UV irradiation enables selective desorption and ionization of products with a chromophoric group. Indeed, a severe limitation of LMMS is its requirement for UV absorbing moieties.

As most lichen compounds have conjugated rings, this analysis method was the first showing ability to correlate analysis to given structures or substructures of the microscopical image. A large variety of lichen metabolites (especially lichen pigments) sublime when submitted to very low pressure, such as the vacuum existing in LAMMA-MS, especially lichen pigments (Mathey 1981). In such conditions, a mild elevation of temperature leads to vaporization of lichen metabolites that further yield mass spectra displaying very prominent parent ions, often corresponding to the base peak of the spectrum.

The tropical lichen *Laurera benguelensis* is characterized by yellow thallus warts that present a marked yellow fluorescence under UV radiation, originating from microcrystals located in the cortex (Mathey 1979). LAMMA spectrum obtained from single microcrystals displayed a characteristic lichexanthone profile while physcion and xanthorin, orange anthraquinone pigments, were distinctly found in the warts containing the fruiting

bodies in additional *Laurera* species (Mathey et al. 1980, 1987, 1994).

LMMS was also successful in detection of a variety of lichen pigments belonging to different structural families (Mathey et al. 1987; Van Roy et al. 1996). However, LAMMA analysis only grants low mass resolution. Hence, unambiguous detection of compounds requires additional data from either NMR or HR mass spectroscopy.

11.4.4.3 Raman and FTIR Spectroscopy

First developed Raman analyses mostly dealt with biodeterioration of monuments and frescoes due to oxalic acid produced by encrusting microlichens, aiming at characterizing the physical and chemical nature of the lichen/substratum system (Edwards et al. 1991). Further works then moved to ecophysiological studies of lichen itself.

In situ Fourier transform Raman spectroscopy was used for identification of pigments and biodegradative calcium oxalate directly within thalli of viable epilithic lichens (*Acarospora* spp.) harvested in contrasted sites from Antarctic and Mediterranean (Holder et al. 2000). Raman-specific fingerprints could be used to recognize two photoprotective pigments: rhizocarpic acid and β -carotene. Near IR excitation (1,064 nm) eliminated possible fluorescence originating from pigments and insensitivity of Raman techniques to water enabled analysis of field fresh samples with a spatial resolution of about a 20 μ m spot diameter. Hydration states of calcium oxalate could be differentiated with different signals between monohydrate (whewellite) and dihydrate (weddelite). Edwards et al. (1998) compared parietin contents of *Xanthoria* lichens harvested in Antarctic and temperate habitats using Raman spectroscopy. Other publications reported on scytonemin detection by Raman spectroscopy from cyanobacteria (*Nostoc* sp., *Chlorogloeopsis* sp., *Scytonema* sp., *Lyngbya* sp.) or from cyanolichen *Collema* species (Wynn-Williams et al. 1999).

Raman spectra of lichen samples colonizing active volcanic environment (Kilauea volcano, Kona, Hawaii) were acquired to decipher biomolecular protective strategies adopted in such

extreme environments (Jorge-Villar and Edwards 2010). Raman profiles were acquired from 16 lichen specimens belonging to eight genera, growing on basaltic lava or on wood substrates. It was shown that chlorophyll and a carotenoid (most likely lutein or astaxanthin) were ubiquitous, but a wide range of protective pigments could be identified as atranorin, gyrophoric acid, parietin, pulvinic acid dilactone, and usnic acid (as well as calcium oxalate mono- and dihydrate in some cases) using specific patterns (Edwards et al. 2003a, b).

Lecanoric acid was characterized by FT-Raman spectroscopy in *Parmotrema tinctorium*, highlighting reliability of Raman spectroscopy for in situ detection of this metabolite from the whole lichen (de Oliveira et al. 2009).

FT-IR spectromicroscopy fits well to the examination of the conspicuous reign of filamentous fungi providing spatially resolved information on cellular biochemical content (Szeghalmi et al. 2007; Jilkine et al. 2008; Isenor et al. 2010).

More recently, Raman spectroscopy and FPA-FTIR were used to image the distribution of usnic acid within *Cladonia arbuscula*, *C. sulphurina*, and *C. uncialis* (Liao et al. 2010). This dibenzofuran-related metabolite was shown to be present in pycnidia and younger branches of *C. arbuscula* and *C. uncialis*, in *C. sulphurina*'s soredia as well as in the spore-forming region of *C. uncialis*' apothecia.

11.4.4.4 Ambient Mass Spectrometry

Recent technical innovations in mass spectrometry now allow detection of molecules in ambient conditions dealing with a large number of compounds in complex matrices and play an important role in various fields such as drug discovery, doping control, forensic identification, and food safety. Open-air sources especially revolutionized the way samples are introduced into the ion source for mass analysis and result in rapid acquisition, without special sample preparation enabling quick and sensitive dereplication. Among these open-air sources is especially worth quoting direct analysis in real-time mass spectrometry (DART-MS) that

is based on the interactions of a sample in a water-containing atmosphere with a gas in a metastable state heated to a temperature up to 350 °C (Cody et al. 2005). DART's detection limit is comprised in the picomolar range and showed satisfying results for chemical fingerprinting of many plants (Kim and Jang 2009). Moreover, a number of lichenic compounds were shown to accumulate in upper cortex (Ozenda and Clauzade 1970). Such a distribution in the most superficial layers enables their detection using ambient mass spectrometry techniques as shown on the cyanolichen *Lichina pygmaea* using DART-MS (Le pogam et al. 2014).

Ambient mass spectrometry methods have to be tried with lichens to measure defense reactions as responses to environmental challenges as successfully applied to the red algae *Callophycus serratus* using DESI imaging (Lane et al. 2009). Other DESI imaging experiments reported on hydrolysis of hydroxynitrile glucosides along leaves wounds of *Lotus japonicus* (Li et al. 2013).

11.4.4.5 Imaging Mass Spectrometry

Imaging mass spectrometry allows to monitor the spatial distribution and abundance of metabolites. Experimental scheme for mass spectrometry imaging experiments can be defined as follows (Fig. 11.11). IMS involves rastering a laser or any other ionization source across a thin section of biological tissue by moving the sample stage in predefined x - y coordinates to generate thousands of position-dependent mass spectra. Sample preparation may be assisted to aid the ion ionization or can remain unassisted depending on both the mechanism of the ion source and the nature of the compounds to be analyzed. Then, data processing is accomplished by displaying ions of interest from a traditional m/z plot to a false color image eventually superimposed on a photograph of the analyzed sample (Greer et al. 2011).

Recently, three-dimensional imaging of metabolites in plant tissues was achieved thanks to LAESI-MS. LAESI-MS relies on tissue ablation with a single laser pulse of 2.94 μm

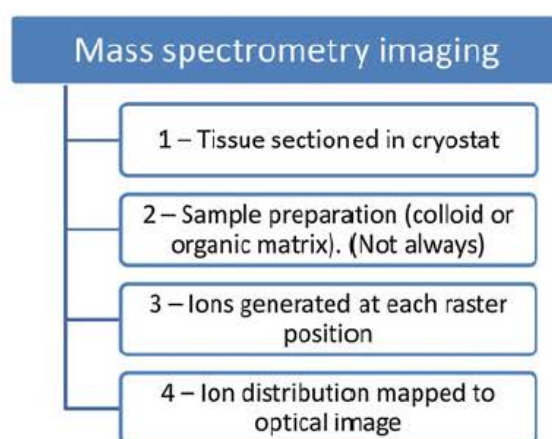


Fig. 11.11 Schematic outline of the workflow in a typical imaging mass spectrometry experiment [adapted from Greer et al. (2011)]

wavelength. O–H vibrations of the native water molecules of the tissue samples absorb the laser pulse energy, leading to ejection of microscopic volumes of the most superficial layers of the sample (as neutral particulates and molecules) that enables establishing depth profiles. This plume is further intercepted by an electrospray that postionizes the ablated material (Nemes and Vertes 2012). 3D-LAESI-MS revealed specific distribution pattern of several molecules within the plant *Aphelandra* in correlation with tissue specificity (Nemes et al. 2009). Common ionization methods applied in imaging mass spectrometry are listed above (Table 11.3).

Although achieved on a wide range of organisms [for review see Esquenazi et al. (2009)], no ambient or imaging mass spectrometry was published until now on lichens to the best of our knowledge.

11.5 Deciphering Metabolic Networks and Partners' Cooperation at the Very Heart of Symbiotic Systems

Systematic analysis of the metabolite composition caused by cellular reactions is called metabolomics (Oliver et al. 1998). A metabolomic approach was developed on *Xanthoria elegans* in 2007 (Aubert et al. 2007). In this study, analysis

Table 11.3 Characteristics of most commonly used imaging mass spectrometry sources

Ionization source	Probe beam	Pressure regime	Spatial resolution (μm)
MALDI	Laser beam	Vacuum (most of the time) or ambient (AP-MALDI)	10–100
SIMS	Ion beam	Vacuum	0, 2–3
DESI	Solvent stream	Ambient	200
NIMS	Laser beam	Vacuum	15–20
LAESI	Infrared laser + electrospray	Vacuum	Lateral: 300–500 Depth: 30–40

Adapted from Lee et al. (2012), Greving et al. (2011)

of polar metabolites was achieved from crude perchloric acid extracts using ^{13}C and ^{31}P NMR spectroscopy to compare chemical profiles of both dry and wet thalli. Such analysis methods afforded the detection of 30 metabolites from the raw extract with no further sample workup (mostly sugars, sugar phosphates, polyols, phosphoenolpyruvate, and nucleotides). The data implied that metabolite composition was affected by stress conditions. Aubert also described increased concentrations of ribitol and mannitol under dry conditions. Sugars are known protectors of cellular substructures when lichens have to survive under dryness (Crowe et al. 1992).

As previously discussed, lichens are able to synthesize unique secondary metabolites. However, the relative contribution of its partners in providing such original compounds remains quite unstudied. This question is especially interesting when both partners possess the enzymatic machinery required to biosynthesize one metabolite [e.g., mycosporine and cyanolichens (Balskus and Walsh 2010)]. Moreover, knowledge about biosynthesis pathway is also a prerequisite for natural compounds production by biotechnological means.

Most current methods used to decipher metabolic pathways are based on stable isotope labeling (Eisenreich and Bacher 2007). Typically, organisms are grown with labeled structures that are most of the time very general precursors (e.g., glucose, acetyl CoA, CO_2 , NH_4 , aminoacids) that will spread in all their possible metabolic fates. Subsequent analysis of enriched biomolecules by either quantitative NMR spectroscopy or mass spectrometry has shown to be a

powerful method for unraveling the dynamics of metabolic networks (Fan et al. 2012). Indeed, according to the detected profiles, metabolic history of the studied metabolite can be traced and then compiled to a comprehensive map about metabolic pathways and fluxes occurring in the network.

Although initially focused on single organisms such as plants or bacteria [for review see Eisenreich and Bacher (2007) and Heinemann and Sauer (2010)], techniques of stable isotope labeling were later applied to multi-organismic systems (Götz et al. 2010).

To our knowledge, only a few labeling studies for biosynthetic-unraveling purposes were reported on lichens. Lines et al. (1989) investigated polyol metabolism in *Xanthoria calcicola* using a ^{13}C NMR spectroscopy approach. More recently, a proof on concept was published in 2011 on the chlorolichen *X. parietina* (Eisenreich et al. 2011). Photobiont cells (*Trebouxia decolorans*) were first harvested alone in a medium containing ^{13}C -glucose, which enabled satisfying labeling of most if not all metabolites according to the authors. In a second step, algae were combined with unmarked mycobiont to reconstitute lichen symbiosis. Therefore, detection of ^{13}C -labeled fungal metabolites is indicative for prior transfer and usage of algal biomass for biosynthetic purposes by the mycobiont. ^{13}C NMR of crude methanol extracts of marked photobionts alone and reconstituted symbiosis by cocultivation with unlabeled fungus bear striking differences that demonstrate substrate transfer and further metabolism by the mycobiont. Closer investigation of those signal patterns shall

provide information regarding (i) the nature of transferred compounds, (ii) the rate of this transfer and eventually, (iii) subsequent transformations occurring within the second partner (Eisenreich et al. 2011).

Such technologies took advantage of tremendous advances in mass spectrometry that now enable microscale mapping of metabolites directly within producing organisms (Esquenazi et al. 2009). Coupling of stable isotope profiling with imaging mass spectrometry enables both tracing and mapping of molecules within its biological system. This approach is especially promising for interfaces or symbiotic systems in order to know the compartment in which a molecule undergoes biotransformation (Jones et al. 2013; Pernice et al. 2012).

11.6 Conclusion

The evaluation of lichen metabolites for therapeutic purposes is generating an increasing interest as their activities are varied and often significant (Boustie et al. 2011). Very few lichen compounds are commercially available, and the thousand known metabolites are only partly or not at all investigated for their medicinal potential (Stocker-Wörgötter 2008). Moreover, lichens appear to harbor a diversity of culturable microorganisms from which original active compounds were recently isolated (Grube et al. 2012).

As lichens grow slowly, both in nature and axenic conditions, analysis must deal with low amounts of crude material. The past few years have witnessed major developments in purification, dereplication, and structure elucidation of lichen compounds, enabling much faster access to sufficient amounts of pure compounds.

Although not described here, innovative strategies were also developed for extracting and separating compounds which facilitate detection and identification of lichen compounds. New extraction methods developed on lichens include supercritical fluid extraction (SFE) involving the so-called supercritical fluids (SCF) (Lisickov et al. 2002; Zizovic et al. 2012) that appears to be a powerful strategy. Although a specific device is

required, the main advantages of these methods are that (i) they display solvating powers similar to liquid organic solvents with higher diffusivity and lower viscosity, (ii) they can provide quantitative or complete extraction (by forcing continuously the fluid to flow through the sample), (iii) the solvating power of the fluid can be adjusted by changing the pressure and/or the temperature, (iv) adding modifiers to a SCF can change its polarity, (v) they avoid solvent residuals and last but not least, (vi) they are chemically inert which avoid chemical artifacts that can be dread when using classical separation procedures (Lang and Wai 2001).

A light fluoruous catch and release approach was another option used to separate three closely related paraconic acids from *Cetraria islandica* allowing the isolation and identification of roccellaric acid from this lichen for the first time (Horhant et al. 2007).

The recent innovations in hyphenated techniques combining separation (HPTLC, HPLC, GC) and detection tools (currently MS, UV, IR) have already had a substantial impact in shortening the timeline for dereplication, isolation, and structure elucidation of the lichen products present in crude extract. Once hampered by methods limitations, lichen study might benefit from tremendous advances in analytical chemistry (MAS-NMR, DART-MS, LC-NMR...) described herein. Consequently, sensitive dereplication of lichen chemodiversity should facilitate focusing on minor, and possibly unknown, compounds. Standardized methods to identify recurrent products and to remove them should be developed in this way. As illustrated, various methods can be performed on solid samples then bypassing chemical artifacts associated with purification processes, giving in some cases direct field information. Furthermore, improvements in imaging techniques pave the way for future investigations into metabolic interactions taking place in lichen miniature ecosystem and might help deciphering ecological relevance of lichens metabolites.

Coupling these approaches with advances in purification, structure elucidation, and streamlining of the screening processes, the timeline for

lichen products drug discovery is shortened similar to that expected for synthetic compounds, now being compatible with the present regime of blitz screening campaigns.

Acknowledgments Jacques Lagabrielle is greatly acknowledged for his support in providing crystal pictures.

References

- Aberhart DJ, Overton KH, Huneck S (1970) Portentol: an unusual polypropionate from the lichen *Roccella portentosa*. *J Chem Soc C* 11:1612–1623
- Adachi S (1965) Thin-layer chromatography of carbohydrates in the presence of bisulfite. *J Chromatogr A* 17:295–299
- Addison JB (1985) Application of pyrolysis-chemical ionisation mass spectrometry to lichenology. *Analyst* 110:933–935
- Alcantara GB, Honda NK, Ferreira MMC, Ferreira AG (2007) Chemometric analysis applied in 1H HR-MAS NMR and FT-IR data for chemotaxonomic distinction of intact lichen samples. *Anal Chim Acta* 595:3–8
- Arup U, Ekman S, Lindblom L, Mattsson J-E (1993) High performance thin layer chromatography (HPTLC), an improved technique for screening lichen substances. *Lichenologist* 25:61–71
- Asplund J, Gauslaa Y (2008) Mollusc grazing limits growth and early development of the old forest lichen *Lobaria pulmonaria* in broadleaved deciduous forests. *Oecologia* 155:93–99
- Asplund J, Solhaug KA, Gauslaa Y (2010) Optimal defense: snails avoid reproductive parts of the lichen *Lobaria scrobiculata* due to internal defense allocation. *Ecology* 91:3100–3105
- Aubert S, Juge C, Boisson A-M, Gout E, Bligny R (2007) Metabolic processes sustaining the reviviscence of lichen *Xanthoria elegans* (link) in high mountain environments. *Planta* 226:1287–1297
- Balskus EP, Walsh CT (2010) The genetic and molecular basis for sunscreen biosynthesis in cyanobacteria. *Science* 329:1653–1656
- Bendz G, Bohman G, Santesson J (1967) Studies on the chemistry of lichens. 5. Separation and identification of the antipodes of usnic acid by thin layer chromatography. *Acta Chem Scand* 21:1376–1377
- Berova N, Di Bari L, Pescitelli G (2007) Application of electronic circular dichroism in configurational and conformational analysis of organic compounds. *Chem Soc Rev* 36:914–931
- Bhattarai HD, Paudel B, Hong SG, Lee HK, Yim JH (2008) Thin layer chromatography analysis of antioxidant constituents of lichens from Antarctica. *J Nat Med* 62:481–484
- Bialonska D, Dayan FE (2005) Chemistry of the lichen *Hypogymnia physodes* transplanted to an industrial region. *J Chem Ecol* 31:2975–2991
- Blasco M, Domeño C, Nerín C (2008) Lichens biomonitoring as feasible methodology to assess air pollution in natural ecosystems: combined study of quantitative PAHs analyses and lichen biodiversity in the Pyrenees Mountains. *Anal Bioanal Chem* 391:759–771
- Bodo B, Molho D (1980) Structure des acides isomuro-nique et neuropogolique, nouveaux acides aliphatiques du lichen *Neuropogon trachycarpus*. *Phytochemistry* 19:1117–1120
- Boustie J, Grube M (2005) Lichens—a promising source of bioactive secondary metabolites. *Plant Genet Resour Charact Util* 3:273–287
- Boustie J, Tomasi S, Grube M (2011) Bioactive lichen metabolites: alpine habitats as an untapped source. *Phytochem Rev* 10:287–307
- Brante G (1949) Iodine as a means of development in paper chromatography. *Nature* 163, 651–651
- Brittain HG (1998) Applications of chiroptical spectroscopy for the characterization of pharmaceutical compounds. *J Pharm Biomed Anal* 17:933–940
- Brodo IM, Sharnoff SD, Sharnoff S (2001) Lichens of North America. Yale University Press, New Haven
- Bychuk IA (1993) Change in the lipid composition of lichens in the spring period. *Chem Nat Compd* 29:582–585
- Cetin H, Tufan-Cetin O, Turk AO, Tay T, Candan M, Yanikoglu A, Sumbul H (2008) Insecticidal activity of major lichen compounds, (–)- and (+)-usnic acid, against the larvae of house mosquito, *Culex pipiens* L. *Parasitol Res* 102:1277–1279
- Cheng S-C, Huang M-Z, Shiea J (2011) Thin layer chromatography/mass spectrometry. *J Chromatogr A* 1218:2700–2711
- Cheng B, Cao S, Vasquez V, Annamalai T, Tamayo-Castillo G, Clardy J, Tse-Dinh Y-C (2013) Identification of anziaic acid, a lichen depside from *Hypotrachyna* sp., as a new topoisomerase poison inhibitor. *PLoS ONE* 8:e60770
- Chollet-Krugler M, Le-Floch M, Articus K, Millot M, Boustie J (2008) Carbon-13 CP-MAS NMR studies of some lichens of the Genus *Cladonia* section *Cladina*. In: *Planta Medica*. Georg Thieme Verlag Stuttgart, Germany, p 1118
- Choma IM, Grzelak EM (2011) Bioautography detection in thin-layer chromatography. *J Chromatogr A* 1218:2684–2691
- Cody RB, Laramée JA, Durst HD (2005) Versatile new ion source for the analysis of materials in open air under ambient conditions. *Anal Chem* 77:2297–2302
- Corcoran O, Spraul M (2003) LC–NMR–MS in drug discovery. *Drug Discov Today* 8:624–631
- Corradi da Silva ML, Iacomini M, Jablonski E, Gorin PA (1993) Carbohydrate, glycopeptide and protein components of the lichen *Sticta* sp. and effect of storage. *Phytochemistry* 33:547–552
- Crowe JH, Hoekstra FA, Crowe LM (1992) Anhydrobi-osis. *Annu Rev Physiol* 54:579–599
- Culbertson CF (1972) Improved conditions and new data for identification of lichen products by standardized thin-layer chromatographic method. *J Chromatogr A* 72:113–125

- Culberson CF, Culberson WL (1978) β -Orcinol derivatives in lichens: biogenetic evidence from *Oropogon loxensis*. *Exp Mycol* 2:245–257
- Culberson CF, Elix JA (1989) Lichen substances. *Methods Plant Biochem* 1:509–535
- Culberson CF, Johnson A (1976) A standardized two-dimensional thin-layer chromatographic method for lichen products. *J Chromatogr A* 128:253–259
- Culberson CF, Johnson A (1982) Substitution of methyltertbutyl ether for diethyl ether in the standardized thin-layer chromatographic method for lichen products. *J Chromatogr A* 238:483–487
- Culberson CF, Kristinsson H-D (1970) A standardized method for the identification of lichen products. *J Chromatogr A* 46:85–93
- Culberson CF, Culberson WL, Johnson A (1977) Non-random distribution of an epiphytic *Lepraria* on two species of *Parmelia*. *Bryologist* 80:201–203
- Culberson CF, Culberson WL, Johnson A (1981) A standardized TLC analysis of β -orcinol depsidones. *Bryologist* 84:16–29
- Czeczuga B, Cifuentes B, Reynaud PA (1988) Carotenoids in lichens from the Canary Islands. *Biochem Syst Ecol* 16:117–118
- Czygan F-C (1976) Carotinoid-Gamitur and-Stoffwechsel der Flechte *Haematomma ventosum* (L.) Massal. s. str. and ihres Phycobionten. *Z Fuer Pflanzenphysiol* 79:438–445
- Dahlman L, Persson J, Näsholm T, Palmqvist K (2003) Carbon and nitrogen distribution in the green algal lichens *Hypogymnia physodes* and *Platismatia glauca* in relation to nutrient supply. *Planta* 217:41–48
- Dailey RN, Montgomery DL, Ingram JT, Siemion R, Raisbeck MF (2008) Experimental reproduction of tumbleweed shield lichen (*Xanthoparmelia chlorochroa*) poisoning in a domestic sheep model. *J Vet Diagn Invest* 20:760–765
- David F, Elix JA, Binsamsudin MW (1990) Two new aliphatic acids from the lichen *Parmotrema praesorediosum*. *Aust J Chem* 43:1297–1300
- Dayan F, Romagni J (2001) Lichens as a potential source of pesticides. *Pestic Outlook* 12:229–232
- De Oliveira LFC, Pinto PCC, Marcelli MP, Dos Santos HF, Edwards HGM (2009) The analytical characterization of a depside in a living species: spectroscopic and theoretical analysis of lecanoric acid extracted from *Parmotrema tinctorum* Del Ex Nyl. lichen. *J Mol Struct* 920:128–133
- Dembitsky VM, Rezanka T, Bychek IA, Shustov MV (1991) Identification of fatty acids from *Cladonia* lichens. *Phytochemistry* 30:4015–4018
- Dembitsky VM, Rezanka T, Bychek IA (1992a) Lipid composition of some lichens. *Phytochemistry* 31:1617–1620
- Dembitsky VM, Rezanka T, Bychek IA (1992b) Fatty acids and phospholipids from lichens of the order Lecanorales. *Phytochemistry* 31:851–853
- Dembitsky VM, Rezanka T, Bychek IA, Shustov MV (1992c) Fatty acid composition of *Parmelia* lichens. *Phytochemistry* 31:841–843
- Dembitsky VM, Rezanka T, Bychek IA (1994) Seasonal variability of lipids and fatty acids in the tree-growing lichen *Xanthoria parietina* L. *J Exp Bot* 45:403–408
- Deschamps JR (2010) X-ray crystallography of chemical compounds. *Life Sci* 86:585–589
- Dmitrenok PS, El'kin YN, Stepanenko LS, Krivoshchekova OE (1987) Fast-atom ionization mass spectra of some lichen metabolites. *Chem Nat Compd* 23:249–250
- Edwards HGM, Farwell DW, Seaward MRD (1991) Raman spectra of oxalates in lichen encrustations on Renaissance frescoes. *Spectrochim Acta Part Mol Spectrosc* 47:1531–1539
- Edwards HGM, Holder JM, Wynn-Williams DD (1998) Comparative FT-Raman spectroscopy of *Xanthoria* lichen-substratum systems from temperate and antarctic habitats. *Soil Biol Biochem* 30:1947–1953
- Edwards HG, Newton EM, Wynn-Williams DD (2003a) Molecular structural studies of lichen substances II: atranorin, gyrophoric acid, fumarprotocetraric acid, rhizocarpic acid, calycin, pulvinic dilactone and usnic acid. *J Mol Struct* 651:27–37
- Edwards HG, Newton EM, Wynn-Williams DD, Coombes SR (2003b) Molecular spectroscopic studies of lichen substances I: parietin and emodin. *J Mol Struct* 648:49–59
- Eisenreich W, Bacher A (2007) Advances of high-resolution NMR techniques in the structural and metabolic analysis of plant biochemistry. *Phytochemistry* 68:2799–2815
- Eisenreich W, Knispel N, Beck A (2011) Advanced methods for the study of the chemistry and the metabolism of lichens. *Phytochem Rev* 10:445–456
- Ejiri H, Sankawa U, Shibata S (1975) Graciliformin and its acetates in *Cladonia graciliformis*. *Phytochemistry* 14:277–279
- Elix JA (1996) Biochemistry and secondary metabolites. *Lichen Biol* 1:154–180
- Elix J, Norfolk S (1975) Synthesis of β -orcinol meta-depsides. *Aust J Chem* 28:2035–2041
- Elix JA (2014) A catalogue of standardized chromatographic data and biosynthetic relationships for lichen substances, 3rd edn. Published by the author, Canberra. <http://www.anbg.gov.au/abrs/lichenlist/Chem%20Cat%203.pdf>
- Ertl L (1951) Über die lichtverhältnisse in laubflechten. *Planta* 39:245–270
- Esquenazi E, Yang Y-L, Watrous J, Gerwick WH, Dorrestein PC (2009) Imaging mass spectrometry of natural products. *Nat Prod Rep* 26:1521–1534
- Ewing DF (1979) ^{13}C substituent effects in monosubstituted benzenes. *Org Magn Reson* 12:499–524
- Exarchou V, Krucker M, van Beek TA, Vervoort J, Gerothanassis IP, Albert K (2005) LC-NMR coupling technology: recent advancements and applications in natural products analysis. *Magn Reson Chem* 43:681–687
- Fahmy AR, Niederwieser A, Pataki G, Brenner M (1961) Dünnschicht-Chromatographie von Aminosäuren auf Kieselgel G. 2. Mitteilung. Eine Schnellmethode zur Trennung und zum qualitativen Nachweis von 22 Aminosäuren. *Helv Chim Acta* 44:2022–2026

- Fan TW-M, Lorkiewicz PK, Sellers K, Moseley HNB, Higashi RM, Lane AN (2012) Stable isotope-resolved metabolomics and applications for drug development. *Pharmacol Ther* 133:366–391
- Feige GB, Lumbsch HT, Huneck S, Elix JA (1993) Identification of lichen substances by a standardized high-performance liquid chromatographic method. *J Chromatogr A* 646:417–427
- Feuerer T, Hawksworth DL (2007) Biodiversity of lichens, including a world-wide analysis of checklist data based on Takhtajan's floristic regions. *Biodivers Conserv* 16:85–98
- Fisher RF (1979) Possible allelopathic effects of reindeer-moss (*Cladonia*) on jack pine and white spruce. *For Sci* 25:256–260
- Freysdottir J, Omarsdottir S, Ingólfssdóttir K, Víkingsson A, Olafsdottir ES (2008) In vitro and in vivo immunomodulating effects of traditionally prepared extract and purified compounds from *Cetraria islandica*. *Int Immunopharmacol* 8:423–430
- Friedman M (2004) Applications of the ninhydrin reaction for analysis of amino acids, peptides, and proteins to agricultural and biomedical sciences. *J Agric Food Chem* 52:385–406
- Furuya T, Shibata S, Iizuka H (1966) Gas-liquid chromatography of anthraquinones. *J Chromatogr A* 21:116–118
- Götz A, Eylert E, Eisenreich W, Goebel W (2010) Carbon metabolism of enterobacterial human pathogens growing in epithelial colorectal adenocarcinoma (Caco-2) Cells. *PLoS ONE* 5:e10586
- Greer T, Sturm R, Li L (2011) Mass spectrometry imaging for drugs and metabolites. *J Proteomics* 74:2617–2631
- Greving MP, Patti GJ, Siuzdak G (2011) Nanostructure-initiator mass spectrometry metabolite analysis and imaging. *Anal Chem* 83:2–7
- Grigsby RD, Jamieson WD, McInnes AG, Maass WSG, Taylor A (1974) The mass spectra of derivatives of polyporic acid. *Can J Chem* 52:4117–4122
- Grube M, Cardinale M, Berg G (2012) 17 Bacteria and the Lichen Symbiosis. *Fungal Associations*, Springer, pp 363–372
- Halama P, Van Haluwin C (2004) Antifungal activity of lichen extracts and lichenic acids. *Biocontrol* 49:95–107
- Hale ME (1983) *The biology of lichens*. Edward Arnold, London
- Hauck M, Huneck S (2007a) Lichen substances affect metal adsorption in *Hypogymnia physodes*. *J Chem Ecol* 33:219–223
- Hauck M, Huneck S (2007b) The putative role of fumarprotocetraric acid in the manganese tolerance of the lichen *Lecanora conizaeoides*. *Lichenologist* 39:301–304
- Hauck M, Willenbruch K, Leuschner C (2009) Lichen substances prevent lichens from nutrient deficiency. *J Chem Ecol* 35:71–73
- Heilman AS, Sharp AJ (1963) A probable antibiotic effect of some lichens on bryophytes. *Rev Bryol Lichenol* 32:215
- Heinemann M, Sauer U (2010) Systems biology of microbial metabolism. *Curr Opin Microbiol* 13:337–343
- Holder JM, Wynn-Williams D, Rull Perez F, Edwards HGM (2000) Raman spectroscopy of pigments and oxalates in situ within epilithic lichens: *Acarospora* from the Antarctic and Mediterranean. *New Phytol* 145:271–280
- Holland PT, Wilkins AL (1979) Mass spectra of some naturally occurring stictane triterpenoids and their trimethylsilyl derivatives. *Org Mass Spectrom* 14:160–166
- Holzmann G, Leuckert C (1990) Applications of negative fast atom bombardment and MS/MS to screening of lichen compounds. *Phytochemistry* 29:2277–2283
- Honegger R (1986) Ultrastructural studies in lichens. *New Phytol* 103:797–808
- Horhant D, Lamer A-CL, Boustie J, Uriac P, Gouault N (2007) Separation of a mixture of paraconic acids from *Cetraria islandica* (L.) Ach. employing a fluorinated tag—catch and release strategy. *Tetrahedron Lett* 48:6031–6033
- Huneck S (1972) Chemie der Flechteninhaltsstoffe, XCI. Chromogluco-side aus Flechten. *J Für Prakt Chem* 314:488–498
- Huneck S (1976) Inhaltsstoffe von *Pyxine coccifera*. *Phytochemistry* 15:799–801
- Huneck S, Himmelreich U (1995) Arthogalin, a cyclic depsipeptide from the lichen *arthothelium galapagoense*. *Z Naturforschung Sect Ba J Chem Sci* 50:1101–1103
- Huneck S, Höfle G (1980) Structure of acaranoic and acarenoic acids. *Phytochemistry* 19:2713–2715
- Huneck S, Schmidt J (1980) Lichen substances—126 mass spectroscopy of natural products—10. Comparative positive and negative ion mass spectroscopy of usnic acid and related compounds. *Biol Mass Spectrom* 7:301–308
- Huneck S, Takeda R (1992) Zur Chemie der Proto- und allo-Proto-lichesterinsäure. *Z Für Naturforschung B J Chem Sci* 47:842–854
- Huneck S, Yoshimura I (1996) *Identification of lichen substances*. Springer, Berlin
- Huneck S, Djerassi C, Becher D, Barber M, Von Ardenne M, Steinfelder K, Tümmeler R (1968) Flechteninhaltsstoffe—XXXI: Massenspektrometrie und ihre anwendung auf strukturelle und stereochemische probleme—CXXIII Massenspektrometrie von depsiden, depsidonen, depsonen, dibenzofuranen und diphenylbutadienen mit positiven und negativen ionen. *Tetrahedron* 24:2707–2755
- Huneck S, Tønsberg T, Bohlmann F (1986) (–)-Allo-pertusaric acid and (–)-dihydropertusaric acid from the lichen *Pertusaria albescens*. *Phytochemistry* 25:453–459

- Huneck S, Feige GB, Lumbsch HT (1994) High performance liquid chromatographic analysis of aliphatic lichen acids. *Phytochem Anal* 5:57–60
- Huovinen K (1987) A standard HPLC method for the analysis of aromatic lichen in progress and problems in lichenology in the eighties. *Bibl Lichenol* 25:457–466
- Hyvärinen M, Koopmann R, Hormi O, Tuomi J (2000) Phenols in reproductive and somatic structures of lichens: a case of optimal defence? *Oikos* 91:371–375
- Ikekawa N, Natori S, Itokawa H, Tobinaga S, Matsui M (1965) Gas chromatography of triterpenes. I. Ursanane, Oleanane, and Lupane Groups. *Chem Pharm Bull (Tokyo)* 13:316–319
- Isenor M, Kaminskyj SG, Rodriguez RJ, Redman RS, Gough KM (2010) Characterization of mannitol in *Curvularia protuberata* hyphae by FTIR and Raman spectromicroscopy. *Analyst* 135:3249–3254
- Jilkine K, Gough KM, Julian R, Kaminskyj SG (2008) A sensitive method for examining whole-cell biochemical composition in single cells of filamentous fungi using synchrotron FTIR spectromicroscopy. *J Inorg Biochem* 102:540–546
- Jones DF, MacMillan J, Radley M (1963) Plant hormones-III. Identification of gibberellic acid in immature barley and immature grass. *Phytochemistry* 2:307–314
- Jones DL, Clode PL, Kilburn MR, Stockdale EA, Murphy DV (2013) Competition between plant and bacterial cells at the microscale regulates the dynamics of nitrogen acquisition in wheat (*Triticum aestivum*). *New Phytol* 200:796–807
- Jorge-Villar SE, Edwards HGM (2010) Lichen colonization of an active volcanic environment: a Raman spectroscopic study of extremophile biomolecular protective strategies. *J Raman Spectrosc* 41:63–67
- Karakus B, Odabasoglu F, Cakir A, Halici Z, Bayir Y, Halici M, Aslan A, Suleyman H (2009) The effects of methanol extract of *Lobaria pulmonaria*, a lichen species, on indometacin-induced gastric mucosal damage, oxidative stress and neutrophil infiltration. *Phytother Res* 23:635–639
- Kim HJ, Jang YP (2009) Direct analysis of curcumin in turmeric by DART-MS. *Phytochem Anal* 20:372–377
- Kinraide WTB, Ahmadjian V (1970) The effects of usnic acid on the physiology of two cultured species of the lichen alga *Trebouxia* Puym. *Lichenologist* 4:234–247
- Kirschbaum U, Wirth V (1997) Les lichens bio-indicateurs: les reconnaître, évaluer la qualité de l'air. E. Ulmer, Paris
- Kutney JP, Sanchez IH, Yee TH (1974) Mass spectral fragmentation studies in usnic acid and related compounds. *Org Mass Spectrom* 8:129–146
- Lane AL, Nyadong L, Galhena AS, Shearer TL, Stout EP, Parry RM, Kwasnik M, Wang MD, Hay ME, Fernandez FM (2009) Desorption electrospray ionization mass spectrometry reveals surface-mediated antifungal chemical defense of a tropical seaweed. *Proc Natl Acad Sci* 106:7314–7319
- Lang Q, Wai CM (2001) Supercritical fluid extraction in herbal and natural product studies—a practical review. *Talanta* 53:771–782
- Lawrey JD (1977) Adaptive significance of O-methylated lichen depsides and depsidones. *Lichenologist* 9:137–142
- Le Pogam P, Legouin B, Le Lamer A-C, Boustie J, Rondeau D (2014) Analysis of the cyanolichen *Lichina pygmaea* metabolites using in situ DART-MS: from detection to thermochemistry of mycosporine serinol. *J Mass Spectrom*, in press
- Lee YJ, Perdian DC, Song Z, Yeung ES, Nikolau BJ (2012) Use of mass spectrometry for imaging metabolites in plants: mass spectrometry for imaging metabolites in plants. *Plant J* 70:81–95
- Letcher RM, Eggers SH (1967) Chemistry of lichen constituents. Part IV. *Tetrahedron Lett* 8:3541–3546
- Li B, Knudsen C, Hansen NK, Jørgensen K, Kannangara R, Bak S, Takos A, Rook F, Hansen SH, Møller BL, Janfelt C, Bjarnholt N (2013) Visualizing metabolite distribution and enzymatic conversion in plant tissues by desorption electrospray ionization mass spectrometry imaging. *Plant J* 74:1059–1071
- Liao C, Piercey-Normore MD, Sorensen JL, Gough K (2010) In situ imaging of usnic acid in selected *Cladonia* spp. by vibrational spectroscopy. *Analyst* 135:3242–3248
- Lines CEM, Ratcliffe RG, Rees TAV, Southon TE (1989) A ¹³C NMR study of photosynthate transport and metabolism in the lichen *Xanthoria calcicola* Oxner. *New Phytol* 111:447–456
- Lisboa BP, Diczfalusy E (1963) Colour reactions for the in situ characterisation of steroid oestrogens on thin-layer chromatograms. *Acta Endocrinol (Copenh)* 43:545–560
- Lisickov K, Najdenova V, Zoltan D (2002) Application of supercritical CO₂ extraction for separation of natural antibiotics from lichens. *Herba Pol* 48:32–39
- Luftmann H, Aranda M, Morlock GE (2007) Automated interface for hyphenation of planar chromatography with mass spectrometry. *Rapid Commun Mass Spectrom* 21:3772–3776
- Lumbsch HT, Kashiwadani H, Streimann H (1993) A remarkable new species in the lichen genus *Placopsis* from Papua New Guinea (lichenized ascomycetes, Agyriaceae). *Plant Syst Evol* 185:285–292
- Luo H, Yamamoto Y, Jeon H-S, Liu YP, Jung JS, Koh YJ, Hur J-S (2011) Production of anti-helicobacter pylori metabolite by the lichen-forming fungus *nephromopsis pallescens*. *J Microbiol* 49:66–70
- Marante FT, Castellano AG, Rosas FE, Aguiar JQ, Barrera JB (2003) Identification and quantitation of allelochemicals from the lichen *Lethariella canariensis*: phytotoxicity and antioxidative activity. *J Chem Ecol* 29:2049–2071
- Mathey A (1979) Contribution a l'étude de la famille des Trypéthéliacées (lichens pyrénomycètes). *Nova Hedwigia* 31:917–935
- Mathey A (1981) LAMMA: new perspectives for lichenology? *Fresenius. J Anal Chem* 308:249–252
- Mathey A, Steffan B, Steglich W (1980) 1, 2-Naphthochinon-Derivate aus Kulturen des Mycosymbionten der Flechte *Trypethelium eluteriae* (Trypetheliaceae). *Liebigs Ann Chem* 1980:779–785

- Mathey A, Van Vaeck L, Steglich W (1987) Investigation of semi-thin cryosections of lichens by laser microprobe mass spectrometry. *Anal Chim Acta* 195:89–96
- Mathey A, Van Roy W, Van Vaeck L, Eckhardt G, Steglich W (1994) In situ analysis of a new perylene quinone in lichens by Fourier-transform laser microprobe mass spectrometry with external source. *Rapid Commun Mass Spectrom* 8:46–52
- Metz H (1961) Dünnschichtchromatographische schnell-analyse bei enzymatischen steroid-umsetzungen. *Naturwissenschaften* 48:569–570
- Mietzsch E, Lumbsch HT, Elix JA (1994) WINTABOLITES (Mactabolites for Windows). Users Man Comput Program Univ Essen 2nd edn. p 54
- Miglietta ML, Lamanna R (2006) 1H HR-MAS NMR of carotenoids in aqueous samples and raw vegetables. *Magn Reson Chem* 44:675–685
- Millot M, Kaouadji M, Champavier Y, Gamond A, Simon A, Chulia AJ (2013) Usnic acid derivatives from *Leprocaulon microscopium*. *Phytochem Lett* 6:31–35
- Mitsuno M (1953) Paper chromatography of lichen substances. I. *Pharm Bull* 1:170–173
- Molnár K, Farkas E (2010) Current results on biological activities of lichen secondary metabolites: a review. *Z Naturforsch C* 65:157–173
- Morlock G, Schwack W (2010) Hyphenations in planar chromatography. *J Chromatogr A* 1217:6600–6609
- Munier R, Macheboeuf M (1949) Microchromatographie de partage des alcaloïdes et de diverses bases azotées biologiques. *Bull Soc Chim Biol (Paris)* 31:1144–1162
- Narui T, Sawada K, Takatsuki S, Okuyama T, Culberson CF, Culberson WL, Shibata S (1998) NMR assignments of depsides and tridepsides of the lichen family Umbilicariaceae. *Phytochemistry* 48:815–822
- Nascimbene J, Tretiach M, Corana F, Lo Schiavo F, Kodnik D, Dainese M, Mannucci B (2014) Patterns of traffic polycyclic aromatic hydrocarbon pollution in mountain areas can be revealed by lichen biomonitoring: a case study in the Dolomites (Eastern Italian Alps). *Sci Total Environ* 475:90–96
- Nash TH (2008) *Lichen biology*. Cambridge University Press, Leiden
- Nemes P, Vertes A (2012) Ambient mass spectrometry for in vivo local analysis and in situ molecular tissue imaging. *TrAC Trends Anal Chem* 34:22–34
- Nemes P, Barton AA, Vertes A (2009) Three-dimensional imaging of metabolites in tissues under ambient conditions by laser ablation electrospray ionization mass spectrometry. *Anal Chem* 81:6668–6675
- Nguyen K-H, Chollet-Krugler M, Gouault N, Tomasi S (2013) UV-protectant metabolites from lichens and their symbiotic partners. *Nat Prod Rep* 30:1490
- Nielsen KF, Smedsgaard J (2003) Fungal metabolite screening: database of 474 mycotoxins and fungal metabolites for dereplication by standardised liquid chromatography–UV–mass spectrometry methodology. *J Chromatogr A* 1002:111–136
- Nimis PL, Skert N (2006) Lichen chemistry and selective grazing by the coleopteran *Lasioderma serricome*. *Environ Exp Bot* 55:175–182
- Nishikawa Y, Michishita K, Kurono G (1973) Studies on the water soluble constituents of lichens. I. Gas chromatographic analysis of low molecular weight carbohydrates. *Chem Pharm Bull (Tokyo)* 21:1014–1019
- Nylander W (1866) *Les lichens du Jardin de Luxembourg*
- Odabasoglu F, Cakir A, Suleyman H, Aslan A, Bayir Y, Halici M, Kazaz C (2006) Gastroprotective and antioxidant effects of usnic acid on indomethacin-induced gastric ulcer in rats. *J Ethnopharmacol* 103:59–65
- Okuyama E, Umeyama K, Yamazaki M, Kinoshita Y, Yamamoto Y (1995) Usnic acid and diffractaic acid as analgesic and antipyretic components of *Usnea diffracta*. *Planta Med* 61:113–115
- Oliver SG, Winson MK, Kell DB, Baganz F (1998) Systematic functional analysis of the yeast genome. *Trends Biotechnol* 16:373–378
- Ozenda P, Clauzade G (1970) *Les lichens: étude biologique et flore illustrée*. Masson Paris
- Parrot D, Jan S, Baert N, Guyot S, Tomasi S (2013) Comparative metabolite profiling and chemical study of *Ramalina siliquosa* complex using LC–ESI–MS/MS approach. *Phytochemistry* 89:114–124
- Patton A, Chism P (1951) Quantitative paper chromatography of amino acids. An evaluation of techniques. *Anal Chem* 23:1683–1685
- Pengsuparp T, Cai L, Constant H, Fong HH, Lin L-Z, Kinghorn AD, Pezzuto JM, Cordell GA, Ingolfssdottir K, Wagner H (1995) Mechanistic evaluation of new plant-derived compounds that inhibit HIV-1 reverse transcriptase. *J Nat Prod* 58:1024–1031
- Pemice M, Meibom A, Van Den Heuvel A, Kopp C, Domart-Coulon I, Hoegh-Guldberg O, Dove S (2012) A single-cell view of ammonium assimilation in coral–dinoflagellate symbiosis. *ISME J* 6:1314–1324
- Polbom K, Steglich W, Connolly JD, Huneck S (1995) Structure of the macrocyclic bis-lactone lepranthin from the lichen *arthonia impolita*; an X-ray analysis. *Z Für Naturforschung B J Chem Sci* 50:1111–1114
- Pöykkö H, Hyvärinen M, Bačkor M (2005) Removal of lichen secondary metabolites affects food choice and survival of lichenivorous moth larvae. *Ecology* 86:2623–2632
- Pyatt FB (1967) The inhibition influence of *Peltigera canina* on the germination and subsequent growth of graminaceous seeds. *Bryologist* 70:326–329
- Ramaut JL (1963a) Chromatographie sur couche mince des depsides et des depsidones. *Bull Sociétés Chim Belg* 72:316–321
- Ramaut JL (1963b) Chromatographie en couche mince des depsidones du β orcinol. *Bull Sociétés Chim Belg* 72:97–101
- Ranković B, Mišvić M, Sukdolac S (2008) The antimicrobial activity of substances derived from the lichens *Physcia aipolia*, *Umbilicaria polyphylla*, *Parmelia caperata* and *Hypogymnia physodes*. *World J Microbiol Biotechnol* 24:1239–1242
- Rezanka T, Dembitsky V (1999a) Novel brominated lipidic compounds from lichens of Central Asia. *Phytochemistry* 51:963–968

- Rezanka T, Dembitsky VM (1999b) Fatty acids of lichen species from Tian Shan Mountains. *Folia Microbiol (Praha)* 44:643–646
- Rezanka T, Guschina IA (2001a) Glycoside esters from lichens of Central Asia. *Phytochemistry* 58:509–516
- Rezanka T, Guschina IA (2001b) Macrolactone glycosides of three lichen acids from *Acarospora gobiensis*, a lichen of Central Asia. *Phytochemistry* 58:1281–1287
- Rikkinen J (1995) What's behind the pretty colours? A study on the photobiology of lichens. Finnish Bryological Society
- Roullier C, Chollet-Krugler M, Pferschy-Wenzig E-M, Maillard A, Rechberger GN, Legouin-Gargadennec B, Bauer R, Boustie J (2011) Characterization and identification of mycosporines-like compounds in cyanolichens. Isolation of mycosporine hydroxyglutamical from *Nephroma laevigatum* Ach. *Phytochemistry* 72:1348–1357
- Russo A, Piovano M, Lombardo L, Garbarino J, Cardile V (2008) Lichen metabolites prevent UV light and nitric oxide-mediated plasmid DNA damage and induce apoptosis in human melanoma cells. *Life Sci* 83:468–474
- Santesson J (1967a) Chemical studies on lichens—III: the pigments of *Thelocarpon epibolum*, *T. laureri* and *Ahlesia lichenicola*. *Phytochemistry* 6:685–686
- Santesson J (1967b) Chemical studies on lichens. 4. Thin layer chromatography of lichen substances. *Acta Chem Scand* 21:1162–1172
- Santesson J (1969) Chemical studies on lichens. 10. Mass spectrometry on lichens. *Ark För Chem* 30:363–377
- Schmeda-Hirschmann G, Tapia A, Lima B, Pertino M, Sortino M, Zacchino S, de Arias AR, Feresin GE (2008) A new antifungal and antiprotozoal depside from the Andean lichen *Protousnea poeppigii*. *Phytother Res* 22:349–355
- Schmidt J, Huneck S, Franke P (1981) Lichen substances—128 Mass spectroscopy of natural products—12. Comparative positive and negative ion mass spectroscopy of nitrogen-containing and ring C cleaved usnic acid derivatives. *Biol Mass Spectrom* 8:293–300
- Seco JM, Quinoa E, Riguera R (2004) The assignment of absolute configuration by NMR. *Chem Rev* 104:17–118
- Sharma J, Hood LV (1965) Thin-layer solubilization chromatography: I Phenols. *J Chromatogr A* 17:307–315
- Shibata S (2000) Yasuhiko Asahina (1880–1975) and his studies on lichenology and chemistry of lichen metabolites. *Bryologist* 103:710–719
- Shibata S, Takito M, Tanaka O (1950) Paper chromatography of anthraquinone pigments. *J Am Chem Soc* 72:2789–2790
- Shrestha G, St. Clair LL (2013) Lichens: a promising source of antibiotic and anticancer drugs. *Phytochem Rev* 12:229–244
- Shukla V, Joshi GP, Rawat MSM (2010) Lichens as a potential natural source of bioactive compounds: a review. *Phytochem Rev* 9:303–314
- Silverstein RM, Bassler GC, Morrill TC (1998) Spectroscopic identification of organic compounds, 5th edn. Wiley, New York
- Stahl E, Kaltenbach U (1961) Anisaldehyde-sulphuric acid for sugars, steroids, and terpenes. *J Chromatogr* 5:35–40
- Stocker-Wörgötter E (2008) Metabolic diversity of lichen-forming ascomycetous fungi: culturing, polyketide and shikimate metabolite production, and PKS genes. *Nat Prod Rep* 25:188–200
- Strack D, Feige GB, Kroll R (1979) Screening of aromatic secondary lichen substances by high-performance liquid-chromatography. *Z Naturforschung CA J Biosci* 34:695–698
- Stuart B (2004) Infrared spectroscopy. Wiley Online Library
- Stuelp PM, Carneiro Leão AMA, Gorin PAJ, Iacomini M (1999) The glucans of *Ramalina celastri*: relation with chemotypes of other lichens. *Carbohydr Polym* 40:101–106
- Sundholm EG (1978) C-13 NMR-spectra of lichen xanthenes—temperature-dependent collapse of long-range couplings to hydrogen-bonded hydroxyl protons. *Acta Chem Scand* 32B:177–181
- Sundholm EG (1979) Syntheses and ¹³C NMR spectra of some 5-chloro-substituted lichen xanthenes. *Acta Chem Scand* 33B:475–482
- Sundholm EG, Huneck S (1980) C-13 NMR-spectra of lichen depsides, depsidones and depsones. 1. Compounds of the orcinol series. *Chem Scr* 16:197–200
- Sundholm EG, Huneck S (1981) C-13 NMR-spectra of lichen depsides, depsidones and depsones. 2. Compounds of the beta-orcinol series. *Chem Scr* 18:233–236
- Szeghalmi A, Kaminskyj S, Gough KM (2007) A synchrotron FTIR microspectroscopy investigation of fungal hyphae grown under optimal and stressed conditions. *Anal Bioanal Chem* 387:1779–1789
- Tabacchi R, Allemand P, Tsoupras G (1991) Direct analysis of lichens by tandem mass spectrometry. *Symbiosis* 11:193–206
- Takeda K, Hara S, Wada A, Matsumoto N (1963) A systematic, simultaneous analysis of steroid saponins by thin-layer chromatography. *J Chromatogr A* 11:562–564
- Tay T, Turk AO, Yilmaz M, Turk H, Kivancc M (2004) Evaluation of the antimicrobial activity of the acetone extract of the lichen *Ramalina farinacea* and its (+)-usnic acid, norstictic acid, and protocetraric acid constituents. *Z Naturforschung C J Biosci* 59:384–388
- Torres A, Hochberg M, Pergament I, Smoum R, Niddam V, Dembitsky VM, Temina M, Dor I, Lev O, Srebnik M (2004) A new UV-B absorbing mycosporine with photo protective activity from the lichenized ascomycete *Collema cristatum*. *Eur J Biochem* 271:780–784
- Tschesche R, Wulff G (1961) Über Saponine der Spirostanolreihe, VII. Über Digitalogenin, ein neues Saponin aus den Samen von *Digitalis purpurea* L. *Chem Ber* 94:2019–2026

- Tschesche R, Lampert F, Snatzke G (1961) Über triterpene: VII. Dünnschicht- und ionenaustauscherpapierchromatographie von triterpenoiden. *J Chromatogr A* 5:217–224
- Van Roy W, Mathey A, Van Vaeck L (1996) In-situ analysis of lichen pigments by Fourier transform laser microprobe mass spectrometry with external ion source. *Rapid Commun Mass Spectrom* 10:562–572
- Vijayakumar CS, Viswanathan S, Kannappa Reddy M, Parvathavarthini S, Kundu AB, Sukumar E (2000) Anti-inflammatory activity of (+)-usnic acid. *Fitoterapia* 71:564–566
- Wachtmeister CA (1952) Studies on the chemistry of lichens. 1. Separation of depside components by paper chromatography. *Acta Chem Scand* 6:818–825
- Wachtmeister CA (1956) Identification of lichen acids by paper chromatography. *Bot Not* 109:313–324
- Wang X-N, Zhang H-J, Ren D-M, Ji M, Yu W-T, Lou H-X (2009) Lobarialides A-C, antifungal triterpenoids from the lichen *Lobaria kurokawae*. *Chem Biodivers* 6:746–753
- Wenkert E, Baddeley GV, Burfitt IR, Moreno LN (1978) Carbon-13 nuclear magnetic resonance spectroscopy of naturally-occurring substances-LVII triterpenes related to lupane and hopane. *Org Magn Reson* 11:337–343
- Whiton JC, Lawrey JD (1984) Inhibition of crustose lichen spore germination by lichen acids. *Bryologist* 87:42–43
- Wilkins AL, Elix JA, Whitton AA (1990) A one- and two-dimensional ¹H and ¹³C NMR study of some lichen triterpenoids of the pyxinol group. *Aust J Chem* 43:411–417
- Wink M, Heinen HJ, Vogt H, Schiebel HM (1984) Cellular localization of quinolizidine alkaloids by laser desorption mass spectrometry (LAMMA 1000). *Plant Cell Rep* 3:230–233
- Wojciechowski ZA, Goad LJ, Goodwin TW (1973) Sterols of the lichen *Pseudevernia furfuracea*. *Phytochemistry* 12:1433–1436
- Wolfender J-L, Ndjoko K, Hostettmann K (2001) The potential of LC-NMR in phytochemical analysis. *Phytochem Anal* 12:2–22
- Woodruff HB, Munk ME (1977) A computerized infrared spectral interpreter as a tool in structure elucidation of natural products. *J Org Chem* 42:1761–1767
- Wynn-Williams DD, Edwards HGM, Garcia-Pichel F (1999) Functional biomolecules of Antarctic stromatolitic and endolithic cyanobacterial communities. *Eur J Phycol* 34:381–391
- Yamamoto Y, Miura Y, Kinoshita Y, Higuchi M, Yamada Y, Murakami A, Ohigashi H, Koshimizu K (1995) Screening of tissue cultures and thalli of lichens and some of their active constituents for inhibition of tumor promoter-induced Epstein-Barr virus activation. *Chem Pharm Bull (Tokyo)* 43:1388–1390
- Yoshimura I, Kinoshita Y, Yamamoto Y, Huneck S, Yamada Y (1994) Analysis of secondary metabolites from lichen by high performance liquid chromatography with a photodiode array detector. *Phytochem Anal* 5:197–205
- Zizovic I, Ivanovic J, Mistic D, Stamenic M, Djordjevic S, Kukic-Markovic J, Petrovic SD (2012) SFE as a superior technique for isolation of extracts with strong antibacterial activities from lichen *Usnea barbata* L. *J Supercrit Fluids* 72:7–14

E. Conclusion

Le mode de vie lichénique, associant un champignon à un partenaire réalisant la photosynthèse (microalgue verte et/ou cyanobactérie) est représenté par plus de 18.500 espèces (Feuerer and Hawksworth, 2007).

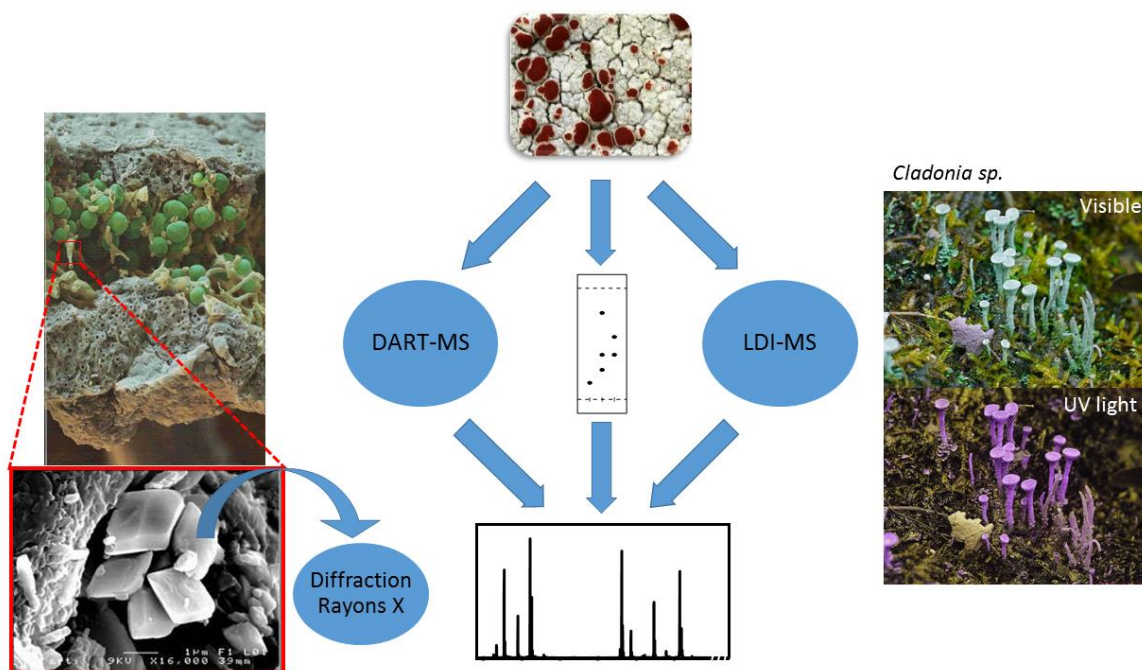
Bien qu'étant parfaitement intégrés aux champignons, la physiologie particulière des lichens est à l'origine d'une chimie unique, avec environ 90% de métabolites secondaires spécifiques aux lichens (Stocker-Wörgötter, 2008). Ces molécules sont façonnées *via* trois voies de biosynthèse (polyacétates/polymalonates, shikimate, mévalonate) inégalement fonctionnelles d'une espèce à l'autre. Il en résulte une vingtaine de noyaux de base diversifiés par des ornements chimiques voire des réarrangements plus complexes. Nous en retirons quelques informations d'intérêt pour notre étude :

- certaines molécules sont récurrentes au sein de nombreuses espèces (e.g acides usnique et stictique, atranorine) ;
- le taux de matière organique extractible par les solvants organiques est compris entre 5% et 25% du poids sec du lichen (nettement supérieur à ce qui obtenu chez les végétaux) (Boustie et al., 2011) ;
- les extraits sont quasi-constamment dominés par quelques voire un seul métabolite majoritaire masquant les autres composés présents dans le lichen ;
- la quantité de lichen à analyser (thalles parfois très petits, lichens multiples sur une surface réduite) peut être très limitée.

Ces différentes caractéristiques soulignent le besoin de techniques de détection très sensibles aussi bien pour passer outre les faibles quantités disponibles que pour contourner « l'arbre qui cache la forêt ».

Les métabolites secondaires jouent un rôle majeur dans la symbiose lichénique. Leur abondance et la présence récurrente de certains d'entre eux évoquent à la fois des activités pléiotropiques et leur caractère incontournable pour le lichen. Un lien étroit existe généralement entre la localisation des métabolites lichéniques et le rôle qu'ils jouent dans le cadre de la symbiose (Hauck et al., 2009a) d'où l'intérêt de pouvoir préciser finement la façon dont les métabolites se distribuent dans le thalle lichénique. Cette observation peut aussi être très informative pour anticiper leurs propriétés physico-chimiques, biologiques... et orienter vers leurs applications potentielles (thérapeutiques par exemple).

APPROCHES DÉRÉPLICATIVES INNOVANTES EN LICHÉNOLOGIE



PARTIE 2 : APPROCHES DÉRÉPLICATIVES INNOVANTES EN LICHÉNOLOGIE

Le chapitre précédent a permis de situer l'intérêt que représentent les lichens en pharmacognosie. La valorisation de leur chimiodiversité unique repose sur la mise en œuvre de procédés de déréplication précoces pour pouvoir y cerner l'originalité structurale en amont d'études phytochimiques.

Les démarches analytiques entreprises dans le cadre de ces travaux se fondent sur des caractéristiques des lichens et/ou de leurs métabolites secondaires ouvrant des perspectives méthodologiques originales.

En premier lieu, ce travail s'est penché sur un protocole de déréplication très utilisé en lichénologie : la Chromatographie Couche Mince (CCM). Les lichénologues utilisent couramment cette technique en se limitant à une caractérisation par rapport à des témoins. Les techniques de couplage actuelles en laboratoire nécessitent un appareillage dédié (spectrophotodensitomètre, HPLC-DAD+/-MS). Soucieux de faire un lien avec l'approche CCM courante en allant au-delà de la caractérisation comparative, nous nous sommes intéressés au couplage CCM-ESI-MS. L'utilisation de cette interface est en plein essor depuis des années mais n'avait pas encore été appliquée aux lichens. Ces travaux se sont inscrits dans le cadre du stage de Master 1 (Spécialité Chimie Moléculaire) d'Aline Pillot réalisé d'Avril à Juin 2015.

En second lieu, nous avons voulu étudier l'intérêt de nouvelles approches de spectrométrie de masse pour une analyse directe de thalles lichéniques. Les métabolites secondaires lichéniques tendent à être sécrétés à la surface des filaments mycéliens pour venir y cristalliser (Honegger, 1986b). De nombreuses études ultrastructurales en microscopie électronique à balayage à basse température ont permis de constater la présence de cristaux de morphologie et de distributions variées au sein de différents lichens. Cette accumulation superficielle des composés lichéniques laisse présager de possibles profilages chimiques *in situ*. La distribution superficielle des composés nous a orientés vers les analyses de lichens en DART-MS.

Dans le prolongement de ces études, l'accumulation sous forme cristalline au sein des thalles lichéniques nous a amenés à explorer récemment l'intérêt de la diffractométrie rayons X. Ces expériences de diffraction ont été menées à l'Ecole Nationale Supérieure de Chimie de Rennes (Dr. Thierry Bataille, Dr. Laurent Le Pollès).

L'absorption UV de la plupart des métabolites secondaires lichéniques nous a conduits à expérimenter le LDI-MS, méthode de spectrométrie de masse pour laquelle la désorption et l'ionisation reposent sur une irradiation laser, avec une longueur d'onde située dans le domaine des UV dans le cas présent. Ces analyses ont fait l'objet d'une collaboration avec l'Université d'Angers (Dr. Andreas Schinkovitz, Pr. Pascal Richomme) et ont utilisé un spectromètre implanté au sein de la plate-forme PIAM (Plate-forme d'Ingénierie et d'Analyses Moléculaires).

I. Analyses de lichens par CCM-ESI-MS

La Chromatographie Couche Mince reste aujourd'hui la technique d'analyse chimique la plus couramment appliquée aux lichens du fait de sa simplicité d'utilisation et du possible profilage de lichens à haut débit par cette approche (Le Pogam et al., 2015a). Les méthodes de détection optiques et chimiques actuellement employées identifient habituellement des groupes structuraux ou la présence de fonctions chimiques mais ne sont pas discriminantes quand il s'agit de distinguer des composés individuels, d'où l'intérêt d'associer la CCM à des techniques d'identification à proprement parler et notamment à la spectrométrie de masse. Le couplage de la CCM à la spectrométrie de masse a donc fait l'objet d'intenses recherches et diverses stratégies analytiques ont émergé pour permettre cette association (Cheng et al., 2011).

Le couplage CCM/MS est à l'origine de contraintes inédites par rapport à d'autres techniques chromatographiques comme l'HPLC ou la GC puisqu'au terme du processus chromatographique, les composés restent adsorbés à la surface de la silice plutôt que d'en être élués par un flux liquide ou gazeux. Deux grandes approches peuvent être mises en œuvre pour permettre le couplage à la spectrométrie de la masse (Morlock and Schwack, 2010) :

- les techniques dites d'élution qui consistent à dissoudre le composé *in situ* pour ensuite l'acheminer vers le spectromètre de masse en maintenant un débit liquide stable. L'interface CAMAG acquise par le laboratoire s'inscrit dans cette première stratégie ;
- les techniques basées sur la désorption font appel à des sources pouvant générer des ions à partir d'une surface comme la CCM. Dans ce second cas de figure, les sources les plus souvent associées à l'analyse de CCM sont le MALDI, le DART, mais également le SIMS (*Secondary Ion Mass Spectrometry*) ou encore le DESI (*Desorption Electro Spray Ionisation*).

Concernant les lichens, si de judicieuses standardisations intervenues au cours des dernières décennies ont permis d'améliorer grandement la fiabilité des identifications de composés lichéniques permises par CCM (Culberson and Kristinsson, 1970; Culberson et al., 1981) (standardisation des solvants de migrations, migrations avec phases mobiles multiples, présence d'étalons internes), la distinction de certains composés (e.g depsides à chaînes aliphatiques, depsidones polaires) reste complexe. Dans de tels cas de figures, des analyses CCM complémentaires doivent être mises en œuvre comme la migration dans d'autres solvants « à la carte » dédiés à la séparation de composés précis (Culberson et al., 1981) ou encore l'hydrolyse acide ou la méthylation par le diazométhane lorsque les composés parents se distinguent mal (Culberson, 1972).

L'intérêt de la spectrométrie de masse couplée à la CCM pour l'identification de composés lichéniques a fait l'objet du stage de Master 1 d'Aline Pillot. Ces analyses CCM/ESI-MS (mode négatif) se sont déroulées en deux temps, s'intéressant d'abord aux seuils de détection de différentes molécules lichéniques pures couvrant les principaux groupes structuraux lichéniques puis une quinzaine de lichens ont ensuite été étudiés par cette approche, livrant des profils chimiques satisfaisants. En parallèle, l'analyse CCM-MS du lichen subantarctique *Usnea trachycarpa* a pu mettre en évidence des signaux ne correspondant à rien de décrit jusqu'à présent dans cette espèce, révélant le potentiel dérégulatif de cette méthode.

Ces travaux ont fait l'objet d'une publication à soumettre dans *The Lichenologist*. Le supplément relatif à ce draft constitue l'Annexe 3 (p. 210). La rédaction de cette publication n'est pas encore finalisée.

Mass spectrometry as a versatile ancillary technique for the rapid *in situ* identification of lichen metabolites directly from TLC plates

Pierre Le Pogam, Aline Pillot, Françoise Le Dévéhat, Anne-Cécile Le Lamer, Béatrice Legouin, Aurélie Sauvager, Alice Gadea, Damien Ertz, Joël Boustie

Abstract:

Thin Layer Chromatography still enjoys a wide-spread popularity among lichenologists as one of the fastest and simplest analytical strategies, remaining today the primary method to assess the chemical content of lichens. The pitfalls associated with this approach are well known as TLC leads to characterize compounds rather than identifying them, which might lead to erroneous assignments, accounting for the long-held interest in hyphenating TLC with dedicated identification tools. As such, commercially available TLC/Mass Spectrometry (MS) interfaces can be easily connected to any brand of mass spectrometer without adjustments. The spots of interest are extracted from the TLC plate to retrieve mass spectrometric signals within a single minute, thereby ensuring proper identification of the chromatographed substances. The outcomes of this hyphenated strategy in the specific field of lichens is illustrated by describing the TLC migration and direct MS analysis of (i) single lichen metabolites of various structural classes and later emphasized through the chemical profiling of crude acetone extracts of (ii) a set of lichens of known chemical composition and at last (iii) applied to a lichen of unknown profile, *Usnea trachycarpa*.

Introduction

As a simple, cost-effective and easy to operate chromatographic technique, Thin Layer Chromatography (TLC) remains today the primary method to assess the chemical content of lichens (Le Pogam *et al.* 2015a). The use of new plates for each separation bypasses memory effects associated to column based chromatographic techniques so that TLC is a fitting tool for the direct analysis of crude extracts with minimal preparation procedures. Likewise, the spotting of many samples on a TLC plate makes this technique appropriate for high-throughput analyses. Despite these advantages, the separative efficiency of this rapid and simple chromatographic technique is usually low and most often leads to characterize compounds rather than properly identifying them.

In the specific field of lichenology, many efforts were undertaken to improve both the reproducibility and the separation efficiency of TLC. Regarding the first aspect, standardized methods for routine identification of lichen products by TLC were published in 1970 (Culberson & Kristinsson 1970). These still widely followed guidelines include three standard solvent systems for migration and assign unknown spots to Rf classes defined by comparison to two common lichen metabolites used as marker controls (atranorin and norstictic acid) to limit Rf varying problems. Identification possibilities can further be narrowed down according to (i) the appearance of the spot under visible light, (ii) the short and longwave UV light exposure color reaction after H₂SO₄ spraying as well as (iii) the microchemical reactions and (iii). In cases when metabolites cannot be satisfactorily separated by TLC, some derivatizations like acidic hydrolysis or methylations proved useful to identify the parent molecule (Culberson 1972). It is noteworthy that two-dimensional TLC was sometimes applied for the separation of complex mixtures (Culberson & Johnson 1976). Secondly, to improve separation efficiency, refined TLC techniques arose including High Performance TLC (HPTLC) that uses gel particles of small diameter as the stationary phase (4-6 μM instead of the nominal 5 to 20 μM for regular TLC plates) to increase the number of interactions with the chromatographed molecules (Siouffi 2005; Sherma 2008). HPTLC separation was performed in the same standardized conditions on a set of 69 lichen substances and their Rf values were collated by Arup and co-workers (Arup *et al.* 1993)..

To characterize unknown metabolites, one can refer to the aforementioned papers that gathered the chromatographic behaviors of lichen metabolites. Informatic tools can now also assist the identification process. For such purposes, LIAS metabolites is a database containing 881 lichen compounds in which the identification of metabolites is guided through a set of characters such as Rf values in standardized solvents, long wavelength UV exposure and microchemical reactions among others (Rambold *et al.* 2014). Although such techniques enable sensitive detection of lichen compounds, these methods are not comprehensive and being based on functional groups, they poorly discriminate between individual compounds. Hence, even when Rf values and spectroscopic characteristics are fully consistent with that of a standard, one should keep in mind that the capacity to determine molecular structures through such detection techniques remains limited and risky (Cheng *et al.* 2011). As such, numerous abusive shortcuts led to erroneous assignments when it comes to discriminate between closely related metabolites. However, by 2016, TLC still remains the prevalent analytical approach to study lichens chemistry often without the support of other analytical approaches.

Such observations account for the long-held interest in the hyphenation of TLC with analytical tools dedicated to proper structural elucidation. For this purpose, mass spectrometry is an attractive candidate as it is one of the most versatile structure elucidative analytical approach by measuring the

mass to charge ratio (m/z ratio) of charged species produced by an ion source and might as well provide further details regarding substructures through fragmentation. Therefore, coupling of planar chromatography with mass spectrometry has been a field of very high level of research over the last decades (Sherma 2010) which resulted in a commercially available TLC-MS interface in the middle of 2009. If these hyphenated approaches garnered a considerable interest in the wider field of natural products, no application to lichen material was described prior to this paper, as far as could be ascertained.

The present study evaluated the adequacy of Negative Ion ElectroSpray Ionization (NI-ESI-MS) for the straightforward identification of lichen metabolites directly from TLC plates. For this purpose, a wide range of lichen substances were analyzed as single molecules to assess both the versatility and the sensitivity of the technique. Subsequently, this TLC hyphenated approach was applied to the crude acetone extracts of a set of lichens of known chemical composition to validate the method in regular TLC conditions. A specific emphasis is given on cases where traditional where traditional methods of detection does not provide a reliable identification of lichen metabolites. At last, the ability of the NI-ESI-TLC-MS to identify unknown molecules is evidenced through the case of the subantarctic lichen *Usnea trachycarpa*.

Material and Methods

Lichen material and compounds

Single compounds used in this manuscript belong to the library of single lichen compounds of UMR CNRS 6226 PNSCM, being isolated and identified through extensive spectroscopic studies during previous phytochemical investigations. Pure compounds were dissolved in acetone and the migration used toluene/acetic acid (17/3) as a mobile phase. Acetone extracts were obtained extracting 1.0 gr of ground lichens with 3 mL of analytical grade solvent. Place of harvest and herbarium codes are given in Table 1 for all species considered in this paper.

Lichens	Voucher specimen	Sampling site, collection date
<i>Cladonia portentosa</i> ^a	JB/05/48	Lot, France, 2005
<i>Cladonia pyxidata</i> ^a	JB/11/133	Savoie, France, 2011
<i>Flavocetraria nivalis</i> ^b	JB/02/37	Pyrénées, France, 2002
<i>Lecidella asema</i> ^a	2014/JYM/04	Bretagne, France, 2014
<i>Lethariella canariensis</i> ^b	JB/04/41	Madère, Portugal, 2004
<i>Ophioparma ventosa</i> ^a	JB/09/58	Tyrol, Austria, 2009
<i>Pannaria rubiginosa</i> ^b		
<i>Pertusaria amara</i> ^a	JB/07/108	Brittany, France, 2007
<i>Pseudevernia furfuracea</i> ^c	JB/00/04	Limousin, France, 2000
<i>Pycnothelia papillaria</i> ^a	JB/?/94	Brittany, France, 2007
<i>Ramalina cuspidata</i> var. <i>stenoclada</i> ^a	JB/11/e495	Brittany, France, 2011
<i>Ramalina siliquosa</i> var. <i>crassa</i> ^a	JB/11/e496	Brittany, France, 2011
<i>Ramalina siliquosa</i> var. <i>zopfii</i> ^a		Brittany, France, 2011
<i>Roccella phycopsis</i> ^d	JB/05/46	Brittany, France, 2005
<i>Tephromela atra</i> ^a	JB/05/e56	Brittany, France, 2005
<i>Usnea trachycarpa</i> ^a	JB/14/203	Iles Kerguelen, France, 2013
<i>Xanthoparmelia pulla</i> ^a	JB/15/204	Ile-de-France, France, 2015
<i>Xanthoria parietina</i> ^a	JB/06/59	Brittany, France, 2006

Table 1 : List of species, sampling locations and dates for the lichens used in the study. Letters indicated as superscripts after lichens' names refer to the solvent system used for the migration of the plate. ^a: toluene/ethyl acetate/formic acid (70/25/5) ; b : toluene/acetic acid (17/3) ; c : toluene/formic acid (85/15) and d : chloroform/acetone 3/1.

Chromatographic procedures

Samples were applied to 10x20 cm silica gel pre-coated 60F254 plates (Merck) by an Automatic TLC Sampler III (Camag). For pure compounds, the analyses were first attempted depositing 10 µL of a dichloromethane solution at 0.1 mg/mL. If the molecule was properly detected at this first concentration, new analyses were performed reducing the concentration of the solution (down to 0.01 mg/mL) and/or the deposited volume (down to 5 µL). In case of unsatisfactory detection from the initial conditions, these parameters were increased with maxima of 0.5 mg/mL and 20 µL. Crude acetone extracts were prepared at a concentration of 0.5 mg/mL in dichloromethane while single molecules were prepared at different concentrations to determine the limits of detection (LOD) and ten microliters aliquots of the samples were applied as 5 mm streaks, 1 cm from the lower edge, unless otherwise specified. Thereafter, each plate was transferred to a pre-saturated development chamber, using the solvent systems described in Table 1. The plates were developed with a fitting solvent mixture to a migration distance of 70 mm. Plates were then monitored under white and ultraviolet light (254 and 365 nm) and the spots to be desorbed were circled with a pencil.

TLC-NI-ESI-MS analysis

The TLC-MS interface (Camag TLC-MS Interface, Muttenz, Switzerland) is fitted with a flowpump of which the inlet is connected to an HPLC pump (TSP Spectra System P1000XR, Thermo Scientific, Waltham, Massachusetts, USA) while the outlet is attached to an expression CMS single quadrupole (Advion) equipped with an ElectroSpray Ionization (ESI) probe. The oval-shaped extraction head (4x2 mm) was used for the extraction of the compounds from the TLC plate. The mass spectra were obtained in situ using a 9/1 mixture of methanol/water (both supplemented with 0.1% formic acid) as extracting solvent with a flow rate of 0.2 mL/min during one minute per spot of interest. Full scan mass spectra were recorded in the Negative-Ion (NI) mode in a mass range of 100 to 1200 Da applying the following parameters: detector gain 1200, ESI voltage 3.5 kV, capillary voltage 180 V, source voltage 20 V, source voltage dynamic 20 V, nebulizer gas pressure 60 psig, desolvation flow gas rate 4L/min, capillary temperature 250°C and gas temperature 20°C. Data processing and evaluation for MS measurement were performed with the Data and Mass Express 2.2.29.2 software (Advion). A didactic overview of the analytical process of TLC-ESI-MS is provided in the Supporting Material.

Results

Analysis of single lichen metabolites

Single lichen metabolites from various structural series were first analyzed by TLC-MS. Both their spectral signatures and limits of detection are collated in Table 2.

Structural class	Compound	Nominal Mass (Da)	R _f	Main signals	Limit of detection (µg)
Depsidés	Atranorin	374	0.79	195+177	0.5
	Evernic acid	332	0.45	331+167	0.5
Depsidones	Variolaric acid	314	0.14	313	2
	Dechlorodiploicin	388	0.62	387	0.1
Dibenzofuran	Usnic acid	344	0.71	343	<0.05

derivatives					
Diphenylethers	β -collatolic acid	526	0.26	525	1
Xanthenes	Secalonic acid D	638	0.28	637	10
Paraconic acid	Lichesterinic acid	324	0.43	323	1
Pulvinic acid derivatives	Vulpinic acid	322	0.88	321	0.1

Table 2 : Mass spectrometric signals and limits of detection for a set of different lichen metabolites encompassing the main structural series. Rf were determined using toluene/acetic acid (170/30) as mobile phase.

Most molecules could be detected in the low microgram range but two tested molecules displayed higher limits of detection: 3-dechlorodiploicin and secalonic acid D. As an illustration, four of these mass spectra are depicted in Figure 1.

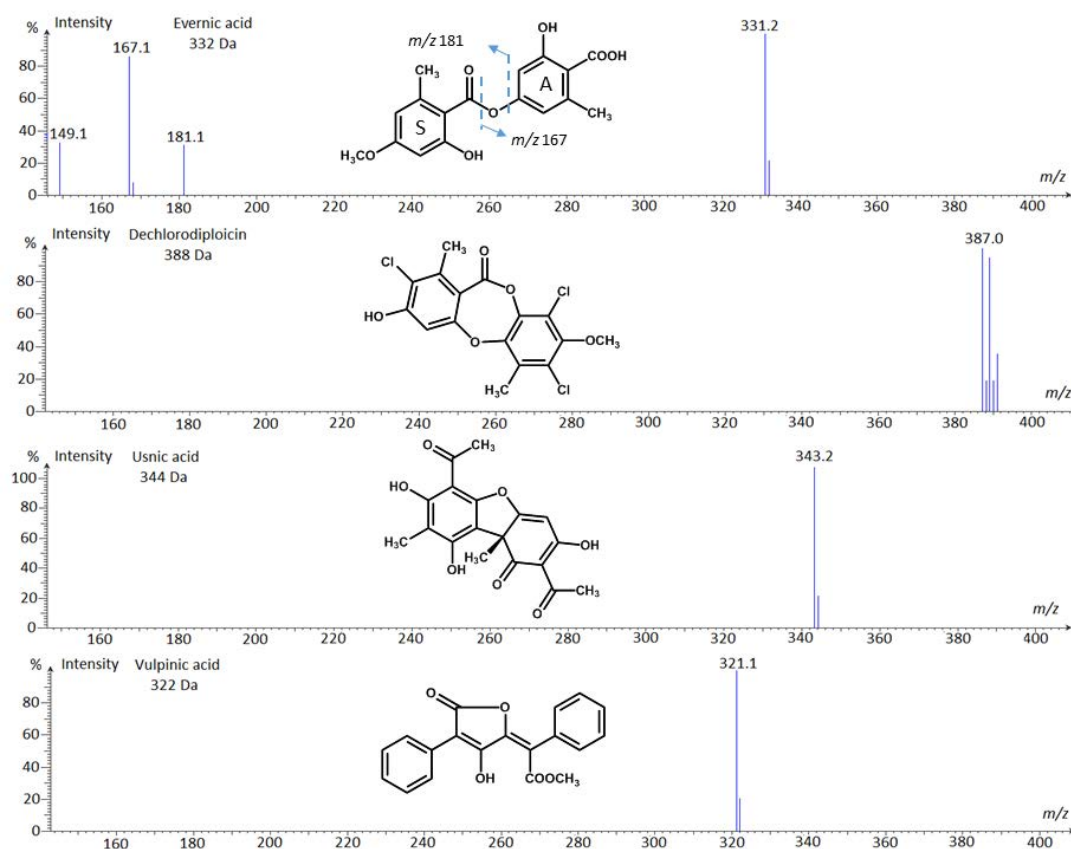


Figure 1: NI-ESI mass spectra recorded directly from TLC plates for some single lichen metabolites (at twice the limit of detection given in table 1). All molecules displayed here exhibit quasi-molecular M-1 signals as base peaks. The fragmentation of evernic acid reveals its monoaromatic building blocks as depicted below. The complex signal pattern of dechlorodiploicin is related to the presence of chlorine atoms in this depsidone.

TLC-NI-ESI-MS Chemical profiling of lichens of known chemical composition

TLC-MS afforded a quick and easy identification of lichen metabolites produced by an array of different lichens enlisted below, with most compounds being detected as quasi-molecular ions (Table 3).

Lichen	Rf*	MS signals (a.m.u.)	Nominal mass (Da)	Compound
<i>Cladonia portentosa</i>	0.62	443+237	444	Perlatolic acid
	0.78	343	344	Usnic acid
<i>Cladonia pyxidata</i>	0.29	471+355	472	Fumarprotocetraric acid
<i>Flavocetraria nivalis</i>	0.71	343	344	Usnic acid
	0.78	351	352	Pinastric acid
	0.88	321	322	Vulpinic acid
<i>Lecidella asema</i>	0.65	359	360	Asemone
	0.75	373	374	3-O-methylasemone
	0.69	393	394	Thiophanic acid
	0.81	407	408	3-O-methylthiophanic acid
<i>Lethariella canariensis</i>	0.03	271	272	Canarione
	0.78	195+177	374	Atranorin
	0.81	407+211+195+177	408	Chloroatranorin
<i>Ophioparma ventosa</i> (without apothecium)	0.34	225+181	420	Thamnolic acid
	0.62	387+209+195	388	Divaricatic acid
	0.77	343	344	Usnic acid
<i>Pannaria rubiginosa</i>	0.79	361	362	Pannarin
<i>Pertusaria amara</i>	0.41	413	414	Subpicrolichenic acid
	0.46	441	442	Picrolichenic acid
<i>Pseudevernia furfuracea</i>	0.36	469	470	Physodic acid
	0.41	483	484	2'-O-methylphysodic acid
	0.79	195 + 177	374	Atranorin
	0.81	407+211+195+177	408	Chloroatranorin
<i>Pycnothelia papillaria</i>	0.58	323	324	Protolichesterinic acid
	0.80	177	374	Atranorin
<i>Ramalina cuspidata</i> var. <i>stenoclada</i>	0.42	371	372	Norstictic acid
<i>Ramalina siliquosa</i> var. <i>crassa</i>	0.19	387	388	Salazinic acid
	0.76	343	344	Usnic acid
<i>Ramalina siliquosa</i> var. <i>zopfii</i>	0.29	343	344	Hypoprotocetraric acid
	0.84	343	344	Usnic acid
<i>Roccella phycopsis</i>	0.06	421+271+181+167	422	Erythrin
	0.41	299	300	Roccellic acid
<i>Tephromela atra</i>	0.31	511	512	α -alectoronic acid
	0.42	525	526	α -collatolic acid
	0.62	411	412	Gangaleioidin
	0.79	195+177	374	Atranorin
<i>Xanthoparmelia pulla</i>	0.64	387+209+195	388	Divaricatic acid
	0.68	415+209+165	416	Stenosporic acid

<i>Xanthoria parietina</i>	0.64	269	270	Emodin
	0.83	Not detected	284	Parietin

Table 3 : Chemical profiling of various lichen species using TLC-NI-ESI-MS: Rf and mass spectrometric signals for detected secondary metabolites. * Solvent systems used as mobile phases are given in Table 1 (Material and Methods).

To further evaluate the extent of the advantages offered by TLC-MS hyphenation, MS detection was attempted on metabolites that are tricky to discriminate using TLC. To assess whether TLC-MS is able to address these routine queries, the TLC depositions associated to these plates were performed manually, according the widely followed guidelines published by Elix & Ernst-Russell (1993).

One such example is that of aliphatic chains-bearing depsides, here emphasized through the specific examples of divaricatic acid (*Ophioparma ventosa*) and perlatolic acid (*Cladonia portentosa*). Even though Rf values of these very common depsides are supposed to discretely increase with the total length of their side chains, their TLC behavior remains virtually identical, precluding their unambiguous assignments. Hence, the reliable TLC identification of these molecules should rely on chromatographing their hydrolysis products which are readily distinguishable (Culberson & Culberson 1966; Culberson 1972). Using MS as an ancillary technique bypasses the mandatory need for chemical derivatization and provides a straightforward and unambiguous identification of these depsides as illustrated in Figure 2.

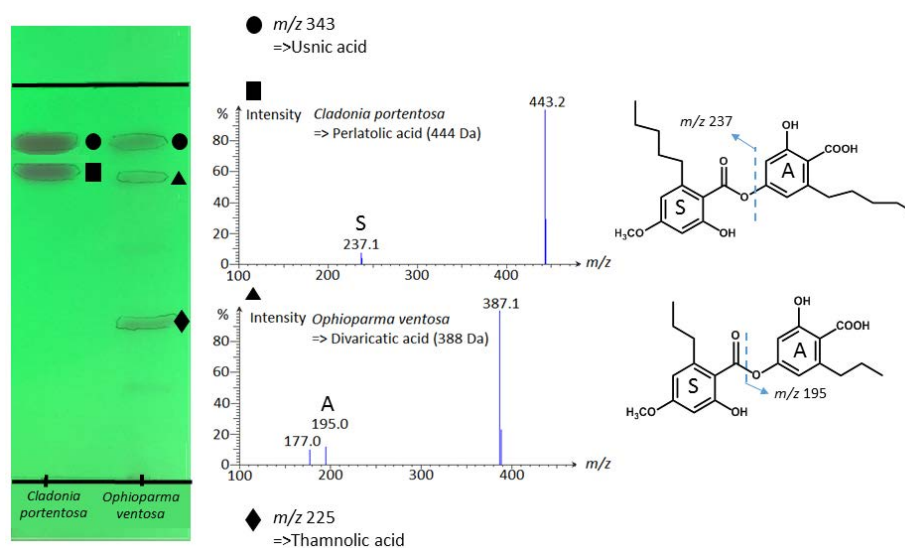


Figure 2: Developed TLC plate (under UV 254 nm) of acetone extracts of *Cladonia portentosa* and *Ophioparma ventosa* and NI-mass spectra of their aliphatic depsides with their chemical structures.

While TLC-MS afforded complete chemical profiles for most lichens described throughout this paper, the specific case of *Xanthoria parietina* is worth mentioning. The TLC-MS profiling of *Xanthoria parietina* only revealed emodin, failing to reveal any further anthraquinone, including the very major parietin. Adversely, the chlorinated xanthenes of *Lecidella asema* could be satisfactorily detected unlike secalonic acid A. The mass spectra obtained from these lichens as well as the chemical formulae of the detected and not detected compounds supporting further discussion are gathered in Figure 3.

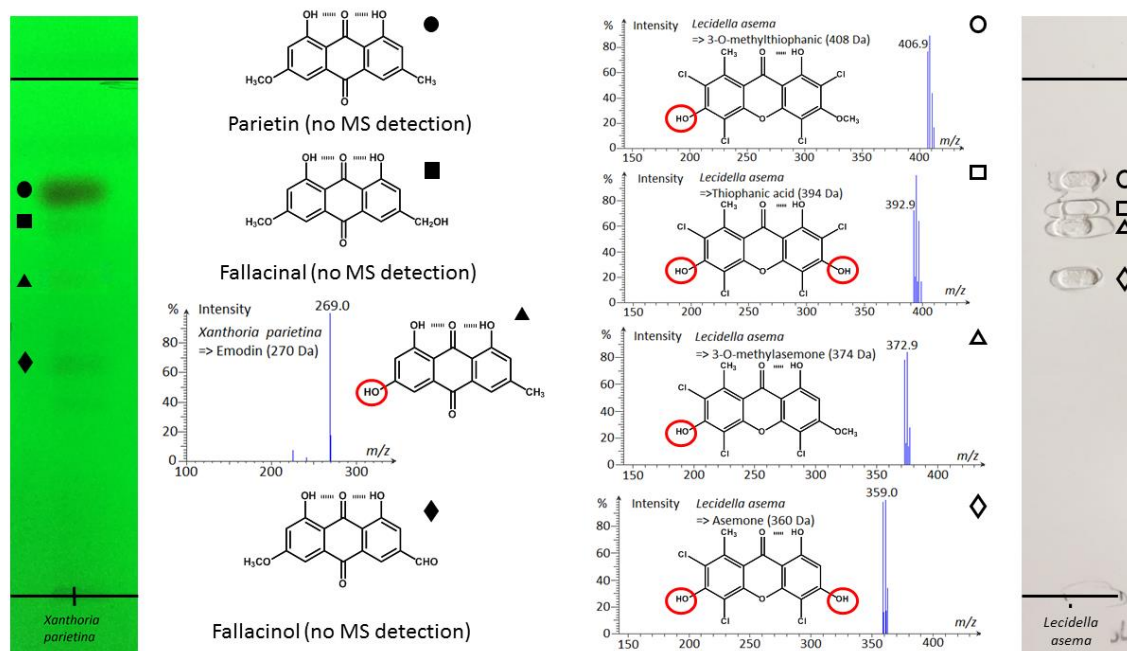


Figure 3: Developed TLC plates of acetone extracts of *Xanthoria parietina* (under UV 254 nm) and *Lecidella asema* (under white light) with NI-mass spectra of the detected compounds. The plate of *Lecidella asema* reveals the imprints left after desorption by the oval elution head. Their chemical structures are represented with a specific emphasis on the chemical features of interest (hydrogen bonds and red circled free phenol groups to support the discussion).

TLC-NI-ESI-MS Chemical profiling of lichens of *Usnea trachycarpa*

As a lichen of unknown composition, the chemical analysis of *Usnea trachycarpa* was of particular significance. This lichen species is known to produce various secondary metabolites including usnic acid, depsidones (norstictic and salazinic acids) and an array of six closely related paraconic acid derivatives (Elix *et al.* 2007). Hence, three couples of isomers differing in the position of the double bond (either exocyclic and endocyclic) were described from this *Usnea*: muronic and isomuronic acids (366 Da), murolic and neuropogolic acids (368 Da) and 13-acetoxyprotolichesterinic and 13-acetoxylichesterinic acids (382 Da), respectively (Bodo & Molho 1980; Ghogomu & Bodo 1982). All these substances could be detected in a straightforward manner even though couples of paraconic acids could not be discriminated by TLC owing to their very close physico-chemical features (Figure 4). Indeed, such derivatives of lichesterinic and protolichesterinic acid are known to be very difficult to separate using classical chromatographic techniques, pledging for the development of refined strategies to purify them (Horhant *et al.* 2007). These analyses also revealed the occurrence of an unknown metabolite with m/z 340.

Lichens	Rf	Signals	Identified metabolite	Nominal mass
<i>Usnea trachycarpa</i>	0.15	387	Salazinic acid	388
	0.24	339	Unidentified compound	340?
	0.27	367	Murolic and/or neuropogolic acids	368
	0.40	365	Muronic and/or isomuronic acids	366
	0.44	371	Norstictic acid	372
	0.44	381	13-acetoxyprotolichesterinic acid and/or 13-acetoxylichesterinic acid	382
	0.85	343	Usnic acid	344

Table 4 : Chemical profiling of *Usnea trachycarpa* using TLC-NI-ESI-MS: Rf (in toluene/ethyl acetate/formic acid 70/25/5) and mass spectrometric signals for detected secondary metabolites.

The chemical profile provided by TLC-NI-ESI-MS was compared to that granted by *in situ* DART-MS, an emerging analytical strategy for the high-throughput chemical profiling of lichens. The NI-DART-MS analysis performed on the whole lichen does not reveal any further metabolite; highlighting the completeness of the information brought by TLC-NI-ESI-MS. The assigned elemental composition of *m/z* 340 provided by DART-HRMS, corresponding to a putative C₁₉H₃₂O₅ (for the neutral species) may support further structural determination.

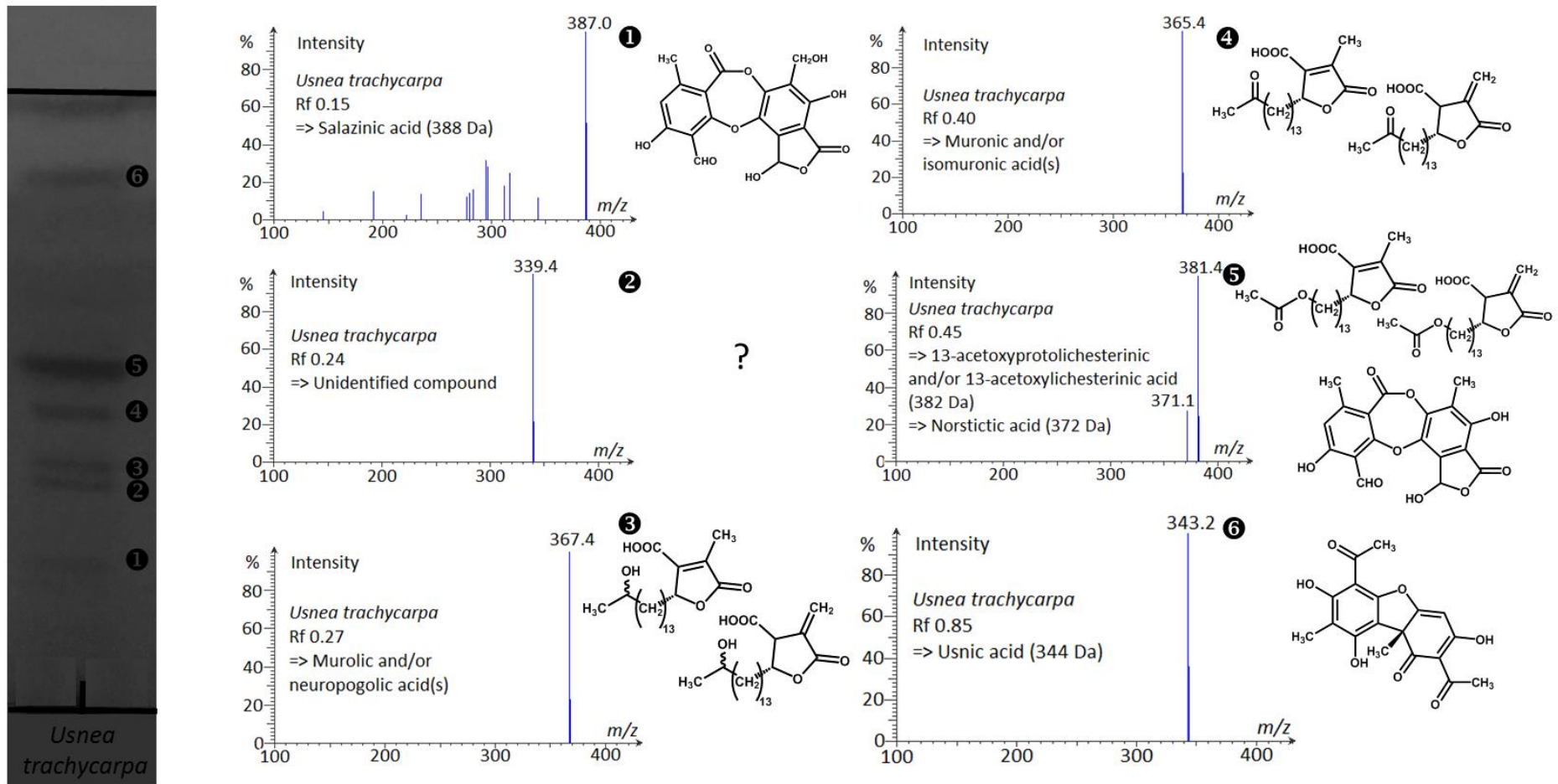


Figure 4: Developed TLC plate of the acetone extract of *Usnea trachycarpa* (under UV 254 nm) with NI-mass spectra of the detected compounds.

Discussion

The overall findings of this study highlight the versatility of mass spectrometric detection to afford an expeditious identification of various lichen structures from all the main structural series directly from regular TLC plates and within a minute. Most interestingly, the mass spectra obtained from lichen compounds most often display prevalent quasi-molecular ions and can thus be easily and straightforwardly interpreted. Among the tested compound that encompass a major part of lichen chemodiversity, only depsides were significantly dissociated. Such fragmentations might be considered as an added value in the identification process of depsides as it provides further clues regarding the monoaromatic subunits of the depside structure, especially when the deprotonated ion is still present in the mass spectrum (e.g erythrin, divaricatic acid, evernic acid, perlatolic acid, chloroatranorin). The observed fragments are indeed released through the cleavage of the ester bond to afford the detection of either the carboxylic acid (S ring) and/or alcohol part (A ring) of the depside. These dissociation are consistent with that described from various mass spectrometry techniques (Huneck *et al.* 1968; Holzmann & Leuckert 1990; Le Pogam *et al.* 2015c). In a rather limited number of cases (i.e atranorin and thamnolic acid), the lack of the deprotonated species complicates the assignment of the metabolite. Yet, the arising of characteristic fragment ions still represents a valuable contribution to the identification process in conjunction with mutually supportive data.

Regarding the sensitivity of the technique, most molecules could be detected in the low microgram range. One can however note that two pure molecules displayed higher limits of detection which emphasize two limitations of the technique. At first, variolaric acid displays a slightly higher limit of detection of 2.0 µg, which is 20-fold that of the other studied depsidone: 3-dechlorodiploicin, indicating that the difficult detection of the former is not related to its depsidone scaffold. This difference is not related to the ionization efficiency of these molecules because the same detection threshold is obtained when directly injecting these two depsidones into the mass spectrometer. Hence, it can be assumed that variolaric acid, as a very polar compound, is hardly extracted from the silica gel, accounting for the higher detection threshold when compared to that of the apolar 3-dechlorodiploicin. This difficult elution of low R_f compounds from the plate might account for the difficult TLC-MS detection of such compounds.

Likewise, secalonic acid D detection by TLC/MS is much less sensitive than that of the other tested compounds. Due to secalonic acid D being the sole single lichen xanthone available during the course of this study, no limit of detection could be determined on a further molecule of this structural group. Nevertheless, the extensive chemical profiling of the xanthone-producing *Lecidella asema* demonstrates that TLC-MS can afford a sensitive detection of xanthenes. A similar phenomenon is reported with the anthraquinones of *Xanthoria parietina* in which the very major parietin (ca. 95%) is not detected by mass spectrometry (Piattelli & de Nicola 1968) whereas the minor emodin (1.5%) is satisfactorily detected. This limitation does not refer to a specific drawback of TLC-MS hyphenation but is related to the ElectroSpray Negative Ionization process that mainly facilitates the formation of deprotonated ions. A closer look at the structure of these undetected compounds reveal that their phenolic groups are in vicinity to a hydrogen bond acceptor moiety. In such cases, the instigation of intramolecular hydrogen bonds prevents the formation of the [M-H]⁻ ions. Conversely, metabolites displaying a free phenolic group could be easily deprotonated and satisfactorily detected (emodin and xanthenes of *Lecidella asema*) (Le Pogam *et al.* 2015c). A possible way to overcome this limitation would be to hyphenate TLC with ion sources that enable the formation of radical ions, bypassing the need to deprotonate the molecule. A good candidate for such purposes is the Laser

Desorption Ionization (LDI) source which was recently proven to afford a complete chemical profile of the lichen *Xanthoria parietina* from its acetone extract (Le Pogam *et al.* 2015c). A few publications reported on successful TLC/LDI-MS hyphenation for the detection of different structural groups (Shariatgorji *et al.* 2009) and we are currently attempting this analytical strategy for the identification of lichen metabolites from TLC plates.

In all these cases, it thus appears that the lower sensitivity observed for these molecules depends on their individual physico-chemical properties rather than on their structural class. These limitations should be kept in mind to account for the poor detection of some lichen compounds.

The adequacy of TLC-MS to discriminate between closely related metabolites is demonstrated here through the expeditious discrimination of aliphatic depsides that remains a vexing problem when using traditional detection approaches of TLC. In this paper, the very closely related perlatolic acid and divaricatic acid are unambiguously discriminated.

A further outcome is that the mass spectra presented in Figures 2 and 3 were obtained from manually spotted plates. Hence, TLC-MS is versatile regarding the amount of extract deposited on the plate and routine manually-prepared TLC plates are perfectly relevant to afford mass spectrometric detection, bypassing the mandatory need for expensive automated deposition facilities. It can therefore be imagined that ambiguous TLC plates regularly prepared by lichenologists could be forwarded to analytical chemistry platforms for subsequent mass spectrometric analyses.

While TLC-NI-ESI-MS appears as a valuable approach for the identification of lichen compounds for chemotaxonomic purposes. This technique might be of interest from a chemist view to evidence original lichen molecules and possibly streamline their isolation, as evidenced here through the example of *Usnea trachycarpa*. The loss of two less CH₂ units between this unknown signal and that of murolic/neuropogolic acids may be indicative of a shorter side chain containing two less CH₂ units than these latter compounds, which would be in agreement with its higher polarity. This finding paves the way for further phytochemical investigation of *Usnea trachycarpa*, to definitely confirm this assumption by elucidating the structure of this metabolite. For such purposes, it is worth noting that the TLC-MS interface also enables collecting the eluted compounds for any further offline analyses, including NMR spectroscopy (Adhami *et al.* 2013).

Acknowledgments

This study was supported by the University of Rennes 1 through the project “Défi Emergent LICHENMASS”. The authors are grateful to Pr. David Rondeau for DART-HRMS analyses that used the mass spectrometry facilities of the DReAM platform of IETR.

References

- Adhami, H.-R., Scherer, U., Kaehlig, H., Hettich, T., Schlotterbeck, G., Reich, E. & Krenn, L. (2013) Combination of Bioautography with HPTLC-MS/NMR: A Fast Identification of Acetylcholinesterase Inhibitors from Galbanum †: HPTLC-MS/NMR: Fast Ache Inhibitor Identification From Galbanum. *Phytochemical Analysis* **24**: 395–400.
- Arup, U., Ekman, S., Lindblom, L. & Mattsson, J.-E. (1993) High performance thin layer chromatography (HPTLC), an improved technique for screening lichen substances. *The Lichenologist* **25**: 61–71.
- Bodo, B. & Molho, D. (1980) Structure des acides isomuronique et neuropogolique, nouveaux acides aliphatiques du lichen *Neuropogon trachycarpus*. *Phytochemistry* **19**: 1117–1120.
- Cheng, S.-C., Huang, M.-Z. & Shiea, J. (2011) Thin layer chromatography/mass spectrometry. *Journal of Chromatography A* **1218**: 2700–2711.

- Culberson, C. F. (1972) Improved conditions and new data for identification of lichen products by standardized thin-layer chromatographic method. *Journal of Chromatography A* **72**: 113–125.
- Culberson, C. F. & Culberson, W. L. (1966) The Identification of Imbricatic Acid and a New Imbricatic Acid-Containing Lichen Species. *The Bryologist* **69**: 192–202.
- Culberson, C. F. & Johnson, A. (1976) A standardized two-dimensional thin-layer chromatographic method for lichen products. *Journal of Chromatography A* **128**: 253–259.
- Culberson, C. F. & Kristinsson, H.-D. (1970) A standardized method for the identification of lichen products. *Journal of Chromatography A* **46**: 85–93.
- Culberson, C. F., Culberson, W. L. & Johnson, A. (1981) A standardized TLC analysis of β -orcinol depsidones. *Bryologist* **84**: 16–29.
- Elix, J. A. & Ernst-Russell, M. A. (1993) A Catalogue of Standardized Thin Layer Chromatographic Data and Biosynthetic Relationships for Lichen Substances. Canberra.
- Elix, J. A., Wirtz, N. & Lumbsch, H. T. (2007) Studies on the chemistry of some *Usnea* species of the *Neuropogon* group (Lecanorales, Ascomycota). *Nova Hedwigia* **85**: 491–501.
- Ghogomu, R. T. & Bodo, B. (1982) Structural elucidation of 13-acetoxylisterinic and 13-acetoxyprotolisterinic acids, two aliphatic lichen metabolites from *Neuropogon trachycarpus*. *Phytochemistry* **21**: 2355–2358.
- Holzmann, G. & Leuckert, C. (1990) Applications of negative fast atom bombardment and MS/MS to screening of lichen compounds. *Phytochemistry* **29**: 2277–2283.
- Horhant, D., Lamer, A.-C. L., Boustie, J., Uriac, P. & Gouault, N. (2007) Separation of a mixture of paraconic acids from *Cetraria islandica* (L.) Ach. employing a fluorine tag—catch and release strategy. *Tetrahedron Letters* **48**: 6031–6033.
- Huneck, S., Djerassi, C., Becher, D., Barber, M., Von Ardenne, M., Steinfelder, K. & Tümmler, R. (1968) Flechteninhaltsstoffe—XXXI: Massenspektrometrie und ihre anwendung auf strukturelle und stereochemische probleme—CXXIII Massenspektrometrie von depsiden, depsidonen, depsonen, dibenzofuranen und diphenylbutadienen mit positiven und negativen ionen. *Tetrahedron* **24**: 2707–2755.
- Le Pogam, P. & Boustie, J. (2016) Xanthones of Lichen Source: A 2016 Update. *Molecules* **21**: 294.
- Le Pogam, P., Herbette, G. & Boustie, J. (2015a) Analysis of Lichen Metabolites, a Variety of Approaches. *Recent Advances in Lichenology* pp. 229–261. India: Springer.
- Le Pogam, P., Legouin, B., Le Lamer, A.-C., Boustie, J. & Rondeau, D. (2015b) Analysis of the cyanolichen *Lichina pygmaea* metabolites using *in situ* DART-MS: from detection to thermochemistry of mycosporine serinol. *Journal of Mass Spectrometry* **50**: 454–462.
- Le Pogam, P., Schinkovitz, A., Legouin, B., Le Lamer, A.-C., Boustie, J. & Richomme, P. (2015c) Matrix-free UV-laser desorption ionization mass spectrometry as a versatile approach for accelerating dereplication studies on lichens. *Analytical Chemistry* **87**: 10421–10428.
- Luftmann, H. (2004) A simple device for the extraction of TLC spots: direct coupling with an electrospray mass spectrometer. *Analytical and bioanalytical chemistry* **378**: 964–968.
- Luftmann, H., Aranda, M. & Morlock, G. E. (2007) Automated interface for hyphenation of planar chromatography with mass spectrometry. *Rapid Communications in Mass Spectrometry* **21**: 3772–3776.
- Morlock, G. & Schwack, W. (2010) Coupling of planar chromatography to mass spectrometry. *TrAC Trends in Analytical Chemistry* **29**: 1157–1171.
- Morlock, G. E. (2014) Background mass signals in TLC/HPTLC–ESI-MS and practical advices for the use of the TLC-MS interface. *Journal of Liquid Chromatography & Related Technologies* **37**: 2892–2914.
- Piattelli, M. & de Nicola, M. G. (1968) Anthraquinone pigments from *Xanthoria parietina* (L.). *Phytochemistry* **7**: 1183–1187.
- Rambold, G., Elix, J. A., Heindl-Tenhunen, B., Köhler, T., Nash III, T. H., Neubacher, D., Reichert, W., Zedda, L. & Triebel, D. (2014) LIAS light – Towards the ten thousand species milestone. *MycKeys* **8**: 11–16.

- Shariatgorji, M., Spacil, Z., Maddalo, G., Cardenas, L. B. & Ilag, L. L. (2009) Matrix-free thin-layer chromatography/laser desorption ionization mass spectrometry for facile separation and identification of medicinal alkaloids. *Rapid Communications in Mass Spectrometry* **23**: 3655–3660.
- Sherma, J. (2008) Planar chromatography. *Analytical chemistry* **80**: 4253–4267.
- Sherma, J. (2010) Planar chromatography. *Analytical chemistry* **82**: 4895–4910.
- Siouffi, A.-M. (2005) From paper to planar: 60 years of thin layer chromatography. *Separation and Purification Reviews* **34**: 155–180.
- Taha, M. N., Krawinkel, M. B. & Morlock, G. E. (2015) High-performance thin-layer chromatography linked with (bio)assays and mass spectrometry – A suited method for discovery and quantification of bioactive components? Exemplarily shown for turmeric and milk thistle extracts. *Journal of Chromatography A* **1394**: 137–147.

II. Nouvelles techniques pour l'analyse de lichens *in situ*

A. Apport déréglicatif du DART-MS

Le développement de méthodes de criblage rapides et de techniques d'identification *in situ* représente aujourd'hui un enjeu majeur dans des domaines aussi variés que la recherche de nouvelles molécules, la sécurité alimentaire, les expertises toxicologiques (Figure 16)... Les avantages de ces approches tiennent à l'accélération du processus déréglicatif en minimisant la préparation de l'échantillon (qui peut être virtuellement nulle) et la durée de l'analyse en elle-même, à l'économie de solvants tout en évitant les artéfacts pouvant être associés aux procédés d'extraction et de purification. Aussi, les techniques de spectrométrie de masse réalisant l'analyse d'échantillons en conditions ambiantes (DART-MS, DESI-MS...) ont connu un essor considérable durant ces dernières années et ont notamment fait montre de leur aptitude à détecter des métabolites secondaires au sein de matrices biologiques variées (notamment de végétaux) voire à y zoner leur répartition (Li et al., 2013).

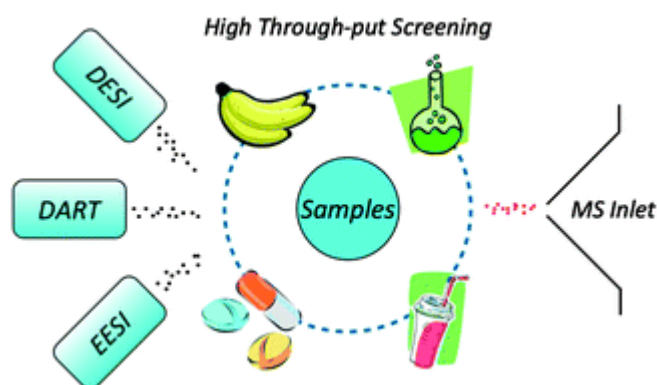


FIGURE 16 : PRINCIPALES TECHNIQUES DE SPECTROMÉTRIE DE MASSE À IONISATION AMBIANTE ET QUELQUES POSSIBLES APPLICATIONS (TIRÉ DE (LI ET AL., 2013))

Pour autant, aucune méthode de spectrométrie de masse ambiante n'avait été appliquée à un quelconque lichen lorsque ces travaux ont été engagés en 2013. Ces méthodes répondent bien à certaines contraintes inhérentes aux lichens comme la faible quantité de matériel disponible et la possibilité d'analyser des spécimens ancrés sur leur support, ce qui revêt un intérêt particulier pour les lichens qui en sont difficilement dissociables (espèces crustacées).

L'apport déréglicatif du DART a été évalué au travers de différents modèles d'étude qui ont été décrits dans plusieurs publications.

a. Profilage chimique de *Lichina pygmaea*

Classification :

- Embranchement : Ascomycètes
- Classe : Lichinomycètes
- Ordre : Lichinales
- Famille : Lichinacées
- Genre : *Lichina*
- Espèce : *pygmaea*

Notre premier modèle d'étude, le cyanolichen *Lichina pygmaea*, est constitué d'un thalle fruticuleux, brun olive à noir lorsqu'il est humide. Il forme des tapis lâches et étendus sur les rochers, de 8 à 10 mm de hauteur. Ses rameaux sont aplatis avec un diamètre de l'ordre de 0.5 mm. Les ascocarpes sont terminaux avec des apothécies apparaissant gonflées, sous la forme de disques punctiformes bruns pâles de 2 mm de diamètre. L'hyménium est constitué d'asques cylindriques étroites contenant chacune 8 spores. Ces dernières sont incolores, simples, ovales et de dimension 22-25 x 12-15 µm. *Lichina pygmaea* possède un cortex bien développé. Les couches sous-corticales et la médulle sous-jacente contiennent le photobionte qui a longtemps été rattaché à des cyanobactéries du genre *Calothrix* mais que de récentes études génétiques rapprocheraient plutôt de *Rivularia* (Ortiz-Álvarez et al., 2015).

Cette espèce a été étudiée pour s'intéresser à la détection de sucres et de composés azotés dont la mycosporine sérinol (Figure 17). Les mycosporines sont des molécules dotées d'un intérêt particulier dans le domaine de la photoprotection. Une analyse phytochimique poussée de ce lichen a été réalisée au sein du laboratoire par une doctorante précédente (Dr. Catherine Roullier, sous la direction du Dr. Marylène Krugler et du Pr. Joël Boustie) (Roullier et al., 2009).



Lichina pygmaea

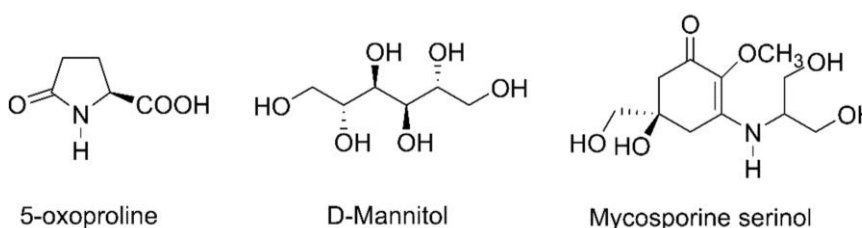


FIGURE 17: PHOTOGRAPHIES DE *LICHINA PYGMAEA* ET STRUCTURE DE SES MÉTABOLITES SECONDAIRES DÉTECTÉS EN DART-MS

La déshydratation de la mycosporine sérinol sous l'effet des conditions d'ionisation DART a été étudiée sur le plan thermodynamique en faisant varier la température de la source d'ions pour avoir accès aux données thermodynamiques de cette réaction et ainsi pouvoir évaluer sa vraisemblance dans le milieu naturel. Ces travaux ont fait l'objet d'une publication dans le *Journal of Mass Spectrometry* qui est fournie dans la suite de ce document. Les groupes structuraux identifiés sont des sucres, des acides aminés et une mycosporine.

Research article

Received: 1 September 2014

Revised: 6 November 2014

Accepted: 19 November 2014

Published online in Wiley Online Library

(wileyonlinelibrary.com) DOI 10.1002/jms.3549

Analysis of the cyanolichen *Lichina pygmaea* metabolites using *in situ* DART-MS: from detection to thermochemistry of mycosporine serinol

Pierre Le Pogam,^a Béatrice Legouin,^a Anne-Cécile Le Lamer,^{a,b} Joël Boustie^a and David Rondeau^{c,d,*}

Direct Analysis in Real Time DART-HRMS is here first applied to the detection of molecules from a lichen, *Lichina pygmaea*. The aim was to propose an innovative method of *in situ* detection of lichen secondary metabolites using the possibilities of elemental composition determination available when a DART source is interfaced with a TOF analyzer. Three kinds of samples have been submitted to DART ionization, *i.e.* an intact thallus, a powder obtained from the crushed lichen and an aqueous extract. *In situ* analysis of crushed lichen, yields an extensive chemical profile, comparable to what is obtained from the aqueous extract, comprising both major polar metabolites described in literature along with some other signals that could correspond to potentially unknown metabolites. One of the detected secondary metabolites, mycosporine serinol, underwent a dehydration reaction prior to its transfer in the gas-phase by DART ionization. The consideration of the thermal transfers involved in the DART ionization process and the possibility to record time-dependent mass spectra through the use of the TOF analyzer allowed establishing Arrhenius plots of this water molecule loss to obtain associated thermodynamic quantities. The low values of corresponding activation enthalpy ($\Delta^\ddagger H_m^\ddagger$ of the order of 25 kJ mol^{-1}) enabled formulating some assumption regarding a possible role of such metabolites in the lichen. Copyright © 2015 John Wiley & Sons, Ltd.

Keywords: DART-MS; *in situ* analysis; lichen metabolites; thermochemistry; Arrhenius plots

Introduction

Lichens are pioneer symbiotic organisms resulting, for most of them, from the association between a fungus and an alga (chlorolichens). In some cases, *i.e.* for 10% of lichens, the green alga is replaced or accompanied by a cyanobacterium, which can absorb atmospheric nitrogen.^[1] Algal or cyanobacterial partners realize photosynthesis and provide sugars and polyols to be metabolized by their fungal associate which corresponds to about 90% of the lichen biomass. These miniature ecosystems can survive in harsh conditions (extreme temperatures, desiccation and UV radiation) which involve production of a vast array of protective compounds. As a result of the symbiosis, unique metabolites are excreted by the fungal hyphae,^[2] most of them being polyphenolic compounds with depside and depsidone structures mostly observed in chlorolichens. Cyanolichens are generally devoid of these hydrophobic metabolites and accumulate high quantities of polysaccharides and other polar compounds.^[3]

Among those original compounds, mycosporines and mycosporine-like amino acids (MAA) are regarded as very promising molecules since they display unique ultraviolet-absorbing capacities based on their common cyclohexenone (*e.g.* mycosporine serinol) or cyclohexenimine conjugated arrangements.^[4] They indeed stand among the strongest UVA absorbing compounds in nature and are also effective against shortwave UVB radiations with λ_{max} ranging from 305 to 360 nm and molecular extinction coefficient (ϵ) of about $40\,000 \text{ l mol}^{-1} \text{ cm}^{-1}$.^[5] Therefore, MAAs and

synthetic derivatives inspired applications as skin care products given the strong need in the cosmetic market for chemically stable, atoxic, potent and broad-spectrum molecules. As an example, Helioguard 365° is a commercial formulation based on MAA shinorine and Porphyrin-334 from the red alga *Porphyra umbilicalis* encapsulated in liposomes to increase their uptake by the skin.^[6] Moreover, their implication in several other processes has been suggested: oxidative stress, salt stress, desiccation, thermal stress, fungal reproduction or as an intracellular nitrogen reservoir.^[7] Detection of these polar and water soluble mycosporines is usually

* Correspondence to: David Rondeau, Institut d'Electronique et de Télécommunication de Rennes (IETR UMR CNRS 6164), Université de Rennes 1, Campus de Beaulieu, 263 Avenue du General Leclerc, 35042 Rennes Cedex, France. E-mail: david.rondeau@univ-rennes1.fr

a Laboratoire de Pharmacognosie, Equipe PNSCM, (ISCR UMR CNRS 6226), Faculté des Sciences Pharmaceutiques et Biologiques, 2 av. du Pr Léon-Bernard, 35042, Rennes Cedex, France

b Université Paul Sabatier Toulouse 3, 118 Route de Narbonne, 31062, Toulouse Cedex 09, France

c Institut d'Electronique et de Télécommunication de Rennes (IETR UMR CNRS 6164), Université de Rennes 1, Campus de Beaulieu, 263 Avenue du General Leclerc, 35042, Rennes Cedex, France

d Université de Bretagne Occidentale, Département de Chimie, 6 avenue le Gorgeu, 29238, Brest Cedex 03, France

DART-MS of cyanolichen *Lichina pygmaea* metabolites

based on LC-DAD-MS (Liquid Chromatography-Diode Array Detector-Mass Spectrometry) profiles requiring time and solvent-consuming extraction and analytical processes that in turn involve the risk of chemical artifacts.^[8] To circumvent such hazards, *in situ* analysis of natural products appears to represent a valuable approach and is required to check location and distribution of identified molecules on a micrometer scale.^[9] As lichen metabolites are generally shown to crystallize on the surface of the hyphae or at least to accumulate in the upper layers of the lichen thallus,^[2,10] their detection might be possible using ambient methods of mass spectrometry.

Recent technical innovations in mass spectrometry allow detection of molecules in ambient conditions, dealing with a large number of compounds in complex matrices and play an important role in various fields such as drug discovery, doping control, forensic identification and food safety.^[11,12] Open air sources especially revolutionized the way samples are introduced into the ion source for mass analysis and result in rapid analysis, without special sample preparation. Those new developments can give an insight into the chemical composition of raw biological matrices and some techniques are even able to show where the metabolites can be found within a sample.^[13] These methods, widely used in the field of plants,^[14–16] have never been applied to lichens, which appear to be a relevant model regarding the aforementioned external distribution of many molecules. Direct Analysis in Real Time (DART) ionization is one of the so-called 'open-air sources' used in 'ambient mass spectrometry' for the analysis of untreated samples and entire objects.^[17,18]

In DART ionization, the sample is positioned between the hot gas outlet of the DART gun and the inlet orifice of the MS. In most cases, a stream containing neutral helium atoms in a long-lived excited-state induces the Penning ionization of ambient water, generating protonated water clusters, such as $(\text{H}_2\text{O})_n\text{H}_3\text{O}^+$, which further participate to the analyte ionization through gas-phase protonation *via* ion/molecule reactions.^[18,19] A Transient Micro-Environment Mechanism (TMEM) was also proposed to account for a direct ionization of the analyte when the DART gas stream is in contact with the sample.^[20] In this case, the TMEM is described as being induced by the desorption of the volatile matrix of the analyte. This is consistent with the fact that the overall DART ionization process intrinsically involves some sample desorption from a surface due to the interaction of the hot helium stream with the exposed sample.^[21] The step of surface desorption leads to relate DART ionization efficiency not only to the proton affinity of the species of interest transferred in the gas phase, but also to the temperature and flow rate of the metastable atom gas and the boiling point of the analyte.^[22] DART-MS has demonstrated its utility in the detection of target substances from different vegetable surfaces^[16] and has already been used for thermal profiling of solids and powders or time-dependent measurements of volatile organic compound release from eucalypts directly submitted to DART-MS analysis.^[23]

For the present paper, we have used the potentialities of the DART source to initiate direct analyses of lichen samples by mass spectrometry. The aim was to propose an innovative method of *in situ* detection of lichen secondary metabolites using the possibilities of the elemental composition determination available when a DART source is interfaced with a Time Of Flight analyzer. The advantages provided by such device were used to analyze a black marine cyanolichen: *Lichina pygmaea* (Lightf.) C. Agardh, in which we previously isolated and identified N-containing compounds, among which mycosporine serinol^[24,25]

Three kinds of samples were then studied, *i.e.* an intact thallus of *L. pygmaea*, a powder obtained from the crushed lichen and an aqueous extract containing mycosporines thanks to a passive diffusion from the lichen thallus in pure water. The reactivity of mycosporine serinol under the desorption/ionization conditions made us consider DART-MS as a relevant platform to reach associated thermochemical data. We thus performed a thermochemical study on mycosporine serinol dehydration using potentialities of the TOF mass spectrometer to record time-dependent mass spectra and to produce a temperature controlled helium stream.

Materials and methods

Materials

L. pygmaea is a black marine fruticose cyanolichen corresponding to the association of a *Calothrix* photobiont and a mycobiont belonging to the Lichinaceae family.^[23] *L. pygmaea* is common on rocks on exposed shores in the upper part of the tidal region. Our samples were collected in December 2007 at 'La Pointe de la Garde' in Dinar (48°38.09'N, 02°08.15'W, Ille-et-Vilaine, France). Lichen thalli were sorted out, washed and dried under ambient atmosphere. Macroscopic and microscopic observations as well as comparison to a reference sample of the REN-ABB herbarium enabled its identification as *L. pygmaea* (Lightf.) C. Agardh. A voucher specimen is kept in the laboratory with the reference JB/07/98. Lichen powders required for our analysis were simply grinded with hand mortar and pestle. *L. pygmaea*'s aqueous extract was performed after a single minute dipping of a piece of uncrushed thallus (roughly 50 mg) within 2 ml of pure water based on the optimum extraction process described elsewhere.^[1] Pure mycosporine serinol was previously extracted and purified from *L. pygmaea* using the method described by Roullier *et al.*^[24] HPLC grade methanol and dichloromethane were supplied by SDS (Peypin, France). PolyEthyleneGlycol (PEG) was purchased from Aldrich-Sigma (Saint-Quentin Fallavier, France). Distilled water was used to perform aqueous extracts.

Mass spectrometry

The analyses of *L. pygmaea* containing samples, *i.e.* intact thallus, powder and aqueous extract, were performed using a JEOL JMS-T100CS (AccuTOF CS) orthogonal time-of-flight (TOF) mass spectrometer (Peabody, MA) equipped with an IonSense DART Source (Danvers, MA). Ultra high purity helium was used as reagent gas at a flow rate of 4 l min^{-1} and under a temperature value of 523 K. DART-MS was used in positive ion mode. The following DART-needle, discharge electrode and the grid electrode voltage values used were 3500, 150 and 250 V, respectively. The voltage values of orifice 1, orifice 2 and the ring lens were set at 15, 5 and 10 V, respectively. The orifice 1 temperature was kept at 80 °C. The detector voltage was set at 2300 V. The mass spectra were recorded every second and with a resolution of 6000 (fwhm definition). The mass scale was calibrated using the $[\text{M}+\text{H}]^+$ ion series of a poly(ethylene glycol) diluted in a dichloromethane/methanol mixture (1:1). To perform accurate mass measurements, the mass drift compensation procedure available on the main program that controls the AccuTOF CS was used to compensate for the m/z drift in the range of m/z 100 to 350. The DART-MS analyses of the intact thallus of *L. pygmaea* were performed by holding the sample between tweezers directly under the helium stream. The DART

analysis of the crushed lichen was performed by presenting a glass rod previously dipped inside the lichen powder. The DART-MS analyses of any liquid samples were performed by depositing 10 μl of a solution containing the sample of interest at the surface of a glass rod located in front of the ion source. For the evaluation of the thermochemical data related to the dehydration reaction of the mycosporine serinol, two samples containing 400 μg of the pure compound in 1 ml of water solution were prepared. DART-MS analyses were performed at different temperature values of the helium stream. These values will be further indicated in the text. A 10- μl sample droplet was submitted to each DART-MS analysis during 2 min without removing the sample positioned under the hot helium stream. After each set of analysis performed from one sample at different temperatures, two procedures were used for the data treatment. With the so-called procedure A, a desired reconstructed ion chromatogram (RIC) was considered from the MS signal of the $[\text{M} + \text{H}]^+$ ion of the mycosporine serinol and its dehydrated form. A drag over a range of 20% of the top of each mono-isotopic peak was done. Note that for the DART mass spectra recorded in the case of the data treatment by the procedure A, two helium flow rate values were used, *i.e.* 4 and 61 min^{-1} . With the so-called procedure B, another sample was analyzed at different temperatures using a unique helium flow rate of 41 min^{-1} . After the 2-min run time, average mass spectra were created by specifying the elapsed time range by right-dragging on the total ion chromatogram (TIC) recorded during the DART analysis. The plots representing the time dependence of the relative amounts of the compound losing a water molecule were obtained by calculating the logarithm of the survival yield (SY) of the mycosporine serinol $[\text{M} + \text{H}]^+$ ion such as:

$$\text{SY} = \frac{I([\text{M} + \text{H}]^+)}{I([\text{M} - \text{H}_2\text{O} + \text{H}]^+) + I([\text{M} + \text{H}]^+)} \quad (1)$$

where, $I([\text{M} + \text{H}]^+)$ and $I([\text{M} - \text{H}_2\text{O} + \text{H}]^+)$ are the intensities of the protonated molecules of the mycosporine serinol and its dehydrated form, respectively. The values of $I([\text{M} + \text{H}]^+)$ and $I([\text{M} - \text{H}_2\text{O} + \text{H}]^+)$ were obtained through the RIC intensities by using the procedure A and the intensities of the mono-isotopic peaks measured on the average mass spectra when the procedure B was chosen.

Thermodynamic analysis

The logarithm of the SY values (see Eqn (1)) obtained from mass spectra recorded at different temperatures were plotted as a function of the time t (s). For plotting the Arrhenius diagram, we have considered that the numerator parameter in Eqn (1) corresponds to the amount of mycosporine serinol that has not reacted and that the sum at the denominator is related to the amount of the metabolite prior to the dehydration reaction. The slope values of the different straight lines $\ln(\text{SY})$ vs t obtained from the linear regressions of the data reported as a function of time for different temperatures can be used to obtain an Arrhenius diagram. The values of these slopes that are related to rate constant $k(T)$ values, are plotted as a function of $1/T$. The linear regression performed from an Arrhenius plot can give the activation parameters of the mycosporine dehydration reaction, *i.e.* the energy (E_a) that is calculated from the slope of the straight line and the pre-exponential factor (A_{pe}) that is obtained from the intercept. The actual temperature of the metastable helium stream exiting the DART gun was obtained by distinguishing the experimental

temperature set by the DART software (T_{set}) from the actual temperatures (T_{actual}) previously measured by Harris *et al.* at different helium flow rate values, *e.g.* 4 and 61 min^{-1} .^[26] By referring to the measured values obtained by these authors, a scaling linear function was used such as:

$$T = T_{actual} = 0.7133 T_{set} + 20.667 \quad (2)$$

and

$$T = T_{actual} = 0.6667 T_{set} + 19.667 \quad (3)$$

for the 41 min^{-1} and 61 min^{-1} flow rates, respectively. Note that the linear regressions were obtained with $R^2 = 0.9997$ and 0.9999 for the Eqns (2) and (3), respectively. The thermochemical data were obtained by formulating the rate constants of dehydration reaction in terms of thermodynamic functions instead of Arrhenius activation parameters. This was done using the Wynne-Jones and Eyring derivation for a unimolecular reaction such as^[27]:

$$k(T) = A_{pe} \exp\left(\frac{-E_a}{RT}\right) = \frac{k_B T}{h} \exp(1) \exp\left(\frac{\Delta_f^\ddagger S_m^\circ}{R}\right) \exp\left(\frac{-\Delta_f^\ddagger H_m^\circ}{RT}\right) \quad (4)$$

where h is Planck's constant, k_B is the Boltzmann's constant and $\Delta_f^\ddagger H_m^\circ$ is the standard molar activation enthalpy such as:

$$\Delta_f^\ddagger H_m^\circ = E_a - RT \quad (5)$$

and $\Delta_f^\ddagger S_m^\circ$ is the standard molar activation entropy such as:

$$\Delta_f^\ddagger S_m^\circ = R \left[\ln(A_{pe}) - \ln\left(\frac{k_B T}{h}\right) - 1 \right] \quad (6)$$

Results and discussion

Chemical profiling of *L. pygmaea*

From the three different samples, a piece of intact thallus was directly submitted to DART-MS analysis. In this case, only diethyl and dibutylphthalates have been detected as their protonated forms which are known to be sensitive to DART-MS analysis.^[28,29] In a first approximation, such results can be attributed either to the absence of any detectable metabolite at the thallus surface or to the DART-MS inadequacy for such purpose. By contrast, the DART-MS analysis of the crushed lichen powder leads to mass spectra exhibiting numerous ions at the m/z ratios ranging from 100 to 350 Th. A representative DART mass spectrum is depicted in Fig. 1(a) and (b), encompassing the m/z ranges from m/z 100 to 200 and m/z 200 to 350, respectively.

The results of the accurate mass measurements performed from the most intense ions observed in the mass spectrum of Fig. 1(a) and (b) are regrouped in Table 1. Each experimental value has been compared with the theoretical mass calculated in an error range of

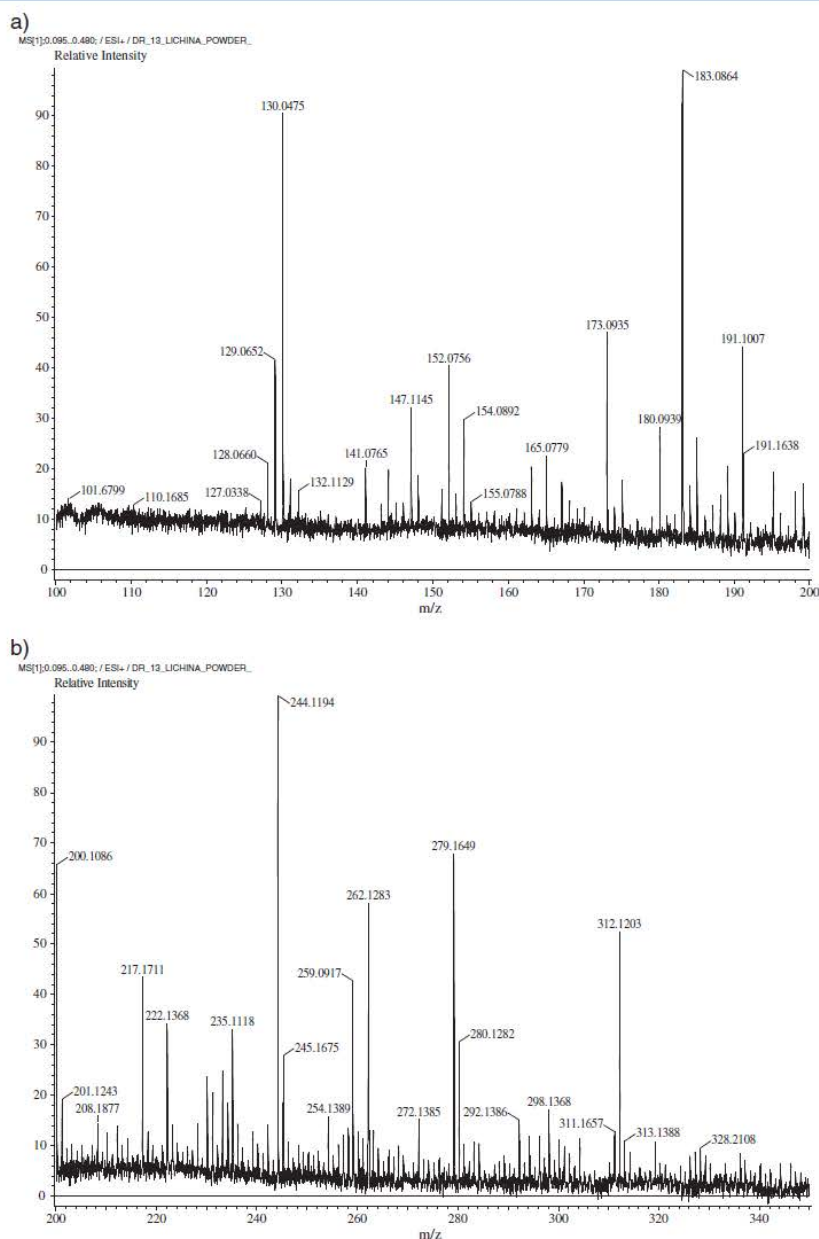
DART-MS of cyanolichen *Lichina pygmaea* metabolites


Figure 1. DART-TOF mass spectrum of a powder formed from the crushed *Lichina pygmaea* (see Table 1 for the attribution of mass measurements): a) encompasses the m/z ranges from 100 to 200 and b) from 200 to 350.

± 10 ppm from candidate compositions encompassing: $C_{5-10}H_{5-20}O_{0-10}N_{0-4}$. One will remark that in Table 1, the proposed formula for the m/z 130.0475 ion, is the only one obtained when an error range of ± 20 ppm was considered.

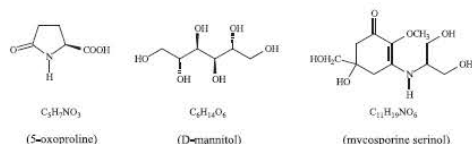
The selected formulae have been compared with secondary metabolites identified from phytochemical studies that we previously performed on *L. pygmaea*.^{124,25} Both major polar metabolites

described within *L. pygmaea* can be identified from this rapid *in situ* characterization. For the present study, the signal at m/z 130 is related to the $[M + H]^+$ ion of the 5-oxoproline. The m/z 183 ion corresponds to the protonated molecule of mannitol. The m/z 244 seems to stem from the dehydration of mycosporine serinol which is detected as its protonated form at m/z 262. The structures of these chemical species are depicted in Fig. 2.

Table 1. Results of exact mass measurements performed from the mass spectrum of the Fig. 1 related to the DART-MS Analysis of a *Lichina pygmaea* powder

Measured mass	Proposed formulae	Calculated mass (error in ppm)
130.0475	C ₅ H ₈ O ₃ N	130.0499 (-18.4)
183.0864	C ₆ H ₁₅ O ₆	183.0863 (+0.5)
	C ₇ H ₁₁ N ₄ O ₂	183.0876 (-6.6)
244.1194	C ₁₁ H ₁₈ NO ₅	244.1180 (+5.7)
	C ₉ H ₁₆ N ₄ O ₄	244.1166 (+11.5)
	C ₁₄ H ₁₆ N ₂ O ₂	244.1207 (-5.4)
262.1283	C ₁₁ H ₂₀ NO ₆	262.1285 (-0.7)
	C ₉ H ₁₈ N ₄ O ₅	262.1272 (+4.2)
	C ₈ H ₂₂ O ₉	262.1258 (+9.6)
312.1203	C ₁₅ H ₂₀ O ₇	312.1203 (0.0)
	C ₁₃ H ₁₈ N ₃ O ₆	312.1190 (+4.2)
	C ₁₆ H ₁₆ N ₄ O ₃	312.1217 (-4.5)

Other signals are detected. The most prominent is the m/z 312 ion that can be attributed to the presence of potentially unknown molecules. The assigned elemental composition propositions may support further structural determinations (see Table 1).


Figure 2. Structures and elemental compositions of the metabolites detected within *Lichina pygmaea* crushed powder.

To study how exhaustive is the detection performed on the crushed lichen, we compared it to the analysis of a classical aqueous extract. Indeed, previous works demonstrated that *L. pygmaea* compounds of interest were well extracted using pure water and uncrushed raw material.^[1] Following such an extraction process, the DART spectrum of the obtained aqueous extract (Fig. 3) displayed a comparable pattern of peaks.

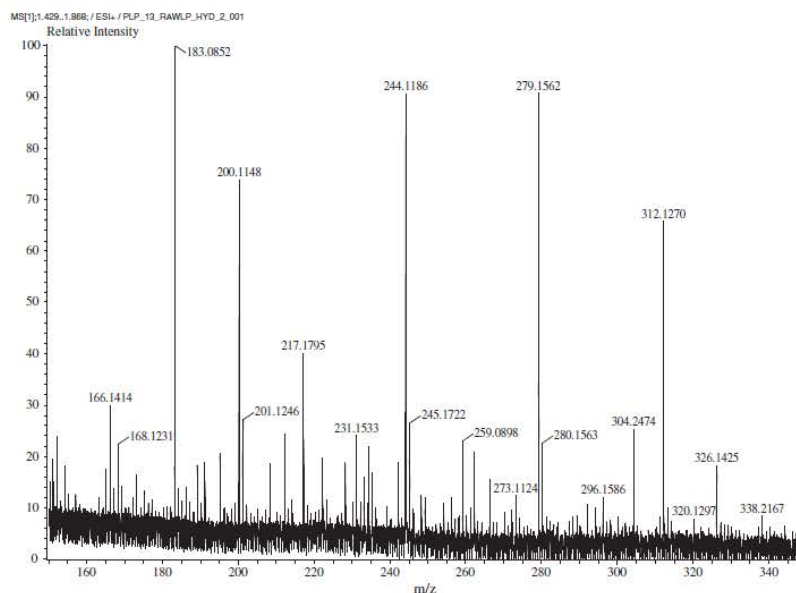
Noteworthy, the relative intensity of the dehydrated mycosporine serinol (m/z 244) relative to that of the m/z 262 ion is higher in the Fig. 3 than in the Fig. 1(b). This accumulation of a metabolite dehydration product in an aqueous extract can be considered as an astonishing result that made us focus on mycosporine serinol's reactivity.

Reactivity of mycosporine serinol

The DART mass spectrum of a pure solution of mycosporine serinol is reported in Fig. 4.

The accurate mass measurements performed from the mass spectrum of the Fig. 4 confirm the detection of mycosporine serinol highlighted in the case of the mass spectra of Figs. 1 and 3. The elemental compositions obtained from candidate formulae are in agreement with the measurements by considering error values of 5.7 and -0.7 ppm for the m/z 244.1192 and m/z 262.1295, respectively. In the higher m/z ratio range, behind the phthalate detections at m/z 279.1598 and 391.2856, one can note the presence of signals over m/z 450. As reported in Table 2, the elemental composition calculated from the m/z 523.2514 ion is in agreement with the detection of a protonated dimer of the mycosporine serinol in the gas phase that can be written: $[C_{11}H_{19}NO_5HC_{11}H_{19}NO_5]^+$.

Likewise, the signals at m/z 487.2299 and m/z 469.2186 are attributed to proton-bound dimers $[C_{11}H_{17}NO_5HC_{11}H_{17}NO_5]^+$ and $[C_{11}H_{17}NO_5HC_{11}H_{15}NO_4]^+$, respectively (see Table 2). They are diagnostic species of a dehydration reaction of the mycosporine serinol


Figure 3. DART mass spectrum of an immersion solution of a *Lichina pygmaea* whole thallus in pure water.

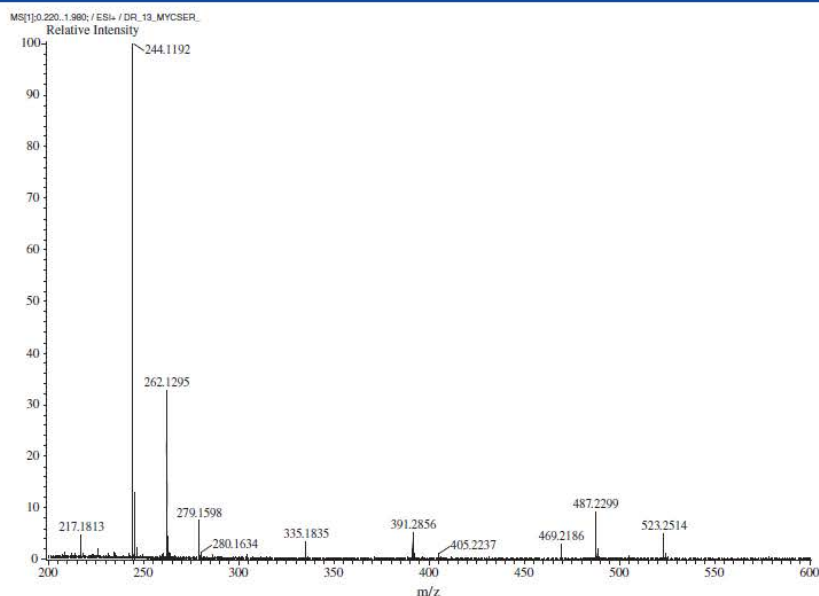
DART-MS of cyanolichen *Lichina pygmaea* metabolites

Figure 4. DART-MS spectrum of a pure solution of mycosporine serinol (1 mg/ml).

Table 2. Results of exact mass measurements performed from the mass spectrum of the Fig. 4 related to the DART-MS analysis of a pure sample of mycosporine serinol

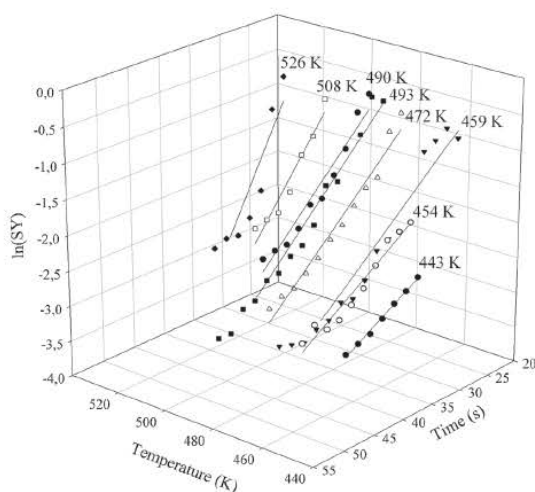
Measured mass	Proposed formulae	Calculated mass (error in ppm)
469.2186	C ₂₂ H ₃₃ N ₂ O ₉	469.2181 (+1.1)
487.2299	C ₂₂ H ₃₃ N ₂ O ₁₀	487.2286 (+2.7)
523.2514	C ₂₂ H ₃₉ N ₂ O ₁₂	523.2498 (+3.0)

prior to its transfer in the gas-phase where each non-covalent dimer is protonated. Note that the detection at a very low relative intensity of an ion at m/z 469 shows the possibility of the occurrence of a double dehydration reaction of mycosporine serinol at the sample surface. Such reactivity can be attributed to the acting mode of the DART source.

The ionization DART-MS processes are indeed based on the production of excited helium atoms that induce a cascade of gas-phase reactions initiated by reagent ions produced from ambient water vapor or other gaseous compounds such as solvent molecule.^[18,30] However, the presence of the analyte in the gas phase is required to observe charged species on the mass spectrum. This is here the role of the ancillary heating element incorporated in the DART source that provides a heated helium gas stream to sustain the transfer of the sample in the gas-phase by evaporation or thermal desorption. The energy then provided for these processes can also be used for a thermal dehydration reaction of a sample such as the mycosporine serinol before its vaporization. In this context, the relatively short time scale of mass spectrum acquisition available with the TOF analyzer can be considered with interest to perform time-resolved measurements. The aim is then to evaluate thermal decomposition rate constants of the mycosporine serinol at different temperatures of the helium gas stream of the DART source.

Thermochemical study of mycosporine serinol's dehydration

The logarithm of the survival yield (SY) (see Eqn (1)) of the protonated mycosporine serinol was plotted as a function of the exposure time to the DART source for different temperatures according to the two procedures A and B previously described in experimental section. The representations of the time dependence of $\ln(\text{SY})$ obtained for different temperature values after data treatment from the two procedures A and B are shown in Figs. 5 and 6, respectively.


Figure 5. Time-dependence of $\ln(\text{SY})$ at different actual temperatures of the helium stream of the DART source. Note that the values have been obtained from the procedure A described in experimental section.

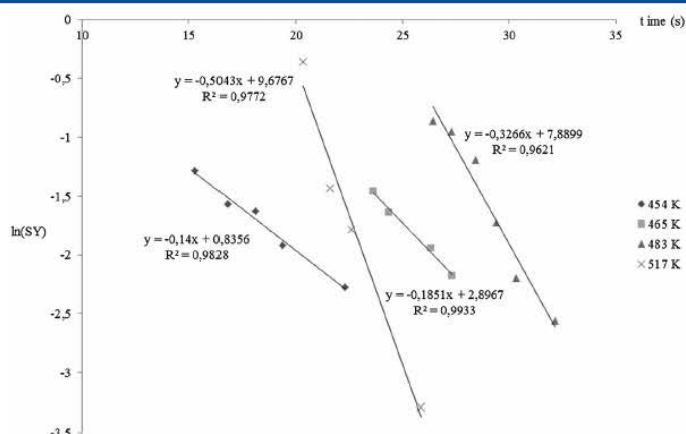


Figure 6. Time dependence of $\ln(SY)$ at different actual temperatures of the helium stream of the DART source, with SY values obtained from mono-isotopic peak intensities measured from average mass spectra (see procedure B in experimental section). Note that the equation of each fit of the experimental with a linear function and the R square are placed close to the plotted corresponding straight line.

For the procedure A, the values of the slopes calculated from the linear fits to the experimental kinetic data are reported in Table 3, with each associated linear regression expressed as the R^2 . For

the procedure B, these values are directly reported in Fig. 6 close to each linear regression. As previously described in experimental section, the data treatment leads to establish Arrhenius plots of $\ln[k(T)]$ vs $1/T$ that are depicted in Fig. 7(a) and 7(b) for the A and B procedures, respectively.

The Arrhenius activation parameters and the thermochemical data can be deduced from each equation written such as:

$$\ln[k(T)] = a(1/T) + b \quad (7)$$

where a represents the slope value of the straight lines obtained by fitting the data plotted in Fig. 7(a) and 7(b) with a linear function and b is the intercept of each Arrhenius plot. From the values of the a and b parameters of the Eqn (7), it is possible to calculate the Arrhenius activation parameters and the thermochemical data that characterize the dehydration reaction of the mycosporine serinol, using the Eqns (5) and (6). The values then obtained are reported in Table 4.

From the data presented in Table 4, it appears that the results obtained from the two data treatment procedures are consistent there between. The very low values of E_a and $\Delta^{\ddagger}H_m^{\ddagger}$ suggest that

Table 3. Temperatures set by the software for a given helium stream flow rate, actual temperature calculated from the Eqns (2) and (3) (see experimental section), values of the coefficient determination of each linear regression and the slope values calculated from the fits of the experimental data with a linear function

Heater set temperature (He flow rate)	Actual temperature (K)	R^2	Slope
225 °C (6 l min ⁻¹)	443 K	0.993	-0.0509
225 °C (4 l min ⁻¹)	454 K	0.945	-0.0604
250 °C (6 l min ⁻¹)	459 K	0.948	-0.0767
250 °C (4 l min ⁻¹)	472 K	0.973	-0.0852
275 °C (4 l min ⁻¹)	490 K	0.958	-0.0920
300 °C (6 l min ⁻¹)	493 K	0.979	-0.0916
300 °C (4 l min ⁻¹)	508 K	0.955	-0.1225
325 °C (4 l min ⁻¹)	526 K	0.897	-0.1778

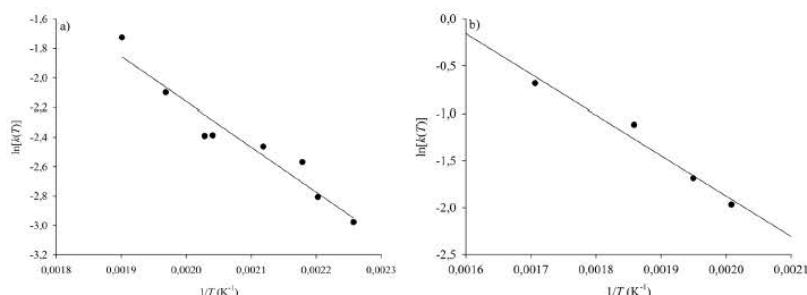


Figure 7. Arrhenius plots for the dehydration reaction of the mycosporine serinol obtained from time resolved mass spectrometry measurements using DART-TOF analysis and data treatment by means of a) procedure A ($R^2 = 0.965$) and b) procedure B ($R^2 = 0.984$) (see experimental section).

DART-MS of cyanolichen *Lichina pygmaea* metabolites

Table 4. Thermochemical data obtained from Arrhenius diagrams plotted for the dehydration reaction of the mycosporine serinol analyzed by time resolved mass spectrometry measurements using DART-TOF analysis and data treatment by means of the procedure A and B described in the experimental section

Thermochemical data	Procedure A	Procedure B
Slopes values (<i>a</i>)	−3067 K ^{−1}	−4300 K ^{−1}
Intercept (<i>b</i>)	3.97	6.72
Activation energy (<i>E_a</i>)	25 kJ mol ^{−1}	36 kJ mol ^{−1}
Arrhenius pre-exponential factor (<i>A_{pe}</i>)	53 s ^{−1}	83 s ^{−1}
Activation enthalpy ($\Delta_r^\ddagger H_m^\circ$) ^a	21 kJ mol ^{−1}	32 kJ mol ^{−1}
Activation entropy ($\Delta_r^\ddagger S_m^\circ$) ^a	−224 J mol ^{−1} K ^{−1}	−201 J mol ^{−1} K ^{−1}

^aCalculated by considering a temperature of 480 K corresponding to the mean actual temperature used in each analytical procedure A and B.

such a dehydration reaction could likely occur with natural stimuli such as a warm-up at ambient temperature or under sun exposure. The magnitude of these values is even in the range of the water vaporization enthalpy.^[31] This is in agreement with the fact that mycosporines are usually considered to act as a chemical agent that participates to the defence against desiccation as proposed elsewhere in literature.^[32–34] One can also propose that this dehydration reaction could lead to a compound which absorbs in the UV range with a higher molar extinction coefficient than the mycosporine itself if the loss of the water molecule yields an insaturation on the cyclohexenone moiety. Such an assumption should be confirmed by molecular modeling.

If the *A_{pe}* factor value cannot be determined with a high accuracy (see Table 4), the corresponding $\Delta_r^\ddagger S_m^\circ$ quantity appears to be characteristic of a surface reaction. For a better examination of such an assertion, one can be referred to the expression of these parameters in the context of the transition state theory (TST) by using statistical thermodynamic that describes the relationship between the *A_{pe}* and the molar activation entropy according to the following formula.^[35,36]

$$A_{pe} = \frac{k_B T}{h} \frac{Q_{tr}^\ddagger \cdot Q_{rot}^\ddagger \cdot Q_{vib}^\ddagger}{Q_{tr} \cdot Q_{rot} \cdot Q_{vib}} = \frac{k_B T}{h} \cdot \exp(1) \cdot \exp\left(\frac{\Delta_r^\ddagger S_m^\circ}{R}\right) \quad (8)$$

In Eqn (8), *k_B* is the Boltzmann constant, *h* is the Planck constant and *Q* and *Q[‡]* are the partition functions for the reactant at the initial state and the activate complex at the transition state, respectively. Note that in Eqn (8), the subscript *tr*, *rot* and *vib* represent the translational, rotational and internal vibrational motions of the molecule, respectively.^[37]

Knowing the value of the reaction entropic barrier of about −200 J mol^{−1} K^{−1} (see Table 4), the examination of Eqn (8) suggests that the mycosporine dehydration reaction involves an unfavorable entropic factor that can be explained as follow. The conversion at the surface of unhindered translational degrees of freedom to a translationally constraint transition state would contribute first to lowering $\Delta_r^\ddagger S_m^\circ$ through the quantity Q_{tr}^\ddagger/Q_{tr} .^[38] The unfavorable entropic factor can also be related to the chemical reactivity of the mycosporine serinol through the water molecule loss reaction. Indeed this one is known to proceed *via* a concerted mechanism involving an activated complex characteristic of a

rearrangement reaction.^[39] With this behavior, internal rotations characterized by low values of vibrational frequency can be converted to out-of-plan vibration of relatively high frequency values leading to vibrational partition functions of the activated complex that differ from the vibrational partition functions then implying $Q_{vib}^\ddagger < Q_{vib}$. One will note that concerning the ratio Q_{rot}^\ddagger/Q_{rot} , the same explanation can be made for the rotational degrees of freedom of the overall reactant and transition state than for the ratio Q_{tr}^\ddagger/Q_{tr} . Nevertheless if the evaluated entropic factor from the time resolved mass spectrometry measurements using DART-TOF analysis of the mycosporine appears unfavorable to a spontaneous process of dehydration, this one is dramatically overcome by a favorable energetic factor highlighted in this study by the evaluation of *E_a* and $\Delta_r^\ddagger H_m^\circ$.

Conclusion

This study demonstrates for the first time the possibility to use DART-MS analysis as well as for *in situ* detection of lichen metabolites than for thermochemical studies of reactions ongoing under the conditions of DART ionization process. DART-MS analyses herein described on our lichenic samples afforded immediate *in situ* detection of most known polar secondary metabolites from *L. pygmaea* without wiping or solvent extraction. Such an immediate access to elemental composition from crushed material emphasizes the potential of DART-MS as an early and refined dereplication tool. In our example, elemental formulae have been proposed for the signal detected at *m/z* 312 which may be attributed to the presence of an unknown secondary metabolite, calling for further investigations. We also report on some preliminary information regarding the distribution of mycosporine serinol within the thallus. Absence of DART-MS detection from the external part of the cortex is suggesting its location in the deep layers of the lichen. Imaging mass spectrometry techniques (MALDI-imaging, TOF-SIMS) are currently undertaken to map more accurately its distribution within the thallus. Given the surprising reactivity of mycosporine serinol, aqueous solutions of other mycosporines were submitted to DART-MS analysis (mycosporine glutamicol and mycosporine glutamicol ethyl-ester) (data not shown). Both of them displayed the same behaviour with a dehydration ongoing. So far, despite having successfully analyzed an array of typical lichen structures using DART-MS (comprising depsides, depsidones, aliphatic acids and quinones),^[40] this dehydration reaction appeared to be somehow specific to mycosporines. Hence, real-time detection of dehydration arising from nitrogen-containing compounds within lichens may serve as a hint to screen for mycosporines.

Besides the use of DART-MS for chemical profiling purposes, the consideration of the thermal transfers in such an ambient ionization source has allowed us to reach thermodynamic quantities associated with the dehydration reaction of one of these metabolites, mycosporine serinol. Such a monitoring is possible thanks to (1) real-time acquisition of mass spectra and (2) the possibility to control the temperature of the helium stream. The low mean activation enthalpy value of this reaction estimated in this paper (~25 kJ mol^{−1}) led us to an assumption regarding the putative role of mycosporine serinol in preventing lichen's dehydration. As *Lichina pygmaea* is an alternatively sea-immersed and atmosphere-dried lichen, this observation could be of concern with its adaptation to environmental stress desiccation.

Therefore, DART-MS, alongside other mass spectrometry, shows promising results in exploration of lichenic chemodiversity and appears as a powerful tool, not only for dereplication but also to get new insights into chemical ecology.

Acknowledgements

This work was supported by the University of Rennes I through the project 'Défi émergent LICHENMASS' and used the mass spectrometry facilities of the DReAM platform of IETR. Thi Thu Tram N' Guyen and Dr. Marylène Chollet-Krugler are greatly acknowledged for providing standards of mycosporines.

References

- [1] C. Roullier, M. Chollet-Krugler, E.-M. Pferschy-Wenzig, A. Maillard, G. N. Rechberger, B. Legouin-Gargadennec, R. Bauer, J. Boustie. Characterization and identification of mycosporines-like compounds in cyanolichens. Isolation of mycosporine hydroxyglutamical from *Nephroma laevigatum* Ach. *Phytochemistry* **2011**, *72*, 1348.
- [2] J. Boustie, M. Grube. Lichens - a promising source of bioactive secondary metabolites. *Plant Genet. Resour.-C* **2005**, *3*, 273.
- [3] S. Huneck, I. Yoshimura. *Identification of lichen substances*. Springer: Berlin, **1996**.
- [4] S. La Barre, C. Roullier, J. Boustie. In *Outstanding marine molecules*, S. La Barre, M. Kornprobst (Eds). Wiley: New-York, **2014**, 333.
- [5] K. H. Nguyen, M. Chollet-Krugler, N. Gouault, S. Tomasi. UV-protectant metabolites from lichens and their symbiotic partners. *Nat. Prod. Rep.* **2013**, *30*, 1490.
- [6] Y. V. Yuan, Y. Athukorala. *Marine cosmeceuticals: trends and prospects*, S. K. Kim (Ed.). Taylor and Francis: Boca Raton, Florida, USA, **2011**, 143.
- [7] A. Oren, N. Gunde-Cimerman. Mycosporines and mycosporine-like amino acids: UV protectants or multipurpose secondary metabolites? *FEMS Microbiol. Lett.* **2007**, *269*, 1.
- [8] W. Van Roy, A. Mathey, L. Van Vaeck. In situ analysis of lichen pigments by Fourier Transform Laser Microprobe Mass Spectrometry with external ion source. *Rapid Commun. Mass Spectrom.* **1996**, *10*, 562.
- [9] C. Liao, M. D. Piercey-Normore, J. L. Sorensen, K. Gough. In situ imaging of usnic acid in selected *Cladonia* spp. by vibrational spectroscopy. *Analyst* **2010**, *135*, 3242.
- [10] P. Ozenda, G. Clauzade. *Les Lichens : étude biologique et flore illustrée*. Masson: Paris, **1970**.
- [11] J. Hajslova, T. Cajka, L. Vaclavik. Challenging applications offered by direct analysis in real time (DART) in food-quality and safety analysis. *TrAC Trends Anal. Chem.* **2011**, *30*, 204.
- [12] L.-P. Li, B.-S. Feng, J.-W. Yang, C.-L. Chang, Y. Bai, H.-W. Liu. Applications of ambient mass spectrometry in high-throughput screening. *Analyst* **2013**, *138*, 3097.
- [13] E. Esquenazi, Y.-L. Yang, J. Watrous, W. H. Gerwick, P. C. Dorrestein. Imaging mass spectrometry of natural products. *Nat. Prod. Rep.* **2009**, *26*, 1521.
- [14] N. Bjarnholt, B. Li, J. D'Alvise, C. Janfelt. Mass spectrometry imaging of plant metabolites - principles and possibilities. *Nat. Prod. Rep.* **2014**, *31*, 818.
- [15] P. Nemes, A. A. Barton, A. Vertes. Three-dimensional imaging of metabolites in tissues under ambient conditions by Laser Ablation Electrospray Ionization mass spectrometry. *Anal. Chem.* **2009**, *81*, 6668.
- [16] R. A. Musah, M. A. Domin, M. A. Walling, J. R. E. Shepard. Rapid identification of synthetic cannabinoids in herbal samples via direct analysis in real time mass spectrometry: Identification of synthetic cannabinoids via DART-MS. *Rapid Commun. Mass Spectrom.* **2012**, *26*, 1109.
- [17] D. J. Weston. Ambient ionization mass spectrometry: current understanding of mechanistic theory, analytical performance and application areas. *Analyst* **2010**, *135*, 661.
- [18] R. B. Cody, J. A. Laramée, H. D. Durst. A Versatile new ion source for the analysis of materials in open air under ambient conditions. *Anal. Chem.* **2005**, *77*, 2297.
- [19] E. S. Chemetsova, G. E. Morlock, I. A. Revelsky. DART mass spectrometry and its applications in chemical analysis. *Russ. Chem. Rev.* **2011**, *80*, 235.
- [20] L. Song, S. C. Gibson, D. Bhandari, K. D. Cook, J. E. Bartmess. Ionization mechanism of positive-ion direct analysis in real time: a transient microenvironment concept. *Anal. Chem.* **2009**, *81*, 10080.
- [21] G. A. Harris, C. E. Falcone, F. M. Fernández. Sensitivity "hot spots" in the direct analysis in real time mass spectrometry of nerve agent simulants. *J. Am. Soc. Mass Spectrom.* **2012**, *23*, 153.
- [22] M. Zhou, J. F. McDonald, F. M. Fernández. Optimization of a direct analysis in real time/time-of-flight mass spectrometry method for rapid serum metabolomic fingerprinting. *J. Am. Soc. Mass Spectrom.* **2010**, *21*, 68.
- [23] S. D. Maleknia, T. M. Vail, R. B. Cody, D. O. Sparkman, T. L. Bell, M. A. Adams. Temperature-dependent release of volatile organic compounds of eucalypts by direct analysis in real time (DART) mass spectrometry. *Rapid Commun. Mass Spectrom.* **2009**, *23*, 2241.
- [24] C. Roullier, M. Chollet-Krugler, A. Bernard, J. Boustie. Multiple dual-mode centrifugal partition chromatography as an efficient method for the purification of a mycosporine from a crude methanolic extract of *Lichina pygmaea*. *J. Chromatogr. B* **2009**, *877*, 2067.
- [25] C. Roullier, M. Chollet-Krugler, P. van de Weghe, F. Lohézic-Le Dévéhat, J. Boustie. A novel aryl-hydrazide from the marine lichen *Lichina pygmaea*: Isolation, synthesis of derivatives, and cytotoxicity assays. *Bioorg. Med. Chem. Lett.* **2010**, *20*, 4582.
- [26] G. A. Harris, D. M. Hostetler, C. Y. Hampton, F. M. Fernández. Comparison of the internal energy deposition of direct analysis in real time and electrospray ionization time-of-flight mass spectrometry. *J. Am. Soc. Mass Spectrom.* **2010**, *21*, 855.
- [27] W. F. K. Wynne-Jones, H. Eyring. Absolute rate of reactions in condensed phases. *J. Chem. Phys.* **1935**, *3*, 492.
- [28] Y. Abe, M. Yamaguchi, M. Mutsuga, Y. Hirahara, M. Kawamura, R. Kikura-Hanajiri, Y. Goda, Y. Kawamura. Discrimination of plasticizers and screening of phthalates in polyvinyl chloride using DART-TOF/MS. *Shokuhin Eiseigaku Zasshi J. Food Hyg. Soc. Jpn.* **2009**, *51*, 160.
- [29] K. Fouyer, O. Lavastre, D. Rondeau. Direct Monitoring of the Role Played by a Stabilizer in a Solid Sample of Polymer Using Direct Analysis in Real Time Mass Spectrometry: The Case of Irgafos 168 in Polyethylene. *Anal. Chem.* **2012**, *84*, 8642.
- [30] J. H. Gross. Direct analysis in real time - a critical review on DART-MS. *Anal. Bioanal. Chem.* **2014**, *406*, 63.
- [31] K. N. Marsh. *Recommended reference materials for the realization of physicochemical properties*. Blackwell Scientific Publications: Oxford, UK, **1987**.
- [32] J. Tirkey, S. P. Adhikary. Cyanobacteria in biological soil crusts of India. *Curr. Sci.* **2005**, *89*, 515.
- [33] A. A. Gorbushina, K. Whitehead, T. Dornieden, A. Niese, A. Schulte, J. I. Hedges. Black fungal colonies as units of survival: hyphal mycosporines synthesized by rock-dwelling microcolonial fungi. *Can. J. Bot.* **2003**, *81*, 131.
- [34] H. Jiang, K. Gao, E. W. Helbling. UV-absorbing compounds in *Porphyra haitanensis* (Rhodophyta) with special reference to effects of desiccation. *J. Appl. Phycol.* **2008**, *20*, 387.
- [35] M. G. Evans, M. Polanyi. Application of the transition-state method to the calculation of reaction velocities, especially in solution. *Trans. Faraday Soc.* **1935**, *31*, 875.
- [36] H. Eyring. Activated complex in chemical reactions. *J. Chem. Phys.* **1935**, *3*, 107.
- [37] K. J. Laidler. *Chemical kinetics*. McGraw-Hill: New-York, **1965**.
- [38] R. B. Hall, A. M. DeSantolo, S. J. Bares. Time resolved measurements of methanol decomposition on Ni (100) utilizing laser induced desorption. *Surf. Sci. Lett.* **1985**, *161*, 533.
- [39] P. J. Robinson, K. A. Holbrook. *Unimolecular reactions*. Wiley-Interscience: New York, **1972**.
- [40] P. Le Pogam, B. Legouin, J. Boustie, D. Rondeau. Detection and chemical reactivity of lichen secondary metabolites using in situ DART-MS. *Proceedings of the EuPA 2013 congress*, Saint-Malo, France, **2013**.

b. Profilage chimique d'*Ophioparma ventosa* et études phytochimiques associées

Un second volet de l'étude DART s'est articulé autour d'un chlorolichen crustacé alpin, *Ophioparma ventosa*.

- Embranchement : Ascomycètes
- Classe : Lécanoromycètes
- Ordre : Lécanorales
- Famille : Ophioparmacées
- Genre : *Ophioparma*
- Espèce : *ventosa*

Ophioparma ventosa est un lichen crustacé dont le thalle est bien délimité au pourtour et qui arbore une couleur jaune plus ou moins nuancée de verdâtre ou de gris. Le thalle, dont l'épaisseur va de 2 à 10 mm, est crevassé et présente une surface aréolée-verruqueuse. La micro-algue verte est de type trébouxioïde. Les apothécies, lécanorines (dont le rebord régresse toutefois au cours du développement), sont caractérisées par une vive coloration rouge-écarlate et mesurent de 2 à 4 mm de diamètre. Les asques contiennent 8 spores incolores contenant 5 à 7 cloisons et sont de dimension 40-50 x 4-5 µm. Une description histologique plus précise de ce lichen est fournie dans la publication relative à l'imagerie des composés au sein de coupes d'*Ophioparma ventosa*.

Ce lichen, de chimie complexe et variable (May, 1997; Skult, 1997), est caractérisé par la présence de polyphénols lichéniques typiques appartenant à plusieurs familles structurales (depsides, dihydrodibenzofurane, naphtoquinone, acides gras, parfois depsidones). Ce lichen arbore de nettes différences de couleur entre ses apothécies de couleur rouge et le reste du thalle qui présente des teintes variables allant du gris au vert en passant par le jaune, ce qui en fait également un modèle de choix pour réaliser de l'histolocalisation. Le profilage DART-MS directement réalisé sur du lichen broyé a permis de générer un profilage chimique complet et a notamment révélé la présence d'acide miriquidique, depside rare et inconnu à ce jour chez *O. ventosa*, soulignant l'intérêt du DART pour la déréplication de polyphénols lichéniques. L'exhaustivité de l'information fournie par le DART-MS a pu être établie par une analyse phytochimique complète de ce lichen. Des analyses comparées des faces supérieure et inférieure de ce lichen au thalle épais livrent également quelques premiers éléments concernant la distribution des composés dans le lichen. Cet axe de travail a donné lieu à un article à paraître en 2016 dans *Phytochemical Analysis* (Le Pogam et al., 2016a). Les documents complémentaires associés à cette publication sont présentés en Annexe 4 (p. 214). Les familles structurales identifiées au DART lors de ce travail sont les suivantes : depsides, depsidones, naphtoquinones, dihydrodibenzofurane et acides gras (Figure 18).



Ophioparma ventosa

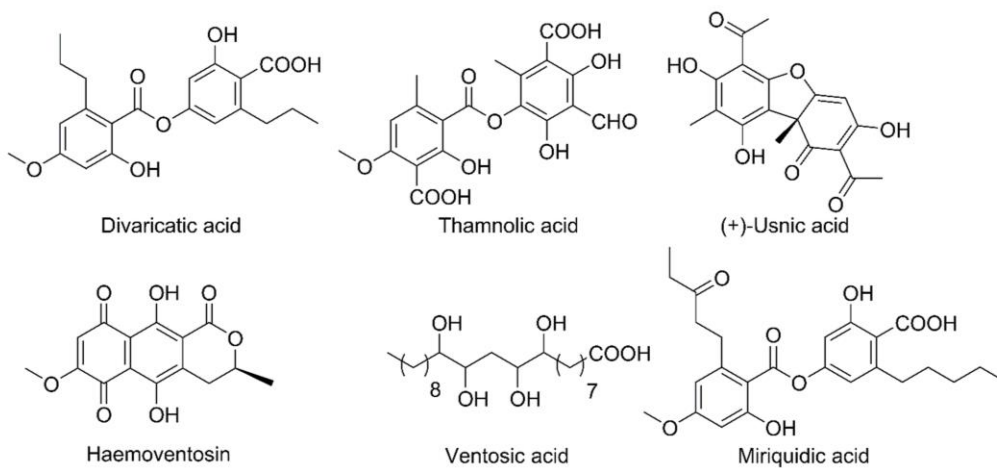


FIGURE 18 : PHOTOGRAPHIE D'*OPHIOPARMA VENTOSA* ET MÉTABOLITES SECONDAIRES ISOLÉS AU COURS DE L'ÉTUDE PHYTOCHIMIQUE ASSOCIÉE

In situ DART-MS as a Versatile and Rapid Dereplication Tool in Lichenology: Chemical Fingerprinting of *Ophioparma ventosa*

Pierre Le Pogam,^a Anne-Cécile Le Lamer,^{a,b,*} Béatrice Legouin,^a Joël Boustie^a and David Rondeau^{c,d,*}

ABSTRACT:

Introduction – Lichens widely occur all over the world and are known to produce unique secondary metabolites with various biological activities.

Objective – To develop high-throughput screening approaches requiring little to no sample preparation to alleviate the dereplication holdup and accelerate the discovery workflow of new structures from lichens.

Methodology – The extracellular distribution of lichen metabolites is incentive for *in situ* chemical profiling of lichens using the ambient mass spectrometry DART-MS. For this purpose, the chlorolichen *Ophioparma ventosa*, producing an array of lichen polyphenolics that encompass the main structural classes associated to lichen chemodiversity, represented a relevant model to assess the versatility of this platform. The feasibility of this approach was first established by analysing the pure compounds known from this species prior to being extended to different solid organs of the lichen.

Results – All tested compounds could be detected in positive and negative ion modes, most often with prevalent protonated or deprotonated molecules. Only depsides underwent a significant in-source fragmentation in both ionisation modes, which should be regarded as an added value for their structural elucidation. *In situ* DART-MS analyses of *Ophioparma ventosa* provided an extensive chemical profile and noteworthy pinpointed miriquidic acid, an unusual lichen depside so far unknown within this species. At last, *in situ* DART-MS granted a first insight into the distribution of the metabolites within the lichen.

Conclusion – DART-MS represents a versatile tool to the wide field of lichenology, facilitating accelerated and sharp analyses of lichens and bypassing costly and tedious procedures of solvent extraction. Copyright © 2016 John Wiley & Sons, Ltd.

Supporting information can be found in the online version of this article.

Keywords: Lichens; polyphenolics; *in situ* DART-MS

Introduction

Lichens are worldwide distributed symbiotic organisms mostly consisting of an association between a fungus and an alga. Valuation of lichens unique metabolites for therapeutic purposes is generating an increasing interest (Shukla *et al.*, 2010) pledging for the development of refined dereplication tools to focus on minor and unknown metabolites. Liquid chromatography-electrospray ionisation-mass spectrometry (LC-ESI-MS) remains the most common dereplication approach in lichenology, often associated with detection in MS/MS or MSⁿ mode (Le Pogam *et al.*, 2015a). Since many lichen metabolites are shown to crystallise on the external surfaces of hyphae (Boustie *et al.*, 2011), new trends in lichenology include *in situ* analysis to get information directly from the natural complex matrix (Le Pogam *et al.*, 2015a).

Some innovative *in situ* approaches rely on recent methods of MS such as desorption electrospray ionisation (DESI) and direct analysis in real time (DART) that create ions outside the instrument, hence giving ability to record mass spectra on samples in their native environment without any preparation or pre-separation (Li *et al.*, 2013). Ions released through the sample surface are transported through the air in a conventional mass spectrometer resulting in straightforward analysis. Owing to their versatility, those ambient MS techniques generated great interest in many fields: high-throughput screening of pharmaceuticals,

environmental analysis, food safety testing, forensics and analyses in the realm of natural products (Cooks *et al.*, 2006). Several advantages can be expected from such approaches: no extraction steps avoiding chemical artefacts, qualitative and quantitative information obtained within a few minutes and direct analysis of genuine

* Correspondence to: Anne-Cécile Le Lamer, Université Paul Sabatier Toulouse 3, 118 Route de Narbonne, 31062, Toulouse Cedex 09, France. Email: anne-cedle.le-lamer@univ-tlse3.fr

** Correspondence to: David Rondeau, Institut d'Electronique et de Télécommunication de Rennes (IETR UMR CNRS 6164), Université de Rennes 1, Campus de Beaulieu, 263 Avenue du General Lederc, 35042, Rennes Cedex, France. Email: david.rondeau@univ-rennes1.fr

^a Laboratoire de Pharmacognosie, Equipe PNSCM (ISCR UMR CNRS 6226), Faculté des Sciences Pharmaceutiques et Biologiques, 2 av. du Pr Léon-Bernard, 35042, Rennes Cedex, France

^b Université Paul Sabatier Toulouse 3, 118 Route de Narbonne, 31062, Toulouse Cedex 09, France

^c Institut d'Electronique et de Télécommunication de Rennes (IETR UMR CNRS 6164), Université de Rennes 1, Campus de Beaulieu, 263 Avenue du General Lederc, 35042, Rennes Cedex, France

^d Département de Chimie, Université de Bretagne Occidentale, 6 avenue le Gorgeu, 29238, Brest Cedex 03, France

In situ DART-MS analysis of the lichen *Ophioparma ventosa*

compounds, including access to the regional distribution of metabolites (Sica *et al.*, 2014).

DART atmospheric pressure ionisation is one of those ambient ionisation sources that enable mass measurements of gas, liquids and solid samples (Li *et al.*, 2013). It involves a stream carrying neutral helium atoms in a metastable (excited) state that induces Penning ionisation of atmospheric water to yield protonated clusters ($\text{H}_2\text{O}_n\text{H}_3\text{O}^+$) that further ionise analytes through gas-phase protonation (Cody *et al.*, 2005). A transient microenvironment mechanism, involving the desorption of the volatile matrix, can also account for a direct ionisation when the gas stream is in contact with the sample (Song *et al.*, 2009). This previous step of surface desorption leads to relate DART ionisation efficiency to the proton affinity of the analytes, but also to the temperature and the flow rate of the metastable atom and to the boiling point of the analyte (Zhou *et al.*, 2010). Patented in 2005, DART-MS showed up as a versatile analytical platform, successfully applied to a variety of samples including biological matrices (Gross, 2014).

Such features prompted us to try *in situ* DART-MS analyses for chemical profiling of lichens. We recently reported on *in situ* DART-HRMS analyses of sugar derivatives and nitrogen-containing metabolites in the cyanolichen *Lichina pygmaea*, highlighting its potential as an accelerated dereplication tool (Le Pogam *et al.*, 2015b). To further evaluate the advantages offered by DART-HRMS in lichenology, its adequacy for *in situ* detection of archetypal lichen polyphenolics such as depsides and depsidones remained to be determined. For this purpose, the chlorolichen *Ophioparma ventosa* was selected as a relevant model since it is described to contain a wide array of typical lichen structures (Skult, 1997; May, 1997). *Ophioparma ventosa* (L.) Norman also represents a well-fitted model to study the spatial allocation of lichen polyphenolics between its blood-red fruiting bodies (apothecia) and the grey/yellowish rest of the lichen (thallus).

A first insight into the chemical profile of our sample of *Ophioparma ventosa* was provided by high performance liquid chromatography-diode array detector-mass spectrometry (HPLC-DAD-MS) analyses of the whole lichen. Preliminary DART experiments using pure compounds classically described within *O. ventosa* were then conducted to study the behaviour of lichen polyphenolics with this ion source. At last, direct *in situ* DART-HRMS analysis of lichen material, including both thallus and apothecia, were achieved and compared to HPLC-DAD-MS and phytochemical investigation.

Experimental

DART-HRMS

All analyses were performed using a JEOL JMS-T100CS (AccuTOF CS) orthogonal time-of-flight (TOF) mass spectrometer (Peabody, MA, USA) equipped with an IonSense DART Source (Danvers, MA) (Model DART 100). Ultra-high purity helium was used as reagent gas at a flow rate of 4 L/min and under a temperature value of 523 K. The following DART-needle, discharge electrode, and the grid electrode voltage values used were 3500, ± 150 , and ± 250 V, respectively. The voltage values of orifice 1, orifice 2, and the ring lens were set at 15, 5, and 10 V, respectively. The orifice 1 temperature was kept at 353 K. The detector voltage was set at 2300 V. The mass spectra were recorded every second with a resolution of 6000 [full width at half maximum (FWHM) definition]. The mass scale was calibrated using the $[\text{M} + \text{H}]^+$ ion series of a polyethylene glycol diluted in a dichloromethane/methanol mixture (1:1) and $[\text{M}-\text{H}]^-$ ion series of a polyethylene glycol sulphate in negative ion (NI) mode (both purchased from Aldrich-Sigma, St Quentin Fallavier, France). To perform accurate mass

measurements, the mass drift compensation procedure available on the main program that controls the AccuTOF CS was used to compensate for the m/z drift in the range of 100 to 500 Da.

DART-MS analyses of the intact pieces of *Ophioparma ventosa* were performed by holding the sample between tweezers directly under the helium stream. DART-MS acquisitions of compounds in solid form and crushed lichens were performed by presenting a glass rod previously dipped inside the powdered compound or crushed lichen. DART-MS analyses of liquid samples were achieved by depositing 10 μL of solution at the surface of a glass rod located in front of the ion source.

To estimate the distribution of the metabolites within *Ophioparma ventosa* thallus, DART helium stream was directed towards both faces of a single piece of thallus. First, the lower face was analysed (0.2–0.5 min) prior to being withdrawn from the source so that all species could disappear from the mass spectrum. During a second period of time (0.6–0.9 min), the upper side of the piece of lichen was analysed. Reconstructed ion chromatograms (RICs) were then considered for m/z values of interest by dragging over the width at 20% of the top of each mono-isotopic peak.

HPLC-DAD-MS

The HPLC system (Prominence Shimadzu, Marne La Vallée, France) was equipped with a Kinetex C₁₈ HPLC column (100 mm \times 4.6 mm – 2.6 μm – 100 Å, Phenomenex) and consisted of a quaternary pump (LC20ADSP), a surveyor autosampler (SIL-20AHT), and a DAD (SPD-M20 A) scanning the wavelength range from 220 to 600 nm. HPLC analysis was performed by gradient elution using the following parameters: A (0.1% formic acid in water) and B (acetonitrile). T: 0 min, 20% B; 0–25 min, 80% B linear; 25–30 min, 100% B linear; 30–35 min, 100% B; 35–40 min, 20% B linear. The flow rate was 0.5 mL/min.

The LC-ESI and ESI-MSⁿ mass spectra were obtained from a LCQ Deca ion trap mass spectrometer (Thermo Finnigan, Villebon sur Yvette, France) equipped with a ESI source (spray voltage 3.5 kV, sheath gas: nitrogen 60 arbitrary units, auxiliary gas: nitrogen 5 arbitrary units, capillary temperature 220 °C and capillary voltage +36 and –27 V) in positive and negative ionisation modes, respectively. The MSⁿ spectra were recorded using conditions described elsewhere (Parrot *et al.*, 2013).

Chemical reagents

Analytical and HPLC grade solvents for extraction and for chromatography were purchased from Carlo Erba Reactifs (Val de Reuil, France). HPLC grade water was obtained by an EasyPure (Barnstead, NH, USA) water purification system. Deuterated solvents were purchased from Euriso-top (Gif-sur-Yvette, France). All other chemicals and standards were available from WWR international (Radnor, PA, USA). Lichen compounds were isolated during previous phytochemical investigation or as described herein.

Lichen material

Ophioparma ventosa was harvested in Obergurgl (Austria) (April 2009) and identified by Pr. J. Boustie. A voucher specimen is kept in the laboratory with the reference JB/09/158. The phytochemical investigation of *O. ventosa* is detailed in the Supporting Information.

Results and discussion

HPLC-DAD-MS analysis of *Ophioparma ventosa* extracts

The chemical profiling of *Ophioparma ventosa* was first assessed by HPLC-DAD-MS analyses of its acetone extract (Fig. S1, Supporting Information). MS analyses were conducted using an ESI source either in PI or NI mode (Table S1, Supporting Information). Haemoventosin (**1**) was the only molecule detected in positive ion (PI) mode, as a $[\text{M} + \text{H}]^+$ of m/z 305 value. This protonated molecule lost a water molecule to yield a m/z 387 fragment ion upon

collision-induced dissociation (CID). All other molecules were only detected using NI mode, which led to characterise the presence of thamnolic acid (2), divaricatic acid (4) and usnic acid (5). Values of m/z ratios of the major peaks detected on the ESI mass spectrum are in agreement with the formation of the $[M-H]^-$ ions from all aforementioned metabolites. CID-MS/MS spectra obtained from the selection of each $[M-H]^-$ parent ion of compounds 2, 4 and 5 show the formation of fragment ions (Table S1).

For the three species 2, 4 and 5, the product ions are consistent with metastable dissociations of $[M-H]^-$ ions of lichen compounds obtained by fast atom bombardment (NI-FAB) (Holzmann and Leuckert, 1990) and laser desorption/ionisation mass spectrometry (NI-LDI-MS) (Le Pogam *et al.*, 2015c) (Table S1). In the case of usnic acid (5), the only fragment ion (m/z 328) that is detected in negative CID-MS/MS from the selection of the m/z 343 ion is due to the loss of a methyl radical leading to an energetically favoured dibenzofuran system as described elsewhere (Huneck and Schmidt, 1980). Such an exception to the "even-electron rule" upon low-energy collision induced decomposition in NI-ESI-MS/MS has been already mentioned when the product ion is a radical anion stabilised by resonance (Cai *et al.*, 2010). LC-MS analysis pinpointed the presence of a fifth metabolite (3), which was not matching with any previous reports on *Ophioparma ventosa*. The exclusive ionisation of this molecule in NI mode and the two co-occurring fragments suggest the presence of a depside. The next step was to compare the chemical profile provided by this benchmark method to that provided by *in situ* DART-MS analyses. Owing to the chemical reactivity that can be associated to the DART-MS ionisation process (Le Pogam *et al.*, 2015b), the expected single compounds were first analysed with this ion source to establish their spectral signatures prior to investigating the lichen material.

DART-HRMS analysis of metabolites expected within *Ophioparma ventosa*

Literature data suggest the possible occurrence of a dozen of metabolites for *Ophioparma ventosa*, covering several major classes of lichen polyphenolics. The investigation of DART mass

spectrometric behaviour was thus extended to some depsidones (stictic acid, norstictic acid, psoromic acid) and a depside (atranorin) alongside molecules identified during HPLC-MS analysis (May, 1997) (Fig. 1). Those molecules were isolated and identified in the laboratory, some of them being purified during the concomitant phytochemical study undertaken on *O. ventosa* (for chemical details, see Supporting Information).

A first outcome is that all the tested compounds could have been detected in both ionisation modes under DART-HRMS conditions. The accurate mass measurements were performed from the most intense ions and each experimental value was compared with the theoretical masses (Table S2 and S3). In all cases, only one molecular formula was proposed.

Dibenzofuran-related usnic acid. As a major and constant component of *Ophioparma ventosa*, and a recurrent metabolite in many lichens, mass spectrometric behaviour of usnic acid under DART conditions was of particular significance. In both ionisation modes, the accurate mass measurements performed from the mass spectrum of a solution of usnic acid led to the detection of prevalent $[M-H]^-$ ($m/z = 343.0826$) and $[M + H]^+$ ions ($m/z = 345.0972$) (Fig. S2; Tables S2 and S3).

The ion observed in Fig. S2(A) at m/z 329.0671 ($C_{17}H_{13}O_7$, Table S2) originates from the loss of a methyl radical from a radical anion of usnic acid. This reactivity has been previously described in the literature during the analysis of lichen compounds in MS using soft negative ionisations (Huneck *et al.*, 1968; Holzmann and Leuckert, 1990; Le Pogam *et al.*, 2015c).

Depsidones. Several depsidones have been described within *Ophioparma ventosa* including stictic, norstictic and psoromic acids (May, 1997). Given the poor solubility of depsidones in most solvents, their analysis was directly achieved using powders rather than solutions. DART-MS analyses were thus carried out by submitting to the warm-up metastable helium stream a glass rod previously dipped into the powdered compound. DART-MS ability to analyse powders is of specific interest for the study of lichen metabolites since many of them are poorly soluble in usual solvents (Kristmundsdóttir *et al.*, 2005). In both ionisation modes, all three

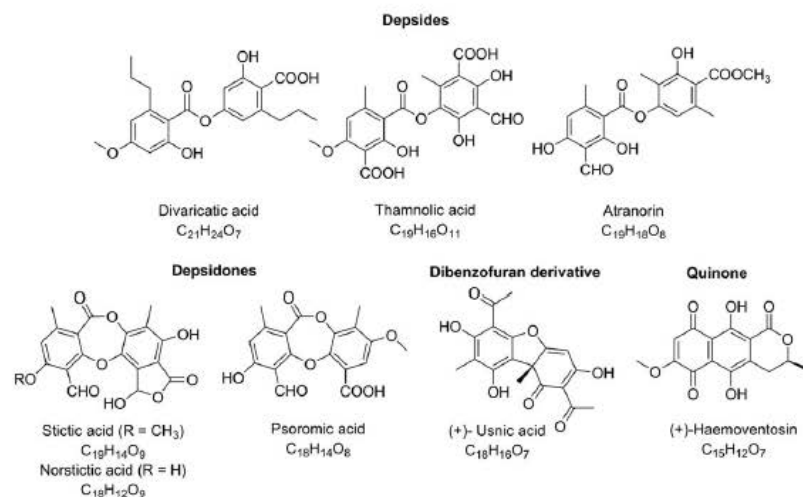


Figure 1. Structure of lichen compounds described in *Ophioparma ventosa*.

In situ DART-MS analysis of the lichen *Ophioparma ventosa*

depsidones were detected through their protonated or deprotonated molecule (Fig. S3–S5; Tables S2 and S3).

Naphthoquinone. Haemoventoin is the main naphthazarin dye accounting for the deep red colour of the apothecia (Le Pogam *et al.*, 2016). A complex pattern of signals appeared during the mass spectrum acquisition, with two successive PI mass spectra (Fig. 2). Whereas only the protonated molecule of haemoventoin is found at the beginning of the DART-MS analysis, two additional signals appear at m/z 303 and 307 framing the m/z 305 ion after a dozen of seconds. This behaviour refers to the bimolecular reactivity of quinone and hydroquinone type compounds (Chambers, 1974). These signals arise through a thermally activated redox reaction between the quinone and hydroquinone functions of haemoventoin (Fig. 2). NI-DART mass spectrum of haemoventoin revealed a similar pattern of signals related to its bimolecular reactivity (Fig. S6). The presence of m/z 304 ion in the NI-DART mass spectrum stems from an electron capture reaction related to the DART process (Fig. 2). This also accounts for the detection of m/z 302 since the diquinone system might not lose a proton.

Depsidides. Literature data suggest possible occurrence of four depsidides within *Ophioparma ventosa*: divaricatic, thamnolic and decarboxythamnolic acids and atranorin (Skult, 1997; May, 1997). Instability of thamnolic acid due to its trend to decarboxylate is a well-established process so that decarboxythamnolic acid was regarded as an artefact rather than a genuine lichen molecule (Culberson *et al.*, 1977, 1986). Therefore, only the behaviour of the three other depsidides under DART-MS conditions was investigated.

The NI-DART mass spectra reported in Fig. 3 displayed prominent signals attributed to the $[M-H]^-$ ions of divaricatic acid [Fig. 3(A)], decarboxythamnolic acid [Fig. 3(B)] and atranorin [Fig. 3(C)] as confirmed by the results of accurate mass measurements (Table S2).

The NI-DART mass spectrum of divaricatic acid can be interpreted straightforward by referring to the NI-ESI-MS/MS results (Table S1), except for an additional m/z 165. This fragment ion might arise from a decarboxylation reaction occurring from m/z 209, respectively. One can note that m/z 177 identified from ESI-MS/MS spectra of divaricatic acid (Table S1) did not show up in NI-DART-MS.

Regarding the NI-DART mass spectrum of thamnolic acid [Fig. 3(B)], the ion of highest m/z ratio (m/z 375) corresponds to the $[M-CO_2-H]^-$ species. As discussed earlier, this one is referenced as being produced by a thermally induced decarboxylation reaction when thamnolic acid is submitted to MS analyses (Culberson *et al.*, 1977). Despite this, m/z 225 and m/z 211 signals observed in the NI-DART-MS of Fig. 3(B) are in agreement with the chemical structures in the case of the ESI-MS/MS experiments performed from the $[M-H]^-$ m/z 419 of thamnolic acid (Table S1).

Finally, the NI-DART-MS spectrum of atranorin [Fig. 3(C)] revealed besides its deprotonated molecule at m/z 373.0926 a signal labelled at m/z 195.0450 corresponding to $C_{13}H_7O_2$ (Table S2), which is inconsistent with the structure of atranorin. This signal is most likely explained by the overlapping peaks of elemental composition $C_{10}H_{11}O_4$ (195.0663) and $C_9H_7O_5$ (195.0299). The molecular formula retrieved from m/z 163.0393 ($C_9H_7O_3$) is consistent with the loss of a methanol molecule from the alcohol moiety of atranorin [see blue arrow in Fig. 3(C)], as described elsewhere (Musharraf *et al.*, 2015). The m/z 177.0191 ion would be rather

due to the loss of water molecule from the m/z 195.0299 ion [see green arrow in Fig. 3(C)].

Alcohol and carboxylic acid moieties might serve as landmarks when screening for depsidides using NI-DART-MS. These specific cleavages of the ester and ether bonds, as depicted on Fig. 3, respectively through the blue and green arrows, are typical fragmentation processes of depsidides described using other sources such as ESI-MS (Bouchoux, 2013), LDI-MS (Le Pogam *et al.*, 2015c) and FAB-MS (Holzmann and Leuckert, 1990).

The PI-DART mass spectrum of atranorin revealed a prevalent protonated molecule at m/z 375 alongside other ions at m/z 179 and 197 [Fig. 4(A)–(D)]. The formation of these species could be due either to a thermal degradation of the analyte before ionisation or to the dissociation of the gaseous ion at m/z 375.1080 from an in source CID. The elemental compositions retrieved for m/z 179.0340 (oxonium ion) and 197.0793 (protonated carboxylic acid) are in agreement with that of fragment ions produced in the interface of the DART source. This zone facilitates the observation of completely desolvated ions by raising the potential difference between focus items delimiting the intermediate pressure area, better defined here as the orifice 1. However, as the electric fields increase, the desolvated ions can also undergo an in source-CID process that leads to the formation of fragment ions. If the relative intensities of low m/z ratio ions produced into the ion source increase with the orifice 1 voltage value while the relative intensity of the higher m/z ratio ion decreases, then the two processes can be related. PI-DART mass spectra of atranorin recorded at different orifice 1 voltage values are displayed in Fig. 4(A)–(D). The intensity of m/z 375 decreases as orifice 1 voltage increases until its complete disappearance for a value of 45 V. It appears that the ion at m/z 197 is the most intense signal when DART mass spectra were recorded at orifice 1 values of 5 V [Fig. 4(A)], 15 V [Fig. 4(B)] and 25 V [Fig. 4(C)]. Its relative intensity decreases as the orifice 1 value reaches 45 V [Fig. 4(D)] whereas the signals at m/z 179 and 165 have increased with the desolvation energy, i.e. from 15 to 45 V [Fig. 4(B)–(D)].

From these observations, a fragmentation mechanism has been proposed (Scheme S1). Note that this putative pathway is supported by MS/MS experiments performed from the protonated molecule of atranorin (Longevialle, 1992; Bouchoux, 2013). Nevertheless, as previously noted in this paper, the ESI in PI mode cannot lead to the observation of the $[M+H]^+$ ion of atranorin.

Since thamnolic acid immediately decarboxylates under DART-MS ionisation conditions, the study of its behaviour can be associated to that of decarboxythamnolic acid with $m/z = 377.0874$ as $[M+H]^+$. As for atranorin, the mass spectrum revealed carboxylic acid and oxonium ions at respective m/z ratios of 227.0556 ($C_{10}H_{11}O_6$), and 209.0444 ($C_{10}H_9O_5$) [Fig. 4(E)]. A third signal at m/z 169.0532 ($C_8H_9O_4$) was in agreement with an alcohol moiety of decarboxythamnolic acid analogous to that observed in NI mode. The elemental composition proposed for 191.0342 ($C_{10}H_7O_4$) is consistent with the loss of a water molecule from the oxonium fragment. The PI-DART-MS analysis of thamnolic acid can lead to a proposition of fragmentation mechanisms regrouped in Scheme S2.

As shown in Fig. 4(F), the PI-DART mass spectrum of divaricatic acid does not lead to detect a characteristic $[M+H]^+$ ion at m/z 389. Therefore, the origin of the ions observed in this PI-DART mass spectrum cannot be investigated, i.e. thermally activated during the warm-up by the helium stream or dissociated by in source CID in the desolvation interface. However, the structures of ions detected in Fig. 4(F) are in accordance with carboxylic acid

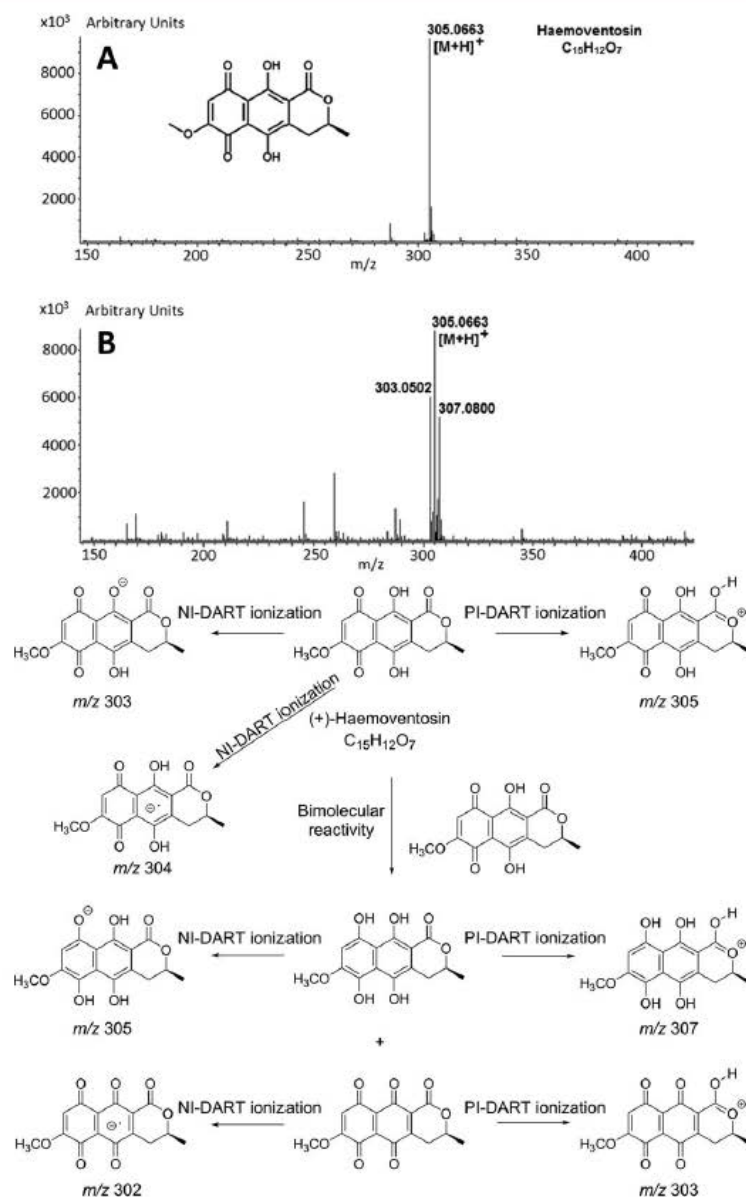


Figure 2. PI-DART-MS successive spectra of haemoventosin (A at $t = 0$ and B at $t = 12$ s) and proposed reactivity of haemoventosin in PI and NI-DART-MS. Note that the sites bearing the charge are arbitrary depicted on the molecular skeleton of each ion in both ionisation modes for a better reading of the scheme.

(211.0966), oxonium (193.0863) and alcohol (197.0808) moieties (Fig. S7).

Fragmentation patterns described from depsides listed earlier can lead to propose three signals as signatures for PI-DART-MS, i.e. carboxylic acid, oxonium and alcohol moieties (Fig. 5), altogether with NI-DART-MS landmarks, i.e. alcohol and carboxylic acid. Such in source-CID process of depsides in both ionisation

modes shall be considered as an added value for their structural elucidation (Fig. 5).

On the whole, DART-MS showed up as a promising tool for detection of lichen metabolites through the detection of protonated and deprotonated molecules (depsidones, usnic acid, haemoventosin and depsides in NI mode). Owing to DART-MS adequacy for detection of typical lichen polyphenolics being

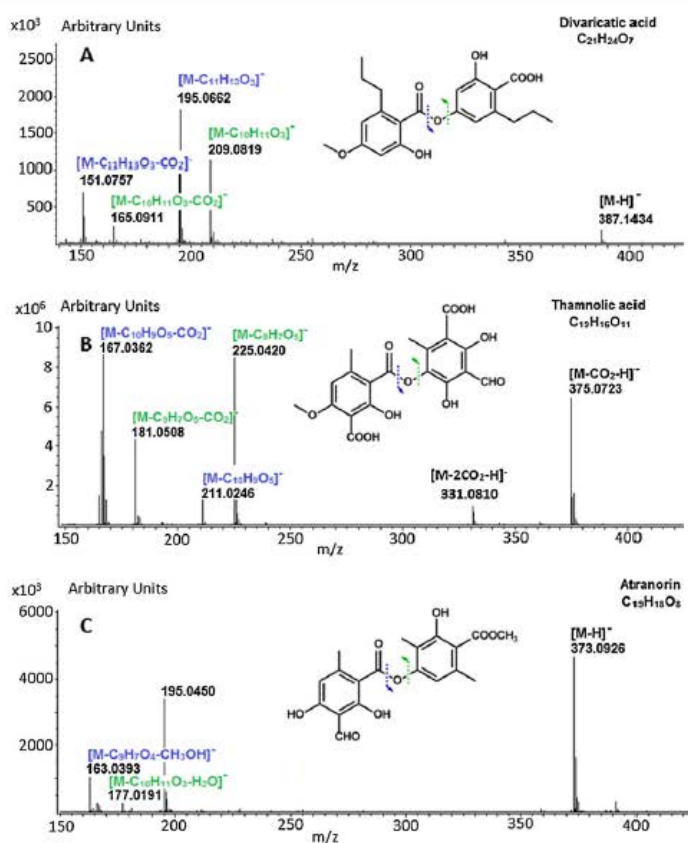


Figure 3. NI-DART-MS spectra of divaricatic acid (A), thamnolic acid (B) and atranorin (C).

demonstrated, *in situ* detection was further attempted from raw lichen material. Diagnostic signals expected for metabolites contained within the sample of *Ophioparma ventosa* are collated in Table 1.

DART-HRMS analyses of *Ophioparma ventosa*

To check whether DART-MS represents a fitting tool for *in situ* chemical fingerprinting of lichens, a first step was to directly analyse the crushed lichen material, including both thallus and apothecia.

In situ analysis of whole crushed lichen. Analyses performed in either PI or NI modes on crushed total lichen instantly revealed some aforementioned molecules.

NI mode mass spectrum [Fig. 6(A); Table S4] displayed peaks standing for divaricatic acid (m/z 195, 209, 387), thamnolic acid (m/z 167, 225, 375), haemovosin (m/z 303, 305) and usnic acid (m/z 343). Of special interest is the occurrence of some unassigned peaks that do not correspond to any pure compound previously analysed (m/z 223, 251, 255, 279, 281, 283 and 403) suggesting the occurrence of additional metabolite(s) within *Ophioparma ventosa*. Interestingly, m/z 223 and 251 most likely correspond to

signals associated to the unidentified compound **3** detected in LC-DAD-MS analysis.

In PI mode [Fig. 6(B); Table S5], signals corresponding to divaricatic acid (m/z 167, 193, 197, 211), thamnolic acid (m/z 169, 227, 377) haemovosin (305) and usnic acid (345) could also be evidenced, as well as unknown peaks (m/z 225, 253 and 405) that correspond to those observed in NI mode, and an additional peak at m/z 235.

The couple of negative and positive ions (respectively m/z 403:405) stood for a molecular formula of $C_{22}H_{44}O_6$, which is consistent with a tetrahydroxyfatty acid previously reported within *Ophioparma ventosa*, ventosic acid (Fig. 6). In the rest of this paper, such couples of ions will be referred to as (m/z xx:yy) where xx and yy are nominal masses of the ions measured in NI- and PI-DART-MS, respectively.

Regarding the other unassigned peaks, signals detected at m/z 223.0989:225.1128 (standing for $C_{12}H_{16}O_4$) and 251.0913:253.1088 (accounting for $C_{13}H_{16}O_5$) were accompanied by a third unassigned signal at m/z 235.0931 (standing for $C_{13}H_{15}O_4$) exclusively observed in PI mode. The joint occurrence of those latter (m/z 253 and 235) differing by H_2O , with the lighter missing in NI mode set typical DART-MS landmarks of a depside, as defined earlier. According to this proposed fragmentation scheme, these fragments might reveal a complete molecular formula of

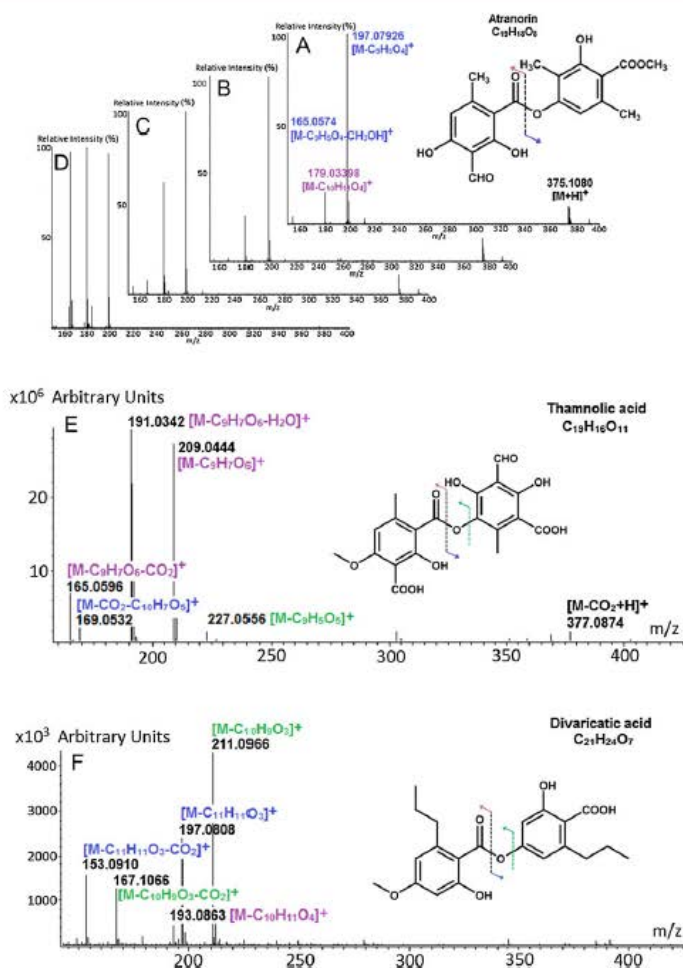


Figure 4. PI-DART-MS spectra of atranorin at increasing orifice 1 voltage values (A = 5 V, B = 15 V, C = 25 V and D = 45 V), PI-DART-MS spectra of thamnolic acid (E) and divaricic acid (F).

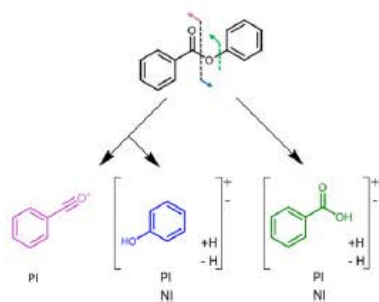


Figure 5. Putative structures of diagnostic ions of depsides submitted to PI- and NI-DART-MS analyses.

$C_{25}H_{30}O_8$ for a nominal mass of 458 Da ($C_{12}H_{16}O_4 + C_{13}H_{15}O_4 - 2H$), which is in agreement with the detection of a deprotonated

molecule at m/z 457 for compound **3** in NI-ESI-MS (Table S1). This pattern of signals has been compared with secondary metabolites described in lichens. Five lichen metabolites displayed such molecular formula, four of them being depsides. Only two of them, glomelliferic acid and miriquidic acid, were compatible with the aforementioned fragmentation process. Such isomers, only differing by the position of the ketone moiety on the side chain, could not be distinguished by MS. A phytochemical investigation enabled identifying this depside as miriquidic acid, reported here for the first time in a sample of *Ophioparma ventosa* (Fig. 6). DART-MS analyses of pure miriquidic acid confirmed this putative fragmentation process that fits the dissociation pathway proposed for the other depsides (Fig. S8; Tables S6 and S7). One should note that miriquidic acid PI and NI DART-MS spectra do not reveal protonated and deprotonated molecules, respectively.

At last, NI-DART-MS spectrum revealed some further signals (m/z 255.2; 279.2; 281.2; 283.2) with that of fatty acids 16:0, 18:2, 18:1 and 18:0, respectively. These series of fatty acids are

Table 1. PI- and NI-DART-MS signals for metabolites occurring within the sample of *Ophioparma ventosa*

	Negative ion (NI) mode signals	Positive ion (PI) mode signals
Usnic acid	329, 343	345
Haemoventosin	302, 303, 304, 305	303, 305, 307
Divaricatic acid	195, 209, 387 (151, 165)	193, 197, 211 (153, 167)
Thamnolic acid	167, 211, 225, 375	169, 209, 227, 377 (165, 191)

Note: numbers indicated between brackets refer to second generation fragments and thus do not stand among the signature signals described earlier.

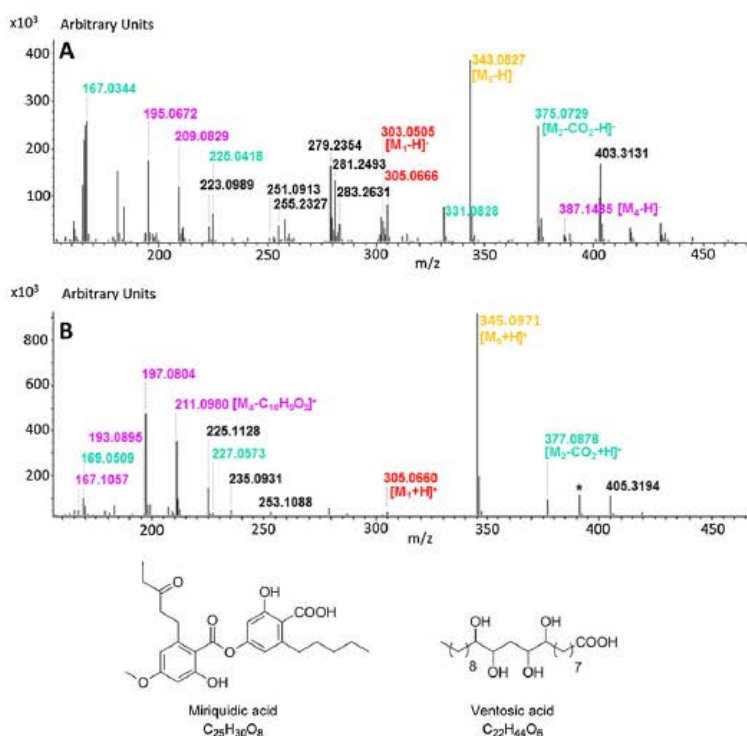


Figure 6. *In situ* DART-MS spectra of whole crushed *Ophioparma ventosa* in (A) NI and (B) PI modes. Numbers associated to the molecules are given according to their retention time using HPLC-MS (see Table S1). Red = haemoventosin; blue = thamnolic acid; purple = divaricatic acid; yellow = usnic acid. Compounds identified within *Ophioparma ventosa* using DART-MS (C).

known to be the most common among lichens and as such, GC-MS analyses of *Ophioparma ventosa* demonstrated the occurrence of palmitic, linoleic, oleic and stearic acids within this lichen (Rycroft *et al.*, 1995). This supports NI-DART-MS adequacy for detection of fatty acids, as recently outlined (Cody *et al.*, 2015).

Then, to reach distribution patterns of secondary metabolites within *Ophioparma ventosa*, apothecia and thallus were separately presented in front of the DART-MS ion source. Given apothecia's thinness (in micrometres), analysis of uncrushed material was presumed to yield an exhaustive chemical profile. Conversely, thallus parts are much thicker (in millimetres) and were thus investigated under both their crushed and entire forms. It can indeed be

hypothesised that metabolites located within the depth of the thallus might remain inaccessible to the helium stream when analysing intact pieces.

***In situ* analysis of apothecia and thallus.** As expected, the analysis of entire (Fig. S9; Tables S8 and S9) and crushed apothecia afforded similar mass spectra. In both PI and NI modes, the spectrum of uncrushed apothecia displayed signals corresponding to divaricatic acid, thamnolic acid, usnic acid, and haemoventosin. Moreover, the signal at m/z 405 attributed to ventosic acid was observed in the PI mode spectrum.

Intact thallus DART-MS analysis yielded a spectrum comprising signal patterns for divaricatic acid, thamnolic acid and usnic acid

in NI mode (Fig. S10; Tables S10 and S11). Thamnic acid occurrence on uncrushed material was only suggested through its alcohol moiety (m/z 169) in PI mode meanwhile all DART-MS landmark signals for this depside (Table 1) could be observed in NI mode. As expected, haemoventosin, the main colouring matter of apothecia was not detected in the thallus.

Analyses carried out on crushed thallus enabled *in situ* detection of the diagnostic compounds with ventosic acid and miriquidic acid in both ionisation modes (Fig. S11; Tables S12 and S13). This might suggest that these latter compounds are mainly located inside the thallus rather than on its surface.

Noteworthy is that PI- and NI-DART-MS spectra acquired from intact pieces of thallus look quite different whereas those obtained from crushed thallus appear to be rather comparable. Indeed, lichen samples are damaged during the course of DART-MS analyses, which requires analyses of two distinct samples to perform PI and NI acquisitions. Differences in chemical profiles might then be explained by the uneven distribution of metabolites within the thallus of *Ophioparma ventosa*. Conversely, grinding the thallus is presumed to average the chemical composition and limit differences between samples of powdered lichen. Given the thickness of *O. ventosa* thallus, we hypothesised that its compounds could be differentially partitioned in the depth of the lichen. This

assumption prompted an estimation of the localisation of *O. ventosa* metabolites using *in situ* DART-MS on a single piece of apotheciate thallus.

In situ estimation of metabolites distribution within *Ophioparma ventosa* thallus. Spatial localisation of metabolites of *Ophioparma ventosa* was evaluated by carefully shooting DART helium stream to the lower (0.2–0.5 min) and upper (0.6–0.9 min) faces of an apotheciate thallus. Both sides displayed different mass spectra, which could be acquired within a single minute analysis.

NI-DART mass spectra corresponding to those two faces are depicted in Fig. 7(A) and (B) (Tables S14 and S15) and reconstructed ion chromatograms associated with m/z values of species of interest are displayed in Fig. 7(C).

As expected, haemoventosin (m/z 305) could only be reported on the upper part of the lichen. Likewise, thamnic acid (m/z 375) was mostly detected from these superficial layers. Usnic acid could be observed in both upper and lower parts of the thallus. However, reconstructed ion chromatogram (at m/z 343) revealed that this compound mostly occurred in the upper layers of the thallus [Fig. 7(C)]. Divaricatic acid (m/z 195) mainly appeared on the spectrum of the inferior face of the lichen. Ventosic acid also seems to occur predominantly in the deepest layers of the lichen,

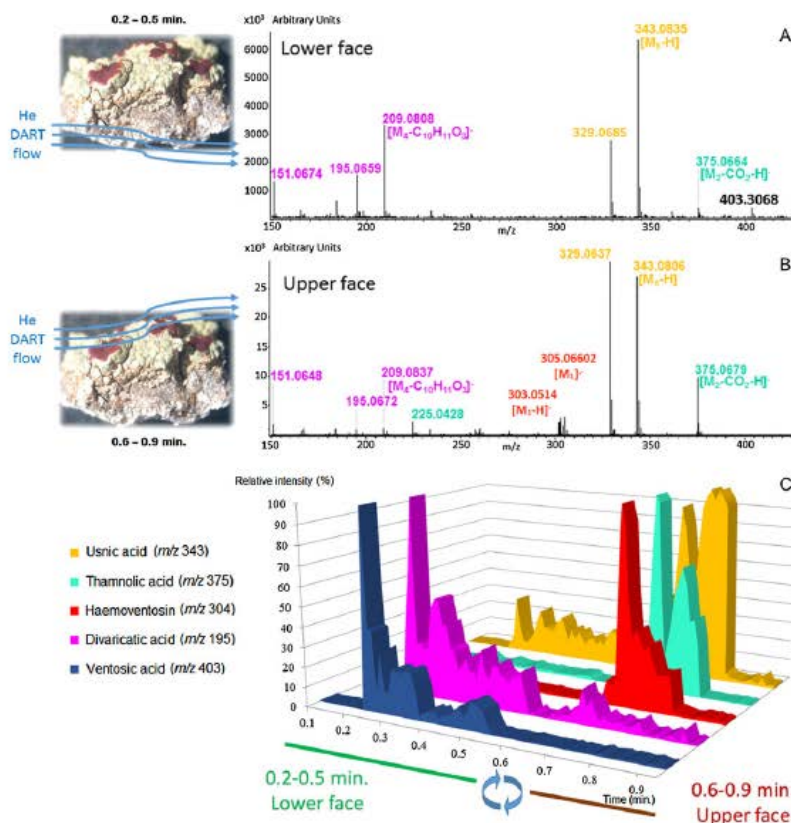


Figure 7. NI-DART-MS spectra of lower (A) and upper (B) faces of *Ophioparma ventosa* apotheciate thallus. Red = haemoventosin; blue = thamnic acid; purple = divaricatic acid; yellow = usnic acid. (C) *In situ* NI-DART-MS acquisition on a piece of intact apotheciate thallus of *O. ventosa* from lower face to upper face: reconstructed ion chromatograms for divaricatic, ventosic, thamnic, usnic acid and haemoventosin versus time.

In situ DART-MS analysis of the lichen *Ophioparma ventosa*

albeit also observed on PI-DART-MS of uncrushed apothecia. Non-detection of miriquidic acid might suggest its location within the depth of the lichen.

In the current study, the ambient DART ionisation process is first applied to the main classes of lichen polyphenolics. DART ionisation could detect all secondary metabolites described within the crustose lichen *Ophioparma ventosa*, encompassing the main structural classes of lichen polyketides. A further advantage of DART-MS is its ability to detect all these metabolites from a single ionisation mode, unlike ESI that requires joint analyses in both ionisation modes to get a complete insight into the chemistry of this lichen. Most mass spectra displayed prevalent protonated or deprotonated molecules enabling the straightforward identification of the compounds. Among tested compounds, only depsides underwent a significant fragmentation and their recurrent dissociation pathways in both ionisation modes should be regarded as an added value for their structural elucidation rather than a drawback.

Furthermore, this versatile analytical platform enabled reaching complete chemical profiles from raw pieces of *Ophioparma ventosa*, without any sample work-up. PI- and NI-DART-MS pinpointed the occurrence of miriquidic acid, a rare depside, here described for the first time within a sample of *O. ventosa*, supporting the adequacy of this device for dereplicative purposes in lichenology. As the chemical knowledge regarding natural substances increases, now encompassing about 1100 secondary metabolites, DART-MS can be considered as a refined dereplication procedure in lichenology. These findings widen the versatility of DART-MS in the more general field of phytochemistry.

In situ DART-MS spectra acquired from different parts of the lichen might shed light on the uneven distribution of metabolites within the thallus of *Ophioparma ventosa*. Since the spatial pattern of metabolites within lichens is presumed to reflect their ecological significance, such information shall advance the understanding of lichen biology. Regarding the specific example of *O. ventosa*, a follow-up study using proper tools of imaging MS is ongoing to get a sharp insight into the localisation of its metabolites.

Acknowledgements

This work was supported by the University of Rennes 1 through the project "Défi emergent LICHENMASS" and used the mass spectrometry facilities of the DReAM platform of IETR (Rennes). The authors are grateful to Dr. Sylvain Guyot (P2M2 platform, INRA, Rennes) for MS/MS analysis and to Aurélie Bernard for her technical assistance.

References

- Bouchoux G. 2013. From the mobile proton to wandering hydride ion: mechanistic aspects of gas-phase ion chemistry. *J Mass Spectrom* **48**: 505–518.
- Boustie J, Tomasi S, Grube M. 2011. Bioactive lichen metabolites: alpine habitats as an untapped source. *Phytochem Rev* **10**: 287–307.
- Cai Y, Mo Z, Rannulu NS, Guan B, Kannupal S, Gibb BC, Cole RB. 2010. Characterization of an exception to the 'even-electron rule' upon low-energy collision induced decomposition in negative ion electrospray tandem mass spectrometry. *J Mass Spectrom* **45**: 235–240.
- Chambers JQ. 1974. Electrochemistry of quinones. In *The chemistry of the quinonoid compounds*, Vol. 2, Patai S, Rappaport Z (eds.). Wiley: New York; 737–791.
- Cody RB, Laramée JA, Durst HD. 2005. Versatile new ion source for the analysis of materials in open air under ambient conditions. *Anal Chem* **77**: 2297–2302.
- Cody RB, McAlpin CR, Cox CR, Jensen KR, Voorhees KJ. 2015. Identification of bacteria by fatty acid profiling with direct analysis in real time mass spectrometry. *Rapid Commun Mass Spectrom* **29**: 1–6.

- Cooks RG, Ouyang Z, Takats Z, Wiseman JM. 2006. Ambient mass spectrometry. *Science* **311**: 1566–1570.
- Culbertson CF, Culbertson WL, Johnson A. 1977. Nonrandom distribution of an epiphytic *Lepraria* on two species of *Parmelia*. *Phytochemistry* **16**: 127–130.
- Culbertson CF, Culbertson WL, Johnson A. 1986. Two new lichen products, elatinic acid and methyl barbatale, from the genus *Haematomma* (Ascomycotina, Haematommataceae). *Mycologia* **78**: 888–891.
- Gross JH. 2014. Direct analysis in real time – a critical review on DART-MS. *Anal Bioanal Chem* **406**: 63–80.
- Holzmann G, Leuckert C. 1990. Applications of negative fast atom bombardment and MS/MS to screening of lichen compounds. *Phytochemistry* **29**: 2277–2283.
- Huneck S, Djerassi C, Becher D, Barber M, Von Ardenne M, Steinfelder K, Tümmler R. 1968. Flechteninhaltsstoffe—XXXI: Massenspektrometrie und ihre anwendung auf strukturelle und stereochemische probleme —CXXIII Massenspektrometrie von depsiden, depsidonen, depsonen, dibenzofuranen und diphenylbutadienen mit positiven und negativen ionen. *Tetrahedron* **24**: 2707–2755.
- Huneck S, Schmidt J. 1980. Phenolische Verbindungen einiger Flechten aus der Familie *Physciaceae*. *Biol Mass Spectrom* **7**: 301–308.
- Kristmundsdóttir T, Jónsdóttir E, Ógmundsdóttir HM, Ingólfssdóttir K. 2005. Solubilization of poorly soluble lichen metabolites for biological testing on cell lines. *Eur J Pharm Sci* **24**: 539–543.
- Le Pogam P, Herbet G, Boustie J. 2015a. Analysis of lichen metabolites: a variety of approaches. In *Recent Advances in Lichenology*, Vol. 2, Upreti DK, Divakar PK, Shukla V, Bajpai R (eds.). Springer: New Delhi; 229–261.
- Le Pogam P, Legouin B, Le Lamer AC, Boustie J, Rondeau D. 2015b. Analysis of the cyanolichen *Lichina pygmaea* metabolites using *in situ* DART-MS: from detection to thermochemistry of mycosporine serinol. *J Mass Spectrom* **50**: 454–462.
- Le Pogam P, Schinkovitz A, Legouin B, Le Lamer AC, Boustie J, Richomme P. 2015c. Matrix-free UV-laser desorption ionisation mass spectrometry as a versatile approach for accelerating dereplication studies on lichens. *Anal Chem* **87**: 10421–10428.
- Le Pogam P, Le Lamer AC, Siva B, Legouin B, Bondon A, Graton J, Jacquemin D, Rouaud I, Ferron S, Obermayer W, Babu KS, Boustie J. 2016. Minor pyranonaphthoquinones from the apothecia of the lichen *Ophioparma ventosa*. *J Nat Prod* **79**: 1005–1011.
- Li LP, Feng BS, Yang JW, Chang CL, Bai Y, Liu HW. 2013. Applications of ambient mass spectrometry in high-throughput screening. *Analyst* **138**: 3097–3103.
- Longevialle P. 1992. Ion-neutral complexes in the unimolecular reactivity of organic cations in the gas phase. *Mass Spectrom Rev* **11**: 157–192.
- May PF. 1997. *Ophioparma lapponica*: a misunderstood species. *Havv Pap Bot* **2**: 213–228.
- Musharaf SG, Kanwal N, Thadhani VM, Choudhary MI. 2015. Rapid identification of lichen compounds based on the structure-fragmentation relationship using ESI-MS/MS analysis. *Anal Methods* **7**: 6066–6076.
- Parrot D, Jan S, Baert N, Guyot S, Tomasi S. 2013. Comparative metabolite profiling and chemical study of *Ramalina siliquosa* complex using LC-ESI-MS/MS approach. *Phytochemistry* **89**: 114–124.
- Rycroft DS, Connolly JD, Huneck S, Himmelreich U. 1995. Revised structure of haemovosin. *Z Naturforsch B* **50**: 1557–1563.
- Shukla V, Joshi GP, Rawat MSM. 2010. Lichens as a potential natural source of bioactive compounds: a review. *Phytochem Rev* **9**: 303–314.
- Sica VP, Raja HA, El-Elmat T, Oberlies NH. 2014. Mass spectrometry imaging of secondary metabolites directly on fungal cultures. *RSC Adv* **4**: 63221–63227.
- Skult H. 1997. Notes on the chemical and morphological variation of the lichen *Ophioparma ventosa* in East Fennoscandia. *Ann Bot Fenn* **34**: 291–297.
- Song L, Gibson SC, Bhandari D, Cook KD, Bartmess JE. 2009. Ionization mechanism of positive-ion direct analysis in real time: a transient micro-environment concept. *Anal Chem* **81**: 10080–10088.
- Zhou M, McDonald JF, Fernández FM. 2010. Optimization of a direct analysis in real time/time-of-flight mass spectrometry method for rapid serum metabolomic fingerprinting. *J Am Soc Mass Spectrom* **21**: 68–75.

Supporting information

Supporting information can be found in the online version of this article.

Lors de l'étude phytochimique d'*Ophioparma ventosa*, il est apparu que ses apothécies concentraient plusieurs pigments tandis que la littérature ne fait état que d'un seul, l'haemoventosine, même si différents articles avaient déjà décrit la présence de pigments non identifiés et présents à l'état de traces dans les organes reproducteurs d'*Ophioparma ventosa* (Rycroft et al., 1995). Sur la base de ce constat, une étude phytochimique des seules apothécies du lichen a été engagée et s'est soldée par l'isolement de six naphthoquinones, dont l'haemoventosine. Pour les cinq autres quinones, l'une d'entre elles, l'anhydrofusarubine lactone est ici décrite pour la première fois chez un lichen tandis que les quatre autres correspondent à de nouvelles structures : l'ophioparmine, deux épimères de la 4-hydroxyhaemoventosine et un isomère de la 4-hydroxyhaemoventosine dont la stéréochimie n'a pas pu être complètement établie (Figure 19). Ces travaux ont été réalisés en collaboration avec le Dr. Bandi Siva, doctorant en chimie à l'époque qui avait été accueilli à Rennes d'avril à juin 2014 (sous la direction du Dr. Suresh K. Babu) dans le cadre du LIA Franco-Indien. Les modélisations de dichroïsme circulaire ont quant à elles été réalisées par le Dr. Jérôme Gratton et le Pr. Denis Jacquemin (CEISAM, Nantes).

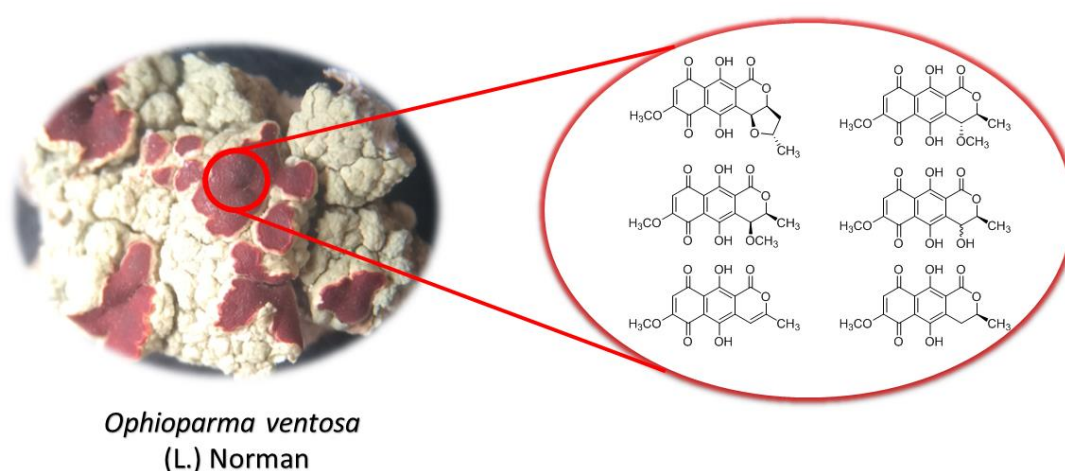


FIGURE 19: NAPHTOQUINONES ISOLÉES AU COURS DE L'ÉTUDE PHYTOCHIMIQUE MENÉE SUR LES APOTHÉCIES D'*OPHIOPARMA VENTOSA*

Cette étude phytochimique et l'élucidation structurale de ces nouvelles structures est décrite au titre d'un article paru dans *Journal of Natural Products* en 2016. Son *supporting material* peut être consulté en Annexe 5 (p. 234).

Minor Pyranonaphthoquinones from the Apothecia of the Lichen *Ophioparma ventosa*

Pierre Le Pogam,[†] Anne-Cécile Le Lamer,^{*,†,‡} Bandi Siva,[§] Béatrice Legouin,[†] Arnaud Bondon,[⊥] Jérôme Graton,^{||} Denis Jacquemin,^{||,∇} Isabelle Rouaud,[†] Solenn Ferron,[†] Walter Obermayer,[¶] K. Suresh Babu,[§] and Joël Boustie^{*,†}

[†]UMR CNRS 6226 ISCR PNSCM, Université de Rennes 1, 2 Avenue du Professeur Léon Bernard, 35043 Rennes, France

[‡]Université Paul Sabatier Toulouse 3, 118 Route de Narbonne, 31062 Toulouse, France

[§]Division of Natural Products Chemistry CSIR, Indian Institute of Chemical Technology, Uppal Road, Hyderabad 500607, India

[⊥]UMR CNRS 6226 ISCR ICMV, Université de Rennes 1, Plate-forme PRISM, CS 34317, 35043 Rennes, France

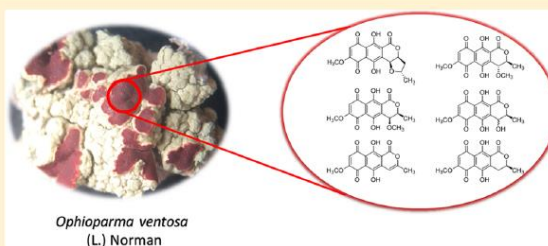
^{||}UMR CNRS 6230, Chimie et Interdisciplinarité: Synthèse, Analyse et Modélisation (CEISAM), Université de Nantes, 2 Rue de la Houssinière, BP 92208, 44322 CEDEX 3 Nantes, France

[∇]Institut Universitaire de France, 1 Rue Descartes, 75231 CEDEX 05 Paris, France

[¶]Institut für Pflanzenwissenschaften, Karl-Franzens-Universität, Holteigasse 6, A-8010 Graz, Austria

Supporting Information

ABSTRACT: Four new quinonoid naphthopyranones, ophioparmin (1), 4-methoxyhaemoventosins (2a and 2b), and 4-hydroxyhaemoventosin (3), together with anhydrofusarubin lactone (4) and haemoventosin (5) were isolated from the fruiting bodies of *Ophioparma ventosa*, a crustose lichen. Their structures were determined by spectroscopic analyses, and the absolute configurations of 1 and 2 were elucidated through experimental and calculated electronic circular dichroism analyses. Compounds 1, 2, and 5 exhibited moderate to strong antioxidant activities. The main pigment haemoventosin exhibited significant cytotoxicity toward a panel of nine cell lines.



Lichens are resilient symbiotic consortia that consist of a fungus and an algal/cyanobacterial partner. As a consequence of this original lifestyle, specific secondary metabolites are produced, and the ever-expanding array of lichen metabolite bioactivities warrants further chemical investigations of these fascinating organisms.¹ Lichens of alpine and polar habitats are of interest because their ability to withstand such stressful conditions is often based on the synthesis of protective compounds.² A focused study on differentiated organs such as apothecia, which represent less than 2% of the thallus weight, is thought to not only facilitate the isolation of minor and specific compounds but also provide a better indication of their ecological significance.

As such, the crustose Alps mountain-living lichen *Ophioparma ventosa* (L.) Norman has been phytochemically investigated by several authors and reported to contain depsides (mainly divaricatic and thamnolic acids), dibenzofuran-related usnic acid, a tetrahydroxyfatty acid (ventosic acid) and some additional compounds, such as psoromic, stictic, and norstictic acids and atranorin, among others.^{3,4} Regarding the intense blood-red color of *O. ventosa* apothecia, Bruun and Lamvik first reported the isolation of its major pigment,

haemoventosin, but they assigned an erroneous furanonaphthoquinone structure.⁵ The correct pyranonaphthoquinone structure of haemoventosin was assigned in 1995.⁶ Several authors reported on the presence of “numerous” minor pigments most likely corresponding to additional quinones,^{4,6} without identifying any of these. Naphthoquinones are a privileged class of secondary metabolites that exhibit a wide range of biological activities, predominantly cytotoxic or antibacterial properties;⁷ however, the biological properties of haemoventosin have not yet been investigated.

The significant cytotoxic and antioxidant activities of the pigment-enriched fraction prompted an undertaking of chemical investigations of the pigments of *Ophioparma ventosa* apothecia. Herein, based on (+)-HRESIMS dereplication of this quinone-enriched fraction, the isolation and structural elucidation of four new quinonoid naphthopyranones, namely, ophioparmin (1), 4-methoxyhaemoventosins (2a and 2b), and 4-hydroxyhaemoventosin (3), are reported. Two known naphthazarinopyranones, anhydrofusarubin lactone (4) and

Received: December 4, 2015

Published: March 2, 2016

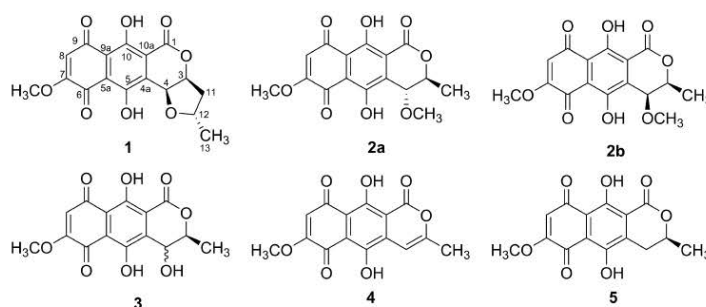


Figure 1. Structures of compounds 1–5.

 Table 1. ^1H (500 MHz) and ^{13}C (125 MHz) NMR Data for 1–3 (CDCl_3)

position	ophioparmin (1)		4-methoxyhaemoventosin (2)			4-hydroxyhaemoventosin (3)	
	δ_{C} , type	δ_{H} , mult. (J in Hz)	δ_{C} , type	δ_{H} , mult. (J in Hz)	δ_{H} , mult. (J in Hz)	δ_{C} , type	δ_{H} , mult. (J in Hz)
1	ND		159.0			157.9	
3	81.7	5.18, dd (4.0, 2.9)	76.5	5.05 dq (7.0, 1.5)	4.54, dq (6.5, 1.5)	74.2	5.14, q (6.9)
4	66.9	5.31, d (2.9)	69.8	4.71 d (1.5)	4.66, d (1.5)	39.2	3.93, s
4-OCH ₃	-	-	57.5	3.46, s	3.46, s		
4a	136.7		136.8			137.9	
5	153.7		153.6			153.3	
5-OH	-	12.29	-	12.25, s	12.29, s	-	11.81, s
5a	115.4		115.4			114.4	
6	188.0		187.6			188.3	
7	160.9		160.2			160.5	
7-OCH ₃	56.8	3.97, s	57.4	3.97, s	3.96, s	56.8	3.90, s
8	111.6	6.25, s	112.5	6.26, s	6.25, s	111.2	6.17, s
9	184.1		183.8			183.6	
9a	113.2		112.7			111.9	
10	156.7		156.2			156.4	
10-OH	-	13.66	-	13.51, s	13.53, s	-	13.52, s
10a	122.1		122.9			123.7	
11 α	41.6	2.00, ddd (14.0, 9.8, 4.0)	18.0	1.28, d (7)	1.62, d (6.5)	19.6	1.35, d (6.9)
11 β		2.67, dd (14.0, 5.5)					
12	76.6	4.60, m					
13	20.6	1.41, d (6)					

(+)-haemoventosin (5), are also described, the former being new to lichens. Owing to the minute amounts of compounds isolated, only 1, 2, and 5 could be assayed for their antioxidant properties. The major pigment, 5, was tested for its *in vitro* inhibition of cell proliferation against a panel of nine different cell lines.

RESULTS AND DISCUSSION

The CH_2Cl_2 extract of the apothecia of *O. ventosa* was washed with a cyclohexane/EtOAc mixture (9/1) to afford a pigment-enriched fraction. The naphthopyranone composition of this fraction was revealed by direct infusion (+)HRESIMS analysis. Indeed, due to their strong chemical homologies, the different dyes could not be separated by HPLC. Accurate mass measurements derived from the most intense ions observed in the mass spectrum (Figure S1, Supporting Information) are collated in Table S2 (Supporting Information). All experimental values were compared with the theoretical mass calculated in an error range of ± 5 ppm from candidate compositions consistent with a quinonoid naphthopyranone core encompassing $\text{C}_{12-20}\text{H}_{10-20}\text{O}_{5-10}$. Eight molecular for-

mulas could be retrieved, among which only haemoventosin⁶ was previously reported from *O. ventosa*.

On the basis of the significant cytotoxic and antioxidant properties of this naphthoquinone-enriched fraction, successive fractionations were performed, including silica gel chromatography and preparative TLC, affording compounds 1, 3, anhydrofusarubin lactone (4), and haemoventosin (5). A second sample of *O. ventosa* was processed, which permitted the identification of the new naphthopyranones 2a and 2b as a mixture of diastereoisomers (Figure 1).

Compound 1 was obtained as an amorphous red powder. The ^{13}C NMR and (+)HRESIMS data established a molecular formula of $\text{C}_{17}\text{H}_{14}\text{O}_8$, consistent with a naphthopyrone derivative, and the UV spectrum of 1 showed absorption maxima at 233, 285, and 501 nm, similar to those of haemoventosin 5. The ^1H NMR and HSQC spectra revealed two hydrogen-bonded hydroxy groups at δ_{H} 13.66 and 12.29; one aromatic proton at δ_{H} 6.25 (1H, s, H-8); three oxygenated methine signals at δ_{H} 5.31 (1H, d, $J = 2.9$ Hz, H-4), 5.18 (1H, dd, $J = 4.0, 2.9$ Hz, H-3), and 4.60 (1H, m, H-12); two diastereotopic methylene hydrogens at δ_{H} 2.67 (1H, dd, $J =$

14.0, 5.5 Hz, H-11 β) and 2.00 (1H, ddd, $J = 14.0, 9.8, 4.0$ Hz, H-11 α); one aromatic methoxy singlet at δ_{H} 3.97 (3H, s, 7-OCH₃); and one aliphatic methyl group at δ_{H} 1.41 (3H, d, $J = 6$ Hz, H-13). These data combined with the ¹³C NMR data obtained from HSQC and HMBC correlations were reminiscent of those of haemoventosin **5** (Table 1). The main difference was the presence of two additional coupled oxygenated methines at $\delta_{\text{H}}/\delta_{\text{C}}$ 5.31/66.9 (H-4) and $\delta_{\text{H}}/\delta_{\text{C}}$ 5.18/81.7 (H-3). HSQC-TOCSY correlations revealed that H-3, H-4, and H-11–H-13 belonged to the same spin system, and the sequence CH₃-13/CH-12/CH₂-11/CH-3/CH-4 could be deduced from cross peaks in the COSY spectrum. HMBC correlations of H-4 with C-5, C-4a, and C-10a showed that C-4 was adjacent to the naphthazarin moiety. The deshielding of H-3 and H-4 and the 11 indices of hydrogen deficiency suggested the presence of a dihydrofurano-fused α -pyrone system to fulfill the molecular formula requirements, although a shortage of material prevented the detection of the α -pyrone carbonyl.^{8–12} Note that the HMBC spectrum did not reveal the H-3 to C-1 cross peak characteristic of a δ -lactone ring. An overview of the spectroscopic behavior of related structures such as lasionectrin;⁸ lichenicolin A;⁹ pentacecillides A, B, and C;¹³ or dihydroisocoumarins¹⁴ revealed that none of them displayed this key correlation. This correlation is also absent from the HMBC spectrum of haemoventosin **5**. In addition, the HMBC spectrum did not reveal any cross-peak between H-4 and H-12, but HMBC correlations between analogous positions in molecules displaying the same fused α -pyrone/tetrahydrofuran substructure are also often lacking (e.g., the isocoumarin series, exserolides A–E,¹⁰ and 11-hydroxy-monocerin¹¹), thus being consistent with the presence of the tetrahydrofuran ring. On the basis of these aforementioned data, the 2D structure of compound **1** was established as depicted in Figure 1. This dihydrofurano-fused α -pyrone system has been reported for a limited number of naphthopyranones,¹⁵ for example, lasionectrin^{8,16} and lichenicolins A and B.⁹ Its fusion with a naphthazarin core is described here for the first time.

Regarding the relative configuration of **1**, NOESY correlations of H-11 α (δ_{H} 2.00) with H-3, H-4, and CH₃-13 showed that these protons and the methyl group are cofacial. The ³ $J_{3,4}$ value of 2.9 Hz is consistent with that described for related compounds having a *cis* junction of the tetrahydrofuran-fused α -pyrone moiety, whereas compounds having a *trans* junction show a lower value.¹⁰ The NOESY correlation between H-11 β (δ_{H} 2.67) and H-12 confined these protons to the opposite face of the tetrahydrofuran ring (Figure 2).

The (3*S*, 4*S*, 12*S*) absolute configuration of **1**, ophioparmin, was subsequently assigned based on a comparison between the

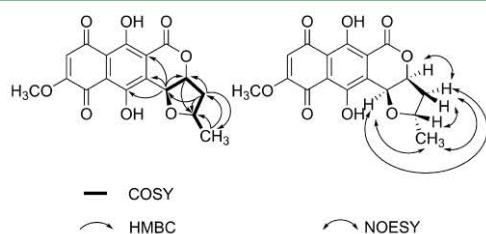


Figure 2. Key COSY (bold bonds, left) and HMBC (¹H → ¹³C) (arrows, left) and key NOESY correlations (double-headed arrows, right) of compound **1**.

calculated (TDDFT) and experimental electronic circular dichroism (ECD) spectra (Figure 3).

The ¹H NMR spectrum of compound **2**, with a molecular formula of C₁₆H₁₄O₈, exhibited many signals analogous to that of compound **5**, but rather than the diastereotopic methylene protons, the spectrum revealed the presence of a second oxygenated methine at δ_{H} 4.71 (1H, d, $J = 1.5$ Hz, H-4) and an aliphatic methoxy group at δ_{H} 3.46 (3H, s, 4-OCH₃) (Table 1). Key HMBC correlations of H-4 with C-4a and C-10a and of 4-OCH₃ with C-4 defined the position of this aliphatic methoxy group at C-4 (Figure 4). The comparison between the calculated and experimental ECD spectra facilitated the identification of **2** as (3*S*,4*R*)-4-methoxyhaemoventosin (Figure 3).

The ¹H NMR spectrum of compound **2** revealed that most of the signals were duplicated to yield minor peaks that overlap more or less completely with the major ones. Two signals are notably modified: the aliphatic methyl group CH₃-11, which was shifted upfield (δ_{H} 1.28 to 1.62), whereas the oxygenated methine H-3 was shielded in the minor form (δ_{H} 5.05 to 4.54) with identical coupling constants. Because the peak associated with the methine H-4 was also slightly shifted (δ_{H} 4.71 for **2a** vs 4.66 for **2b**), compound **2** was hypothesized to be a mixture of diastereoisomers with the major form **2a** (as suggested from the ECD data of the mixture) and the minor form **2b** in a 2:1 ratio. Overlapping signals arising from the common scaffold of **2a** and **2b** prevented the determination of ¹³C NMR data related to the minor compound **2b**. The ECD data of a diastereoisomeric mixture can still provide valuable information, particularly when the calculated ECD spectrum shows an excellent fit with the experimental spectrum of the mixture, as in Figure 3C. Because each component contributes to the overall electronic circular dichroism spectrum with a weight comparable to its molar fraction, the entire spectrum is expected to reflect that of the predominant compound.¹⁷ A proof-of-principle study established the reliability of ECD data on an epimeric mixture through the example of tetracyclin and 4-epitetracyclin.¹⁸ Regarding the identical vicinal coupling constants for H-3 and H-4 between **2a** and **2b**, NMR studies in related dihydro-2-pyrone indicated that small values of the vicinal coupling between H-3 and H-4 suggest a synclinal (*gauche*) effect but do not allow distinction between the *cis* (axial–equatorial) and *trans* (equatorial–equatorial) orientations of H-3 and H-4, only excluding a *trans*-diaxial arrangement of these protons.^{19–21} This further supported the hypothesis of two diastereoisomers, suggesting that **2b** might represent a 3,4-*cis* isomer. Considering the identical configurations of C-3 in **1**, **2a**, and **5** and assuming that oxidation at C-4 occurs after cyclization during the biosynthesis process,²² **2b** is hypothesized to correspond to (3*S*,4*S*)-4-methoxyhaemoventosin. This hypothesis is further supported by the interpretation of the ¹H NMR chemical shift differences of the oxygenated methine and the aliphatic methyl of the two isomers. Indeed, signals located in the shielding zone of the benzene ring are located in an axial or axial-like position (CH₃-11 in **2a** and H-3 in **2b**), whereas deshielded signals refer to moieties located in an equatorial position (CH₃-11 in **2b** and H-3 in **2a**), as assessed on closely related systems.²³ Given the impossibility of an axial/axial configuration due to the low magnitude of the vicinal coupling constant between H-3 and H-4, the axial position of H-3 implies the equatorial position of H-4, thus confirming the 3,4-*cis* configuration of **2b**.

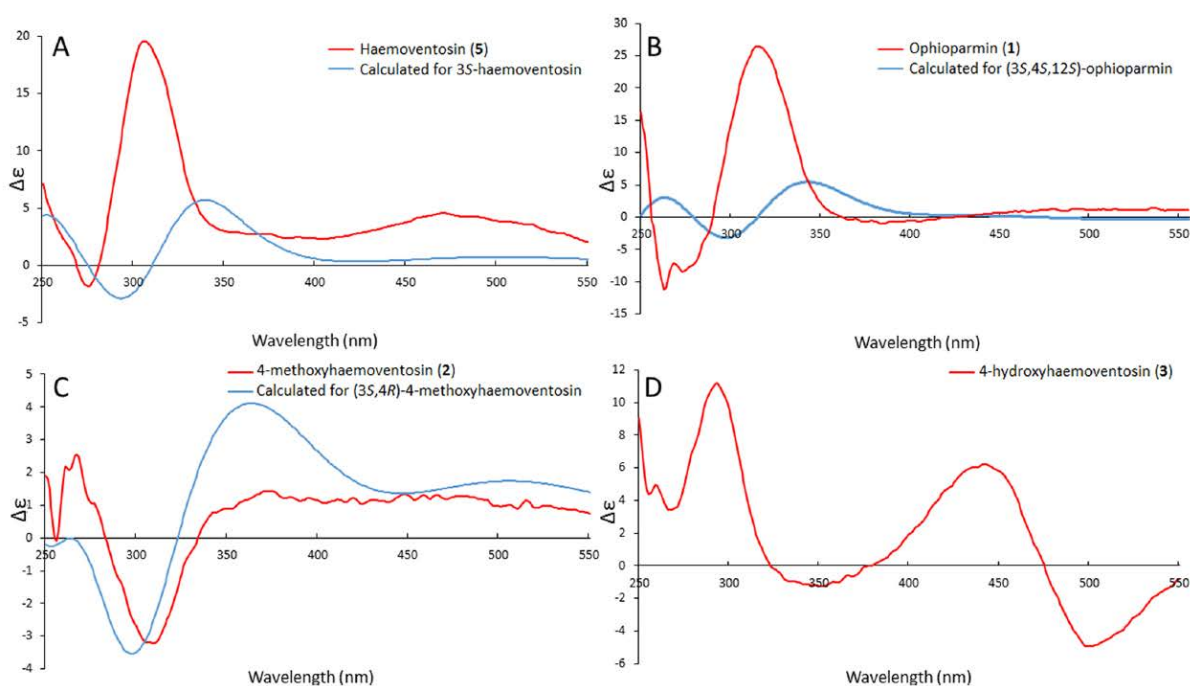


Figure 3. Comparison of the experimental ECD spectra of 1 (B), 2 (C), and 5 (A) and calculated ECD spectra for the stereoisomers shown in Figure 1. Experimental ECD spectrum of 3 (D).

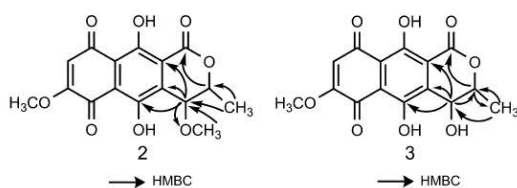


Figure 4. Diagnostic HMBC correlations ($^1\text{H} \rightarrow ^{13}\text{C}$) of compounds 2 and 3.

Compound 3 could be assigned a molecular formula of $\text{C}_{15}\text{H}_{12}\text{O}_8$, which differs from haemoventosin 5 by an additional oxygen atom. Their ^1H NMR spectra exhibited close similarities, but that of 3 lacked the diastereotopic methylene signals of haemoventosin 5, which were replaced by an oxygenated methine (δ_{H} 3.93), suggesting the replacement of one diastereotopic proton by a hydroxy group (Table 1). Indeed, HMBC correlations between H-4 and C-3, C-4a, C-5, and C-10a validated the C-4 location of this hydroxy group

(Figure 4), and compound 3 was thus identified as 4-hydroxyhaemoventosin.

The absolute configuration of 3 could not be established through comparison between the calculated and experimental ECD spectra, which provided no clear-cut match, irrespective of the absolute configuration used in TDDFT. The chemical shifts of the oxygenated methine and the aliphatic methyl, reminiscent of that of 2a, indicated the equatorial position of H-3. The positive Cotton effect observed at approximately 260 nm in the ECD spectrum can be correlated to the P-helicity of the heterocyclic ring (Figure 3).²⁴ Collectively, these results suggested the 3S-configuration, which is shared with the metabolites described herein. Assuming the H-3 α_{eq} orientation of 3, either a *trans* H-3 α_{eq} – H-4 β_{eq} or a *cis* H-3 α_{eq} – H-4 α_{ax} might account for the absence of coupling between H-3 and H-4, hence precluding the assignment of the C-4 configuration.

Compound 4 was identified as anhydrofusarubin lactone on the basis of its ^1H and ^{13}C NMR data.^{25,26} This naphthoquinone was previously isolated from the phytopatho-

Table 2. Cytotoxicity Against Cultured Cell Lines (IC_{50}) and Antioxidant Activity Results

tested compound or fraction	cytotoxic activity		antioxidant activity	
	B16	HaCaT	DPPH	NBT
pigment fraction	$6.30 \pm 0.8 \mu\text{g mL}^{-1}$	$3.30 \pm 0.8 \mu\text{g mL}^{-1}$	$>500 \mu\text{g mL}^{-1}$	$8.30 \pm 1.4 \mu\text{g mL}^{-1}$
1	$>10 \mu\text{M}$	$>10 \mu\text{M}$	-	$49.90 \pm 4.0 \mu\text{M}$
2	-	-	-	$6.10 \pm 1.2 \mu\text{M}$
5	$2.40 \pm 0.4 \mu\text{M}$	$14.20 \pm 1.0 \mu\text{M}$	$>500 \mu\text{g mL}^{-1}$	$1.90 \pm 0.4 \mu\text{M}$
doxorubicin	$0.43 \pm 0.13 \mu\text{M}$	$0.53 \pm 0.07 \mu\text{M}$	-	-
vincristine	$0.50 \pm 0.35 \mu\text{M}$	$0.65 \pm 0.20 \mu\text{M}$	-	-
gallic acid	-	-	$7.20 \pm 0.3 \mu\text{g mL}^{-1}$	-
ascorbic acid	-	-	-	$22.10 \pm 7.1 \mu\text{M}$

genic fungus *Fusarium solani*, but this is its first report from a lichen, even though closely related molecules such as fusarubin, anhydrofusarubin lactol, and coronatoquinone are all known from lichen sources.^{27–29} Compound **5** was identified as (+)-haemoventosin by comparison of its ¹H and ¹³C NMR data and optical activity with an earlier report on the structural reassessment of this compound.⁶

The cytotoxicity of the pigment-enriched fraction was investigated against B16 murine melanoma and HaCaT human keratinocyte cell lines, revealing significant cytotoxic activities with respective IC₅₀ values of 6.3 ± 0.8 μg mL⁻¹ and 3.3 ± 0.8 μg mL⁻¹. This semipurified extract exhibited strong antioxidant properties via an NBT test with an IC₅₀ value of 8.3 ± 1.4 μg mL⁻¹ compared to that of ascorbic acid used as a positive control (3.8 ± 1.2 μg mL⁻¹). Owing to a shortage of material, only **1** and **5** could be evaluated for their cytotoxicity (Table 2). Only the latter exhibited a significant cytotoxicity, which prompted a further study of its bioactivity on seven other cell lines. Compound **5** exhibited significant cytotoxic activity toward all cell lines, with IC₅₀ values ranging from 3 to 10 μM (Figure S20, Supporting Information).

Compounds **1**, **2**, and **5** were tested for radical-scavenging activity against superoxide anion (O₂^{-•}), and compound **5** was also tested against 2,2-diphenyl-1-picrylhydrazyl (DPPH) radicals. No compounds or fractions exhibited activity during a DPPH assay (IC₅₀ > 3000 μM), which may be explained by the intramolecular hydrogen bonds between phenolic hydroxy groups and quinone moieties of all the structures described herein.³⁰ As superoxide anion scavengers, compound **1** exhibited moderate activity, with an IC₅₀ value of 50 ± 4 μM, whereas compounds **2** and **5** both exhibited stronger activities than that of ascorbic acid used as a positive control (Table 2).

In summary, new minor quinonoid naphthopyranones ophioparmin (**1**), 4-methoxyhaemoventosins (**2a** and **2b**) and 4-hydroxyhaemoventosin (**3**), as well as the known anhydrofusarubin lactone (**4**) and haemoventosin (**5**), were isolated from the apothecia of the lichen *O. ventosa*. Compounds **1**, **2**, and **5** exhibit moderate to strong antioxidant activities, and **5** exhibits a significant cytotoxic effect against a panel of nine cell lines. These pigments appear to be exclusively located in the fruiting bodies of the lichen, and ongoing mass spectrometric imaging should support this assumption. Reproductive structures are often reported to produce other lichen compounds than the remaining thallus³¹ or known to be more concentrated in phenols compared to somatic tissues.³² This is consistent with the optimal defense theory that predicts the allocation of defensive compounds to structures that are the most valuable for the fitness of the organism. Regarding the specific example of *O. ventosa*, the presence of such quinones might account for the atypical bacterial communities sheltered by its apothecia, selecting bacterial strains that are able to withstand such a cytotoxic mixture.³³ Because these molecules concentrate at the surface of the fruiting bodies, their spreading at the surface of the spores might be beneficial to outcompete other microorganisms. Finally, these compounds might act as antioxidant and UV screening filters to protect spores during their maturation within asci.

EXPERIMENTAL SECTION

General Experimental Procedures. Optical rotations were recorded using a PerkinElmer 341 automatic polarimeter at 293 K at the sodium line; [α]_D are given in 10⁻¹ deg·cm⁻².

Electronic circular dichroism and corresponding UV–visible spectra were recorded using a Jasco J-815 ECD spectrometer. 1D and 2D NMR spectra were recorded in CDCl₃ using a 500 MHz spectrometer equipped with a TCI cryoprobe at the PRISM core facility (Rennes, France). HRMS data on the quinone-enriched fraction were measured using a Thermo Fisher Scientific Q Exactive equipped with an ESI source by direct injection at a rate of 400 nL·min⁻¹ at the CRMPO (Centre Régional de Mesures Physiques de l'Ouest, Rennes 1), and the measurements were performed in positive-ion mode. Analytical grade solvents for extraction and chromatography were purchased from VWR International (Pennsylvania, USA). Open column chromatography was performed on silica gel (40–63 μm, Kieselgel, Merck) in normal phase and at atmospheric pressure. The preparative TLC plates used for purification were glass backed (20 × 20 cm) and normal phase silica plates (250 μm thickness) purchased from Macherey-Nagel (Düren, Germany). Solutions were applied to the preparative plate at 12 mm from the lower edge using an automatic TLC sampler III device (Camag, Muttenz, Switzerland) as streaks with a 160 mm length. The preparative TLCs were developed in dedicated solvent systems, and the plates were allowed to fully air-dry prior being rerun in the same solvent system. Migrations were thus repeated until a good separation could be achieved between the closely related naphthopyranones. Subsequently, the silica was scraped off the plate, and the band of interest was desorbed in CH₂Cl₂/MeOH (95/5) three times (30 min each).

Plant Material. Two samples of *Ophioparma ventosa* were harvested for this study:

- Sample 1 was harvested in Tyrol (Austria), 500 m south of Obergurgl (elevation 1800–1850 m). The lichen was collected and identified by one of the authors (J.B.) in 04/2009. A voucher specimen was deposited at the herbarium of PNSCM laboratory with the reference JB/09/158.
- Sample 2 was harvested in Styria (Austria) at the south of the lake Großer Winterleitensee (elevation 1950–2000 m). The specimen was collected and identified by one of the authors (W.O.) in 09/2014. A voucher specimen (No. 13218a) was deposited at the herbarium GZU.

Extraction and Purification of Compounds. Out of 100 g of thallus, the meticulous dissection of *O. ventosa*'s apothecia from sample 1 yielded 1 g of apothecia that was powdered and extracted with CH₂Cl₂ (4 × 10 mL, 4 h) to afford a total of 100 mg of extract. This raw extract was washed three times with a 9:1 mixture of cyclohexane/EtOAc to afford 40 mg of a naphthoquinone-enriched fraction. This fraction was subsequently chromatographed on silica gel using a cyclohexane/EtOAc/CH₂Cl₂/MeOH gradient system (1:0:0:0 to 0:0:1:1 via 0:1:0:0) to yield seven fractions (F1–F7). Fraction F7 (20 mg), which was primarily composed of naphthazarin pigments, was selected for further purification using column chromatography based on a CH₂Cl₂/MeOH (1:0 to 7:3), affording five subfractions (F71 to F75). Subfraction F74 (8 mg) was subjected to a preparative TLC in a toluene/EtOAc/formic acid (70/25/5) solvent system. Five consecutive runs were required to achieve a proper separation of the compounds. Three bands were desorbed from this plate, affording anhydrofusarubin lactone (**4**) (1 mg), haemoventosin (**5**) (1.8 mg), and ophioparmin (**1**) (0.4 mg). Subfraction F75 (6 mg) was also subjected to preparative TLC in CH₂Cl₂/

EtOAc/formic acid (88/10/2), and the plate was developed twice. This second plate yielded 0.4 mg of 4-hydroxyhaemovosin (2).

Likewise, 1.1 g of apothecia could be recovered from sample 2. Apothecia were ground using a mortar and pestle prior to extracting the powdered material with CH_2Cl_2 (4×10 mL) at room temperature for 4 h.

The different extracts were combined to yield a total mass of 115 mg, which was subjected to silica gel column chromatography using a cyclohexane/EtOAc/ CH_2Cl_2 /MeOH gradient system (8:2:0:0 to 0:0:1:1) to yield five main fractions (F'1-F'5). Fraction F'4 (20 mg) was separated by preparative TLC using the same protocol as described earlier for fraction F74 on the basis of its observed similarities with the latter. Owing to the higher weight of this fraction, the material was applied to three TLC plates. After five runs each, these plates afforded a total of 6 mg of haemovosin (5) and 0.2 mg of ophioparmin (1). Three successive preparative TLC runs from fraction F'5 (4.5 mg) in a toluene/EtOAc/formic acid (70/25/5) solvent system afforded 0.7 mg of 4-methoxyhaemovosin (2).

Ophioparmin (1). Red amorphous powder. UV (MeCN), λ_{max} (log ϵ) 233 (4.57), 285 (4.23), 501 (4.02); ECD ($c = 0.9$ mM, MeCN) λ_{max} ($\Delta\epsilon$) 258 (−11.21), 311 (26.38); ^1H NMR and ^{13}C NMR data, see Table 1; (+)-HRESIMS m/z 369.05830 $[\text{M} + \text{Na}]^+$ (calcd for $\text{C}_{17}\text{H}_{14}\text{O}_8\text{Na}$, 369.05809).

4-Methoxyhaemovosins (2a, 2b). Red amorphous powder. UV (MeCN), λ_{max} (log ϵ) 231 (3.50), 291 (3.05), 501 (2.97); ECD ($c = 0.5$ mM, MeCN) λ_{max} ($\Delta\epsilon$) 267 (2.55), 309.5 (−3.20), 374.0 (1.44); ^1H NMR and ^{13}C NMR data, see Table 1; (+)-HRESIMS m/z 357.0580 $[\text{M} + \text{Na}]^+$ (calcd for $\text{C}_{16}\text{H}_{14}\text{O}_8\text{Na}$, 357.05809).

4-Hydroxyhaemovosin (3). Red amorphous powder. UV (MeCN), λ_{max} (log ϵ) 228 (3.31), 289 (2.90), 490 (2.72); ECD ($c = 0.5$ mM, MeCN) λ_{max} ($\Delta\epsilon$) 267.5 (3.42), 293.5 (11.17), 352 (−1.24), 441.5 (+6.24), 499.5 (−4.97); ^1H NMR and ^{13}C NMR data, see Table 1; (+)-HRESIMS m/z 343.04240 $[\text{M} + \text{Na}]^+$ (calcd for $\text{C}_{15}\text{H}_{12}\text{O}_8\text{Na}$, 343.04244).

Anhydrofusarubin lactone (4). Purple amorphous powder. ^1H NMR (CDCl_3 , 500 MHz): 14.22 (1H, s, OH-10), 12.78 (1H, s, OH-5), 6.85 (1H, s, H-4), 6.32 (1H, s, H-8), 3.97 (3H, s, OMe-7), 2.38 (3H, s, Me-11). ^{13}C NMR (CDCl_3 , 500 MHz): 184.8 (C-6), 180.5 (C-9), 162.7 (C-3), 160.8 (C-10), 160.0 (C-7), 155.2 (C-5), 141.4 (C-4a), 114.0 (C-10a), 113.4 (C-5a), 111.4 (C-8), 108.1 (C-9a), 98.2 (C-4), 57.0 (OMe-7), 20.6 (C-11); (+)-HRESIMS m/z 325.03200 $[\text{M} + \text{Na}]^+$ (calcd for $\text{C}_{15}\text{H}_{10}\text{O}_7\text{Na}$, 325.03187).

Haemovosin (5). Red bronze-shimmering amorphous powder. $[\alpha]_{\text{D}}^{20} + 550$ (c 0.02, CH_2Cl_2). UV (MeCN), λ_{max} (log ϵ) 232 (3.40), 293 (2.97), 501 (2.88); ECD ($c = 0.7$ mM, MeCN) λ_{max} ($\Delta\epsilon$) 276 (−1.76), 306.5 (20.31), 489 (4.22); ^1H NMR (CDCl_3 , 500 MHz): 13.70 (1H, s, OH-10), 12.25 (1H, s, OH-5), 6.23 (1H, s, H-8), 4.60 (1H, m, H-3), 3.97 (3H, s, OMe-7), 3.35 (1H, dd, $J = 17.5$, 3 Hz), 2.73 (1H, dd, $J = 17.5$, 11 Hz, H-4), 1.56 (3H, $J = 8$ Hz, Me-11). ^{13}C NMR (CDCl_3 , 500 MHz): 188.2 (C-6), 183.6 (C-9), 160.4 (C-7), 160.0 (C-1), 157.2 (C-10), 152.7 (C-5), 141.4 (C-4a), 122.8 (C-10a), 114.1 (C-5a), 111.1 (C-8), 110.5 (C-9a), 74.0 (C-3), 56.4 (OMe-7), 29.1 (C-4), 20.0 (C-11); (+)-HRESIMS m/z 327.04750 $[\text{M} + \text{Na}]^+$ (calcd for $\text{C}_{15}\text{H}_{12}\text{O}_7\text{Na}$, 327.04752).

COMPUTATIONAL DETAILS

All DFT calculations were performed using the latest version of the Gaussian09 program.³⁴ The B3LYP/6-311++G(2d,p) level of theory was selected to conduct the conformational analyses of the four haemovosin derivatives (1–3, 5), taking into account the various possible enantiomeric or diastereoisomeric structures. The harmonic frequencies were computed analytically at the same level of theory to characterize the stationary points as true minima. Owing to the strong structural similarities between the various derivatives, the common scaffold has been thoroughly investigated only for the haemovosin 5 (Figure 3), and the resulting features were transposed to structures 1–3. The naphthazarin nucleus appears as a rigid moiety with possible rotation of the C-7 methoxy group and the C-5 and C-10 hydroxy groups. The most stabilized structure involves both hydroxy groups intramolecularly hydrogen-bonded to the quinone carbonyl moieties, and the methoxy substituent repelled from the vicinal carbonyl group. This geometry represents more than 90% of the relative conformational population, irrespective of whether the solvent effects (MeCN) are considered, through Polarizable Continuum Model (PCM) calculations.³⁵ The ECD spectra were computed for these structures considering various plausible configurations at C-3 and C-4. The ECD spectra were computed with the same functional and basis set as the structures, namely, B3LYP/6-311++G(2d,p), using a time-dependent density functional theory (TD-DFT) implementation. For these calculations, 50 excited states were determined, and the solvent effects were systematically included using the PCM model. Only the spectra clearly corresponding to their experimental counterparts are presented.

Antioxidant Testing. The scavenging activity of the pigment-enriched fraction and of compound 5 on the 2,2-diphenyl-1-picrylhydrazyl free radical (DPPH) was measured as described elsewhere.³⁶ For the same compounds, measurement of superoxide anion scavenging activity in 96-well microplates was based on the published nonenzymatic method with some modifications. The reaction mixture in the sample wells consisted of NADH (78 μM), NBT (50 μM), PMS (10 μM), and lichen compounds (350, 116, 39, and 13 μM). The reagents were dissolved in 16 mM tris-hydrochloride buffer at pH = 8, except for all the lichen compounds, which were dissolved in DMSO. After 5 min of incubation at room temperature, the spectrophotometric measurement was performed at 560 nm against a blank sample without PMS. Ascorbic acid was used as a positive control. The percentage inhibition at steady state for each dilution was used to calculate the IC_{50} values. This provided the amount of antioxidant required (measured as the concentration of the stock solution added to the reaction mixture) to scavenge 50% of $\text{O}_2^{\cdot -}$, with lower values indicating more effective scavenging of $\text{O}_2^{\cdot -}$. All tests were conducted in triplicate, and the results were averaged.

Cell Culture and Survival Assays. The cytotoxic activity of the pigment-enriched fraction and of compound 5 was determined against B16 murine melanoma and HaCaT human keratinocyte cell lines as described elsewhere.^{37,38}

The in vitro inhibition of cell proliferation of 5 was determined using a panel of 6 representative cell lines, namely, Huh7D12 (differential hepatocellular carcinoma), Caco 2 (differentiating colorectal adenocarcinoma), MDA-MB-231 (breast carcinoma), HCT-116 (actively proliferating colorectal carcinoma), PC3 (prostate carcinoma), NCI-H2 (lung carcinoma), and diploid skin fibroblasts as normal cell lines for control. Cells were grown as described elsewhere.³⁹ The inhibition of cell proliferation was assessed as in Coulibaly et al.²⁸

ASSOCIATED CONTENT

Supporting Information

The Supporting Information is available free of charge on the ACS Publications website at DOI: 10.1021/acs.jnatprod.5b01073.

Copies of 1D (^1H , ^{13}C) and 2D NMR and ECD spectra for compounds 1–5 as well as details regarding the cytotoxic activity of compound 5 (PDF)

■ AUTHOR INFORMATION

Corresponding Authors

*E-mail: anne-cecile.le-lamer@univ-tlse3.fr.

*E-mail: joel.boustie@univ-rennes1.fr.

Notes

The authors declare no competing financial interest.

■ ACKNOWLEDGMENTS

This work was supported by the University of Rennes 1 through the project “Défi emergent LICHENMASS”. This research was conducted within the context of the International Associated Laboratory Indo-French Joint Laboratory for Sustainable Chemistry at Interfaces. The authors thank Professor P. Uriac for his insightful support. Dr. P. Jehan and Dr. N. Le Yondre, CRMPO Rennes, are gratefully acknowledged for performing mass spectrometry measurements and for fruitful discussions. The authors are also indebted to Dr. R. Le Guével (Impacell) for performing the in vitro test of cell proliferation inhibition on haemoventosin. Dr. Stéphane La Barre is acknowledged for improving the English style of the manuscript.

■ REFERENCES

- Boustie, J.; Grube, M. *Plant Genet. Resour.* **2005**, *3*, 273–287.
- Boustie, J.; Tomasi, S.; Grube, M. *Phytochem. Rev.* **2011**, *10* (3), 287–307.
- Skult, H. *Annales Botanici Fennici; JSTOR* **1997**, 291–297.
- May, P. F. *Harv. Pap. Bot.* **1997**, *2* (2), 213–228.
- Bruun, T.; Lamvik, A. *Acta Chem. Scand.* **1971**, *25* (2), 483–486.
- Rycroft, D. S.; Connolly, J. D.; Huneck, S.; Himmelreich, U. *Z. Naturforsch., B: J. Chem. Sci.* **1995**, *50* (10), 1557–1563.
- Sunasse, S. N.; Davies-Coleman, M. T. *Nat. Prod. Rep.* **2012**, *29* (5), 513–535.
- El Aouad, N.; Pérez-Moreno, G.; Sánchez, P.; Cantizani, J.; Ortiz-López, F. J.; Martín, J.; González-Menéndez, V.; Ruiz-Pérez, L. M.; González-Pacanowska, D.; Vicente, F.; Bills, G.; Reyes, F. *J. Nat. Prod.* **2012**, *75* (6), 1228–1230.
- He, H.; Bigelis, R.; Yang, H. Y.; Chang, L.-P.; Singh, M. P. *J. Antibiot.* **2005**, *58* (11), 731–736.
- Li, R.; Chen, S.; Niu, S.; Guo, L.; Yin, J.; Che, Y. *Fitoterapia* **2014**, *96*, 88–94.
- Sappapan, R.; Sommit, D.; Ngamrojjanavanich, N.; Pengprecha, S.; Wiyakrutta, S.; Sriubolmas, N.; Pudhom, K. *J. Nat. Prod.* **2008**, *71* (9), 1657–1659.
- Aldridge, D. C.; Turner, W. B. *J. Chem. Soc. C* **1970**, *18*, 2598–2600.
- Yamazaki, H.; Ōmura, S.; Tomoda, H. *J. Antibiot.* **2009**, *62* (4), 207–211.
- Haritakun, R.; Sappan, M.; Suvannakad, R.; Tasanathai, K.; Isaka, M. *J. Nat. Prod.* **2009**, *73* (1), 75–78.
- Donner, C. D. *Nat. Prod. Rep.* **2015**, *32* (4), 578–604.
- Poral, V. L.; Furkert, D. P.; Brimble, M. A. *Org. Lett.* **2015**, *17* (24), 6214–6217.
- Berova, N.; Di Bari, L.; Pescitelli, G. *Chem. Soc. Rev.* **2007**, *36* (6), 914–931.
- Miller, R. F.; Sokoloski, T. D.; Mitscher, L. A.; Bonacci, A. C.; Hoener, B.-A. *J. Pharm. Sci.* **1973**, *62* (7), 1143–1147.
- Hutchings, M. G.; Chippendale, A. M.; Shukla, R.; McPartlin, M. *Tetrahedron* **1991**, *47* (37), 7869–7874.
- Jeon, J.; Julianti, E.; Oh, H.; Park, W.; Oh, D.-C.; Oh, K.-B.; Shin, J. *Tetrahedron Lett.* **2013**, *54* (24), 3111–3115.
- Magid, A. A.; Voutquenne-Nazabadioko, L.; Moroy, G.; Moretti, C.; Lavaud, C. *Phytochemistry* **2007**, *68* (19), 2439–2443.
- Han, Y.-S.; Van der Heijden, R.; Verpoorte, R. *Plant Cell, Tissue Organ Cult.* **2001**, *67* (3), 201–220.
- Okuno, T.; Oikawa, S.; Goto, T.; Sawai, K.; Shirahama, H.; Matsumoto, T. *Agric. Biol. Chem.* **1986**, *50* (4), 997–1001.
- Krohn, K.; Bahramsari, R.; Flörke, U.; Ludewig, K.; Kliche-Spory, C.; Michel, A.; Aust, H.-J.; Draeger, S.; Schulz, B.; Antus, S. *Phytochemistry* **1997**, *45* (2), 313–320.
- Parisot, D.; Devys, M.; Férézou, J.-P.; Barbier, M. *Phytochemistry* **1983**, *22* (5), 1301–1303.
- Tatum, J. H.; Baker, R. A.; Berry, R. E. *Phytochemistry* **1989**, *28* (1), 283–284.
- Elix, J. A.; Wardlaw, J. H. *Aust. J. Chem.* **2002**, *51*, 2–3.
- Elix, J. A.; Wardlaw, J. H. *Australas. Lichenol.* **2001**, *49*, 10–11.
- Ernst-Russell, M. A.; Elix, J. A.; Chai, C. L.; Rive, M. J.; Wardlaw, J. H. *Aust. J. Chem.* **2000**, *53* (4), 303–306.
- Honda, N. K.; Lopes, T. I. B.; Costa, R. C. S.; Coelho, R. G.; Yoshida, N. C.; Rivarola, C. R.; Marcelli, M. P.; Spielmann, A. A. *Orbital - Electron. J. Chem.* **2015**, *7* (2), 99–107.
- Nybakken, L.; Asplund, J.; Solhaug, K. A.; Gauslaa, Y. *J. Chem. Ecol.* **2007**, *33* (8), 1607–1618.
- Hyvärinen, M.; Koopmann, R.; Hormi, O.; Tuomi, J. *Oikos* **2000**, *91* (2), 371–375.
- Hodkinson, B. P.; Gottel, N. R.; Schadt, C. W.; Lutzoni, F. *Environ. Microbiol.* **2012**, *14* (1), 147–161.
- Frisch, M.; Trucks, G. W.; Schlegel, H. B.; Scuseria, G. E.; Robb, M. A.; Cheeseman, J. R.; Scalmani, G.; Barone, V.; Mennucci, B.; Petersson, G. A.; Nakatsui, H.; Caricato, M.; Li, X.; Hratchian, H. P.; Izmaylov, A. F. I.; Bloino, J.; Zheng, G.; Sonnenberg, J. L.; Hada, M.; Ehara, M.; Toyota, K.; Fukuda, R.; Hasegawa, J.; Ishida, M.; Nakajima, T.; Honda, Y.; Kitao, O.; Nakai, H.; Vreven, T.; Montgomery, J. A. J.; Peralta, J. E.; Ogliaro, F.; Bearpark, M.; Heyd, J. J.; Brothers, E.; Kudin, K. N.; Staroverov, V. N.; Keith, T.; Kobayashi, R.; Normand, J.; Raghavachari, K.; Rendell, A.; Burant, J. C.; Iyengar, S. S.; Tomasi, J.; Cossi, M.; Rega, N.; Millam, J. M.; Klene, M.; Knox, J. E.; Cross, J. B.; Bakken, V.; Adamo, C.; Jaramillo, J.; Gomperts, R.; Stratmann, R. E.; Yazyev, O.; Austin, A. J.; Cammi, R.; Pomelli, C.; Ochterski, J. W.; Martin, R. L.; Morokuma, K.; Zakrzewski, V. G.; Voth, G. A.; Salvador, P.; Dannenberg, J. J.; Dapprich, S.; Daniels, A. D.; Farkas, O.; Foresman, J. B.; Ortiz, J. V.; Cioslowski, J.; Fox, D. J. *Gaussian 09*; Gaussian, Inc.: Wallingford, CT, 2009.
- Tomasi, J.; Mennucci, B.; Cammi, R. *Chem. Rev.* **2005**, *105* (8), 2999–3094.
- Ismed, F.; Lohézic-Le Dévéhat, F.; Delalande, O.; Sinbandhit, S.; Bakhtiar, A.; Boustie, J. *Fitoterapia* **2012**, *83* (8), 1693–1698.
- Millot, M.; Tomasi, S.; Studzinska, E.; Rouaud, I.; Boustie, J. *J. Nat. Prod.* **2009**, *72*, 2177–2180.
- Bézivin, C.; Tomasi, S.; Rouaud, I.; Delcros, J.-G.; Boustie, J. *Planta Med.* **2004**, *70* (9), 874–877.
- Coulibaly, W. K.; Paquin, L.; Bénie, A.; Békro, Y.-A.; Le Guével, R.; Ravache, M.; Corlu, A.; Bazureau, J. P. *Med. Chem. Res.* **2015**, *24* (4), 1653–1661.

c. Profilage chimique de lichen divers pour la détection d'autres classes structurales

L'adaptabilité du DART-MS à d'autres groupes structuraux a été décrite secondairement dans d'autres papiers qui ne se focalisent pas directement sur les travaux entrepris dans le cadre de cette thèse :

- La déréplication de xanthones directement depuis un thalle de *Lecidella asema* non broyé en DART positif dans une revue parue dans *Molecules* en 2016 (Le Pogam and Boustie, 2016). Le texte intégral de cette publication est fourni en Annexe 6 (p. 257).
- La détection de dérivés de l'acide pulvinique au travers du profilage *in situ* de thalles entiers de *Vulpicida pinastri* (Legouin et al., *submitted.*).
- L'analyse d'acides paraconiques depuis des fragments entiers d'*Usnea trachycarpa* (cf. chapitre CCM-MS) (Annexe 3, p. 210).

B. Déréplication par diffraction par poudres des rayons X : application à quelques lichens appartenant au genre *Cladonia*

Plus encore que la présence des métabolites secondaires lichéniques en surface des filaments mycéliens, leur cristallisation extracellulaire (Honegger, 1986b) représente une opportunité pour développer des méthodologies analytiques innovantes.

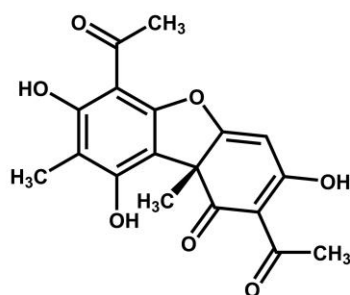
L'identification des métabolites secondaires lichéniques selon la morphologie des cristaux qu'ils forment représente l'une des premières méthodes pour identifier les molécules issues du lichen. Cette approche historique développée par Asahina reposait sur les cristallisations d'extraits lichéniques totaux dans des systèmes de solvants particuliers (Shibata, 2000). Si cette technique d'identification rudimentaire ne permettait généralement d'apprécier que le métabolite majoritaire, la variété de formes et de couleurs obtenue par ce procédé dit de microcristallisation est très conséquente (Huneck and Yoshimura, 1996). De nos jours, la diffraction de monocristal par rayons X représente sans doute la technique analytique la plus informative, livrant jusqu'à la stéréochimie absolue d'une molécule (Deschamps, 2010). Les analyses par diffraction des rayons X en pharmacognosie interviennent donc dans les stades ultimes de l'étude phytochimique, à des seules fins d'élucidation structurale de molécules isolées (Gaudêncio and Pereira, 2015).

L'absence de méthode de déréplication fondée sur la diffraction rayons X tient certainement au fait que peu de matrices naturelles cristallisent autant leurs métabolites secondaires que les lichens. Compte-tenu du caractère très inhabituel de cette méthode en déréplication, les principes de la diffraction des rayons X par la matière cristallisée sont brièvement rappelés en Annexe 2 (p. 200).

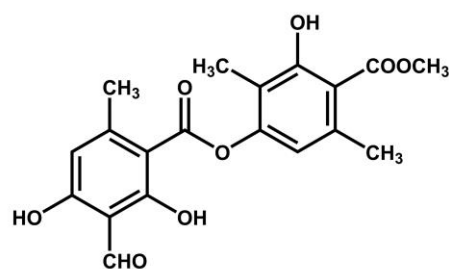
Des essais en diffraction par poudre des rayons X ont été menés sur trois lichens du genre *Cladonia* relativement difficiles à distinguer sur la seule base de critères morphologiques : *Cladonia arbuscula*, *C. ciliata* et *C. rangiferina*. Ces trois lichens présentent des profils chimiques simples (comprenant un ou deux métabolites secondaires dominants) et qui en font de bons candidats pour la mise au point de nouvelles méthodes analytiques. En ce sens, ces *Cladonia* avaient déjà été étudiés au moyen d'une autre approche déréplivative innovante (Miglietta and Lamanna, 2006) : la RMN ¹³C du solide (C-13 CP MAS NMR pour *Cross Polarization Magic Angle Spinning*) (Figure 20).


Cladonia portentosa

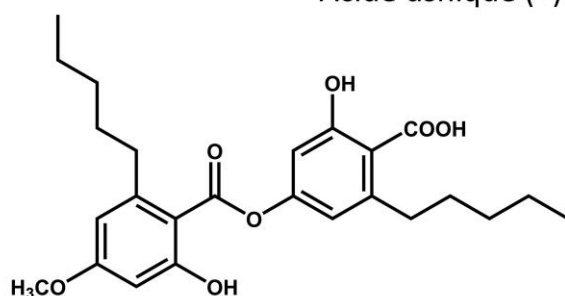
Cladonia rangiferina

Cladonia ciliata var. *tenuis*


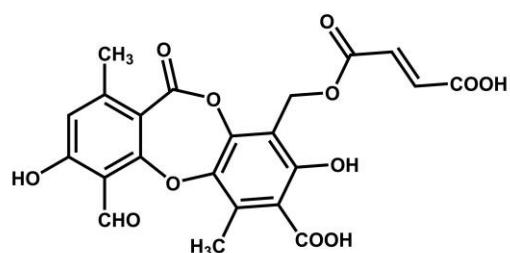
Acide usnique (+)



Atranorine



Acide perlatolique



Acide fumarprotocétrarique

FIGURE 20 : *CLADONIA* UTILISÉS LORS DES ANALYSES DÉRÉPLICATIVES PAR DIFFRACTION DE RAYONS X : PHOTOGRAPHIES ET MÉTABOLITES SECONDAIRES MAJORITAIRES.

Les diagrammes de diffraction ont été enregistrés à l'aide d'un diffractomètre de rayons X sur poudre haute résolution PANalytical Empyrean opérant en géométrie Bragg-Brentano θ - θ . La longueur d'onde $K\alpha$ du cuivre ($\lambda K\alpha_1 = 1.5406 \text{ \AA}$, $\lambda K\alpha_2 = 1.5444 \text{ \AA}$) est sélectionnée à l'aide d'un miroir multicouches plan. Les échantillons sont positionnés sur des porte-échantillons silicium afin d'éviter la contribution du fond continu aux diagrammes de diffraction. La statistique de comptage est adaptée en fonction de la réponse du détecteur 2D. Le traitement des données est effectué à l'aide du logiciel PANalytical Highscore.

Les analyses sont directement effectuées sur des lichens broyés pendant deux minutes (hachoir-mixeur Seb Rondo 500) et les diffractogrammes permettent de retrouver des signatures spectrales correspondant à celles des composés attendus (Chollet-Krugler et al., 2008). Les broyats sont tamisés sur deux grilles (80 et 125 μm) pour évaluer le rapport phases cristallines/phases amorphes au sein de ces différentes fractions. Quatre échantillons ont donc été considérés pour chaque lichen : le lichen broyé non tamisé, les particules supérieures à 125 μm , la fraction allant de 80 à 125 μm et les particules inférieures à 80 μm .

Concernant *Cladonia portentosa*, les études menées en RMN du solide avaient permis de caractériser dans l'échantillon la présence des acides usnique et perlatolique. La diffractométrie rayons X permet de détecter ces deux espèces (Figure 21).

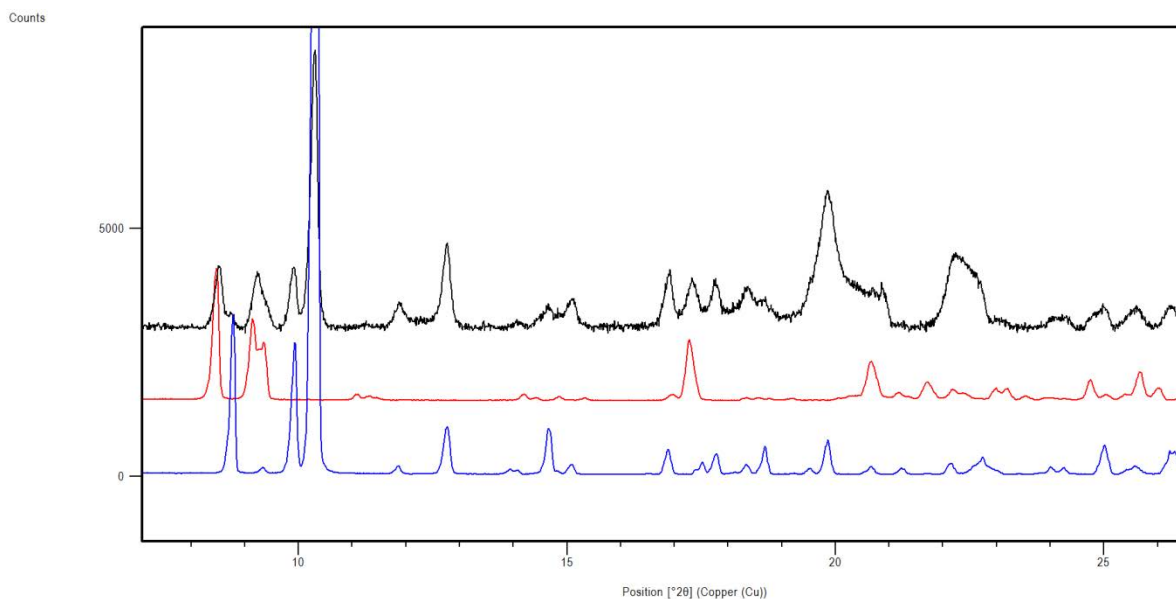


FIGURE 21: DIFFRACTOGRAMMES RAYONS X SUR POUDRES RELATIFS À *CLADONIA PORTENTOSA* ET À SES MÉTABOLITES SECONDAIRES. NOIR, POUDRE TOTALE DE LICHEN SANS TAMISAGE (APRÈS SOUSTRACTION DU FOND CONTINU) ; ROUGE, ACIDE PERLATOLIQUE ; BLEU, ACIDE USNIQUE.

La comparaison des diagrammes de diffraction du *Cladonia portentosa* mixé selon le tamisage est donnée (Figure 22).

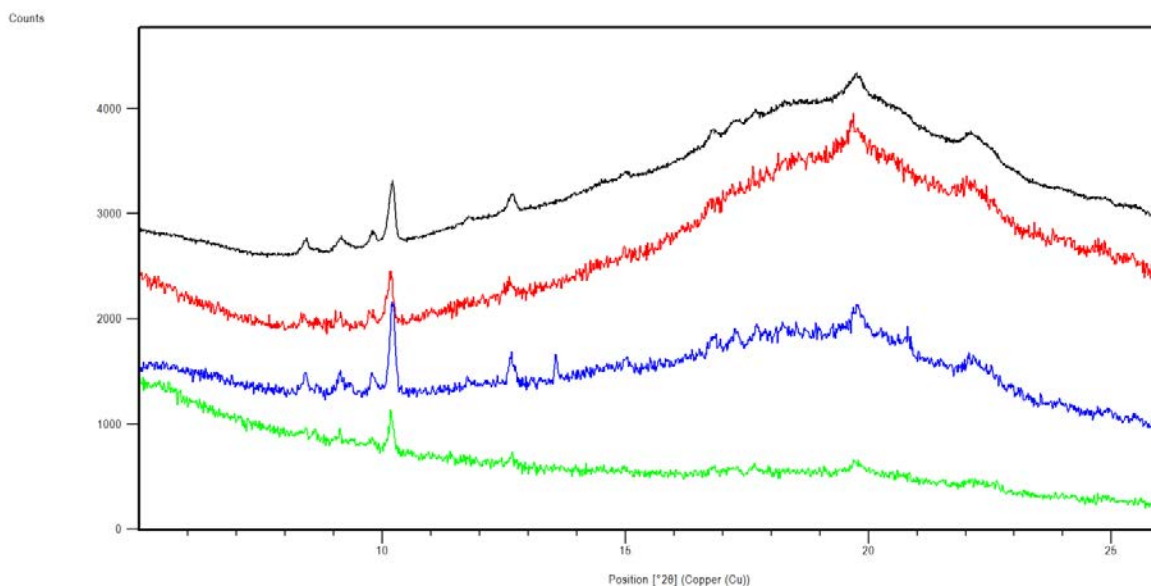


FIGURE 22: DIFFRACTOGRAMMES RAYONS X SUR POUDRES RELATIFS À *CLADONIA PORTENTOSA* : NOIR, NON TAMISÉ ; ROUGE, FRACTION SUPÉRIEURE À 125 μm ; BLEU, GRAINS COMPRIS ENTRE 80 ET 125 μm ET VERT, GRAINS INFÉRIEURS À 80 μm.

Le fond continu, caractéristique de phases amorphes est particulièrement notable pour les fractions non traitées et de granulométrie > 125 μm. La contribution est moindre pour la fraction comprise entre 80 et 125 μm et le rapport phases cristallines/phases amorphes y semble le plus élevé. Le tamisage à

grains < 80 µm supprime efficacement la contribution des amorphes mais ne permet pas de récupérer une fraction cristalline importante.

Le diffractogramme de l'acide usnique correspond à des cristaux orthorhombiques déjà décrits dans la littérature (Jones and Palmer, 1950). Afin de visualiser ces cristaux et de voir si deux populations cristallines peuvent être distinguées, des thalles de *Cladonia portentosa* ont été visualisés en Microscopie Electronique à Balayage. Ces analyses ont été menées au Centre de microscopie électronique à balayage et microanalyse (CMEBA) par Francis Gouttefangeas et Loïc Joanny. L'analyse de podétions intacts révèle la présence de nombreux cristaux à la surface des filaments mycéliens (Figure 23).

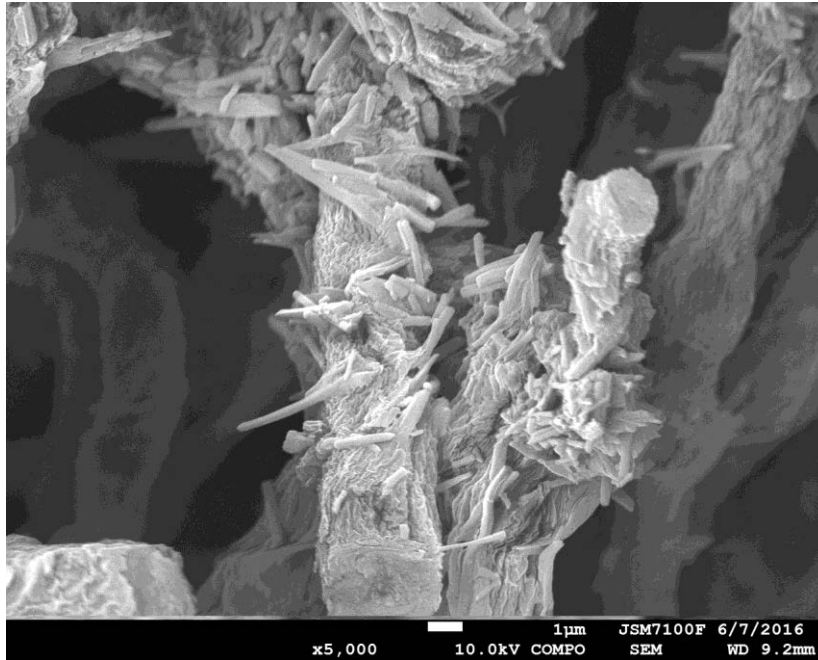


FIGURE 23: FORMATIONS CRISTALLINES À LA SURFACE DU CORTEX SUPÉRIEUR DE *CLADONIA PORTENTOSA* OBSERVÉES EN MICROSCOPIE ÉLECTRONIQUE À BALAYAGE (x 5000)

Cette présence superficielle et la forme des cristaux évoquent l'acide usnique, molécule présentant une distribution corticale chez de nombreux lichens (McEvoy et al., 2006; Nybakken and Julkunen-Tiitto, 2006). L'acide perlatolique étant décrit comme un composé médullaire (Hauck et al., 2009a), l'étude de coupes transversales de podétions est nécessaire pour voir si les cristaux de ce depside sont morphologiquement distincts de ceux d'acide usnique. De façon notable, un gradient de cristaux est observé le long des podétions avec une présence nettement plus importante dans les tissus jeunes (haut des podétions) que dans les parties basales du lichen, en accord avec les données de la littérature concernant l'acide usnique (Mirando and Fahselt, 1978).

Cladonia rangiferina quant à lui contient de l'acide fumarprotocétrarique et de l'atranorine. Ces deux molécules peuvent être caractérisées directement depuis le lichen broyé et non tamisé (Figure 24).

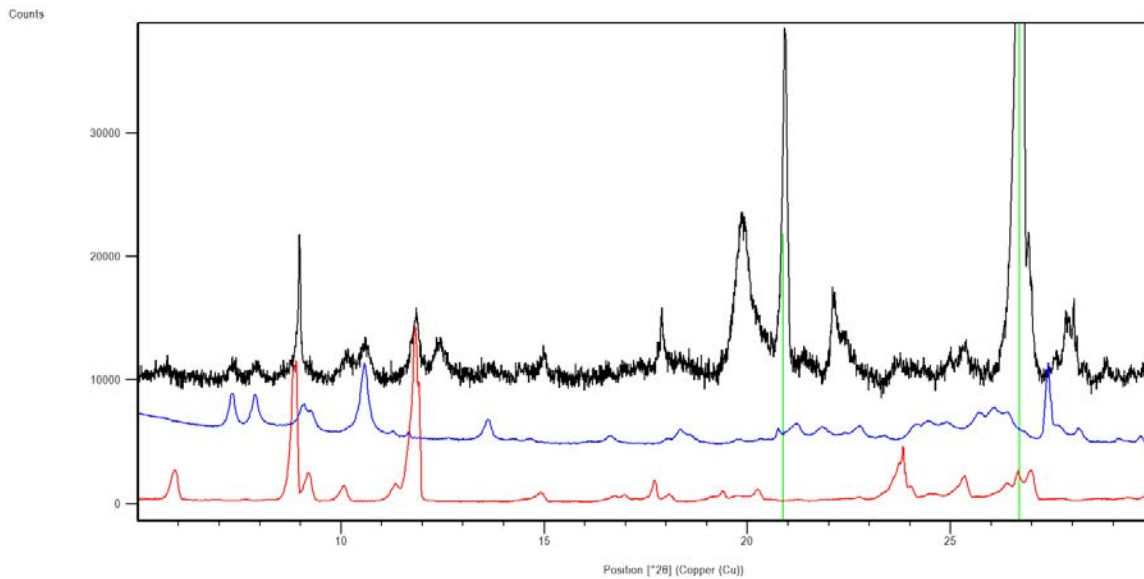


FIGURE 24 : DIFFRACTOGRAMMES RAYONS X SUR POUDRES RELATIFS À *CLADONIA RANGIFERINA* ET À SES MÉTABOLITES SECONDAIRES. NOIR, POUDRE TOTALE DE LICHEN SANS TAMISAGE (APRÈS SOUSTRACTION DU FOND CONTINU) ; BLEU, ACIDE FUMARPROTOCÉTRARIQUE ; ROUGE, ATRANORINE. LES PICS MARQUÉS EN VERT SONT ASSOCIÉS À LA PRÉSENCE DE QUARTZ DANS L'ÉCHANTILLON.

Le tamisage n'exerce pas d'influence notable sur l'analyse du diagramme pour ce lichen (Figure 25).

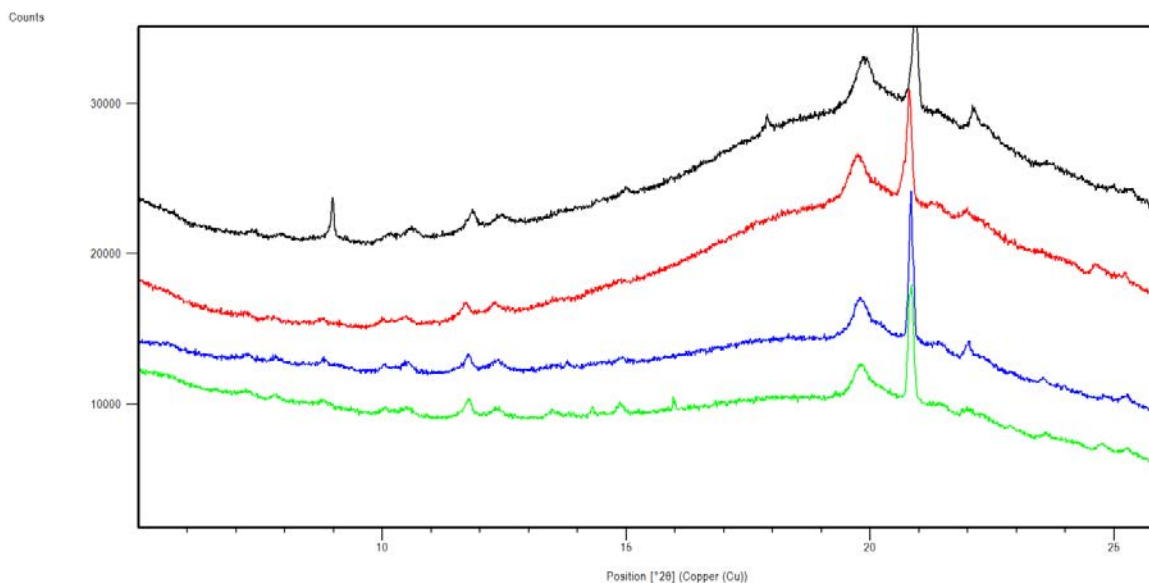


FIGURE 25 : DIFFRACTOGRAMMES RAYONS X SUR POUDRES RELATIFS À *CLADONIA RANGIFERINA* : NOIR, NON TAMISÉ ; ROUGE, FRACTION SUPÉRIEURE À 125 μm ; BLEU, GRAINS COMPRIS ENTRE 80 ET 125 μm ET VERT, GRAINS INFÉRIEURS À 80 μm.

Dernier lichen étudié pour l'heure par diffraction par les rayons X, *Cladonia ciliata* var. *tenuis* est un lichen caractérisé par la présence d'acide usnique (Hauck and Jürgens, 2008). Cette molécule parvient à être détectée directement depuis le lichen broyé et non tamisé (Figure 26)

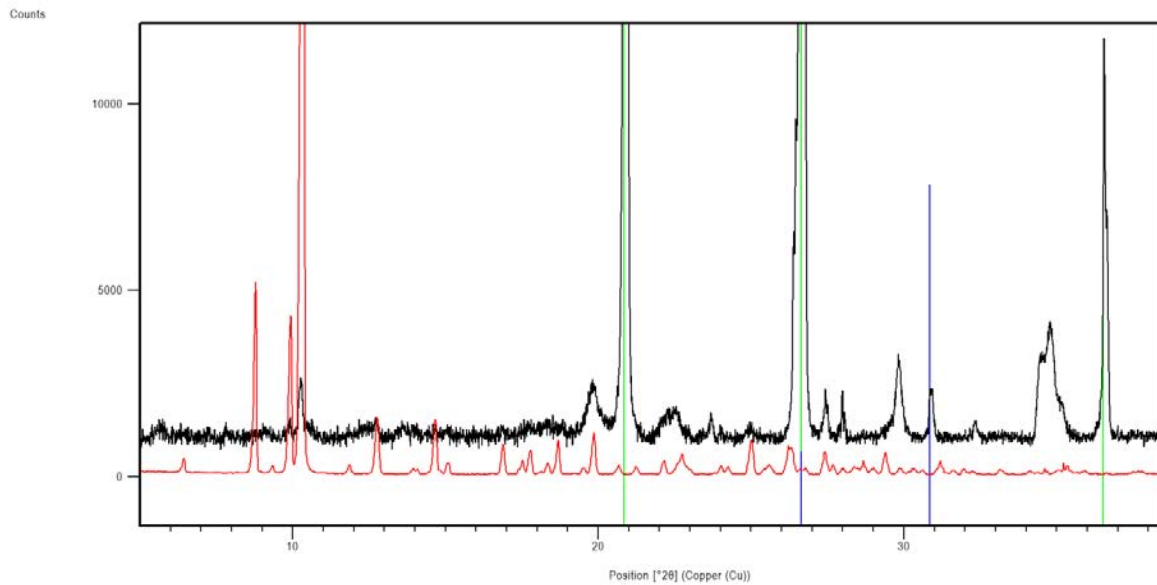


FIGURE 26: DIFFRACTOGRAMMES RAYONS X SUR POUDRES RELATIFS À *CLADONIA CILIATA* ET À L'ACIDE USNIQUE. NOIR, POUDRE TOTALE DE LICHEN SANS TAMISAGE (APRÈS SOUSTRACTION DU FOND CONTINU) ; ROUGE, ACIDE USNIQUE. LES PICS MARQUÉS EN VERT SONT ASSOCIÉS À LA PRÉSENCE DE QUARTZ DANS L'ÉCHANTILLON ET CELUI EN BLEU CORRESPOND À LA PRÉSENCE DE NaCl.

Une nouvelle fois, le tamisage $80\ \mu\text{m} < \text{grains} < 125\ \mu\text{m}$ semble le plus adapté mais l'identification se fait correctement avec l'échantillon non tamisé (Figure 27).

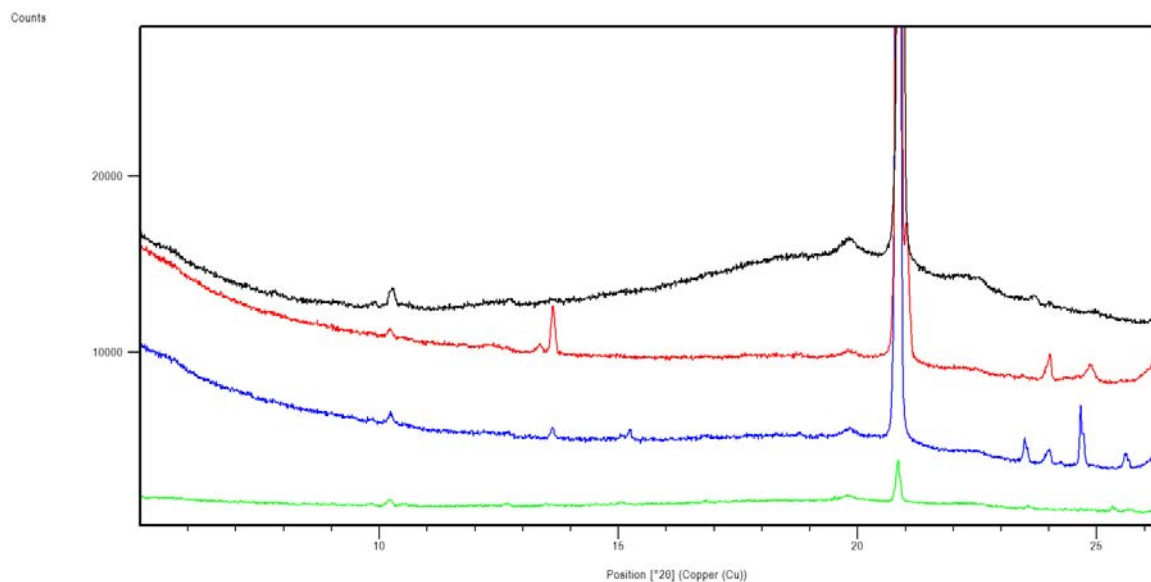


FIGURE 27: DIFFRACTOGRAMMES RAYONS X SUR POUDRES RELATIFS À *CLADONIA CILIATA* : NOIR, NON TAMISÉ ; ROUGE, FRACTION SUPÉRIEURE À 125 μm ; BLEU, GRAINS COMPRIS ENTRE 80 ET 125 μm ET VERT, GRAINS INFÉRIEURS À 80 μm .

Si ces premiers résultats démontrent la faisabilité de cette approche très originale, des compléments sont à prévoir pour estimer le potentiel de la diffraction de poudres aux rayons X pour le profilage chimique de lichens broyés, notamment l'analyse de lichens de chimie plus complexe. Pour appliquer la méthode à de véritables fins déréplicatives, une banque de données compilant les diffractogrammes de composés lichéniques devra être constituée.

III. Apport du LDI-MS pour la déréplication de lichens

Le LDI-MS s'inscrit dans les méthodes d'ionisation/désorption laser dont la déclinaison analytique la plus fréquemment rencontrée est le MALDI (Matrix Assisted Laser Desorption and Ionization Mass Spectrometry). De telles analyses requièrent l'adjonction de molécules de matrice absorbant à la longueur d'onde du laser utilisé. Les mécanismes régissant l'ionisation MALDI sont complexes et restent encore débattus aujourd'hui mais il est admis que l'irradiation laser désorbe et ionise dans un premier temps les molécules de matrice puis qu'un transfert de charge intervient pour permettre ensuite la détection des analytes (Karas et al., 1987; Zenobi and Knochenmuss, 1998). Il y a de fait une détection conjointe des analytes et des molécules de matrice, ce qui va obscurcir le signal dans les régions de basses masses molaires (typiquement en dessous de 700 à 1.000 unités de masse atomique selon la matrice utilisée) (Figure 28). Ce phénomène dit d'interférences matricielles explique que cette méthode de spectrométrie de masse soit plutôt orientée vers la détection de molécules de masses molaires élevées et à ce titre notamment la protéomique. Les techniques de désorption/ionisation laser représentent pourtant des candidats attractifs pour la déréplication car ces analyses sont très rapides, peu coûteuses et peuvent être automatisées (Manna et al., 2011; Pavarini et al., 2012).

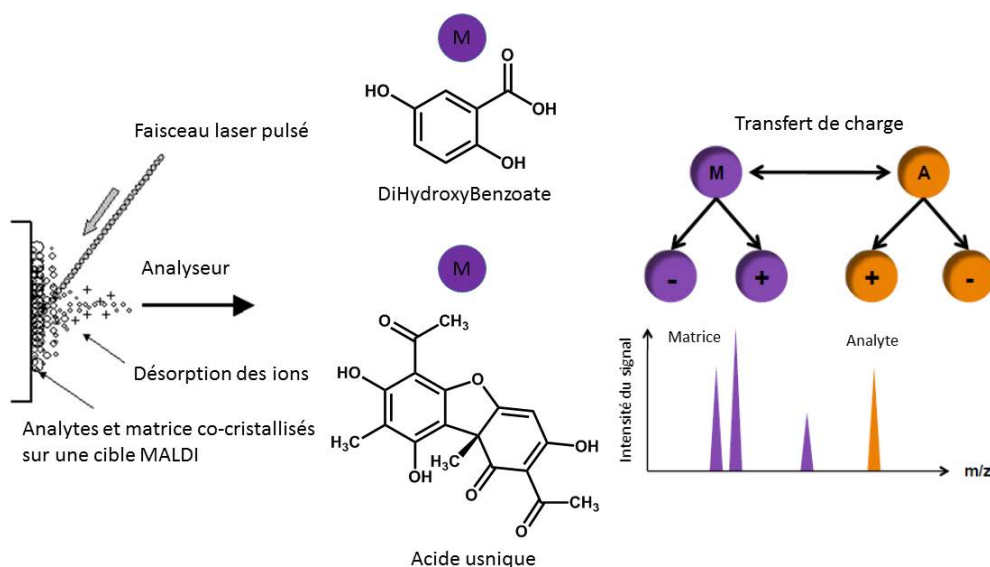


FIGURE 28 : PRINCIPE DE L'IONISATION MALDI ET HOMOLOGUES STRUCTURALES ENTRE LE DIHYDROXYBENZOATE (MATRIE COMMERCIALE) ET L'ACIDE USNIQUE

Sur la base de l'absorption UV de la majorité des métabolites secondaires lichéniques et des similitudes structurales entre les polyphénols lichéniques et des matrices commercialement disponibles, il a pu être établi que l'acide usnique présente des propriétés matriciales indiquant par la même que ce composé est capable de s'auto-ioniser *i.e* sans avoir besoin d'y adjoindre une matrice (Schinkovitz and Richomme, 2015). Au travers de l'analyse de 25 composés purs représentatifs de la chimiodiversité lichénique, l'auto-ionisabilité des molécules lichéniques appartenant à 11 grands groupes structuraux de métabolites lichéniques a pu être caractérisée. Dans un second temps, le potentiel déréplicatif du LDI en mode d'ionisation négatif a été évalué sur une quinzaine d'extraits lichéniques de composition connue. Du fait de l'ionisation douce déclenchée par la source LDI, les spectres permettent généralement une identification facile des métabolites, le plus souvent par leurs ions quasi-moléculaires. L'aptitude du LDI à former des radicaux permet de détecter des espèces difficilement déprotonables en mode négatif (e.g quinones instiguant des liaisons hydrogène intramoléculaires) non détectables dans ce même mode en ESI. L'ensemble des données en lien avec le LDI est compilé dans un article paru en 2015 dans *Analytical Chemistry* et intitulé « Matrix-Free UV-Laser Desorption and Ionization Mass Spectrometry ». Les données complémentaires de cette publication font l'objet de l'Annexe 7 (p. 288).

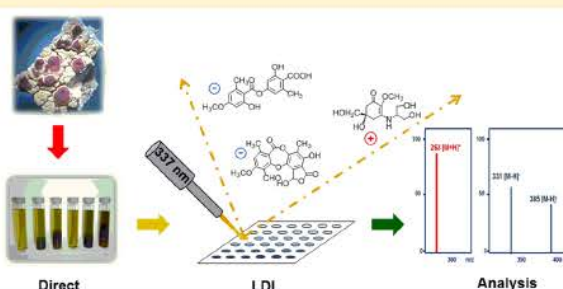
Matrix-Free UV-Laser Desorption Ionization Mass Spectrometry as a Versatile Approach for Accelerating Dereplication Studies on Lichens

Pierre Le Pogam,[†] Andreas Schinkovitz,[‡] Béatrice Legouin,[†] Anne-Cécile Le Lamer,^{†,§} Joël Boustie,^{*,†} and Pascal Richomme^{*,‡}[†]Université de Rennes 1, UMR CNRS 6226 PNSCM, 2 Avenue du Professeur Léon Bernard, 35043 Rennes, France[‡]Université d'Angers, EA 921 SONAS/SFR 4207 QUASAV, 16 Boulevard Daviers, 49100 Angers, France[§]Université Paul Sabatier Toulouse 3, 118 Route de Narbonne, 31062 Toulouse, France

Supporting Information

ABSTRACT: The present study examined the suitability of laser desorption/ionization time-of-flight mass spectrometry (LDI-MS) for the rapid chemical fingerprinting of lichen extracts. Lichens are known to produce a wide array of secondary metabolites. Most of these compounds are unique to the symbiotic condition but some can be found in many species. Therefore, dereplication, that is, the rapid identification of known compounds within a complex mixture is crucial in the search for novel natural products. Over the past decade, significant advances were made in analytical techniques and profiling methods specifically adapted to crude lichen extracts, but LDI-MS has never been applied in this context.

However, most classes of lichen metabolites have UV chromophores, which are quite similar to commercial matrix molecules used in matrix-assisted laser desorption ionization (MALDI). It is consequently postulated that these molecules could be directly detectable by matrix-free LDI-MS. The present study evaluated the versatility of this technique by investigating the LDI properties of a vast array of single lichen metabolites as well as lichen extracts of known chemical composition. Results from the LDI experiments were compared with those obtained by direct ESI-MS detection as well as LC-ESI-MS. It was shown that LDI ionization leads to strong molecular ion formation with little fragmentation, thus, facilitating straightforward spectra interpretation and representing a valuable alternative to time-consuming LC-MS analysis.



Lichens are self-sustaining partnerships between a filamentous fungus and a photosynthetic partner (eukaryotic algae and cyanobacterium). These structurally complex symbiotic organisms can survive in harsh conditions including extreme temperature, desiccation, UV radiation, and high saline concentration.¹ They have further developed protective mechanisms to resist intense light exposure, including the synthesis of many UV protectants.² Lichens were reported to produce over 1200 secondary metabolites among which only a relatively small number (50–60) occur in nonsymbiotic fungi or higher plants.³ These unique metabolites exhibit an impressive range of biological effects including antibiotic, antifungal, anticancer, antiprotozoan, and anti-HIV activities.⁴ As some lichen substances are frequently observed in many species, successful harnessing of this outstanding reservoir relies on refined dereplicative approaches.⁵ In this context, Liquid Chromatography–Mass Spectrometry (LC-MS), allowing the characterization of metabolites by mass spectra profiling and retention times, represents the standard method for analyzing the chemical composition of lichens. However, the development of high-throughput screening approaches that require little to no sample prepurification may offer new perspectives in terms of

dereplication studies. On one hand, such methods may be based on innovative techniques such as Direct Analysis in Real Time Mass Spectrometry (DART-MS) facilitating chemical profiling directly from untreated lichen material.⁶ On the other hand, the adaptation of already existing methods may also yield significant advances in the field. In this respect, the direct detection of lichen compounds by laser desorption ionization (LDI) represents an interesting approach that has not been studied so far. To the best of the authors' knowledge, the only application of laser-desorption ionization mass spectrometry on lichens is a MALDI experiment on Chilean lichens targeting the analysis of soluble proteins.⁸

Many lichen compounds show close structural similarity to known MALDI matrices and may therefore exhibit similar ionization properties as recently shown for usnic acid.⁷

Independently from their potential matrix effects, phenolic compounds should exhibit autoionization upon laser light exposure. Consequently, these compounds should be directly

Received: July 6, 2015

Accepted: September 17, 2015

Published: September 17, 2015

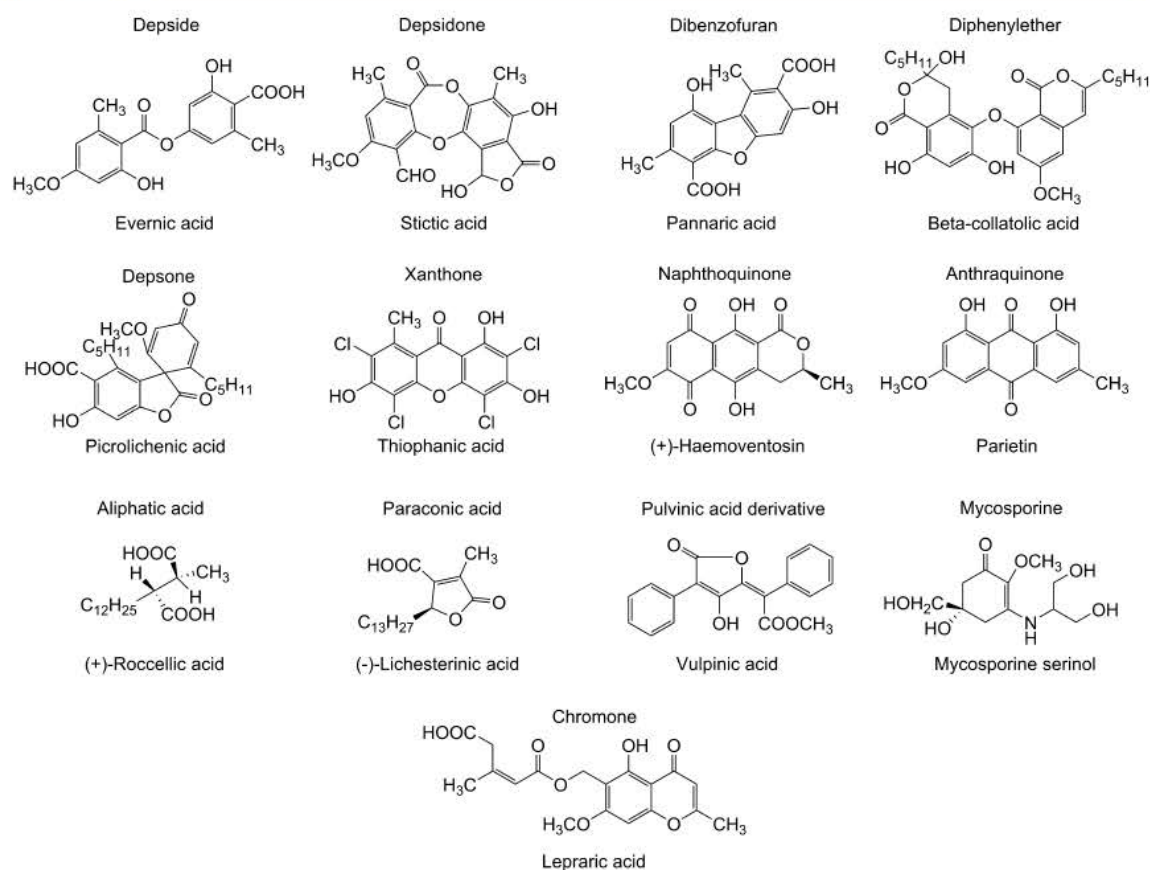


Figure 1. Structures of secondary lichen metabolites. Each compound represents one typical class of lichenic compounds studied in this work.

detectable by LDI, without matrix support. With this in mind, the present study evaluated the self-ionization properties of a wide range of chemically diverse lichen compounds such as depsides, depsidones, dibenzofurans, depsones, diphenylethers, pulvinic acid derivatives, anthraquinones, naphthoquinones, xanthonnes, chromones, and aliphatic and paraconic acids. Additionally, compound complex mixtures such as crude lichen extracts were also analyzed, and the results from the LDI experiments were compared to those obtained by direct injection ESI-MS and classical LC-DAD-ESIMS. This latter approach facilitated the estimation of the number of genuine compounds, supported structural assignments, and also added evidence to the proposed fragmentation pathways.

EXPERIMENTAL SECTION

Mass Spectrometry and Instrument Settings. LDI experiments were carried out on a Bruker Biflex III time-of-flight (TOF) mass spectrometer (Bruker Daltonik, Bremen, Germany) equipped with a 337 nm pulsed nitrogen laser (model VSL-337i, Laser Sciences Inc., Boston, MA). Spectra were acquired in the linear positive and negative mode within mass range of 20 to 2000 Da. The acceleration voltage was 19 kV, for both the positive and negative ionization modes, pulse ion extraction was 200 ns, and laser frequency was 5 ns. Experiments were performed within a laser energy range of 30–80% (46.2–103.2 μJ), depending on sample requirements. For LDI analyses, single molecules and extracts were prepared at a concentration of 10 mg mL⁻¹ in dichloromethane (DCM) or a mixture of DCM and pyridine 9:1 (v/v),

depending on sample solubility. Mycosporine serinol was dissolved in distilled water.

For direct injection, ESI-MS solutions of single compounds and lichen extracts were prepared in DCM at concentrations of 0.5 and 1.0 mg mL⁻¹, respectively. These samples were introduced into an expression CMS single quadrupole (Advion) using a mixture of MeOH/water (+0.1% formic acid) 9:1 (v/v) at a flow rate of 200 $\mu\text{L min}^{-1}$.

Full scan mass spectra were recorded in the negative ion mode in a mass range of 100 to 1200 Da, applying the following parameters: detector gain 1200, ESI voltage 3.5 kV, capillary voltage 180 V, source voltage 20 V, source voltage dynamic 20 V, nebulizer gas pressure 60 psig, desolvation gas flow rate 4 L min⁻¹, capillary temperature 250 °C, and source gas temperature 50 °C. Full scan mass spectra were recorded in the positive ion mode in a mass range of 100 to 1200 Da using the following parameters: detector gain 1200, ESI voltage 3.5 kV, capillary voltage 180 V, source voltage 40 V, source voltage dynamic 0 V, nebulizer gas pressure 60 psi, dissolution gas flow rate 4 L min⁻¹, capillary temperature 250 °C, and source gas temperature 20 °C. Data processing and evaluation for MS measurement was performed with the Data and Mass Express 2.2.29.2 software (Advion).

The LC-ESI and ESI mass spectra were all obtained from the same single quadrupole analyzer (Advion, Ithaca, U.S.A.). The MS system was coupled to a HPLC system (Prominence Shimadzu, Marne La Vallée, France) equipped with a Kinetex C18 HPLC column (100 \times 4.6 mm, 2.6 μm , 6A, Phenomenex) and consisting of a quaternary pump (LC20ADSP), a

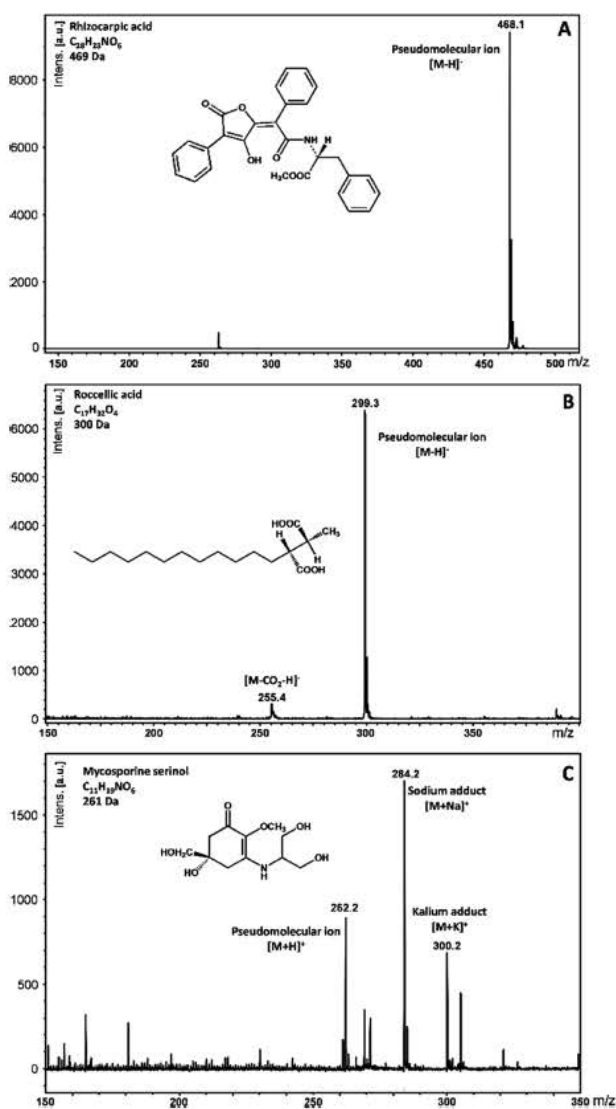


Figure 2. LDI spectra of rhizocarpic acid (A) and roccellic acid (B), both negative mode, and LDI spectra of mycosporine serinol, positive mode (C).

surveyor autosampler (SIL-20AHT), and a diode array detector (SPD-M20A). HPLC analyses were performed by gradient elution using the following parameters: A (0.1% formic acid in water) and B (acetonitrile); T , 0 min, 20% B; 0–25 min, 80% B linear; 25–30 min, 100% B linear; 30–35 min 100% B; 35–40 min 20% B linear. The flow rate was 200 $\mu\text{L min}^{-1}$.

Compounds and Lichen Material. Single compounds used in this manuscript all belong to the library of single lichenic compounds of UMR CNRS 6226 PNCSM, being isolated during previous phytochemical investigations. All specimens except the crustose alpine lichen *Ophioparma ventosa* have been harvested in France and are representative for different morphologies. Place of harvest and herbarium codes of studied lichens are given in Supporting Information (Table S-1). For all lichens, 5.0 g of the air-dried thallus were ground with mortar and pestle, before being extracted with 50.0 mL of analytical grade acetone for 9 h at room

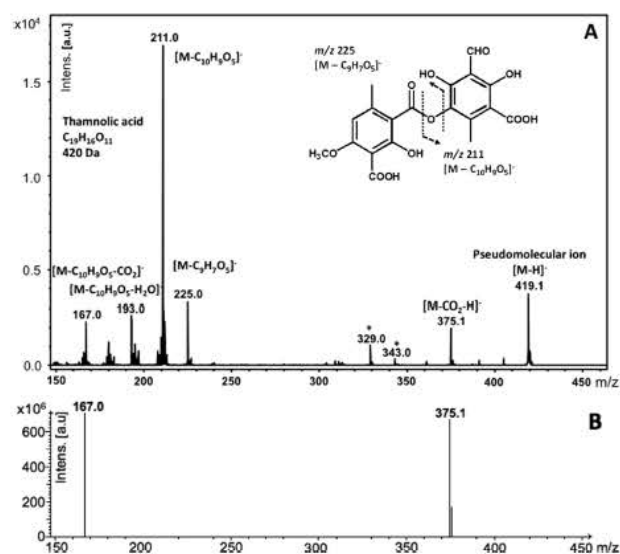


Figure 3. Negative LDI-MS (A) and ESI-MS (B) of thamnolic acid; *contamination of usnic acid.

temperature. Extracts were then split for ESI-MS and LDI-MS experiments.

RESULTS AND DISCUSSION

Autoionizability of Lichen Metabolites. The LDI-MS analyses of main classes of lichen compounds were first performed on a selection of single molecules covering most expected chemodiversity within lichens. A selection of molecules detected in LDI-MS is depicted in Figure 1, and a complete list of all molecules detected in this study is provided in the Supporting Information (Table S1).

Initial experiments were performed in linear negative ionization mode. Most of the LDI-ionized compounds like rhizocarpic acid exhibited at least some UV absorption at the irradiation wavelength of the N_2 laser (337 nm; Figure 2A). Interestingly, also paraconic and aliphatic acids displaying no UV absorption at 337 nm ionized quite well upon laser irradiation (e.g., roccellic acid, see Figure 2B). This suggests that the presence of a carboxylic function on its own is sufficient to trigger negative ionization. Among tested molecules, only mycosporine serinol, displaying a strong UV absorption,⁹ required positive-ion mode (Figure 2C).

Being a soft ionization method, LDI yielded clean spectra with strong molecular ions and little fragmentation for the vast majority of the analyzed molecules. In many cases, the molecular or pseudomolecular ion was observed as the base peak. From all tested compounds, only depsides and diphenylethers exhibited notable fragmentation, which could be explained by the cleavage of ester and ether bonds. For depsides, both the carboxylic acid and the alcohol fragment were observed, but the latter exhibited a much stronger signal. This specific cleavage is typical for didepsides and is often followed by loss of water from the alcohol moiety (Figure 3).^{10–12}

In parallel to LDI-MS experiments, all samples were also studied by direct injection ESI-MS and results are outlined in Table 1. Contrary to LDI, some depsides did not show up as pseudomolecular ions in the ESI spectra, as shown for atranorin (Figure S-2) and thamnolic acid (Figure 3).

Table 1. Negative mode LDI and ESI signal patterns for single molecules (underlined species refer to base peaks) (Mycosporine serinol was analyzed in positive-ion mode)

structural family	molecule	molecular formula	monoisotopic mass	LDI-MS (m/z)	ESI-MS (m/z)
depsides	atranorin ^{10,11,17}	C ₁₉ H ₁₈ O ₈	374.10	<u>373</u> , 195, 177, 163	195, 177, <u>151</u>
	divaricatic acid ¹²	C ₂₁ H ₂₄ O ₇	388.15	387, 209, <u>195</u> , 177, 151	<u>387</u> , (209), 195
	evernic acid	C ₁₇ H ₁₆ O ₇	332.09	<u>331</u> , 181, 167, 149, 123	<u>331</u> , 181, 167
	thamnolic acid ¹²	C ₁₉ H ₁₆ O ₁₁	420.07	419, 375, 225, <u>211</u> , 193, 167	<u>375</u> , 167
depsidones	lobaric acid	C ₂₅ H ₂₈ O ₈	456.18	<u>455</u>	<u>455</u>
	stictic acid	C ₁₉ H ₁₄ O ₉	386.06	<u>385</u> , 357, 341	<u>385</u> , 357, 341
	variolaric acid	C ₁₆ H ₁₀ O ₇	314.04	<u>313</u>	<u>313</u> , 269
dibenzofurans and related	pannaric acid	C ₁₆ H ₁₂ O ₇	316.06	<u>315</u>	<u>315</u> , 297, 271
	usnic acid	C ₁₈ H ₁₆ O ₇	344.09	<u>343</u> , 329	<u>343</u>
diphenylethers	β -collatolic acid	C ₂₉ H ₃₄ O ₉	526.22	<u>525</u> , 280	<u>525</u>
	lobarin	C ₂₅ H ₃₀ O ₉	474.19	473, <u>411</u> , 238	<u>473</u> , 411, 385
	sakisacaulon A	C ₂₄ H ₃₀ O ₇	430.20	429, <u>385</u> , 251	<u>429</u> , 385
xanthenes	secalonic acid D	C ₃₂ H ₃₀ O ₁₄	638.16	<u>637</u>	<u>637</u>
	thiophanic acid	C ₁₄ H ₆ Cl ₄ O ₅	393.90	<u>393</u>	<u>393</u>
naphthoquinone	haemoventoin	C ₁₅ H ₁₂ O ₇	304.06	<u>304</u>	not detected
anthraquinones	chrysophanol	C ₁₅ H ₁₀ O ₄	254.06	<u>254</u>	not detected
	emodin	C ₁₅ H ₁₀ O ₅	270.05	<u>269</u>	<u>269</u>
	parietin	C ₁₆ H ₁₂ O ₅	284.07	<u>284</u>	not detected
	lepralic acid	C ₁₆ H ₁₈ O ₈	362.10	383, 339, <u>235</u> , 203	not detected
aliphatic and paraconic acids	roccellic acid	C ₁₇ H ₃₂ O ₄	300.23	<u>299</u> , 255	<u>299</u>
	lichesteric acid	C ₁₉ H ₃₂ O ₄	324.23	<u>323</u>	<u>323</u>
pulvinic acid derivatives	epanorin	C ₂₅ H ₂₅ NO ₆	435.17	<u>434</u>	<u>434</u>
	rhizocarpic acid	C ₂₈ H ₂₃ NO ₆	469.15	<u>468</u>	<u>468</u>
	vulpinic acid	C ₁₉ H ₁₄ O ₅	322.08	<u>321</u>	<u>321</u>
mycosporine (positive mode)	mycosporine serinol	C ₁₁ H ₁₉ NO ₆	261.12	300, <u>284</u> , 262	545, 300, <u>284</u> , 262

Proposed cleavages are consistent with previously described dissociation pathways.¹¹

Fragments observed in the diphenylethers spectra are presumed to come from a cleavage of the ether bond. While the first fragment could be identified in a straightforward manner, the second one showed up one mass unit lower than expected. This might be explained by the loss of a hydrogen radical, as previously described for diphenylether,¹³ but also for phenolic hydroxyl groups of flavonoids in negative-ion mode MALDI-MS.¹⁴ A typical example for diphenylether fragmentation is provided by the LDI spectrum of sakisacaulon A (Figure 4).

Furthermore, the analysis of quinones highlighted a specific advantage of LDI-MS over ESI-MS. While quinones were easily detected in LDI, their signals were, except for emodin,

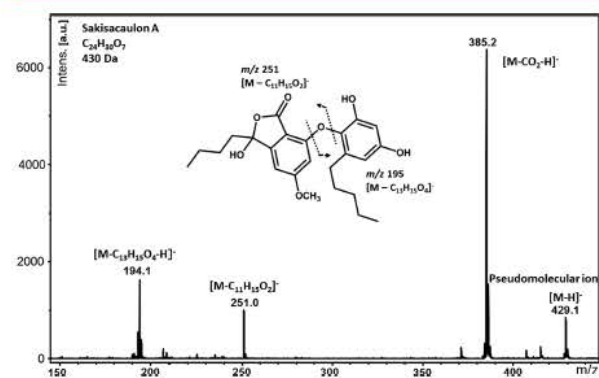


Figure 4. Negative mode LDI spectrum of sakisacaulon A and its proposed dissociation pathway.

constantly absent in ESI-MS. Chrysophanol (Figure 5A), haemoventoin, and parietin all exhibited molecular radical ions $[M]^{*-}$ in LDI, whereas emodin displayed a pseudomo-

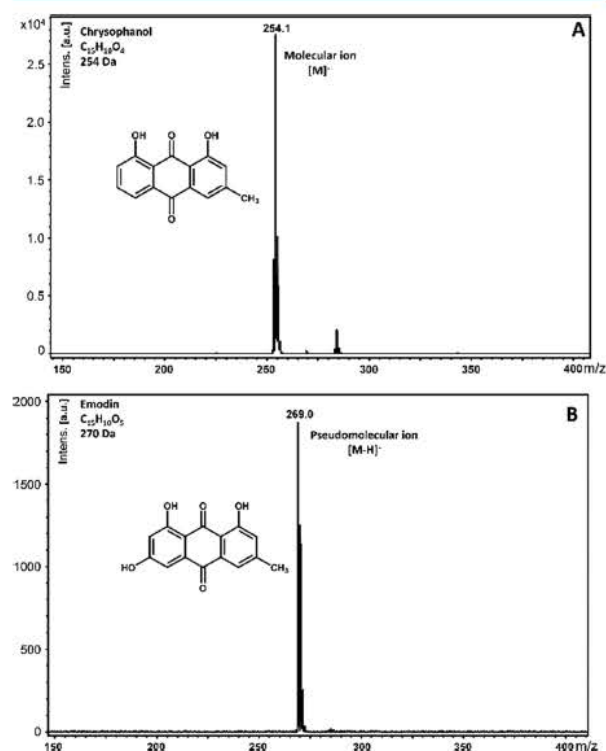


Figure 5. Negative LDI-MS of chrysophanol (A) and emodin (B).

Table 2. Lichen Extracts Yielding Similar Spectra in Negative LDI and ESI-MS

lichens	molecule	LDI-MS (<i>m/z</i>)	ESI-MS (<i>m/z</i>)	major compounds identified in the sample and consistent literature data
<i>Cladonia portentosa</i> ^a	usnic acid	343, 329, 259	343	usnic acid, perlatolic acid ^{19,20}
	perlatolic acid	443, 237, 223, 205, 179	443, 237, 223	
<i>Flavocetraria nivalis</i> ^b	pinastric acid	351	351	pinastric acid, usnic acid, vulpinic acid ²¹
	usnic acid	343, 329	343	
	vulpinic acid	321	321	
<i>Lecidella asema</i> ^b	asemone	359	359	asemone, 3- <i>O</i> -methylasemone, thiophanic acid, 3- <i>O</i> -methylthiophanic acid ¹⁸
	3- <i>O</i> -methylasemone	373	373	
	thiophanic acid	393	393	
	3- <i>O</i> -methylthiophanic acid	407	407	
<i>Pertusaria amara</i> ^a	picrolichenic acid	441, 397	441	picrolichenic acid, subpicrolichenic acid ^{22,23}
	subpicrolichenic acid	413	413	
<i>Ramalina cuspidata</i> var. <i>stenoclada</i> ^a	norstictic acid	371, 327	371	norstictic acid, usnic acid ²⁴
	usnic acid	343	343	
	unassigned signal	387	387	
<i>Ramalina siliquosa</i> var. <i>crassa</i> ^a	salazinic acid	387	387	salazinic acid, usnic acid ²⁴
	usnic acid	343	343	
<i>Roccella phycopsis</i> ^a	roccellic acid	299	299	roccellic acid, erythrin ²⁵
	erythrin	421, 317, 271, 167, 149	421, 167	
<i>Tephromela atra</i> ^a	α/β -collatolic acid	525, 280	525, 280	α - and β -collatolic acids, α -alectoronic acid, atranorin ²⁶
	α -alectoronic acid	511	511, 483	
	gangaleoidin	411	411	
	atranorin	373, 195, 177, 163	195, 151	
	unassigned signal	543	543	
<i>Usnea filipendula</i> ^b	salazinic acid	387	387	salazinic acid, usnic acid ^{19,27,28}
	usnic acid	343, 329, 259	343	
<i>Vulpicida pinastri</i> ^b	pinastric acid	351	351	pinastric acid, usnic acid, vulpinic acid ^{29,30}
	usnic acid	343, 329	343	
	vulpinic acid	321	321	

^aSamples (crude extracts) in which the outlined single compounds were isolated from their respective crude extract. ^bSamples (crude extracts) in which the outlined single compounds were identified by HPLC/DAD/MS.

lecular ion $[M - H]^-$ (Figure 5B). This is most reasonably explained by the different modes of ionization observed in ESI and LDI. For the latter, both the formation of the radical and pseudomolecular ions are possible.¹⁵ On the other hand, ESI is mainly a pseudomolecular ion-forming method.¹⁶ This explains why solely emodin could be observed in ESI. A closer look on the structure of these four compounds also helps understanding their respective preferences in terms of ion formation. Chrysophanol, haemovosin, and parietin all have their phenolic groups in close vicinity to a hydrogen bond acceptor moiety (carbonyl), preventing the formation of $[M - H]^-$. This is not the case for the phenolic group of emodin in position 3, which can be easily deprotonated to form $[M - H]^-$.

Analysis of Lichen Extracts. Subsequent to the LDI-MS analysis of single compounds, the LDI technique was further evaluated on complex mixtures, such as crude extracts originating from various lichen species of known chemical composition. There again, LDI was compared with direct injection ESI-MS. Additional HPLC-DAD-MS analyses were performed on all samples in order to determine the number of genuine compounds occurring within the samples and support observed fragmentation patterns. Overall, LDI-MS experiments yielded chemical profiles that were in good agreement with previously published works and at least equal to those obtained by ESI-MS (Table 2). In some cases, an

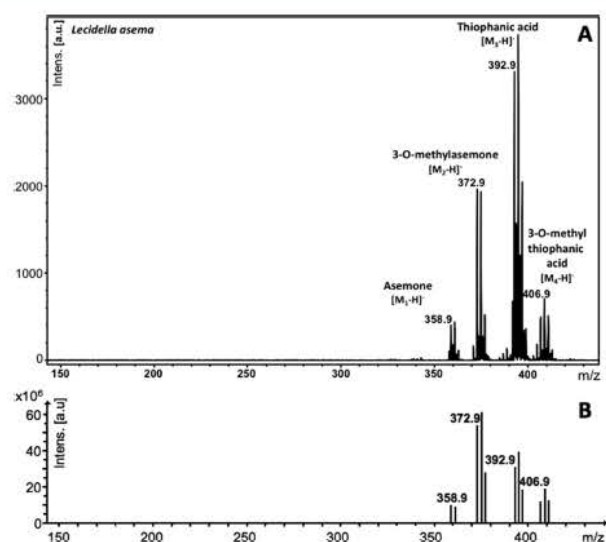


Figure 6. LDI-MS (A) and ESI-MS (B) negative-ion mode spectra of the acetone extract of *Lecidella asema*.

even wider range of compounds was detected by LDI-MS (Table 3). All LDI and ESI spectra are displayed in

Table 3. Lichen Extracts Displaying a More Detailed Chemical Profile in Negative LDI than in ESI

lichen	molecule	LDI-MS (m/z)	ESI-MS (m/z)	major compounds reported in literature
<i>Diploicia canescens</i> ^a	diploicin	421	421	diploicin, dechlorodiploicin, secalonic acids, chloroatranorin ³⁶
	dechlorodiploicin	387	387	
	secalonic acids	637	not detected	
	chloroatranorin	407, 229, 211, 195	not detected	
<i>Evernia prunastri</i> ^b	usnic acid	343	not detected	usnic acid, evernic acid, chloroatranorin, ³⁸ atranorin ^{11,27,37}
	evernic acid	331, 167	331, 181, 167	
	chloroatranorin	407, 229, 211, 195	229, 195, 185, 151	
	atranorin	373, 195, 177	195, 151 (all in common with chloroatranorin)	
<i>Ophioparma ventosa</i> ^a	usnic acid	343, 329	343	usnic acid, divaricatic acid, thamnolic acid, miriquidic acid, haemoventosin ³⁹
	divaricatic acid	387, 209, 195, 177	387, 209, 195, 181	
	thamnolic acid	419, 375, 225, 211, 167	375, 225, 211, 193, 181, 167	
	miriquidic acid	457, 223	not detected	
<i>Pseudevernia furfuracea</i> ^b	haemoventosin	304	not detected	atranorin, physodic acid, 3-OH physodic acid, 2'-O-methylphysodic acid, chloroatranorin, α -alectoronic acid ^{40,41}
	atranorin	373, 195, 177, 163	195, 177, 151 (all in common with chloroatranorin)	
	physodic acid	469	469, 425	
	3-OH physodic acid	485	485	
	2'-O-methylphysodic acid	not detected	483	
	chloroatranorin	407, 211, 195, 163	229, 195, 185, 151	
<i>Roccella fuciformis</i> ^a	α -alectoronic acid	511	511	erythrin, lepranic acid, roccelic acid ²⁵
	erythrin	421, 271, 167, 149	421, 271, 167	
<i>Xanthoria parietina</i> ^b	lepranic acid	235, 203	not detected	emodin, fallacinal, fallacinalol, parietin, parietinic acid ^{42–46}
	emodin	269	269	
	fallacinal	298	not detected	
	fallacinalol	300	not detected	
	parietin	284	not detected	
parietinic acid	314	not detected		

^aSamples (crude extracts) in which the outlined single compounds were isolated from their respective crude extract. ^bSamples (crude extracts) in which the outlined single compounds were identified by HPLC/DAD/MS.

Supporting Information (Figures S2–S43 and S44–S81, respectively).

The extracts of *Cladonia portentosa*, *Flavocetraria nivalis*, *Lecidella asema*, *Pertusaria amara*, *Ramalina siliquosa* var. *crassa*, *Tephromela atra*, *Usnea filipendula*, and *Vulpicida pinastri* yielded equivalent results for both methods and are summarized in Table 2. Any of the reported major compounds could be detected by LDI and ESI.

However, it is worth mentioning that automated LDI experiments were far less time-consuming since all 15 samples could be analyzed within 30 min. As a representative example, the crude extract analysis of *L. asema*, displaying all expected chlorinated xanthenes,¹⁸ is outlined in Figure 6.

For other lichen extracts such as *Diploicia canescens*, *Roccella fuciformis*, and *Ophioparma ventosa*, LDI-MS yielded more detailed chemical profiles than ESI-MS, as shown in Table 3. Highlighting this specific advantage of LDI, three representative examples will be consecutively discussed in detail. For *Evernia prunastri* (Figure 7), the LDI spectrum permitted the detection of usnic acid, atranorin, and chloroatranorin by their pseudomolecular ions, while these signals were entirely missing in the ESI spectrum. Solely evernic acid could be

detected by both methods. In the case of chloroatranorin, the ESI limitation of the missing $[M - H]^-$ ion could be bypassed by the close inspection of the characteristic isotopic pattern of its chlorinated fragments. However, in the case of the concurrent presence of atranorin and chloroatranorin, which neither showed $[M - H]^-$ (e.g., *E. prunastri* or *Pseudevernia furfuracea*, Table 3), the two compounds could not be distinguished by ESI since they both shared the same fragmentation pattern. Noteworthy, usnic acid, which was missing in the ESI-MS spectra of *E. prunastri* and *Ramalina cuspidata* var. *stenoclada* could be detected when LC-MS was used instead of direct injection ESI. The authors assume that the missing detection of usnic acid is most reasonably due to ion suppression effects resulting from direct injection, as previously described in the literature for ESI and APCI-MS experiments.³¹

As previously discussed for single compounds, haemoventosin, chrysophanol, and parietin, LDI induces the formation of molecular and pseudomolecular ions, while ESI exclusively forms pseudomolecular ions. The same effect was also observed when studying the crude extract of *Xanthoria parietina* (Table 3). There the main constituents (fallacinal,

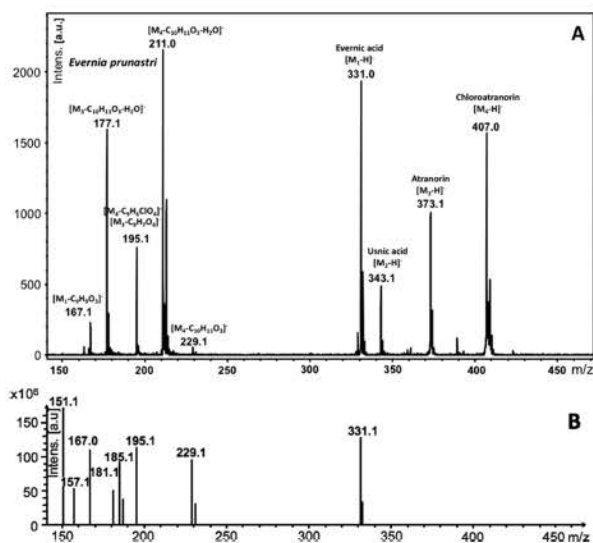


Figure 7. Compared negative-ion mode LDI (A) and ESI-MS (B) spectra of the acetone extract of *Evernia prunastri*.

parietin, and parietinic acid) were detected by their molecular radical ions $[M]^-$, while these signals were naturally missing in the ESI spectrum. Only emodin was detected in both LDI and ESI-MS (Figures S-43 and S-81, respectively).

Finally the LDI spectrum of *Ophioparma ventosa* (Figure 8) revealed all expected metabolites. Of special interest are

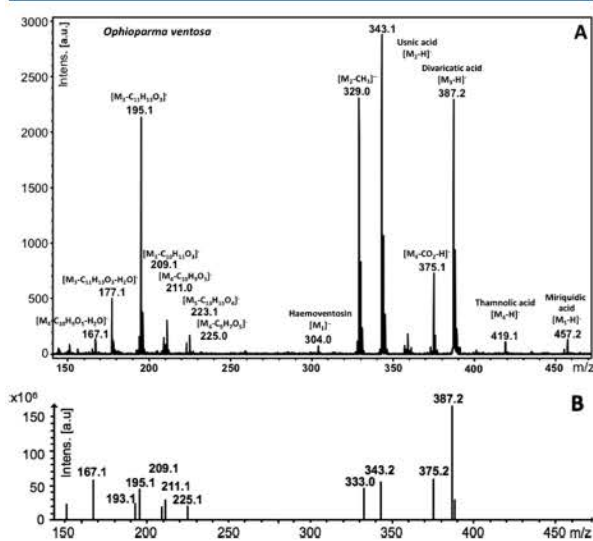


Figure 8. Comparison of negative LDI (A) and ESI-MS (B) spectra of *Ophioparma ventosa* acetone extract.

signals corresponding to miriquidic acid, the pseudomolecular ion of thamnolic acid and the radical molecular anion of haemovosin. Indeed, ESI-MS detection of this latter required a switch to positive-ion mode, which does not enable detection of any other metabolite, emphasizing the advantageous versatility of negative LDI-MS. This time-saving aspect represents one of the most valuable advantages of LDI as it allows accelerated sample processing and data analysis. Besides, LDI facilitated the detection of thamnolic acid in its

unfragmented state. The compound is very easily decarboxylated and always accompanied by decarboxythamnolic acid, which is regarded as an artifact rather than the product of an enzyme-mediated reaction.³² The detection of unfragmented thamnolic acid therefore highlights the softness of LDI ionization, indicating a significant advantage of LDI over ESI.

CONCLUSION

Up to today, only a few reports on the LDI detection of phenolic compounds exist, and to the best of the authors' knowledge, the present work represents the first analysis conducted on lichen compounds and extracts. Benefiting from the photoabsorbing properties observed for most groups of lichen metabolites, LDI can be directly conducted without any matrix support. The versatility of this approach was assessed in comparison to LC-ESI-MS and direct injection ESI-MS. It was found that LDI covers a wider range of analytes within one ionization mode, as shown for some depsides, but also for quinones (fallacinal, parietin, parietinic acid, and haemovosin). The effect is explained by the observation that LDI facilitates both $[M]^-$ and $[M - H]^-$ ion formation, while negative ESI preferably forms $[M - H]^-$ ions. Further advantages of LDI are its low cost, the possibility of automation (high-throughput screening), and that little to no sample preparation is required. Furthermore, the auto-ionizability of lichen polyphenols opens up new avenues for the screening of related natural compounds in plants and bacteria. Whether the method may also be used for quantitative applications and which limit of detection and sensitivity can be expected warrants further investigation. Further, it should be kept in mind that all presented MS data are acquired in low resolution, including any limitation coming along with it. However, the use of high-resolution mass spectrometry and tandem MS detectors should allow the analysis of even more complex samples and the direct identification of new compounds. So far, LDI-MS has only been performed on a rather limited number of chemical groups such as stilbenes,³³ flavonoids,³⁴ naphthodianthrones,³⁴ and phenylphenalenones.³⁵ With this in mind, the method represents an interesting field of contemporary research, which could be extended to many technical applications in the near future. Currently a follow up study is investigating the LDI-MS imaging and histolocalization of lichenic metabolites within lichen thalli. In conclusion, LDI-MS adds a versatile tool to the wide field of lichenology, facilitating direct and sharp analysis of lichen metabolites.

ASSOCIATED CONTENT

Supporting Information

The Supporting Information is available free of charge on the ACS Publications website at DOI: 10.1021/acs.analchem.5b02531.

Additional information as noted in text (PDF)

AUTHOR INFORMATION

Corresponding Authors

*E-mail: joel.boustie@univ-rennes1.fr.

*E-mail: pascal.richomme@univ-angers.fr.

Notes

The authors declare no competing financial interest.

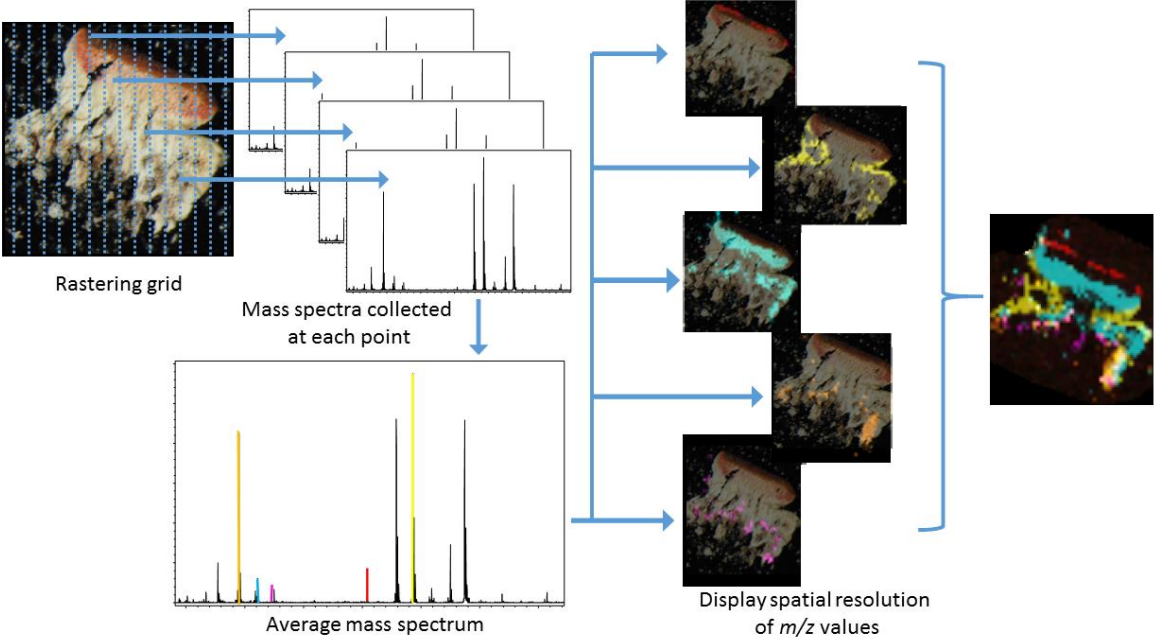
ACKNOWLEDGMENTS

This work was supported by the University of Rennes 1 through Project “Défi émergent LICHENMASS” and through the use of the mass spectrometry facilities of the PIAM platform of the University of Angers. Dr. Marylène Chollet-Krugler, Dr. Françoise Lohézic-Le Dévéhat, and Pr. Sophie Tomasi are greatly acknowledged for providing mycosporine serinol, *Lecidella asema*, and *Pertusaria amara* extracts. The authors are also grateful to Aurélie Bernard for her technical assistance.

REFERENCES

- (1) Boustie, J.; Grube, M. *Plant Genet. Resour.* **2005**, *3*, 273–287.
- (2) Nguyen, K.-H.; Chollet-Krugler, M.; Gouault, N.; Tomasi, S. *Nat. Prod. Rep.* **2013**, *30*, 1490–1508.
- (3) Elix, J. A.; Stocker-Worgotter, E. *Lichen Biology*; Cambridge University Press: New York, 2008; pp 104–133.
- (4) Shrestha, G.; St. Clair, L. L. *Phytochem. Rev.* **2013**, *12*, 229–244.
- (5) Le Pogam, P.; Herbette, G.; Boustie, J. *Recent Advances in Lichenology*; Springer: New York, 2015; pp 229–261.
- (6) Le Pogam, P.; Legouin, B.; Le Lamer, A.-C.; Boustie, J.; Rondeau, D. *J. Mass Spectrom.* **2015**, *50*, 454–462.
- (7) Schinkovitz, A.; Richomme, P. *J. Mass Spectrom.* **2015**, *50*, 270–274.
- (8) Santos, L. S.; Soriano, M.; del, P. C.; Mirabal-Gallardo, Y.; Carrasco-Sanchez, V.; Nachtigall, F. M.; Pereira, I.; Pereira, E. *Braz. Arch. Biol. Technol.* **2015**, *58* (2), 244–253.
- (9) La Barre, S.; Roullier, C.; Boustie, J. *Outstanding Marine Molecules: Chemistry, Biology, Analysis*; Wiley: New York, 2014; pp 333–360.
- (10) Huneck, S.; Schmidt, J. *Herzogia* **2006**, *19*, 199–203.
- (11) Hiserodt, R. D.; Swijter, D. F.; Mussinan, C. J. *J. Chromatogr. A* **2000**, *888*, 103–111.
- (12) Holzmann, G.; Leuckert, C. *Phytochemistry* **1990**, *29*, 2277–2283.
- (13) De Maaijer-Gielbert, J.; Somogyi, Á.; Wysocki, V. H.; Kistemaker, P. G.; Weeding, T. L. *Int. J. Mass Spectrom. Ion Processes* **1998**, *174*, 81–94.
- (14) Yamagaki, T.; Watanabe, T.; Tanaka, M.; Sugahara, K. *J. Am. Soc. Mass Spectrom.* **2014**, *25*, 88–94.
- (15) Kudaka, I.; Asakawa, D.; Mori, K.; Hiraoka, K. *J. Mass Spectrom.* **2008**, *43*, 436–446.
- (16) Mann, M. *Org. Mass Spectrom.* **1990**, *25*, 575–587.
- (17) Tabacchi, R.; Allemand, P.; Tsoupras, G. *Symbiosis* **1991**, *11*, 193–206.
- (18) Leuckert, C.; Knoph, J.-G. *Lichenologist* **1992**, *24*, 383–397.
- (19) Arup, U.; Ekman, S.; Lindblom, L.; Mattsson, J.-E. *Lichenologist* **1993**, *25*, 61–71.
- (20) Chollet-Krugler, M.; Le-Floch, M.; Articus, K.; Millot, M.; Boustie, J. *Planta Med.* **2008**, *74* (09), PC132.
- (21) Sundset, M. A.; Kohn, A.; Mathiesen, S. D.; Præsteng, K. E. *Naturwissenschaften* **2008**, *95*, 741–749.
- (22) Elix, J. A.; Calanasan, C. A.; Archer, A. W. *Aust. J. Chem.* **1991**, *44*, 1487–1493.
- (23) Bonny, S.; Paquin, L.; Carrié, D.; Boustie, J.; Tomasi, S. *Anal. Chim. Acta* **2011**, *707* (1–2), 69–75.
- (24) Parrot, D.; Jan, S.; Baert, N.; Guyot, S.; Tomasi, S. *Phytochemistry* **2013**, *89*, 114–124.
- (25) Parrot, D.; Peresse, T.; Hitti, E.; Carrié, D.; Grube, M.; Tomasi, S. *Phytochem. Anal.* **2015**, *26*, 23–33.
- (26) Millot, M.; Tomasi, S.; Sinbandhit, S.; Boustie, J. *Phytochem. Lett.* **2008**, *1*, 139–143.
- (27) Asplund, J.; Bokhorst, S.; Wardle, D. A. *Soil Biol. Biochem.* **2013**, *66*, 10–16.
- (28) MacGillivray, T.; Helleur, R. *J. Anal. Appl. Pyrolysis* **2001**, *58*, 465–480.
- (29) Kowalski, M.; Hausner, G.; Piercey-Normore, M. D. *Mycoscience* **2011**, *52*, 413–418.
- (30) Backor, M.; Bodnarova, M. *Thaiszia - J. Bot* **2002**, *12*, 173–178.
- (31) Antignac, J.-P.; de Wasch, K.; Monteau, F.; De Brabander, H.; Andre, F.; Le Bizec, B. *Anal. Chim. Acta* **2005**, *529*, 129–136.
- (32) Culberson, C. F.; Culberson, W. L.; Johnson, A. *Phytochemistry* **1977**, *16*, 127–130.
- (33) Hamm, G.; Carre, V.; Poutaraud, A.; Maunit, B.; Frache, G.; Merdinoglu, D.; Muller, J.-F. *Rapid Commun. Mass Spectrom.* **2010**, *24*, 335–342.
- (34) Holscher, D.; Shroff, R.; Knop, K.; Gottschaldt, M.; Crecelius, A.; Schneider, B.; Heckel, D. G.; Schubert, U. S.; Svatos, A. *Plant J.* **2009**, *60*, 907–918.
- (35) Holscher, D.; Fuchser, J.; Knop, K.; Menezes, R. C.; Buerkert, A.; Svatos, A.; Schubert, U. S.; Schneider, B. *Phytochemistry* **2015**, *116*, 239–245.
- (36) Millot, M.; Tomasi, S.; Studzinska, E.; Rouaud, I.; Boustie, J. *Nat. Prod.* **2009**, *72*, 2177–2180.
- (37) Legaz, M. E.; Avalos, A.; Torres, M.; de Escribano, M. I.; González, A.; Martín-Falquina, A.; Pérezurria, E.; Vicente, C. *Environ. Exp. Bot.* **1986**, *26*, 385–396.
- (38) Culberson, C. F. *Bryologist* **1970**, *73*, 177–377.
- (39) Le Pogam P.; Legouin B.; Le Lamer A.-C.; Boustie J.; Rondeau D. XXIIth GP2A Conference, Faculty of Pharmacy, Nantes, France, August 28–29, 2014, communication.
- (40) Culberson, W. L.; Culberson, C. F.; Johnson, A. *Mycologia* **1977**, *69*, 604–614.
- (41) Manrique, E.; López, F. *Bryologist* **1991**, *94* (2), 207–212.
- (42) Piattelli, M.; de Nicola, M. G. *Phytochemistry* **1968**, *7*, 1183–1187.
- (43) Sargent, M. V.; Smith, D. O.; Elix, J. A. *J. Chem. Soc. C* **1970**, No. 2, 307–311.
- (44) Söchting, U.; Lutzoni, F. *Mycol. Res.* **2003**, *107* (11), 1266–1276.
- (45) Söchting, U. *Bibl. Lichenol.* **1997**, *68*, 135–144.
- (46) Arup, U.; Söchting, U.; Frödén, P. *Nord. J. Bot.* **2013**, *31* (1), 016–083.

HISTOLOCALISATION DE COMPOSÉS LICHÉNIQUES



PARTIE 3 : HISTOLOCALISATION DE COMPOSÉS LICHÉNIQUES

I. État de l'art

Un second grand axe de travail entrepris dans le cadre de cette thèse avait pour objectif de préciser la distribution tissulaire des métabolites lichéniques.

Peu de travaux se sont penchés jusqu'à présent sur l'histolocalisation fine des composés lichéniques bien que la répartition inhomogène de composés lichéniques ait pu être constatée au sein du thalle de plusieurs lichens, vraisemblablement en lien avec le rôle écologique de ces molécules. Il est ainsi souvent constaté que les organes reproducteurs du lichen vont concentrer davantage de polyphénols que le reste du thalle, sans doute pour procurer une défense chimique à ces précieux organes pour la pérennisation de l'espèce (Asplund et al., 2010; Hyvärinen et al., 2000). La caractérisation de ces aires de distribution repose essentiellement sur des méthodes chimiques (réactions thallines) ou optiques (profils de fluorescence UV) (Kauppi and Verseghe—Patay, 1990) qui dans les deux cas distinguent mal les composés individuels (cf. Chapitre CCM-MS) ou sur des extractions d'organes ciblés suivies d'une étude phytochimique traditionnelle mais dans ce cas de figure, les détails fins de la répartition des molécules sont perdus. La seule étude ayant réalisé une véritable histo-localisation de composés lichéniques est une analyse par spectromicroscopies infrarouge et Raman ayant précisé la distribution de l'acide usnique au sein de différentes espèces de *Cladonia*, atteignant une résolution spatiale de l'ordre de 15 μm (Liao et al., 2010).

L'essor relativement récent de l'imagerie par spectrométrie de masse (MSI pour *Mass Spectrometry Imaging*) offre de nouvelles techniques pour accéder à la distribution spatiale des composés présents dans un échantillon. Schématiquement, l'acquisition de ces données se décompose en quelques grandes étapes (Esquenazi et al., 2009) (Figure 29):

- la **préparation de l'échantillon** est plus ou moins longue et exigeante selon la nature de l'ionisation mise en œuvre (e.g pulvérisation de la matrice dans le cadre des analyses MALDI...);
- la seconde étape représente l'**acquisition des données** à proprement parler. Pour ce faire, l'échantillon est déplacé pour permettre à la source d'en ioniser différentes positions selon un quadrillage prédéfini. Un spectre de masse est alors généré en chacun de ces points ;
- le troisième temps correspond à un **traitement graphique** des données. Chacun des signaux d'intérêt va être associé à une couleur qui sera ensuite utilisée pour représenter la présence du composé avec une intensité d'autant plus marquée que le composé est abondant. Les molécules peuvent ensuite être associées à leur structure histologique d'appartenance en superposant les aires de distributions ioniques à une image optique de l'échantillon.

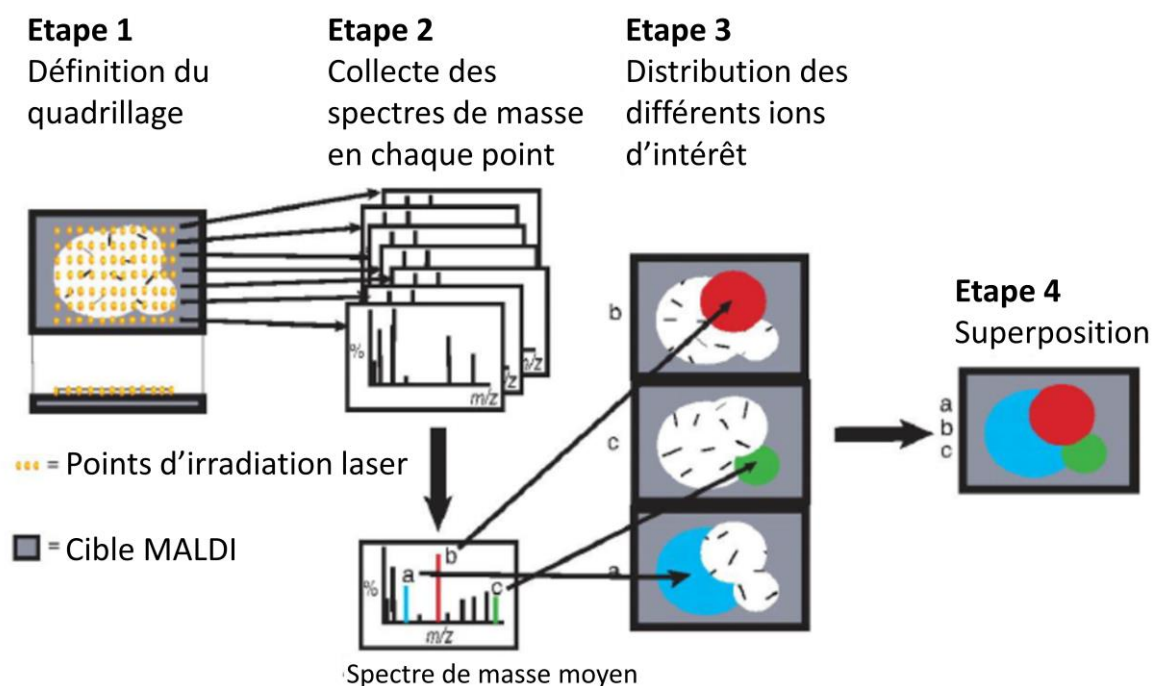


FIGURE 29: PRINCIPE DE L'ACQUISITION DES DONNÉES EN IMAGERIE PAR SPECTROMÉTRIE DE MASSE LDI (ADAPTÉ DE (GREER ET AL., 2011))

Les sources d'ion les plus classiquement employées en imagerie par spectrométrie de masse sont le MALDI, le DESI et le SIMS. À noter que des analyses LAESI (*Laser Ablation ElectroSpray Ionization*) ont permis de réaliser de l'histolocalisation tridimensionnelle au sein de feuilles d'*Aphelandra squarrosa* (Nemes and Vertes, 2009).

Compte-tenu de l'ionisation satisfaisante des composés en LDI, les analyses d'imagerie par spectrométrie de masse entreprises dans le cadre de cette thèse ont été engagées avec cette source d'ions. Le LDI-MSI a été utilisé au service de deux problématiques différentes qui vont être abordées séquentiellement au titre de cette troisième partie :

- l'histolocalisation des composés polyphénoliques au sein du thalle d'*Ophioparma ventosa*. Ces analyses ont fait appel aux appareillages de la plate-forme BIA de l'INRA de Nantes dans le cadre d'une collaboration avec Audrey Geairon et le Docteur Hélène Rogniaux ;
- l'imagerie de la mycosporine sérinol au sein du cyanolichen *Lichina pygmaea* pour tenter de mieux comprendre la contribution des symbiontes dans la biosynthèse de ces composés. Cette thématique s'accompagne d'une étude concernant l'équipement génétique des partenaires réalisée en collaboration avec le Dr. Yanyan Li (UMR 7245 CNRS/MNHN, Paris 5). Les premières étapes de ces travaux de biologie moléculaire ont fait appel à l'expertise du Pr. Annie Guiller (Université Jules Verne, Amiens).

II. Distribution tissulaire des composés produits par *Ophioparma ventosa* par LDI-MSI : écologie chimique

L'étude de la répartition des métabolites secondaires au sein du lichen *Ophioparma ventosa* a été engagée sur la base des analyses DART-MS qui indiquaient une répartition asymétrique des composés qu'il contient (comparatif face supérieure vs. face inférieure). La localisation tissulaire de l'acide miriquidique, depside que nous avons décrite pour la première fois chez *Ophioparma ventosa* représentait un intérêt supplémentaire à cette analyse d'imagerie. Les métabolites secondaires principaux isolés à partir de ce lichen ont pu être imagés avec une résolution spatiale de l'ordre de 50 μm à partir de coupes réalisées par un cryotome (40 μm d'épaisseur) (plate-forme H2P2, Dr. Alain Fautrel) ou manuellement à la lame de rasoir. Les contours de distribution des composés sont cohérents avec les rôles écologiques précédemment décrits pour ces différentes molécules.

Ces analyses sont compilées dans un article devant être soumis très prochainement à Scientific Reports. Une version avancée de ce draft est fournie à la suite tandis que les données complémentaires peuvent être consultées en Annexe 8 (p. 323).

SCIENTIFIC REPORTS

OPEN Spatial mapping of lichen specialized metabolites using LDI-MSI: chemical ecology issues for *Ophioparma ventosa*

Received: 14 July 2016
Accepted: 27 October 2016
Published: 24 November 2016

Pierre Le Pogam^{1,2}, Béatrice Legouin¹, Audrey Geairon³, Hélène Rogniaux³,
Françoise Lohézic-Le Dévéhat¹, Walter Obermayer⁴, Joël Boustie^{1,4} &
Anne-Cécile Le Lamer^{1,5,8}

Imaging mass spectrometry techniques have become a powerful strategy to assess the spatial distribution of metabolites in biological systems. Based on auto-ionisability of lichen metabolites using LDI-MS, we herein image the distribution of major secondary metabolites (specialized metabolites) from the lichen *Ophioparma ventosa* by LDI-MSI (Mass Spectrometry Imaging). Such technologies offer tremendous opportunities to discuss the role of natural products through spatial mapping, their distribution patterns being consistent with previous chemical ecology reports. A special attention was dedicated to miriquidic acid, an unexpected molecule we first reported in *Ophioparma ventosa*. The analytical strategy presented herein offers new perspectives to access the sharp distribution of lichen metabolites from regular razor blade-sectioned slices.

Lichens are a world-widespread consortium of fungal and photosynthetic partners. The high specialization in lichen tissue metabolism leads to diverse metabolite distribution corresponding to secondary metabolites, preferably named specialized metabolites. For example, lichens tend to allocate their most efficient grazing-deterrent compounds to their reproductive parts that are the most valuable for lichen fitness, in agreement with the optimal defense theory¹. The discovery of such distribution patterns most often relies on extraction of targeted tissues for chemical analyses, sometimes guided by specific features of the analytes such as UV fluorescence². Many lichen compounds can also be stained by exogenously applied chemicals (spot tests on cortex, medulla or apothecium). Both approaches appear limited since sharp details of distribution are lost when analyzing bulk tissues, while techniques based on functional group histochemistry do not distinguish between individual compounds and lead to distortions of localization. MSI techniques underwent significant technological improvements during the last decade so that they gained considerable importance in the field of plant metabolites imaging, the most prevalent method being MALDI-MSI (Matrix Assisted Laser Desorption and Ionization)³. We first reported on auto-ionisability of all main classes of lichenic compounds using matrix-free LDI-MS and emphasized the potential of this technique as a blitz-screening compatible dereplication tool⁴. Indeed, lichen analytes did not require a chemical matrix for ionization avoiding the tricky step of matrix spraying and the interference between the high matrix ion background in the low mass range and sample metabolites. Lack of matrix is also a tremendous advantage in the field of imaging since applying MALDI matrices complicates sample preparation for imaging and might disturb the native distribution of the studied metabolites⁵. *Ophioparma ventosa* (L.) Norman., also referred to as the Alpine bloodspot owing to its blood-red fruiting bodies (apothecia) and a grayish thallus, represents a well-fitted model to investigate the tissue-specific accumulation of lichen metabolites. Preliminary DART-MS experiments emphasized specific distribution patterns of *O. ventosa* specialized metabolites between

¹Université Rennes 1, UMR CNRS 6226 PNSCM, 2 Avenue du Pr. L. Bernard, 35043 Cedex, France. ²Institut d'Électronique et de Télécommunications de Rennes, Université Rennes 1, UMR CNRS 6164, 263 Avenue du Général Leclerc, 35042 Cedex, France. ³INRA, UR 1268 Biopolymers Interactions Assemblies F-44316 Nantes, France. ⁴Universität Graz, Institut Karl Franzens, Holteigasse 6, A-8010 Graz, Austria. ⁵Université Toulouse 3 Paul Sabatier, UFR Pharmacie, 118 Route de Narbonne, 31062 Toulouse, France. ⁶These authors contributed equally to this work. Correspondence and requests for materials should be addressed to P.L.P. (email: pierre.lepogam.alluard@gmail.com) or J.B. (email: joel.boustie@univ-rennes1.fr)

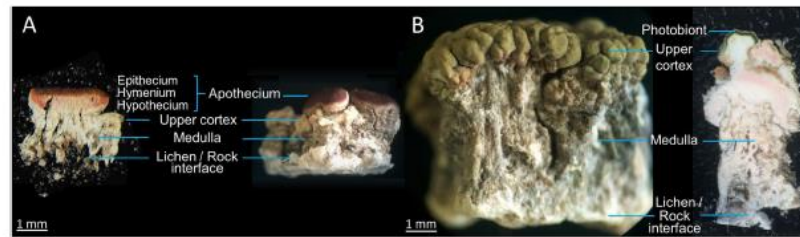


Figure 1. Lateral macroscopic views of *O. ventosa* from both sampling sites revealing the different anatomical features alongside a cryosectioned piece of an apotheciate thallus (Tyrol sample) (A) and a hand-cut piece of a non-apotheciate thallus (Styria sample) (B).

the apothecia and the thallus and within the depth of its thick thallus paving the way for imaging mass spectrometric analyses on this lichen⁶. The structural diversity of specialized metabolites described in this lichen (Figure S1)⁷ also makes it a relevant model to demonstrate the broader applicability of LDI-MSI in the wide field of lichenology. Besides, the material investigated here was of specific interest as it contained miriquidic acid, a rare depside which was solely described for this species on this particular sample collected in Austrian Alps⁶. Given the aggressiveness of *O. ventosa* and its trend to overrun neighbouring lichens, an hypothesis to explain the arising of this additional molecule is that it might be acquired from overgrown lichens rather than being biosynthesized by *O. ventosa* itself, as previously suggested for other additional metabolites^{7,8}. In our specific case, locally occurring miriquidic acid-producing lichen species represent likely candidates to account for the presence of this depside within our sample (e.g. *Miriquidica garovaglii*)⁹. It was therefore worth checking (i) how miriquidic acid was distributed in a piece of thallus and (ii) whether miriquidic acid was ascribed to the basal layers of the lichen, as expected if acquired from overgrown lichens. In our study, we intended to image the distribution pattern of specialized metabolites from *O. ventosa* with a specific insight into miriquidic acid. LDI-MSI could establish the spatial mapping of all specialized metabolites known from our sample with a spatial resolution of 50 μm including miriquidic acid and even one of the trace pigments recently described within the apothecia of *O. ventosa* (Figure S1)¹⁰. Their distribution patterns are consistent with the ecological roles previously proposed for these metabolites.

Results

Lichen material and preparation of the slices. *Ophioparma ventosa* appears as a crustose epilithic lichen forming large patches reaching up to 15 cm diameter. Its blood-red fruiting bodies (=apothecia) are delimited by an algae-containing external rim concolour with the rest of the thallus called thallin margin. The appearance of this species is known to be highly variable regarding the color and the thickness of the thallus^{8,7}. Hence, two different samples from Austrian Alps were considered during the course of this manuscript to take into account the morphological variety of this lichen. The first sample, referred to as Tyrol sample, was collected in the Tyrol state in southwest Austria (Fig. 1A). It exhibits a yellowish colour and a rather thin thallus structure (1–3 mm). The second lichen displaying a greenish colour and a thick thallus (3–10 mm) was collected in the state of Styria, in the southeast of Austria (Styria sample) (Fig. 1B).

The histological structures of slices containing and lacking apothecia obtained from both lichen samples are displayed in Fig. 1. The cross section of an apothecium reveals the hymenium which represents the spore-bearing layer of the fruiting body. The epithecium is the red tissue present at the surface of the hymenium layer, formed by the branching of the ends of the paraphyses above the asci. Conversely, the hypothecium refers to the hyphal layer beneath the hymenium in an apothecium. The hypothecium of *O. ventosa* is faint pink, especially in its basal parts¹¹. *Ophioparma ventosa* develops an internally-stratified thallus typical of the so-called heteromerous lichens divided into three main layers that are upper cortex, photobiont layer and medulla. The algal cells, in the present case belonging to the *Trebouxia* genus, are arranged in a discrete layer immediately below the upper cortex. Due to the areolate structure of the thallus, the algae trailing the upper cortex might arise in an anticlinal orientation. The thickest lichen layer, named medulla, is the histological layer present below the photobiont to the surface of the rock. As a crustose lichen, *O. ventosa* lacks a lower cortex. Its fungal filaments extend downwards into the rock substrate from its entire surface, forming an hyphal layer inside the rock. The layer could be 7–12 times as thick as the thallus present at the surface of the rock¹². Therefore, the lichen cannot be removed from its substratum without being damaged which accounts for the poor integrity of the lower parts of the thallus, which might further crumble upon slicing.

Two different slicing procedures were applied to the lichen material for samples of both locations: cryosectioning (Fig. 1A) and hand-cutting (Fig. 1B). For the cryosectioning procedure, the use of organic solvents was avoided to circumvent de-localization of hydrophobic metabolites of *O. ventosa* and 40 μm thick transverse sections were cut from frozen pieces of thallus resulting in a significant crumbling of the medulla. Hand-cutting merely used a razor blade, as regularly performed by lichenologists, to afford undamaged slices with a thickness exceeding 100 μm .

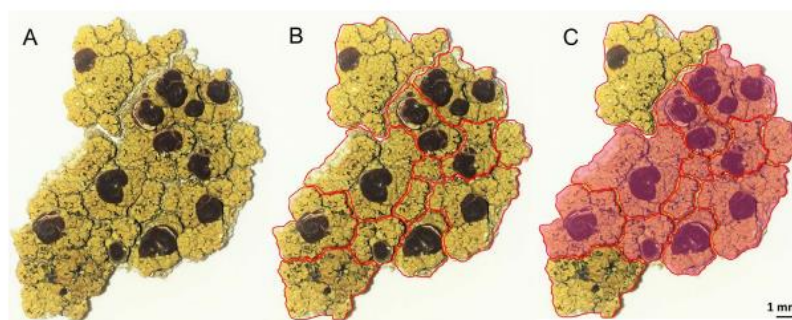


Figure 2. Longitudinal distribution of miriquidic acid in a piece of *Ophioparma ventosa* thallus (Tyrol sample). Piece of thallus (A). Division of a piece of thallus in small fragments (B). Rose patches refer to areas containing miriquidic acid, as revealed by TLC monitoring (C).

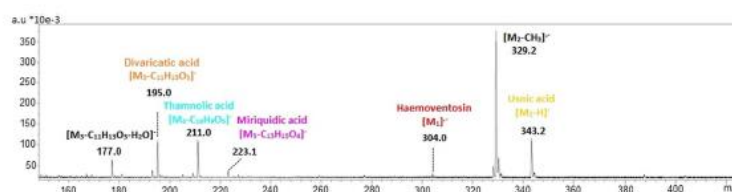


Figure 3. Negative-ion mode LDI mass spectrum of a dichloromethane extract of *Ophioparma ventosa* displaying ions selected for imaging mass spectrometry with related colors.

Chemical investigation of micro-samples of *O. ventosa*. To assess whether miriquidic acid was evenly distributed in the thallus, we first checked the chemical profile of 50 random pieces of thallus from the Styria sample. Each fragment was cut into upper and lower halves to monitor their chemical content by Thin Layer Chromatography (TLC) (Figure S2). These micro-analyses revealed that miriquidic acid occurs in only two of them, and when it is present, it seems confined to the lower part of the medulla. Then, the distribution of miriquidic acid was studied in the specific context of a piece of thallus taken from the Tyrol sample. For this purpose, several pieces of lichen were divided into small fragments in accordance with the areolate structure of the thallus as depicted in Fig. 2B and S3. TLC monitoring of each fragment confirmed that miriquidic acid did not occur in every fragment and it is noteworthy that the lichen fragments containing this depside appeared contiguous to one another, defining patches as displayed in Fig. 2C and S3. Once again, miriquidic acid was ascribed to the lower half of the thallus pieces. Hence, these results indicate an uneven longitudinal distribution of miriquidic acid and allowed us to select pieces of lichen containing or lacking miriquidic acid for LDI-MSI experiments.

355 nm-UV Laser desorption/ionization time of flight (LDI-TOF) detection of *O. ventosa* specialized metabolites. We recently outlined that lichen metabolites ionized under UV irradiation with a conventional nitrogen laser (337 nm) fitted to the MALDI instrument⁴. Since the present study uses a spectrometer with a 355 nm smartbeam laser, a dichloromethane extract of *Ophioparma ventosa* was analyzed as a control to check if compounds could still be ionized at this different wavelength without matrix assistance. This preliminary analysis revealed that a 355 nm laser triggers a satisfying ionization of all main compounds encountered within our *O. ventosa* sample, with comparable fragmentation patterns. Signals from this mass spectrum were thus assigned by comparison to prior 337 nm – LDI analysis⁴. Names and structures of specialized metabolites described from *O. ventosa* are given in Figure S1.

Deprotonated usnic acid (m/z 343) and the molecular ion of haemoventosin (m/z 304) were selected to image the distribution of these metabolites. Depsides underwent a significant fragmentation under 355 nm laser desorption ionization similar to that triggered at 337 nm so that divaricatic, miriquidic and thamnolic acids were better detected through their fragments than their deprotonated molecule. Depsides were consequently imaged by their alcohol moieties, released through breakage of their ester bond as previously reported (divaricatic acid: m/z 195, miriquidic acid: m/z 223 and thamnolic acid: m/z 211)⁴ (Fig. 3).

LDI-MSI of *O. ventosa* specialized metabolites. *In situ* assessment of *O. ventosa* specialized metabolites is displayed on two series of mass spectrometric images from the two sampling sites (Tyrol: Fig. 4 and S4

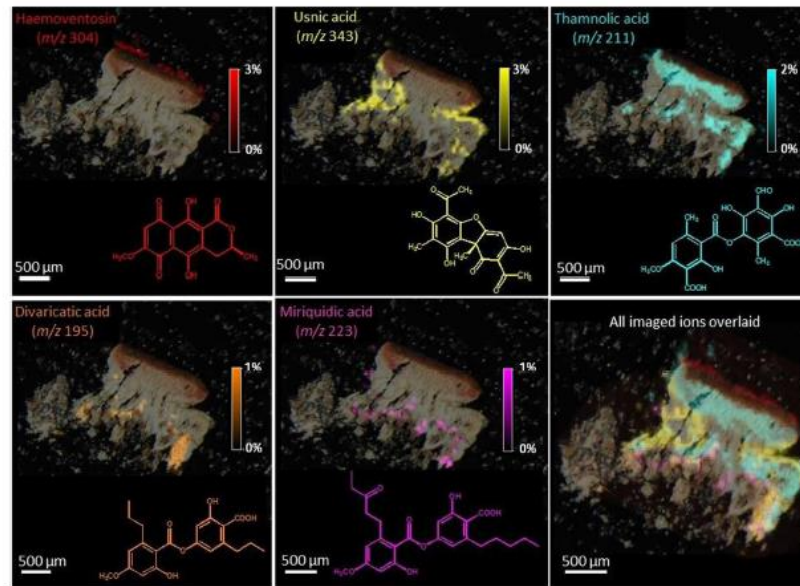


Figure 4. From left to right: Molecular images of haemoventosin, usnic acid, divaricatic acid, thamnolic acid, miriquidic acid and all overlaid ions in a cryosectioned piece of an apotheciate piece of thallus from the Tyrol sample of *Ophioparma ventosa*. Intensities of ions in the imaged spots are color coded using a heat map with relative intensities given as indicated on the color scale bars.

and Styria; Fig. 5 and S5). A first outcome is that LDI-MSI afforded ion images of similar qualities from both 40 µm thick cryosectioned slices and ca. 100 µm hand-cut sections. Then, the distribution patterns retrieved from the lichens of both sampling sites and from either apotheciate or non-apotheciate pieces of thallus are similar. Specialized metabolites could be imaged with a resolution of 50 µm, showing organized and specific spatial allocations for each compound, which do not overlap.

Haemoventosin was localized in the red epihymenial layer. While this molecule remains the major pigment of the fruiting bodies, we recently isolated a variety of minor pyranonaphthoquinones from the apothecia of *O. ventosa*¹⁰. Their trace amounts limited their imaging but 4-hydroxyhaemoventosin could be ascribed to the red epihymenial layer, thus being co-localized with haemoventosin (Fig. 6). Usnic acid is densely distributed above the *Trebouxia* photobiont layer and along internal furrows. Thamnolic acid is confined to the hypothecium and upper medulla parts of the lichen, associated with faint pink-colored patches. At last, divaricatic and miriquidic acids are allocated to the lower medulla of the lichen extending downwards to the lichen/rock interface. Molecular images acquired from samples not displaying miriquidic acid in both Tyrol and Styria lichens are presented in Figures S4 and S5.

Overall, these results were in full agreement with those provided by DART-MS which ascribed haemoventosin, usnic and thamnolic acids to the upper part of the thallus whereas divaricatic acid was rather detected from the lower half of the lichen⁹. Non-detection of miriquidic acid from the previous DART-MS investigated pieces of thallus might refer to the uneven allocation of this depside.

Discussion

LDI-MSI appears as a versatile approach for lichen metabolites mapping. Regarding the thickness of the slices, regular slices obtained using a razor blade are perfectly suitable for imaging purposes, bypassing the mandatory need for expensive slicing facilities. Haemoventosin, usnic acid, divaricatic acid and thamnolic acid are diagnostic compounds of *Ophioparma ventosa*^{8,7}. Their occurrence in each slice supports their taxonomic value, and their organized, non-overlapping and constant distribution patterns suggests a specific ecological relevance for each of them.

As expected, pigments such as haemoventosin and its minor derivative 4-hydroxyhaemoventosin are confined to the apothecia, especially to the epithecium. The reproductive structures are often reported to produce specific lichen compounds or known to be more concentrated in phenols than the remaining thallus¹³, in accordance with the optimal defense theory¹⁴. Haemoventosin belongs to a structural class (quinones) exerting a wide array of biological activities of ecological significance including antibiotic, antifungal¹⁵ and cytotoxic properties¹⁰. Moreover, haemoventosin putatively acts as a UV screening filter to protect spores during their maturation within

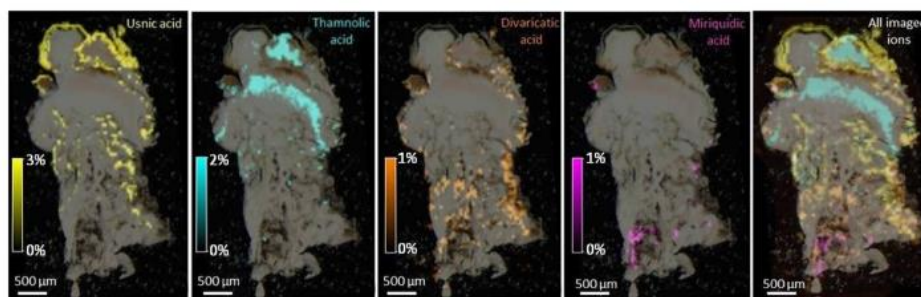


Figure 5. From left to right: Molecular images of usnic acid, divaricatic acid, thamnolic acid, miriquidic acid and all overlaid ions in a hand-cut piece of an apotheciate piece of thallus from the Styria sample of *Ophioparma ventosa*. Intensities of ions in the imaged spots are color coded using a heat map with relative intensities given as indicated on the color scale bars.

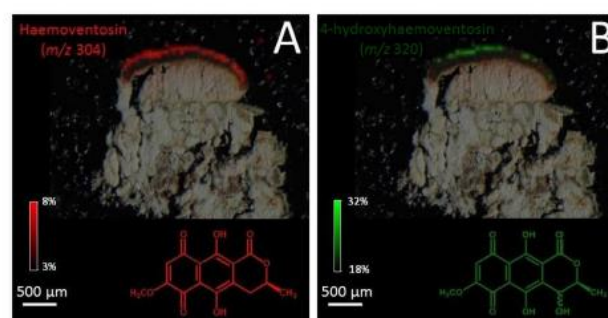


Figure 6. Molecular images of naphthazarine pigments in the Tyrol sample of *Ophioparma ventosa* (A): haemoventosin m/z 304 and (B): 4-hydroxyhaemoventosin m/z 320). Intensities of ions in the imaged spots are color coded using a heat map with relative intensities given as indicated on the color scale bars.

asci. As haemoventosin forms a film at the surface of asci apices, this quinone most likely spreads on spore surface which might be a beneficial effect for the initial steps of spore germination, by inhibiting the growth of competing microorganisms. Lichens were also found to host substantial communities of non photo-autotrophic bacteria, that are increasingly regarded as integrated partners of the lichen symbiosis¹⁶. It was presumed that the arising of haemoventosin was linked to the establishment of the atypical bacterial communities of *O. ventosa*, selecting bacterial strains able to withstand such metabolites^{16,17}.

LDI-MSI revealed usnic acid to be concentrated in cortical areas that contain the photobiont. Through the use of vibrational spectromicroscopy approaches and scanning electron microscopy, comparable distribution patterns were evidenced in different lichens^{18,19}. In the context of lichen symbiosis, the photobionts display an increased resilience suggesting that a substantial photoprotection is provided by the cortical mycobiont layer above the photobiont. Given the strong UV absorption of usnic acid²⁰, its cortical distribution suggests its involvement in photoprotection of the sensitive algal layer^{13,21}. However, the arising of this phytotoxic mycobiont-derived product^{22–25} at the surface of the algal partner²⁶, or even within it²⁷, might appear surprising. Usnic acid was indeed proven to act as an allelochemical exerting phytotoxic effects that are nevertheless higher towards free-living alga than on aposymbiotically grown lichen photobionts. This shall be regarded as an adaptation resulting from long term co-evolution of these algae with fungi that produce toxic specialized metabolites²⁸. To maintain a harmonious growth pattern of the thallus, the mycobiont, whose growth capacities are limited, has to regulate the metabolism and the division rate of its photobiont through chemicals^{29,30}. More widely, usnic acid displays pleiotropic effects including strong antibacterial effects³¹, antifeedant activity, toxicity towards herbivorous insects^{32,33} and metal-binding properties under acidic conditions³⁴ that might lower availability of toxic ions to photobiont cells³⁵. It is worth pointing out that usnic acid also occurs in deeper parts of the lichen thallus, where it defines reticulated structures. This secondary distribution pattern can be understood by referring to the brain-like growth of *O. ventosa* thallus: when new squamules are developed on the surface, the old surface of the lichen (including cortex and

algae) gets buried in a self-overgrowing process. The deep furrows of usnic acid might then refer to the former localization of the photobionts.

Thamnolic acid was found to be mainly located in the upper part of the medulla for both samples, but also within hypothecial tissue for apotheciate samples (Fig. 4). A few works previously reported on thamnolic acid distribution within lichen thalli, most often arising in the sub-apothecial tissues as well as in the hypothecial and thalline tissues³⁶. Regarding *Ophioparma* species, thamnolic acid is given responsible for the pink color of the basal hypothecium layers (Fig. 1B)^{11,37}. This depside is found in a wide array of lichens growing on acidic substrata as *O. ventosa* that displays a mid pH range of 4.4³⁸. With a pK_{a1} of 2.8, thamnolic acid might represent a selective advantage to cope with increasing acidic air and rain pollution^{39–41}. Likewise, one can imagine that thamnolic acid produced by *O. ventosa* might help outcompeting other lichens growing in its environment in acidifying conditions. As an example, the commonly associated *Rhizocarpon geographicum* was proven to be severely damaged by acid rain⁴². Spatial allocation of compounds involved in control of acidity tolerance in lichens is not considered to play a key role in their functioning⁴¹. However, hypothecium represents a very valuable tissue for lichen fitness. Therefore, the partitioning of thamnolic acid might be regarded as a further example of the optimal defense theory.

LDI-MSI spatial mapping allocated divaricatic acid to the lower parts of the medulla, even at the interface with the rock for the Tyrol sample, thus making divaricatic acid a candidate to account for chemical weathering⁴³. Some lichen substances in direct contact with the mineral surfaces of porous rocks were reported to increase mineral dissolution rates and may contribute in the chemical weathering process^{45–47}. Indeed, in a comparative study of the lichen-rock interface of different epilithic lichens, the mean weathering depth beneath *O. ventosa* was much thicker than with the other lichens⁴³. Divaricatic acid was among the first molecules reported to occur in the rock beneath epilithic lichens and the only *O. ventosa* metabolite that has been detected in the weathered rock^{43,48}. Besides, cation-chelating properties of lichen substances that accumulate on the outer surface of the hyphae might also step in metal ion homeostasis and heavy metal tolerance^{49–51}. As such, divaricatic acid was proven to promote Cu²⁺ uptake⁵² by adsorbing this ion. Since Cu stands among the rarest micronutrients, divaricatic acid might be crucial in supplying this cofactor. Promotion of the uptake of metals needed as micronutrients might then broaden the ecological niche of lichens in nutrient-poor habitats⁵².

We first reported on the presence of miriquidic acid in a sample of *O. ventosa* collected in the Tyrol state in Austria⁶. Alongside aforementioned metabolites that are constant in this lichen, a vast array of additional molecules could be occasionally detected including atranorin, stictic, norstictic, psoromic, salazinic, gyrophoric, alectoronic and α -collatolic acids⁷. Since lichens belonging to the *Ophioparma* taxa grow aggressively, one current hypothesis for the origin of such additional compounds is that they could be acquired from overgrown lichens. This assumption is further strengthened by the co-occurrence of lichens containing such specialized metabolites in their close environment. As an example, in the course of its study on Finnish *O. ventosa* samples, Skult reported on the “unexpected” presence of atranorin in some of its specimens^{8,11}, assuming that atranorin might arise from a contamination in the thick prothallus⁸. Likewise, May suggested that the thick thallus of *O. ventosa* might easily hide the remnants of long overgrown lichens to account for the arising of atranorin and additional depsidones in some specimens⁷. As such, the occurrence of host-synthesized substances was recently observed in the lichenicolous lichen *Miriquidica invadens* that accumulates 5-O-methylhiassic acid from the parasitized *Sporastatia polyspora*⁵³. Regarding our samples, miriquidic acid might stem from overgrown species containing this depside which are described in both sampling sites such as the squamulose *Miriquidica garovaglii*. LDI-MSI analysis revealed that miriquidic acid was located in the basal medullary layer of the thallus. Such a basal distribution appears to be compatible with an acquisition from overgrown lichens. Moreover, analysis of further slices obtained from the same thallus do not reveal the presence of miriquidic acid. This validates the uneven longitudinal distribution highlighted earlier, and therefore supports the acquisition from a parasitized lichen, rather than a new *O. ventosa* chemotype.

LDI-MSI is here first described as a powerful tool for molecular mapping of compounds in lichen sections. From a methodological perspective, some advantageous features are worth being stressed. At first, the lack of matrix facilitates sample preparation and ensures an optimal spatial resolution. Likewise, the versatility of the technique regarding the thickness of the slice can lead to image the distribution of metabolites from regular hand-made slices. This micro-scale mapping enabled to establish the distribution pattern of all the molecules identified from our sample of *O. ventosa* and supported the putative ecological significances of most of them. Imaging of miriquidic acid reveals a distribution pattern compatible with its acquisition through overgrown lichen thalli. Considering such aspects, LDI-MSI approaches might represent new opportunities to decipher molecular strategies underlying dynamism and equilibrium in a saxicolous lichen mosaic. Little is known about aspects conferring advantage and factors promoting stability in multi-species communities but chemistry and allelopathy are presumed to be of paramount importance⁵⁴ as recently proven for endophytes⁵⁵. Therefore, delineating chemical interactions ongoing at marginal contacts between lichen thalli might advance the understanding of such complex relationships.

LDI-MSI techniques might also shed light on poorly known metabolic processes lying at the very heart of these fascinating symbioses. Many aspects of this association yet have to be characterized regarding the exact identity of the transferred metabolites and subsequent fate of the translocated material in fungal tissue⁵⁶. This lack of knowledge most likely stems from difficulties in investigating such metabolic interactions both *in situ* and at high spatial resolution. Addressing these shortcomings, LDI-MSI provides new opportunities for the investigations of many aspects of the lichen symbiosis, including the dynamics of cellular interaction. Imaging mass spectrometry techniques combined with stable isotope labelling can track the spatio-temporal dynamics of metabolic interactions in symbiotic systems⁵⁷. A proof of principle on *Xanthoria parietina*, using pre-labeled photobiont, an unlabeled mycobiont and a reconstituted lichen by co-cultivation of the two partners, indicated the transfer and usage of algal metabolites for biosynthetic purposes by the mycobiont⁵⁸. Altogether, this study highlights

the interest of LDI-imaging mass spectrometry as a simple and versatile strategy to assess the distribution of metabolites within lichens and more widely paves the way for its future application to polyphenolic structures in the wider realm of natural products. The narrow correlation between the localization of the compounds and their presumed ecological significance demonstrates the relevance of LDI-MSI as a privileged tool for chemical ecology studies.

Methods

Lichen material. Two samples of *Ophioparma ventosa* of different thicknesses were harvested: a first sample was collected in Tyrol (Austria), 500 meters south of Obergurgl (elevation 1800–1850 m). The lichen was collected and identified by one of the authors (J.B.) in 04/2009. A voucher specimen was deposited at the herbarium of laboratory PNSCM with the reference JB/09/158. This sample is referred to as Tyrol. Sample 2 was harvested in Styria (Austria) at the south of the lake Grosser Winterleitensee (elevation 1950–2000 m). The specimen was collected and determined by one of the authors (W.O.) in 09/2014. A voucher specimen (No. 13218a) was deposited at the herbarium GZU. In the rest of the manuscript, this sample is identified as Styria.

Sample preparation for LDI mass spectrometry imaging. Forty microns-thick transverse frozen sections were cut using a cryostat (Leica, Milton Keynes, UK) and fixed on a carbon-conductive adhesive tape which was in turn fixed on an indium tin oxide (ITO) slide (Bruker Daltonics, Bremen, Germany, cat no 237001).

All MSI measurements were performed using an Autoflex-Speed MALDI-TOF/TOF spectrometer (Bruker Daltonics, Bremen, Germany) equipped with a Smartbeam laser (355 nm, 1000 Hz) and controlled using the Flex Control 3.4 software package. The mass spectrometer was operated with a negative polarity in the reflectron mode. Spectra were acquired in the mass range of m/z 100–600 for all (x, y) coordinates corresponding to the imaged tissue.

The laser raster size was set at 50 microns. The signal was initially optimized by manually adjusting the laser power and the number of laser shots fired. Accordingly, full-scan MS experiments were run by accumulating 400 satisfactory laser shots per raster position, and using the laser power leading to the best signal-to-noise ratio. Image acquisition was performed using the Flex Imaging 4.0 (Bruker Daltonics) software package. The correlation of the target plate with the optical image was performed from three distinct teaching points following the procedure of the Flex Imaging software (Bruker Daltonics).

References

- Hyvärinen, M., Koopmann, R., Hormi, O. & Tuomi, J. Phenols in reproductive and somatic structures of lichens: a case of optimal defence? *Oikos* **91**, 371–375, doi: 10.1034/j.1600-0706.2000.910217 (2000).
- Kauppi, M. & Versegny—Patay, K. Determination of the distribution of lichen substances in the thallus by fluorescence microscopy. In *Annales Botanici Fennici* 189–202 (JSTOR, 1990).
- Bjarnholt, N., Li, B., D'Alvise, J. & Janfelt, C. Mass spectrometry imaging of plant metabolites – principles and possibilities. *Natural Products Reports* **31**, 818–837, doi: 10.1039/C3NP70100J (2014).
- Le Pogam, P. et al. Matrix-free UV-laser desorption/ionization mass spectrometry as a versatile approach for accelerating dereplication studies on lichens. *Analytical Chemistry* **87**, 10421–10428, doi: 10.1021/acs.analchem.5b02531 (2015).
- Hölscher, D. et al. Matrix-free UV-laser desorption/ionization (LDI) mass spectrometric imaging at the single-cell level: distribution of secondary metabolites of *Arabidopsis thaliana* and *Hypericum* species: Matrix-free UV-LDI mass spectrometric imaging at the single-cell level. *The Plant Journal* **60**, 907–918, doi: 10.1111/j.1365-3113.2009.04012.x (2009).
- Le Pogam, P., Le Lamer, A.-C., Legouin, B., Boustie, J. & Rondeau, D. *In situ* dart-ms as a versatile and rapid dereplication tool in lichenology: chemical fingerprinting of *Ophioparma ventosa*. *Phytochemical Analysis* in press, doi: 10.1002/pca.2635 (2016).
- May, P. F. *Ophioparma lapponica* – a misunderstood species. *Harvard Papers in Botany* **2**, 213–228 (1997).
- Skult, H. Notes on the chemical and morphological variation of the lichen *Ophioparma ventosa* in east fennoscandia. In *Annales Botanici Fennici* 291–297 (JSTOR, 1997).
- Rambold, G. & Schwab, A. Rusty coloured species of the lichen genus *Miriacidica* (Lecanoraceae). *Nordic Journal of Botany* **10**, 117–121, doi: 10.1111/j.1756-1051.1990.tb01757 (1990).
- Le Pogam, P. et al. Minor pyranonaphthoquinones from the apothecia of the lichen *Ophioparma ventosa*. *Journal of natural products* **79**, 1005–1011, doi: 10.1021/acs.jnatprod.5b01073 (2016).
- Rogers, R. W. & Hafellner, J. *Haematomma* and *Ophioparma*: two superficially similar genera of lichenized fungi. *The Lichenologist* **20**, 167–174, doi: 10.1017/S0024282988000179 (1988).
- Bjelland, T. & Ekman, S. Fungal diversity in rock beneath a crustose lichen as revealed by molecular markers. *Microbial Ecology* **49**, 598–603, doi: 10.1007/s00248-004-0101-z (2005).
- Nybakken, L., Asplund, J., Solhaug, K. A. & Gauslaa, Y. Forest successional stage affects the cortical secondary chemistry of three old forest lichens. *Journal of chemical ecology* **33**, 1607–1618, doi: 10.1007/s10886-007-9339-5 (2007).
- Spiteller, P. Chemical defence strategies of higher fungi. *Chemistry - A European Journal* **14**, 9100–9110, doi: 10.1002/chem.200800292 (2008).
- Donner, C. D. Naphthopyranones – isolation, bioactivity, biosynthesis and synthesis. *Natural Product Reports* **32**, 578–604, doi: 10.1039/C4NP00127C (2015).
- Hodkinson, B. P., Götzel, N. R., Schadt, C. W. & Lutzoni, F. Photoautotrophic symbiont and geography are major factors affecting highly structured and diverse bacterial communities in the lichen microbiome: Prokaryotic communities of the lichen microbiome. *Environmental Microbiology* **14**, 147–161, doi: 10.1111/j.1462-2920.2011.02560.x (2012).
- Grube, M. & Berg, G. Microbial consortia of bacteria and fungi with focus on the lichen symbiosis. *Fungal Biology Reviews* **23**, 72–85, doi: 10.1016/j.fbr.2009.10.001 (2009).
- Ahmadjian, V. & Jacobs, J. B. Artificial re-establishment of lichens IV. comparison between natural and synthetic thalli of *Usnea strigosa*. *The Lichenologist* **17**, 149–165, doi: 10.1017/S0024282988000179 (1985).
- Liao, C., Piercey-Normore, M. D., Sorensen, J. L. & Gough, K. *In situ* imaging of usnic acid in selected *Cladonia* spp. by vibrational spectroscopy. *Analyst* **135**, 3242–3248, doi: 10.1039/C0AN00533A (2010).
- Lohézic-Le Dévéhat, F., Legouin, B., Couteau, C., Boustie, J. & Coiffard, L. Lichenic extracts and metabolites as UV filters. *Journal of Photochemistry and Photobiology B: Biology* **120**, 17–28, doi: 10.1016/j.jphotobiol.2013.01.009 (2013).
- Bjerke, J. W., Lerfall, K. & Elvebakk, A. Effects of ultraviolet radiation and PAR on the content of usnic and divaricatic acids in two arctic-alpine lichens. *Photochemical & Photobiological Sciences* **1**, 678–685, doi: 10.1039/b203399b (2002).

22. Kinraide, W. T. B. & Ahmadjian, V. The effects of usnic acid on the physiology of two cultured species of the lichen alga *Trebouxia* puyum. *The Lichenologist* **4**, 234–247, doi: 10.1017/S0024282970000270 (1970).
23. Bačkor, M., Hudák, J., Repčák, M., Ziegler, W. & Bačkorová, M. The influence of pH and lichen metabolites (vulpinic acid and (+)-usnic acid) on the growth of the lichen photobiont *Trebouxia irregularis*. *The Lichenologist* **30**, 577–582, doi: 10.1006/lich.1998.0166 (1998).
24. Gardner, C. R. & Mueller, D. M. Factors affecting the toxicity of several lichen acids: effect of pH and lichen acid concentration. *American Journal of Botany* **68**, 87–95 (1981).
25. Inoue, H. Site of inhibition of usnic acid at oxidizing side of photosystem 2 of spinach chloroplasts. *Photosynthetica* **21**, 88–90 (1987).
26. Honegger, R. Ultrastructural studies in lichens. *New phytologist* **103**, 797–808, doi: 10.1111/j.1469-8137.1986.tb00854 (1986).
27. Avalos, A. & Vicente, C. The occurrence of lichen phenolics in the photobiont cells of *Evernia prunastri*. *Plant Cell Reports* **6**, 74–76, doi: 10.1007/BF00269744 (1987).
28. Bačkor, M., Klemová, K., Bačkorová, M. & Ivanova, V. Comparison of the phytotoxic effects of usnic acid on cultures of free-living alga *Scenedesmus quadricauda* and aposymbiotically grown lichen photobiont *Trebouxia erici*. *Journal of Chemical Ecology* **36**, 405–411, doi: 10.1007/s10886-010-9776-4 (2010).
29. Feige, B. Probleme der flechtenphysiologie. *Nova Hedwigia* **30**, 725–774 (1978).
30. Vainshtein, E. & Takhtadzhan, E. Physiological changes in the lichen alga *Trebouxia* during cultivation. *Fiziologiya Rastenii* **28**, 1037–1044 (1981).
31. Cocchietto, M., Skert, N., Nimis, P. & Sava, G. A review on usnic acid, an interesting natural compound. *Naturwissenschaften* **89**, 137–146, doi: 10.1007/s00114-002-0305-3 (2002).
32. Emmerich, R., Giez, J., Lange, O. L. & Proksch, P. Toxicity and antifeedant activity of lichen compounds against the polyphagous herbivorous insect *Spodoptera littoralis*. *Phytochemistry* **33**, 1389–1394, doi: 10.1016/0031-9422(93)85097-B (1993).
33. Nimis, P. & Skert, N. Lichen chemistry and selective grazing by the coleopteran *Lasioderma serricornis*. *Environmental and Experimental Botany* **55**, 175–182, doi: 10.1016/j.enxvpt.2004.10.011 (2006).
34. Hauck, M., Jürgens, S.-R., Willenbruch, K., Huneck, S. & Leuschner, C. Dissociation and metal-binding characteristics of yellow lichen substances suggest a relationship with site preferences of lichens. *Annals of Botany* **103**, 13–22, doi: 10.1093/aob/mcn202 (2008).
35. Kalinowska, R., Bačkor, M. & Pawlik-Skowrońska, B. Parietin in the tolerant lichen *Xanthoria parietina* (L.) th. fr. increases protection of *Trebouxia* photobionts from cadmium excess. *Ecological Indicators* **58**, 132–138, doi: 10.1016/j.ecolind.2015.05.055 (2015).
36. Kantvilas, G. & Elix, J. A. The genus *Ramboldia* (Lecanoraceae): a new species, key and notes. *The Lichenologist* **39**, 135, doi: 10.1017/S0024282907006469 (2007).
37. Hawksworth, D. L. The chemical constituents of *Haematomma ventosum* (L.) massal in the british isles. *The Lichenologist* **4**, 248–255, doi: 10.1017/S0024282970000282 (1970).
38. Wirth, V. *Die Flechten baden-württembergs* vol. 2 (Ulmer Stuttgart, 1995).
39. Wirth, V. Zur ausbreitung, herkunft und Ökologie anthropogen geförderter rinden-und holzflechten. *Tuexenia* 523–535 (1985).
40. Hauck, M. & Jürgens, S.-R. Utric acid controls the acidity tolerance of lichens. *Environmental Pollution* **156**, 115–122, doi: 10.1016/j.envpol.2007.12.033 (2008).
41. Hauck, M., Jürgens, S.-R., Huneck, S. & Leuschner, C. High acidity tolerance in lichens with fumarprotocetraric, perlatolic or thamnolic acids is correlated with low pKa1 values of these lichen substances. *Environmental Pollution* **157**, 2776–2780, doi: 10.1016/j.envpol.2009.04.022 (2009).
42. Mahaney, W., Wilson, E., Boyer, M. & Hancock, R. Marginal bleaching of thalli of *Rhizocarpon* as evidence for acid rain in the norra storfjället, sweden. *Environmental Pollution* **87**, 71–75, doi: 10.1016/S0269-7491(99)80010-4 (1995).
43. Bjelland, T. The occurrence of biomineralization products in four lichen species growing on sandstone in western norway. *The Lichenologist* **34**, 429–440, doi: 10.1006/lich.2002.0413 (2002).
44. Ascaso, C., Galvan, J. & Ortega, C. The pedogenic action of *Parmelia conspersa*, *Rhizocarpon geographicum* and *Umbilicaria pustulata*. *The Lichenologist* **8**, 151–171, doi: 10.1017/S0024282976000236 (1976).
45. Purvis, O. W., Elix, J. A., Broomhead, J. A. & Jones, G. C. The occurrence of copper—norstictic acid in lichens from cupriferous substrata. *The Lichenologist* **19**, 193–203, doi: 10.1017/S0024282987000161 (1987).
46. Purvis, O. W., Elix, J. A. & Gaul, K. L. The occurrence of copper-psoromic acid in lichens from cupriferous substrata. *The Lichenologist* **22**, 345–354, doi: 10.1017/S002428299000038X (1990).
47. Cuny, D. et al. Cellular impact of metal trace elements in terricolous lichen *Diploschistes muscorum* (scop.) r. sant.—identification of oxidative stress biomarkers. *Water, Air, and Soil Pollution* **152**, 55–69, doi: 10.1023/B:WATE.0000015332.94219.f (2004).
48. Bjelland, T. & Thorseth, I. H. Comparative studies of the lichen—rock interface of four lichens in vingen, western norway. *Chemical Geology* **192**, 81–98, doi: 10.1016/S0009-2541(02)00193-6 (2002).
49. Hauck, M. Susceptibility to acidic precipitation contributes to the decline of the terricolous lichens *Cetraria aculeata* and *Cetraria islandica* in central europe. *Environmental pollution* **152**, 731–735, doi: 10.1016/j.envpol.2007.06.046 (2008).
50. Pawlik-Skowrońska, B. & Bačkor, M. Zn/pb-tolerant lichens with higher content of secondary metabolites produce less phytochelatin than specimens living in unpolluted habitats. *Environmental and Experimental Botany* **72**, 64–70, doi: 10.1016/j.enxvpt.2010.07.002 (2011).
51. Hauck, M. & Huneck, S. Lichen substances affect metal adsorption in *Hypogymnia physodes*. *Journal of Chemical Ecology* **33**, 219–223, doi: 10.1007/s10886-006-9225-6 (2006).
52. Hauck, M., Willenbruch, K. & Leuschner, C. Lichen substances prevent lichens from nutrient deficiency. *Journal of Chemical Ecology* **35**, 71–73, doi: 10.1007/s10886-008-9584-2 (2009).
53. Hafellner, J., Obermayer, W. & Tretsch, M. *Miriquidica invadens*, an obligate youth parasite on *Sporastatia*, with remarks and a key to species of the *M. griseoatra* group. *The Lichenologist* **46**, 303–331, doi: 10.1017/S002428291400005X (2014).
54. Armstrong, R. A. & Welch, A. R. Competition in lichen communities. *Symbiosis* **43**, 1–12 (2007).
55. Combès, A. et al. Chemical communication between the endophytic fungus *Paraconiothyrium variable* and the phytopathogen *Fusarium oxysporum*. *PLoS ONE* **7**, e47313, doi: 10.1371/journal.pone.0047313 (2012).
56. Stocker-Wörgötter, E., Hager, A. & Elix, J. A. Intraspecific chemical variation within the crustose lichen genus *Haematomma*: anthraquinone production in selected cultured microorganisms as a response to stress and nutrient supply. *Phytochemistry Reviews* **8**, 561–569, doi: 10.1007/s11101-009-9149-1 (2009).
57. Pernice, M. et al. A single-cell view of ammonium assimilation in coral—dinoflagellate symbiosis. *The ISME journal* **6**, 1314–1324, doi: 10.1038/ismej.2011.196 (2012).
58. Eisenreich, W., Knispel, N. & Beck, A. Advanced methods for the study of the chemistry and the metabolism of lichens. *Phytochemistry Reviews* **10**, 445–456, doi: 10.1007/s11101-011-9215-3 (2011).

Acknowledgements

This work was supported by the University of Rennes 1 through Project “Défi emergent LICHENMASS” and through the use of the mass spectrometry facilities of the BIBS platform of INRA UR 1268, Nantes. The authors gratefully acknowledge Dr. Alain Fautrel (University of Rennes 1, H2P2 platform, Biosit, Rennes) for cryosectioning.

Author Contributions

W.O. and J.B. collected and identified the lichen material, P.L.P., A.C.L.L., B.L. and J.B. conceived the experiments, P.L.P., A.C.L.L., A.G. and H.R. conducted the experiments, P.L.P., A.C.L.L., B.L., W.O. and J.B. analyzed the results. All authors reviewed the manuscript.

Additional Information

Supplementary information accompanies this paper at <http://www.nature.com/srep>

Competing financial interests: The authors declare no competing financial interests.

How to cite this article: Le Pogam, P. *et al.* Spatial mapping of lichen specialized metabolites using LDI-MSI: chemical ecology issues for *Ophioparma ventosa*. *Sci. Rep.* 6, 37807; doi: 10.1038/srep37807 (2016).

Publisher's note: Springer Nature remains neutral with regard to jurisdictional claims in published maps and institutional affiliations.



This work is licensed under a Creative Commons Attribution 4.0 International License. The images or other third party material in this article are included in the article's Creative Commons license, unless indicated otherwise in the credit line; if the material is not included under the Creative Commons license, users will need to obtain permission from the license holder to reproduce the material. To view a copy of this license, visit <http://creativecommons.org/licenses/by/4.0/>

© The Author(s) 2016

III. Étude de la contribution des symbiontes dans la biosynthèse de composés : application à la biosynthèse de la mycosporine sérinol de *Lichina pygmaea* par une approche alliant imagerie par spectrométrie de masse et génétique

Une autre problématique ayant conduit à des analyses d'imagerie LDI est la biosynthèse des mycosporines au sein du cyanolichen *Lichina pygmaea*. Ces métabolites secondaires étant décrits aussi bien chez les cyanobactéries que chez les champignons, la contribution des différents partenaires de la symbiose lichénique dans l'élaboration de ces structures n'est pas actuellement connue. En ce sens, il peut être intéressant de savoir lequel des symbiontes concentre ces molécules ainsi que de s'intéresser au contenu génétique des partenaires pour voir qui est doté de l'arsenal enzymatique permettant d'assurer cette biosynthèse.

A. Mycosporines : données structurales et connaissances sur leur biosynthèse

Les mycosporines et les acides aminés mycosporine-like (ou MAA pour *Mycosporine Amino Acids*) sont des métabolites secondaires contenant un noyau cyclohexénone ou cyclohexéminine. Les délocalisations électroniques prenant place au sein de ces motifs structuraux sont à l'origine d'une photo-absorption très marquée dans le domaine des ultraviolets, avec un maximum d'absorption respectivement centré sur 310 et 330 nm pour des coefficients d'extinction molaire atteignant 40.000 L mol⁻¹ cm⁻¹ (Oren and Gunde-Cimerman, 2007) (Figure 30). Par ailleurs, l'hydrosolubilité, la photostabilité et l'atotoxicité de ces molécules en font d'intéressants candidats pour le développement de filtres solaires (La Barre et al., 2014).

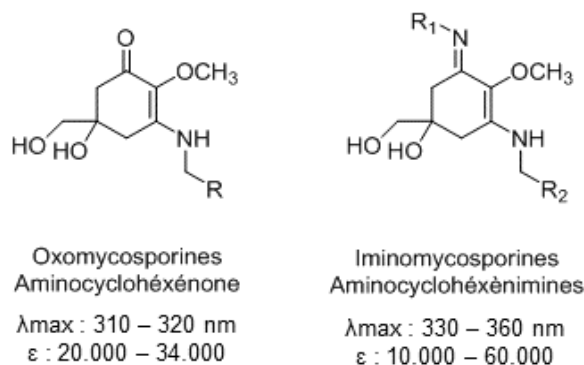


FIGURE 30: NOYAUX DES OXO- ET DES IMINOMYCOSPORINES ET DONNÉES SPECTRALES ASSOCIÉES.

Les mycosporines ont été décrites au sein d'organismes variés : d'abord isolées chez un champignon (le Basidiomycète *Stereum hirsutum* (Favre-Bonvin et al., 1976)), des MAA ont par la suite rapidement été isolées à partir de coraux (Ito and Hirata, 1977). Dès 1977, des mycosporines *sensu lato* ont été mises en évidence à partir d'organismes variés comprenant :

- d'autres champignons (e.g *Aureobasidium pullulans* (Kogej et al., 2006), *Botrytis cinerea* (Arpin et al., 1977), *Rhodoturula minuta* (Pérez et al., 2006)...)
- des cyanobactéries (dont *Calothrix sp* (Sinha et al., 2003), *Nostoc commune* (Garcia-Pichel and Castenholz, 1993), *Scytonema sp.* (Sinha et al., 2003) notamment) ;
- des algues
 - o rouges (genre *Bangia* (Boedeker and Karsten, 2005), *Bostrychia* (Karsten et al.,

- 2000), ou encore *Neuroglossum* (Hoyer et al., 2002) ;
- o vertes (e.g *Boodlea* (Karsten et al., 1998), *Caulerpa* (Gröniger et al., 2000), diverses espèces du genre *Prasiola* (Karsten et al., 2005)...);
- o brunes (e.g *Desmaretia menziesii* (Karentz et al., 1991), *Hydroclathrus clathratus* (Gröniger et al., 2000)) ;
- et même occasionnellement à partir de mollusques ou de poissons, lesquels les accumulent vraisemblablement par voie alimentaire (Helbling et al., 2002; Newman et al., 2000).

De façon générale, les oxomycosporines sont rencontrées chez des champignons tandis que les iminomycosporines sont retrouvées chez les coraux et les cyanobactéries (La Barre et al., 2014).

L'originalité chimique et la large distribution phylogénique des mycosporines leur ont rapidement valu un intérêt considérable de la part de la communauté scientifique. Pour autant, les aspects moléculaires aussi bien que génétiques sous-tendant leur biosynthèse restent imparfaitement connus jusqu'au début des années 2010. Sur la base de simples considérations structurales, il a été envisagé que les mycosporines soient obtenues à partir d'un intermédiaire bien connu de la voie du shikimate : le 3-déhydroquinone (Rastogi et al., 2010) (3-DQ). Selon cette voie canonique du shikimate, associée à l'obtention des acides aminés aromatiques ainsi que de nombreux métabolites secondaires, le 3-désoxy-D-arabinoheptulose est converti en 3-DQ sous l'action d'une enzyme, la DéHydroQuinone Synthase (DHQS) (Ganem, 1978). Des éléments de preuve indirects suggèrent en effet que le 3-DQ est un intermédiaire de biosynthèse des mycosporines (Portwich and Garcia-Pichel, 2003). La découverte ultérieure de voies métaboliques qualifiées de DHQS-like suggère rapidement que la biosynthèse des mycosporines puisse transiter par d'autres intermédiaires que le 3-déhydroquinone (Flatt and Mahmud, 2007).

Selon une approche bioinformatique, Starcevic et al. mettent en évidence dans le génome d'une anémone de mer (*Nematostella vectensis*) la présence d'un homologue de DHQS présentant d'importantes homologies avec un gène issu de chloroplastes de dinoflagellés, lequel est fusionné à un gène codant pour une O-MéthylTransférase (O-MT). Ce gène O-MT est également présent chez *N. vectensis* sans toutefois être associé à un gène DHQS, lequel apparaît à distance dans le génome. Les auteurs voient en ces gènes de vraisemblables candidats pour la biosynthèse des mycosporines dans la mesure où toutes les mycosporines comportent un groupement méthyle (Starcevic et al., 2008).

Parallèlement, il apparaît de plus en plus clairement que les protéines de la famille DHQS ne se limitent pas à la réaction DHQS canonique telle qu'indiquée plus haut. Les bactéries font appel à tout un arsenal d'enzymes DHQS-like impliquant des substrats et produits différents de telle sorte que le 3-DQ n'en représente pas un intermédiaire métabolique consensuel (Flatt and Mahmud, 2007) (Figure 31, Figure 32). L'analyse phylogénique d'enzymes DHQS bactériennes et fongiques permet de regrouper les protéines correspondantes suivant la nature des substrats et/ou des produits correspondants. Cinq groupes ont ainsi pu être distingués, quatre d'entre eux étant associés à des produits connus mais un dernier groupe relié à des familles fongiques et cyanobactériennes ne peut être rapproché d'aucun produit connu (Wu et al., 2007). Ce groupe inconnu se distingue par la structure différente de son site actif laissant présager de possibles nouveaux substrats et/ou produits. Dans la mesure où cette sous-famille de DHQS se révèle très similaire au gène DHQS-like décrit chez *Nematostella vectensis*, cette sous-famille semble représenter une base vraisemblable pour la biosynthèse des mycosporines (Wu et al., 2007).

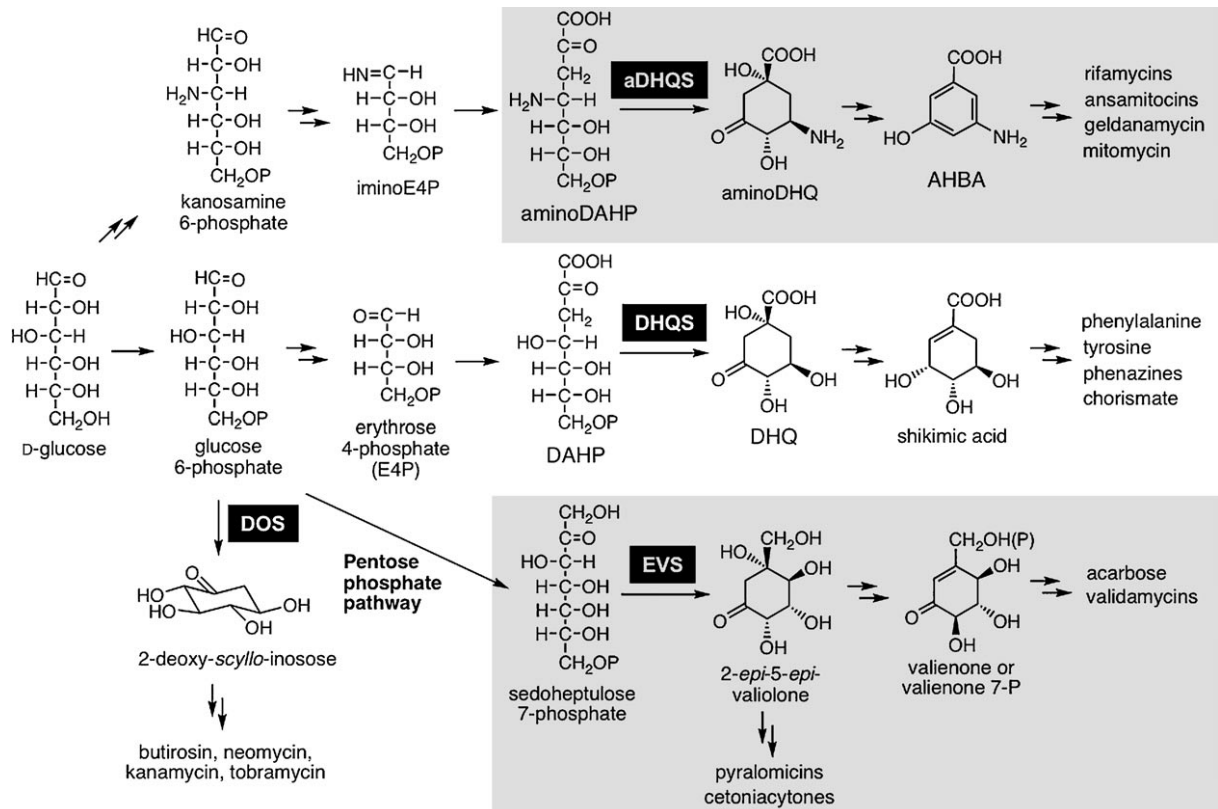


FIGURE 31 : PRODUITS ISSUS DES VOIES MÉTABOLIQUES INITIÉES PAR DHQS ET LES ENZYMES DHQS-LIKE. DOS = 2-DEOXY-SCYLLO-INOSOSE SYNTHASE, EVS = 2-EPI-5-EPI-VALIOLONE SYNTHASE, DHQS = DEHYDROQUINATE SYNTHASE, ADHQS= AMINO DEHYDROQUINATE SYNTHASE (WU ET AL., 2007).

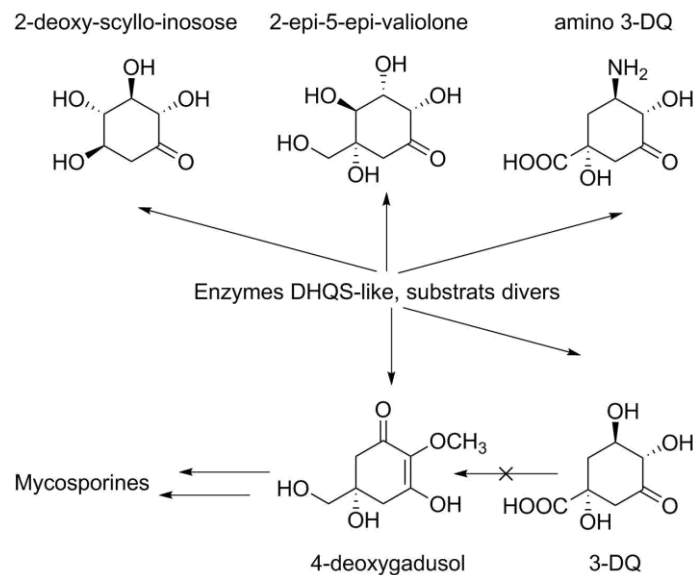


FIGURE 32: MOTIFS STRUCTURAUX OBTENUS SOUS L'ACTION DE DIFFÉRENTES ENZYMES DHQS-LIKE. LE 4-DÉSOXYGADUSOL EST OBTENU DIRECTEMENT ET NON PAR L'INTERMÉDIAIRE DE 3-DQ (ADAPTÉ DE (SCHMIDT, 2011)).

La comparaison du génome de quatre cyanobactéries différentes dont une seule produit des mycosporines (*Anabaena variabilis* PCC 7937) a permis d'apprécier la combinaison de DHQS et de O-MT au sein de cette seule souche. Le gène DHQS associé à cette biosynthèse diffère toutefois des

DHQS canoniquement rencontrées chez les cyanobactéries et des recherches d'homologies de séquences internucléotidiques BLAST révèlent que cette enzyme se rapproche davantage de la 2-*epi*-5-*epi*-valiolone synthase fongique, enzyme d'importance pour la biosynthèse de cyclitols en C₇ à partir du sedoheptulose (Figure 31) et dont la séquence réactionnelle présente des homologies avec la réaction catalysée par la DHQS canonique (Wu et al., 2007). À noter qu'au sein du génome d'*Anabaena variabilis* PCC 7937, la présence d'un second gène DHQS, canonique cette fois et non associé à un gène O-MT, est vraisemblablement associée à la voie du shikimate en catalysant quant à lui la production de 3-DQ (Singh et al., 2010). Ce DHQS canonique est d'ailleurs rencontré chez chacune des quatre souches, indifférent de leur statut de producteur ou de non-producteur de mycosporine.

Les dernières précisions apportées à ce jour concernant la biosynthèse des mycosporines ont pu être apportées la même année (Balskus and Walsh, 2010). Les recherches d'homologies de séquences inter-nucléotidiques entreprises par ces auteurs à partir des gènes DHQS et O-MT de l'anémone de mer *Nematostella vectensis* ont permis de révéler des clusters homologues dans le génome de dinoflagellés, de cyanobactéries et de champignons, ce qui semble effectivement corrélé à la large distribution phylogénique de ces molécules.

De plus, l'étude des hits en question dans leur contexte génomique a révélé que les phases ouvertes de lecture (*Open Reading Frames*) correspondant aux gènes de DHQS et de O-MT étaient constamment accompagnées d'un troisième cadre ouvert de lecture usuellement annoté comme correspondant à une protéine virtuelle. Cette troisième séquence génique est caractérisée par la présence de domaines structuraux permettant de l'affilier au groupe des ATP-grasp, enzymes connues pour catalyser la formation de liaisons peptidiques (Galperin and Koonin, 1997) et pouvant être ici imputées à la fonctionnalisation de la cyclohexénone par un acide aminé. Enfin, de façon très intéressante, sont également notées des différences de contexte génomique entre les hits cyanobactériens et fongiques. En effet, les cyanobactéries comprennent une seconde séquence additionnelle à même de coder pour une enzyme catalysant la formation de liaisons peptidiques, il peut s'agir d'un second domaine ATP-grasp mais également d'un *Non Ribosomal Protein Synthase* (NRPS). Cette différence pourrait fournir une base génétique au constat selon lequel les cyanobactéries synthétisent des iminomycosporines contrairement aux champignons qui s'arrêtent au stade oxomycosporine. À la place de ce quatrième gène, les champignons possèdent des réductases (Balskus and Walsh, 2010; Schmidt, 2011).

L'expression hétérologue des gènes associés à la biosynthèse des mycosporines d'*Anabaena variabilis* (cyanobactérie productrice de shinorine, une iminomycosporine (Singh et al., 2008)) a été réalisée chez *Escherichia coli* afin de valider l'implication des gènes dans cette biosynthèse en recueillant les intermédiaires de biosynthèse obtenus au moyen de différentes constructions géniques (Balskus and Walsh, 2010). Il en ressort :

- que le cluster entier (DHQS + O-MT + ATP-grasp + NRPS) permet effectivement d'obtenir la shinorine ;
- que la construction déficiente en NRPS (comparable à un hit fongique, 3 ORF seulement) est à l'origine d'une séquence de synthèse incomplète, prématurément interrompue au stade de la mycosporine glycine ;
- pour finir, le modèle seulement doté de DHQS et d'O-MT s'arrête à un stade encore plus précoce : le 4-désoxygadusol.

Ainsi, Balskus et Walsh ont démontré d'une part que les hits identifiés correspondent effectivement à un cluster de gènes impliqué dans la biosynthèse des mycosporines mais ont également permis de valider l'identité de plusieurs intermédiaires de cette voie métabolique (Balskus and Walsh, 2010) (Figure 33).

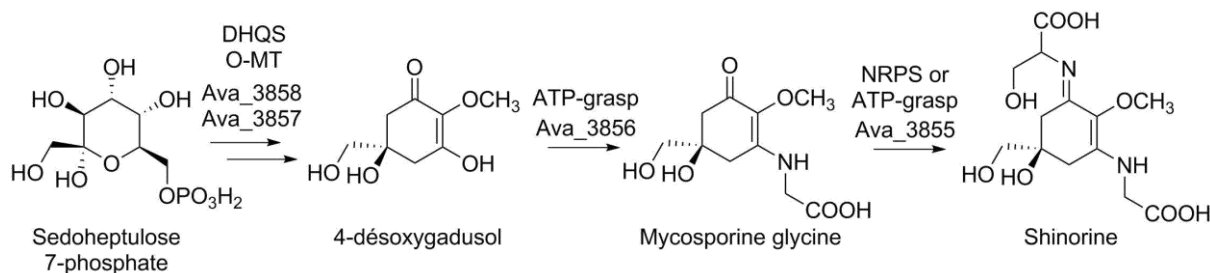


FIGURE 33: BIOSYNTÈSE DE LA SHINORINE CHEZ *ANABAENA VARIABILIS* D'APRÈS BALSUKS ET WALSH : STRUCTURES CHIMIQUES DES DIFFÉRENTS INTERMÉDIAIRES ET ENZYMES IMPLIQUÉES.

Par ailleurs, ces auteurs fournissent également un substratum génétique pour expliquer la distribution différentielle des oxo- et des iminomycosporines respectivement entre les champignons et les cyanobactéries.

Les mycosporines ont également été décrites chez différents lichens, ce qui pose d'intéressantes questions quant à la contribution des partenaires de cette association puisque que chacun des règnes retrouvé dans la symbiose lichénique (champignon, algue ou cyanobactérie) est décrit comme capable de réaliser la synthèse de ces métabolites dans des conditions de vie autonomes. Les mycosporines ont, dans un premier temps, été constamment isolées à partir de cyanolichens, ce qui a laissé présager de l'implication des cyanobactéries dans la biosynthèse des mycosporines rencontrées chez les lichens. La récente caractérisation au laboratoire de mycosporines à partir de chlorolichens du genre *Dermatocarpon* (Nguyen et al., 2015) démontre qu'au moins dans certains cas de figure la biosynthèse des mycosporines lichéniques n'est pas assurée par les cyanobactéries. La localisation tissulaire des mycosporines a été rapidement perçue comme un élément clé pour comprendre leur biosynthèse dans le cadre de la symbiose lichénique mais les techniques d'imagerie utilisées jusqu'à présent ne permettaient pas d'atteindre une résolution spatiale suffisante pour discerner le contenu en mycosporines des partenaires de la symbiose lichénique dans le cadre classique de lichens bipartites. Toutefois, certains lichens tripartites confinent les cyanobactéries dans des compartiments morphologiques distincts et parfois volumineux : les céphalodies. Le profilage chimique comparé du thalle et des céphalodies du lichen tripartite *Stereocaulon philippinense* semble indiquer une différence dans le contenu en mycosporines de ces deux compartiments (Roullier et al., 2011) :

- le thalle lichénique contient une molécule ayant un λ_{\max} de 310 nm, évocateur d'une oxomycosporine (aminocyclohexénone) ;
- les céphalodies renferment quant à elle un métabolite avec un λ_{\max} de 340 nm, suggérant une iminomycosporine.

La biosynthèse des mycosporines a davantage été considérée dans le cadre d'une autre symbiose : celle des coraux hermatypiques consistant en une endosymbiose qui réunit un hôte affilié aux cnidaires et une algue unicellulaire (zooxanthelle). Chez le corail modèle *Stylophora pistillata*, Shick a démontré que la biogenèse des mycosporines sous l'effet d'irradiations UV opère en deux temps (Figure 34) (Shick, 2004). Dans un premier temps sont biosynthétisées des mycosporines connues de la zooxanthelle *Symbiodinium* cultivée seule. Lors d'une seconde phase, ces mycosporines qualifiées de primaires décroissent au profit de mycosporines qui ne sont pas connues de ces zooxanthelles et qui sont alors dites secondaires. Sur la base de cette séquence, Shick propose que les mycosporines primaires soient biosynthétisées par les zooxanthelles puis transférées aux cellules coralliennes qui les métaboliseraient alors en mycosporines secondaires. Il est toutefois important de relever qu'aucune base génétique n'accrédite le scénario de Shick. Histologiquement, les mycosporines se localisent dans l'épiderme des polypes coralliens. Il est également constaté que ces molécules sont allouées prioritairement aux zones les plus exposées aux radiations solaires, en accord avec leur rôle de filtre UV. Cette localisation des mycosporines limite la dépendance du corail vis-à-vis de son partenaire lors des épisodes de blanchissement (ou *bleaching*) lors desquels la zooxanthelle est

expulsée, dans le cas où les mycosporines seraient effectivement synthétisées par cette dernière (La Barre et al., 2014). De récentes études ont démontré que le corail *Acropora digitata* détient l'ensemble du cluster de gènes associé à la biosynthèse des mycosporines suggérant que le cnidaire est à même d'assurer indépendamment la biosynthèse de ces composés photoprotecteurs (Shinzato et al., 2011). Un transfert horizontal de gènes a été suggéré mais aucune preuve expérimentale n'accrédite pour l'instant cette hypothèse (Shinzato et al., 2011). De fait, l'effective contribution des partenaires de cette symbiose dans l'édification de ces composés demeure inconnue à ce jour.

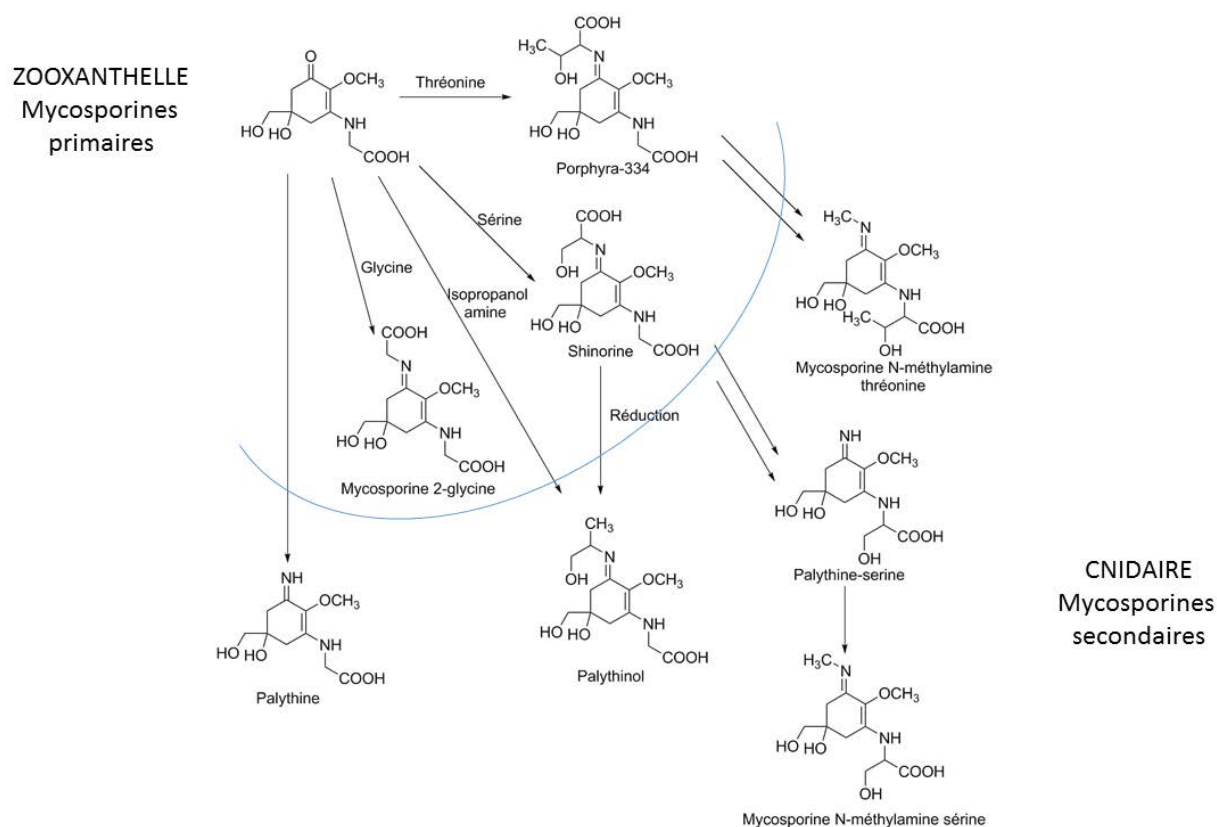
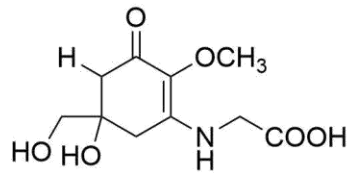


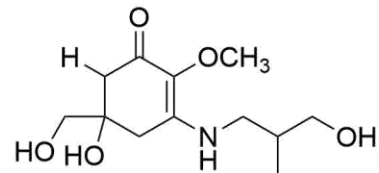
FIGURE 34: HYPOTHÈSE DE SHICK CONCERNANT LA BIOSYNTHÈSE DES MYCOSORINES CHEZ LES CORAUX HERMATYPIQUES, ADAPTÉ DE (SHICK ET AL., 1999). CE SCÉNARIO BIOGÉNÉTIQUE EST INSPIRÉ PAR LA SÉQUENCE DE BIOSYNTHÈSE DES MYCOSORINES CHEZ LES CORAUX. LA RÉCENTE DÉCOUVERTE DU CLUSTER DE 4 GÈNES CHEZ LE CNIDAIRE ANTHOZOAIRE *ACROPORA DIGITATA* SEMBLE ALLER À L'ENCONTRE DE CETTE HYPOTHÈSE (SHINZATO ET AL., 2011).

Les structures chimiques des mycosporines rencontrées chez les lichens ainsi que les références décrivant leur isolement sont fournies dans la figure suivante (Figure 35):



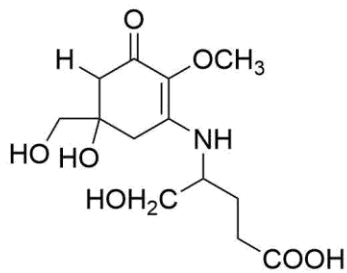
Mycosporine glycine

Collema sp.
Peltula sp.
Gonohymenia sp. | Büdel et al., 1997
Lichina pygmaea de la Coba et al., 2009



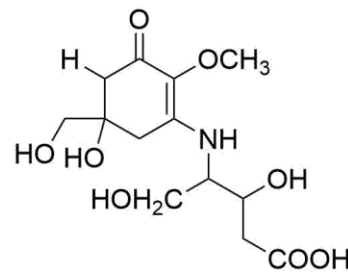
Mycosporine sérinol

Collema cristatum Torres et al., 2004
Lichina pygmaea Roullier et al., 2009



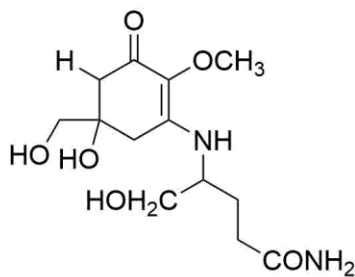
Mycosporine glutamicol

Degelia plumbea Roullier et al., 2011
Dermatocarpon luridum
Dermatocarpon miniatum | Nguyen et al., 2015



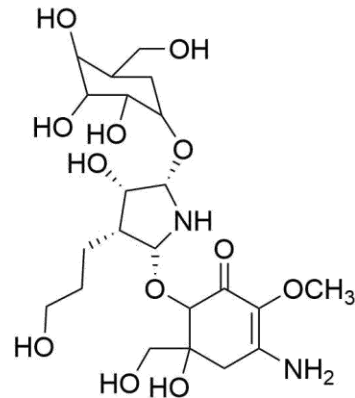
Mycosporine hydroxyglutamicol

Nephroma laevigatum Roullier et al., 2011



Mycosporine glutaminol

Dermatocarpon luridum
Dermatocarpon miniatum | Nguyen et al., 2015



Collemin A

Collema cristatum Torres et al., 2004

FIGURE 35 : STRUCTURES CHIMIQUES DES MYCOSPORINES ISOLÉES DE LICHENS INDIQUANT LE NOM DU LICHEN PRODUISANT CE COMPOSÉ ET LES RÉFÉRENCES DE LA PUBLICATION DÉCRIVANT LEUR ISOLEMENT. LES NOMS DE LICHENS INDIQUÉS EN BLEU CORRESPONDENT AUX CYANOLICHENS TANDIS QUE CEUX ÉCRITS EN VERT SONT DES CHLOROLICHENS. RÉFÉRENCES : (BÜDEL ET AL., 1997; TORRES ET AL., 2004; DE LA COBA ET AL., 2009; ROULLIER ET AL., 2009, 2011; NGUYEN ET AL., 2015).

B. Investigation moléculaire (LDI-MSI) et génétique de *Lichina pygmaea*

a. Stratégie générale

Pour progresser dans la compréhension de la biosynthèse des mycosporines chez les lichens, deux axes de travail complémentaires ont été entrepris chez le cyanolichen producteur de mycosporine sérinol déjà étudié en DART-MS, *Lichina pygmaea* (Figure 36):

- des analyses d'imagerie pour cerner la localisation tissulaire des mycosporines et préciser dans le cas présent quel(s) partenaire(s) de la symbiose les accumule(nt). Deux approches sont envisagées pour répondre à cette question : le LDI imaging et la spectromicroscopie Raman ;
- en parallèle, le matériel génétique des deux partenaires de la symbiose est étudié séparément. Cette approche complémentaire est très importante dans le cas présent car il est possible que les mycosporines se redistribuent comme c'est le cas chez les coraux et que leur distribution ne préjuge pas de l'implication des tissus qui les accumulent dans leur biosynthèse, à l'image de l'acide usnique d'*Ophioparma ventosa* qui est rencontré au sein de la couche algale tout en étant produit par le champignon (Abdel-Hameed et al., 2016a). Le recueil séparé de la cyanobactérie et du champignon a été possible par microdissection capture laser (plate-forme H2P2, Dr. Alain Fautrel).

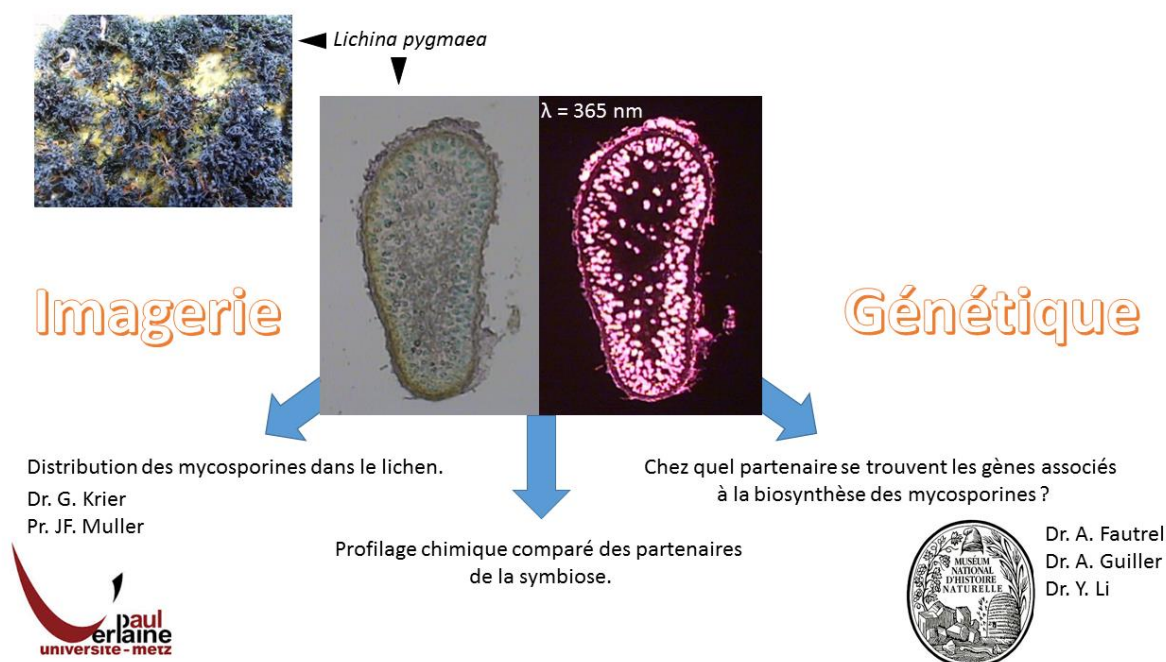


FIGURE 36 : APPROCHES RETENUES POUR ÉTUDIER LA CONTRIBUTION DES SYMBIOTES DANS LA BIOSYNTÈSE DES MYCOSPORINES CHEZ *LICHINA PYGMAEA* (PHOTOGRAPHIE : PIERRE LE POGAM ET ALAIN FAUTREL)

b. Approches retenues pour histolocaliser les mycosporines

i. Spectromicroscopie Raman

La spectromicroscopie Raman ou formellement spectromicroscopie de vibration par diffusion Raman étudie les transitions vibrationnelles sur la base d'un processus de diffusion de la lumière.

Lorsqu'un échantillon transparent est soumis à une onde électromagnétique monochromatique, une majeure partie des ondes va être transmise tandis qu'une faible proportion d'entre elles va être diffusée. Dans ce dernier cas de figure, la direction de propagation des ondes change pour ne plus obéir aux lois de l'optique géométrique.

L'analyse en fréquence des ondes permet de caractériser (Kneipp et al., 1999) (Figure 37):

- une composante de longueur d'onde identique à celle du faisceau incident, il y a dans ce cas diffusion élastique (= diffusion Rayleigh);
- une composante de longueur d'onde différente de celle du faisceau incident, il y a alors diffusion inélastique (= diffusion Raman).

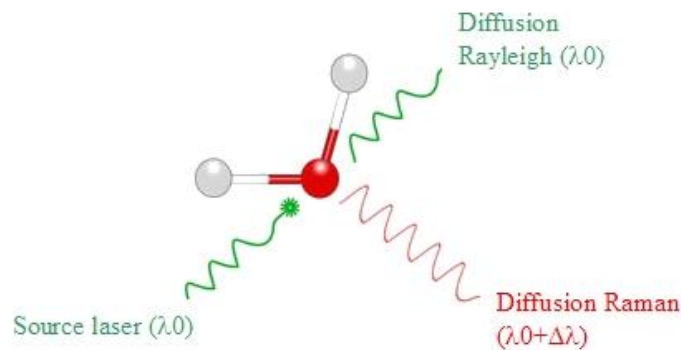


FIGURE 37: DIFFUSION RAYLEIGH ET DIFFUSION RAMAN

[HTTP://WWWZ.IFREMER.FR/RD_TECHNOLOGIQUES/MOYENS/LABORATOIRES/SPECTROSCOPIES-TECHNIQUES-DE-MESURES-IN-SITU/SPECTROSCOPIE-RAMAN](http://wwwz.ifremer.fr/rd_technologiques/moyens/laboratoires/spectroscopies-techniques-de-mesures-in-situ/spectroscopie-raman)

Selon la fréquence des photons incidents, plusieurs phénomènes peuvent intervenir (Kneipp et al., 1999) (Figure 38).

- Lorsque le photon incident correspond à l'énergie d'un niveau de vibration, l'énergie du photon peut être absorbée. C'est la base de la spectroscopie infrarouge.
- Lorsque le photon incident est d'une énergie très supérieure à celle d'une énergie de vibration, il peut y avoir diffusion:
 - o élastique si les photons incident et diffusé sont de même énergie;
 - o Raman en cas de diffusion inélastique avec deux possibilités:
 - un effet Stokes si le photon diffusé est d'énergie plus faible que celle du photon incident. Dans ce cas de figure, le photon incident lègue à la molécule au repos une quantité d'énergie qui correspond à la transition de l'état vibrationnel fondamental à l'état excité ($E_{vib0} \rightarrow E_{vib1}$);
 - une contribution anti-Stokes se rapportant à la diffusion de photons de plus haute énergie. La molécule excitée cède au photon incident une quantité d'énergie permettant le retour de l'état excité à l'état fondamental.

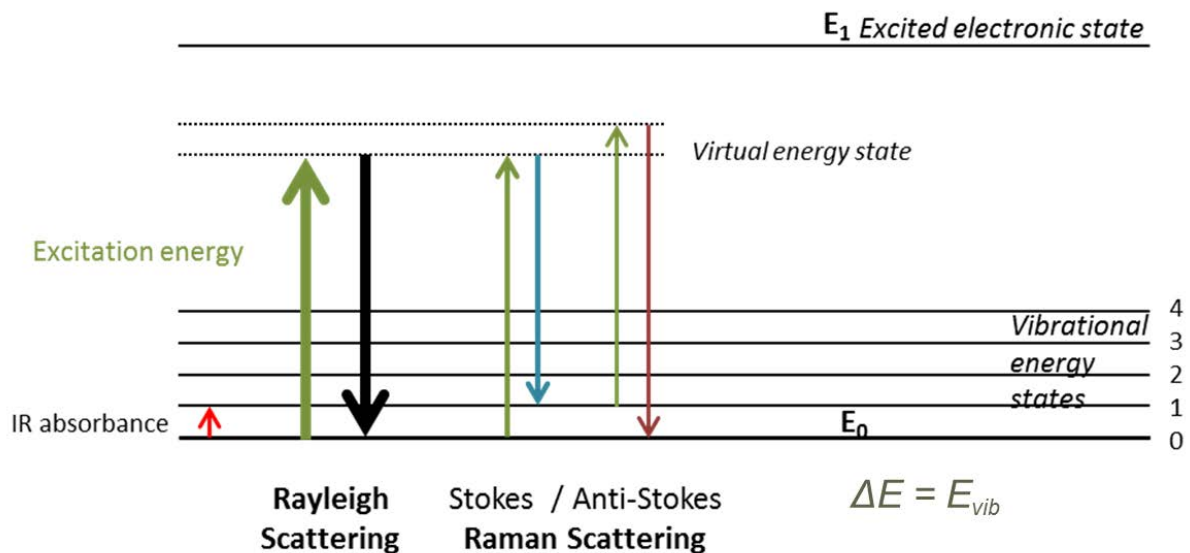


FIGURE 38: BASES QUANTIQUES DES DIFFÉRENTES TECHNIQUES DE SPECTROSCOPIE VIBRATIONNELLE
[HTTPS://WWW.SURFGROUP.BE/RAMAN](https://www.surfgroup.be/raman)

Les fréquences des raies Raman sont exprimées en nombre d'ondes rapportées à la raie excitatrice prise comme origine. Ces raies sont reliées aux énergies de vibration de la molécule et signent la présence de motifs structuraux ou de groupes fonctionnels (Naumann et al., 1991). Caractéristiquement, les raies Stokes sont d'une intensité très supérieure à celles des anti-Stokes (d'un facteur 10^3 environ), c'est donc sur ces raies que se focalise l'essentiel des études entreprises en spectroscopie Raman (Kneipp et al., 1999) (Figure 39).

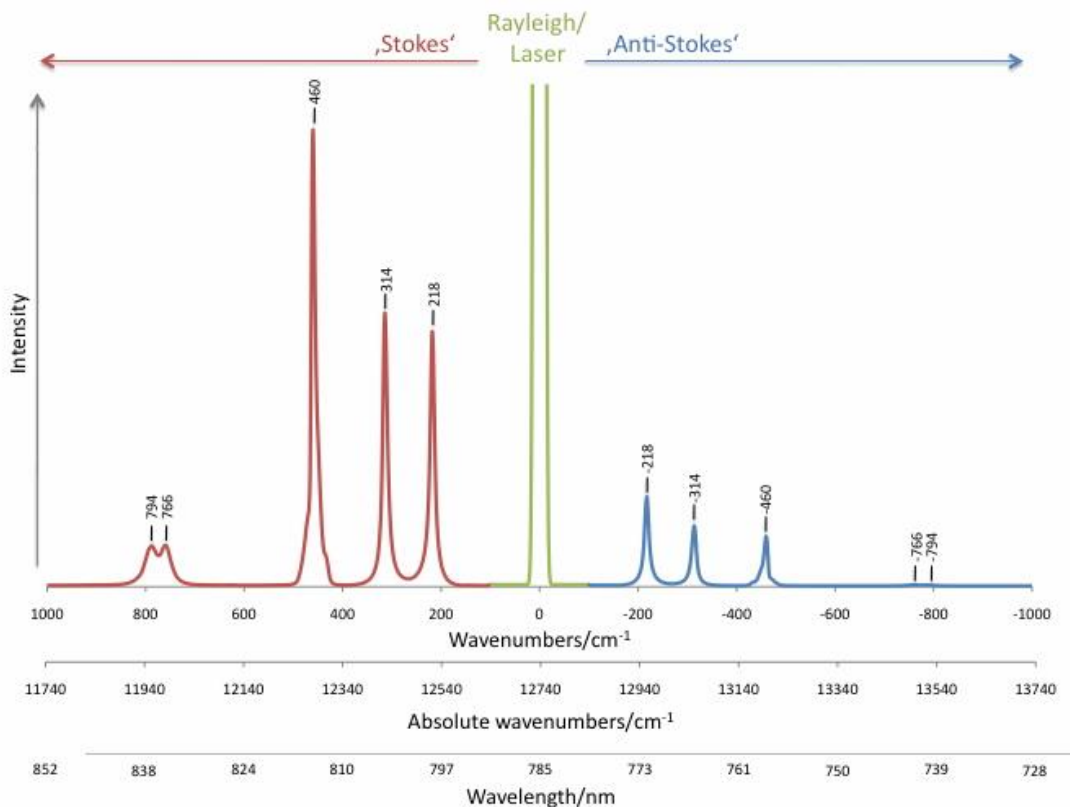


FIGURE 39: SPECTRE RAMAN : RAIES STOKES ET ANTI-STOKES
[HTTP://WWW.RAMAN.DE/HTMLEN/BASICS/INTENSITYENG.HTML](http://www.raman.de/htmlen/basics/intensityeng.html)

La spectromicroscopie Raman est une technique d'histolocalisation permettant d'atteindre une résolution spatiale d'une extrême précision : 1 μm x 1 μm (contre 10 μm x 10 μm pour la spectroscopie infrarouge à transformée de Fourier) (Thygesen et al., 2003). Ces deux modalités de spectromicroscopie vibrationnelle ont été appliquées à différents lichens du genre *Cladonia* pour y cartographier la distribution de l'acide usnique (Liao et al., 2010). En ce qui concerne les mycosporines, les signaux Raman caractérisant diverses mycosporines ont été décrits dans la littérature (Edwards et al., 2007; Vitek et al., 2010).

ii. Imagerie par spectrométrie de masse LDI à 266 nm

Bien qu'étant ionisée en LDI à 337 nm, la mycosporine sérinol n'est pas détectée en faisant appel à l'appareillage LDI-imaging utilisé lors de la cartographie des métabolites secondaires d'*Ophioparma ventosa* qui utilise un laser émettant à 355 nm (INRA de Nantes, plate-forme BIA, Audrey Geairon et Docteur Hélène Rogniaux).

Pour tenter d'atteindre une meilleure détection de la mycosporine sérinol, des essais de désorption/ionisation laser à une autre longueur d'onde ont été réalisés. Ces analyses ont été menées à la plateforme de spectrométrie de masse du Laboratoire de Chimie et Physique – Approche Multi échelle des Milieux Complexes (LCP-A2MC) à Metz (Université de Lorraine) par les Drs. Gabriel Krier, Lionel Vernex-Loiset et le Pr. Jean-François Muller. Ces analyses ont fait appel à un LDI-TOF de marque Bruker Daltonics et de type Reflex IV dont le module de désorption/ionisation est constitué soit d'un laser pulsé azote ($\lambda = 337$ nm) soit d'un laser pulsé Nd:YAG quadruplé ($\lambda = 266$ nm), dotés dans les deux cas d'un système d'atténuation variable de l'énergie laser au point d'impact.

Ces analyses indiquent une plus grande sensibilité de détection de la mycosporine sérinol à la longueur d'onde de 266 nm. Des fragments de thalle sont dans un second temps directement fixés à la surface du porte-échantillon métallique pour tenter de repérer la mycosporine sérinol à la surface du lichen intact. Ces analyses directes ne permettent pas de caractériser la mycosporine sérinol à la surface du thalle de *Lichina pygmaea*. Cette non-détection va dans le sens des conclusions issues des analyses DART-MS qui ne parvenaient pas à caractériser cette molécule depuis le lichen intact mais seulement broyé, ce qui pouvait laisser penser que ces molécules ne se localisent pas à la surface du lichen. Un test de dopage des fragments de thalle par la mycosporine sérinol (1 μL à 10^{-3} M) s'avère quant à lui positif. Les analyses d'imagerie sur des coupes de *Lichina pygmaea* sont actuellement en cours.

iii. Profilage chimique de cellules pures micro-disséquées

Une autre possibilité pour l'analyse comparée des partenaires est le profilage (e.g UHPLC-qTOF-MS) de cellules pures obtenues par microdissection capture laser. De telles approches ont déjà été appliquées pour comparer les métabolites secondaires de différents types cellulaires chez des végétaux (Jaiswal et al., 2014a, 2014b; Chen et al., 2015).

c. Recherche des gènes du cluster de biosynthèse des mycosporines

i. Procédures expérimentales

1. Matériel lichénique

L'échantillon de *Lichina pygmaea* utilisé dans cette étude a été récolté à Locmariaquer (Morbihan, Bretagne, France) par Joël Boustie, qui l'a également identifié. Un spécimen est conservé dans

l'herbier du Laboratoire de Pharmacognosie de l'UFR de Pharmacie de Rennes 1 sous le code JB/16/175.

2. Recueil isolé des partenaires de la symbiose

Pour recueillir séparément les deux partenaires de la symbiose, nous avons eu recours à un micro-dissecteur capture laser (LCM). Cette technique est utilisée pour obtenir des populations de cellules pures à partir de sections histologiques contenant des types cellulaires variés. La sélection des cellules à collecter est effectuée par l'opérateur sur la base de critères morphologiques, par observation microscopique (Bonner et al., 1997; Emmert-Buck et al., 1996).

Un laser IR est incorporé dans l'axe optique de la platine du microscope et est employé pour faire fondre un film de polymère thermolabile. Ce polymère est localisé sur la face inférieure d'un bouchon de tube Eppendorf de qualité optique. Le polymère ne fond qu'au voisinage de l'impulsion laser et en se liquéfiant capture les cellules situées dans le champ du microscope (Espina et al., 2006). Des pigments sont incorporés dans le polymère plastique à la fois pour absorber une partie de l'irradiation laser et ainsi limiter les dégâts infligés aux constituants cellulaires mais également pour mieux visualiser les aires où le polymère fondu se répand (Espina et al., 2006). Par la suite, le retrait du polymère de la surface de la coupe emporte les cellules qui y sont emprisonnées, les dissociant de leur tissu d'origine (Figure 40). Différents tampons d'extraction permettent ensuite de remettre en suspension les cellules à partir de leur matrice de polymère et d'en libérer les molécules d'intérêt (Espina et al., 2006). Éventuellement, un second laser émettant dans l'UV peut être utilisé pour aider à découper les contours des cellules à prélever et ainsi faciliter le processus d'exérèse.

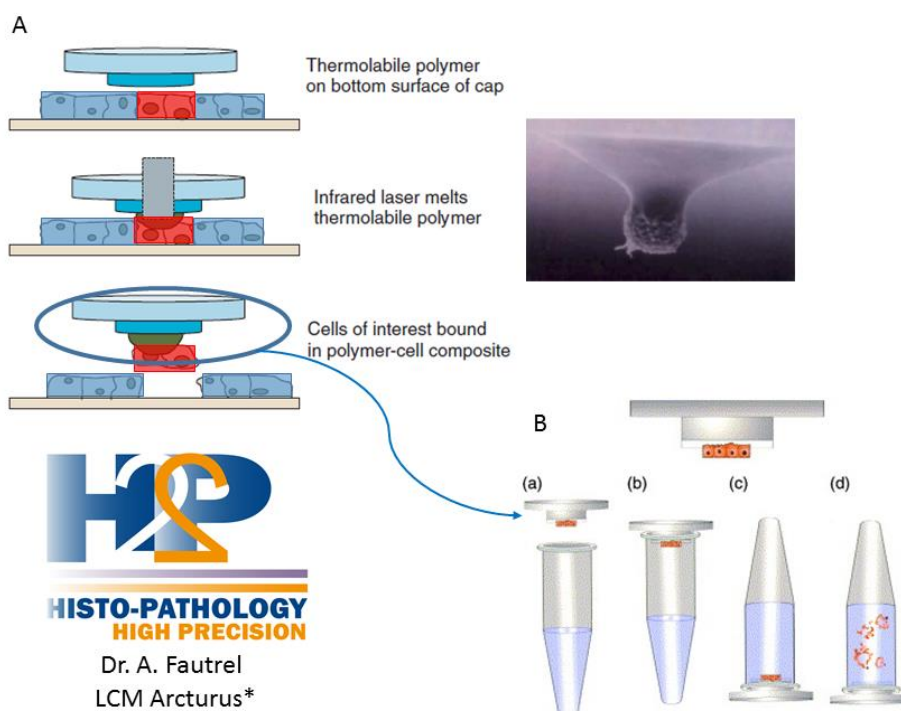


FIGURE 40: ILLUSTRATION DU PROCESSUS DE MICRO-DISSECTION CAPTURE LASER **A-** DIFFÉRENTES ÉTAPES PERMETTANT LA CAPTURE DES CELLULES DANS UN FILM DE POLYMÈRE FONDU SOUS L'ACTION D'UNE IRRADIATION UV (ADAPTÉ DE (ESPINA ET AL., 2006)) ET **B –** LE BOUCHON PORTANT LES CELLULES CAPTURÉES S'ADAPTE SUR UN TUBE EPPENDORF ET DES TAMPONS DE LYSE PERMETTENT D'EXTRAIRE LE TYPE DE BIOMOLÉCULES D'INTERÊT (TIRÉ DE (SIMONE ET AL., 1998)).

L'appareillage utilisé, implanté dans la plate-forme d'histopathologie H2P2 (Université de Rennes 1, Dr. Alain Fautrel) est de type Arcturus Veritas (Applied Biosystems, Life Technologies, Saint-Aubin, France). Les cellules ont été recueillies sur des coupes d'une épaisseur de 10µm obtenues à l'aide

d'un cryostat Leica en prenant le lichen en masse dans de l'OCT (*Optimal Cutting Temperature*). Le laser infrarouge a été ajusté pour produire des spots compris entre 10 et 15 μm de diamètre, permettant la capture des populations de cellules microdisséquées sur des bouchons CapSure LCM caps (Excilone, Elancourt, France).

3. Extraction de l'ADN génomique de *Lichina pygmaea* (lichen total ou champignon microdisséqué) et de *Rivularia sp.* (cyanobactérie microdisséquée).

Cette méthode dérivée de l'approche développée par Dellaporta et al. en 1983 (Dellaporta et al., 1983) a fait appel à un kit commercial d'extraction d'ADN végétal DNeasy Plant Mini Kit (Qiagen). Le surnageant contenant l'ADN génomique est purifié par deux colonnes en tandem selon le protocole fourni par le fabricant. Le principe de ces méthodes d'extraction est détaillé en Annexe 9 (p. 327). Les extractions ont porté soit sur le lichen total soit sur des populations de cellules issues de microdissection-capture laser.

Concernant le lichen total, environ 30 mg de lichen ont été broyés avec mortier et pilon en utilisant de l'azote liquide. Le broyat est re-suspendu dans un tampon de lyse DNAeasy Plant Mini Kit (Qiagen) puis homogénéisé à l'aide d'un appareil FastPrep-24™ 5G (MB Biomedicals, fungi program) en présence de Lysing Matrix Y (MB Biomedicals).

La purification a fait appel à un mini kit DNAeasy Plant (Qiagen) suivant le protocole décrit en Annexe 9.

Au terme de ce protocole, 100 μL de solution d'ADN à 200 ng/ μL ont pu être obtenus, pour un total de 20 μg d'ADNg ($\text{DO}_{260}/\text{DO}_{280} = 1.7$). La concentration d'ADN a été évaluée au moyen d'un spectrophotomètre NanoVue (GE Healthcare Life Science).

4. Recherche des gènes par PCR dégénérée et purification des amplicons

Au terme de l'extraction de l'ADN génomique, la recherche de séquences génétiques d'intérêt est effectuée par PCR. Les PCR ont utilisé un thermocycleur GenePro (Bioer Inc.). La présence de deux des trois gènes du cluster présomptif de biosynthèse des mycosporines a été recherchée : DHQS et ATP-grasp. Du fait de l'implication des O-MT dans de nombreuses voies métaboliques, ce gène ne saurait être fiablement relié à la biosynthèse des mycosporines. Des amorces fongiques et cyanobactériennes ont été désignées pour chacun de ces deux gènes avec pour DHQS deux paires d'amorces fongiques et un set d'amorces cyanobactériennes et pour ATP-grasp un set de primers fongiques et deux paires de primers cyanobactériens.

a. Désignation des amorces cyanobactériennes

Des recherches d'homologies de séquence BLASTp ont utilisé comme sondes les séquences protéiques DHQS-like (Ava_3858) et ATP-grasp (Ava_3856) associées à la biosynthèse des mycosporines chez *Anabaena variabilis*. Les séquences homologues identifiées d'autres cyanobactéries ont été retirées, plus particulièrement celles reliées à des souches proches du genre *Calothrix*. Les alignements de séquence ont été réalisés avec Clustal Omega pour identifier les motifs conservés et sont présentés en Annexe 9 de ce manuscrit (Figure 74 et Figure 75). Les amorces dégénérées sont désignées manuellement de sorte à amplifier des fragments d'environ 300-400 pb. Les amorces retenues sont les suivantes :

DegATP_1_F (HKYWL): 5'- GAAAGTCAYAARTAYTGGYT-3'
DegATP_1_R (WIMQE): 5'-AAAYTCYTG CATDATCCA-3'
DegATP_2_F (YAIECNP): 5'-TACGCAATYGARTGYAAAYCC-3'
DegATP_2_R (IDFNIGK): 5'-TTCCCGATRTTRAARTCDAT- 3'
DegDHQS_F (RNGMAE): 5'-CGTAACGGNATGGCNGA-3'
DegDHQS_R (HGHAVN): 5'-TTC ACTGCRTGNCCRTG-3'

b. Désignation des amorces fongiques

Des recherches d'homologies de séquence BLASTp ont été menées sur la base des séquences protéiques DHQS-like et ATP-grasp de *Magnaporthe oryzae*. Les alignements de séquence (présentés en Annexe 9 : Figure 76 et Figure 77) et le choix des amorces se sont déroulés selon le protocole indiqué plus haut. Les amorces suivantes ont été retenues :

ATPgrasp_fungi_deg_F (ELLMHY): 5'- GARCTNCTNATGCAYTA-3'
ATPgrasp_fungi_deg_R (IECNPR): 5'-CGNGGRTTRCAYTCRAT-3'
DHQS_fungi_deg_F1 (IGEKAK): 5'-ATHGGNGARAARGCNA-3'
DHQS_Fungi_deg_R1 (IKVAVN): 5'-TARTTNACNGCNACYTTDAT-3'
DHQS_Fungi_deg_F2 (RNGFAE): 5'-CGNAAYGGNTTYGCNGA-3'
DHQS_Fungi_deg_R2 (AYGHTW): 5'-CATNGTRTGNCCRTANGC-3'

c. Conditions de PCR

Les PCR ont été réalisées dans un volume total de 25 µL contenant 1 µL (échantillons microdisséqués) ou 2 µL (lichen total) d'ADN génomique, 2,5 µL de tampon 10x Key Buffer, 1 µL supplémentaire de MgCl₂ à 25 mM (pour atteindre une concentration finale de 2,5 mM), 1,2 µL de DMSO, 4 ou 8 µL d'amorces sens et anti-sens (25 µM) (amorces cyanobactériennes et fongiques, respectivement), 0,2 µL de Taq ADN polymérase (VWR), dH₂O : qsp 25 µL.

Les conditions de PCR ont été les suivantes : une étape de dénaturation initiale à 95°C pendant 2 minutes, 45 cycles contenant une étape de dénaturation à 95°C pendant 20 secondes, 45 secondes d'hybridation à 42°C et 45 secondes d'élongation à 72°C et une étape d'élongation finale à 72°C pendant 10 minutes.

La validité des conditions de PCR pour les amorces cyanobactériennes a été évaluée sur une souche productrice de mycosporines : *Calothrix* sp. PCC 6303.

Les produits de PCR sont ensuite analysés par électrophorèse sur gel d'agarose (1,2%). Les fragments amplifiés sont excisés sous lumière UV puis l'ADN en est extrait au moyen d'un kit NucleoSpin Gel and PCR Clean-up (Macherey-Nagel) suivant les indications du fabricant.

5. Sous-clonage des produits PCR

Les gènes sont insérés dans le vecteur pCR2.1-TOPO à l'aide d'un kit de sous-clonage TOPO® TA Cloning® (ThermoFisher Scientific) dans le but d'en réaliser le séquençage. Le principe de cette méthode est décrit en Annexe 9.

Le mélange de ligation est le suivant :

Réactif	Volume
Produit PCR purifié	2.4 µL
Solution Saline	1 µL
Eau	1.6 µL
Vecteur TOPO	1 µL

La réaction de ligation se déroule sur une nuit à température ambiante.

6. Transformation des cellules et sélection des clones recombinants

Des bactéries *Escherichia coli* DH10b ont été transformées avec la réaction de ligation TOPO. Les transformants ont été sélectionnés sur le milieu LB (*Lysogeny Broth*) gélosé supplémenté par de la kanamycine (50 µg/mL). Les cultures ont été incubées à 37°C pendant une nuit. L'insertion du fragment PCR a été criblé à l'aide du test X-Gal (dit bleu-blanc). Le principe de ce criblage est détaillé en Annexe 9.

7. Purification de l'ADN plasmidique

Au terme de ce protocole, les colonies contenant les plasmides recombinants sont mises à cultiver en milieu LB liquide à 37°C pendant une nuit. L'ADN plasmidique doit ensuite être isolé spécifiquement en éliminant l'ADN du chromosome bactérien par un protocole de lyse alcaline (Bimboim and Doly, 1979). Le protocole de lyse alcaline et le principe de la méthode sont décrits en Annexe 9.

8. Séquençage

Le séquençage est effectué par une prestation de service (Eurofins MWG Oregon). Le séquençage des plasmides fait appel aux amorces M13 (-21) flanquant le site d'insertion du transgène.

ii. Premiers résultats sur l'équipement génétique des symbiotes

La recherche de ces gènes a été effectuée sur lichen total et sur cyanobactérie microdisséquée et devrait être à l'avenir appliquée à du champignon microdisséqué. Différentes amorces ont été employées pour caractériser la présence du cluster de gènes associé à la biosynthèse des mycosporines.

- Pour les amorces fongiques : deux sets de primers ont été utilisés pour caractériser DHQS, et un pour rechercher une séquence ATP-grasp.
- Pour les amorces cyanobactériennes : un set de primers pour cibler DHQS et deux autres pour ATP-grasp.

Les résultats des recherches de gènes menées depuis la cyanobactérie microdisséquée sont consignés ci-après (Figure 41) :

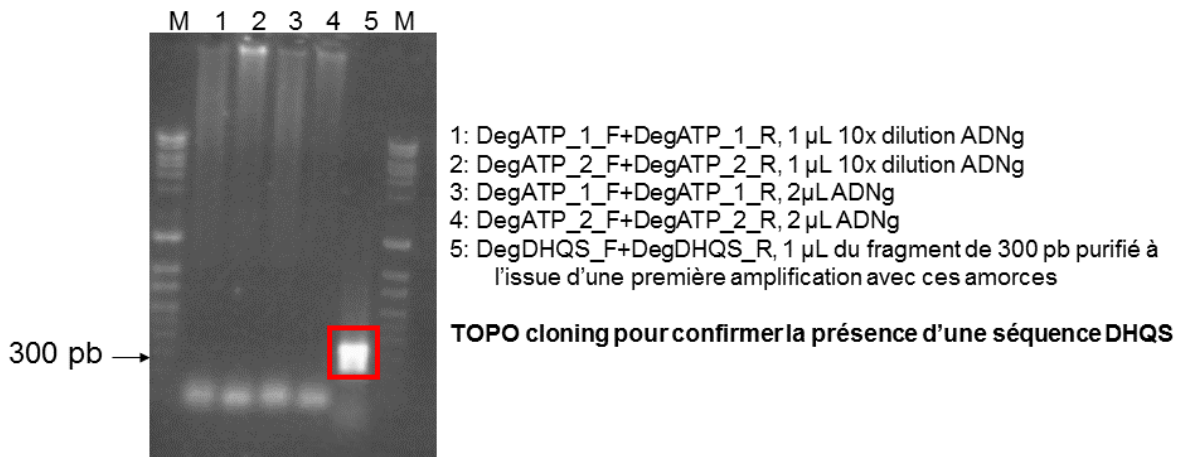


FIGURE 41 : RECHERCHE DES GÈNES DHQS-LIKE ET ATP-GRASP (AMORCES CYANOBACTERIENNES DANS LES DEUX CAS) AU SEIN DE LA CYANOBACTÉRIE MICRODISSÉQUÉE (*RIVULARIA*)

La séquence du fragment amplifié par les amorces DHQS-like est donnée en Annexe 9 (Figure 81).

Des recherches d'homologies de séquence inter-nucléotidiques BLASTx sont menées sur ce fragment. Son plus proche homologue (92% d'identité de séquence) est un gène impliqué dans la biosynthèse des mycosporines décrit chez la cyanobactérie *Rivularia* sp. PCC 7116, cette dernière étant dotée du cluster de gènes complet pour assurer la biosynthèse des mycosporines (Figure 42).

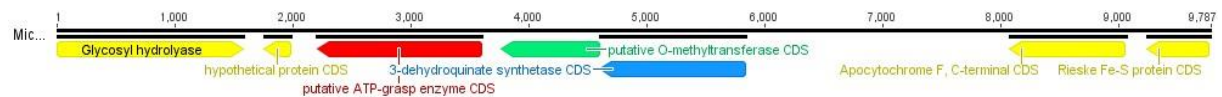


FIGURE 42 : CLUSTER DE GÈNES ASSOCIÉ À LA BIOSYNTHÈSE DES MYCOSPORINES CHEZ *RIVULARIA* SP. PCC 7116

Si les photobiontes de *Lichina pygmaea* sont traditionnellement associés au genre *Calothrix*, la récente caractérisation moléculaire des cyanobiontes de différents *Lichina* (dont *Lichina pygmaea*) suggère plutôt que le champignon lichénisant s'associe en réalité à des cyanobactéries du genre *Rivularia* dans cette espèce (Ortiz-Álvarez et al., 2015).

Pour l'instant, les recherches de gènes fongiques n'ont été menées qu'à partir du lichen total, et non encore sur du champignon microdisséqué. Tandis que les deux jeux d'amorces ciblant d'éventuels gènes DHQS-like ne permettent pas d'amplification par PCR, deux fragments différents (de 400 et 600 pb) sont détectés avec les amorces ATP-grasp fongiques (Figure 43).

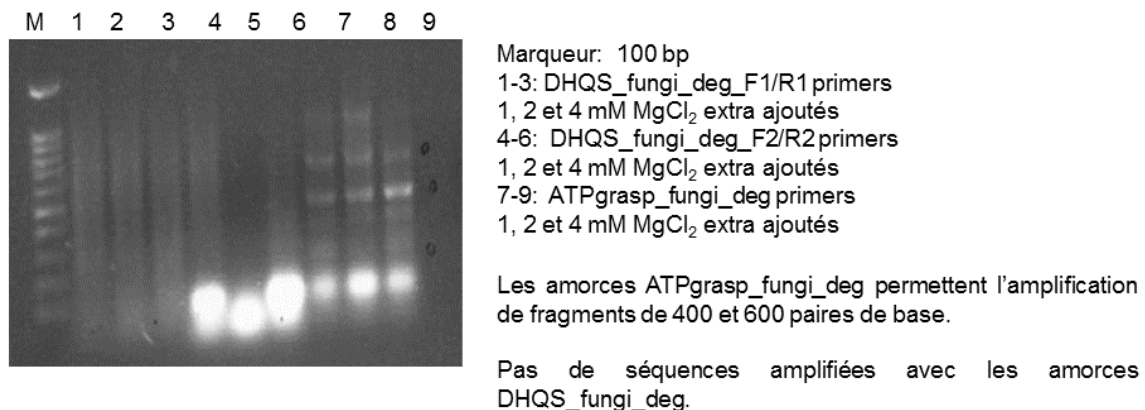


FIGURE 43 : RECHERCHE DES GÈNES DHQS-LIKE ET ATP-GRASP (AMORCES FONGIQUES DANS LES DEUX CAS) AU SEIN DU LICHEN TOTAL.

À ce stade, ces résultats pourraient laisser penser que la cyanobactérie serait dotée du gène DHQS tandis que le champignon posséderait dans son génome le gène ATP-grasp.

Pour valider ces résultats préliminaires, cyanobactéries et lichen total ont été soumis à des PCR au moyen des amorces désignées pour chacun des deux partenaires (Figure 44). L'amplification par les amorces ATP-grasp fongiques depuis le lichen total et non depuis la cyanobactérie est un élément supplémentaire en faveur de l'origine fongique de ces gènes. Le séquençage de ce gène est en cours. En revanche, il est plus surprenant de constater qu'une séquence est amplifiée au moyen des amorces ATP-grasp cyanobactériennes alors qu'aucun gène n'avait pu être amplifié de la cyanobactérie micro-disséquée. Il apparaît donc vraisemblable que ces séquences soient amplifiées à partir de cyanobactéries épiphytes (Grube et al., 2015) plutôt qu'à partir du cyanobionte primaire. Cette hypothèse est aussi accréditée par l'absence d'amplification à partir de l'ADN de cyanobactérie microdisséquée. La complexité considérable de l'écosystème lichénique peut donner lieu à des interférences liées à l'amplification de séquences microbiennes et non à celles issues des partenaires principaux de la symbiose. Ce risque légitime le besoin de recourir à des échantillons microdisséqués plutôt qu'au lichen total pour s'affranchir autant que possible de ces contaminations. Aussi, l'investigation génétique de champignon micro-disséqué apparaît indispensable pour la poursuite de ces travaux.

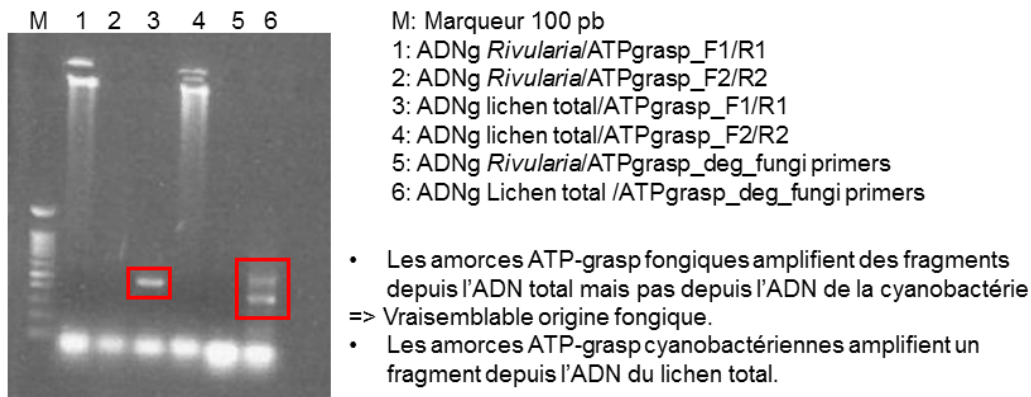


FIGURE 44 : RÉSUMÉ DES AMPLIFICATIONS DE GÈNES ATP-GRASP

La bande amplifiée par la première paire d'amorces cyanobactériennes ATP-grasp a été sous-clonée puis séquencée au moyen d'amorces M13 (-21). Deux populations de clones distincts sont en fait disintguées et leurs séquences sont données en Figure 82, Annexe 9. Les homologies de séquence sont ensuite recherchées par BLASTx (Figure 45).

>ATPCyano_pair 1_Total lichen gDNA clone 1

Description (five first hits)	Query cover	E value	Ident	Accession
ATP-grasp domain-containing protein [<i>Pleurocapsa</i> sp. PCC 7319]	99%	1e-85	81%	WP_019509604.1
ATP-grasp enzyme [<i>Myxosarcina</i> sp. GI1]	99%	5e-84	78%	WP_036482405.1
DUF201 domain-containing protein [<i>Stanieria cyanosphaera</i>]	99%	3e-80	77%	WP_015192873.1
hypothetical protein [<i>Synechococcus</i> sp. PCC 7335]	99%	7e-80	77%	WP_006456065.1
hypothetical protein STA3757_07780 [<i>Stanieria</i> sp. NIES-3757]	99%	7e-80	75%	BAU63414.1

>ATPCyano_pair 1_Total lichen gDNA clone 2

Description (five first hits)	Query cover	E value	Ident	Accession
ATP-grasp domain-containing protein [Trichodesmium erythraeum]	99%	3e-80	74%	WP_011612489.1
ATP-grasp domain-containing protein [Lyngbya sp. PCC 8106]	98%	6e-67	65%	WP_009783739.1
ATP-grasp domain protein [Lyngbya aestuarii]	99%	1e-65	62%	WP_023068529.1
ATP-grasp enzyme [Scytonema tolypotherichoides]	99%	8e-62	60%	WP_048866499.1
hypothetical protein [Oscillatoria sp. PCC 10802]	99%	1e-61	62%	WP_017716159.1

FIGURE 45 : RECHERCHE DES SÉQUENCES HOMOLOGUES (BLASTx) DES FRAGMENTS DE GÈNE AMPLIFIÉS PAR LES AMORCES ATP-LIKE CYANOBACTÉRIENNES SUR LE LICHEN TOTAL MAIS PAS SUR *RIVULARIA SP*

Concernant les gènes DHQS-like, les amorces fongiques n'amplifient pas de fragments dans le génome cyanobactérien. En revanche, plusieurs fragments sont amplifiés lorsque les amorces cyanobactériennes sont utilisées sur le lichen total (Figure 46). Leur sous-clonage est actuellement en cours.

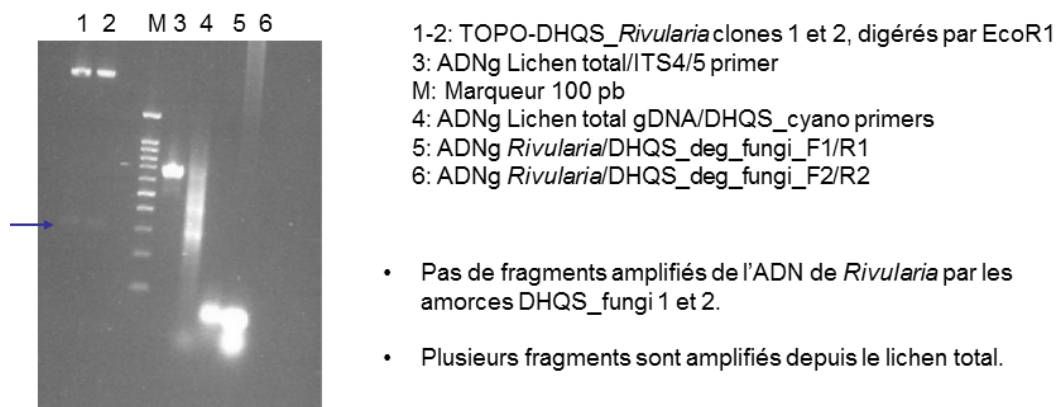


FIGURE 46 : RÉSUMÉ DES AMPLIFICATIONS DE GÈNES DHQS-LIKE

Il apparaît donc que ces séquences géniques proviennent également de cyanobactéries autres que le cyanobionte lichénique, ce d'autant plus que les séquences homologues ne sont pas décrites à partir de *Rivularia*. L'étude de champignons microdisséqués plutôt que de lichen total devrait permettre de contourner cet écueil.

Les données pouvant être retirées des travaux de biologie moléculaire à l'achèvement de cette thèse sont consignées dans ce tableau :

Primers	Matériel		
	Cyanobactérie <i>Rivularia sp.</i>	Champignon <i>Lichina pygmaea</i> F	Lichen total <i>Lichina pygmaea</i>
DHQS-Cy	Oui	Analyses	Non
ATP-grasp-Cy 1	Non		Oui ?
ATP-grasp-Cy 2	Non	En Cours	Non
DHQS-F 1	Non		Non
DHQS-F 2	Non		Non
ATP-grasp-F	Non		Oui

La réelle absence d'ATP-grasp du génome du cyanobionte est en passe d'être vérifiée au moyen d'amorces spécifiquement désignées à partir de séquences d'ATP-grasp de cyanobactéries du genre *Rivularia*. De la même façon, l'utilisation d'autres amorces doit être considérée avant d'exclure la présence de DHQS des cellules de champignon.

L'exploration du contexte génomique des différentes séquences repérées pourrait également être effectuée au moyen de techniques de *Genome Walking* (Leoni et al., 2011) afin d'apprécier le cluster de biosynthèse dans son ensemble. Tandis que le gène O-MT intervient dans trop de voies métaboliques pour pouvoir être relié sans discernement à la biosynthèse des mycosporines, sa présence contiguë à celle d'un gène DHQS-like serait très évocatrice de cette voie de biosynthèse (Balskus and Walsh, 2010; Singh et al., 2010).

À terme, les gènes séquencés devraient permettre de désigner des amorces pour localiser la présence de séquences d'ADN ou d'ARNm au sein des coupes de lichens. Des approches combinées émergent pour relier l'activité métabolique de cellules individuelles à leur identité taxonomique et/ou à leur distribution tissulaire. Tandis que la localisation des métabolites repose sur des techniques de d'imagerie par spectrométrie de masse telles que précédemment décrites (e.g (MA)LDI-MSI), les techniques FISH permettent d'analyser le contenu génétique de cellules individuelles. Les analyses de type (MA)LDI-FISH émergent donc comme des stratégies privilégiées pour étudier les interactions microbiennes *in situ*. Ainsi, Kaltenpoth *et al.* ont pu relier la production d'antibiotiques à la surface de cocons de guêpe *Philanthus* à la présence de bactéries symbiotiques *Streptomyces philanthi* (Kaltenpoth et al., 2016). Dans notre cas de figure, ne pouvant exclure que le cluster entier de biosynthèse soit présent chez les deux partenaires, à l'instar de ce qui a été rapporté chez le corail *Acropora digitata*, la recherche de séquences géniques exprimées (ARNm) devrait être privilégiée pour statuer sur la réelle implication des associés dans la biosynthèse de ces métabolites secondaires.

CONCLUSIONS/PERSPECTIVES



CONCLUSION GÉNÉRALE/PERSPECTIVES

Les lichens représentent des organismes pionniers dont l'extraordinaire résilience tient pour partie à la constitution d'un arsenal de défense chimique unique dans le vivant (Stocker-Wörgötter, 2008). Cette chimiodiversité légitime l'intérêt grandissant suscité par les lichens en pharmacognosie, d'autant plus que ces composés sont dotés d'activités biologiques variées et souvent significatives (Shukla et al., 2010; Shrestha and St. Clair, 2013). Outre cet aspect, les métabolites secondaires jouent également un rôle important dans la phylogénie des lichens, ce qui représente un autre intérêt à explorer la chimie de ces organismes (Hawksworth, 1973; Frisvad et al., 2008).

Ce travail a été mené selon deux grands axes. Cette thèse s'est d'abord penchée sur le développement de nouveaux outils permettant de réaliser du profilage chimique à haut débit. Les stratégies analytiques retenues se sont adossées à des caractéristiques particulières des composés lichéniques ou de leurs métabolites.

L'accumulation des métabolites secondaires dans les tissus superficiels du lichen, voire leur cristallisation à la surface des filaments mycéliens, a été perçue comme une opportunité pour développer des méthodes de détection *in situ*. Une méthode de spectrométrie de masse à ionisation ambiante, le DART-MS, a démontré son aptitude à générer des profils chimiques complets à partir d'extraits acétoniques mais également de poudre de thalles voire de thalles natifs. De nombreuses classes structurales ont ainsi pu être détectées par le DART, aussi bien en modes positif que négatif : depsides, depsidones, dibenzofuranes, naphtoquinones, xanthones (Le Pogam and Boustie, 2016), acides paraconiques, dérivés de l'acide pulvinique et mycosporines (Le Pogam et al., 2015b) soulignant la polyvalence de cette méthode en lichénologie.

De plus, les spectres de masse fournis par le DART restent généralement simples à interpréter car ils contiennent le plus souvent des ions quasi-moléculaires prédominants. Seuls les depsides révèlent des fragmentations véritablement prononcées. En mode négatif, les dissociations décrites pour ces composés s'avèrent comparables à celles obtenues en utilisant d'autres sources (ESI, FAB...) et des signatures spectrales récurrentes ont pu être observées en mode positif. L'intérêt du DART pour la déréplication a été démontré en étudiant un lichen modèle : *Ophioparma ventosa*. La mise en évidence d'un depside rare et jusqu'alors jamais décrit dans cette espèce, l'acide miriquidique, a été le point de départ d'investigations plus poussées. Chez ce même lichen, il a également pu être établi que le DART permet une première estimation de la distribution de métabolites secondaires au sein du thalle en révélant des profils chimiques différents entre les faces supérieure et inférieure de cette espèce (Le Pogam et al., 2016a).

Au cours des différentes analyses engagées sur le lichen modèle *Ophioparma ventosa*, il est apparu que ce lichen accumulait dans ses apothécies de nombreux pigments non caractérisés structuralement. Une étude phytochimique ciblée sur les seules apothécies de ce lichen a alors été engagée. Tandis que l'haemoventosine était le seul pigment chimiquement identifié au sein des organes reproducteurs d'*Ophioparma ventosa*, cinq autres pyranonaphtoquinones ont pu y être isolées et identifiées : un premier pigment connu chez les champignons mais nouveau chez les lichens – l'anhydrofusarubine lactone – ainsi que quatre nouvelles structures : l'ophioparmine, deux épimères de la 4-méthoxyhaemoventosine ((3S,4R)- et (3S,4S)-4-méthoxyhaemoventosines et un isomère de la 3S-4-hydroxyhaemoventosine dont la configuration absolue du carbone 3 n'a pas pu être déterminée (Le Pogam et al., 2016b).

Le DART-MS représente donc un outil déréplicatif de choix en lichénologie en permettant l'analyse de très petites quantités de lichens (un fragment de thalle suffit) mais également avec une préparation de l'échantillon virtuellement nulle consistant au maximum à broyer le lichen. Enfin, des informations complémentaires à l'analyse de l'échantillon peuvent être obtenues en faisant varier la température. Ainsi, la source DART a été mise à profit pour étudier les constantes thermodynamiques associées à

la déshydratation de la mycosporine sérinol. À notre connaissance, l'utilisation du DART à de telles fins thermodynamiques n'a pas été décrite auparavant dans la littérature (Le Pogam et al., 2015b).

La seconde approche de spectrométrie de masse retenue dans le cadre de ces travaux est le LDI. Du fait de la forte absorption UV et d'une relative homologie structurale des molécules lichéniques avec certaines matrices commerciales, il a été observé que tous les grands groupes de métabolites lichéniques sont ionisables sans devoir y adjoindre de matrices en mode négatif (= auto-ionisables). L'analyse d'extraits acétoniques totaux de lichens couvrant la chimie de ces organismes dans sa diversité a démontré la polyvalence du LDI pour leur profilage chimique. L'ionisation douce déclenchée par le LDI livre des spectres dominés le plus souvent par l'ion déprotoné et, ici aussi, seuls les depsides fragmentent de façon significative, toujours en lien avec les fragmentations constatées en ayant recours à d'autres sources d'ions. Il est à noter que la possibilité offerte par le LDI de générer des ions radicalaires permet la détection d'espèces qui peuvent difficilement l'être en faisant appel à d'autres sources d'ions (e.g quinones difficilement déprotonables car engageant des liaisons hydrogène intramoléculaires) (Le Pogam et al., 2015c).

Les analyses LDI ne nécessitent que très peu de préparation puisqu'il s'agit simplement de préparer un extrait acétonique total et de le déposer à la surface de cibles MALDI. Cette méthode de déréplication fait appel à peu de matière première puisque les analyses LDI requièrent 0,7 µL d'une solution à 10 mg/mL. Les analyses LDI sont par ailleurs peu onéreuses et sont automatisables, permettant d'analyser une trentaine d'échantillons en l'espace d'une heure à une heure trente.

L'auto-ionisabilité des métabolites secondaires lichéniques pourrait amener à évaluer leurs propriétés matriciales, à l'instar de ce qui avait initialement été réalisé pour l'acide usnique (Schinkovitz and Richomme, 2015).

Si ces stratégies analytiques innovantes offrent de nouvelles perspectives pour le criblage de lichens à haut débit, les instrumentations permettant ces analyses font appel à des compétences avancées en chimie analytique pour piloter et entretenir de tels équipements. Aussi, la CCM reste encore à l'heure actuelle la méthode d'identification des composés lichéniques la plus largement employée par les lichénologues. Les limites associées à cette approche sont bien connues dans la mesure où il s'agit de caractériser les molécules et non de les identifier. Ce travail s'est donc également penché sur la possibilité d'identifier les familles structurales lichéniques par CCM-NI-ESI-MS. La détection par spectrométrie de masse depuis la plaque CCM s'avère généralement sensible avec des composés détectés pour la plupart dès 1 µg. L'intérêt de ce couplage est mis en évidence dans des cas de figure où la distinction des composés lichéniques est réputée difficile (depsides à longues chaînes aliphatiques, depsidones polaires...). Deux limites doivent être gardées à l'esprit :

- les composés polaires ont une détection moins sensible, sans doute du fait de leur désorption plus difficile depuis la plaque de silice ;
- les composés difficilement déprotonables ne sont pas détectés en CCM-NI-ESI-MS. Cette limite n'est pas liée à l'interface CCM-MS mais est une limite du processus d'ionisation ESI qui ne permet pas la formation d'ions radicalaires.

Tandis que les avantages associés aux méthodes DART-MS et LDI-MS demeurent évidents en termes de temps de préparation des échantillons et de l'analyse en elle-même, le manque de données complémentaires à l'appui (e.g temps de rétention, spectre UV/Vis) peut entraver l'identification non ambiguë de certains métabolites secondaires (Sica et al., 2015). À titre d'exemple, les limites associées à la déréplication des lichens par le DART et/ou le LDI peuvent être mises en évidence au travers du profilage de *Lecidella asema*, lichen producteur de xanthones chlorées présentant de nombreuses isoméries possibles. L'identification se fonde alors sur les données préalables de la littérature concernant la chimie de ce lichen mais la spectrométrie de masse ne livre aucune donnée spectrale en faveur de l'un ou l'autre des isomères. Parmi les perspectives envisageables pour obtenir davantage d'informations tout en conservant une approche sans couplage

chromatographique, nous pensons en priorité à la spectrométrie de mobilité ionique couplée à la spectrométrie de masse (IM-MS pour *Ion Mobility – Mass Spectrometry*). L'IM-MS associe à la mesure des masses une seconde dimension de séparation tenant compte de la structure des ions en phase gazeuse (Kanu et al., 2008). Pour réaliser cette séparation supplémentaire, une cellule de mobilité ionique est introduite en aval de la source d'ions et en amont de l'analyseur (Figure 47). Au sein de cette chambre règne une pression relativement élevée de gaz tampon (typiquement de 5 Torr environ avec un gaz inerte comme l'hélium ou l'azote) et un champ électrique relativement faible. L'énergie thermique fournie aux ions par les collisions avec le gaz tampon doit être supérieure à celle acquise par le champ électrique imposé aux ions (Gabelica, 2006). De fait, les processus de diffusion dominent dans la cellule de dérive de telle sorte que la migration des ions dans cette chambre est assimilable à une diffusion dirigée (Kanu et al., 2008). Plus l'ion adopte une conformation compacte, moins il est freiné par les collisions et plus sa vitesse de migration dans cette cellule sera élevée, et inversement. L'introduction de molécules chirales dans ce gaz inerte a permis la séparation en phase gazeuse de différents énantiomères (Dwivedi et al., 2006).

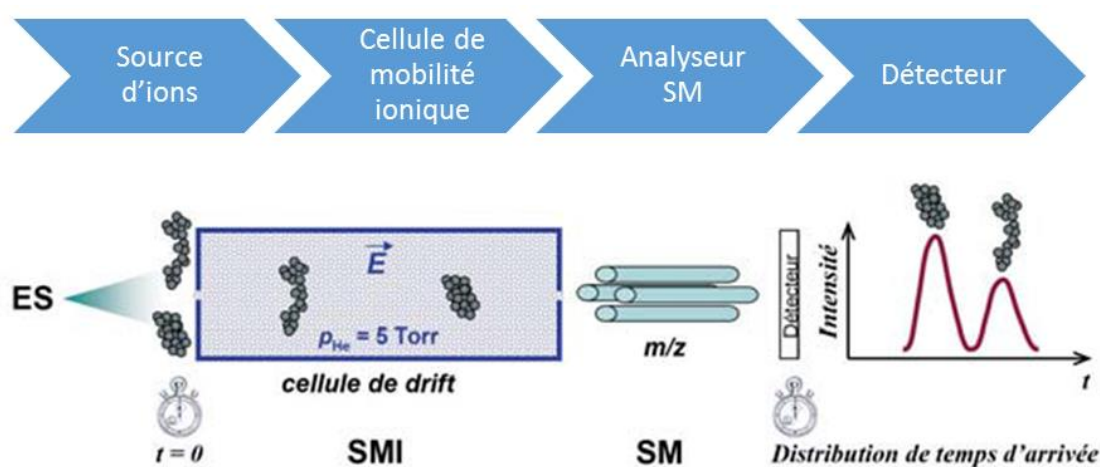


FIGURE 47: PRINCIPE DE LA SPECTROMÉTRIE DE MOBILITÉ IONIQUE COUPLÉE À LA SPECTROMÉTRIE DE MASSE (ADAPTE DE (GABELICA, 2006))

Si le couplage de la cellule de mobilité ionique aux techniques de désorption/ionisation laser est rencontré de façon courante dans la littérature, l'association de la mobilité ionique au DART-MS est une approche qui n'a été décrite que récemment (Harris et al., 2011; Räsänen et al., 2014).

L'absence d'extraction et la possibilité de travailler à partir de très petites quantités d'échantillons font également du DART-MS une technique privilégiée pour l'analyse de matériels d'intérêt patrimonial en minimisant la quantité de matière première à prélever au sein de spécimens historiques (Adams, 2011; Selvius DeRoo and Armitage, 2011). De telles perspectives revêtent un intérêt tout particulier dans le contexte de l'équipe PNSCM qui héberge l'herbier Des Abbayes, collection d'une importance majeure compilant environ 1.300 espèces (pour ca. 11.000 spécimens) dont certains ont plus de 100 ans (Delmail et al., 2012). Dans ce même souci de préservation d'échantillons précieux, il est intéressant de noter que la littérature comporte quelques analyses d'empreintes d'échantillons plutôt que de l'échantillon directement au moyen d'approches connexes de spectrométrie de masse comme le DESI-MS (Ifa et al., 2011; Müller et al., 2011). Pour ce faire, les analytes sont transférés de la matière première à une membrane de nature variable en y pressant l'échantillon pour que les analytes s'y adsorbent (papier ordinaire, surfaces poreuses dérivées du Téflon)... Cette approche semble d'autant plus applicable aux lichens que leurs métabolites secondaires se localisent en surface des filaments mycéliens du fait de la cristallisation des métabolites lichéniques à la surface des filaments fongiques, laissant présager d'une adsorption aisée de ces molécules bien accessibles (Stocker-Wörgötter, 2008).

Concernant le couplage de la CCM à la spectrométrie de masse, des alternatives peuvent être envisagées à la méthode CCM-ESI-MS décrite dans ce manuscrit. Parmi les autres techniques l'approche CCM-LDI-MS peut être citée. De telles analyses restent rares à ce jour avec un premier article basé sur cette approche paru en 2009 et décrivant la détection d'alcaloïdes quaternaires (donc déjà chargés positivement) de la plante *Berberis barandana* (Shariatgorji et al., 2009). Différents avantages peuvent être attendus du couplage CCM-LDI-MS face au couplage CCM-ESI-MS :

- la rapidité de l'analyse. L'éluion des composés à partir des bandes d'intérêt en CCM-ESI-MS requiert une minute suivie de quatre à cinq autres minutes pour ramener le courant ionique total à son niveau basal et ainsi permettre l'analyse d'une nouvelle bande ;
- la possibilité de parcourir des surfaces. D'une façon rigoureusement analogue à l'imagerie LDI présentée dans le chapitre « Histolocalisation » de cette thèse, le laser peut parcourir l'ensemble de pistes de migration en CCM pour ensuite y cartographier les différents signaux (Batubara et al., 2015; Cheng et al., 2011). Cette analyse systématique de l'ensemble de la piste de migration permet de s'affranchir de l'étape préalable de repérage des positions à analyser, avec le biais de ne pas rechercher les composés non visualisés en amont (e.g acide roccelique non visible aux longueurs d'onde de lecture UV classique 254 et 365 nm mais ionisable en LDI).

En contrepartie, le laser UV employé en LDI ne pénètre que peu la silice dans son épaisseur, l'analyte ne peut en être désorbé que depuis les couches les plus superficielles de la plaque CCM. Par voie de conséquence, une perte de sensibilité par rapport à l'ionisation CCM-ESI-MS, qui désorbe les composés dans l'épaisseur de la plaque, peut être attendue (Fuchs et al., 2009).

L'extension de nos essais de diffraction de poudres lichéniques aux rayons X devrait permettre de mieux cerner le potentiel dérégicatif de cette approche.

Les conclusions et les perspectives associées au volet dérégicatif sont reprises dans la Figure 48.

DART-MS	LDI-MS
<p>Analyses de lichens solides</p> <ul style="list-style-type: none">• Pas de préparation et analyses très courtes• Analyse de très faibles quantités de matériel non extrait : un fragment de thalle suffit• Pas d'artefacts liés aux solvants• Premières données sur la localisation tissulaire des composés	<p>Analyses d'extraits acétoniques totaux</p> <ul style="list-style-type: none">• Préparation de l'échantillon très limitée• Durée de l'analyse très courte et possible automatisation• Analyses de très faibles quantités d'extrait: 0.7 µL d'une solution à 10mg/mL
<p>Ionisation des métabolites lichéniques</p> <ul style="list-style-type: none">• Généralement détection en modes positif et négatif• Molécules généralement peu fragmentées (hors depsides)... mais réactivité chimique parfois importante et chauffage pouvant dégrader les molécules instables thermiquement (e.g acide thamnolique).• Pour les depsides, fragmentations consensuelles dans les deux modes.	<p>Ionisation des métabolites lichéniques</p> <ul style="list-style-type: none">• Très essentiellement en mode négatif (sauf mycosporines)• Ionisation douce : peu de fragmentation (seules les depsides et souvent l'ion déprotoné reste observable)• Possibilité de détecter des espèces radicalaires: avantage pour détecter des espèces établissant des liaisons hydrogène intramoléculaire comme de nombreuses quinones et xanthones lichéniques
<p>Perspectives</p> <ul style="list-style-type: none">• Couplage à la spectrométrie de mobilité ionique• Analyse d'échantillons d'intérêt patrimonial (e.g spécimens Herbier des Abbayes) voire d'empreintes obtenues par adsorption sur une surface	<p>Perspectives</p> <ul style="list-style-type: none">• Couplage à la spectrométrie de mobilité ionique• Analyses de plaques CCM en LDI• Évaluation des propriétés matriciales de métabolites lichéniques autres que l'acide usnique

FIGURE 48 : RÉSULTATS ET PERSPECTIVES ASSOCIÉS AU DART-MS ET AU LDI-MS À L'ISSUE DE CES TRAVAUX

Un autre enjeu de cette thèse gravitait autour de l'histolocalisation des composés lichéniques dans le thalle. Dans la mesure où la distribution des métabolites secondaires dans le lichen est souvent en lien avec leurs rôles écologiques, l'imagerie par spectrométrie de masse peut représenter un puissant outil au service de questions d'écologie chimique. De la même façon, ces données spatiales peuvent fournir des clés pour comprendre les séquences de biosynthèse de métabolites secondaires chez ces organismes symbiotiques.

Sur la base de la distribution irrégulière des molécules d'*Ophioparma ventosa* constatée par analyses DART-MS, les premières analyses d'imagerie LDI ont porté sur des coupes transversales d'*Ophioparma ventosa*. Les cinq molécules majoritaires de ce lichen (haemoventosine, acides usnique, divaricatique, thamnolique et miriquidique) ont pu être imagées avec une résolution spatiale atteignant 50 μm et leurs distributions vont dans le sens des hypothèses d'écologie chimique précédemment décrites dans la littérature. Il est à noter que l'un des nouveaux pigments présent à l'état de trace, la 4-hydroxyhaemoventosine a même pu être imagé. Concernant l'acide miriquidique, molécule décrite pour la première fois chez *O. ventosa* au titre de ce travail, sa distribution dans les parties basales du lichen et sa présence longitudinale inhomogène sont compatibles avec son acquisition à partir de thalles produisant ce depside et parasités par ce lichen. Hypothèse d'autant plus vraisemblable que ce depside se concentre pour devenir un métabolite majoritaire au niveau de certaines parties du thalle et totalement manquer au niveau d'autres fragments (considérés longitudinalement). Il peut être supposé que les portions de thalle concentrant cette molécule correspondent aux régions du lichen s'étant développées sur des thalles qui pourraient être ceux de *Miriquidica garovaglii*, la présence de ce dernier étant avérée sur les rochers où l'on a pu récolter *O. ventosa*.

De telles approches devraient également permettre de préciser quel(s) partenaire(s) de la symbiose accumule(nt) les métabolites secondaires du lichen pour cerner la contribution de chacun dans leur biosynthèse. S'il est généralement admis que la biosynthèse des polyphénols lichéniques est imputable aux champignons (à partir des sucres transmis par le photobionte), les mycosporines - molécules notamment connues chez des champignons, des cyanobactéries et des algues vertes - ont une origine plus difficile à établir chez les lichens dans la mesure où chacun des partenaires de la symbiose est connu comme pouvant produire des mycosporines lorsqu'il vit isolément.

Pour mieux comprendre la biosynthèse des mycosporines chez les lichens, un projet alliant imagerie par spectrométrie de masse et génétique a été engagé sur le cyanolichen modèle *Lichina pygmaea* :

- l'imagerie par spectrométrie de masse a dû faire l'objet de quelques ajustements et un appareil doté d'une longueur d'onde de 266 nm a été employé pour assurer une détection plus efficace des mycosporines. Si la détection de ces composés s'avère effectivement plus sensible à cette seconde longueur d'onde, ces analyses d'imagerie par spectrométrie de masse n'ont pas encore permis de préciser la distribution de la mycosporine sérinol au sein de coupes de ce cyanolichen. Une autre approche envisagée pour visualiser la distribution de la mycosporine sérinol est la spectromicroscopie Raman, équipement récemment arrivé au sein de la plate-forme H2P2 ;
- en parallèle, des études de biologie moléculaire ont été menées en collaboration avec le MNHN pour analyser le bagage génétique du champignon et de la cyanobactérie. Le recueil séparé des deux symbiontes a pu être réalisé par microdissection-capture laser. La recherche de gènes appartenant au cluster de biosynthèse des mycosporines a permis de caractériser une séquence DHQS-like au sein du génome de la cyanobactérie. Le troisième segment génique, ATP-grasp, a pu quant à lui être caractérisé dans l'ADN isolé à partir du lichen total au moyen d'amorces d'ATP-grasp fongiques. Des analyses similaires portant sur le champignon micro-disséqué sont en cours pour relier ces gènes au mycobionte en présence. A l'inverse, le gène ATP-grasp n'a pas pu être caractérisé chez la cyanobactérie et le gène DHQS n'a pas été identifié dans la mycobionte pour l'instant. Des conditions de PCR faisant appel à d'autres amorces sont prévues pour statuer sur la réelle absence de ces gènes.

Les méthodes envisageables pour l'histolocalisation de composés lichéniques ainsi que les problématiques où cette information spatiale est d'intérêt sont résumés dans la Figure 49.

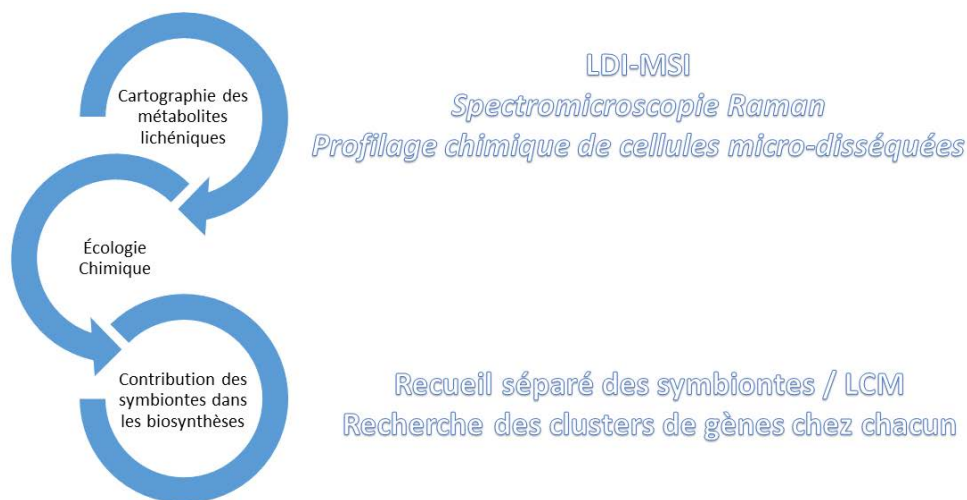


FIGURE 49 : MÉTHODOLOGIES ENVISAGEABLES POUR ÉTABLIR LA DISTRIBUTION TISSULAIRE DE MÉTABOLITES LICHÉNIQUES ET PROBLÉMATIQUES DANS LESQUELLES CES ANALYSES PEUVENT S'INSCRIRE

Ces développements méthodologiques appliqués aux lichens ont été facilités par la présence de molécules cristallisées à la surface des structures fongiques ou des photobiotés associés. La distribution de ces métabolites au sein des lichens est un élément d'importance en taxonomie et leur repérage a rapidement été un sujet d'étude pour les lichénologues qui ont développé des approches variées dès le 19^{ème} siècle (caractérisation chimique, reconnaissance cristalline au microscope des composés majoritaires, développement de méthodes standardisées en CCM et HPLC, analyse Raman...). C'est aussi à l'heure actuelle un enjeu d'importance pour repérer en amont des molécules d'intérêt que ce soit pour la taxonomie, une valorisation thérapeutique des métabolites, une compréhension de leur rôle au sein du lichen ou de l'environnement biotique ou abiotique associé. Tirant profit de nouvelles méthodes analytiques et d'appareillages performants, nos travaux permettent d'améliorer le niveau d'information pour la réalisation de profils chimiques rapides et fiables. Ils s'inscrivent dans un prolongement et une complémentarité avec d'autres techniques qui méritent d'être explorées sur ces organismes modèles. Nous pouvons citer la cristallographie pour laquelle nous avons eu des résultats très encourageants mais aussi d'autres techniques (Raman, proche IR...) dont la miniaturisation des appareillages permet un accès de plus en plus aisé, y compris sur le terrain. Un autre avantage à souligner est la possibilité d'avoir des informations fiables avec des quantités infimes de matériel, permettant par exemple d'avoir des approches quasiment non-destructives. Nous pensons ici à des applications sur des échantillons d'herbier mais aussi à la génération de données métabolomiques dont le traitement adéquat peut être une source éclairante d'information...

Le couplage de ces données chimiques à des données de biologie est un élément essentiel à la compréhension de mécanismes clés pour le mode de fonctionnement de ces organismes singuliers, des approches holistiques semblant nécessaires pour apprécier le fonctionnement de cet éco-système dans sa complexité. Nous espérons par exemple que notre approche sur la biosynthèse des mycosporines sera prochainement finalisée et ne doutons pas que certains de ces résultats auront des applications bien au-delà de l'étude des lichens proprement dite.

BIBLIOGRAPHIE

- Abdel-Hameed, M., Bertrand, R.L., Piercey-Normore, M.D., Sorensen, J.L., 2016a. Putative identification of the usnic acid biosynthetic gene cluster by de novo whole-genome sequencing of a lichen-forming fungus. *Fungal Biol.* 120, 306–316. doi:10.1016/j.funbio.2015.10.009
- Abdel-Hameed, M., Bertrand, R.L., Piercey-Normore, M.D., Sorensen, J.L., 2016b. Identification of 6-Hydroxymellein Synthase and Accessory Genes in the Lichen *Cladonia uncialis*. *J. Nat. Prod.* in press.
- Adams, J., 2011. Analysis of printing and writing papers by using direct analysis in real time mass spectrometry. *Int. J. Mass Spectrom.* 301, 109–126. doi:10.1016/j.ijms.2010.07.025
- Adeboya, M.O., Edwards, R.L., Lassøe, T., Maitland, D.J., Shields, L., Whalley, A.J., 1996. Metabolites of the higher fungi. Part 29. Maldoxin, maldoxone, dihydromaldoxin, isodihydromaldoxin and dechlorodihydromaldoxin. A spirocyclohexadienone, a depsidone and three diphenyl ethers: Keys in the depsidone biosynthetic pathway from a member of the fungus genus *Xylaria*. *J. Chem. Soc. [Perkin 1]* 1419–1425.
- Ainsworth, G.C., 2008. *Ainsworth & Bisby's Dictionary of the Fungi*. CABI.
- Armaleo, D., Sun, X., Culberson, C., 2011. Insights from the first putative biosynthetic gene cluster for a lichen depside and depsidone. *Mycologia* 103, 741–754.
- Armstrong, R.A., Welch, A.R., 2007. Competition in lichen communities. *Symbiosis* 43, 1–12.
- Arpin, N., Favre-Bonvin, J., Thivend, S., 1977. Structure de la mycosporine 2, nouvelle molécule, isolée de *Botrytis cinerea*. *Tetrahedron Lett.* 18, 819–820.
- Asplund, J., Solhaug, K.A., Gauslaa, Y., 2010. Optimal defense: snails avoid reproductive parts of the lichen *Lobaria scrobiculata* due to internal defense allocation. *Ecology* 91, 3100–3105.
- Asplund, J., Solhaug, K.A., Gauslaa, Y., 2009. Fungal depsidones – an inducible or constitutive defence against herbivores in the lichen *Lobaria pulmonaria*? *Basic Appl. Ecol.* 10, 273–278. doi:10.1016/j.baae.2008.04.003
- Aubert, S., Juge, C., Boisson, A.-M., Gout, E., Bligny, R., 2007. Metabolic processes sustaining the reviviscence of lichen *Xanthoria elegans* (Link) in high mountain environments. *Planta* 226, 1287–1297.
- Avalos, A., Vicente, C., 1987. The occurrence of lichen phenolics in the photobiont cells of *Evernia prunastri*. *Plant Cell Rep.* 6, 74–76.
- Bačkor, M., Klemová, K., Bačkorová, M., Ivanova, V., 2010. Comparison of the Phytotoxic Effects of Usnic Acid on Cultures of Free-Living Alga *Scenedesmus quadricauda* and Aposymbiotically Grown Lichen Photobiont *Trebouxia erici*. *J. Chem. Ecol.* 36, 405–411. doi:10.1007/s10886-010-9776-4
- Balskus, E.P., Walsh, C.T., 2010. The genetic and molecular basis for sunscreen biosynthesis in cyanobacteria. *Science* 329, 1653–1656.
- Batubara, A., Carolan, V.A., Loadman, P.M., Sutton, C., Shnyder, S.D., Clench, M.R., 2015. Thin-layer chromatography/matrix-assisted laser desorption/ionisation mass spectrometry and matrix-assisted laser desorption/ionisation mass spectrometry imaging for the analysis of phospholipids in LS174T colorectal adenocarcinoma xenografts treated with the vascular disrupting agent DMXAA. *Rapid Commun. Mass Spectrom.* 29, 1288–1296.
- Beaumont, P.C., Edwards, R.L., Elsworth, G.C., 1968. Constituents of the higher fungi. Part VIII. The blueing of *Boletus* species. Variegatic acid, a hydroxytetronic acid from *Boletus* species and a reassessment of the structure of boletol. *J. Chem. Soc. C Org.* 2968–2974.
- Bel-Vialar, S., 2002. L'électroporation *in vivo* chez l'embryon. *Médecine/Sciences* 18, 91–96. doi:10.1051/medsci/200218191

- Bialońska, D., Dayan, F.E., 2005. Chemistry of the lichen *Hypogymnia physodes* transplanted to an industrial region. *J. Chem. Ecol.* 31, 2975–2991.
- Bimboim, H.C., Doly, J., 1979. A rapid alkaline extraction procedure for screening recombinant plasmid DNA. *Nucleic Acids Res.* 7, 1513–1523.
- Bjelland, T., Thorseth, I.H., 2002. Comparative studies of the lichen–rock interface of four lichens in Vingen, western Norway. *Chem. Geol.* 192, 81–98.
- Bjerke, J.W., Lerfall, K., Elvebakk, A., 2002. Effects of ultraviolet radiation and PAR on the content of usnic and divaricatic acids in two arctic-alpine lichens. *Photochem. Photobiol. Sci.* 1, 678–685. doi:10.1039/b203399b
- Boedeker, C., Karsten, U., 2005. The occurrence of mycosporine-like amino acids in the gametophytic and sporophytic stages of *Bangia* (Bangiales, Rhodophyta). *Phycologia* 44, 403–408.
- Bonner, R.F., Emmert-Buck, M., Cole, K., Pohida, T., others, 1997. Laser capture microdissection: molecular analysis of tissue. *Science* 278, 1481–1483.
- Bonny, S., Paquin, L., Carrié, D., Boustie, J., Tomasi, S., 2011. Ionic liquids based microwave-assisted extraction of lichen compounds with quantitative spectrophotodensitometry analysis. *Anal. Chim. Acta* 707, 69–75. doi:10.1016/j.aca.2011.09.009
- Boustie, J., Tomasi, S., Grube, M., 2011. Bioactive lichen metabolites: alpine habitats as an untapped source. *Phytochem. Rev.* 10, 287–307. doi:10.1007/s11101-010-9201-1
- Bowler, P.A., Rundel, P.W., 1975. Reproductive strategies in lichens. *Bot. J. Linn. Soc.* 70, 325–340.
- Brandt, A., de Vera, J.-P., Onofri, S., Ott, S., 2015. Viability of the lichen *Xanthoria elegans* and its symbionts after 18 months of space exposure and simulated Mars conditions on the ISS. *Int. J. Astrobiol.* 14, 411–425. doi:10.1017/S1473550414000214
- Bringmann, G., Lang, G., Steffens, S., Günther, E., Schaumann, K., 2003. Evariquinone, isoemicellin, and stromemycin from a sponge derived strain of the fungus *Emericella varicolor*. *Phytochemistry* 63, 437–443.
- Brunauer, G., Hager, A., Krautgartner, W.D., Tuerk, R., Stocker-Wörgötter, E., 2006. Experimental studies on *Lecanora rupicola* (L.) Zahlbr.: chemical and microscopical investigations of the mycobiont and re-synthesis stages. *The Lichenologist* 38, 577–585.
- Brundrett, M.C., 2009. Mycorrhizal associations and other means of nutrition of vascular plants: understanding the global diversity of host plants by resolving conflicting information and developing reliable means of diagnosis. *Plant Soil* 320, 37–77.
- Büdel, B., Karsten, U., Garcia-Pichel, F., 1997. Ultraviolet-absorbing scytonemin and mycosporine-like amino acid derivatives in exposed, rock-inhabiting cyanobacterial lichens. *Oecologia* 112, 165–172.
- Büdel, B., Lange, O.L., 1991. Water Status of Green and Blue-green Phycobionts in Lichen Thalli after Hydration by Water Vapor Uptake: Do They Become Turgid? *Bot. Acta* 104, 361–366.
- Bud'ova, J., Backer, M., Backorova, M., Zidzik, J., 2006. Usnic acid and copper toxicity in aposymbiotically grown lichen photobiont *Trebouxia erici*. *Symbiosis* 42, 169–174.
- Bycroft, B.W., Roberts, J.C., 1963. The structure of nidulin. *J. Org. Chem.* 28, 1429–1430.
- Cao, S., Lee, A.S.Y., Huang, Y., Flotow, H., Ng, S., Butler, M.S., Buss, A.D., 2002. Agonodepsides A and B: two new depsides from a filamentous fungus F7524. *J. Nat. Prod.* 65, 1037–1038. doi:10.1021/np010626i
- Cardarelli, M., Serino, G., Campanella, L., Ercole, P., Nardone, F.D.C., Alesiani, O., Rossiello, F., 1997. Antimitotic effects of usnic acid on different biological systems. *Cell. Mol. Life Sci.* 53, 667–672.
- Cardinale, M., Puglia, A.M., Grube, M., 2006. Molecular analysis of lichen-associated bacterial communities. *FEMS Microbiol. Ecol.* 57, 484–495.
- Cardinale, M., Vieira de Castro, J., Müller, H., Berg, G., Grube, M., 2008. *In situ* analysis of the bacterial community associated with the reindeer lichen *Cladonia arbuscula* reveals predominance of *Alphaproteobacteria*: Lichen-associated bacterial community. *FEMS Microbiol. Ecol.* 66, 63–71. doi:10.1111/j.1574-6941.2008.00546.x

- Cetin, H., Tufan-Cetin, O., Turk, A.O., Tay, T., Candan, M., Yanikoglu, A., Sumbul, H., 2008. Insecticidal activity of major lichen compounds, (-)- and (+)-usnic acid, against the larvae of house mosquito, *Culex pipiens* L. *Parasitol. Res.* 102, 1277–1279. doi:10.1007/s00436-008-0905-8
- Chen, G.-D., Chen, Y., Gao, H., Shen, L.-Q., Wu, Y., Li, X.-X., Li, Y., Guo, L.-D., Cen, Y.-Z., Yao, X.-S., 2013. Xanthoquinodins from the Endolichenic Fungal Strain *Chaetomium elatum*. *J. Nat. Prod.* 76, 702–709. doi:10.1021/np400041y
- Cheng, S.-C., Huang, M.-Z., Shiea, J., 2011. Thin layer chromatography/mass spectrometry. *J. Chromatogr. A* 1218, 2700–2711.
- Chen, Y., Xu, L., Zhao, Y., Zhao, Z., Chen, H., Yi, T., Qin, M., Liang, Z., 2015. Tissue-specific metabolite profiling and quantitative analysis of ginsenosides in *Panax quinquefolium* using laser microdissection and liquid chromatography–quadrupole/time of flight-mass spectrometry. *Chem. Cent. J.* 9, 1–13.
- Chollet-Krugler, M., Le-Floch, M., Articus, K., Millot, M., Boustie, J., 2008. Carbon-13 CP-MAS NMR studies of some lichens of the Genus *Cladonia* section *Cladina*. *Planta Med.* 74, PC132.
- Chomcheon, P., Wiyakrutta, S., Sriubolmas, N., Ngamrojanavanich, N., Kengtong, S., Mahidol, C., Ruchirawat, S., Kittakoop, P., 2009. Aromatase inhibitory, radical scavenging, and antioxidant activities of depsidones and diaryl ethers from the endophytic fungus *Corynespora cassicola* L36. *Phytochemistry* 70, 407–413. doi:10.1016/j.phytochem.2009.01.007
- Chooi, Y.-H., 2008. Genetic Potential of Lichen-Forming Fungi in Polyketide Biosynthesis (Ph. D). RMIT, Viet-Nam.
- Cook, W.E., Raisbeck, M.F., Cornish, T.E., Williams, E.S., Brown, B., Hiatt, G., Kreeger, T.J., 2007. Paresis and death in elk (*Cervus elaphus*) due to lichen intoxication in Wyoming. *J. Wildl. Dis.* 43, 498–503.
- Culberson, C.F., 1972. Improved conditions and new data for identification of lichen products by standardized thin-layer chromatographic method. *J. Chromatogr. A* 72, 113–125. doi:10.1016/0021-9673(72)80013-X
- Culberson, C.F., Culberson, W.L., Johnson, A., 1981. A standardized TLC analysis of β -orcinol depsidones. *Bryologist* 84, 16–29.
- Culberson, C.F., Culberson, W.L., Johnson, A., 1977. Nonrandom Distribution of an Epiphytic *Lepraria* on Two Species of *Parmelia*. *The Bryologist* 80, 201–203. doi:10.2307/3242539
- Culberson, C.F., Dibben, M.J., 1972. 2-O-Methylperlatolic and 2'-O-Methylperlatolic acids: two new lichen depsides from *Pertusaria*. *Bryologist* 75, 362–365.
- Culberson, C.F., Kristinsson, H.-D., 1970. A standardized method for the identification of lichen products. *J. Chromatogr. A* 46, 85–93.
- Dailey, R.N., Montgomery, D.L., Ingram, J.T., Siemion, R., Vasquez, M., Raisbeck, M.F., 2008. Toxicity of the lichen secondary metabolite (+)-usnic acid in domestic sheep. *Vet. Pathol. Online* 45, 19–25.
- Davies, J., Wang, H., Taylor, T., Warabi, K., Huang, X.-H., Andersen, R.J., 2005. Uncialamycin, a new enediyne antibiotic. *Org. Lett.* 7, 5233–5236.
- De la Coba, F., Aguilera, J., Figueroa, F.L., De Gálvez, M.V., Herrera, E., 2009. Antioxidant activity of mycosporine-like amino acids isolated from three red macroalgae and one marine lichen. *J. Appl. Phycol.* 21, 161–169.
- Dellaporta, S.L., Wood, J., Hicks, J.B., 1983. A plant DNA miniprep: version II. *Plant Mol. Biol. Report.* 1, 19–21.
- Delmail, D., Chambet, A., Boustie, J., 2012. The lichenical collection of Professor Henry Des Abbayes incorporated in the herbarium of the University of Rennes 1. *Taxon* 61, 263–264.
- De Medeiros, L.S., Abreu, L.M., Nielsen, A., Ingmer, H., Larsen, T.O., Nielsen, K.F., Rodrigues-Filho, E., 2015. Dereplication-guided isolation of depsides thielavins S–T and lecanorins D–F from the endophytic fungus *Setophoma* sp. *Phytochemistry* 111, 154–162. doi:10.1016/j.phytochem.2014.12.020

- De Medeiros, L.S., Murgu, M., de Souza, A.Q., others, 2011. Antimicrobial depsides produced by *Cladosporium uredinicola*, an endophytic fungus isolated from *Psidium guajava* fruits. *Helv. Chim. Acta* 94, 1077–1084.
- Deschamps, J.R., 2010. X-ray crystallography of chemical compounds. *Life Sci.* 86, 585–589.
- Desprez-Loustau, M.-L., Robin, C., Buee, M., Courtecuisse, R., Garbaye, J., Suffert, F., Sache, I., Rizzo, D.M., 2007. The fungal dimension of biological invasions. *Trends Ecol. Evol.* 22, 472–480.
- De Vera, J.-P., Schulze-Makuch, D., Khan, A., Lorek, A., Koncz, A., Möhlmann, D., Spohn, T., 2014. Adaptation of an Antarctic lichen to Martian niche conditions can occur within 34 days. *Planet. Space Sci.* 98, 182–190.
- Dower, W.J., Miller, J.F., Ragsdale, C.W., 1988. High efficiency transformation of *E. coli* by high voltage electroporation. *Nucleic Acids Res.* 16, 6127–6145.
- Durazo, F.A., Lassman, C., Han, S.H., Saab, S., Lee, N.P., Kawano, M., Saggi, B., Gordon, S., Farmer, D.G., Yersiz, H., others, 2004. Fulminant liver failure due to usnic acid for weight loss. *Am. J. Gastroenterol.* 99, 950–952.
- Dwivedi, P., Wu, C., Matz, L.M., Clowers, B.H., Siems, W.F., Hill, H.H., 2006. Gas-phase chiral separations by ion mobility spectrometry. *Anal. Chem.* 78, 8200–8206.
- Edwards, H.G., Vandenabeele, P., Jorge-Villar, S.E., Carter, E.A., Perez, F.R., Hargreaves, M.D., 2007. The Rio Tinto Mars analogue site: an extremophilic Raman spectroscopic study. *Spectrochim. Acta. A. Mol. Biomol. Spectrosc.* 68, 1133–1137.
- Emmerich, R., Giez, I., Lange, O.L., Proksch, P., 1993. Toxicity and antifeedant activity of lichen compounds against the polyphagous herbivorous insect *Spodoptera littoralis*. *Phytochemistry* 33, 1389–1394.
- Emmert-Buck, M.R., Bonner, R.F., Smith, P.D., Chuaqui, R.F., Zhuang, Z., Goldstein, S.R., Weiss, R.A., Liotta, L.A., 1996. Laser capture microdissection. *Science* 274, 998–1001.
- Endo, T., Takahagi, T., Kinoshita, Y., Yamamoto, Y., Sato, F., 1998. Inhibition of photosystem II of spinach by lichen-derived depsides. *Biosci. Biotechnol. Biochem.* 62, 2023–2027.
- Espina, V., Wulfkühle, J.D., Calvert, V.S., VanMeter, A., Zhou, W., Coukos, G., Geho, D.H., Petricoin, E.F., Liotta, L.A., 2006. Laser-capture microdissection. *Nat. Protoc.* 1, 586–603.
- Esquenazi, E., Yang, Y.-L., Watrous, J., Gerwick, W.H., Dorrestein, P.C., 2009. Imaging mass spectrometry of natural products. *Nat. Prod. Rep.* 26, 1521–1534.
- Favre-Bonvin, J., Arpin, N., Brevard, C., 1976. Structure de la mycosporine (P 310). *Can. J. Chem.* 54, 1105–1113.
- Ferguson, B.A., Dreisbach, T.A., Parks, C.G., Filip, G.M., Schmitt, C.L., 2003. Coarse-scale population structure of pathogenic *Armillaria* species in a mixed-conifer forest in the Blue Mountains of northeast Oregon. *Can. J. For. Res.* 33, 612–623.
- Feurerer, T., Hawksworth, D.L., 2007. Biodiversity of lichens, including a world-wide analysis of checklist data based on Takhtajan's floristic regions. *Biodivers. Conserv.* 16, 85–98. doi:10.1007/s10531-006-9142-6
- Fisher, R.F., 1979. Possible allelopathic effects of reindeer-moss (*Cladonia*) on jack pine and white spruce. *For. Sci.* 25, 256–260.
- Flatt, P.M., Mahmud, T., 2007. Biosynthesis of aminocyclitol-aminoglycoside antibiotics and related compounds. *Nat. Prod. Rep.* 24, 358–392.
- Fontaine, K.M., Beck, A., Stocker-Wörgötter, E., Piercey-Normore, M.D., 2012. Photobiont Relationships and Phylogenetic History of *Dermatocarpon luridum* var. *luridum* and Related *Dermatocarpon* Species. *Plants* 1, 39–60. doi:10.3390/plants1020039
- Friedl, T., Büdel, B., 1996. Photobionts, in: *Lichen Biology*. Cambridge University Press, pp. 9–26.
- Frisvad, J.C., Andersen, B., Thrane, U., 2008. The use of secondary metabolite profiling in chemotaxonomy of filamentous fungi. *Mycol. Res.* 112, 231–240. doi:10.1016/j.mycres.2007.08.018
- Fuchs, B., Süchs, R., Nimptsch, A., Schiller, J., 2009. MALDI-TOF-MS directly combined with TLC: a review of the current state. *Chromatographia* 69, 95–105.

- Gabelica, V., 2006. Intérêt de la spectrométrie de mobilité ionique pour l'étude de la conformation et des assemblages non-covalents de biomolécules. *Spectra Anal.* 251, 21–27.
- Galiulin, R.V., 2003. To the 150th anniversary of the birth of Evgraf Stepanovich Fedorov (1853–1919) Irregularities in the fate of the theory of regularity. *Crystallogr. Rep.* 48, 899–913.
- Galperin, M.Y., Koonin, E.V., 1997. A diverse superfamily of enzymes with ATP-dependent carboxylate—amine/thiol ligase activity. *Protein Sci.* 6, 2639–2643.
- Ganem, B., 1978. From glucose to aromatics: recent developments in natural products of the shikimic acid pathway. *Tetrahedron* 34, 3353–3383.
- Garcia-Pichel, F., Castenholz, R.W., 1993. Occurrence of UV-absorbing, mycosporine-like compounds among cyanobacterial isolates and an estimate of their screening capacity. *Appl. Environ. Microbiol.* 59, 163–169.
- Gargas, A., DePriest, P.T., Grube, M., Tehler, A., 1995. Multiple origins of lichen symbioses in fungi suggested by SSU rDNA phylogeny. *Science* 268, 1492–1495.
- Gaspar, A., Matos, M.J., Garrido, J., Uriarte, E., Borges, F., 2014. Chromone: a valid scaffold in medicinal chemistry. *Chem. Rev.* 114, 4960–4992.
- Gaudêncio, S.P., Pereira, F., 2015. Dereplication: racing to speed up the natural products discovery process. *Nat. Prod. Rep.* 32, 779–810.
- Gauslaa, Y., 2004. Lichen palatability depends on investments in herbivore defence. *Oecologia* 143, 94–105. doi:10.1007/s00442-004-1768-z
- Gavériaux, J.-P., 2006. Les lichens et l'évolution de la classification des êtres vivants. *Bull. Inf.-Assoc. Fr. Lichénologie* 31, 65–74.
- Giez, I., Lange, O.L., Proksch, P., 1994. Growth retarding activity of lichen substances against the polyphagous herbivorous insect *Spodoptera littoralis*. *Biochem. Syst. Ecol.* 22, 113–120. doi:10.1016/0305-1978(94)90001-9
- Gill, M., Kiefel, M.J., 1994. Pigments of fungi. XXXVII. Pseudoquinone, a new naphthalenoid pulvinic acid from the fungus *Pisolithus arhizus*. *Aust. J. Chem.* 47, 1967–1977.
- Gill, M., Steglich, W., 1987. Pigments of Fungi (Macromycetes), in: *Fortschritte Der Chemie Organischer Naturstoffe / Progress in the Chemistry of Organic Natural Products, Fortschritte Der Chemie Organischer Naturstoffe / Progress in the Chemistry of Organic Natural Products*. Springer Vienna, pp. 1–297.
- Golojuch, S.T., Lawrey, J.D., 1988. Quantitative variation in vulpinic and pinastric acids produced by *Tuckermannopsis pinastris* (lichen-forming Ascomycotina, *Parmeliaceae*). *Am. J. Bot.* 75, 1871–1875.
- Greer, T., Sturm, R., Li, L., 2011. Mass spectrometry imaging for drugs and metabolites. *J. Proteomics* 74, 2617–2631.
- Grinhut, T., Hadar, Y., Chen, Y., 2007. Degradation and transformation of humic substances by saprotrophic fungi: processes and mechanisms. *Fungal Biol. Rev.* 21, 179–189. doi:10.1016/j.fbr.2007.09.003
- Gröniger, A., Sinha, R.P., Klisch, M., Häder, D.-P., 2000. Photoprotective compounds in cyanobacteria, phytoplankton and macroalgae—a database. *J. Photochem. Photobiol. B* 58, 115–122.
- Grube, M., Berg, G., 2009. Microbial consortia of bacteria and fungi with focus on the lichen symbiosis. *Fungal Biol. Rev.* 23, 72–85. doi:10.1016/j.fbr.2009.10.001
- Grube, M., Cardinale, M., de Castro, J.V., Müller, H., Berg, G., 2009. Species-specific structural and functional diversity of bacterial communities in lichen symbioses. *ISME J.* 3, 1105–1115.
- Grube, M., Cernava, T., Soh, J., Fuchs, S., Aschenbrenner, I., Lassek, C., Wegner, U., Becher, D., Riedel, K., Sensen, C.W., Berg, G., 2015. Exploring functional contexts of symbiotic sustain within lichen-associated bacteria by comparative omics. *ISME J.* 9, 412–424.
- Guo, B., Dai, J.-R., Ng, S., Huang, Y., Leong, C., Ong, W., Carté, B.K., 2000. Cytotoxic Acids A and B: Novel Tridepside Inhibitors of hCMV Protease from the Endophytic Fungus *Cytonaema* Species. *J. Nat. Prod.* 63, 602–604. doi:10.1021/np990467r

- Ha, L.D., Hansen, P.E., Duus, F., Pham, H.D., Nguyen, L.-H.D., 2012. Oliveridepsidones A-D, antioxidant depsidones from *Garcinia oliveri*: Oliveridepsidones. *Magn. Reson. Chem.* 50, 242–245. doi:10.1002/mrc.2862
- Harris, G.A., Kwasnik, M., Fernández, F.M., 2011. Direct analysis in real time coupled to multiplexed drift tube ion mobility spectrometry for detecting toxic chemicals. *Anal. Chem.* 83, 1908–1915.
- Hauck, M., 2008. Metal homeostasis in *Hypogymnia physodes* is controlled by lichen substances. *Environ. Pollut.* 153, 304–308.
- Hauck, M., Huneck, S., 2007a. The putative role of fumarprotocetraric acid in the manganese tolerance of the lichen *Lecanora conizaeoides*. *The Lichenologist* 39, 301–304.
- Hauck, M., Huneck, S., 2007b. Lichen substances affect metal adsorption in *Hypogymnia physodes*. *J. Chem. Ecol.* 33, 219–223.
- Hauck, M., Jürgens, S.-R., 2008. Usnic acid controls the acidity tolerance of lichens. *Environ. Pollut.* 156, 115–122. doi:10.1016/j.envpol.2007.12.033
- Hauck, M., Jürgens, S.-R., Huneck, S., Leuschner, C., 2009a. High acidity tolerance in lichens with fumarprotocetraric, perlatolic or thamnolic acids is correlated with low pKa1 values of these lichen substances. *Environ. Pollut.* 157, 2776–2780. doi:10.1016/j.envpol.2009.04.022
- Hauck, M., Jurgens, S.-R., Willenbruch, K., Huneck, S., Leuschner, C., 2008. Dissociation and metal-binding characteristics of yellow lichen substances suggest a relationship with site preferences of lichens. *Ann. Bot.* 103, 13–22. doi:10.1093/aob/mcn202
- Hauck, M., Willenbruch, K., Leuschner, C., 2009b. Lichen substances prevent lichens from nutrient deficiency. *J. Chem. Ecol.* 35, 71–73.
- Hawksworth, D.L., 1988. The variety of fungal-algal symbioses, their evolutionary significance, and the nature of lichens. *Bot. J. Linn. Soc.* 96, 3–20.
- Hawksworth, D.L., 1973. Some advances in the study of lichens since the time of EM Holmes. *Bot. J. Linn. Soc.* 67, 3–31.
- Helbling, E.W., Menchi, C.F., Villafañe, V.E., 2002. Bioaccumulation and role of UV-absorbing compounds in two marine crustacean species from Patagonia, Argentina. *Photochem. Photobiol. Sci.* 1, 820–825.
- Herrero-Yudego, P., Martín-Pedrosa, M., Norato, J., Vicente, C., 1989. Some features about Usnic Acid Accumulation and its Movement between the Symbionts of the Lichen, *Evernia prunastri*. *J. Plant Physiol.* 135, 170–174.
- Hillenbrand, M., Zapp, J., Becker, H., 2004. Depsides from the petals of *Papaver rhoeas*. *Planta Med.* 70, 380–382.
- Hoffman, M.T., Arnold, A.E., 2010. Diverse bacteria inhabit living hyphae of phylogenetically diverse fungal endophytes. *Appl. Environ. Microbiol.* 76, 4063–4075.
- Holder, J.M., Wynn-Williams, D., Rull Perez, F., Edwards, H.G.M., 2000. Raman spectroscopy of pigments and oxalates in situ within epilithic lichens: *Acarospora* from the Antarctic and Mediterranean. *New Phytol.* 145, 271–280.
- Honegger, R., 2012a. Differential gene expression within the cyanobacterial cell population of a lichen thallus. *New Phytol.* 196, 657–660.
- Honegger, R., 2012b. The symbiotic phenotype of lichen-forming ascomycetes and their endo- and epibionts., in: Hock, B. (Ed.), *Fungal Associations*. Springer Berlin Heidelberg, Berlin, Heidelberg, pp. 288–326.
- Honegger, R., 2000. Simon Schwendener (1829-1919) and the dual hypothesis of lichens. *The Bryologist* 103, 307–313.
- Honegger, R., 1998. The lichen symbiosis—what is so spectacular about it? *The Lichenologist* 30, 193–212.
- Honegger, R., 1995. Experimental studies with foliose macrolichens: fungal responses to spatial disturbance at the organismic level and to spatial problems at the cellular level during drought stress events. *Can. J. Bot.* 73, 569–578.

- Honegger, R., 1986a. Ultrastructural studies in lichens. I. Haustorial types and their frequencies in a range of lichens with trebouxoid photobionts. *New Phytol.* 103, 785–795.
- Honegger, R., 1986b. Ultrastructural studies in lichens. *New Phytol.* 103, 797–808.
- Honegger, R., Axe, L., Edwards, D., 2013. Bacterial epibionts and endolichenic actinobacteria and fungi in the Lower Devonian lichen *Chlorolichenomycites salopensis*. *Fungal Biol.* 117, 512–518. doi:10.1016/j.funbio.2013.05.003
- Hoyer, K., Karsten, U., Wiencke, C., 2002. Induction of sunscreen compounds in Antarctic macroalgae by different radiation conditions. *Mar. Biol.* 141, 619–627.
- Hulien, M.L., Lekse, J.W., Rosmus, K.A., Devlin, K.P., Glenn, J.R., Wisneski, S.D., Wildfong, P., Lake, C.H., MacNeil, J.H., Aitken, J.A., 2015. An Inquiry-Based Project Focused on the X-ray Powder Diffraction Analysis of Common Household Solids. *J. Chem. Educ.* 92, 2152–2156.
- Huneck, S., Yoshimura, I., 1996. Identification of lichen substances. Springer.
- Hyvärinen, M., Koopmann, R., Hormi, O., Tuomi, J., 2000. Phenols in reproductive and somatic structures of lichens: a case of optimal defence? *Oikos* 91, 371–375.
- Ifa, D.R., Srimany, A., Eberlin, L.S., Naik, H.R., Bhat, V., Cooks, R.G., Pradeep, T., 2011. Tissue imprint imaging by desorption electrospray ionization mass spectrometry. *Anal. Methods* 3, 1910–1912. doi:10.1039/c1ay05295k
- Ingolfssdottir, K., 2002. Usnic acid. *Phytochemistry* 61, 729–736.
- Inokoshi, J., Takagi, Y., Uchida, R., Masuma, R., Ōmura, S., Tomoda, H., 2010. Production of a new type of amidepsine with a sugar moiety by static fermentation of *Humicola* sp. FO-2942. *J. Antibiot. (Tokyo)* 63, 9–16.
- Ito, C., Itoigawa, M., Mishina, Y., Tomiyasu, H., Litaudon, M., Cosson, J.-P., Mukainaka, T., Tokuda, H., Nishino, H., Furukawa, H., 2001. Cancer chemopreventive agents. New depsidones from *Garcinia* plants. *J. Nat. Prod.* 64, 147–150.
- Ito, S., Hirata, Y., 1977. Isolation and structure of a mycosporine from the zoanthid *Palythoa tuberculosa*. *Tetrahedron Lett.* 18, 2429–2430.
- Jaiswal, Y., Liang, Z., Guo, P., Ho, H.-M., Chen, H., Zhao, Z., 2014a. Tissue-Specific Metabolite Profiling of *Cyperus rotundus* L. Rhizomes and (+)-Nootkatone Quantitation by Laser Microdissection, Ultra-High-Performance Liquid Chromatography–Quadrupole Time-of-Flight Mass Spectrometry, and Gas Chromatography–Mass Spectrometry Techniques. *J. Agric. Food Chem.* 62, 7302–7316.
- Jaiswal, Y., Liang, Z., Ho, A., Wong, L., Yong, P., Chen, H., Zhao, Z., 2014b. Distribution of toxic alkaloids in tissues from three herbal medicine *Aconitum* species using laser micro-dissection, UHPLC–QTOF MS and LC–MS/MS techniques. *Phytochemistry* 107, 155–174.
- Jones, F.T., Palmer, K.J., 1950. Optical, Crystallographic and X-Ray Diffraction Data for Usnic Acid. *J. Am. Chem. Soc.* 72, 1820–1822.
- Jordan, W.P., 1970. The Internal Cephalodia of the Genus *Lobaria*. *The Bryologist* 73, 669–681. doi:10.2307/3241279
- Kallio, P., Heinonen, S., 1971. Influence of short-term low temperature on net photosynthesis in some subarctic lichens. *Rep. Kevo Subarct. Res. Stn.* 8, 63–72.
- Kaltenpoth, M., Strupat, K., Svatoš, A., 2016. Linking metabolite production to taxonomic identity in environmental samples by (MA) LDI-FISH. *ISME J.* 10, 527–531.
- Kanu, A.B., Dwivedi, P., Tam, M., Matz, L., Hill, H.H., 2008. Ion mobility–mass spectrometry. *J. Mass Spectrom.* 43, 1–22.
- Kappen, L., 1993. Plant activity under snow and ice, with particular reference to lichens. *Arctic* 46, 297–302.
- Kappen, L., Schroeter, B., Scheidegger, C., Sommerkorn, M., Hestmark, G., 1996. Cold resistance and metabolic activity of lichens below 0 C. *Adv. Space Res.* 18, 119–128.
- Karas, M., Bachmann, D., Bahr, U. el, Hillenkamp, F., 1987. Matrix-assisted ultraviolet laser desorption of non-volatile compounds. *Int. J. Mass Spectrom. Ion Process.* 78, 53–68.

- Karentz, D., McEuen, F.S., Land, M.C., Dunlap, W.C., 1991. Survey of mycosporine-like amino acid compounds in Antarctic marine organisms: potential protection from ultraviolet exposure. *Mar. Biol.* 108, 157–166.
- Karsten, U., Friedl, T., Schumann, R., Hoyer, K., Lembcke, S., 2005. Mycosporine-like amino acids and phylogenies in green algae: *Prasiola* and its relative from the *Trebouxiphyceae* (Chlorophyta). *J. Phycol.* 41, 557–566.
- Karsten, U., Sawall, T., West, J., Wiencke, C., 2000. Ultraviolet sunscreen compounds in epiphytic red algae from mangroves. *Hydrobiologia* 432, 159–171.
- Karsten, U., Sawall, T., Wiencke, C., 1998. A survey of the distribution of UV-absorbing substances in tropical macroalgae. *Phycol. Res.* 46, 271–279.
- Kauppi, M., Versegny—Patay, K., 1990. Determination of the distribution of lichen substances in the thallus by fluorescence microscopy. *Ann. Bot. Fenn.* 27, 189–202.
- Kawahara, N., Nozawa, K., Nakajima, S., Kawai, K., Yamazaki, M., 1988. Isolation and structures of novel fungal depsidones, emeguisins A, B, and C, from *Emericella unguis*. *J. Chem. Soc. [Perkin 1]* 2611–2614.
- Kneipp, K., Kneipp, H., Itzkan, I., Dasari, R.R., Feld, M.S., 1999. Ultrasensitive Chemical Analysis by Raman Spectroscopy. *Chem. Rev.* 99, 2957–2976. doi:10.1021/cr980133r
- Kogej, T., Gostinčar, C., Volkmann, M., Gorbushina, A.A., Gunde-Cimerman, N., 2006. Mycosporines in extremophilic fungi—novel complementary osmolytes? *Environ. Chem.* 3, 105–110.
- Kranner, I., Beckett, R., Hochman, A., Nash, T.H., 2008. Desiccation-Tolerance in Lichens: A Review. *The Bryologist* 111, 576–593. doi:10.1639/0007-2745-111.4.576
- La Barre, S., Roullier, C., Boustie, J., 2014. Mycosporine-Like Amino Acids (MAAs) in Biological Photosystems, in: *Outstanding Marine Molecules: Chemistry, Biology, Analysis*. Wiley, New York, pp. 333–360.
- Lambers, H., Teste, F.P., 2013. Interactions between arbuscular mycorrhizal and non-mycorrhizal plants: do non-mycorrhizal species at both extremes of nutrient availability play the same game? *Plant Cell Environ.* 36, 1911–1915.
- Lange, O.L., 1966. CO₂-Gaswechsel der Flechte *Cladonia alcornis* nach langfristiger Aufenthalt bei tiefen Temperaturen. *Flora* 156, 500–502.
- Lange, O.L., Allan Green, T.G., Melzer, B., Meyer, A., Zellner, H., 2006. Water relations and CO₂ exchange of the terrestrial lichen *Teloschistes capensis* in the Namib fog desert: Measurements during two seasons in the field and under controlled conditions. *Flora* 201, 268–280. doi:10.1016/j.flora.2005.08.003
- Lange, O.L., Kappen, L., 1972. Photosynthesis of lichens from Antarctica, in: *Antarctic Terrestrial Biology*. Wiley Online Library, Washington, pp. 83–95.
- Lang, G., Cole, A.L.J., Blunt, J.W., Robinson, W.T., Munro, M.H.G., 2007. Excelsione, a depsidone from an endophytic fungus isolated from the New Zealand endemic tree *Knightia excelsa*. *J. Nat. Prod.* 70, 310–311. doi:10.1021/np060202u
- Larson, D.W., 1989. The impact of ten years at -20° C on gas exchange in five lichen species. *Oecologia* 78, 87–92.
- Larson, D.W., 1987. The absorption and release of water by lichens. *Bibl. Lichenol.* 25, 1–360.
- Larson, D.W., 1978. Patterns of lichen photosynthesis and respiration following prolonged frozen storage. *Can. J. Bot.* 56, 2119–2123. doi:10.1139/b78-253
- Lawrey, J.D., 2009. Chemical defense in lichen symbioses, in: *Defensive Mutualism in Microbial Symbiosis*. CRC Press, Taylor and Francis group, pp. 167–176.
- Lawrey, J.D., 1986. Biological role of lichen substances. *Bryologist* 89, 111–122.
- Lawrey, J.D., 1983. Lichen Herbivore Preference: A Test of Two Hypotheses. *Am. J. Bot.* 70, 1188–1194. doi:10.2307/2443288
- Lawrey, J.D., 1980. Correlations between lichen secondary chemistry and grazing activity by *Pallifera varia*. *Bryologist* 83, 328–334.
- Lawrey, J.D., 1977. Adaptive significance of O-methylated lichen depsides and depsidones. *The Lichenologist* 9, 137–142.

- Lawrey, J.D., Diederich, P., 2003. Lichenicolous fungi: interactions, evolution, and biodiversity. *The Bryologist* 106, 80–120.
- Le Dévéhat, F., Thüs, H., Abasq, M.-L., Delmail, D., Boustie, J., 2014. Oxidative Stress Regulation in Lichens and Its Relevance for Survival in Coastal Habitats, in: *Advances in Botanical Research*. Elsevier, pp. 467–503.
- Legaz, M.E., Vicente, C., de Armas, R., 2011. Bioproduction of depsidones for pharmaceutical purposes, in: *Drug Development - A Case Study Based Insight into Modern Strategies*. INTECH Open Access Publisher.
- Leoni, C., Volpicella, M., De Leo, F., Gallerani, R., Ceci, L.R., 2011. Genome walking in eukaryotes. *Febs J.* 278, 3953–3977.
- Le Pogam, P., Boustie, J., 2016. Xanthonones of Lichen Source: A 2016 Update. *Molecules* 21, 294.
- Le Pogam, P., Herbette, G., Boustie, J., 2015a. Analysis of Lichen Metabolites, a Variety of Approaches, in: *Recent Advances in Lichenology*. Springer, India, pp. 229–261.
- Le Pogam, P., Legouin, B., Le Lamer, A.-C., Boustie, J., Rondeau, D., 2015b. Analysis of the cyanolichen *Lichina pygmaea* metabolites using *in situ* DART-MS: from detection to thermochemistry of mycosporine serinol. *J. Mass Spectrom.* 50, 454–462.
- Le Pogam, P., Le Lamer, A.-C., Legouin, B., Boustie, J., Rondeau, D., 2016a. *In situ* DART-MS as a versatile and rapid dereplication tool in lichenology: chemical fingerprinting of *Ophioparma ventosa*. *Phytochem. Anal.* 27, in press.
- Le Pogam, P., Le Lamer, A.-C., Siva, B., Legouin, B., Bondon, A., Graton, J., Jacquemin, D., Rouaud, I., Ferron, S., Obermayer, W., Babu, K.S., Boustie, J., 2016b. Minor pyranonaphthoquinones from the apothecia of the lichen *Ophioparma ventosa*. *J. Nat. Prod.* 79, 1005–1011. doi:10.1021/acs.jnatprod.5b01073
- Le Pogam, P., Schinkovitz, A., Legouin, B., Le Lamer, A.-C., Boustie, J., Richomme, P., 2015c. Matrix-free UV-laser desorption ionization mass spectrometry as a versatile approach for accelerating dereplication studies on lichens. *Anal. Chem.* 87, 10421–10428. doi:10.1021/acs.analchem.5b02531
- Letrouit-Galinou, M.-A., 1968. The Apothecia of the Discolichens. *The Bryologist* 71, 297. doi:10.2307/3241116
- Lewis, D.H., 1973. Concepts in Fungal Nutrition and the Origin of Biotrophy. *Biol. Rev.* 48, 261–277. doi:10.1111/j.1469-185X.1973.tb00982.x
- Liao, C., Piercey-Normore, M.D., Sorensen, J.L., Gough, K., 2010. *In situ* imaging of usnic acid in selected *Cladonia* spp. by vibrational spectroscopy. *Analyst* 135, 3242–3248.
- Liba, C.M., Ferrara, F.I.S., Manfio, G.P., Fantinatti-Garboggini, F., Albuquerque, R.C., Pavan, C., Ramos, P.L., Moreira-Filho, C.A., Barbosa, H.R., 2006. Nitrogen-fixing chemo-organotrophic bacteria isolated from cyanobacteria-deprived lichens and their ability to solubilize phosphate and to release amino acids and phytohormones. *J. Appl. Microbiol.* 101, 1076–1086.
- Ligrone, R., Carafa, A., Lumini, E., Bianciotto, V., Bonfante, P., Duckett, J.G., 2007. Glomeromycotean associations in liverworts: a molecular, cellular, and taxonomic analysis. *Am. J. Bot.* 94, 1756–1777.
- Li, G., Wang, H., Zhu, R., Sun, L., Wang, L., Li, M., Li, Y., Liu, Y., Zhao, Z., Lou, H., 2012. Phaeosphaerins A–F, Cytotoxic Perylenequinones from an Endolichenic Fungus, *Phaeosphaeria* sp. *J. Nat. Prod.* 75, 142–147. doi:10.1021/np200614h
- Li, L.-P., Feng, B.-S., Yang, J.-W., Chang, C.-L., Bai, Y., Liu, H.-W., 2013. Applications of ambient mass spectrometry in high-throughput screening. *The Analyst* 138, 3097–3103. doi:10.1039/c3an00119a
- Lipnicki, L.I., 2015. The role of symbiosis in the transition of some eukaryotes from aquatic to terrestrial environments. *Symbiosis* 65, 39–53.
- Li, Q., Zhang, X., Cao, J., Guo, Z., Lou, Y., Ding, M., Zhao, Y., 2015. Depside derivatives with anti-hepatic fibrosis and anti-diabetic activities from *Impatiens balsamina* L. flowers. *Fitoterapia* 105, 234–239. doi:10.1016/j.fitote.2015.07.007

- Lohézic-Le Dévéhat, F., Legouin, B., Couteau, C., Boustie, J., Coiffard, L., 2013. Lichenic extracts and metabolites as UV filters. *J. Photochem. Photobiol. B* 120, 17–28.
- Lutzoni, F., Miadlikowska, J., 2009. *Lichens. Curr. Biol.* 19, R502–R503.
- Lutzoni, F., Pagel, M., Reeb, V., 2001. Major fungal lineages are derived from lichen symbiotic ancestors. *Nature* 411, 937–940. doi:10.1038/35082053
- Malloch, D.W., Pirozynski, K.A., Raven, P.H., 1980. Ecological and evolutionary significance of mycorrhizal symbioses in vascular plants (a review). *Proc. Natl. Acad. Sci.* 77, 2113–2118.
- Manna, J.D., Reyzer, M.L., Latham, J.C., Weaver, C.D., Marnett, L.J., Caprioli, R.M., 2011. High-throughput quantification of bioactive lipids by MALDI mass spectrometry: application to prostaglandins. *Anal. Chem.* 83, 6683–6688.
- Marante, F.T., Castellano, A.G., Rosas, F.E., Aguiar, J.Q., Barrera, J.B., 2003. Identification and quantitation of allelochemicals from the lichen *Lethariella canariensis*: phytotoxicity and antioxidative activity. *J. Chem. Ecol.* 29, 2049–2071.
- Marchuk, D., Drumm, M., Saulino, A., Collins, F.S., 1991. Construction of T-vectors, a rapid and general system for direct cloning of unmodified PCR products. *Nucleic Acids Res.* 19, 1154.
- May, P.F., 1997. *Ophioparma lapponica* - a misunderstood species. *Harv. Pap. Bot.* 2, 213–228.
- McEvoy, M., Nybakken, L., Solhaug, K.A., Gauslaa, Y., 2006. UV triggers the synthesis of the widely distributed secondary lichen compound usnic acid. *Mycol. Prog.* 5, 221–229. doi:10.1007/s11557-006-0514-9
- Meier, J.L., Chapman, R.L., 1983. Ultrastructure of the lichen *Coenogonium interplexum* Nyl. *Am. J. Bot.* 70, 400–407.
- Miglietta, M.L., Lamanna, R., 2006. 1H HR-MAS NMR of carotenoids in aqueous samples and raw vegetables. *Magn. Reson. Chem.* 44, 675–685.
- Millbank, J.W., Kershaw, K.A., 1970. Nitrogen Metabolism in Lichens: Iii. Nitrogen Fixation by Internal Cephalodia in *Lobaria pulmonaria*. *New Phytol.* 69, 595–597. doi:10.1111/j.1469-8137.1970.tb07611.x
- Millot, M., Tomasi, S., Sinbandhit, S., Boustie, J., 2008. Phytochemical investigation of *Tephromela atra*: NMR studies of collatolic acid derivatives. *Phytochem. Lett.* 1, 139–143. doi:10.1016/j.phytol.2008.07.004
- Millot, M., Tomasi, S., Studzinska, E., Rouaud, I., Boustie, J., 2009. Cytotoxic Constituents of the Lichen *Diploicia canescens*. *J. Nat. Prod.* 72, 2177–2180. doi:10.1021/np9003728
- Mirando, M., Fahselt, D., 1978. The effect of thallus age and drying procedure on extractable lichen substances. *Can. J. Bot.* 56, 1499–1504.
- Mittler, R., 2002. Oxidative stress, antioxidants and stress tolerance. *Trends Plant Sci.* 7, 405–410. doi:10.1016/S1360-1385(02)02312-9
- Morlock, G., Schwack, W., 2010. Coupling of planar chromatography to mass spectrometry. *TrAC Trends Anal. Chem.* 29, 1157–1171.
- Mosbach, K., 1969. Biosynthesis of lichen substances, products of a symbiotic association. *Angew. Chem. Int. Ed. Engl.* 8, 240–250.
- Muggia, L., Gueidan, C., Knudsen, K., Perlmutter, G., Grube, M., 2013. The lichen connections of black fungi. *Mycopathologia* 175, 523–535.
- Müller, T., Oradu, S., Ifa, D.R., Cooks, R.G., Kräutler, B., 2011. Direct Plant Tissue Analysis and Imprint Imaging by Desorption Electrospray Ionization Mass Spectrometry. *Anal. Chem.* 83, 5754–5761. doi:10.1021/ac201123t
- Murtagh, G.J., Dyer, P.S., Crittenden, P.D., 2000. Reproductive systems: sex and the single lichen. *Nature* 404, 564–564.
- Naumann, D., Helm, D., Labischinski, H., Giesbrecht, P., 1991. The characterization of microorganisms by Fourier-transform infrared spectroscopy (FT-IR), in: *Modern Techniques for Rapid Microbiological Analysis*. VCH, New York, pp. 43–96.
- Neff, G.W., Rajender Reddy, K., Durazo, F.A., Meyer, D., Marrero, R., Kaplowitz, N., 2004. Severe hepatotoxicity associated with the use of weight loss diet supplements containing ma huang or usnic acid. *J. Hepatol.* 41, 1062–1064.

- Nemes, P., Vertes, A., 2009. Laser ablation electrospray ionization for atmospheric pressure, *in vivo*, and imaging mass spectrometry. *Anal. Chem.* 79, 8098–8106.
- Newman, S.J., Dunlap, W.C., Nicol, S., Ritz, D., 2000. Antarctic krill (*Euphausia superba*) acquire a UV-absorbing mycosporine-like amino acid from dietary algae. *J. Exp. Mar. Biol. Ecol.* 255, 93–110.
- Ngoupayo, J., Tabopda, T.K., Ali, M.S., Tsamo, E., 2008. Alpha-Glucosidase Inhibitors from *Garcinia brevipedicellata* (Clusiaceae). *Chem. Pharm. Bull. (Tokyo)* 56, 1466–1469.
- Nguyen, K.-H., Chollet-Krugler, M., Gouault, N., Tomasi, S., 2013. UV-protectant metabolites from lichens and their symbiotic partners. *Nat. Prod. Rep.* 30, 1490–1508. doi:10.1039/c3np70064j
- Nguyen, T.T.T., Chollet-Krugler, M., Lohézic-Le Dévéhat, F., Rouaud, I., Boustie, J., 2015. Mycosporine-like compounds in Chlorolichens: isolation from *Dermatocarpon luridum* and *Dermatocarpon miniatum*, and their photoprotective properties. *Planta Medica Lett.* 2, e1–e5.
- Nielsen, J., Nielsen, P.H., Frisvad, J.C., 1999. Fungal depside, guisinol, from a marine derived strain of *Emericella unguis*. *Phytochemistry* 50, 263–265.
- Nimis, P.L., Skert, N., 2006. Lichen chemistry and selective grazing by the coleopteran *Lasioderma serricorne*. *Environ. Exp. Bot.* 55, 175–182. doi:10.1016/j.envexpbot.2004.10.011
- Nybakken, L., Helmersen, A.-M., Gauslaa, Y., Selås, V., 2010. Lichen Compounds Restrained Lichen Feeding by Bank Voles (*Myodes glareolus*). *J. Chem. Ecol.* 36, 298–304. doi:10.1007/s10886-010-9761-y
- Nybakken, L., Julkunen-Tiitto, R., 2006. UV-B induces usnic acid in reindeer lichens. *Lichenologist* 38, 477–486.
- Nybakken, L., Solhaug, K.A., Bilger, W., Gauslaa, Y., 2004. The lichens *Xanthoria elegans* and *Cetraria islandica* maintain a high protection against UV-B radiation in Arctic habitats. *Oecologia* 140, 211–216.
- Oren, A., Gunde-Cimerman, N., 2007. Mycosporines and mycosporine-like amino acids: UV protectants or multipurpose secondary metabolites? *FEMS Microbiol. Lett.* 269, 1–10.
- Ortiz-Álvarez, R., de los Ríos, A., Fernández-Mendoza, F., Torralba-Burrial, A., Pérez-Ortega, S., 2015. Ecological Specialization of Two Photobiont-Specific Maritime Cyanolichen Species of the Genus *Lichina*. *PLOS ONE* 10, e0132718. doi:10.1371/journal.pone.0132718
- Øvstedal, D.O., Smith, R.L., 2001. Lichens of Antarctica and South Georgia: a guide to their identification and ecology. Cambridge University Press, Cambridge.
- Palmqvist, K., Campbell, D., Ekblad, A., Johansson, H., 1998. Photosynthetic capacity in relation to nitrogen content and its partitioning in lichens with different photobionts. *Plant Cell Environ.* 21, 361–372.
- Parrot, D., Jan, S., Baert, N., Guyot, S., Tomasi, S., 2013. Comparative metabolite profiling and chemical study of *Ramalina siliquosa* complex using LC–ESI-MS/MS approach. *Phytochemistry* 89, 114–124. doi:10.1016/j.phytochem.2013.02.002
- Parrot, D., Peresse, T., Hitti, E., Carrie, D., Grube, M., Tomasi, S., 2015. Qualitative and Spatial Metabolite Profiling of Lichens by a LC-MS Approach Combined With Optimised Extraction: Metabolite Profiling by Lc-ms of Lichens Combined With Optimized Extraction. *Phytochem. Anal.* 26, 23–33. doi:10.1002/pca.2532
- Pavarini, D.P., da Silva, D.B., Carollo, C.A., Portella, A.P.F., Latansio-Aidar, S.R., Cavalin, P.O., Oliveira, V.C., Rosado, B.H.P., Aidar, M.P.M., Bolzani, V.S., Lopes, N.P., Joly, C.A., 2012. Application of MALDI-MS analysis of Rainforest chemodiversity: a keystone for biodiversity conservation and sustainable use: JMS letters. *J. Mass Spectrom.* 47, 1482–1485. doi:10.1002/jms.3100
- Pérez, P., Libkind, D., del Carmen Diéguez, M., Summerer, M., Sonntag, B., Sommaruga, R., van Broock, M., Zagarese, H.E., 2006. Mycosporines from freshwater yeasts: a trophic cul-de-sac? *Photochem. Photobiol. Sci.* 5, 25–30.
- Permana, D., Abas, F., Maulidiani, F., Shaari, K., Stanslas, J., Ali, A.M., Lajis, N.H., 2005. Atroviridone B, a new prenylated depsidone with cytotoxic property from the roots of *Garcinia atroviridis*. *Z. Für Naturforschung C* 60, 523–526.

- Portwich, A., Garcia-Pichel, F., 2003. Biosynthetic pathway of mycosporines (mycosporine-like amino acids) in the cyanobacterium *Chlorogloeopsis* sp. strain PCC 6912. *Phycologia* 42, 384–392.
- Pöykkö, H., Hyvärinen, M., 2003. Host preference and performance of lichenivorous *Eilema* spp. larvae in relation to lichen secondary metabolites. *J. Anim. Ecol.* 72, 383–390.
- Pöykkö, H., Hyvärinen, M., Bačkor, M., 2005. Removal of lichen secondary metabolites affects food choice and survival of lichenivorous moth larvae. *Ecology* 86, 2623–2632.
- Purvis, O.W., Elix, J.A., Broomhead, J.A., Jones, G.C., 1987. The occurrence of copper—norstictic acid in lichens from cupriferous substrata. *The Lichenologist* 19, 193–203.
- Purvis, O.W., Elix, J.A., Gaul, K.L., 1990. The occurrence of copper-psoromic acid in lichens from cupriferous substrata. *The Lichenologist* 22, 345–354.
- Raggio, J., Pintado, A., Ascaso, C., De La Torre, R., De Los Ríos, A., Wierzchos, J., Horneck, G., Sancho, L. g., 2011. Whole Lichen Thalli Survive Exposure to Space Conditions: Results of Lithopanspermia Experiment with *Aspicilia fruticulosa*. *Astrobiology* 11, 281–292. doi:10.1089/ast.2010.0588
- Rai, A.N., Bergman, B., 2002. Cyanolichens. *Biol. Environ. Proc. R. Ir. Acad.* 102, 19–22.
- Rao, D.N., LeBlanc, F., 1965. A possible role of atranorin in the lichen thallus. *Bryologist* 68, 284–289.
- Räsänen, R.-M., Dwivedi, P., Fernández, F.M., Kauppila, T.J., 2014. Desorption atmospheric pressure photoionization and direct analysis in real time coupled with travelling wave ion mobility mass spectrometry. *Rapid Commun. Mass Spectrom.* 28, 2325–2336. doi:10.1002/rcm.7028
- Rastogi, R.P., Sinha, R.P., Singh, S.P., Häder, D.-P., others, 2010. Photoprotective compounds from marine organisms. *J. Ind. Microbiol. Biotechnol.* 37, 537–558.
- Reynertson, K.A., Wallace, A.M., Adachi, S., Gil, R.R., Yang, H., Basile, M.J., D’Armiento, J., Weinstein, I.B., Kennelly, E.J., 2006. Bioactive depsides and anthocyanins from Jaboticaba (*Myrciaria cauliflora*). *J. Nat. Prod.* 69, 1228–1230.
- Richardson, D.H., 2002. Reflections on lichenology: achievements over the last 40 years and challenges for the future. *Can. J. Bot.* 80, 101–113.
- Rodriguez, R.J., White Jr, J.F., Arnold, A.E., Redman, R.S., 2009. Fungal endophytes: diversity and functional roles. *New Phytol.* 182, 314–330. doi:10.1111/j.1469-8137.2009.02773.x
- Romagni, J.G., Dayan, F.E., 2002. Structural Diversity of Lichen Metabolites and Their Potential Use, in: Upadhyay, R.K. (Ed.), *Advances in Microbial Toxin Research and Its Biotechnological Exploitation*. Springer US, pp. 151–169.
- Roullier, C., Chollet-Krugler, M., Bernard, A., Boustie, J., 2009. Multiple dual-mode centrifugal partition chromatography as an efficient method for the purification of a mycosporine from a crude methanolic extract of *Lichina pygmaea*. *J. Chromatogr. B* 877, 2067–2073.
- Roullier, C., Chollet-Krugler, M., Pferschy-Wenzig, E.-M., Maillard, A., Rechberger, G.N., Legouin-Gargadennec, B., Bauer, R., Boustie, J., 2011. Characterization and identification of mycosporines-like compounds in cyanolichens. Isolation of mycosporine hydroxyglutamicol from *Nephroma laevigatum* Ach. *Phytochemistry* 72, 1348–1357.
- Rubio, C., Fernández, E., Hidalgo, M.E., Quilhot, W., 2002. Effects of solar UV-B radiation in the accumulation of rhizocarpic acid in a lichen species from alpine zones in Chile. *Bol. Soc. Chil. Quím.* 47, 67–72. doi:10.4067/S0366-16442002000100012
- Rukachaisirikul, V., Naklue, W., Phongpaichit, S., Towatana, N.H., Maneenoon, K., 2006. Phloroglucinols, depsidones and xanthenes from the twigs of *Garcinia parvifolia*. *Tetrahedron* 62, 8578–8585. doi:10.1016/j.tet.2006.06.059
- Rundel, P.W., 1978. The ecological role of secondary lichen substances. *Biochem. Syst. Ecol.* 6, 157–170. doi:10.1016/0305-1978(78)90002-9
- Rüther, U., 1980. Construction and properties of a new cloning vehicle, allowing direct screening for recombinant plasmids. *Mol. Gen. Genet.* 178, 475–477.
- Rycroft, D.S., Connolly, J.D., Huneck, S., Himmelreich, U., 1995. Revised structure of haemovosin. *Z Naturforsch B* 50, 1557–1563.

- Sala, T., Sargent, M.V., 1981. Depsidone synthesis. Part 16. Benzophenone–grisa-3', 5'-diene-2', 3-dione–depsidone interconversion: a new theory of depsidone biosynthesis. *J. Chem. Soc. [Perkin 1]* 855–869.
- Sancho, L.G., De la Torre, R., Horneck, G., Ascaso, C., de los Rios, A., Pintado, A., Wierzchos, J., Schuster, M., 2007. Lichens survive in space: results from the 2005 LICHENS experiment. *Astrobiology* 7, 443–454.
- Sancho, L.G., de la Torre, R., Pintado, A., 2008. Lichens, new and promising material from experiments in astrobiology. *Fungal Biol. Rev.* 22, 103–109.
- Schinkovitz, A., Richomme, P., 2015. Usnic acid and its versatility as MALDI matrix. *J. Mass Spectrom.* 50, 270–274.
- Schmidt, E.W., 2011. An Enzymatic Route to Sunscreens. *ChemBioChem* 12, 363–365. doi:10.1002/cbic.201000709
- Schneider, P., Bouhired, S., Hoffmeister, D., 2008. Characterization of the atromentin biosynthesis genes and enzymes in the homobasidiomycete *Tapinella panuoides*. *Fungal Genet. Biol.* 45, 1487–1496. doi:10.1016/j.fgb.2008.08.009
- Selosse, M.-A., Boullard, B., Richardson, D., 2011. Noël Bernard (1874–1911): orchids to symbiosis in a dozen years, one century ago. *Symbiosis* 54, 61–68.
- Selosse, M.-A., Richard, F., He, X., Simard, S.W., 2006. Mycorrhizal networks: des liaisons dangereuses? *Trends Ecol. Evol.* 21, 621–628. doi:10.1016/j.tree.2006.07.003
- Selvius DeRoo, C., Armitage, R.A., 2011. Direct identification of dyes in textiles by direct analysis in real time-time of flight mass spectrometry. *Anal. Chem.* 83, 6924–6928.
- Shariatgorji, M., Spacil, Z., Maddalo, G., Cardenas, L.B., Ilag, L.L., 2009. Matrix-free thin-layer chromatography/laser desorption ionization mass spectrometry for facile separation and identification of medicinal alkaloids. *Rapid Commun. Mass Spectrom.* 23, 3655–3660.
- Shechtman, D., Blech, I., Gratias, D., Cahn, J.W., 1984. Metallic phase with long-range orientational order and no translational symmetry. *Phys. Rev. Lett.* 53, 1951.
- Shibata, S., 2000. Yasuhiko Asahina (1880–1975) and his studies on lichenology and chemistry of lichen metabolites. *The Bryologist* 103, 710–719.
- Shick, J.M., 2004. The continuity and intensity of ultraviolet irradiation affect the kinetics of biosynthesis Accumulation and conversion of mycosporine-like amino acids (MAAs) in the coral *Stylophora pistillata*. *Limnol. Oceanogr.* 49, 442–458.
- Shick, J.M., Romaine-Lioud, S., Ferrier-Pages, C., Gattuso, J.P., 1999. Ultraviolet-B radiation stimulates shikimate pathway-dependent accumulation of mycosporine-like amino acids in the coral *Stylophora pistillata* despite decreases in its population of symbiotic dinoflagellates. *Limnol. Oceanogr.* 44, 1667–1682.
- Shinzato, C., Shoguchi, E., Kawashima, T., Hamada, M., Hisata, K., Tanaka, M., Fujie, M., Fujiwara, M., Koyanagi, R., Ikuta, T., others, 2011. Using the *Acropora digitifera* genome to understand coral responses to environmental change. *Nature* 476, 320–323.
- Shrestha, G., St. Clair, L.L., 2013. Lichens: a promising source of antibiotic and anticancer drugs. *Phytochem. Rev.* 12, 229–244. doi:10.1007/s11101-013-9283-7
- Shukla, V., Joshi, G.P., Rawat, M.S.M., 2010. Lichens as a potential natural source of bioactive compounds: a review. *Phytochem. Rev.* 9, 303–314.
- Shuman, S., 1994. Novel approach to molecular cloning and polynucleotide synthesis using *Vaccinia* DNA topoisomerase. *J. Biol. Chem.* 269, 32678–32684.
- Sica, V.P., Raja, H.A., El-Elimat, T., Kertesz, V., Van Berkel, G.J., Pearce, C.J., Oberlies, N.H., 2015. Dereplicating and spatial mapping of secondary metabolites from fungal cultures *in situ*. *J. Nat. Prod.* 78, 1926–1936. doi:10.1021/acs.jnatprod.5b00268
- Sierankiewicz, J., Gatenbeck, S., 1973. The biosynthesis of nidulin and trisdechloronornidulin. *Acta Chem Scand* 27, 2710–2716.
- Simone, N.L., Bonner, R.F., Gillespie, J.W., Emmert-Buck, M.R., Liotta, L.A., 1998. Laser-capture microdissection: opening the microscopic frontier to molecular analysis. *Trends Genet.* 14, 272–276.

- Singh, S.P., Klisch, M., Sinha, R.P., Häder, D.-P., 2010. Genome mining of mycosporine-like amino acid (MAA) synthesizing and non-synthesizing cyanobacteria: A bioinformatics study. *Genomics* 95, 120–128.
- Singh, S.P., Klisch, M., Sinha, R.P., Häder, D.-P., 2008. Effects of Abiotic Stressors on Synthesis of the Mycosporine-like Amino Acid Shinorine in the Cyanobacterium *Anabaena variabilis* PCC 7937. *Photochem. Photobiol.* 84, 1500–1505.
- Sinha, R.P., Ambasht, N.K., Sinha, J.P., Häder, D.-P., 2003. Wavelength-dependent induction of a mycosporine-like amino acid in a rice-field cyanobacterium, *Nostoc commune*: role of inhibitors and salt stress. *Photochem. Photobiol. Sci.* 2, 171–176.
- Skult, H., 1997. Notes on the chemical and morphological variation of the lichen *Ophioparma ventosa* in East Fennoscandia, in: *Annales Botanici Fennici*. JSTOR, pp. 291–297.
- Slansky, F., 1979. Effect of the lichen chemicals atranorin and vulpinic acid upon feeding and growth of larvae of the yellow-striped armyworm, *Spodoptera ornithogalli*. *Environ. Entomol.* 8, 865–868.
- Solhaug, K.A., Gauslaa, Y., 1996. Parietin, a photoprotective secondary product of the lichen *Xanthoria parietina*. *Oecologia* 108, 412–418.
- Soyer-Gobillard, M.-O., 1985. Edouard Chatton (1883–1947) ou l'Essor de la protistologie moderne. *Arch. Für Protistenkd.* 130, 161–164. doi:10.1016/S0003-9365(85)80058-0
- Starcevic, A., Akthar, S., Dunlap, W.C., Shick, J.M., Hranueli, D., Cullum, J., Long, P.F., 2008. Enzymes of the shikimic acid pathway encoded in the genome of a basal metazoan, *Nematostella vectensis*, have microbial origins. *Proc. Natl. Acad. Sci.* 105, 2533–2537.
- Steglich, W., Furtner, W., Prox, A., 1969. Mushroom pigments. 3. Xerocomic acid and gomphidic acid, 2 chemotaxonomically interesting pulvinic acid derivatives from *Gomphidius glutinosus* (Schff) Fr. *Z. Für Naturforschung Teil B Chem. Biochem. Biophys. Biol.* 24, 941–942.
- Stocker-Wörgötter, E., 2015. Biochemical diversity and ecology of lichen-forming fungi: lichen substances, chemosyndromic variation and origin of polyketide-type metabolites (biosynthetic pathways), in: Upreti, D.K., Divakar, P.K., Shukla, V., Bajpai, R. (Eds.), *Recent Advances in Lichenology*. Springer India, New Delhi, pp. 161–179.
- Stocker-Wörgötter, E., 2008. Metabolic diversity of lichen-forming ascomycetous fungi: culturing, polyketide and shikimate metabolite production, and PKS genes. *Nat Prod Rep* 25, 188–200. doi:10.1039/B606983P
- Sundset, M.A., Kohn, A., Mathiesen, S.D., Præsteng, K.E., 2008. *Eubacterium rangiferina*, a novel usnic acid-resistant bacterium from the reindeer rumen. *Naturwissenschaften* 95, 741–749. doi:10.1007/s00114-008-0381-0
- Sureram, S., Kesornpun, C., Mahidol, C., Ruchirawat, S., Kittakoop, P., 2013. Directed biosynthesis through biohalogenation of secondary metabolites of the marine-derived fungus *Aspergillus unguis*. *RSC Adv* 3, 1781–1788. doi:10.1039/C2RA23021F
- Takani, M., Yajima, T., Masuda, H., Yamauchi, O., 2002. Spectroscopic and structural characterization of copper (II) and palladium (II) complexes of a lichen substance usnic acid and its derivatives. Possible forms of environmental metals retained in lichens. *J. Inorg. Biochem.* 91, 139–150.
- Takenaka, Y., Tanahashi, T., Nagakura, N., Hamada, N., 2000. Production of xanthonones with free radical scavenging properties, emodin and sclerotiorin by the cultured lichen mycobionts of *Pyrenula japonica*. *Z. Für Naturforschung C* 55, 910–914.
- Tanahashi, T., Takenaka, Y., Ikuta, Y., Tani, K., Nagakura, N., Hamada, N., 1999. Xanthonones from the cultured lichen mycobionts of *Pyrenula japonica* and *Pyrenula pseudobufonia*. *Phytochemistry* 52, 401–405. doi:10.1016/S0031-9422(99)00235-6
- Taylor, T., Hass, H., Kerp, H., 1997. A cyanolichen from the Lower Devonian Rhynie chert. *Am. J. Bot.* 84, 992–992.
- Thomas, R., 2001. A biosynthetic classification of fungal and Streptomyces fused-ring aromatic polyketides. *ChemBioChem* 2, 612–627.
- Thygesen, L.G., Løkke, M.M., Micklander, E., Engelsen, S.B., 2003. Vibrational microspectroscopy of food. Raman vs. FT-IR. *Trends Food Sci. Technol.* 14, 50–57.

- Timdal, E., 1989. The production of rhodocladonic acid in *Cladonia bacilliformis* and *C. norvegica* triggered by the presence of a lichenicolous mite. *Graph. Scr.* 2, 125–127.
- Tønsberg, T., Holtan–Hartwig, J., 1983. Phycotype pairs in *Nephroma*, *Peltigera* and *Lobaria* in Norway. *Nord. J. Bot.* 3, 681–688.
- Torres, A., Hochberg, M., Pergament, I., Smoum, R., Niddam, V., Dembitsky, V.M., Temina, M., Dor, I., Lev, O., Srebniak, M., Enk, C.D., 2004. A new UV-B absorbing mycosporine with photo protective activity from the lichenized ascomycete *Collema cristatum*. *Eur. J. Biochem.* 271, 780–784.
- Toudic, B., 2015. Qu'est-ce qu'un cristal? *Reflets Phys.* 18–24.
- Turner, A., Chen, S.-N., Nikolic, D., van Breemen, R., Farnsworth, N.R., Pauli, G.F., 2007. Coumaroyl iridoids and a depside from cranberry (*Vaccinium macrocarpon*). *J. Nat. Prod.* 70, 253–258.
- Umezawa, H., Shibamoto, N., Naganawa, H., Ayukawa, S., Matsuzaki, M., Takeuchi, T., Kono, K., Sakamoto, T., 1974. Isolation of lecanoric acid, an inhibitor of histidine decarboxylase from a fungus. *J. Antibiot. (Tokyo)* 27, 587–596.
- Van der Heijden, M.G., Martin, F.M., Selosse, M.-A., Sanders, I.R., 2015. Mycorrhizal ecology and evolution: the past, the present, and the future. *New Phytol.* 205, 1406–1423.
- Van der Sar, S.A., Blunt, J.W., Cole, A.L.J., Din, L.B., Munro, M.H.G., 2005. Dichlorinated Pulvinic Acid Derivative from a Malaysian *Scleroderma* sp. *J. Nat. Prod.* 68, 1799–1801. doi:10.1021/np0503395
- Van Haluwyn, C., Asta, J., Gavériaux, J.-P., 2009. Guide des lichens de France: lichens des arbres. Belin.
- Vítek, P., Edwards, H.G.M., Jehlička, J., Ascaso, C., De los Ríos, A., Valea, S., Jorge-Villar, S.E., Davila, A.F., Wierzechos, J., 2010. Microbial colonization of halite from the hyper-arid Atacama Desert studied by Raman spectroscopy. *Philos. Trans. R. Soc. Lond. Math. Phys. Eng. Sci.* 368, 3205–3221.
- Wachtmeister, C.A., 1958. Studies on the chemistry of lichens. XI. Structure of picrolichenic acid. *Acta Chem. Scand.* 12, 147–164.
- Whiton, J.C., Lawrey, J.D., 1984. Inhibition of crustose lichen spore germination by lichen acids. *Bryologist* 87, 42–43.
- Whiton, J.C., Lawrey, J.D., 1982. Inhibition of *Cladonia cristatella* and *Sordaria fimicola* ascospore germination by lichen acids. *Bryologist* 85, 222–226.
- Whittaker, R.H., 1969. New concepts of kingdoms of organisms. *Science* 163, 150–163.
- Winner, M., Giménez, A., Schmidt, H., Sontag, B., Steffan, B., Steglich, W., 2004. Unusual pulvinic acid dimers from the common fungi *Scleroderma citrinum* (common earthball) and *Chalciporus piperatus* (peppery bolete). *Angew. Chem. Int. Ed.* 43, 1883–1886.
- Wirth, V., 1985. Zur Ausbreitung, Herkunft und Ökologie anthropogen geförderter Rinden- und Holzflechten. *Tuexenia* 523–535.
- Wu, X., Flatt, P.M., Schlörke, O., Zeeck, A., Dairi, T., Mahmud, T., 2007. A comparative analysis of the sugar phosphate cyclase superfamily involved in primary and secondary metabolism. *ChemBioChem* 8, 239–248.
- Wynn-Williams, D.D., Edwards, H.G.M., Garcia-Pichel, F., 1999. Functional biomolecules of Antarctic stromatolitic and endolithic cyanobacterial communities. *Eur. J. Phycol.* 34, 381–391.
- Xu, X., Liu, L., Zhang, F., Wang, W., Li, J., Guo, L., Che, Y., Liu, G., 2014. Identification of the first diphenyl ether gene cluster for pesthelic acid biosynthesis in plant endophyte *Pestalotiopsis fici*. *ChemBioChem* 15, 284–292.
- Xu, Y.-J., Chiang, P.-Y., Lai, Y.-H., Vittal, J.J., Wu, X.-H., Tan, B.K.H., Imiyabir, Z., Goh, S.-H., 2000. Cytotoxic prenylated depsidones from *Garcinia parvifolia*. *J. Nat. Prod.* 63, 1361–1363. doi:10.1021/np000141e
- Zenobi, R., Knochenmuss, R., 1998. Ion formation in MALDI mass spectrometry. *Mass Spectrom. Rev.* 17, 337–366.

- Zhang, F., Li, L., Niu, S., Si, Y., Guo, L., Jiang, X., Che, Y., 2012. A Thiopyranchromenone and Other Chromone Derivatives from an Endolichenic Fungus, *Preussia africana*. *J. Nat. Prod.* 75, 230–237. doi:10.1021/np2009362
- Zhang, F., Liu, S., Lu, X., Guo, L., Zhang, H., Che, Y., 2009. Allenyl and Alkynyl Phenyl Ethers from the Endolichenic Fungus *Neurospora terricola*. *J. Nat. Prod.* 72, 1782–1785. doi:10.1021/np900512k

Annexe 1 : Biosynthèse des métabolites secondaires lichéniques

A. Voie des polyacétates/polymalonates

La voie des polyacétates-polymalonates est associée à une très large majorité de composés lichéniques et concentre les motifs structuraux typiques des lichens. Les polyacétates fongiques sont biosynthétisés par des méga-enzymes dotées de domaines fonctionnels modulaires : les PolyKetideSynthase abrégées PKS (Thomas, 2001). L'incorporation en série d'unités acétylCoA par réactions de Claisen successives donne lieu à des dérivés linéaires de type poly- β -cétoester.

La diversité des polyacétates est ensuite liée au choix de l'unité de départ (starter), des unités d'extension, à la longueur de la chaîne (liée aux nombre de modules que comporte l'enzyme), à des cyclisations régiospécifiques et enfin à d'éventuelles modifications enzymatiques en aval (post-PKS). La diversification des polyacétates peut être apportée par la présence de domaines optionnels pouvant assurer tout ou partie de ces modifications : réduire le groupement cétone en alcool (domaine kétoréductase), déshydrater cet alcool (domaine déhydratase) et éventuellement réduire cette double liaison (domaine énoylréductase) (Thomas, 2001).

a. Polyacétates aromatiques

Pour une très importante partie des polyacétates lichéniques, la condensation des unités acétyl-CoA et malonyl CoA conduit à la formation d'une chaîne en C-8 qui, par aldolisation interne ou condensation de Claisen, livre l'acide orsellinique ou le méthylphloroacétophénone.

La condensation de ces structures de base pour livrer des composés di- (le plus souvent), tri- voire parfois tétracycliques introduit la variété des polyphénols lichéniques qui vont diverger selon la nature des groupements reliant ces différents motifs (Figure 50) :

- des couplages de type **estérification** sont rencontrés chez les depsides, depsidones et depsones (représentées en bleu) ;
- une **étherification** intervient dans l'obtention des depsidones, dibenzofuranes et diphényléthers (vert) ;
- un **couplage oxydant**, permettant d'accéder à des jonctions C-C, est rencontré chez les dibenzofuranes et les depsones (rouge).

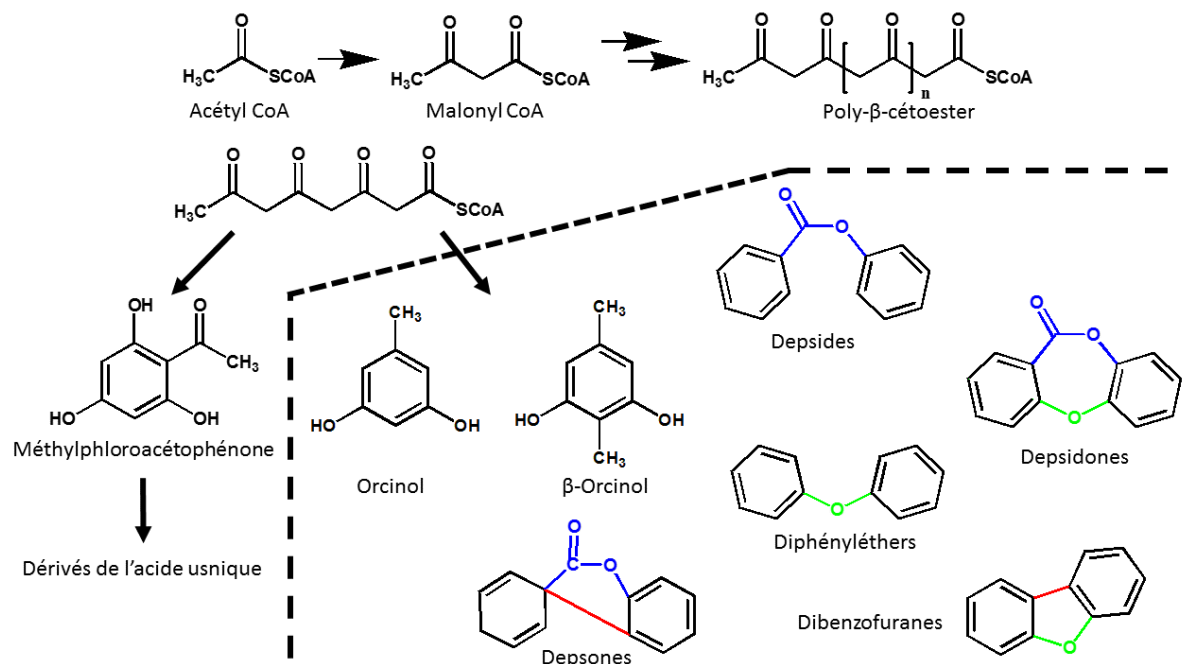


FIGURE 50 : FAMILLES STRUCTURALES DE MÉTABOLITES LICHÉNIQUES OBTENUES PAR CONDENSATIONS D'UNITÉS MONOAROMATIQUES.

1. Depsides

La réaction d'estérification entre deux noyaux orcinol donne naissance aux didepsides (la plupart du temps désignés sous le nom de depsides). En de plus rares occasions, la condensation de trois ou quatre unités livre des tri- et tétradepsides.

Le noyau depside reste très essentiellement associé aux lichens. Ce motif structural est parfois retrouvé chez des champignons non lichénisés souvent ornementé de substituants qui ne sont pas rencontrés chez les depsides lichéniques : on peut ainsi citer les agonodepsides A et B (didepsides isolés d'un ascomycète non identifié porteurs de deux groupements 1-méthyl-prop-1-ényl (Cao et al., 2002), le guisinol (porteur d'un exemplaire de ce même substituant isolé du champignon marin *Emericella unguis* (Nielsen et al., 1999)), les lécanorines B à F (obtenus à partir de champignons endophytes et contenant des cycles aromatiques polyméthylés (de Medeiros et al., 2011, 2015) mais également la stromémycine C-hétéroside de depside (*Emericella varicolor* (Bringmann et al., 2003)). Cependant, il arrive parfois que des depsides lichéniques soient isolés à partir de champignons non lichénisants : c'est notamment le cas de l'acide lécanorique qui a pu être isolé à partir d'un *Pyricularia* (Umezawa et al., 1974). En de plus rares occasions, des tridepsides ont pu être caractérisés chez des champignons non lichénisants : peuvent ainsi être citées les acides cytoniques isolés de champignons endophytiques du genre *Cytonaema* (Guo et al., 2000), différentes thielavines issues de champignons endophytes *Setophoma sp.* (de Medeiros et al., 2015) et *Cladosporium uredinicola* (de Medeiros et al., 2011) ou encore des tridepsides greffés à des acides aminés, les amidepsines, issues d'*Humicola sp* (Inokoshi et al., 2010). Il est d'ailleurs à noter que cette dernière souche produit également de l'acide gyrophorique, tridepside couramment rencontrée chez les lichens. Plus rarement, des depsides ont été isolés de végétaux, notamment de *Papaver rhoeas* (Hillenbrand et al., 2004), *Myrciaria cauliflora* (Reynertson et al., 2006), *Vaccinium macrocarpon* (Turner et al., 2007) et *Impatiens balsamina* (Li et al., 2015) mais la structure de leurs composants monoaromatiques suggère qu'ils dérivent de la voie du shikimate.

2. Depsidones

Les depsidones correspondent à deux noyaux orcinoliques unis à la fois par une liaison ester et par un éther (Legaz et al., 2011; Sierankiewicz and Gatenbeck, 1973). Plus récemment, Armaleo *et al.* ont pu établir l'implication vraisemblable d'une PolyKetideSynthase (PKS) dans l'oxydation de depsides en depsidones en décrivant un cytochrome P450 associé au cluster d'une PKS, CgrPKS16 (Armaleo et al., 2011). Néanmoins, la synthèse des depsidones peut impliquer des mécanismes plus complexes. Cette seconde voie repose sur le couplage oxydatif d'une benzophénone pour livrer un intermédiaire grisadiènedione pouvant à son tour se réarranger en depsidone (Sureram et al., 2013). Un tel schéma de biosynthèse est accrédité par des réactions chimiques impliquant cette séquence benzophénone/grisadiènedione/depsidone (Sala and Sargent, 1981) et également par la co-occurrence de la grisadiènedione et de la depsidone correspondante au sein d'un même champignon (Adeboya et al., 1996). Ces séquences de biosynthèse sont présentées dans la Figure 51.

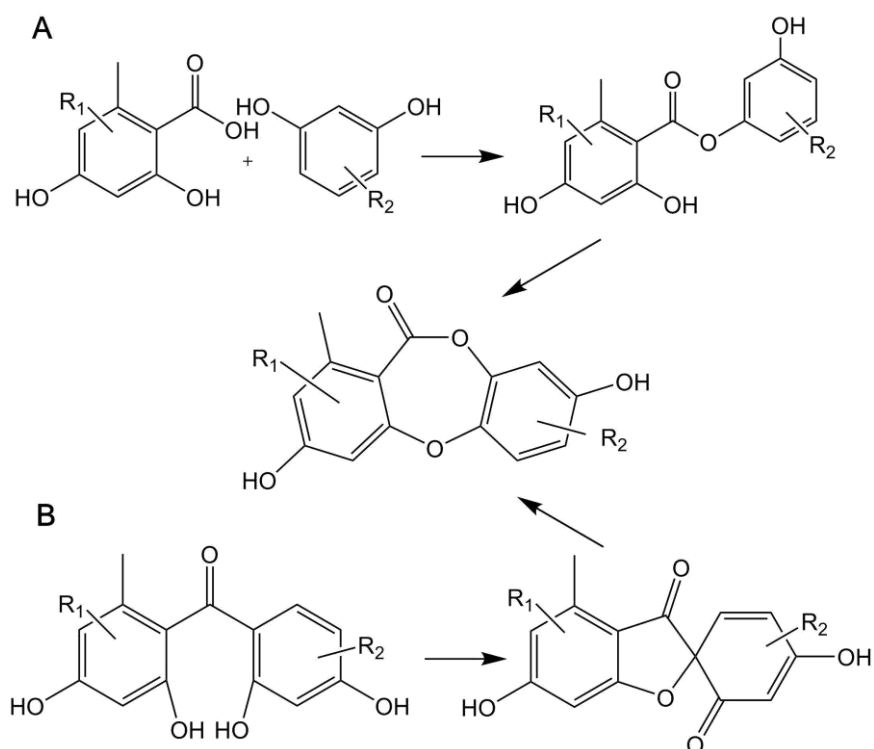


FIGURE 51 : VOIES DE BIOSYNTÈSE DES DEPSIDONES

À l'instar des depsides, les depsidones sont parfois rencontrées hors des lichens. Elles sont particulièrement représentées chez les plantes du genre *Garcinia*. Ornées de groupements prényles, ces structures sont à la confluence des voies des acétates-polymalonates et du mévalonate. Quelques exemples incluent : les atrovirisidones (Permana et al., 2005), les brevipsidones (Ngoupayo et al., 2008), les garcidepsidones (Xu et al., 2000), les garcinisidones (Ito et al., 2001), les oliveridepsidones (Ha et al., 2012), les parvifolidones (Rukachaisirikul et al., 2006). Quelques depsidones ont également été décrites de champignons non lichénisés : les corynésidones (Chomcheon et al., 2009), les eméguisines (Kawahara et al., 1988), l'excelsione (Lang et al., 2007), la folipastatine et la niduline (Bycroft and Roberts, 1963) en sont quelques exemples.

3. Depsones

Les depsones résultent de l'association entre deux noyaux orcinoliques par une liaison ester et un couplage oxydant. Seules 8 molécules appartenant à cette série ont été identifiées chez les lichens jusqu'à présent. Il est admis que les depsones résultent d'un couplage oxydant de depsides tel qu'indiqué sur la Figure 52. À titre d'exemple, l'acide picrolichéinique, première depsonne découverte (Wachtmeister, 1958), comporte deux unités de type penténylrésorcinol au même titre que l'acide colensoïque (depsidone), que les acides 2-O-méthylperlatolique et 2-O-méthylanziaïque (depsides) et que l'acide épiphorellique I (diphényléther). La découverte des acides 2-O-méthylperlatolique et 2'-O-méthylperlatolique dans 6 espèces du genre *Pertusaria* (Culberson and Dibben, 1972) accrédite la filiation biogénétique proposée ci-dessus (Figure 52).

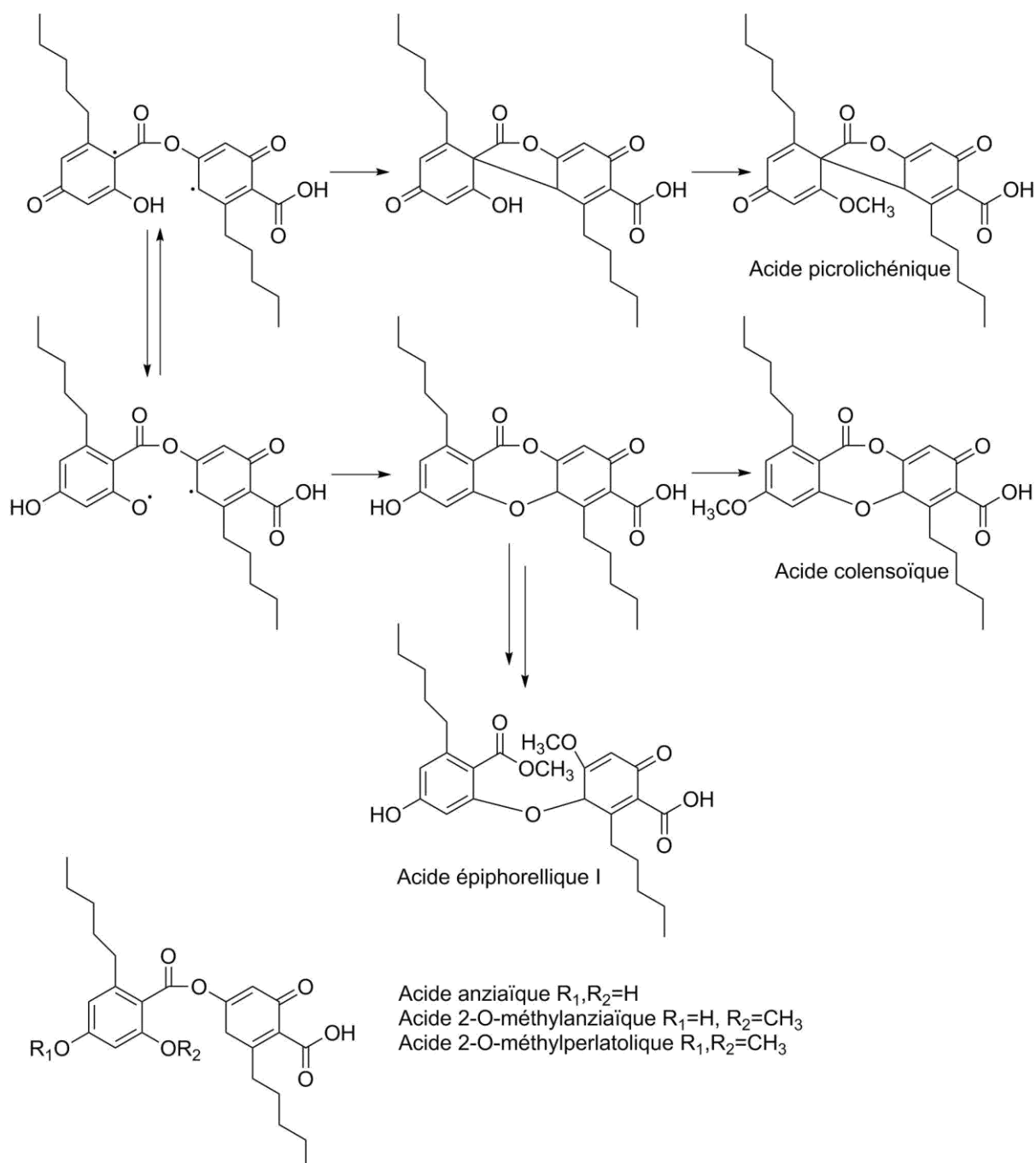


FIGURE 52 : BIOSYNTÈSE PROPOSÉE POUR LES DEPSONES ET FILIATIONS BIOGÉNÉTIQUES POSSIBLES AVEC QUELQUES DEPSIDES, DEPSIDONES ET DIPHÉNYLETERS QUI LEUR SONT STRUCTURALEMENT APPARENTÉES (ADAPTÉ DE (CHOOI, 2008)).

4. Dibenzofuranes et acide usnique

Parmi ces composés, la biosynthèse de l'acide usnique a été la plus étudiée. Ce composé n'est pas considéré comme un dibenzofurane au sens strict en raison de la non-aromaticité de son cycle C. L'acide usnique résulte du couplage oxydant entre deux unités de méthylphloroacétophénone selon la séquence indiquée Figure 53 (Ingolfsdottir, 2002).

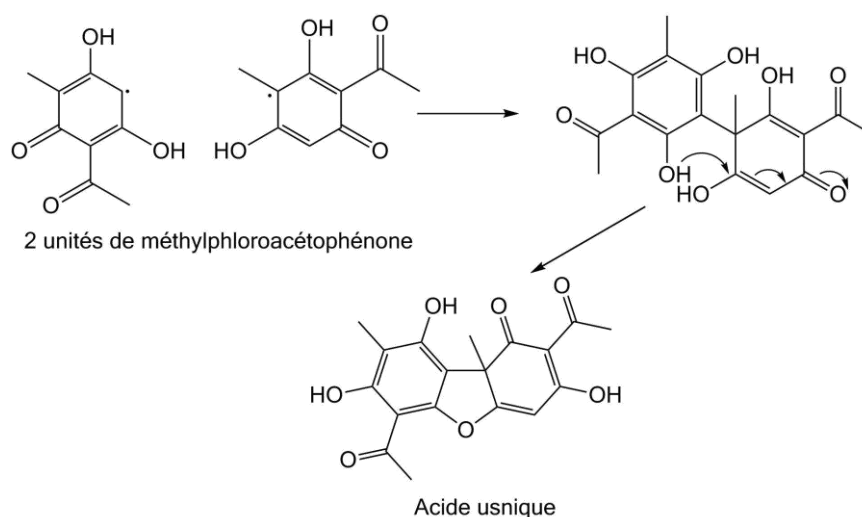


FIGURE 53 : BIOSYNTÈSE DE L'ACIDE USNIQUE (ADAPTÉ DE (INGOLFSDDOTTIR, 2002))

Aucune étude ne s'est penchée sur la biosynthèse de dibenzofuranes *stricto sensu* mais des propositions extrapolées sur la base du mécanisme démontré pour l'acide usnique ont été formulées par Mosbach (Mosbach, 1969). Les dibenzofuranes seraient également le fait de couplages oxydants entre deux unités monoaromatiques mais l'absence de groupements méthyles aux sites de couplage radicalaire permettrait de maintenir l'aromaticité des deux cycles. Contrairement à l'acide usnique, ces dibenzofuranes vraies correspondent à des hétérodimères (Figure 54).

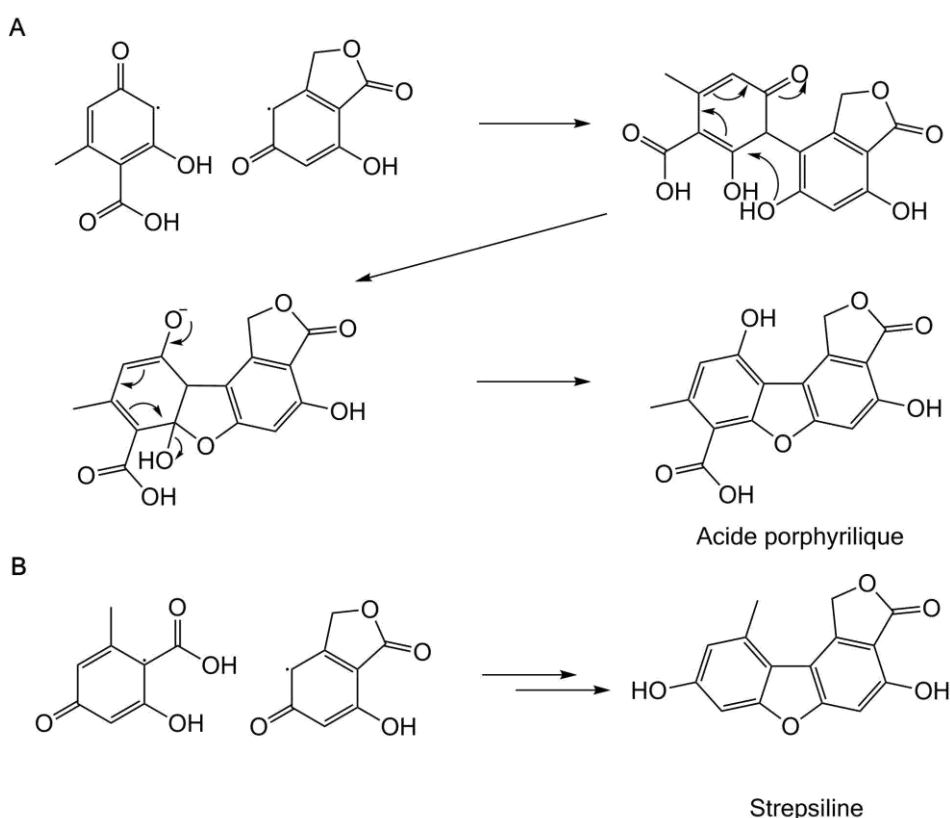


FIGURE 54 : BIOSYNTÈSE DE DIBENZOFURANES *SENSU STRICTO* (ADAPTÉ DE (CHOOI, 2008))

5. Diphényléthers

Groupe structural moins représenté chez les lichens, les diphényléthers sont souvent perçus comme des catabolites de depsidones. A ce titre, il est souvent noté que les diphényléthers sont fréquemment isolés en parallèle de depsidones qui leur sont structurellement apparentées (Adeboya et al., 1996; Chomcheon et al., 2009; Millot et al., 2009). Un tel scénario biogénétique a été invoqué pour expliquer la présence de buelline (diphényléther) à partir de la diploïcine (depsidone) (Millot et al., 2009) (Figure 55).

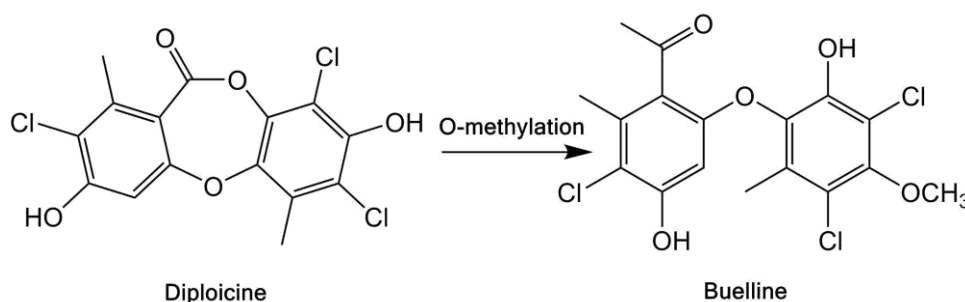


FIGURE 55 : POSSIBLE TRANSFORMATION DE LA DIPLOÏCINE EN BUELLINE

La récente découverte d'un cluster de gènes associé à la production d'un diphényléther (l'acide pesthaïque) chez le champignon endophyte *Pestalotiopsis fici* propose toutefois un autre scénario biosynthétique initié par une anthraquinone (Xu et al., 2014). Cette autre voie de biogenèse sera traitée en aval de la partie abordant les quinones.

6. Quinones, xanthones et chromones

Ces classes de métabolites secondaires ne sont absolument pas spécifiques des lichens et sont largement décrites à partir de plantes et de champignons non lichénisés. La biosynthèse des quinones résulte de la cyclisation d'un intermédiaire poly- β -cétoster selon le mécanisme indiqué ci-dessous (Figure 56). La diversité des quinones dépend de la longueur du poly- β -cétoster initial et est également le fait d'enzymes qui vont pouvoir introduire une variété de substituants différents en aval du travail des PKS. De façon notable, les quinones fongiques et les quinones bactériennes ont des procédés de biosynthèse qui divergent par des régiospécificités différentes dans la cyclisation du polyacétate initial. Cette spécificité fait que les quinones associées à ces deux règnes présentent théoriquement des structures non redondantes (Thomas, 2001).

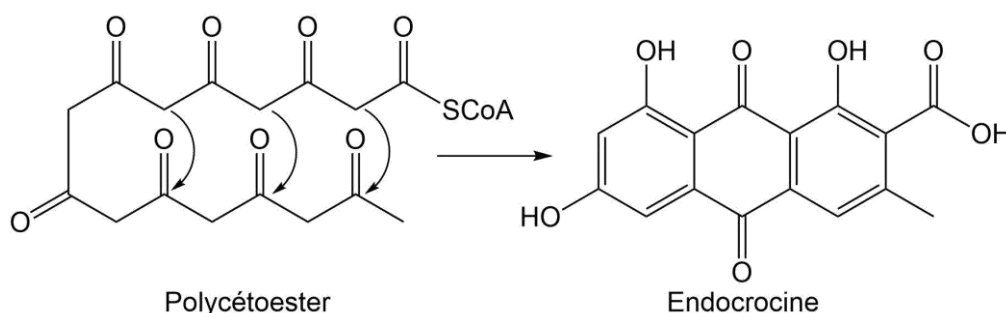
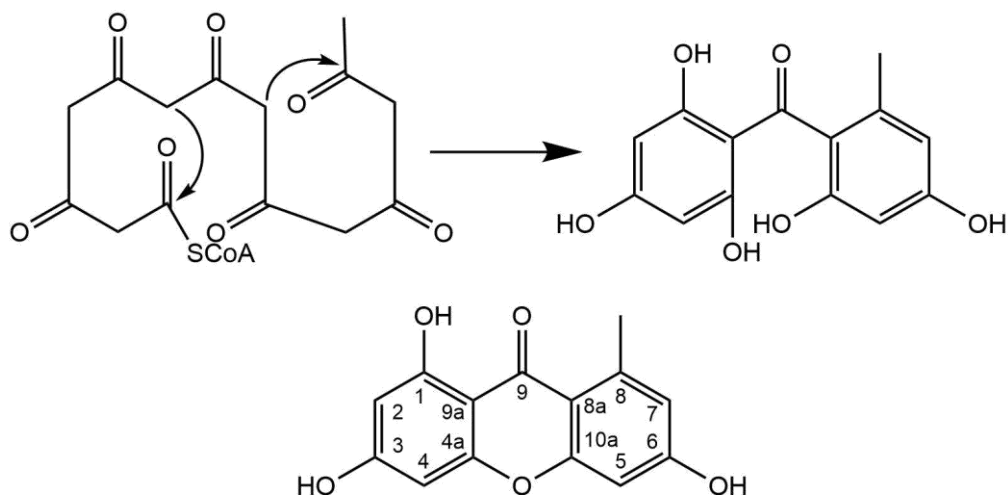


FIGURE 56: BIOSYNTÈSE DES QUINONES À PARTIR DE L'INTERMÉDIAIRE POLY- β -CÉTOESTER

Les xanthones représentent également un noyau fréquemment rencontré chez les lichens. Bien que ce noyau retrouvé chez près de 2.000 molécules naturelles soit essentiellement rencontré chez des plantes (80% d'entre elles), la voie de biosynthèse en œuvre chez les champignons diverge de celle rencontrée chez les végétaux. En effet, chez les plantes, les xanthones sont issues d'une biosynthèse convergente entre la voie du shikimate et la voie des polyacétates/polymalonates tandis que les

xanthones lichéniques sont générées par la seule voie des polyacétates. Ces voies de biosynthèse divergentes sont à l'origine de patterns de substitution entre les xanthones fongiques et végétales et de fait, sur la petite centaine décrite à partir des lichens, moins de 10 sont également rencontrées chez des plantes ou des champignons non lichénisants. Le procédé le plus courant de biosynthèse implique un repliement du poly- β -cétate comme indiqué Figure 57 pour donner un intermédiaire benzophénone qui cyclise ensuite pour livrer les xanthones de type lichéxanthone.



Lichexanthone-type xanthone
Common substitution pattern :
1,3,6-trihydroxy-8-methylxanthone

FIGURE 57: BIOSYNTÈSE DES XANTHONES AYANT UN PATTERN D'OXYGÉNATION DE TYPE LICHEXANTHONE (LE POGAM AND BOUSTIE, 2016).

Un procédé de biosynthèse plus complexe, reposant sur un intermédiaire anthraquinone permet d'atteindre les structures de type thioméline et acides sécaloniques après dimérisation (Figure 58).

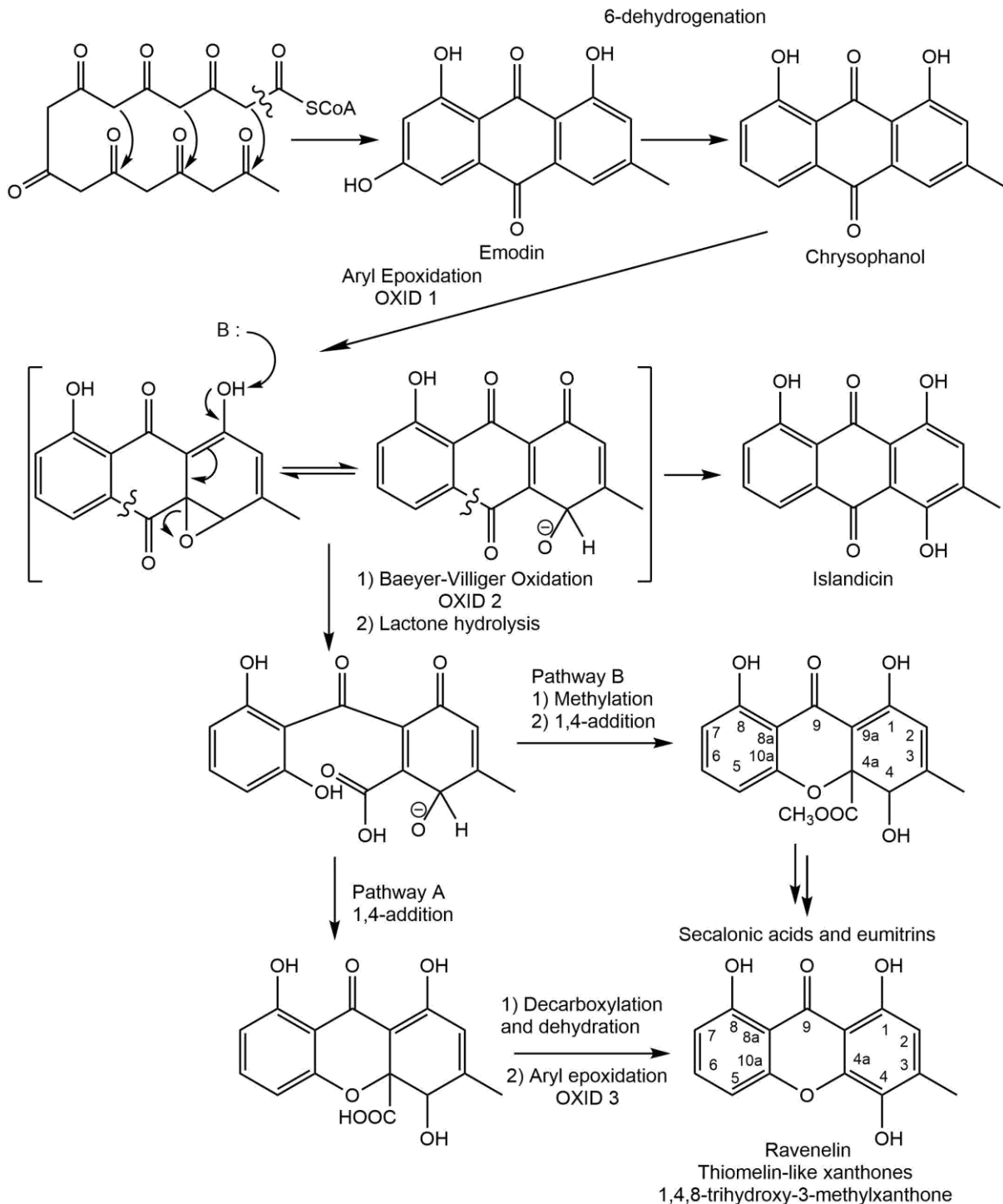


FIGURE 58: BIOSYNTÈSE DES XANTHONES AFFILIÉES A LA THIOMÉLINE ET AUX BISXANTHONES DE TYPE ACIDE SÉCALONIQUE ET EUMITRINE (LE POGAM AND BOUSTIE, 2016).

Un état des lieux sur les xanthones d'origine lichénique a été publié en 2016 dans *Molecules*, le texte intégral de cette publication est disponible en Annexe 6.

Parfois isolées à partir de lichens, les chromones, molécules surtout rencontrées chez les végétaux et parfois chez des champignons non lichénisants (pour revue voir (Gaspar et al., 2014)) sont obtenues par cyclisation de penta-acétates linéaires selon le mécanisme indiqué ci-dessous (Romagni and Dayan, 2002) (Figure 59).

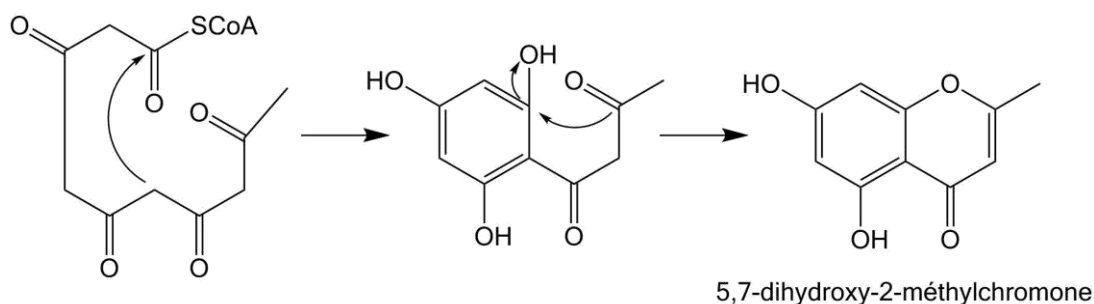


FIGURE 59: BIOSYNTÈSE DES CHROMONES

Comme indiqué plus haut, l'obtention de diphényléthers à partir de l'endocrocine a pu être démontrée par une approche génétique. La décarboxylation puis la méthylation de cette molécule livrent dans un premier temps le physcion dont le clivage oxydatif va engendrer une benzophénone. Cette dernière, sous l'influence d'une DiHydroGéodine Oxydase (DHGO) donne un spiro-intermédiaire de type grisadiénedione pouvant se réarranger en diphényléther (Xu et al., 2014) (Figure 60).

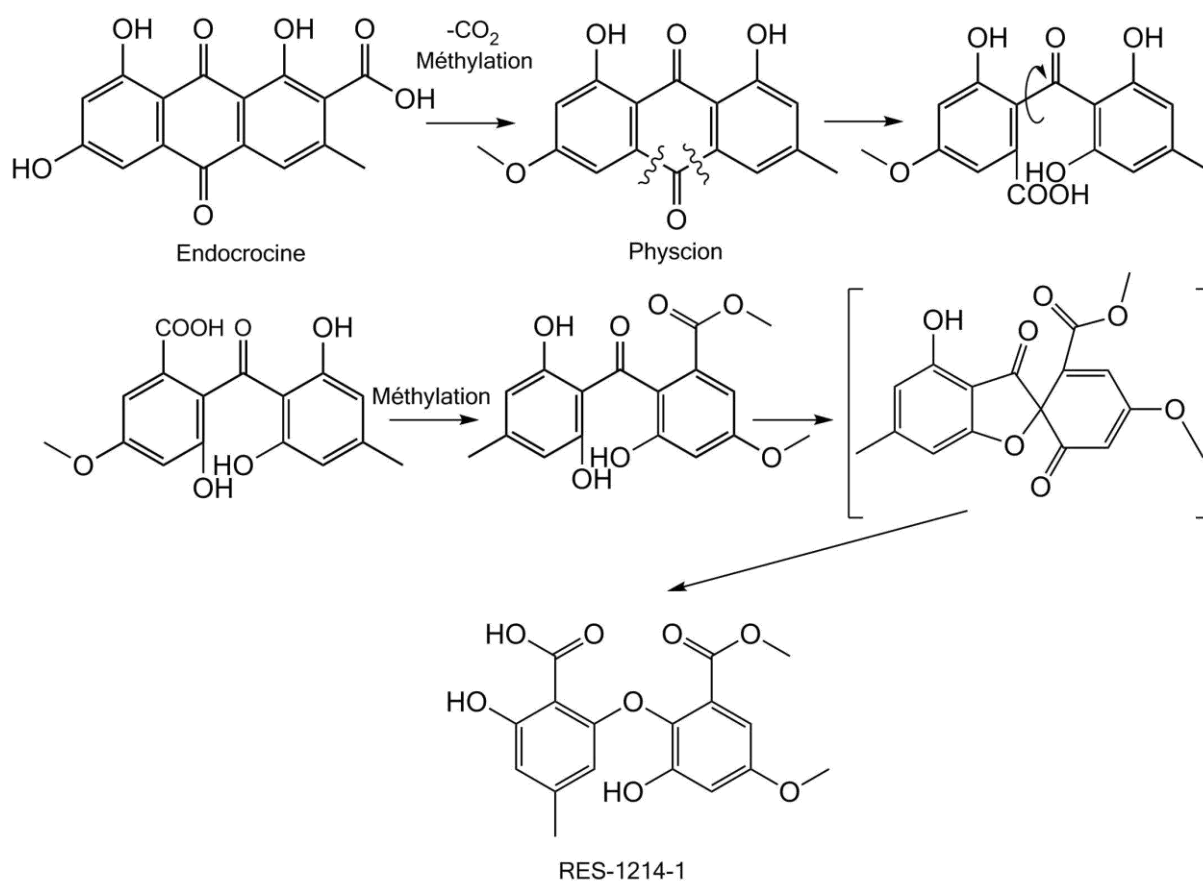


FIGURE 60: BIOSYNTÈSE DE DIPHÉNYLÉTERS VIA UN INTERMÉDIAIRE ANTHRAQUINONE (ADAPTÉ DE (XU ET AL., 2014)).

b. Polyacétates non aromatiques

Certains acides lichéniques sont obtenus par aldolisation d'une chaîne alconyl-CoA avec une unité d'acide cétonique. Trois groupes structuraux peuvent ainsi être obtenus (Figure 61):

- Les γ -lactones
- Les diacides aliphatiques
- Les triacides aliphatiques

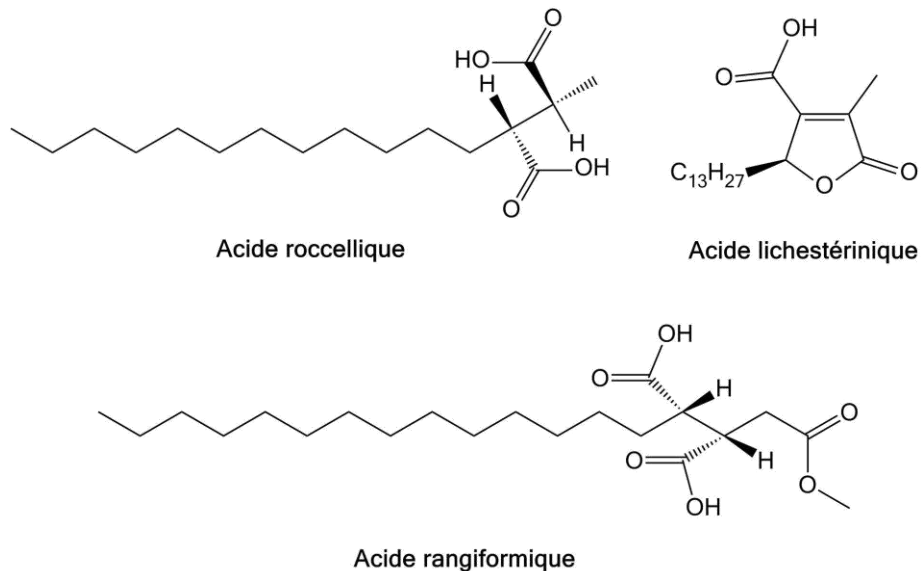


FIGURE 61 : FORMULES CHIMIQUES DE QUELQUES ACIDES ALIPHATIQUES LICHÉNIQUES.

B. Voie de l'acide mévalonique

Chez les lichens, la voie du mévalonate mène essentiellement aux di- et triterpènes, aux stéroïdes et aux caroténoïdes. Ces dérivés ont pour unité de base l'isoprène, obtenu à partir de l'acétylCoA. Les conditions de l'isopenténylpyrophosphate (unité en C_5) peuvent livrer soit le géranylpyrophosphate (C_{20}), précurseur de diterpènes et de caroténoïdes, soit le squalène (C_{30}), précurseur des stéroïdes et des terpènes (Figure 62).

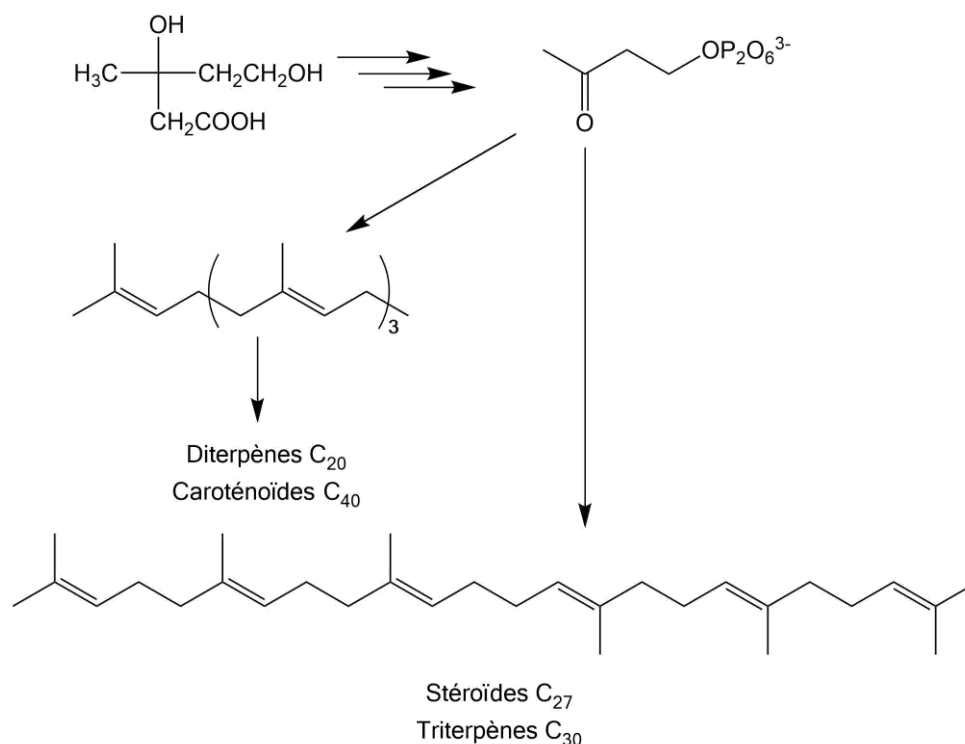


FIGURE 62: FAMILLES STRUCTURALES ISSUES DE LA VOIE DU MÉVALONATE

C. Voie de l'acide shikimique

Cette voie de biosynthèse permet d'obtenir des acides aminés aromatiques qui vont chez les plantes être les précurseurs des flavonoïdes, des coumarines et des alcaloïdes. Cet axe métabolique intervient en revanche assez peu chez les lichens où il est essentiellement associé à la production des dérivés de l'acide pulvinique. La dimérisation de l'acide phénylpyruvique livre dans un premier temps des dérivés terphénylquinones comme l'acide polyporique selon la séquence réactionnelle indiquée dans la Figure 63 (Schneider et al., 2008). La coupure oxydative du cycle médian permet la constitution d'une γ -lactone pour atteindre le squelette final des dérivés de l'acide pulvinique comme indiqué ci-dessous (Gill and Steglich, 1987). Non spécifiques des lichens, les dérivés de l'acide pulvinique aussi bien que les terphénylquinones sont rencontrés chez de nombreux Basidiomycètes (Beaumont et al., 1968; Gill and Kiefel, 1994; Steglich et al., 1969; van der Sar et al., 2005; Winner et al., 2004).

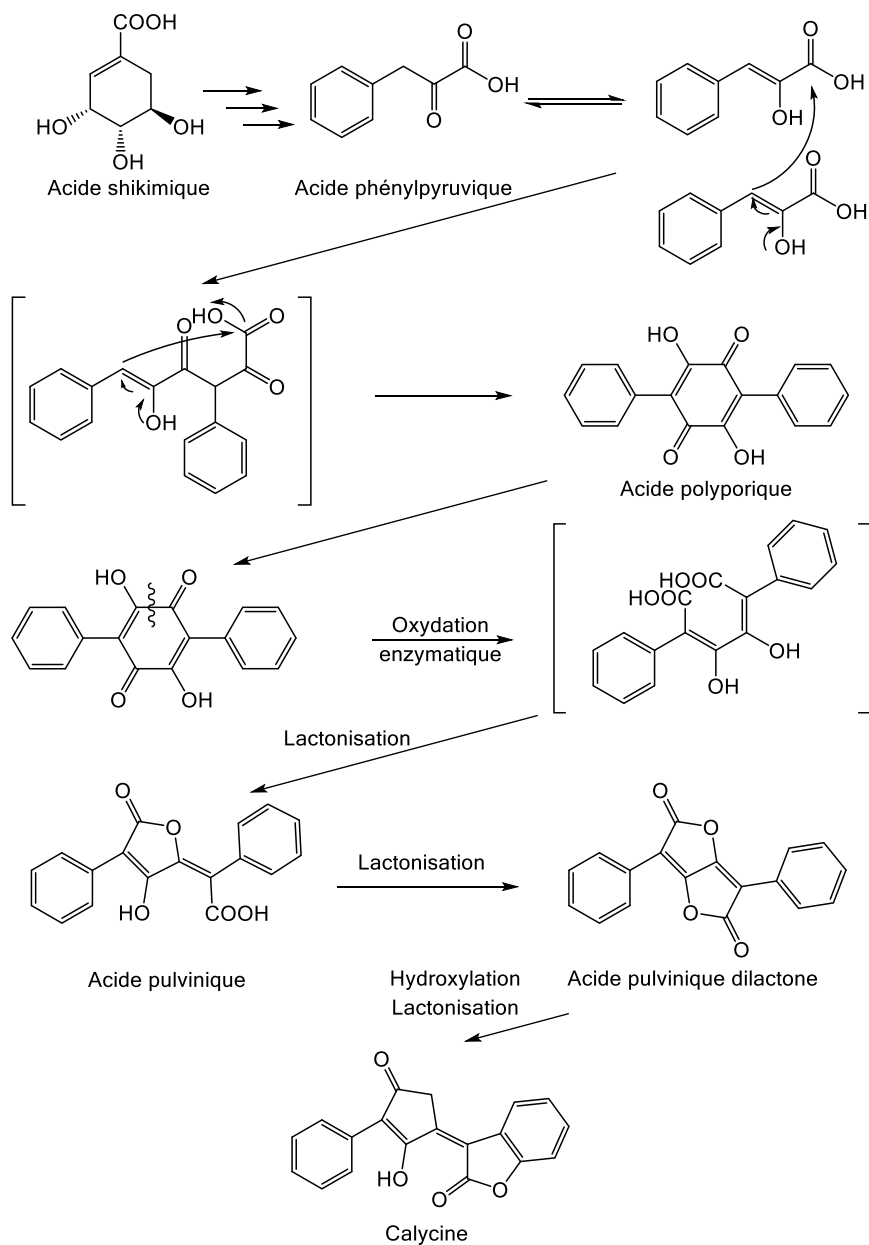


FIGURE 63: BIOSYNTÈSE DES DÉRIVÉS DE L'ACIDE PULVINIQUE (GILL AND STEGLICH, 1987)

Annexe 2 : Généralités sur la diffraction des rayons X par la matière cristallisée

A. Concepts cristallographiques de base

L'état cristallin se définit traditionnellement comme un arrangement triplement périodique de la matière à l'échelle atomique. Depuis 1992 toutefois, l'IUCr (International Union of Crystallography) définit les cristaux comme des objets physiques donnant lieu à des pics de diffraction essentiellement fins (au sens où l'information structurale est principalement contenue dans des pics répondant à la loi de Bragg).

L'approche traditionnelle de la cristallographie est associée à un certain nombre de définitions fondamentales :

La **maille élémentaire** représente une unité de base (période) à partir de laquelle l'ensemble du cristal peut être engendré par opérations de translations.

Ce volume élémentaire est caractérisé par une origine O et trois vecteurs de base non colinéaires **a**, **b** et **c**. Les paramètres de maille correspondent aux normes de ces trois vecteurs et aux angles α , β et γ qui existent entre eux, définissant sept **systèmes cristallins** (Figure 64).

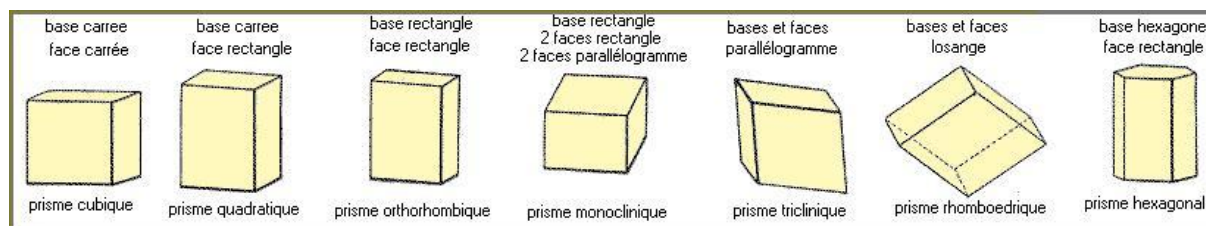


FIGURE 64: LES SEPT SYSTÈMES CRISTALLINS

On définit ensuite l'ensemble des points O' vérifiant :

$OO' = ma + nb + pc$ avec m, n et p des nombres entiers relatifs. Les points O' sont appelés des **nœuds** et l'ensemble de ces nœuds constitue le **réseau cristallin primitif**.

L'arrangement des atomes, molécules ou ions au sein de cette maille prend le nom de **motif** (Figure 65).

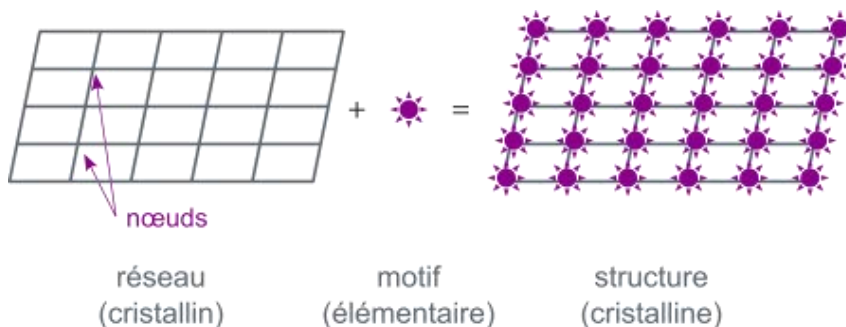


FIGURE 65 : NOTIONS DE BASE EN CRISTALLOGRAPHIE : NŒUDS, RÉSEAU ET MOTIF.

Chacun des systèmes cristallins est caractérisé par un certain nombre de symétries qui sont de trois ordres :

- Centrale
- Plane
- Axiale

Lorsqu'il existe une invariance par rotation, on dit qu'il y a symétrie d'ordre n lorsque la rotation en question correspond à un angle de $2\pi/n$ radians, avec $n = 2, 3, 4$ ou 6 . La symétrie d'ordre 5 (comme celle d'ordres supérieurs) est proscrite puisqu'il est impossible de paver l'espace euclidien avec des pentagones et icosaèdres (analogues tridimensionnels des pentagones).

La notion de maille primitive associée au réseau défini par le motif ne décrit pas l'ensemble des réseaux cristallins réels. En effet, la convention impose que le repère de la maille élémentaire adopte des axes colinéaires aux symétries du réseau. La conséquence est alors qu'une maille peut contenir plus d'un nœud du réseau ($1, 2$ ou 4). En admettant qu'un motif constitue le nœud du réseau, on obtient alors 4 types de mailles :

- P (Primitive) : comme décrit précédemment, les nœuds du réseau sont confondus avec les sommets de la maille ;
- I (pour l'allemand *Innenzentriert*, centrée) : si l'on positionne l'origine de la maille sur un nœud du réseau, il existe un second nœud au centre de cette maille. Celle-ci contient alors 2 motifs ;
- F (Faces centrées) : si l'on positionne l'origine de la maille sur un nœud du réseau, il existe trois autres nœuds au sein de la maille, chacune au centre d'une face non parallèle aux deux autres ;
- A, B ou C (selon l'axe concerné) : seule une des faces de la maille possède un nœud en son centre.

Tous les systèmes cristallins possèdent une forme primitive P mais pas tous les types de réseaux. L'ensemble des combinaisons système cristallin/type de maille aboutit aux 14 réseaux de Bravais (Figure 66).

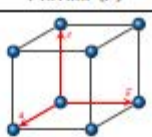
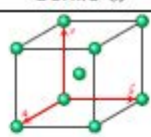
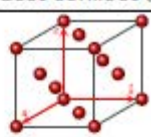
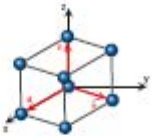
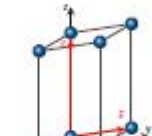
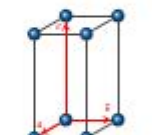
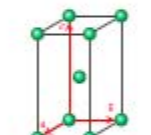
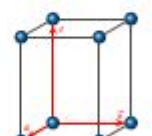
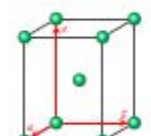
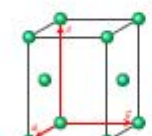
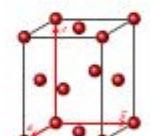
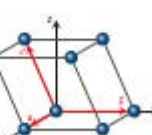
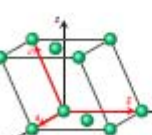

Multiplicité	m = 1	m = 2		m = 4
Type de réseau	Primitif (P)	Centré (I)	Bases centrées (C)	Faces centrées (F)
Cubique $a = b = c$ $\alpha = \beta = \gamma$				
Rhomboédrique $a = b = c$ $\alpha = \beta = \gamma \neq 90^\circ$				
Hexagonal $a = b \neq c$ $\alpha = \beta = 90^\circ$ $\gamma = 120^\circ$				
Quadratique $a = b \neq c$ $\alpha = \beta = \gamma = 90^\circ$				
Orthorhombique $a \neq b \neq c$ $\alpha = \beta = \gamma = 90^\circ$				
Monoclinique $a \neq b \neq c$ $\alpha = \gamma = 90^\circ$ $\beta \neq 90^\circ$				
Triclinique $a \neq b \neq c$ $\alpha \neq \beta \neq \gamma \neq 90^\circ$				

FIGURE 66 : LES 14 RÉSEAUX DE BRAVAIS

Enfin, le cristal est caractérisé par son groupe d'espace désignant l'ensemble des opérations de symétrie laissant invariante sa structure périodique. L'ensemble des combinaisons de tous les opérateurs de symétrie permet ainsi d'obtenir 230 groupes d'espace, compilés dans les tables internationales de cristallographie. Ces groupes décrits de façon purement mathématique, représentent les 230 façons de distribuer périodiquement des objets dans un espace triplement euclidien (Galiulin, 2003).

Du fait de l'invariance par translation, il existe une infinité de plans atomiques parallèles à un plan atomique donné. Si l'on considère un réseau de vecteurs de base \mathbf{a} , \mathbf{b} et \mathbf{c} , soit un plan d'équation normale :

$$h.x/\mathbf{a}+k.y/\mathbf{b}+l.z/\mathbf{c}=1$$

Les longueurs OA, OB et OC découpées par ce plan sur les axes valent : a/h , b/k et c/l .

Si le réseau est un réseau cristallin et A, B et C des nœuds de ce réseau, il peut être écrit :

$$OA = x = u \cdot \mathbf{a} \text{ (avec } u \text{ entier)}$$

$$OB = y = v \cdot \mathbf{b}$$

$$OC = z = w \cdot \mathbf{c}$$

L'équation de ce **plan réticulaire** est alors $h \cdot u + k \cdot v + l \cdot w = 1$. Le plan réticulaire étant défini comme un plan passant par au moins trois nœuds du réseau. Une infinité de plans parallèles à ce plan existe. Cette infinité de plans équidistants, désignés par les **indices de Miller** (=indices hkl) contient l'ensemble des nœuds du réseau.

Les indices de Miller d'une famille de plans réticulaires sont donc les inverses des longueurs découpées sur les axes par le premier plan de la famille ne contenant pas l'origine.

À ce réseau direct, ou réel, correspond un **réseau réciproque** de vecteurs \mathbf{a}^* , \mathbf{b}^* et \mathbf{c}^* définis tels que :

$$\mathbf{a} \cdot \mathbf{a}^* = \mathbf{b} \cdot \mathbf{b}^* = \mathbf{c} \cdot \mathbf{c}^* = 1$$

et

$$\mathbf{a} \cdot \mathbf{b}^* = \mathbf{a} \cdot \mathbf{c}^* = \mathbf{b} \cdot \mathbf{a}^* = \mathbf{b} \cdot \mathbf{c}^* = \mathbf{c} \cdot \mathbf{a}^* = \mathbf{c} \cdot \mathbf{b}^* = 0.$$

De cette première équation, il peut être déduit que les nœuds du réseau réciproque vérifient :

$$OO'^* = h\mathbf{a}^* + k\mathbf{b}^* + l\mathbf{c}^* \text{ (où } h, k \text{ et } l \text{ sont des nombres entiers et premiers entre eux, les indices de Miller).}$$

De la seconde équation, il ressort qu'un vecteur rangée du réseau réciproque est normal à un vecteur rangée du réseau réel.

B. Rappels généraux sur la diffraction

La définition traditionnelle du cristal comme étant la répétition triplement périodique d'un motif de base s'est récemment heurtée à la découverte d'objets présentant un ordre à grande distance sans répétition d'une maille comme les quasi-cristaux. La symétrie de translation de tels objets est retrouvée dans des espaces de dimension supérieure à celle de l'espace physique (Toudic, 2015). La diffraction des quasi-cristaux diffère radicalement de celles des autres cristaux, en présentant des symétries de rotation interdites *i.e* incompatibles avec le pavage d'espaces euclidiens (e.g symétries d'ordre 5 (Shechtman et al., 1984)).

Depuis 1992, les cristaux sont définis comme un matériel présentant un profil de diffraction essentiellement fin.

En ce sens, la diffraction mise en œuvre lors d'études cristallographiques par rayons X est rigoureusement analogue à celle observée avec de la lumière visible mais également avec des sons, des vagues ou encore des neutrons : c'est la signature de la nature ondulatoire d'un phénomène. La diffraction résulte de la rencontre d'une onde avec un obstacle ou une ouverture d'une grandeur comparable à celle de la longueur d'onde et se traduit par un étalement des directions de propagation de l'onde à la rencontre de cet objet diffractant. Le phénomène de diffraction est le résultat de l'interférence des ondes.

Thomas Young a démontré expérimentalement le caractère ondulatoire de la lumière au moyen du montage dit des fentes de Young (Figure 67). Dans cette expérience sur l'interférence, on considère une source ponctuelle de lumière monochromatique émettant des fronts d'onde semi-circulaires. Lorsque cette lumière atteint un écran portant deux fentes, elle est diffractée par chacune d'elles qui vont alors se comporter comme des sources secondaires de lumière (principe de Huygens-Fresnel). Les ondes lumineuses se propageant à partir de ces fentes se chevauchent alors et produisent des interférences. Ces interférences se manifestent où un écran intercepte la lumière sous la forme de franges brillantes et de franges sombres qui alternent.

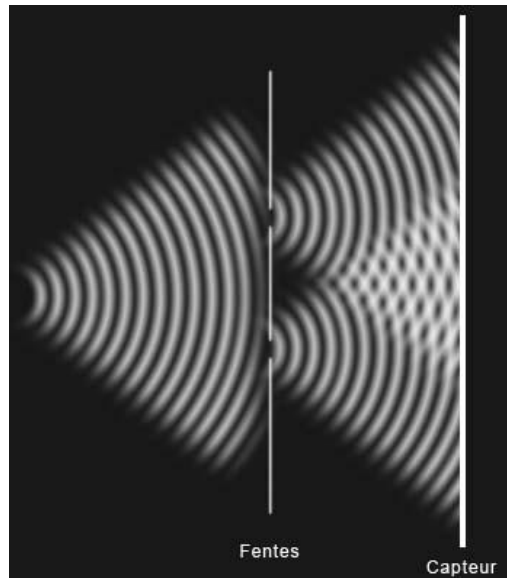


FIGURE 67: MONTAGE EXPÉRIMENTAL DÉRIVÉ DES FENTES DE YOUNG CARACTÉRISANT LES NOTIONS D'INTERFÉRENCE ET DE DIFFRACTION LUMINEUSES.

Lorsque les ondes passent à travers les deux fentes, elles sont en phase puisqu'elles font partie de la même onde incidente. Toutefois, après avoir traversé les fentes, les ondes qui en sont issues doivent parcourir des distances différentes pour atteindre un même point de l'écran. Cette différence de distance est désignée sous le terme de **différence de marche** (ΔL).

Lorsque ΔL est nulle ou égale à un nombre entier de longueurs d'onde, les ondes arrivent parfaitement en phase au point commun. L'interférence est constructive et il y a une frange claire.

A l'inverse, si ΔL correspond à un nombre impair de demies longueurs d'onde, les interférences sont destructives et la frange est sombre.

Pour analyser la structure interne de la matière, où les distances sont de l'ordre d'une dizaine d'Angstroms, il faut donc faire appel à des ondes d'une période avoisinante : les rayons X. Ainsi, la première analyse par diffraction des rayons X par von Laue démontre à la fois :

- la nature ondulatoire des rayons X, rayonnement découvert en 1895 par Wilhelm Röntgen (Prix Nobel de physique 1901) et dont la nature n'était pas encore connue ;
- que le cristal est bien formé d'un réseau périodique de particules.

Les éléments diffractants représentent les plans réticulaires régulièrement espacés de distances interréticulaires d_{hkl} telles que définies plus haut. L'image de diffraction d'une onde sur une distribution de matière correspond à la transformée de Fourier de cette distribution, ce qui revient à introduire un réseau dual du réseau réel appelé réseau réciproque. De la position des tâches peut être déduit le système cristallin et de l'intensité des tâches de diffraction sont retrouvées la nature et la position des atomes dans la maille.

C. Conditions de diffraction des rayons X par la matière cristallisée

L'interaction de faisceaux de rayons X avec la matière est à l'origine d'émissions dans toutes les directions d'un rayonnement de même longueur d'onde et de phase cohérente. Tandis que le phénomène livre des ondes de très faible amplitude dans le cas de la diffusion d'un atome ou d'un électron, la structure périodique de milieux cristallisés est à l'origine d'interférences d'ondes cohérentes qui engendrent des tâches de diffraction par analogie à l'expérience de Young décrite plus tôt.

La diffraction se produit à un angle déterminé par l'équidistance d_{hkl} des plans réticulaires comme indiqué sur la Figure 68.

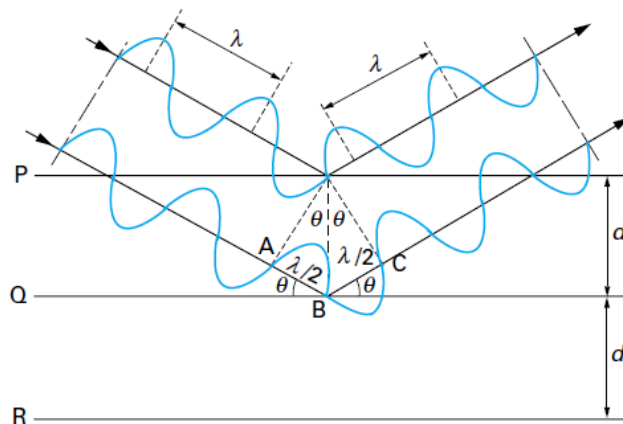


FIGURE 68 : GÉOMÉTRIE ILLUSTRANT LES CONDITIONS DE DIFFRACTION PAR LES RAYONS X (LOI DE BRAGG)

Les conditions de diffraction sont remplies lorsque la différence de marche (ΔL) entre les rayons ($AB + BC$) est égale à un nombre entier de longueurs d'onde, ce qui revient à écrire :

$$\Delta L = AB + BC = n\lambda \text{ (avec } n \text{ un nombre entier naturel)}$$

En ayant en même temps par trigonométrie :

$$AB + BC = 2d \cdot \sin\theta$$

Dès lors, la diffraction a lieu lorsque les conditions de Bragg sont vérifiées selon :

$$n\lambda = 2d \cdot \sin\theta.$$

Une expression équivalente à la loi de Bragg (dite condition de Laue) formule une condition nécessaire et suffisante pour qu'une onde soit diffractée par un réseau cristallin. A ces fins, Laue introduit un vecteur de diffraction ΔK exprimé comme étant la différence des vecteurs d'onde des faisceaux incident et diffusé.

$$\Delta K = K_d - K_i = d^*_{hkl}$$

Il y a diffraction si le vecteur de diffraction ΔK est un vecteur du réseau réciproque (si les extrémités des vecteurs d'onde incidents et diffractés sont des nœuds du réseau réciproque) (Figure 69).

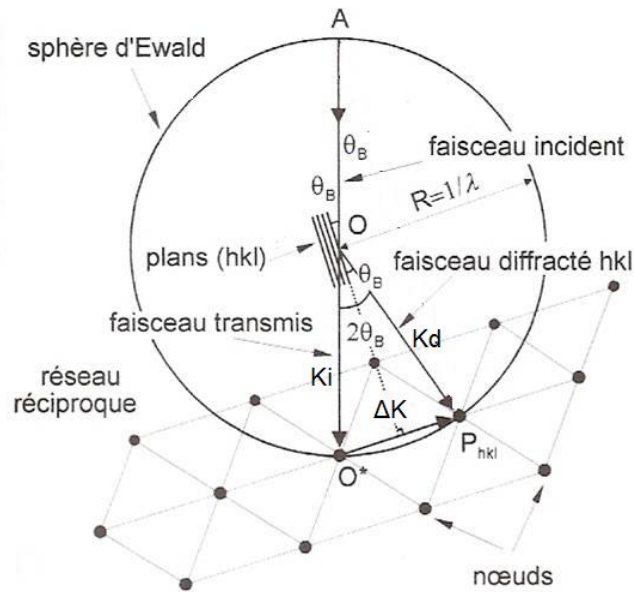


FIGURE 69: SCHÉMA ILLUSTRANT LES CONDITIONS DE DIFFRACTION DE LAUE

De là, il est aisément démontré que tous les points hkl du réseau réciproque croisant la sphère de rayon $1/\lambda$, dite sphère d'Ewald (Figure 70), répondent à l'équation de Bragg :

$$d_{hkl} = 2 \sin \theta / \lambda \text{ (Bragg) avec } d_{hkl}^* = 1/d_{hkl}$$

$$d_{hkl}^* = 2x \cdot \sin \theta \text{ (Laue).}$$

Ce qui revient à $x = 1/\lambda$.

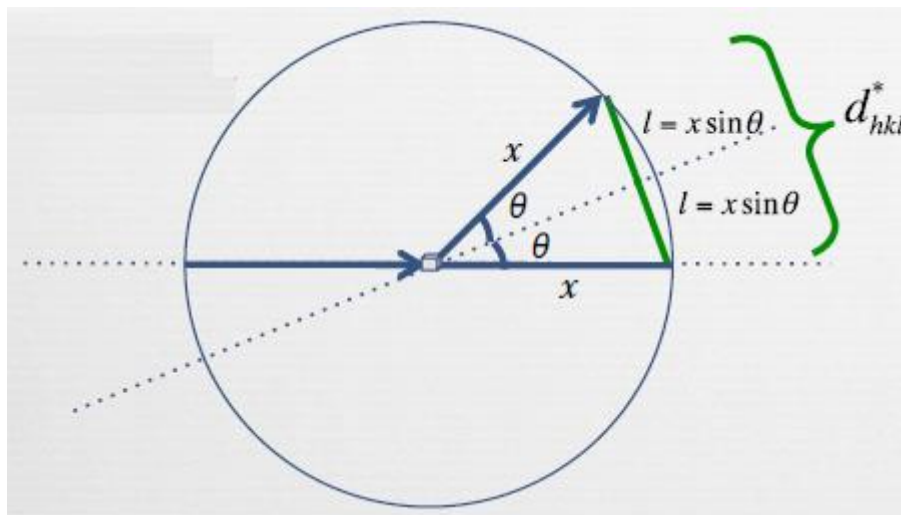


FIGURE 70: DÉTERMINATION DU RAYON DE LA SPHÈRE D'EWALD

D. Techniques de diffraction de rayons X

La mise en œuvre expérimentale d'analyses par diffraction de rayons X peut se faire selon deux approches différentes :

- L'analyse de monocristal (de dimensions généralement submillimétriques)
- L'analyse de poudres cristallines (ensemble de microcristaux orientés aléatoirement).

a. Diffraction de monocristal

En diffraction de monocristal, le cristal sélectionné est monté sur une tête goniométrique permettant sa rotation dans les trois directions de l'espace pour faire varier l'angle θ . Les tâches de diffraction qui vont être observées correspondent à l'ensemble des vecteurs de diffraction ΔK satisfaisant les conditions de Laue définies plus haut. Il s'agit donc de considérer dans l'espace du réseau réciproque la sphère de rayon $1/\lambda$ centrée sur le cristal (sphère d'Ewald) qui, selon la direction de diffraction par rapport au réseau du cristal, va pouvoir intercepter différents nœuds du réseau réciproque. À chacune de ces coïncidences, le vecteur de diffraction correspond à un vecteur reliant l'origine du réseau réciproque à l'un de ces nœuds et est objectivé par une tâche de diffraction (Figure 71).

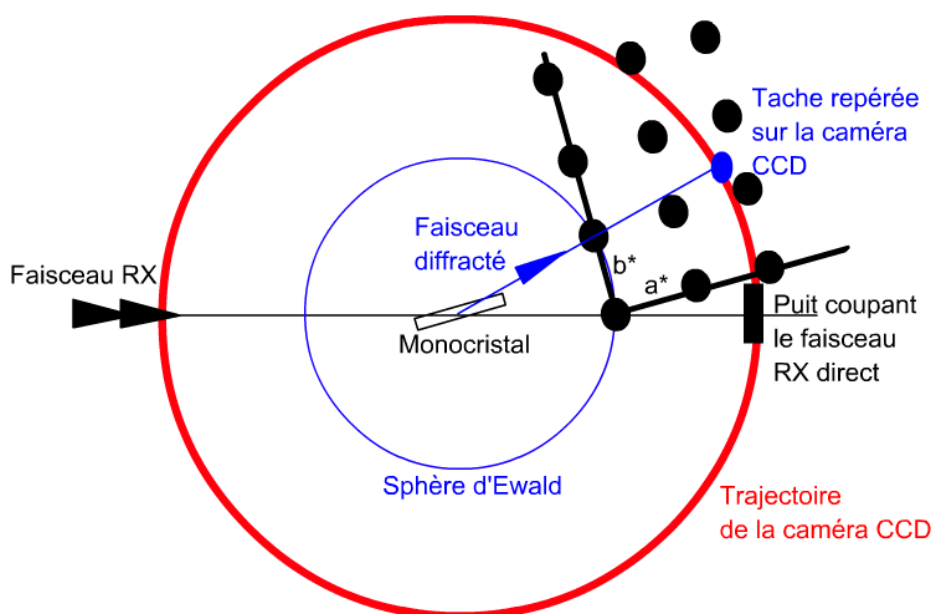


FIGURE 71 : FORMATION DES TÂCHES DE DIFFRACTION LORS DE LA ROTATION DU MONOCRISTAL (REPRÉSENTATION 2D). FIGURE TIRÉE DE [HTTP://CULTURESCIENCESPHYSIQUE.ENS-LYON.FR/RESSOURCE/DIFFRACTION-RAYONS-X-TECHNIQUES-DETERMINATION-STRUCTURE.XML](http://culturesciencesphysique.ens-lyon.fr/ressource/diffraction-rayons-x-techniques-determination-structure.xml)

Le traitement numérique des positions observées des tâches de diffraction et de leurs intensités permet de remonter à la structure complète de la molécule.

b. Diffraction sur poudres

Si l'échantillon n'est pas monocristallin, il est possible d'avoir recours à la technique de diffraction sur poudre. Ces poudres étant constituées de microcristaux se présentant dans toutes les orientations cristallines possibles, l'espace réciproque peut être projeté selon une seule dimension (Figure 72).

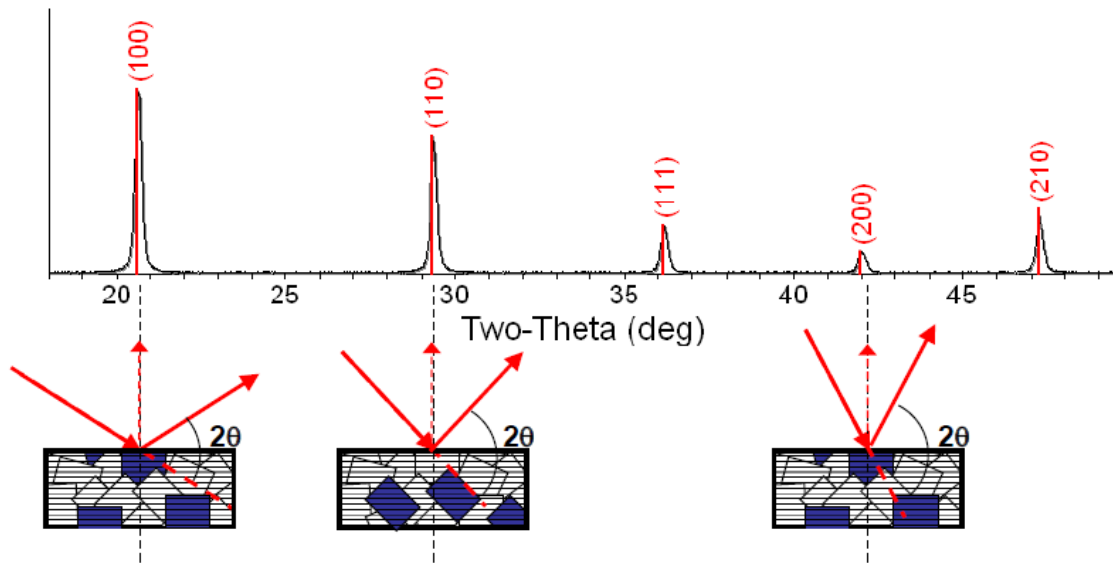


FIGURE 72: DIFFRACTOGRAMME SUR POUDRE D'ÉCHANTILLONS MICROCRISTALLINS

En conséquence, l'échantillon est placé au centre d'un goniomètre et le balayage de l'angle de diffraction est réalisé par exemple selon une géométrie de réflexion dite Bragg-Brentano (plus communément θ - 2θ ou θ - θ) qui assure une rotation à vitesse angulaire constante θ de l'échantillon tandis que le détecteur avec sa fente réceptrice placée sur le point de focalisation tourne autour de l'échantillon avec une vitesse 2θ . L'ensemble des données associé à ces analyses peut être synthétisé dans un diffractogramme reliant l'intensité détectée à l'angle de déviation 2θ .

Chaque composant cristallin est à l'origine d'un ensemble de pics unique dans le diffractogramme. Par conséquent, la confrontation du diffractogramme d'un mélange de cristaux à celui des différents composés purs doit permettre d'identifier les constituants cristallins d'un mélange de composition inconnue (Hulien et al., 2015) (Figure 73).

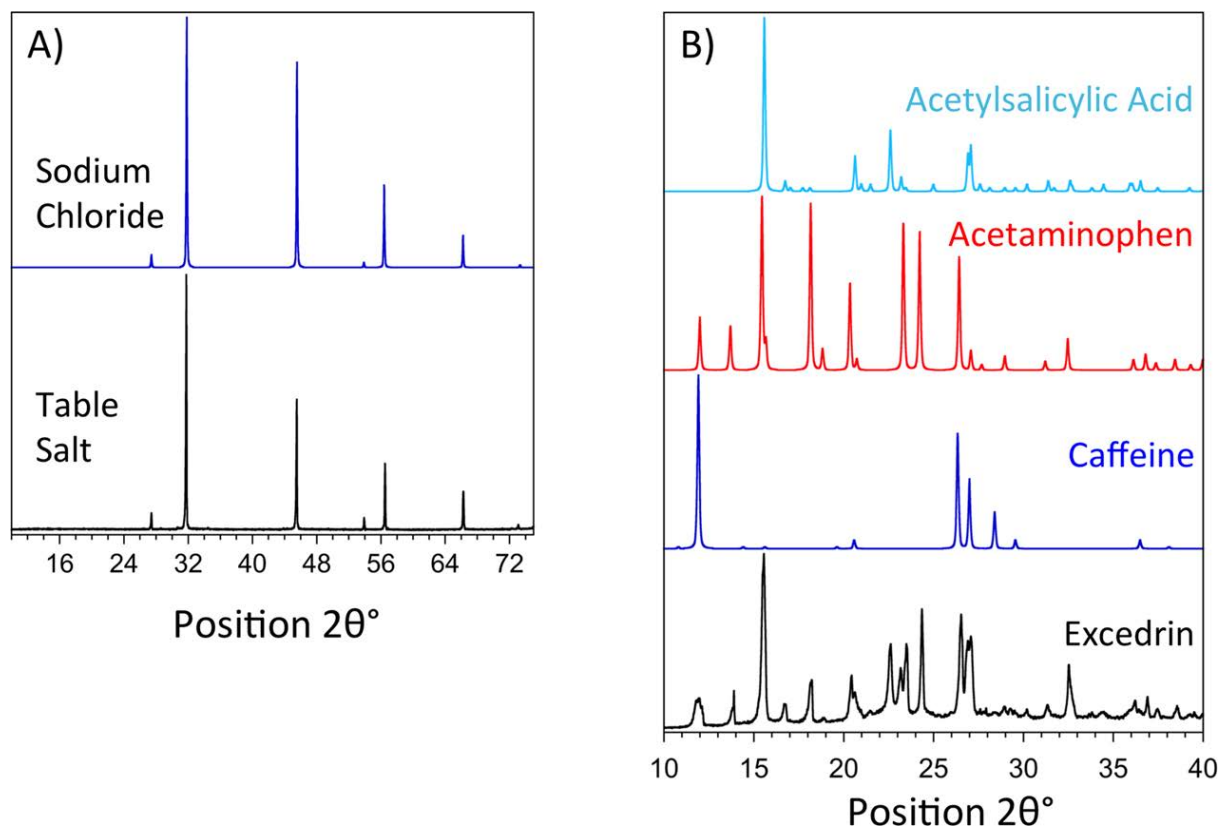


FIGURE 73: DIFFRACTOGRAMME DE POUDRES AUX RAYONS X DE SELS DE TABLE ET DE LA SPÉCIALITÉ EXCEDRIN°. LES DIFFRACTOGRAMMES DE RÉFÉRENCE ASSOCIÉS AUX PRODUITS CRISTALLINS PURS SONT FOURNIS SUR LE DIFFRACTOGRAMME TOTAL. LES ORDONNÉES PRÉSENTENT L'INTENSITÉ DU SIGNAL DE DIFFRACTION, NORMALISÉ SUR LE SIGNAL LE PLUS INTENSE (HULIEN ET AL., 2015).

Annexe 3 : Supporting Material TLC-MS draft

Mass spectrometry as a versatile ancillary technique for the rapid *in situ* identification of lichen metabolites directly from TLC plates

Pierre Le Pogam, Aline Pillot, Françoise Le Dévéhat, Anne-Cécile Le Lamer, Béatrice Legouin, Aurélie Sauvager, Alice Gadea, Damien Ertz, Joël Boustie

Analytical process of TLC/MS hyphenation

The hyphenation of TLC with mass spectrometry long represented an analytical challenge as the analytes remain adsorbed at the surface of the silica plate after the migration unlike column-based chromatographic techniques in which compounds are eluted due to a gas or liquid flow. A possible way to solve the apparent incompatibility between the static planar chromatography and the need for a stable supply of liquid sample into the mass spectrometer was the development of elution-based techniques to transfer the TLC-separated compounds into a solvent stream (Morlock & Schwack 2010). A prototype developed and reported by Luftmann in 2004 first addressed this shortcoming with a TLC-MS interface that mostly consisted of a stainless steel plunger that contains a solvent inlet and an outlet capillary (Luftmann 2004). This elution head can be pressed onto the region of interest of the plate to form a tight seal with the carrier foil owing to its cutting edge. The solvent can enter the desorption area through a small hole present at the periphery of the disk when the valve is switched to elution mode, dissolve the compounds and be forwarded to the mass spectrometer via the outlet capillary. A frit is present at the entrance of this latter to prevent silica particles from clogging downwards (Luftmann *et al.* 2007). From the proof-of-concept described by Luftmann, the commercially available devices include several improvements comprising a laser-light cross to target more accurately the zone to be desorbed. An automated cleaning of the elution head through N₂ flux can be performed on commercial interfaces to eliminate residual clumpy layer particles that might remain at the surface of the cutting edge (Morlock & Schwack 2010). An insight into the TLC/MS interface used in this work is presented in Figure 1.

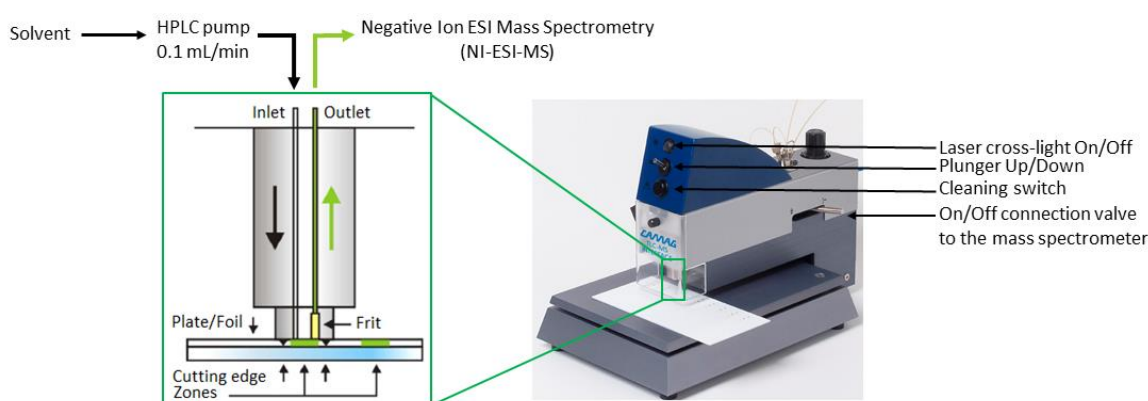


Figure S1: Overview of the TLC-MS interface available from CAMAG (images taken from CAMAG website <http://www.copybook.com/pharmaceutical/companies/camag/articles/tlc-mass-spectrometry>). When the elution head is lowered and the valve switched to elution mode, the solvents move through the head and elute the zone previously positioned by the laser crosshairs. The extracted compound is then transferred online into the mass spectrometer but can also be collected in a vial for further offline analyses. When the valve is in bypass position, the solvent flow is directed into the mass spectrometer.

During the analysis of an extract, several mass spectrometric detection can be achieved on different spots of the plates. The ionization process is monitored in real time through the Total Ion Chromatogram (TIC) which is a chromatogram obtained by summing up intensities of all mass spectral peaks belonging to the same scan. Mass spectra can then be retrieved by left dragging along the TIC regions of interest. As recommended elsewhere, the impact of background signals originating from the plate and solvent residues on the mass spectra was reduced by subtracting a background

mass spectrum obtained from a blank position of the plate (Morlock 2014; Taha *et al.* 2015). Afterwards, when screening for a specific signal (e.g quasi-molecular ion of an expected metabolite), Reconstructed Ion Chromatogram (RIC) can be retrieved for a particular m/z value. This function is also of interest when the signal to noise ratio (S/N) is poor and it is questionable whether the peaks are related to genuine molecules or to artefacts. Hence, if signals are ascribed to a single desorption area, it can reliably be assigned to an authentic molecule signal. Adversely, if the Reconstructed Ion Chromatogram results in a permanent signal or in a peak present at each desorption spot, it can be assumed that it corresponds to an artefact. This whole analytical process is presented in Figure 2, illustrated by the example of *Pertusaria amara* chemical profiling.

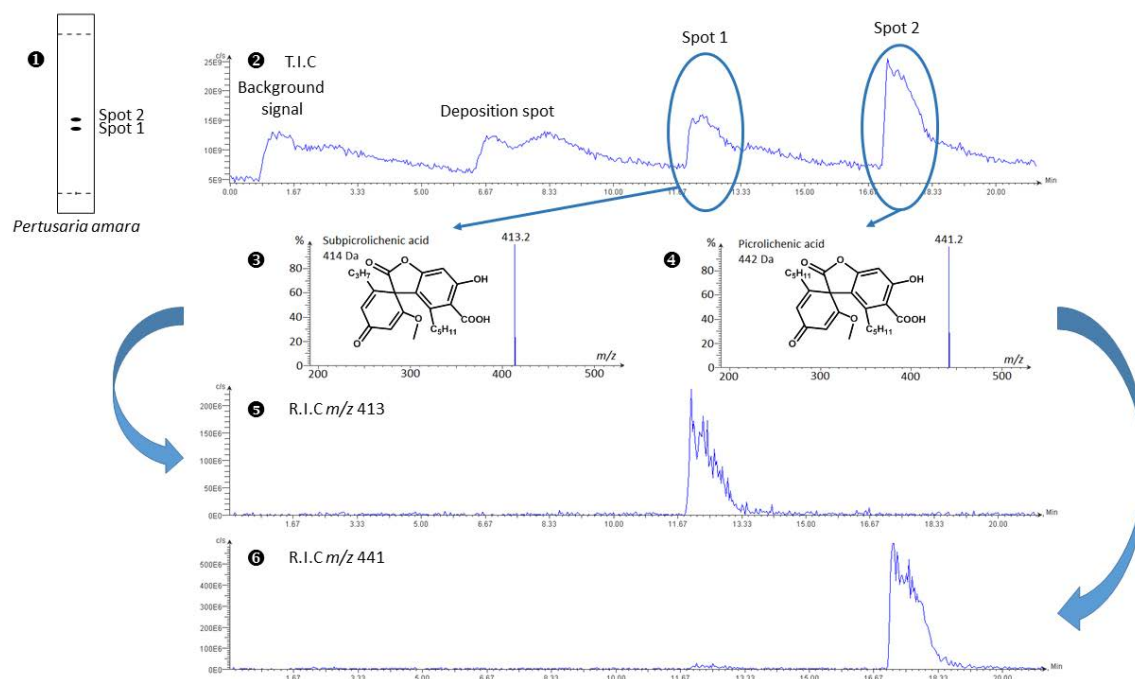


Figure S2 : Workflow diagram of TLC-MS analysis: chemical profiling of *Pertusaria amara*. TLC of the crude acetone extract of *P. amara* (1), Total Ion Chromatogram obtained from the TLC-NI-ESI-MS analysis of *P. amara* (2), NI-ESI mass spectrum retrieved from Spot 1 (Subpicrolichenic acid, 3) and Spot 2 (Picrolichenic acid, 4) and Reconstructed Ion Chromatograms retrieved from m/z 413 (5) and m/z 441 (6).

Settings of DART-MS analyses

DART-HRMS analyses were performed using a JEOL JMS-T100CS (AccuTOF CS) orthogonal time-of-flight (TOF) mass spectrometer (Peabody, MA) equipped with an IonSense DART Source (Danvers, MA). Ultra-high purity helium was used as reagent gas at a flow rate of 4 L min^{-1} and under a temperature value of 523 K. The following DART-needle, discharge electrode, and the grid electrode voltage values used were 3500, 150, and 250 V, respectively. The voltage values of orifice 1, orifice 2, and the ring lens were set at 15, 5, and 10 V, respectively. The orifice 1 temperature was kept at 353 K. The detector voltage was set at 2300 V. The mass spectra were recorded every second with a resolution of 6000 (fwhm definition). The mass scale was calibrated using the $[M-H]^-$ ion series of a poly(ethyleneglycol) sulfate diluted in a $\text{CH}_2\text{Cl}_2/\text{MeOH}$ mixture (1:1). To perform accurate mass measurements, the mass drift compensation procedure available on the main program that controls the AccuTOF CS was used to compensate for the m/z drift in the range of m/z 100 to 500. DART-MS analysis of the intact pieces of *Usnea trachycarpa* were performed by holding unprocessed pieces of lichen between tweezers directly under the helium stream.

DART-MS analysis of *Usnea trachycarpa*

To retrieve the elemental composition of the unknown compound of *Usnea trachycarpa*, a DART-HRMS analysis was attempted from the whole lichen. From an intact piece of *Usnea trachycarpa*, negative-ion mode (NI) DART-MS displayed signals that could be attributed to all paraconic acids detected using the TLC-MS approach. The corresponding mass spectrum is presented in Figure S1 and the associated exact mass measurements are collated in Table S1.

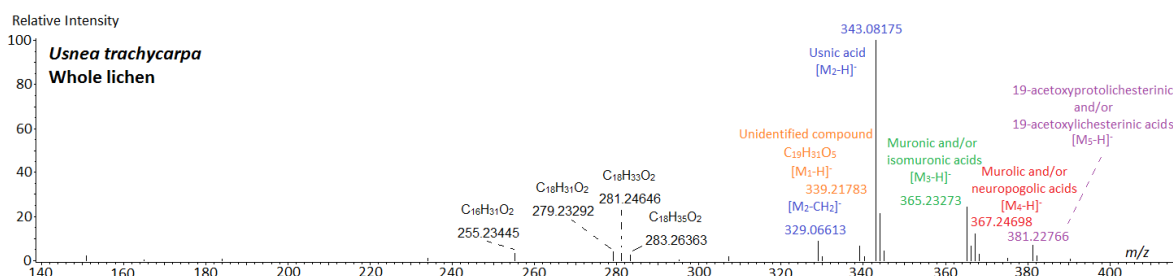


Figure S3 : Negative-ion mode DART-MS spectrum of a solid piece of *Usnea trachycarpa*.

Table S1: Results of exact mass measurements performed from the mass spectrum of the Fig. S3 related to the NI-DART-MS of a whole piece of *Usnea trachycarpa*.

Measured mass	Proposed formulae	Calculated mass (error in ppm)	Assignment
255.23445	C ₁₆ H ₃₁ O ₂	255.23240 (8.03)	C ₁₆ :0
279.23292	C ₁₈ H ₃₁ O ₂	279.23240 (1.86)	C ₁₈ :2
281.24646	C ₁₈ H ₃₃ O ₂	281.24805 (-5.66)	C ₁₈ :1
283.26363	C ₁₈ H ₃₅ O ₂	283.26370 (-0.27)	C ₁₈ :0
329.06727	C ₁₇ H ₁₃ O ₇	329.06613 (3.47)	Fragment of usnic acid
339.21783	C₁₉H₃₁O₅	339.21715 (2.00)	Unknown compound
343.08175	C ₁₈ H ₁₅ O ₇	343.08178 (-0.07)	Usnic acid
365.23273	C ₂₁ H ₃₃ O ₅	365.23280 (-0.17)	Murolic/Isomurolic acid(s)
367.24698	C ₂₁ H ₃₅ O ₅	367.24845 (-4.00)	Murolic/Neuropogolic acid(s)
381.22766	C ₂₁ H ₃₃ O ₆	381.22771 (-0.15)	19- acetoxyprotolichesterinic/19- acetoxylichesterinic acid(s)

Annexe 4 : Supporting Material Phytochem. Anal. 2016; 27: 354-363.

In situ DART-MS as a versatile and rapid dereplication tool in lichenology: chemical fingerprinting of the chlorolichen *Ophioparma ventosa*

Pierre Le Pogam¹, Anne-Cécile Le Lamer^{1,2*}, Béatrice Legouin¹, Joël Boustie¹, David Rondeau^{3,4*}

¹ Laboratoire de Pharmacognosie, Equipe PNSCM, (ISCR UMR CNRS 6226), Faculté des Sciences Pharmaceutiques et Biologiques, 2 av. du Pr Léon-Bernard, 35042, Rennes Cedex, France

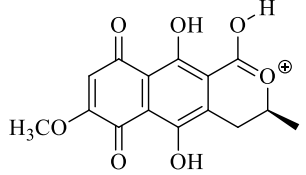
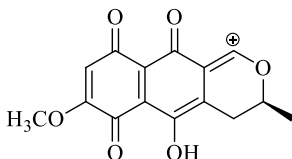
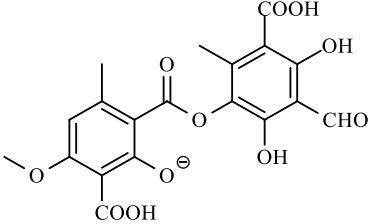
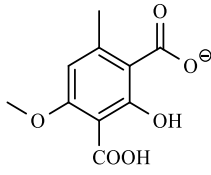
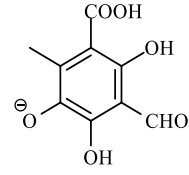
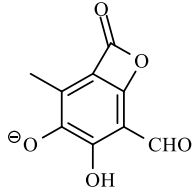
² Université Paul Sabatier Toulouse 3, 118 Route de Narbonne, 31062, Toulouse Cedex 09, France

³ Institut d'Electronique et de Télécommunication de Rennes (IETR UMR CNRS 6164), Université de Rennes 1, Campus de Beaulieu, 263 Avenue du General Leclerc, 35042, Rennes Cedex, France

⁴ Université de Bretagne Occidentale, Département de Chimie, 6 avenue le Gorgeu, 29238, Brest Cedex 03, France

E-mail : anne-cecile.le-lamer@univ-tlse3.fr; david.rondeau@univ-rennes1.fr.

Table S5 Retention times (RT), structures of parent and product ions detected in LC-MS-MS analysis of an *Ophioparma ventosa* acetone extract. Note that R.I. represents the Relative Intensity of the product ions detected in MS-MS mode. * Analysis performed in positive-ion mode.

No.	Compound name (R.T.)	Proposed structure for the detected parent ion (m/z)	Proposed structure for the product ions at 35 eV of collision energy (m/z; R.I. %)		
1*	Haemoventosin (9.1 min.)	 <p>(m/z 305)</p>	 <p>(m/z 287 ; 100)</p>		
2	Thamnolic acid (10.3 min.)	 <p>(m/z 419)</p>	 <p>(m/z 225 ; 49)</p>	 <p>(m/z 211 ; 100)</p>	 <p>(m/z 193 ; 10)</p>
3	Unassigned signals (14.2 min.)	(m/z 457)	(m/z 251 ; 23), (m/z 223 ; 100), (m/z 205 ; 9)		

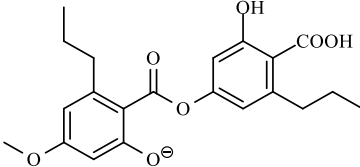
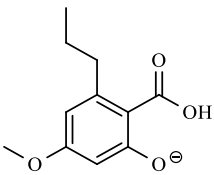
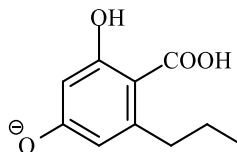
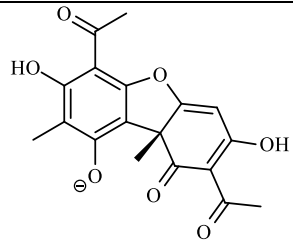
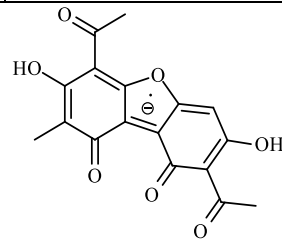
<p>4</p>	<p>Divaricatic acid (14.6 min.)</p>	 <p>(<i>m/z</i> 387)</p>	 <p>(<i>m/z</i> 209 ; 0.9)</p>	 <p>(<i>m/z</i> 195 ; 100)</p>
<p>5</p>	<p>Usnic acid (15.8 min.)</p>	 <p>(<i>m/z</i> 343)</p>	 <p>(<i>m/z</i> 328 ; 8)</p>	

Table S2 Results of exact mass measurements in negative-ion mode DART-HRMS of single molecules.

Compound	Measured Mass	Proposed formulae	Calculated Mass (error in ppm)
Usnic acid	343.08259	C ₁₈ H ₁₅ O ₇	343.08233 (0.75)
	329.06914	C ₁₇ H ₁₃ O ₇	329.06668 (7.47)
Stictic acid	385.05742	C ₁₉ H ₁₃ O ₉	385.05651 (2.36)
Norstictic acid	371.03964	C ₁₈ H ₁₅ O ₈	371.04086 (3.29)
Psoromic acid	357.06230	C ₁₈ H ₁₃ O ₈	357.06159 (1.98)
Haemoventosin	305.06612	C ₁₅ H ₁₃ O ₇	305.06668 (1.83)
	304.05670	C ₁₅ H ₁₂ O ₇	304.05885 (7.07)
	303.04957	C ₁₅ H ₁₁ O ₇	303.05100 (4.72)
	302.04368	C ₁₅ H ₁₀ O ₇	302.04265 (3.39)
Atranorin	373.09263	C ₁₉ H ₁₇ O ₈	373.09289 (0.69)
	195.04498	C ₁₃ H ₇ O ₂ *	195.04406 (4.71)
	177.01907	C ₉ H ₅ O ₄	177.01824 (4.69)
	163.03933	C ₉ H ₇ O ₃	163.03897 (2.21)
Thamnolic/ Decarboxythamnolic acids	375.07227	C ₁₈ H ₁₅ O ₉	375.07216 (0.29)
	331.08096	C ₁₇ H ₁₅ O ₇	331.08233 (4.13)
	225.04199	C ₁₀ H ₉ O ₆	225.04046 (6.79)
	211.02463	C ₉ H ₇ O ₆	211.02481 (0.85)
	181.05082	C ₉ H ₉ O ₄	181.05063 (1.05)
	167.03616	C ₈ H ₇ O ₄	167.03498 (7.06)
	137.06014	C ₈ H ₉ O ₂	137.06080 (4.81)
Divaricatic acid	387.14340	C ₂₁ H ₂₃ O ₇	387.14493 (3.95)
	343.15524	C ₂₀ H ₂₃ O ₅	343.15510 (0.40)
	209.08192	C ₁₁ H ₁₃ O ₄	209.08193 (0.04)
	195.06620	C ₁₀ H ₁₁ O ₄	195.06628 (0.41)
	165.09106	C ₁₀ H ₁₃ O ₂	165.09210 (6.29)
	151.07570	C ₉ H ₁₁ O ₂	151.07645 (4.96)

*Formula not consistent with atranorin structure

Table S3 Results of exact mass measurements in positive-ion mode DART-HRMS for single molecules.

Compound	Measured Mass	Proposed formulae	Calculated Mass (error in ppm)
Usnic acid	345.09724	C ₁₈ H ₁₇ O ₇	345.09688 (1.04)
	327.08650	C ₁₈ H ₁₅ O ₆	327.08631 (0.58)
Stictic acid	387.07094	C ₁₉ H ₁₅ O ₉	387.07106 (0.31)
Norstictic acid	373.05541	C ₁₈ H ₁₃ O ₉	373.05580 (1.04)
Psoromic acid	359.07610	C ₁₈ H ₁₅ O ₈	359.07614 (0.11)
Haemoventosin	307.07998	C ₁₅ H ₁₅ O ₇	307.08123 (4.07)
	305.06627	C ₁₅ H ₁₃ O ₇	305.06558 (2.26)
	303.05018	C ₁₅ H ₁₁ O ₇	303.04993 (0.82)
Atranorin	375.10799	C ₁₉ H ₁₉ O ₈	375.10744 (1.46)
	197.07926	C ₁₀ H ₁₃ O ₄	197.08084 (8.01)
	179.03398	C ₉ H ₇ O ₄	179.03389 (0.50)
	165.05736	C ₉ H ₉ O ₃	165.05462 (16.60)
Thamnolic / Decarboxythamnolic acid	377.08736	C ₁₈ H ₁₇ O ₉	377.08671 (1.72)
	227.05557	C ₁₀ H ₁₁ O ₆	227.05501 (2.46)
	209.04443	C ₁₀ H ₉ O ₅	209.04445 (0.09)
	191.03417	C ₁₀ H ₇ O ₄	191.03389 (1.46)
	169.05324	C ₈ H ₉ O ₄	169.04954 (21.88)
Divaricatic acid	165.05963	C ₉ H ₉ O ₃	165.05462 (30.35)
	211.09664	C ₁₁ H ₁₅ O ₄	211.09649 (0.71)
	197.08081	C ₁₀ H ₁₃ O ₄	197.08084 (0.15)
	193.08628	C ₁₁ H ₁₃ O ₃	193.08592 (1.86)
	167.10663	C ₁₀ H ₁₅ O ₂	167.10666 (0.18)
153.09102	C ₉ H ₁₃ O ₂	153.09101 (0.06)	

Table S4 Results of exact mass measurements performed from the mass spectrum of the Fig. 6A related to the NI-DART-MS analysis of crushed whole *Ophioparma ventosa*.

Measured mass	Proposed formulae	Calculated mass
167.03437	C ₈ H ₇ O ₄	167.03498 (3.65)
195.06722	C ₁₀ H ₁₁ O ₄	195.06628 (4.81)
209.08288	C ₁₁ H ₁₃ O ₄	209.08193 (4.54)
223.09889	C ₁₂ H ₁₅ O ₄	223.09758 (5.87)
225.04180	C ₁₀ H ₉ O ₆	225.04046 (5.95)
251.09130	C ₁₃ H ₁₅ O ₅	251.09250 (4.77)
255.23272	C ₁₆ H ₃₁ O ₂	255.23296 (0.94)
279.23540	C ₁₈ H ₃₁ O ₂	279.23296 (8.74)
281.24930	C ₁₈ H ₃₃ O ₂	281.24861 (2.45)
283.26310	C ₁₈ H ₃₅ O ₂	283.26426 (4.09)
303.05054	C ₁₅ H ₁₁ O ₇	303.05103 (1.61)
305.06661	C ₁₅ H ₁₃ O ₇	305.06668 (0.22)
331.08279	C ₁₇ H ₁₅ O ₇	331.08233 (1.39)
343.08273	C ₁₈ H ₁₅ O ₇	343.08233 (1.16)
375.07291	C ₁₈ H ₁₅ O ₉	375.07216 (1.99)
387.14849	C ₂₁ H ₂₃ O ₇	387.14493 (9.19)

Table S5 Results of exact mass measurements performed from the mass spectrum of the Fig. 6B related to the PI-DART-MS analysis of crushed whole *Ophioparma ventosa*.

Measured mass	Proposed formulae	Calculated mass (error in ppm)
167.10566	C ₁₀ H ₁₅ O ₂	167.10666 (5.98)
169.05090	C ₈ H ₉ O ₄	169.04954 (8.04)
193.08954	C ₁₁ H ₁₃ O ₃	193.08592 (18.74)
197.08045	C ₁₀ H ₁₃ O ₄	197.08084 (1.97)
211.09804	C ₁₁ H ₁₅ O ₄	211.09649 (7.34)
225.11284	C ₁₂ H ₁₇ O ₄	225.11214 (3.11)
235.09309	C ₁₃ H ₁₅ O ₄	235.09649 (14.46)
227.05729	C ₁₀ H ₁₁ O ₆	227.05501 (10.04)
253.10878	C ₁₃ H ₁₇ O ₅	253.10705 (6.83)
303.05066	C ₁₅ H ₁₁ O ₇	303.04993 (2.41)
305.06597	C ₁₅ H ₁₃ O ₇	305.06558 (1.28)
307.08035	C ₁₅ H ₁₅ O ₇	307.08123 (2.86)
345.09706	C ₁₈ H ₁₇ O ₇	345.09688 (0.52)
377.08785	C ₁₈ H ₁₇ O ₉	377.08671 (3.02)
405.31938	C ₂₂ H ₄₅ O ₆	405.32107 (4.17)

Table S6 Results of exact mass measurements performed from the mass spectrum of the Fig. S8A related to the NI-DART-MS analysis of miriquidic acid.

Measured mass	Proposed formulae	Calculated mass (error in ppm)
179.10794	C ₁₁ H ₁₅ O ₂	179.10775 (1.06)
207.10215	C ₁₂ H ₁₅ O ₃	207.10267 (2.51)
223.09726	C ₁₂ H ₁₅ O ₄	223.09758 (1.43)
251.09204	C ₁₃ H ₁₅ O ₅	251.09250 (1.83)

Table S7 Results of exact mass measurements performed from the mass spectrum of the Fig. S8B related to the PI-DART-MS analysis of miriquidic acid.

Measured mass	Proposed formulae	Calculated mass (error in ppm)
181.12132	C ₁₁ H ₁₇ O ₂	181.12231 (5.47)
209.11739	C ₁₂ H ₁₇ O ₃	209.11722 (0.81)
225.11319	C ₁₂ H ₁₇ O ₄	225.11214 (4.66)
235.09703	C ₁₃ H ₁₅ O ₄	235.09649 (2.29)
253.10760	C ₁₃ H ₁₇ O ₅	253.10705 (2.17)

Table S8 Results of exact mass measurements performed from the mass spectrum of the Fig. S9A related to the NI-DART-MS analysis of a whole apothecium of *Ophioparma ventosa*.

Measured mass	Proposed formulae	Calculated mass (error in ppm)
167.03343	C ₈ H ₇ O ₄	167.03498 (9.27)
195.06682	C ₁₀ H ₁₁ O ₄	195.06628 (2.76)
209.08242	C ₁₁ H ₁₃ O ₄	209.08193 (2.34)
225.03991	C ₁₀ H ₉ O ₆	225.04046 (2.44)
303.05158	C ₁₅ H ₁₁ O ₇	303.05103 (1.81)
305.06633	C ₁₅ H ₁₃ O ₇	305.06668 (1.14)
329.06685	C ₁₇ H ₁₃ O ₇	329.06668 (0.51)
343.08233	C ₁₈ H ₁₅ O ₇	343.08233 (0.00)
375.07107	C ₁₈ H ₁₅ O ₉	375.07216 (2.90)
387.14363	C ₂₁ H ₂₃ O ₇	387.14493 (3.35)

Table S9 Results of exact mass measurements performed from the mass spectrum of the Fig S9B related to the PI-DART-MS analysis of a whole apothecium of *Ophioparma ventosa*.

Measured mass	Proposed formulae	Calculated mass (error in ppm)
153.08907	C ₉ H ₁₃ O ₂	153.09101 (12.67)
167.10675	C ₁₀ H ₁₅ O ₂	167.10666 (0.54)
169.04942	C ₈ H ₉ O ₄	169.04954 (0.71)
193.08634	C ₁₁ H ₁₃ O ₃	193.08592 (2.17)
197.08157	C ₁₀ H ₁₃ O ₄	197.08084 (3.70)
209.04645	C ₁₀ H ₉ O ₅	209.04445 (9.56)
211.09657	C ₁₁ H ₁₅ O ₄	211.09649 (0.38)
227.05567	C ₁₀ H ₁₁ O ₆	227.05501 (2.90)
303.04973	C ₁₅ H ₁₁ O ₇	303.04993 (0.65)
305.06488	C ₁₅ H ₁₃ O ₇	305.06558 (2.29)
307.08035	C ₁₅ H ₁₅ O ₇	307.08123 (2.86)
345.09792	C ₁₈ H ₁₇ O ₇	345.09688 (3.01)
377.09027	C ₁₈ H ₁₇ O ₉	377.08671 (9.44)
405.32290	C ₂₂ H ₄₅ O ₆	405.32107 (4.51)

Table S10 Results of exact mass measurements performed from the mass spectrum of the Fig. S10A related to the NI-DART-MS analysis of a whole piece of thallus of *Ophioparma ventosa*.

Measured mass	Proposed formulae	Calculated mass (error in ppm)
167.03526	C ₈ H ₇ O ₄	167.03498 (1.67)
195.06554	C ₁₀ H ₁₁ O ₄	195.06628 (3.79)
209.08198	C ₁₁ H ₁₃ O ₄	209.08193 (0.23)
211.02481	C ₉ H ₇ O ₆	211.02413 (3.22)
225.04131	C ₁₀ H ₉ O ₆	225.04046 (3.77)
329.06615	C ₁₇ H ₁₃ O ₇	329.06668 (1.61)
343.08178	C ₁₈ H ₁₅ O ₇	343.08233 (1.60)
375.07147	C ₁₈ H ₁₅ O ₉	375.07216 (1.83)

Table S11 Results of exact mass measurements performed from the mass spectrum of the Fig. S10B related to the PI-DART-MS analysis of a whole piece of thallus of *Ophioparma ventosa*.

Measured mass	Proposed formulae	Calculated mass (error in ppm)
153.09005	C ₉ H ₁₃ O ₂	153.09101 (6.27)
167.10730	C ₁₀ H ₁₅ O ₂	167.10666 (3.82)
169.05152	C ₈ H ₉ O ₄	169.04954 (11.71)
193.08610	C ₁₁ H ₁₃ O ₃	193.08592 (0.93)
197.08104	C ₁₀ H ₁₃ O ₄	197.08084 (1.01)
211.09674	C ₁₁ H ₁₅ O ₄	211.09649 (1.18)
345.09743	C ₁₈ H ₁₇ O ₇	345.09688 (1.59)

Table S12 Results of exact mass measurements performed from the mass spectrum of the Fig. S11A related to the NI-DART-MS analysis of crushed thallus of *Ophioparma ventosa*.

Measured mass	Proposed formulae	Calculated mass (error in ppm)
167.03484	C ₈ H ₇ O ₄	167.03498 (0.84)
195.06661	C ₁₀ H ₁₁ O ₄	195.06628 (1.69)
209.08204	C ₁₁ H ₁₃ O ₄	209.08193 (0.53)
223.09806	C ₁₂ H ₁₅ O ₄	223.09758 (2.15)
225.04180	C ₁₀ H ₉ O ₆	225.04046 (5.95)
251.09225	C ₁₃ H ₁₅ O ₅	251.09250 (0.99)
255.23272	C ₁₆ H ₃₁ O ₂	255.23296 (0.94)
279.23370	C ₁₈ H ₃₁ O ₂	279.23296 (2.65)
281.25050	C ₁₈ H ₃₃ O ₂	281.24861 (6.72)
283.26470	C ₁₈ H ₃₅ O ₂	283.26426 (1.55)
329.06541	C ₁₇ H ₁₃ O ₇	329.06668 (3.86)
343.08199	C ₁₈ H ₁₅ O ₇	343.08233 (0.99)
375.07146	C ₁₈ H ₁₅ O ₉	375.07216 (1.86)
387.14540	C ₂₁ H ₂₃ O ₇	387.14849 (7.98)
403.30641	C ₂₂ H ₄₃ O ₆	403.30651 (0.25)

Table S13 Results of exact mass measurements performed from the mass spectrum of the Fig. S11B related to the PI-DART-MS analysis of crushed thallus of *Ophioparma ventosa*.

Measured mass	Proposed formulae	Calculated mass (error in ppm)
169.05122	C ₈ H ₉ O ₄	169.04954 (9.93)
193.08647	C ₁₁ H ₁₃ O ₃	193.08592 (2.84)
197.08172	C ₁₀ H ₁₃ O ₄	197.08084 (4.46)
211.09811	C ₁₁ H ₁₅ O ₄	211.09649 (7.64)
225.11268	C ₁₂ H ₁₇ O ₄	225.11214 (2.39)
227.05525	C ₁₀ H ₁₁ O ₆	227.05501 (1.05)
235.09815	C ₁₃ H ₁₅ O ₄	235.09649 (7.06)
253.11076	C ₁₁ H ₁₅ O ₄	253.10705 (14.65)
345.09689	C ₁₈ H ₁₇ O ₇	345.09688 (0.01)
377.08774	C ₁₈ H ₁₇ O ₉	377.08671 (2.73)
405.32067	C ₂₂ H ₄₅ O ₆	405.32107 (0.98)

Table S14 Results of exact mass measurements performed from the mass spectrum of the Fig. 7A related to the NI-DART-MS analysis of the lower face of the thallus of *Ophioparma ventosa*.

Measured mass	Proposed formulae	Calculated mass (error in ppm)
151.06743	C ₉ H ₁₁ O ₂	151.07645 (60)
195.06594	C ₁₀ H ₁₁ O ₄	195.06628 (0.74)
209.08084	C ₁₁ H ₁₃ O ₄	209.08193 (5.23)
329.06849	C ₁₇ H ₁₃ O ₇	329.06668 (24.85)
343.08351	C ₁₈ H ₁₅ O ₇	343.08233 (3.44)
375.06644	C ₁₈ H ₁₅ O ₉	375.07216 (15.25)
403.30680	C ₂₂ H ₄₃ O ₆	403.30651 (14.16)

Table S15 Results of exact mass measurements performed from the mass spectrum of the Fig. 7B related to the NI-DART-MS analysis of the upper face of the thallus of *Ophioparma ventosa*.

Measured mass	Proposed formulae	Calculated mass (error in ppm)
151.06483	C ₉ H ₁₁ O ₂	151.07645 (77)
195.06723	C ₁₀ H ₁₁ O ₄	195.06628 (4.87)
209.08368	C ₁₁ H ₁₃ O ₄	209.08193 (8.37)
225.04280	C ₁₀ H ₉ O ₆	225.04046 (10.40)
305.06602	C ₁₅ H ₁₃ O ₇	305.06668 (2.16)
329.06374	C ₁₇ H ₁₃ O ₇	329.06668 (8.93)
343.08064	C ₁₈ H ₁₅ O ₇	343.08233 (4.92)
375.06793	C ₁₈ H ₁₅ O ₉	375.07216 (11.28)

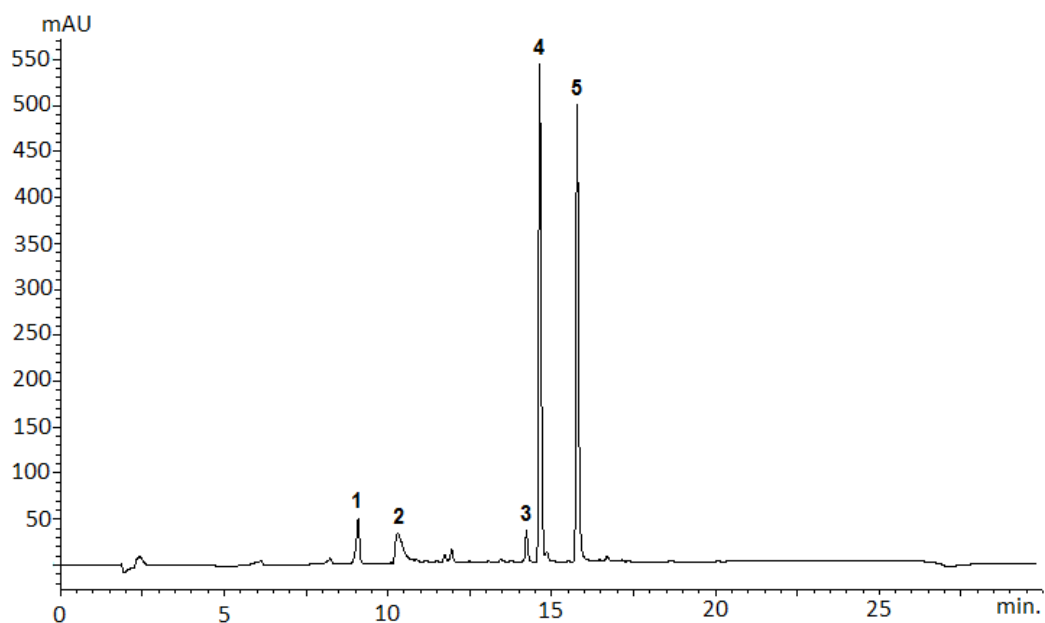


Fig. S1. DAD chromatogram at 280 nm of an acetone extract of *Ophioparma ventosa*. 1: haemoventin, 2: thamnolic acid, 3: unidentified compound, 4: divaricatic acid, 5: usnic acid.

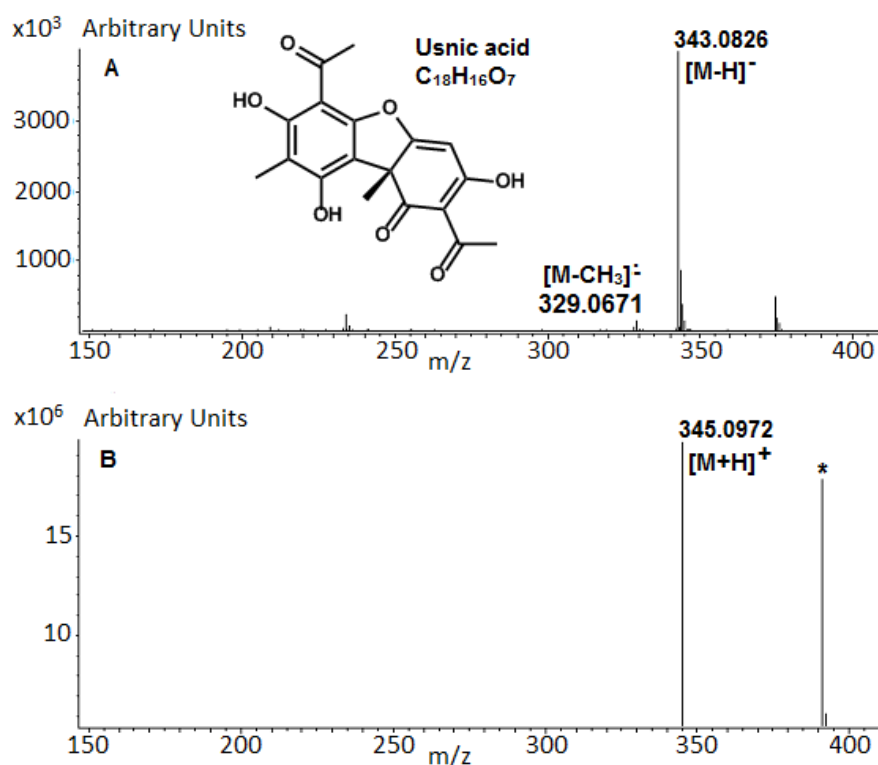


Fig. S2. DART-MS spectra of usnic acid in negative (A) and positive ion (B) mode. * Peak of the di(2-ethylhexyl)phthalate $[M + H]^+$.

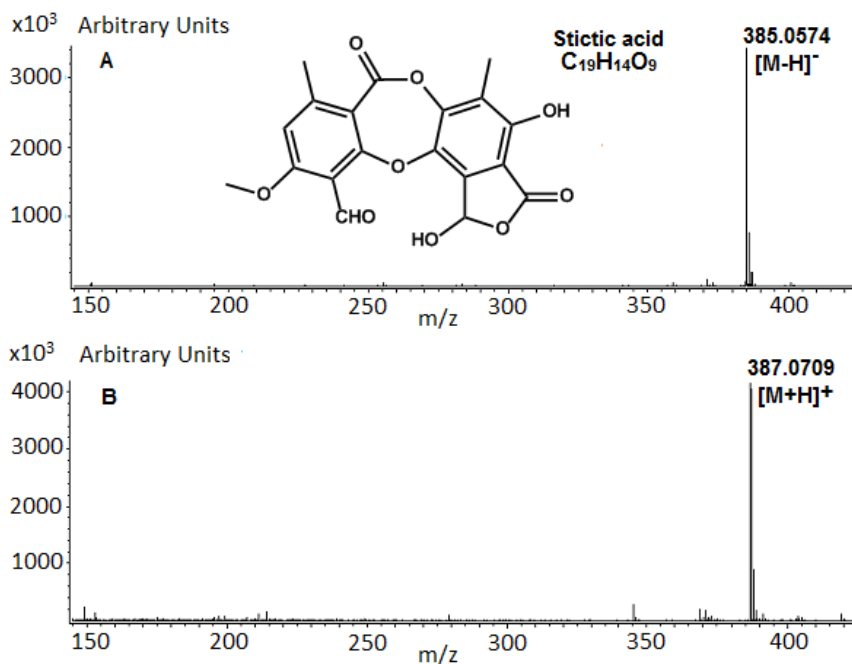


Fig. S3. DART-MS spectra of stictic acid in negative (A) and positive ion mode (B).

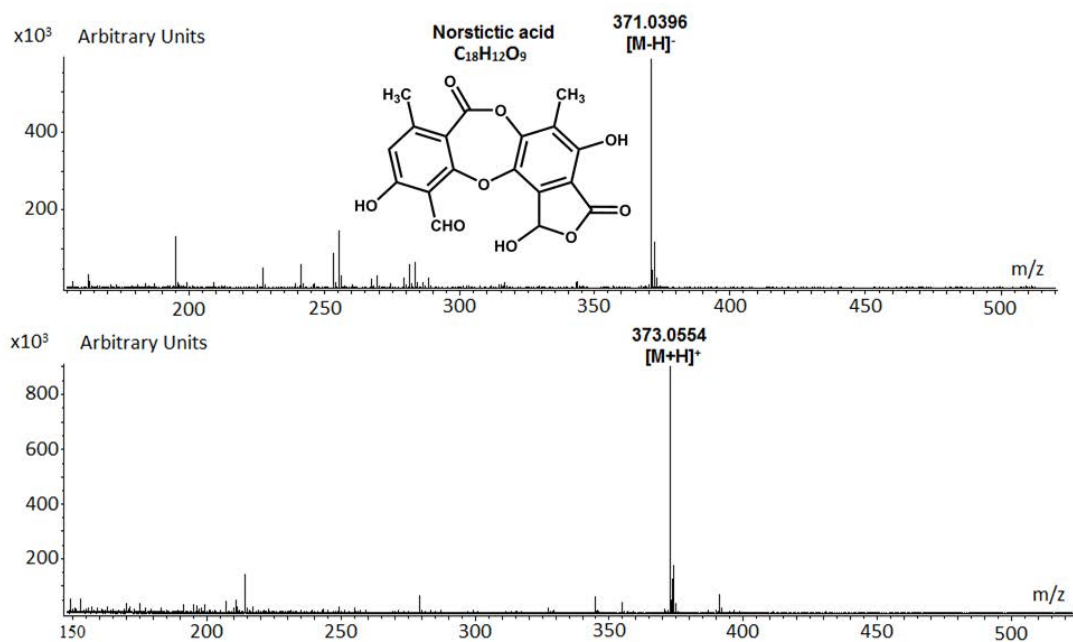


Fig. S4 DART mass spectra of norstictic acid in negative (A) and positive-ion mode (B).

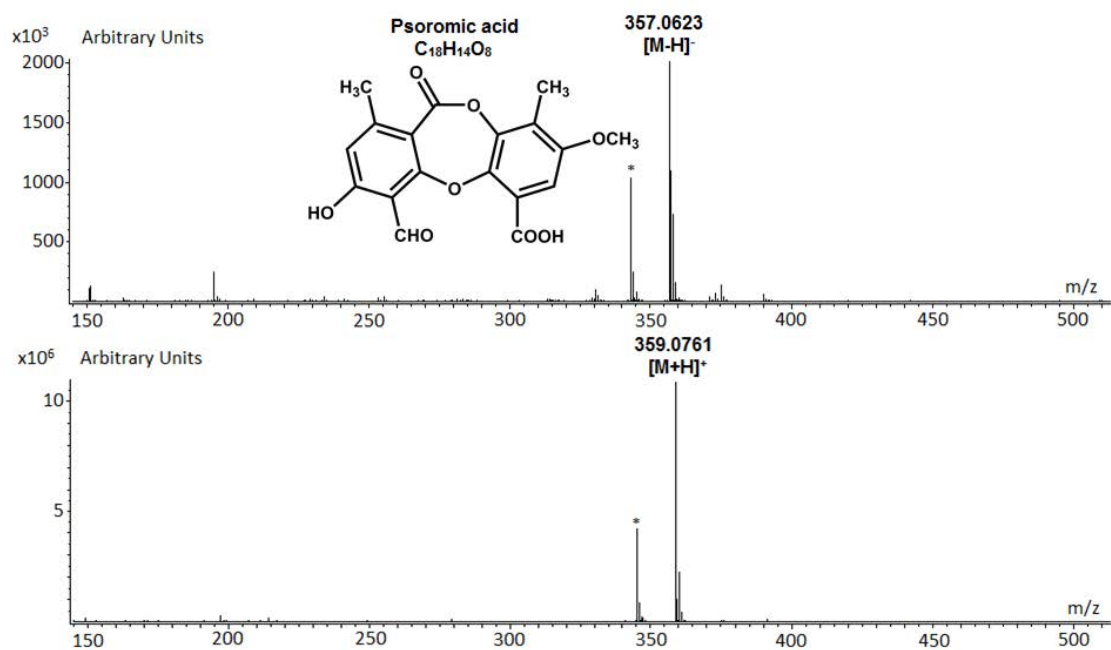


Fig. S5. DART mass spectra of psoromic acid in negative (A) and positive-ion mode (B).

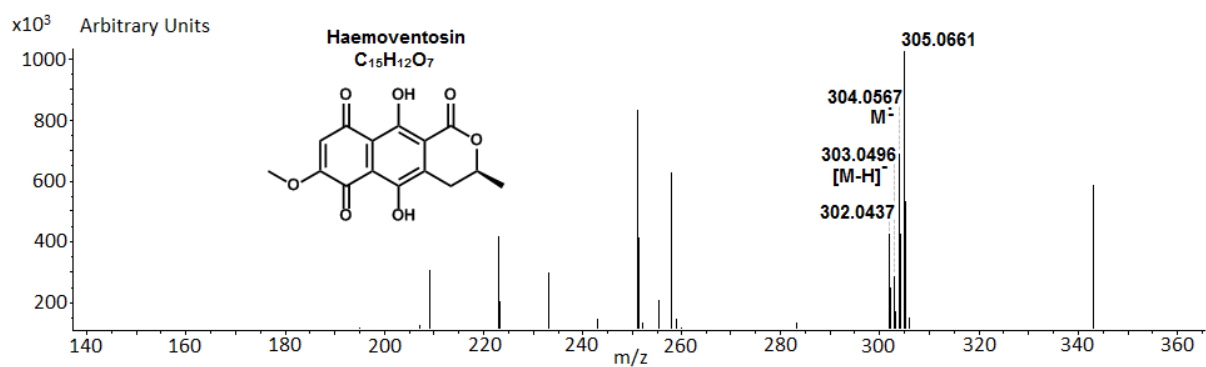


Fig. S6. NI-DART-MS mass spectrum of haemoventosin.

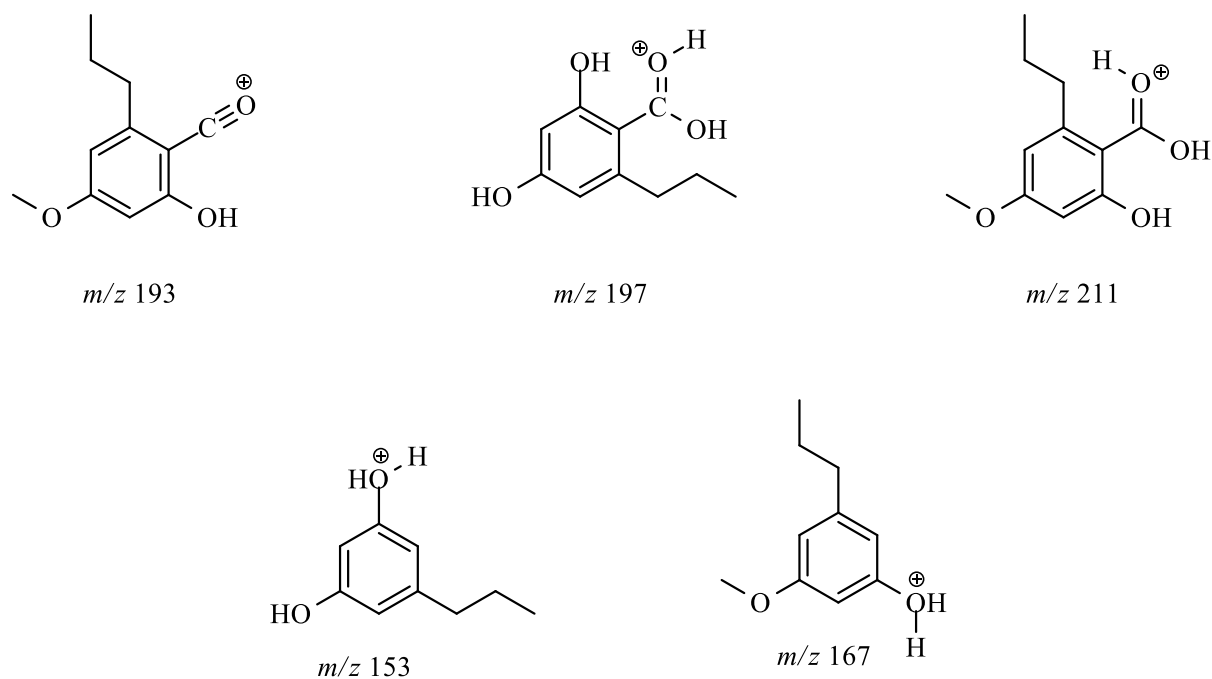


Fig. S7. Proposed fragment ions of divaricatic acid in PI-DART-MS.

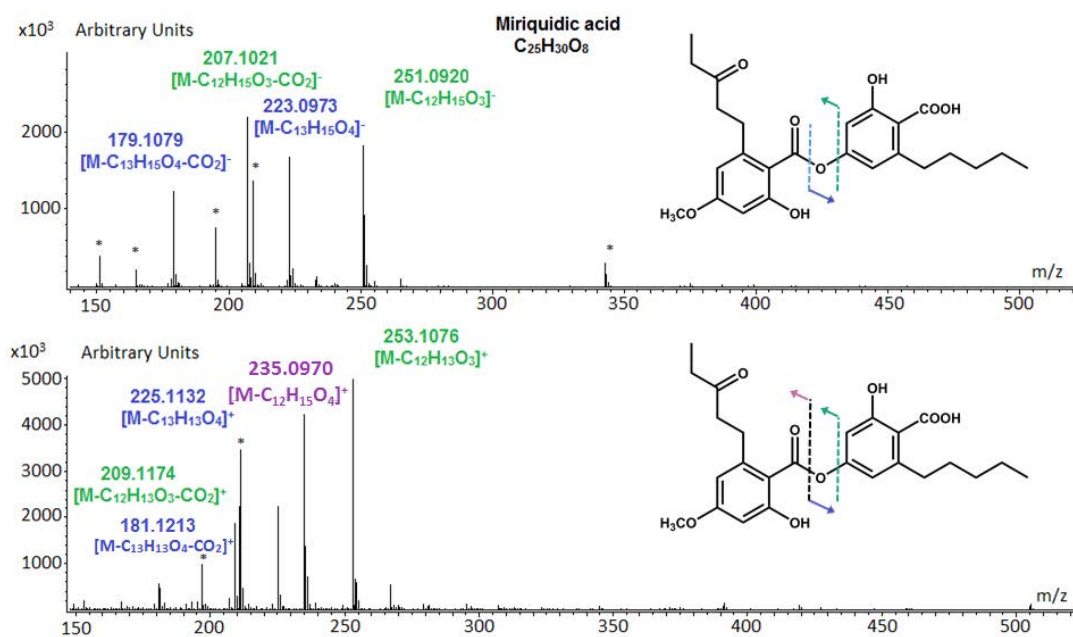


Fig. S8. DART mass spectra of miriquidic acid in negative (A) and positive-ion mode (B).

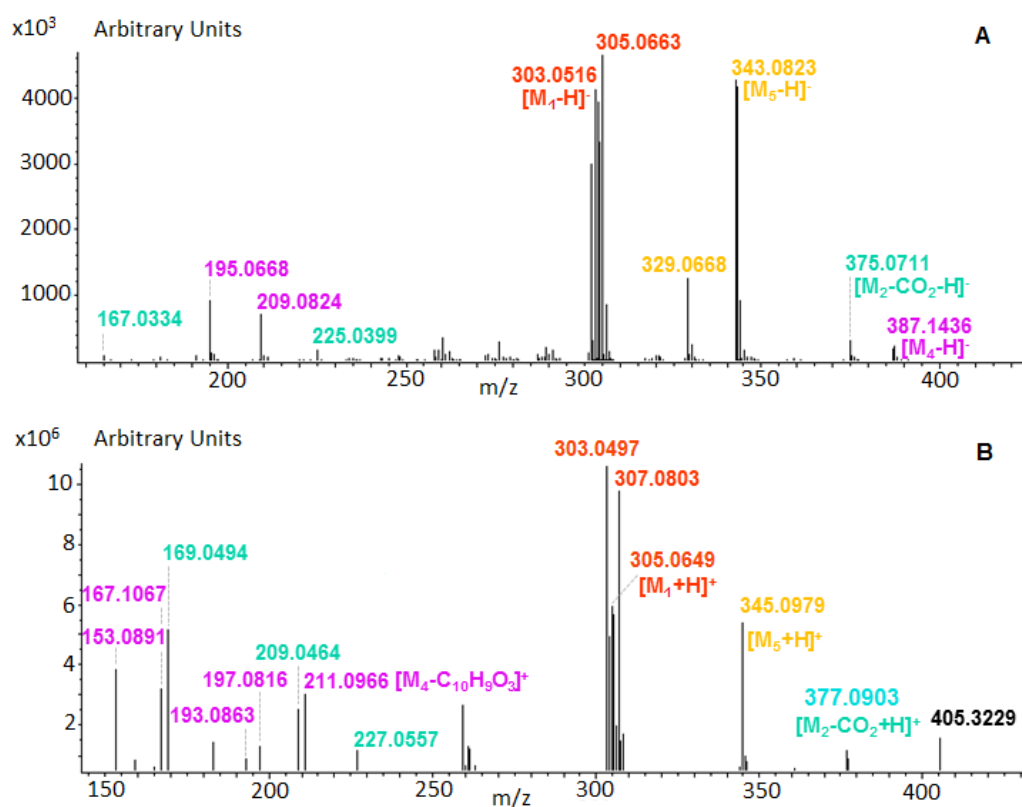


Fig. S9. *In situ* DART-MS spectra of uncrushed apothecia of *Ophioparma ventosa* in (A) negative and (B) positive ion modes. Red = haemoventosin; blue = thamnolic acid; purple = divaricatic acid; yellow = usnic acid.

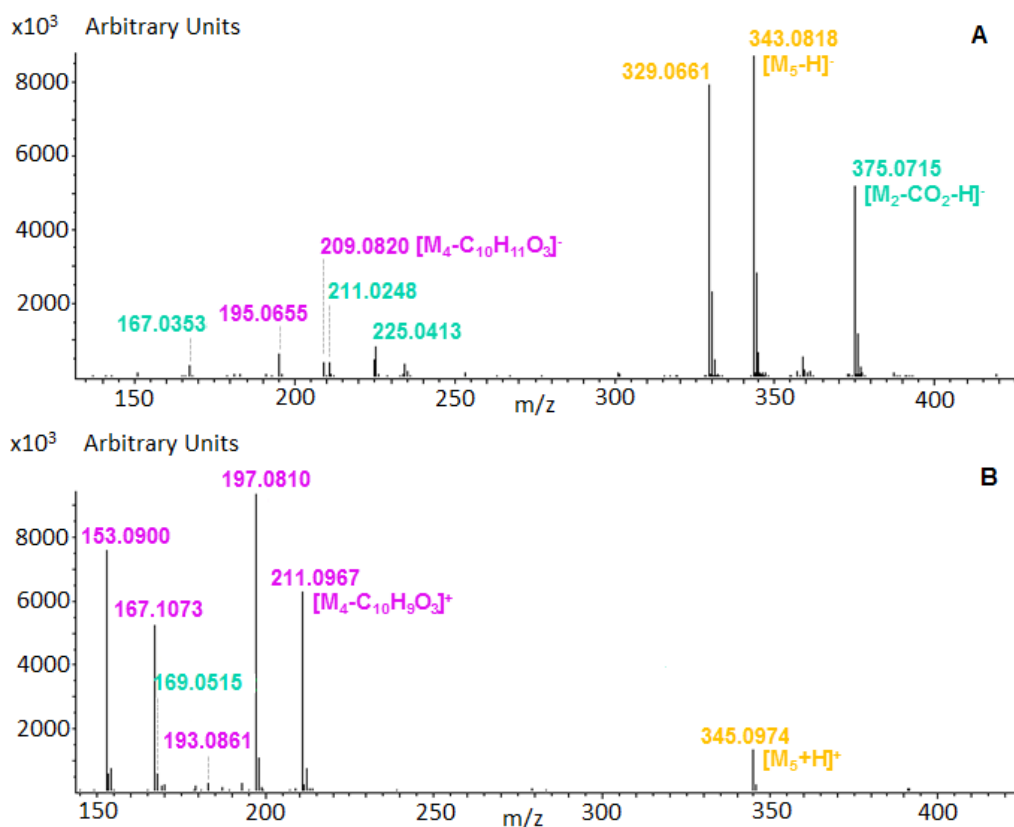


Fig. S10. *In situ* DART-MS spectra of intact thallus of *Ophioparma ventosa* in (A) negative and (B) positive ion modes. Blue = thamnolic acid; purple = divaricatic acid; yellow = usnic acid.

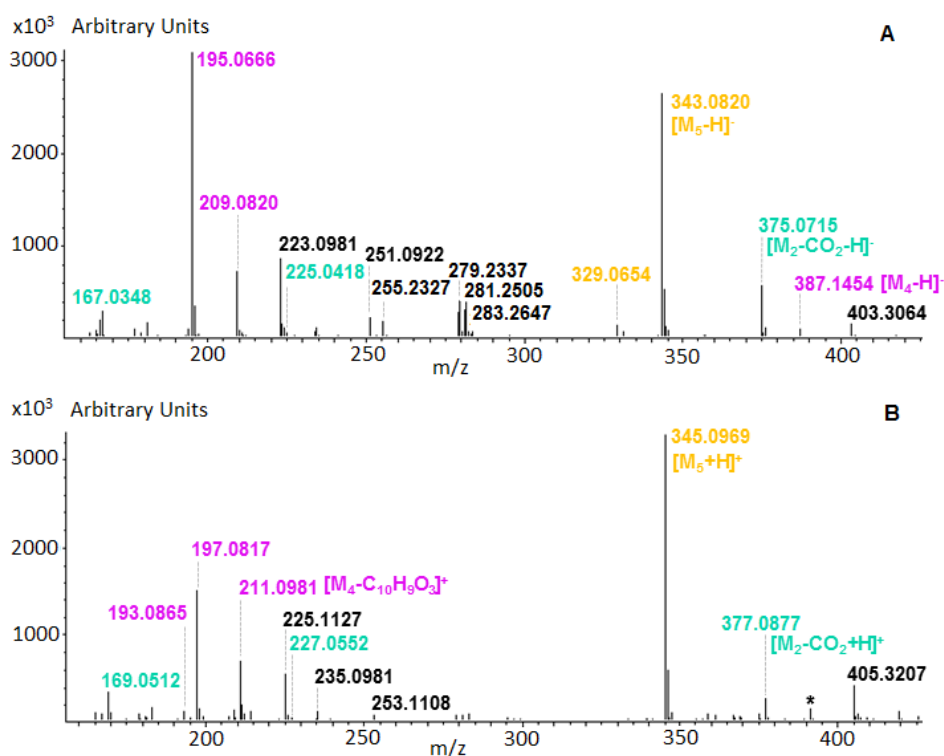
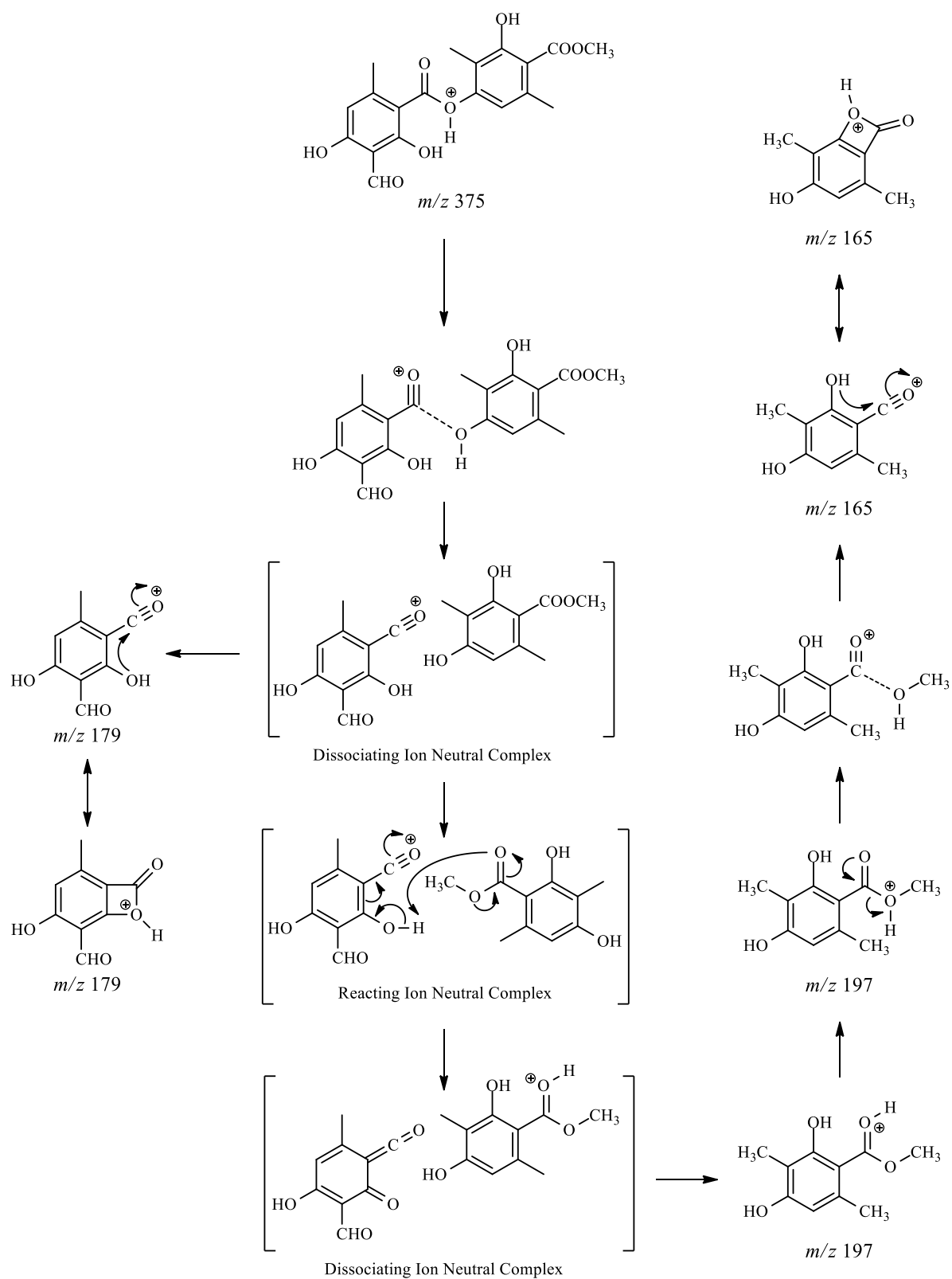
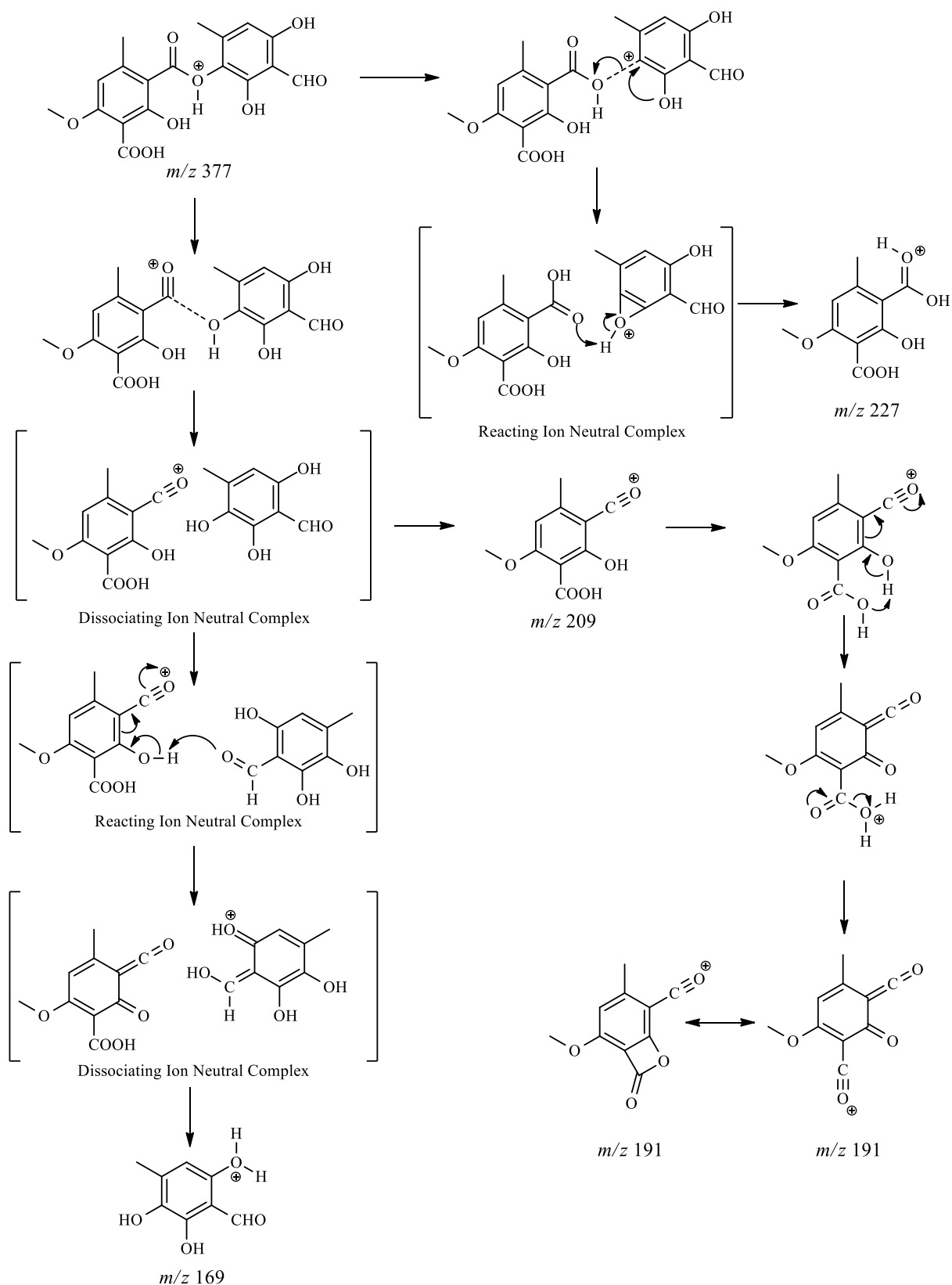


Fig. S11. *In situ* DART-MS spectra of crushed thallus of *Ophioparma ventosa* in (A) negative and (B) positive ion modes. Blue = thamnolic acid; purple = divaricatic acid; yellow = usnic acid.



Scheme S1 Proposed fragmentation pathway of atranorin in PI-DART-MS.

The scheme 1 concerns the in-source CID of the protonated molecule of atranorin in PI-DART-MS. The dissociation pathways written in the scheme 1, take into account a protonation site that leads to the bond enhancement and the formation of a ion-neutral complex (INC) that can dissociate or react by proton abstraction into the INC at relatively lower energy values (Bowen, 1991; Longevialle, 1992; Bouchoux, 2013). The formation of all the ions present in the DART mass spectra of Fig. 8 can be interpreted through the dissociation pathways depicted in Scheme 1. The m/z 197 and 179 ions, respectively corresponding to carboxylic acid and oxonium moieties, are due to competitive dissociations into an INC. At low desolvation conditions inducing lower dissociation energies, the proton transfer into the INC can occur and the formation of the m/z 197 ion can be observed with the separation of the two partners constituting the INC. At higher OR1 voltage value, the direct dissociation channel take place instead of the reactivity of the INC. In this case, the relative intensity of the m/z 179 ion increases on the mass spectra. Finally, the m/z 165 ion can be interpreted as the product of a secondary dissociation of the m/z 197 ion (from which it differs by a methanol molecule) since its formation requires higher desolvation energy and its relative intensity reaches a maximum when the m/z 197 intensity begins to decrease.



Scheme S2 Proposed fragmentation pathway of decarboxythamnolic acid in PI-DART-MS.

Phytochemical investigation of Ophioparma ventosa

The air-dried powdered material of *O. ventosa* (100 gr.) was successively macerated at room temperature with solvents of increasing polarity: *n*-heptane, dichloromethane and ethyl acetate (2 times with 300 ml, 12 h followed by 3h).

The *n*-heptane extract (800 mg) was repeatedly concentrated *in vacuo* to give a *n*-heptane precipitate (427 mg) mostly containing usnic and divaricatic acids. Those latter were repeatedly suspended in Et₂O to selectively precipitate usnic acid (220 mg). The supernatant (200 mg), enriched in divaricatic acid, was then submitted to a silica gel column chromatography (CC) using a cyclohexane/CH₂Cl₂/MeOH gradient (9:1:0 to 0:0:1) to yield six fractions (H1 - H6). Fraction H4 (28.8 mg) was purified by precipitation in CHCl₃ affording 6 mg of divaricatic acid.

The CH₂Cl₂ extract (3.5 g) was allowed to dry at room temperature, giving a CH₂Cl₂ precipitate (850 mg) and a CH₂Cl₂ filtrate (2.6 g). This latter was evaporated *in vacuo* and then repeatedly suspended in Et₂O leading to an Et₂O precipitate (2.2 g) and an Et₂O filtrate (1.4 g). The Et₂O precipitate (750 mg) was chromatographed by silica gel CC with a CH₂Cl₂/AcOEt/MeOH gradient system (1:0:0 to 0:1:1) to give 6 fractions (DP1 - DP6). Fractions DP2 and DP3 were combined (11 mg) and submitted to a preparative TLC eluted with toluene/Et₂O/formic acid (70:25:2) that enabled to isolate haemoventosin (3.5 mg).

A second sample of powdered thalli of *O. ventosa* (17 g) was directly extracted with AcOEt (200 mL) yielding 150 mg of crude extract. 55 mg of thamnolic acid were purified from the dry residue after washing with CH₂Cl₂ (5 x 3 mL) and AcOEt (3 x 3 mL).

All compounds were identified by comparison of their NMR spectra, mass spectrometric data and optical rotation with the literature (Huneck and Yoshimura, 1996).

Fractionation of the previous Et₂O filtrate (1.4 g) on a silica gel CC using a cyclohexane/CH₂Cl₂/MeOH gradient (8:2:0 to 0:1:1) afforded nine fractions (DF1 - DF9). Fraction DF7 (154 mg) was selected for further purification by silica gel CC using the same gradient yielding seven subfractions (DF7.1 - DF7.7). Subfractions DF7.6 (12 mg) and DF7.7 (24 mg) were both applied to a Sephadex LH-20 CC eluted with a CH₂Cl₂/EtOAc/methanol gradient (1:0:0 to 0:0:1) resulting in isolation of miriquidic acid (5 mg) after precipitation in MeOH.

Annexe 5 : Supporting Material J. Nat. Prod. 2016 ; 79(4) :
1005-1011

Minor quinonoid naphthopyrones from apothecia of the lichen *Ophioparma ventosa*

*Pierre Le Pogam*¹, *Anne-Cécile Le Lamer*^{1,2}, *Bandi Siva*³, *Béatrice Legouin*¹, *Arnaud Bondon*⁴, *Jérôme Graton*⁵, *Denis Jacquemin*^{5,6}, *Isabelle Rouaud*¹, *Solemn Ferron*¹, *Walter Obermayer*⁷, *K. Suresh Babu*³, *Joël Boustie*¹.

¹UMR CNRS 6226 ISCR PNSCM, Université de Rennes 1, 2 Avenue du Professeur Léon Bernard, 35043 Rennes, France.

²Université Paul Sabatier Toulouse 3, 118 Route de Narbonne, 31062 Toulouse, France.

³Division of Natural Products Chemistry CSIR, Indian Institute of Chemical Technology, Uppal Road, Hyderabad 500607, India.

⁴UMR CNRS 6226 ISCR ICMV, Université de Rennes 1, Plate-forme PRISM, CS 34317, 35043 Rennes, France

⁵UMR CNRS 6230, Chimie et Interdisciplinarité : Synthèse, Analyse et Modélisation (CEISAM), Université de Nantes, 2 Rue de la Houssinière – BP 92208, 44322 Nantes Cedex 3, France.

⁶Institut Universitaire de France, 1 Rue Descartes, 75231 Paris Cedex 05, France.

⁷Institut für Pflanzenwissenschaften, Karl-Franzens-Universität, Holteigasse 6, A-8010 Graz, Austria.

- I. Materials for pigment-enriched fraction.
 - S1. Positive-ion mode NanoHRESIMS profile of pigment-enriched fraction.
 - S2. Retrieved elemental composition of positive-ion mode NanoHRESIMS major peaks of pigment-enriched fraction.

- II. Materials for ophioparmin (**1**)
 - S3. ^1H NMR (CDCl_3 , 500 MHz) of **1**
 - S4. COSY spectrum (CDCl_3 , 500 MHz) of **1**
 - S5. COSY/TOCSY spectrum (CDCl_3 , 500 MHz) of **1**
 - S6. HSQC spectrum (CDCl_3 , 500 MHz) of **1**
 - S7. HMBC spectrum (CDCl_3 , 500 MHz) of **1**
 - S8. COSY (bold) and HMBC (arrows) correlations of **1**
 - S9. NOESY spectrum (CDCl_3 , 500 MHz) of **1**

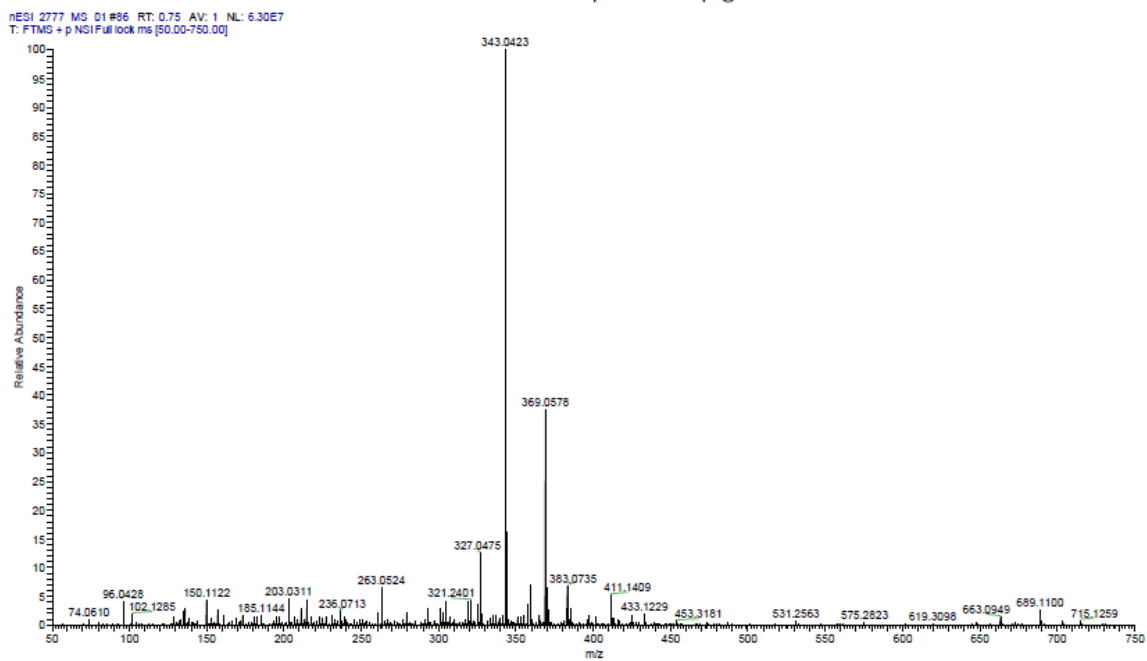
- III. Materials for 4-methoxyhaemoventosin (**2**)
 - S10. ^1H NMR (CDCl_3 , 500 MHz) of **2**
 - S11. COSY spectrum (CDCl_3 , 500 MHz) of **2**
 - S12. HSQC spectrum (CDCl_3 , 500 MHz) of **2**
 - S13. HMBC spectrum (CDCl_3 , 500 MHz) of **2**
 - S14. HMBC (arrows) correlations of **2**

- IV. Materials for 4-hydroxyhaemoventosin (**3**)
 - S15. ^1H NMR (CDCl_3 , 500 MHz) of **3**
 - S16. HSQC spectrum (CDCl_3 , 500 MHz) of **3**
 - S17. HMBC spectrum (CDCl_3 , 500 MHz) of **3**
 - S18. HMBC (arrows) correlations of **3**

- V. Material for anhydrofusarubin lactone (**4**)
 - S19. ^1H NMR (CDCl_3 , 500 MHz) of **4**

- VI. Material for haemoventosin (**5**)
 - S20. ^1H NMR (CDCl_3 , 500 MHz) of **5**
 - S21. Cytotoxicity of **5** using a panel of 7 cell lines

S1. Positive-ion mode NanoHRESIMS profile of pigment-enriched fraction

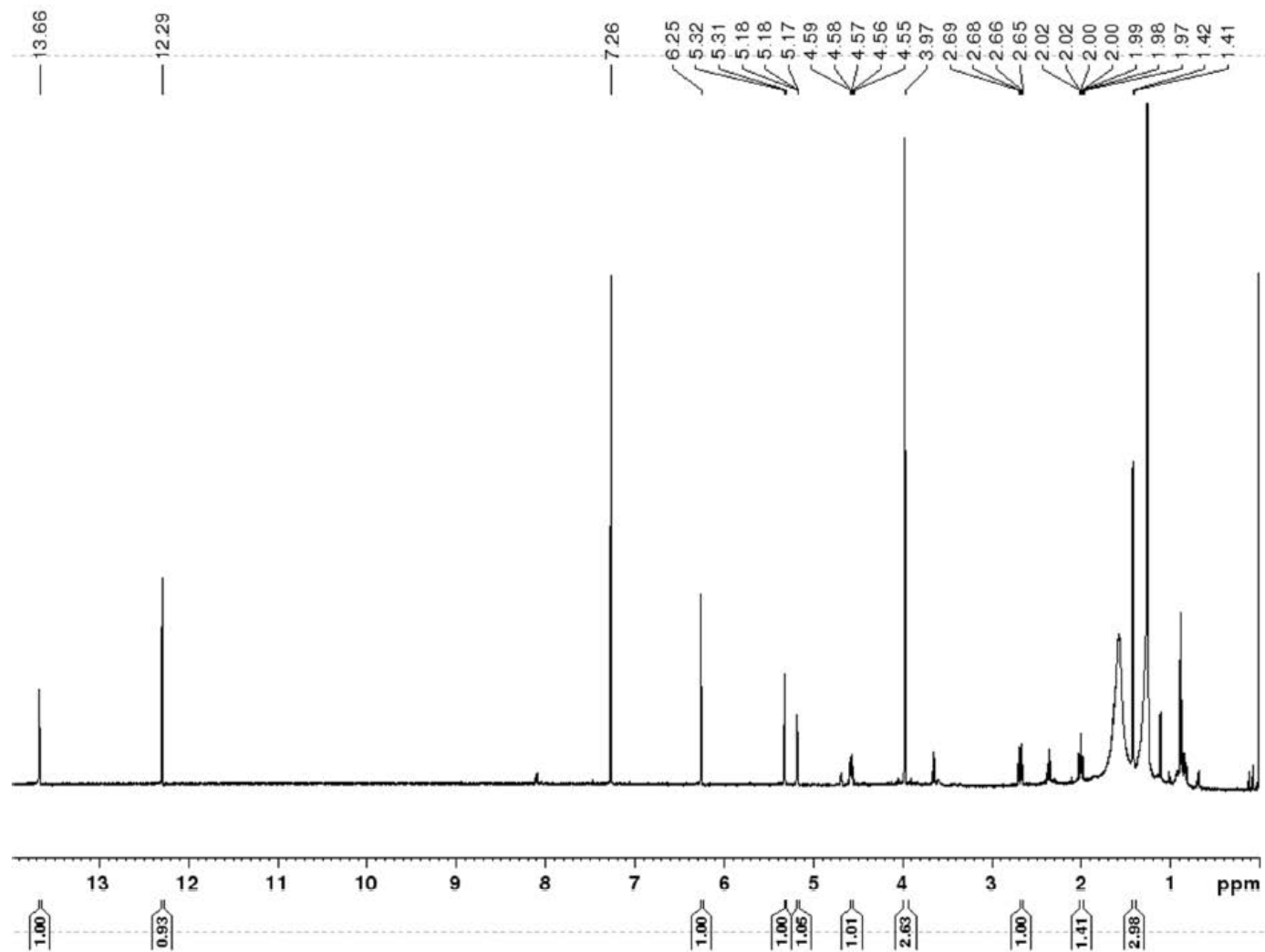


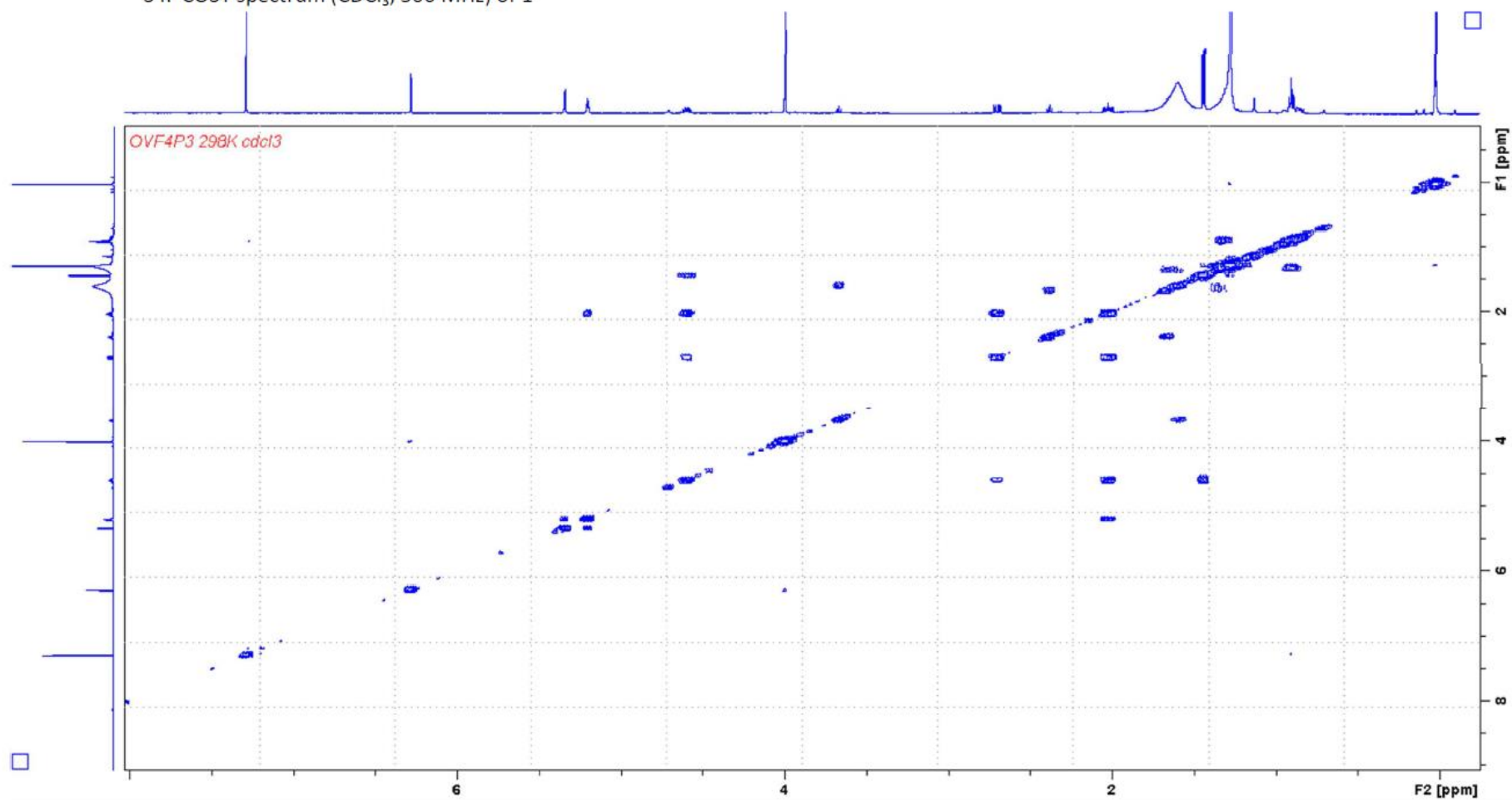
S2. Retrieved elemental composition of positive-ion mode NanoHRESIMS major peaks of the pigment-enriched fraction.

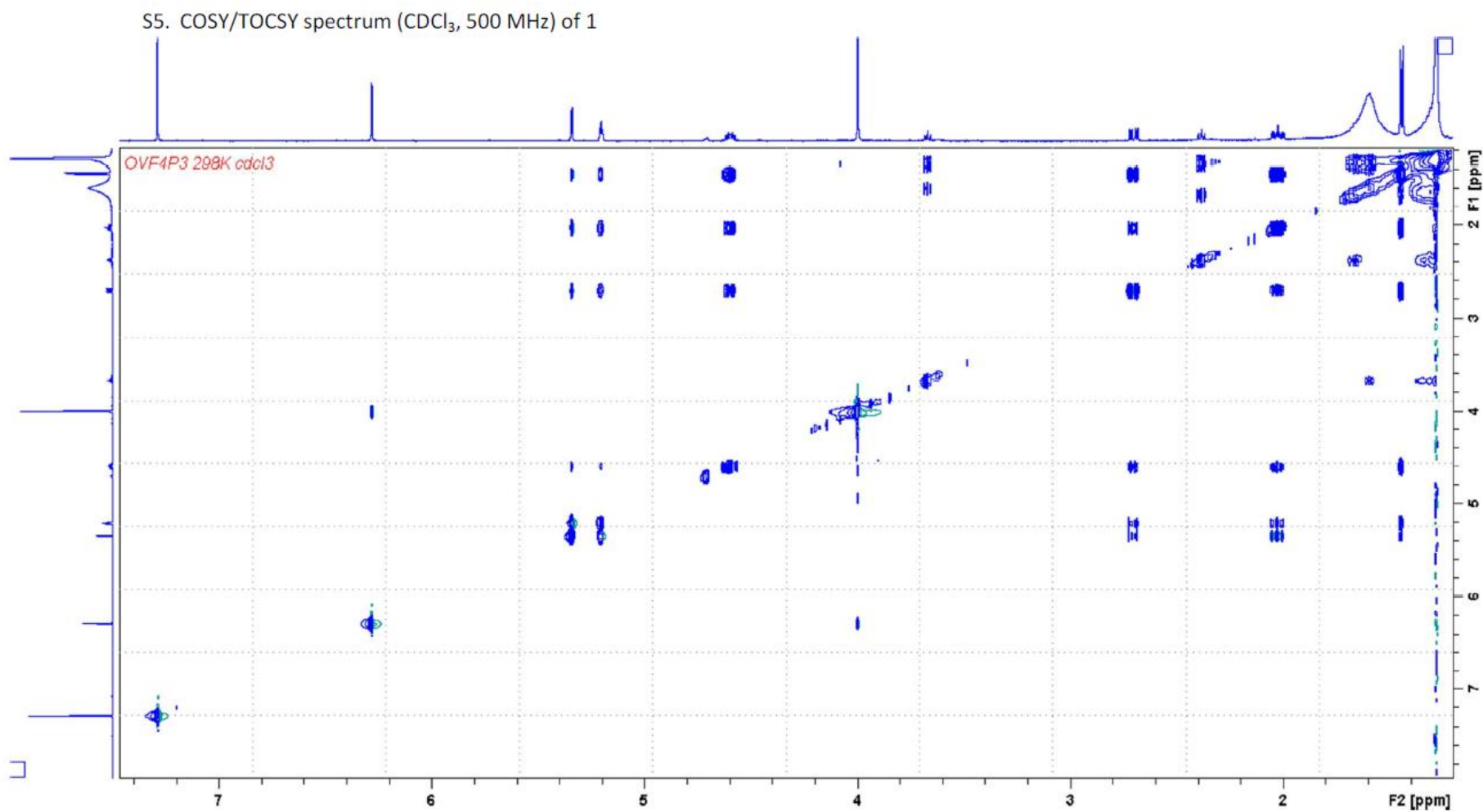
m/z	Intensity	Relative	Theo. Mass	Delta (ppm)	Composition	Identification
343.04235	56883868	100	343.04244	-0.25	C15 H12 O8 Na	4-hydroxyhaemoventosin (3)
369.05785	21900272	38.5	369.05809	-0.64	C17 H14 O8 Na	Ophioparmin (1)
327.0476	7870470.5	13.84	327.04752	0.23	C15 H12 O7 Na	Haemoventosin (5)
263.05243	6273552	11.03	263.05261	-0.7	C11 H12 O6 Na	
411.14102	4011858	7.05	411.14142	-0.98	C21 H24 O7 Na	Divaricatic acid
383.07352	3985133.8	7.01	383.07374	-0.56	C18 H16 O8 Na	
359.01628	3353377.8	5.9	359.01622	0.17	C18 H8 O7 Na	
215.06749	3159354	5.55	215.06787	-1.75	C11 H12 O3 Na	
203.03107	3148826.5	5.54	203.03148	-2.04	C9 H8 O4 Na	
321.24012	2968336.8	5.22	321.24002	0.34	C18 H34 O3 Na	
319.22446	2809529.8	4.94	319.22437	0.31	C18 H32 O3 Na	
293.24491	2668366.8	4.69	293.2451	-0.64	C17 H34 O2 Na	
211.09374	2449126.3	4.31	211.09408	-1.59	C9 H16 O4 Na	
325.03195	2436766.5	4.28	325.03187	0.22	C15 H10 O7 Na	Anhydrofusarubin lactone (4)
357.05797	2176772.8	3.83	357.05809	-0.33	C16 H14 O8 Na	4-methoxyhaemoventosin (2)
157.08322	2123446.3	3.73	157.08352	-1.86	C6 H14 O3 Na	
305.24509	1913303.4	3.36	305.2451	-0.02	C18 H34 O2 Na	
303.22944	1844170.1	3.24	303.22945	-0.05	C18 H32 O2 Na	
371.07353	1807822.3	3.18	371.07374	-0.56	C17 H16 O8 Na	
231.02618	1791374.6	3.15	231.02639	-0.93	C10 H8 O5 Na	
261.08783	1720905	3.03	261.0886	-2.95	C16 H14 O2 Na	
261.10957	1646988.6	2.9	261.10973	-0.59	C13 H18 O4 Na	
197.07808	1521087.8	2.67	197.07843	-1.76	C8 H14 O4 Na	
279.22936	1452110.3	2.55	279.22945	-0.33	C16 H32 O2 Na	
185.11449	1424935.8	2.5	185.11482	-1.77	C8 H18 O3 Na	
385.03175	1400423.5	2.46	385.03187	-0.32	C20 H10 O7 Na	
335.21934	1377668.8	2.42	335.21928	0.18	C18 H32 O4 Na	
195.09883	1348236.3	2.37	195.09917	-1.75	C9 H16 O3 Na	
173.07812	1337691.5	2.35	173.07843	-1.77	C6 H14 O4 Na	
383.31292	1324849.9	2.33	383.31318	-0.68	C21 H44 O4 Na	
239.16143	1323011.4	2.33	239.16177	-1.41	C12 H24 O3 Na	
207.09885	1241546.5	2.18	207.09917	-1.54	C10 H16 O3 Na	
223.13013	1234563.3	2.17	223.13047	-1.49	C11 H20 O3 Na	
197.11445	1192634.4	2.1	197.11482	-1.86	C9 H18 O3 Na	
225.10939	1186437.8	2.09	225.10973	-1.51	C10 H18 O4 Na	

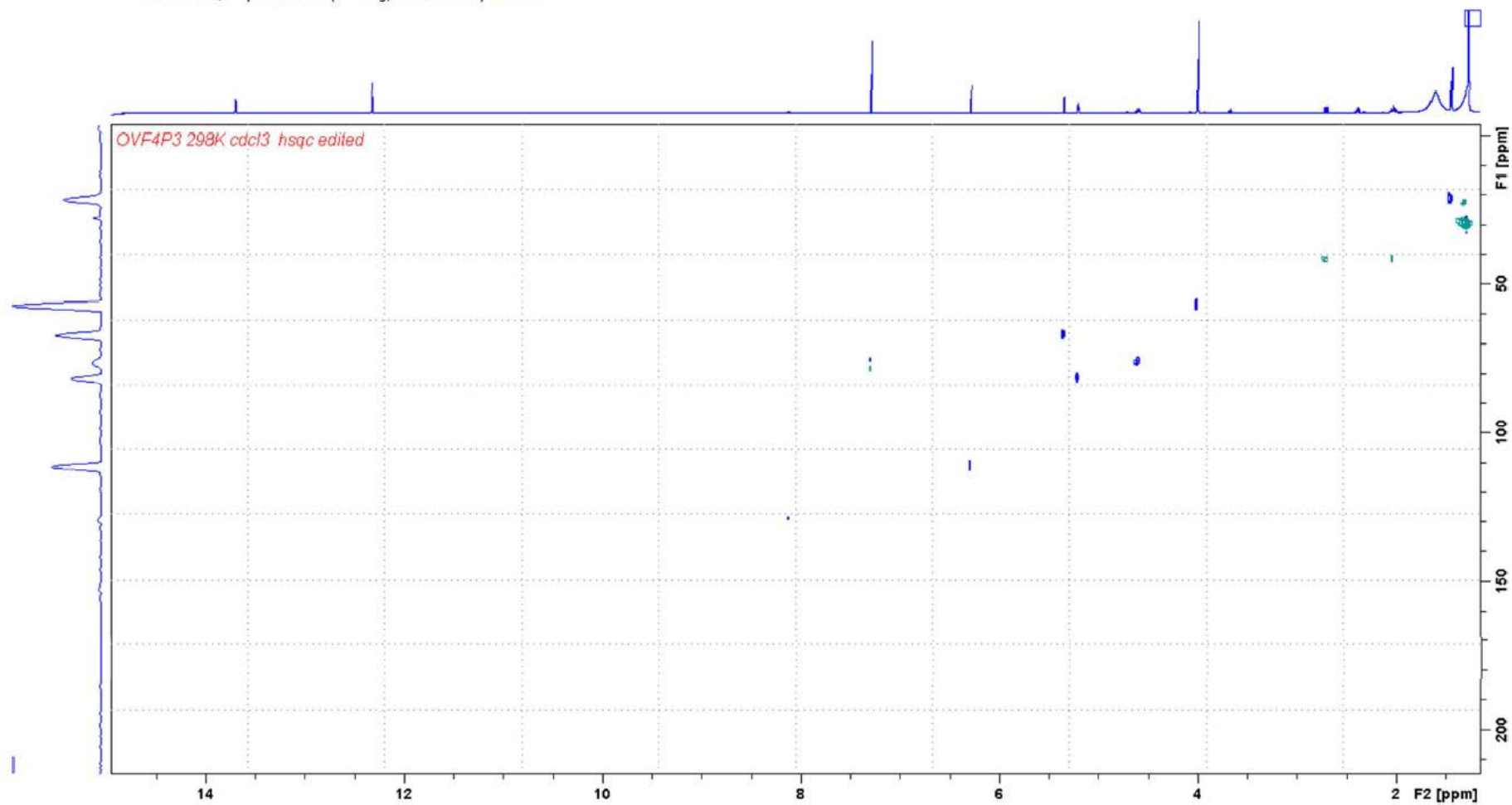
Table S2 : Elemental compositions retrieved for all major peaks detected in positive-ion mode NanoHRESIMS. Lines outlined in blue refer to possible quinonoid naphthopyrones structures (i.e candidate compositions encompassing C₁₂₋₂₀H₈₋₂₀O₅₋₁₀).

S3. ^1H NMR (CDCl_3 , 500 MHz) of **1**

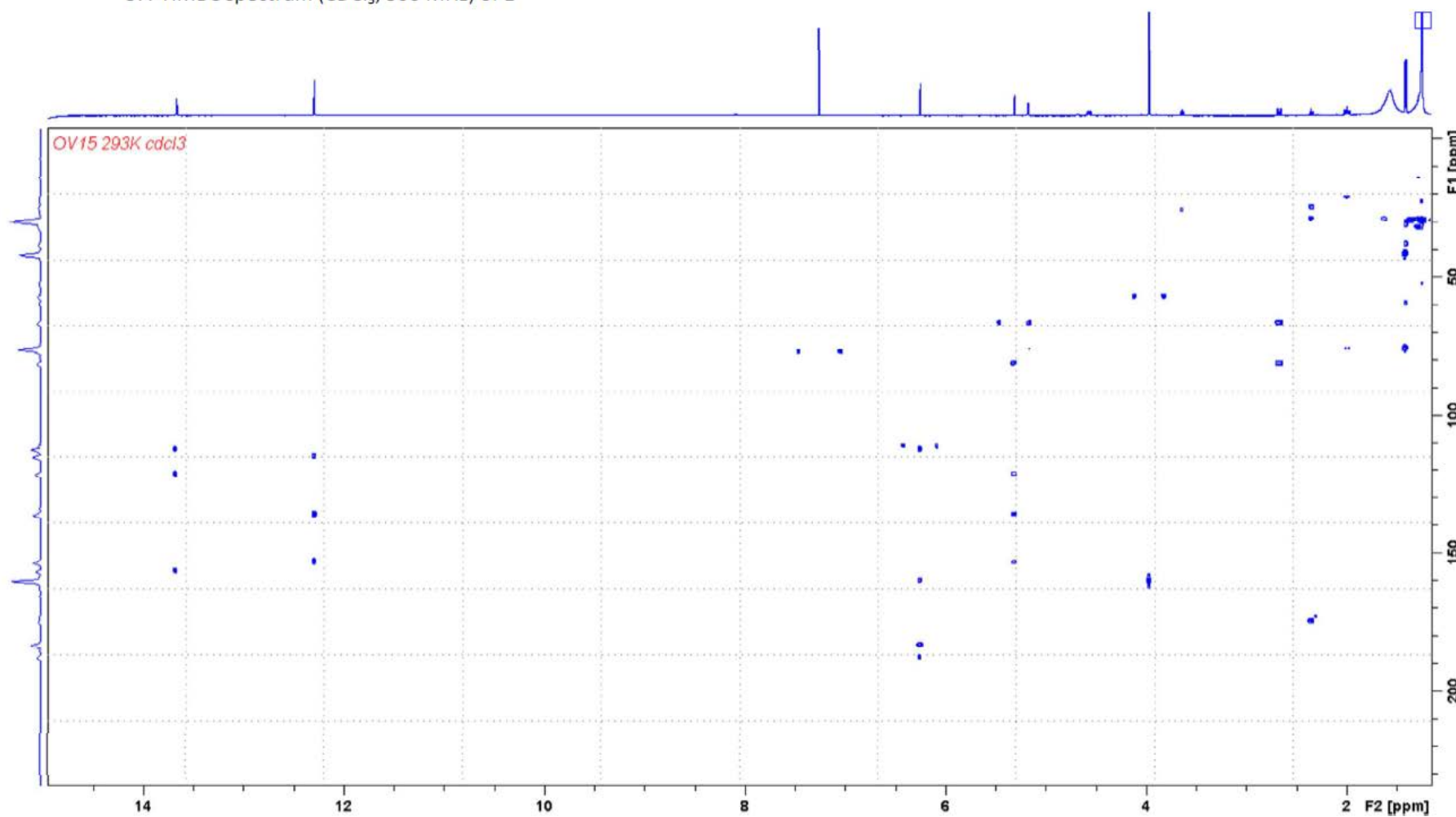


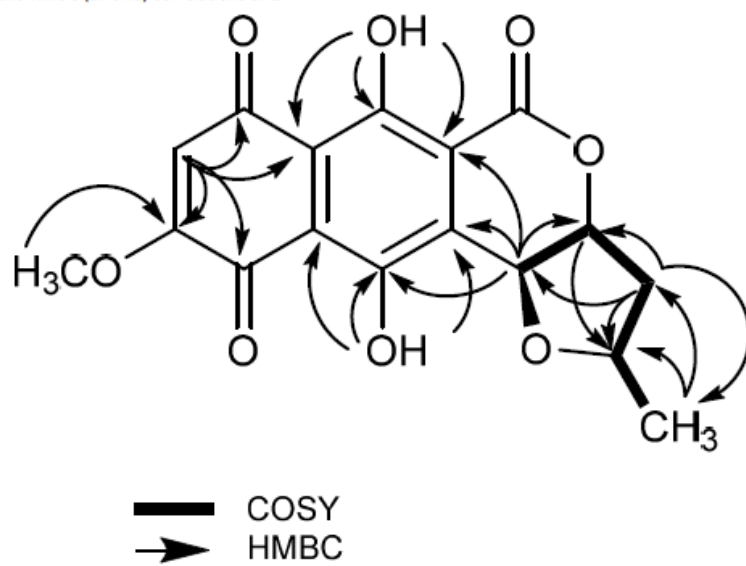
S4. COSY spectrum (CDCl₃, 500 MHz) of 1



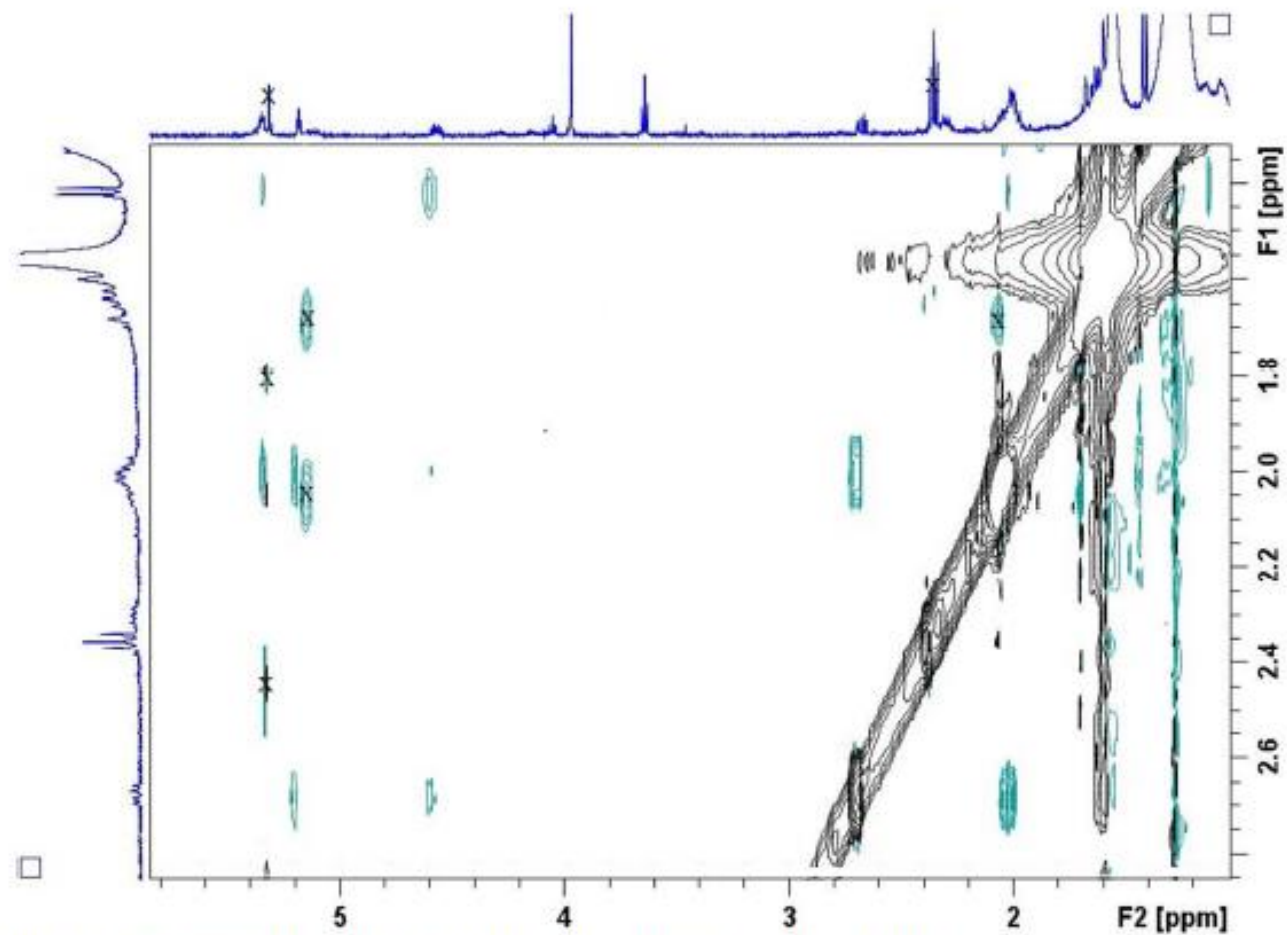
S6. HSQC spectrum (CDCl₃, 500 MHz) of 1

S7. HMBC spectrum (CDCl₃, 500 MHz) of 1

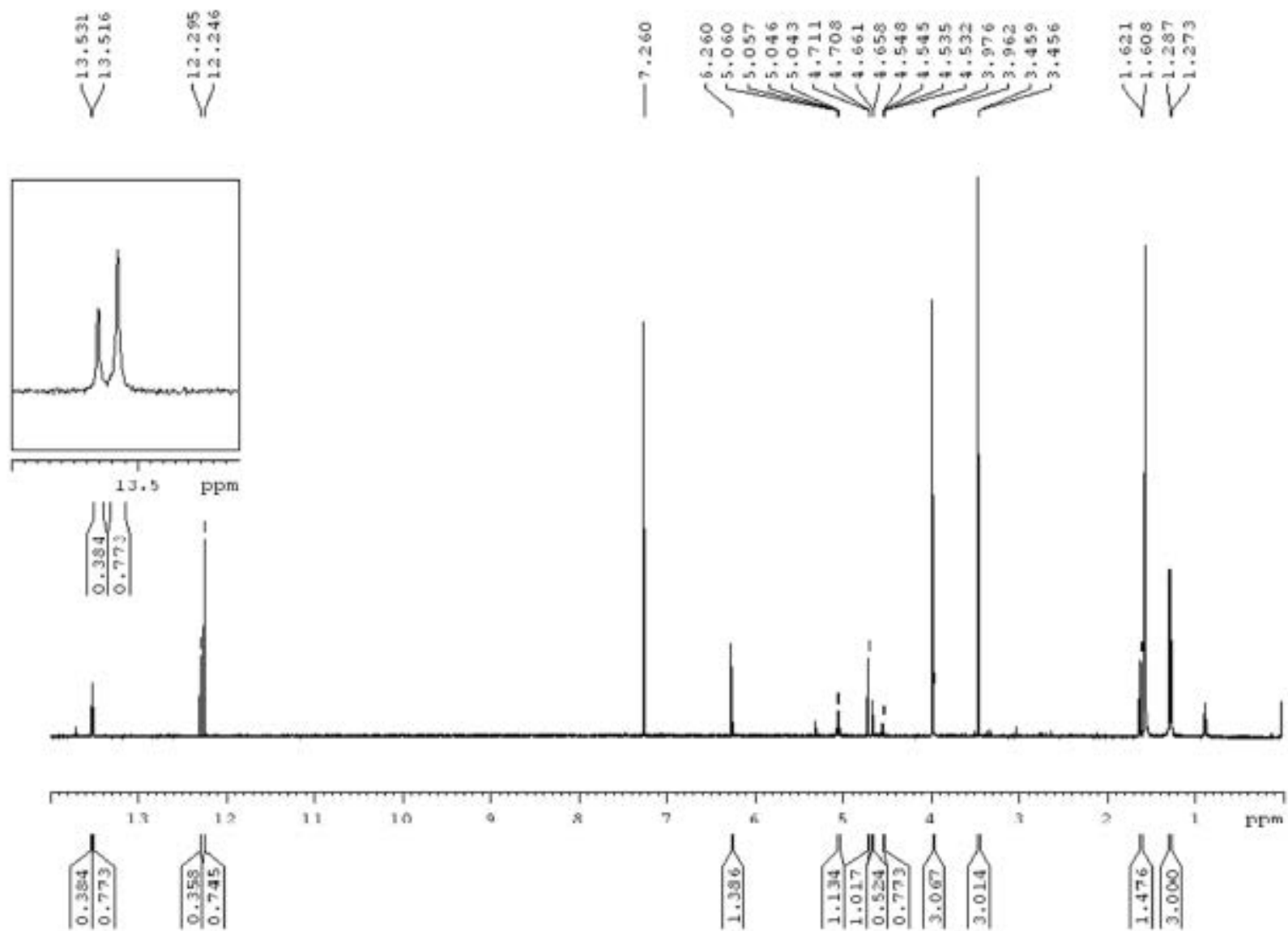


S8. Key COSY (bold) and HMBC (arrows) correlations of **1**.

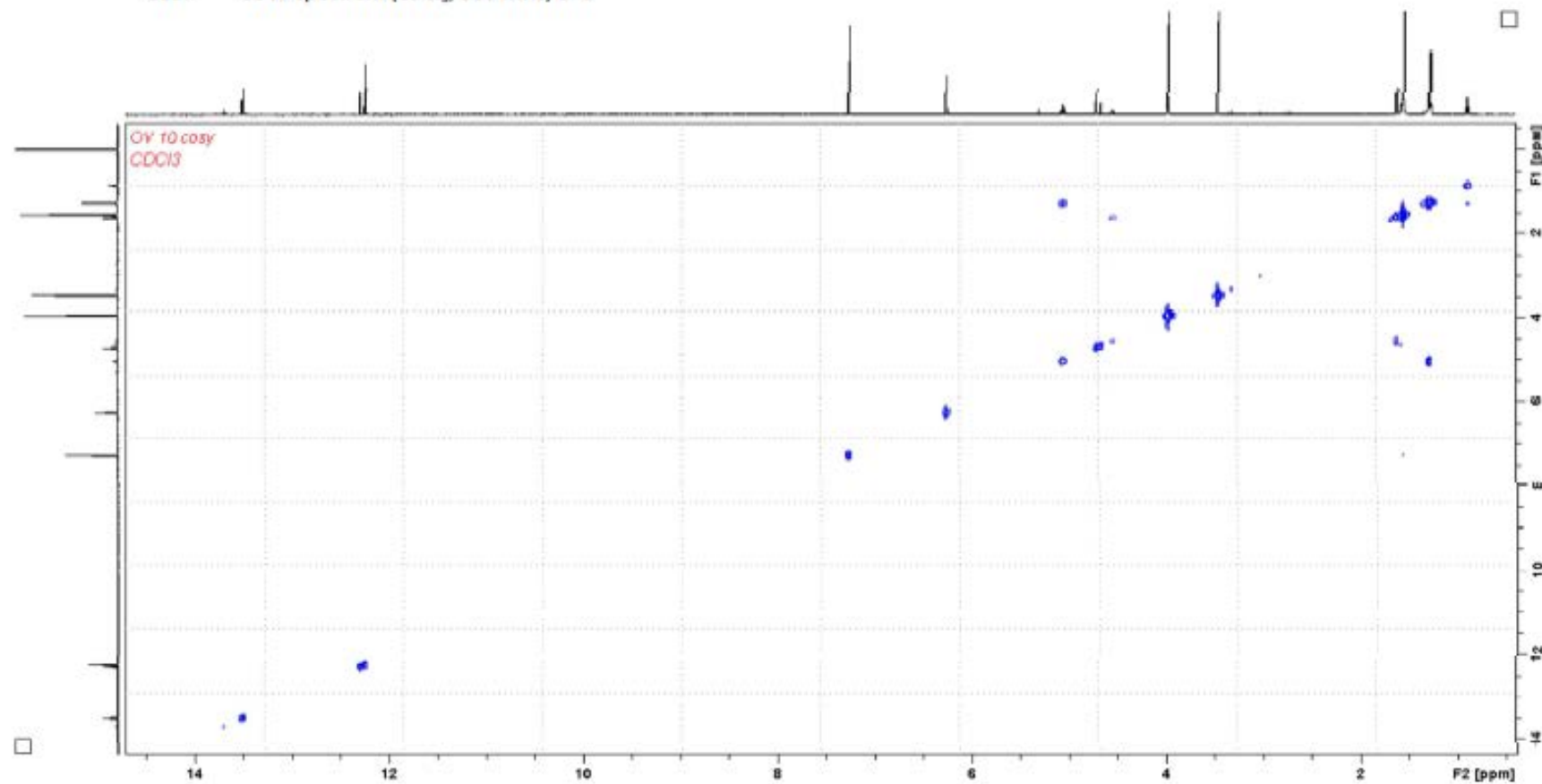
S9. NOESY spectrum (CDCl₃, 500 MHz) of **1**

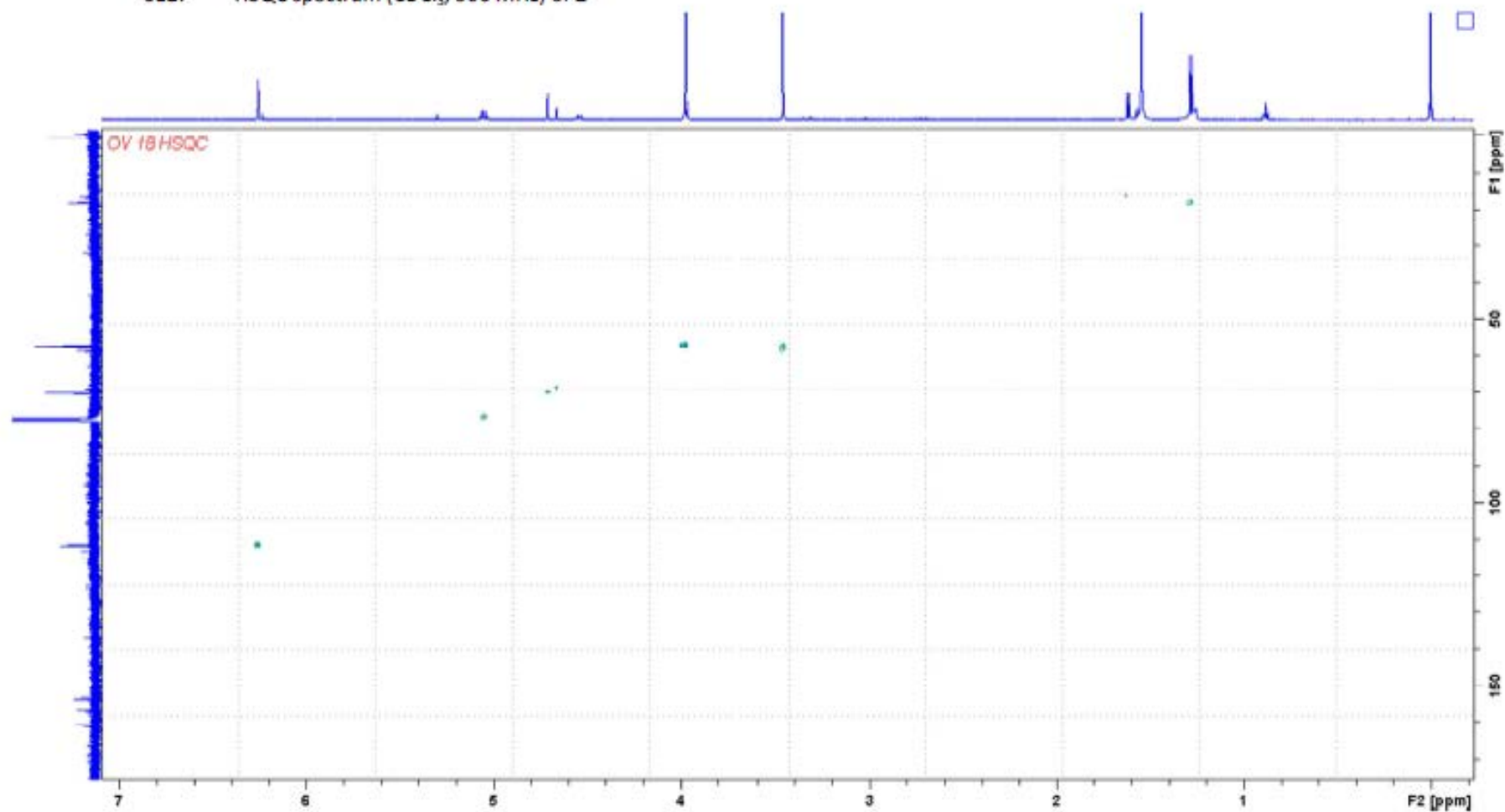


*Strikethrough signals refer to peaks appeared upon long storage of **1** thus not belonging to the native molecule.

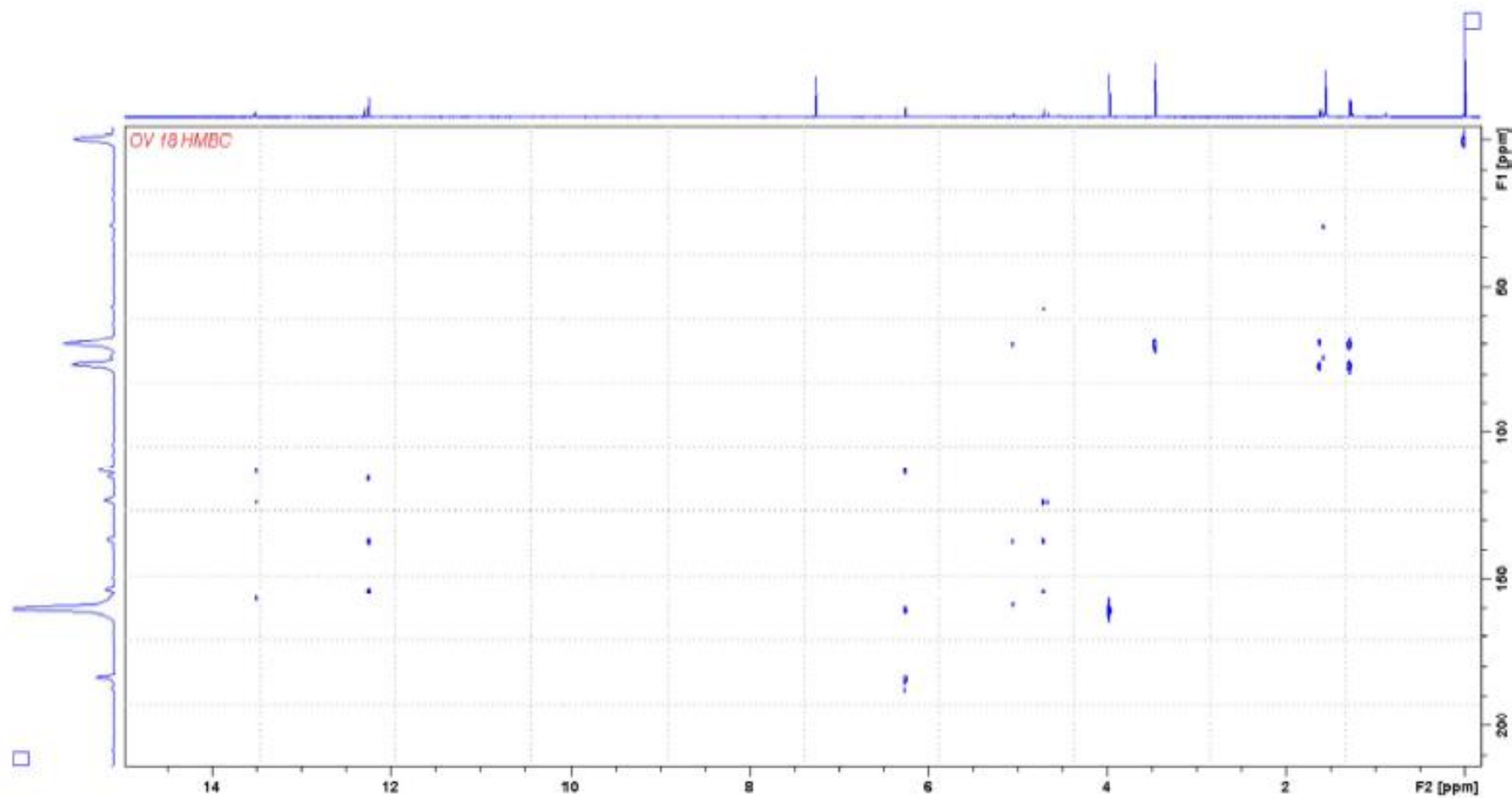
S10. ^1H NMR (CDCl_3 , 500 MHz) of **2**

S11. COSY spectrum (CDCl₃, 500 MHz) of 2

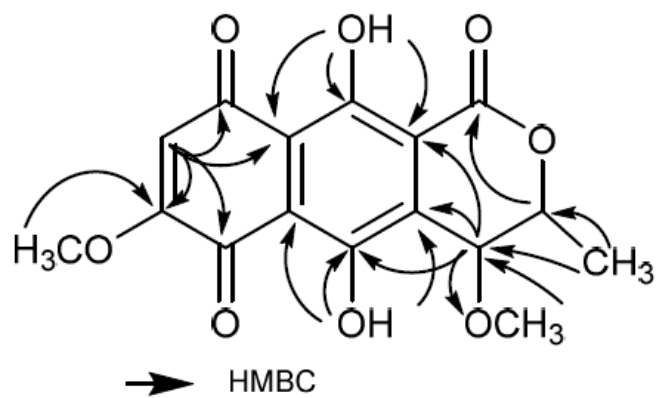


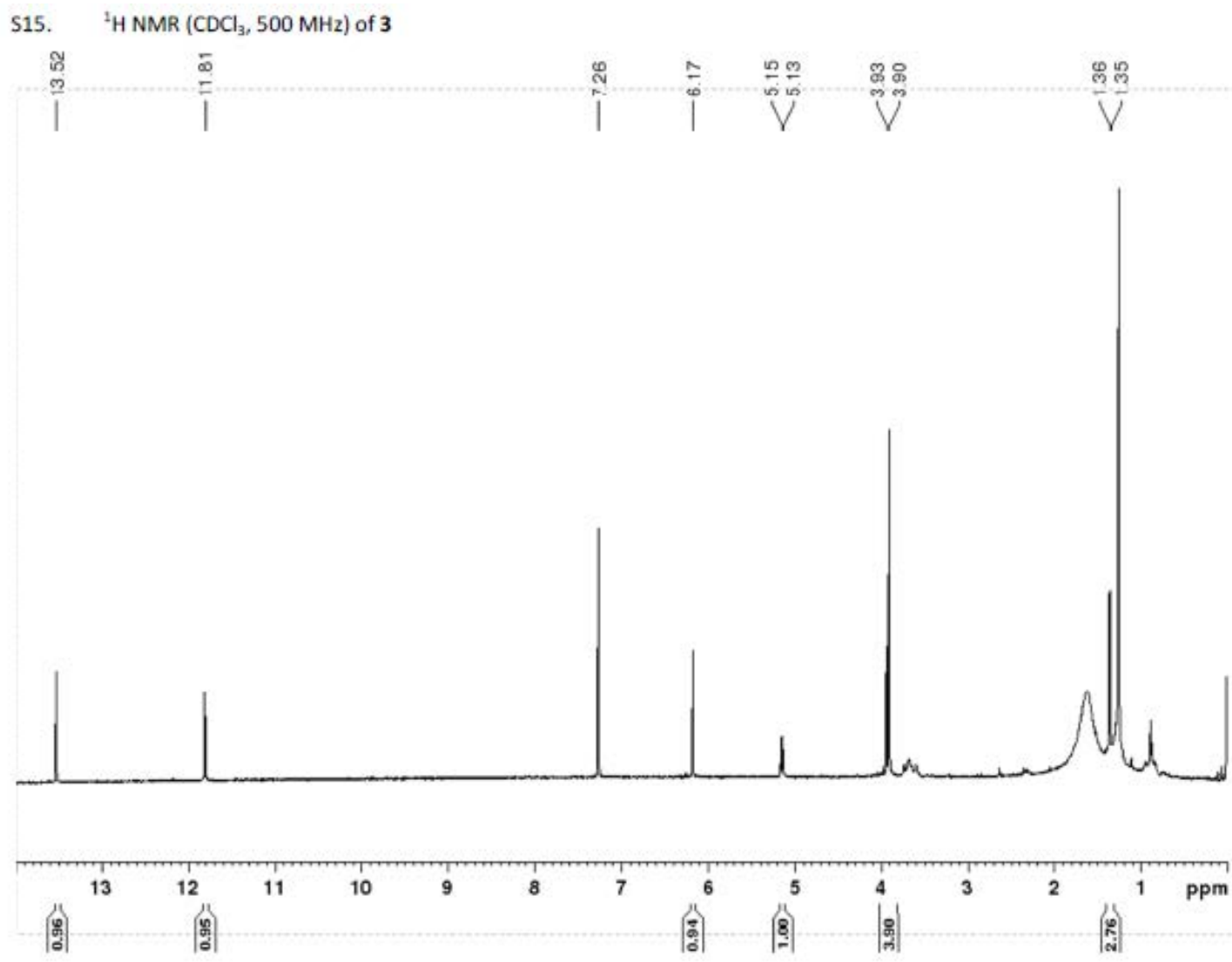
S12. HSQC spectrum (CDCl₃, 500 MHz) of 2

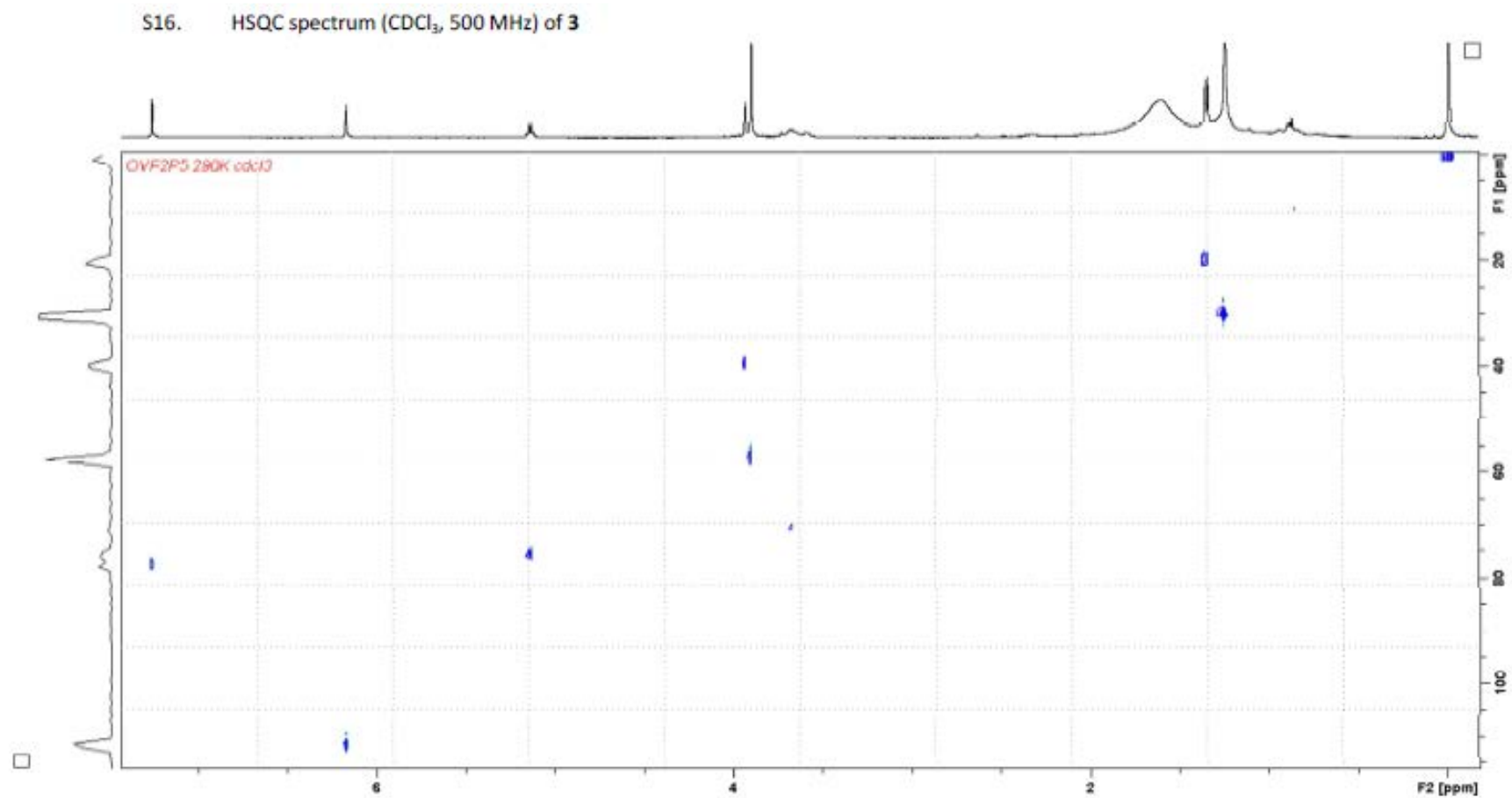
S13. HMBC spectrum (CDCl₃, 500 MHz) of 2



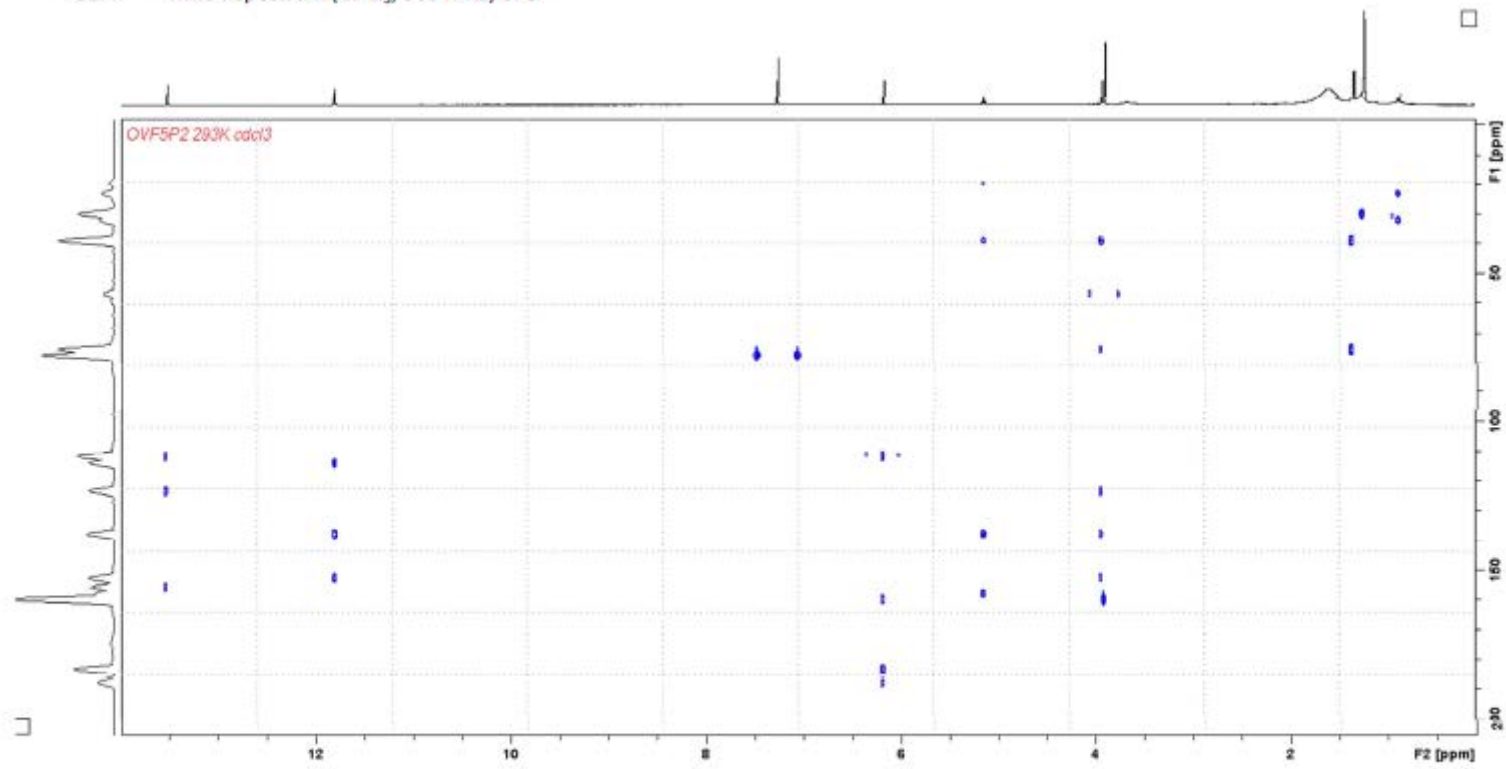
S14. HMBC (arrows) correlations of 2.

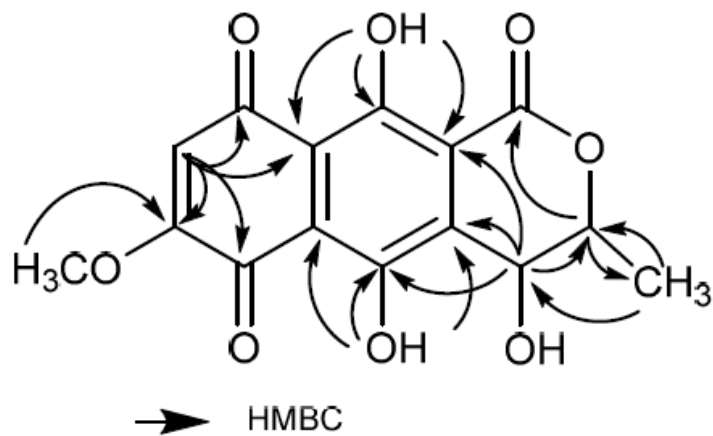




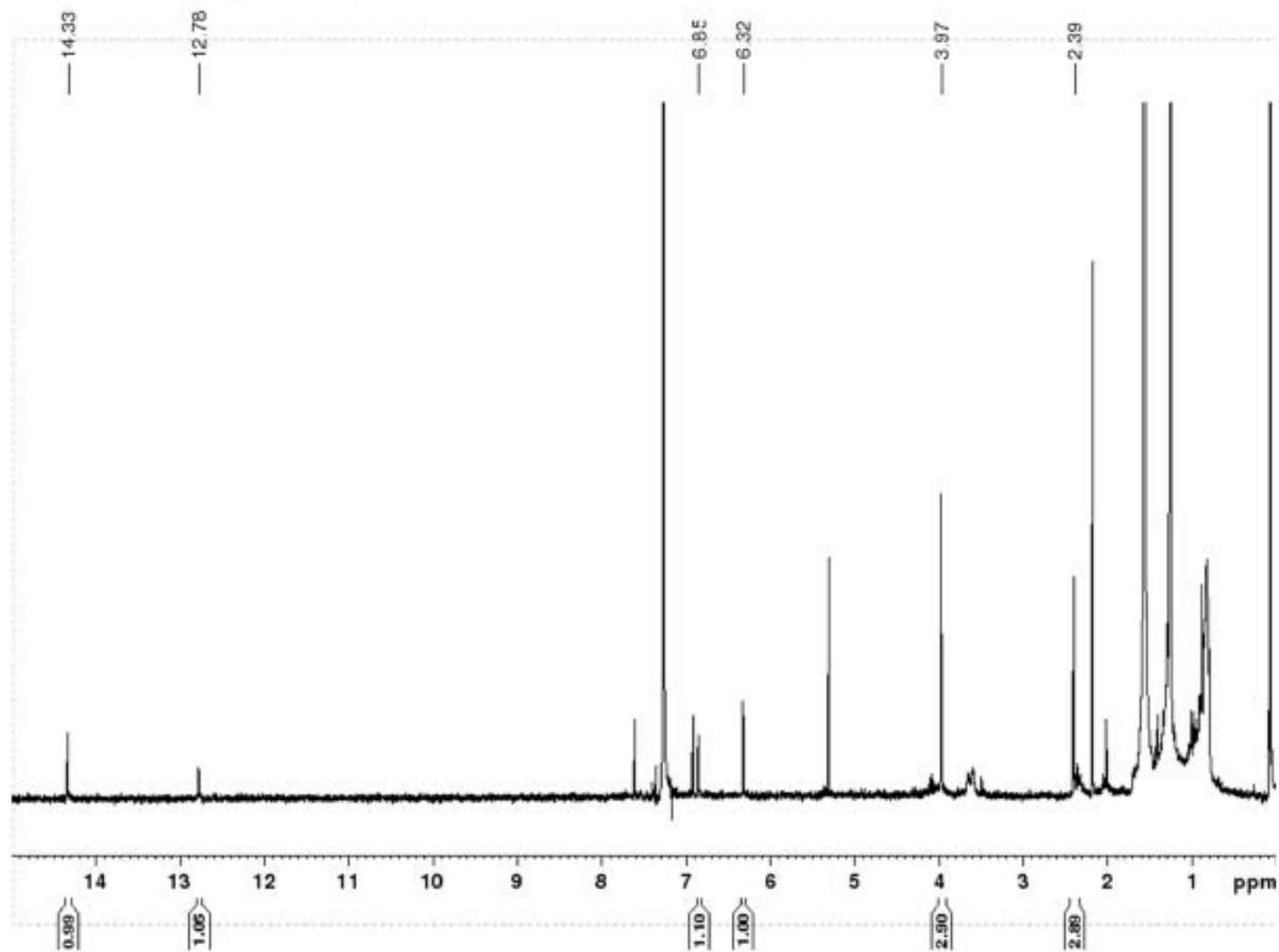


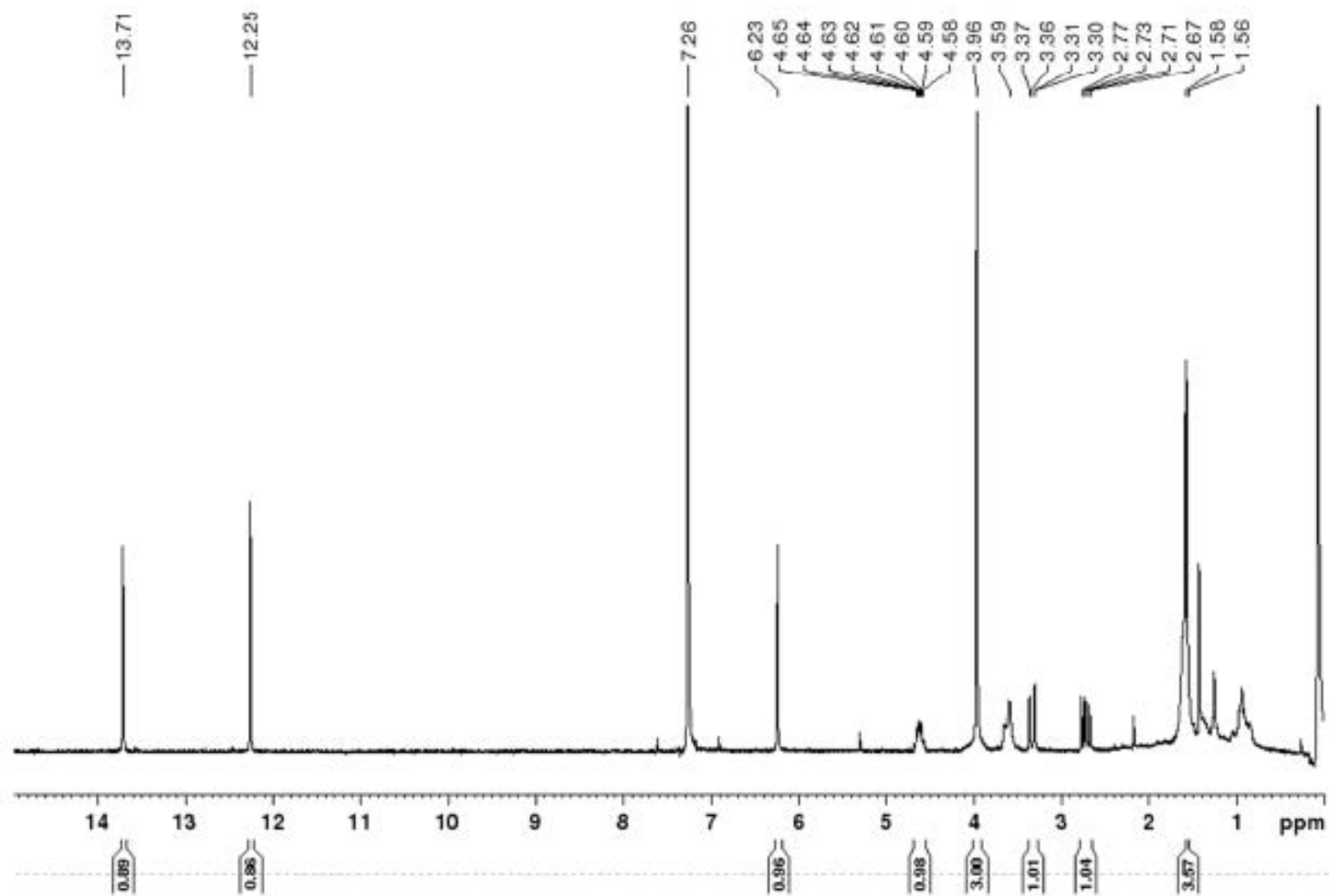
S17. HMBC spectrum (CDCl₃, 500 MHz) of **3**



S18. HMBC (arrows) correlations of **3**

S19. ^1H NMR (CDCl_3 , 500 MHz) of 4



S20. ^1H NMR (CDCl_3 , 500 MHz) of **5**

S21. Cytotoxicity of **5** using a panel of 7 cell lines

	IC ₅₀ (μM) of compounds						
	Huh7D12	Caco2	MDA-MB-231	HCT116	PC3	NCI-H2	Fibroblasts
Haemoventosin (5)	3	4	10	2.6	4	2.5	4
Roscovitin	15	16	15	9	12	18	7
Doxorubicin	0.06	0.03	0.03	0.08	0.09	0.04	0.04
Paclitaxel	0.008	0.014	0.021	0.003	0.004	0.02	> 0.25

Annexe 6 : Molecules 2016 ; 21(3) : 294



Review

Xanthonnes of Lichen Source: A 2016 Update

Pierre Le Pogam and Joël Boustie *

Laboratoire de Pharmacognosie, Equipe PNSCM, (ISCR UMR CNRS 6226), Faculté des Sciences Pharmaceutiques et Biologiques, 2 Avenue du Professeur Léon Bernard, 35043, Rennes Cédex, France; pierre.lepogam-alluard@univ-rennes1.fr

* Correspondence: joel.boustie@univ-rennes1.fr; Tel.: +33-0223-237-840

Academic Editor: Derek J. McPhee

Received: 25 January 2016 ; Accepted: 23 February 2016 ; Published: 2 March 2016

Abstract: An update of xanthonnes encountered in lichens is proposed as more than 20 new xanthonnes have been described since the publication of the compendium of lichen metabolites by Huneck and Yoshimura in 1996. The last decades witnessed major advances regarding the elucidation of biosynthetic schemes leading to these fascinating compounds, accounting for the unique substitution patterns of a very vast majority of lichen xanthonnes. Besides a comprehensive analysis of the structures of xanthonnes described in lichens, their bioactivities and the emerging analytical strategies used to pinpoint them within lichens are presented here together with physico-chemical properties (including NMR data) as reported since 1996.

Keywords: biosynthesis; polyketides; fungi; NMR spectroscopy; bioactivity; lichexanthone; islandicin; thiomelin; secalonic acids

1. Introduction

Xanthonnes are ubiquitous polyphenolic compounds displaying a common 9*H*-xanthen-9-one scaffold [1]. Bioactivities of these compounds depend on their tricyclic core as well as on the nature and/or position of their highly diverse substituents, making them a “privileged structure” [2] likely to bind a variety of targets [3]. Thus, more than 250 of them were shown to display significant bioactivities including antimicrobial, antioxidant and cytotoxic activities [4]. Even though xanthonnes might be regarded as non-specific lichen compounds compared to other structural classes (e.g., depsides, depsidones, dibenzofurans...), the specific biosynthetic pathway of fungal xanthonnes results in novel substitution patterns, highlighting the interest of lichen xanthonnes. Furthermore, since the compendium of lichen substances established by Huneck and Yoshimura in 1996 [5], various xanthonnes of unexpected structures were isolated from lichen sources, further strengthening the interest in the chemodiversity of this source. This review aims at gathering all the recent data regarding the lichen xanthonnes that has appeared since 1996. A brief insight is given into the biosynthetic schemes of lichen xanthonnes with a focus on elements accounting for their specific substitution. Subsequently, the structures of all lichen xanthonnes isolated since 1996 are given and their available physico-chemical properties, including NMR data, are further compiled alongside their published bioactivities.

2. Current Data Regarding the Biosynthesis of Xanthonnes within Lichens

As with most lichen metabolites [6], the biosynthesis of xanthonnes proceeds through the polyacetate/polymalonate pathway, featuring the internal cyclization of a single folded polyketide chain. Two distinct series of xanthonnes are obtained, depending on this folding pattern.

Most lichen xanthonnes arise through the folding of a polyketide intermediate as described by Cacho *et al.* [7], resulting in structures displaying a methyl group in position 8 (Figure 1). Aldol condensation and Claisen-type cyclization and release and yield a benzophenone intermediate

that might spontaneously dehydrate to obtain the central pyrone core. This biosynthetic scheme gives rise to the common oxygen substitution pattern of lichexanthone and norlichexanthone (1,3,6-trihydroxy-8-methylxanthone).

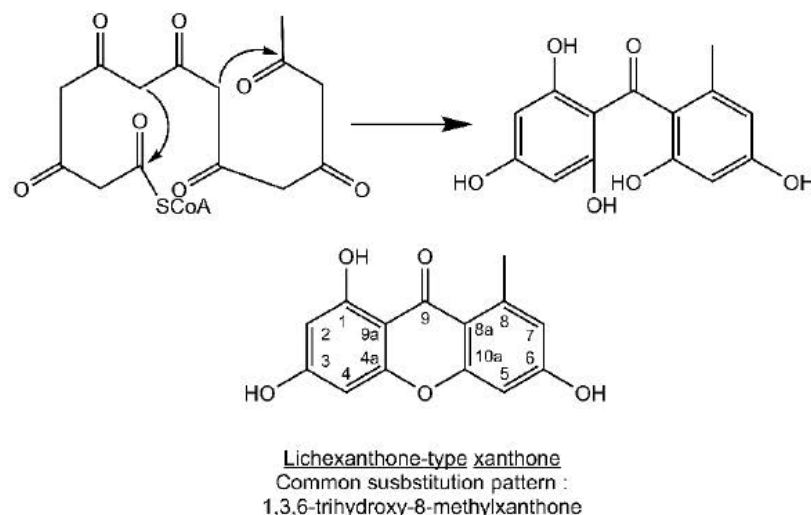


Figure 1. Proposed biosynthetic pathway for lichexanthone-type lichen xanthenes. Adapted from [7].

In contrast, a limited number of structures arise via a distinct biosynthetic pathway that leads to the ravenelin skeleton, with the methyl group in position 3. This biosynthetic scheme begins with the widespread anthraquinone emodin as a precursor [8] (Figure 2). To begin with, the hydroxyl group on C-6 of the emodin disappears (yielding chrysophanol) as it was observed in cell-free preparations of the fungus *Pyrenochaeta terrestris* [9,10]. The hydroxyl group on C-4 is then incorporated after the oxidative ring opens [11]. Deeper insights into this latter biosynthetic event were discussed by Henry and Townsend [12], who proposed an aryl epoxidation across an A-ring edge of chrysophanol to yield an intermediate that lost its A-ring aromaticity. Under this scheme, this intermediate, stabilized by a hydrogen bond between its newly formed phenol group and the neighboring quinone group, recovers its A-ring aromaticity to grant islandicin as a shunt product. An alternative for this intermediate is to undergo a second oxidation, most likely by the same P450 oxygenase, to afford a Baeyer-Villiger cleavage of the central quinone ring to yield an *ortho* carboxybenzophenone that might follow several metabolic fates. A first possibility is the 1,4-addition of a B-ring phenol to the A-ring dienone followed by dehydration and decarboxylation to access ravenelin-like xanthenes after a final oxidation [12]. This results in xanthenes displaying an archetypical 1,4,8-trihydroxy-3-methylxanthone skeleton. A second metabolic pathway, granting access to eumitrins and secalonics acids, is assumed to include a methylation of the carboxy group to prevent its subsequent elimination after a similar 1,4-addition. Finally, a subsequent 1,2-addition to the benzophenone intermediate leads to further cores similar to that of tajixanthone produced by *Aspergillus varicolor*, a skeleton thus far unknown from lichens.

It is noteworthy that the xanthone nucleus of plants is of mixed biosynthetic origin with the A-ring being acetate-derived whereas shikimic acid pathway-derived 3-hydroxybenzoic acid gives rise to the C-ring (Figure 3). Aromatization of the side chain leads to a freely rotating benzophenone intermediate that can further cyclize to yield the xanthone core. Regioselective oxidative coupling can then yield a 1,3,7-trihydroxyxanthone (*Hypericum androsaemum*) or 1,3,5-trihydroxyxanthone (*Centaureum erythraea*) [4].

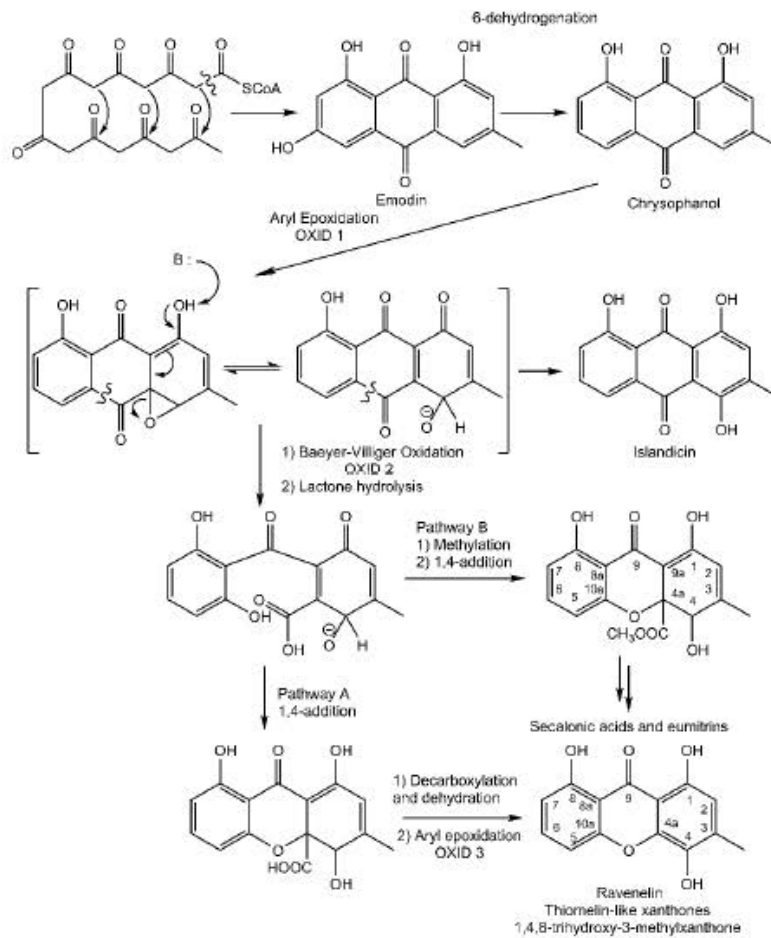


Figure 2. Proposed biosynthetic pathway for thiomelin-type lichen xanthones. Adapted from [12].

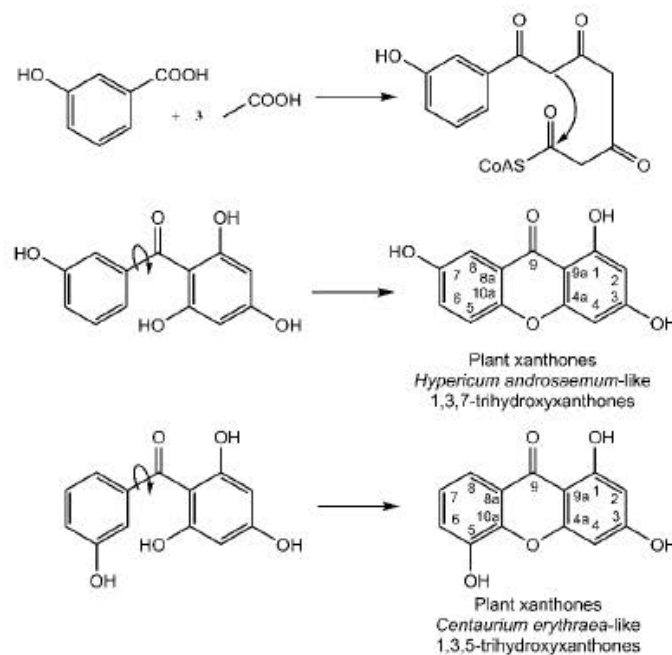


Figure 3. Biosynthesis of xanthones within plants.

Given these different biosynthetic pathways, only few lichen xanthenes are known from non-lichenized organisms. However, some can be produced by higher plants, such as lichexanthone (e.g., *Anthocleista djalensis* [13], *Croton cuneatus* [14], *Cupania cinerea* [15], *Feroniella lucida* [16], *Minquartia guianensis* [17], *Zanthoxylum microcarpum* [18], *Z. valens* [18]), vinetorin (*Hypericum ascyron* [19]). Likewise, non-lichenized fungi have the ability to synthesize some lichen xanthenes, such as lichexanthone from various *Penicillium* [20], norlichexanthone from *Penicillium patulum* [21] and the endolichenic fungus *Ulocladium* [22]; 1,3,6-trihydroxy-8-methylxanthone (also known as griseoxanthone C) is a precursor of aflatoxins—a group of significant environmental mycotoxins—first reported from *Penicillium patulum* [23]. Secalonic acids are also mycotoxins produced by a wide array of fungi [24].

Likewise, very few xanthenes are common to higher plants and fungi, with some such examples being 1,7-dihydroxyxanthone (known from the plants *Vismia parviflora* [25] and *Weddelina squamulosa* [26] while also being produced by a *Penicillium* strain [27]) 1,8-dihydroxy-3-methoxy-6-methylxanthone (plant *Cassia obtusifolia* [28] and fungus *Astrocystis* sp. BCC 22166 [29]), pinselin (plant *Cassia occidentalis* [30] and several fungal strains including an endophytic *Phomopsis* sp. [31], *Talaromyces bacillosporus* [32] and the marine-derived *Engyodontium album* [33]), 6-*O*-methyl-2-deprenylrheediaxanthone B (plant *Garcinia vieillardii* [34] and fungus *Phomopsis* sp. [31]), as well as 8-desoxygartanin (produced by both *Garcinia mangostana* and *Streptomyces rishiriensis* 265-P5921 (according to the Dictionary of Natural Products)). It can therefore be stated that xanthenes are highly unique to each realm, legitimating joint efforts on higher plants, non-lichenized fungi and lichens to widen the chemical diversity of these privileged structures.

Recent data regarding the number of naturally occurring xanthenes are scarce, with the last numbered record of 278 xanthenes listed by Vieira and Kijjoa more than 10 years ago [3]. By January 2016, the Dictionary of Natural Products revealed a dramatic increase in the number of natural xanthenes with *ca.* 2000 occurrences of xanthenes *sensu lato* (*i.e.*, including their reduced derivatives di-, tetra- and hexahydroxanthenes). These considerable efforts might be explained by the discovery of promising leads such as the anti-angiogenic molecule Vadimezan (AS 404) which is currently undergoing phase III clinical trials as a tumor vascular-disrupting agent [35,36], as well as the pleiotropic pharmacological activities of mangosteen xanthenes which have garnered considerable interest from the scientific community [37,38]. Obviously, plants remain the prevalent source of xanthenes, concentrating almost 80% of natural xanthenes. Non-lichenized fungi represent a further 15% while lichens account for the remaining 5% (Figure 4).

ORIGIN OF NATURALLY OCCURRING XANTHONES

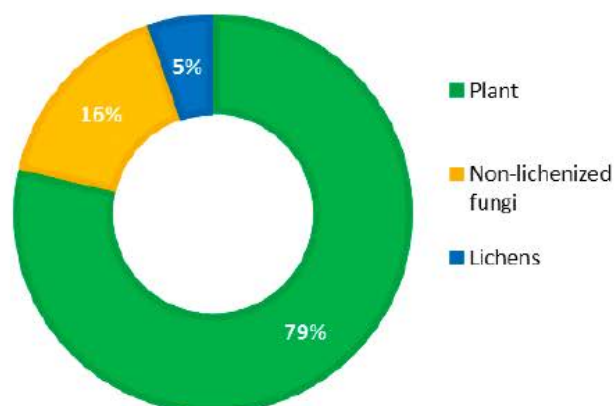


Figure 4. Pie diagram showing the distribution of source organisms for 1940 naturally occurring xanthenes (established by consultation of the Dictionary of Natural Products, 15 January 2016).

Structural diversity of lichen xanthenes mostly stems from variations in the orientation and degree of chlorination of the norlichexanone or ravenelin core, as well as from the position and extent of methylation of the phenolic groups. Elix and Crook tremendously advanced the understanding of chlorination and methylation processes affecting the xanthone core. Through the example of 40 different species of lichens, theoretical biosynthetic schemes mirroring the sequence of biogenetic events leading to the joint occurrence of xanthenes among lichens were constructed [39]. This results in chemosyndromes in which the biosynthetic intermediates can be expected alongside the final xanthone. As an example, isoarthothelin (=2,5,7-trichloronorlichexanone) might be biosynthesized from 2,4-dichloronorlichexanone and 2,5-dichloronorlichexanone. Therefore, the joint occurrence of these species is referred to as the isoarthothelin chemosyndrome [40].

Further structural modifications might be taken into account to extend the chemodiversity of lichen xanthenes. Important contributors to the chemical diversity of xanthenes are prenyl groups which are most often incorporated as dimethylallyl moieties [41]. Generally speaking, prenylated secondary metabolites are of paramount interest since their bioactivities are often distinct from those of their non-prenylated precursors [42]. Even though prenylxanthenes have been known to come from fungi for a long time [43], no reports of such xanthenes were made by the time Huneck and Yoshimura published their compendium of lichen substances [5] since the first lichen prenylxanthenes were reported by Rezanka *et al.* in 2002 [44]. Underlying biosynthetic pathways were recently outlined within the prenylxanthone-producing fungus *Aspergillus nidulans*, through the identification of prenyltransferase genes belonging to the fungal indole prenyltransferases, so far known for their involvement in the prenylation of amino acids [45]. Glycosylations represent another kind of functionalization recently evidenced from lichen xanthenes through the examples of umbilicaxanthosides A and B [44] and hirtusneanoside [46].

The diversity of lichen xanthenes is also extended through some dimeric xanthenes. Although the identification of key dimerization processes still warrants further investigation, xanthone dimers are most likely obtained after the biaryl linkage of monomers. This hypothesis is preferred to that of a tandem biosynthetic pathway which would involve a side-by-side cyclization of a double-length polyketide, especially since the discovery of the long-sought-after monomeric units of secalonic acids (the so-called blennolides) within the fungus *Blennoria* sp. [47]. Enzymatically mediated or not, it is admitted that the dimerization would involve a xanthyonyl radical that subsequently couples to electron donors. Resonance contributors of this delocalized aryl radical might then account for the reactivity of *ortho* and *para* C positions [24].

Reductive dearomatizations are sometimes observed on xanthenes to yield dihydro-, tetrahydro- or hexahydroxanthenes. To date, in lichens, such reduced species were only observed from dimeric xanthenes: secalonic acids, hirtusneanoside and eumitrin A1 (bis tetrahydroxanthenes) and eumitrin A2, B and T (unsymmetrical tetrahydro- and hexahydroxanthenes). Overall, a vast majority of xanthenes reported from lichens have a monomeric and fully aromatized structure.

3. Contribution of the Symbiotic Partners

Even though xanthenes from free-living fungi are well known, a plant-fungus collaboration has been suggested for several lichen xanthenes. As an example, the typical lichen xanthone 2,7-dichlorolichexanone could be isolated from the lichen *Lecanora dispersa* [48]. However, when the fungus was cultivated in the absence of the alga, the xanthone production was diverted to other secondary metabolites being produced instead (e.g., depsidones such as pannarin and related compounds). A further consistent example is that of *Lecanora rupicola*. This lichen is known to produce metabolites of various polyketide classes: lecanoric acid (depsides), hematommic and orsellinic acids (monocyclic phenols), eugenitol and sordidone (chromones) and arthothelin (xanthone). The whole chemosyndrome could be produced from axenically grown mycobionts, with the notable exception of arthothelin [49], suggesting a likely metabolic cooperation between the symbiotic partners. Likewise, dimeric xanthenes eumitrins are produced by the lichen *Physconia distorta* but not by its isolated

mycobiont [50]. Adversely, axenic cultures of the mycobiont of *Pyrenula japonica* and *P. pseudobufonia* revealed the biosynthesis of xanthenes that cannot be evidenced from the lichen as a whole (see further), suggesting their significance in the pre-lichenized condition [51,52].

A total of 72 xanthenes containing one to four chlorine atoms are currently known from lichens. Even though recent studies have shed light on chlorinated xanthone biosynthesis, no study has focused on their degradation. Dechlorination of organochlorines can be achieved by some bacterial strains, referred to as organohalide respirers. Such bacteria comprise the famous *Dehalococcoides mccartyi* that has gathered attention because of its ability to dechlorinate a large array of anthropogenic pollutants [53–55]. Later on, related bacteria were also reported from an unpolluted environment, suggesting their involvement in homeostatic chlorine cycling [56–58]. Therefore, a contribution from the rich bacterial communities sheltered by lichens can be envisaged. Notably, some such organohalide respirers belong to the Firmicutes phylum [59], which is represented among the bacterial diversity hosted by lichens [60–62]. However, comparative studies of bacterial populations harvested by chlorinated xanthenes producing lichens and lichens lacking such metabolites are mandatory for validating this assumption. Given the close structural homologies between chlorinated xanthenes and polychlorinated biphenyls (PCB) and dibenzo-*p*-dioxins (dioxins), such bacterial strains might be of paramount interest for bioremediation purposes [59]. Acting as alternative electron acceptors, chlorinated xanthenes might serve as biostimulants to speed up the remediation at contaminated sites [59,63].

4. Analytical Chemistry: From Detection to Structure Elucidation

Although widespread among lichens, the long neglect of xanthenes compared to other structural classes most likely arises from initial confusion in structural assignments between isomers and the subsequent difficulties in distinguishing the large number of co-occurring isomers [64]. However, the reliability of structural assignments tremendously increased over the last decades as refined dereplicative processes were developed. By 1993, a normalized reverse phase HPLC technique defined retention indices for 393 lichen products—including 55 xanthenes—revealing that numerous xanthone isomers had different retention times [65]. Likewise, standardized TLC procedures were defined [66–68], with specific guidelines dedicated to xanthenes [69]. A further enhancement of the normalized HPLC procedure was its subsequent hyphenation with a photodiode array detector to screen for xanthenes based on their specific UV/Vis spectra [70]. As fluorescent substances, the color of lichen metabolites in long-wave UV light has been used for a long time as a hint to determine their structural class, especially for TLC. While the color of xanthenes at such wavelengths is expected to range from bright yellow to orange, anthraquinones vary from bright red to vermilion and pulvinic acid derivatives appear yellowish [71]. At last, depsides and depsidones generally fluoresce blue to white or shades of grey, although atranorin gives a yellow hue [72]. Such features paved the way for fluorescence microscopy studies undertaken on semi-thin sections of lichens to explore the location of lichen metabolites across sections of a range of macrolichens [73]. However, an obvious limitation of this approach is that it only depends on the structural group scaffold and therefore it does not discriminate between individual compounds. Structural assignments have now been confirmed by the unambiguous synthesis of most lichen xanthenes [74–76]. A further strategy to improve the information granted by the aforementioned separative techniques is the subsequent detection by mass spectrometry. If HPLC-MS of lichen extracts is now widely used for lichen dereplication, with the possible detection of xanthenes, no TLC-MS reports have yet been made to the best of the authors' knowledge [77]. To date, no standardized liquid chromatography-UV-mass spectrometry methodology has been published on lichen metabolites. However, a few non-specific lichen xanthenes (lichexanthone, norlichexanthone, secalononic acid D) can be found in the fungal database established by Nielsen and Smedsgaard [78]. As far as mass spectrometry is concerned, various lichen xanthenes were shown to be ionizable in negative-ion mode LDI-MS (Laser Desorption and Ionization), directly providing a complete chemical fingerprint from the complete acetone extract of the chloroxanthone-containing

Lecidella asema, without the need for matrix assistance [79]. Lately, the ambient ionization technique DART-MS revealed its potent ability in examining lichen secondary metabolites *in situ* [80]. As shown below, the analysis of a whole piece of *Lecidella asema* shows an exhaustive chemical profile (Figure 5).

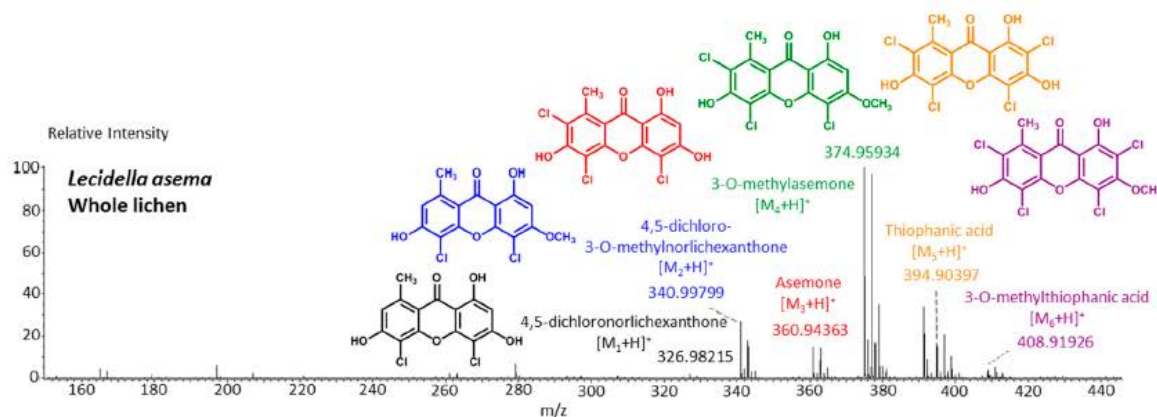


Figure 5. Positive-ion mode DART-MS spectrum of a solid piece of *Lecidella asema*. Experimental conditions as described in [80].

However, regarding the specific example of lichen xanthenes, the lack of mutually supportive data such as chromatographic retention times and/or UV/Vis spectra precludes the differentiation of isomers and is a severe limitation of such methods. Possible ways to overcome such limitations while keeping an *in situ* approach might be the use of a droplet microjunction surface sampling probe and subsequent coupling with HPLC-DAD-MS(MS) to perform separation and therefore to collect retention time and UV/Vis data as obtained with more traditional dereplication protocols [81]. Even though such enhancements might shorten the time lapse for drug discovery through pinpointing and streamlining the isolation of original compounds, NMR analysis remains mandatory for elucidating structure, especially for highly isomeric structures such as xanthenes. For a long time, the poor sensitivity of NMR precluded the structure elucidation of numerous minor to trace compounds. However, since 2000, significant improvements in reducing the operational sample amount and concentration addressed this shortcoming, especially through the use of low-volume tube probes and capillary probes coupled with cryogenically cooled radiofrequency coils [82]. Such innovations pave the way for the full characterization by one-dimensional (1D) and two-dimensional (2D) NMR of natural products in vanishingly small amounts (down to one nanomole) in reasonable time frames [82,83]. This increased sensitivity is of special significance in the field of lichenology since (i) the collection of bulk quantities of material is often hard to achieve and (ii) the high degree of accumulation of the major metabolites in lichens remains a major pitfall when studying their phytochemistry [84].

Together with analytical achievements, informatics tools were also developed to alleviate the dereplication holdup. A computer software named Wintabolites[®] was dedicated to the identification of lichen metabolites from an original database of 550 compounds, including HPLC retention indices, TLC-Rf values, UV/visible colors of TLC spots and thalline reactions to guide their identification [85]. A most valuable upgrade of this informatics approach is LIAS metabolites (A Global Information for Lichenized and non-lichenized Ascomycetes) [86], a database compiled by Pr. J.A. Elix with additions by Pr. K. Kalb. Extended to 881 secondary metabolites as of January 2016, this database now includes mass spectrometry data besides HPLC and TLC standardized chromatographic values. Useful information regarding the structural class of the metabolites and biosynthetically related compounds is also given [87].

5. Structures and Bioactivities of Lichen Xanthones

It is noteworthy that lichen xanthones described up to 1996 most often belonged to the two basic cores described earlier with canonical substitution patterns. Today, 62 molecules displaying the lichexanthone scaffold and 19 molecules following the thiomelin substitution pattern (Figure 2) have been described. However, the logical biosynthetic sequences delineated by Elix and Crook [39] enable the prediction of putative intermediates that have not yet been reported from lichens. These putative intermediates might represent eight additional lichexanthone derivatives and three other thiomelin-type xanthones. Interestingly, a number of xanthone species described as putative in 1996 [5] have been purified since then. Such species include 7-chlorolichexanthone (*Lecanora schofieldii* [88]), 2,4-dichloro-3-*O*-methylnorlichexanthone (*Pertusaria aceroae* and *P. calderae* [89]), 2,5-dichloro-3-*O*-methylnorlichexanthone (obtained from *Calopadia fusca* [90] among others), 3,6-di-*O*-methylthiophanic acid from *Calopadia subcoerulescens* [90] and *Phyllopsora chodatunica* [91]), 4,5,7-trichlorolichexanthone (*Sporopodium leprosum* [92]) and 2,4,7-trichloro-3-*O*-methylnorlichexanthone (*Calopadia perpallida* [90]). Chlorinations and methylations from these cores can directly account for the structures of most lichen xanthones described by Huneck and Yoshimura. This diversity of lichen xanthones has to be extended to the vast array of secalonic acid and eumitrin derivatives identified by their chromatographic data but for which their minute amounts have so far hampered their NMR structure elucidation. Such tetrahydroxanthone dimers might represent privileged metabolites given their structural homology with the promising anti-tumor compound phomoxanthone A [93]. One might also take into account the putative monomeric units of secalonic acids and eumitrins, none of them being identified from lichen sources so far.

Besides these fully rationalized structures, a limited number of metabolites exhibit structural variations that are more or less difficult to explain. As an example, demethylchodatun displays a methoxy group in position 4 that might be introduced by a xanthone oxidase on this trichlorinated norlichexanthone derivative. Another unusual modification of the lichexanthone series is the occurrence of two acetyl groups in erythrommone. The chemical structures of xanthones with trivial names discussed in this manuscript are enlisted in Figure 6.

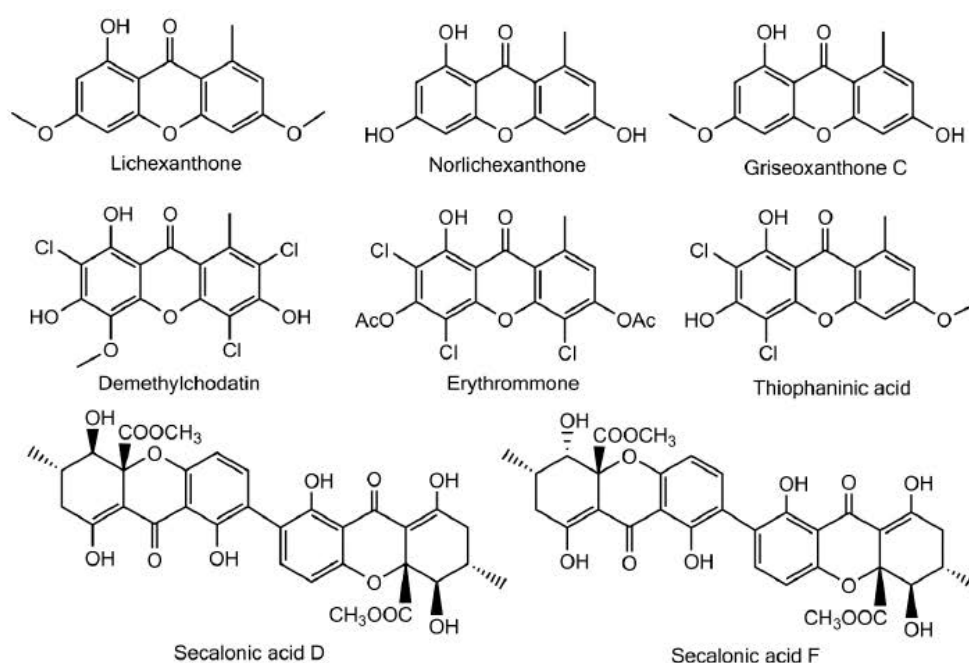


Figure 6. Chemical structures of xanthones with trivial names discussed in this manuscript.

However, 22 lichen xanthenes display unusual structural features that make their biosynthetic intermediates tricky to unravel (including a series of 16 related species described by Rezanka and colleagues [44,94], see further). Three such species were already mentioned in the compendium established by Huneck and Yoshimura [5]: the absence of a methyl substituent in 1,8-dihydroxy-3,6-dimethoxyxanthone is biogenetically difficult to explain, as are the two methyl substituents of 1,7-dihydroxy-2,4-dichloro-6,8-dimethylxanthone and of 1-hydroxy-2,4-dichloro-6,8-dimethylxanthone, obtained from *Rinodina thiomela*.

As of 2016, a total of 103 xanthenes were isolated from lichens, implying the presence of 11 further species as biosynthetic intermediates. This chemodiversity will soon be enriched with an extensive array of unidentified tetrahydrobixanthenes and their associated monomeric units.

Very few lichen xanthenes have been investigated to date for their bioactivities. Lichexanthone exerts a weak activity against *Mycobacterium tuberculosis* [95] and *M. aurum* [96]. Despite this mild activity, a dihydropyrane xanthone derivative of lichexanthone revealed an antimycobacterial activity comparable to that of drugs commonly used to treat tuberculosis [97]. Lichexanthone and griseoxanthone C exhibit strong antibiotic effects towards *Bacillus subtilis* with respective IC₅₀ values of 2.25 and 1.29 µM, but only the former inhibited the growth of methicillin-resistant *Staphylococcus aureus* (IC₅₀: 21 µM) [22]. No anti-parasitic activity of lichexanthone could be observed towards *Plasmodium falciparum* and *Trypanosoma brucei* [15]. Lichexanthone also displays sperm mobility-enhancing properties [98] and induces the production of NO by murine macrophages which might reveal their activation [99]. Lichexanthone revealed no cytotoxic activity against murine melanoma B16F10, human melanoma UACC-62 and fibroblast cells NIH/3T3 [100]. At last, lichexanthone was found to be effective against the dengue vector *Aedes aegypti* [98].

Norlichexanthone was shown to display promising cytotoxic activities [101]. Indeed, norlichexanthone caused 100% inhibition of p56^{lck} tyrosine kinase at 200 µg/mL [102] and inhibited the activity of the protein kinases aurora-B, PIM1 and VEGF-R2 with mean IC₅₀ values ranging from 0.3 to 12 µM [103]. Norlichexanthone also promotes the expression of the insulin-sensitizing, anti-diabetic and anti-atherogenic protein adiponectin within cultured ST-13 adipocytes [104]. Dayan and Romagni also reported on the fungicidal effect of thiophanic (Figure 5) and thiophaninic acids [105]. Alongside many other lichen compounds, Huneck and Schreiber reported on the allelopathic effect of thiophanic acid towards a wide array of higher plants [106].

As most structural classes of lichen metabolites, xanthenes display strong UV-absorbing properties, predominantly in the wavelength range of UVA [107]. Indeed, lichexanthone synthesis could be triggered in juvenile mycelia of *Haematomma fluorescens* as a response to a 365 nm UV light exposure, emphasizing its protective role as a light filter [108]. Deposition of xanthenes in the cortical layers further suggests their involvement in the protection of the UV-sensitive algal layer [109,110]. Such properties might be of utmost interest when urgently needing new materials to outperform the currently used UV-photoprotective products [111]. A Time-Dependent Density Functional Theory (TD-DFT) modelization recently delineated the electronic transitions accounting for the UV/Vis spectra of secalonic acids. This revealed that absorption wavelengths and molecular extinction coefficients obtained from these bisxanthenes were comparable to that of UVA-referent sunscreens, which might stem from the structural homologies shared by the commercially available avobenzone and the phenyl-β-diketo moiety of xanthenes [112].

6. New Lichen Xanthenes Described since 1996: Discussion, Physico-Chemical Properties (Including NMR Data) and Bioactivities

The past 20 years witnessed the isolation of 23 further lichen xanthenes. It is noteworthy that those new xanthenes displayed original substitution patterns and revealed original moieties compared to the previous state of the art.

Cultures of the spore-derived mycobionts of *Pyrenula japonica* and *P. pseudobufonia* afforded a series of five new ravenelin-type lichen xanthenes, the first reports of such xanthenes from aposymbiotically

grown lichen mycobionts. A first report elucidated the structures of 1,5,8-trihydroxy-3-methylxanthone, 1,8-dihydroxy-5-methoxy-3-methylxanthone and 1,7-dihydroxy-3-methylxanthone [51] while a second one established the occurrence of 1,8-dihydroxy-3-hydroxymethyl-5-methoxyxanthone and 1,4,8-trihydroxy-5-methoxy-3-methylxanthone, typically associated with the thiomelin pathway [52]. Notably, 1,7-dihydroxy-3-methylxanthone stands among the rare xanthenes also described from plants (*Cassia occidentalis* [113]) and also from an Ascomycete fungus [114]. Surprisingly, all molecules described from this series lack the 4-hydroxy group with four of them displaying an unusual oxygenated substituent at C5 instead. In one case, position 2 is oxygenated, which is a unique structural feature among the lichen xanthenes described so far. One will note that 1,7-dihydroxy-3-methylxanthone also lacks the oxygenated substituent on C8 which is replaced by a unique hydroxyl substituent on C7, an unprecedented structural peculiarity for a lichen xanthone. Finally, the oxidation of the methyl group into a hydroxymethyl for one of these molecules is also new to lichen xanthenes. Of special interest is that these compounds could not be identified from the whole lichen, whereas they are constantly isolated from mycobionts harvested in highly unrelated sampling sites (one in Japan and one in the USA), which might point to their biological significance in the prelichenized condition. Notably, 1,5,8-trihydroxy-3-methylxanthone and 1,2,8-trihydroxy-5-methoxy-3-methylxanthone displayed stronger antioxidant activities than α -tocopherol via the DPPH radical test [52]. Besides, 1,7-dihydroxy-3-methylxanthone also exerts a moderate Mono Amine Oxidase-inhibiting activity [114].

Two highly unusual glycosylated prenylxanthenes were subsequently identified from the Ural lichen *Umbilicaria proboscidea* [44]. Umbilicaxanthoside A is a C2-monoprenyl xanthone having a β -D-glucopyranose unit anchored at position O-7, whereas umbilicaxanthoside B stands for a C2,C8-diprenylxanthone with a disaccharide β -D-glucopyranose-(1 \rightarrow 4)- β -D-glucopyranose moiety at O-7. These compounds were the first prenylated xanthenes to be isolated from a lichen source and glycosides are not frequently encountered in lichens [84]. Besides, both molecules reveal a highly unusual oxygenation pattern, rendering their biosynthetic pathway tricky to delineate. A follow-up study carried out on the same lichen identified 14 acylated xanthone O-glycosides corresponding to linolenoyl, lineoyl, palmitoleoyl, oleoyl, palmitoyl, eicosenoyl and stearoyl esters of both umbilicaxanthosides A and B [94]. Fragmentation patterns obtained by LC-APCI-MS were highly informative and could establish the nature of the esterified fatty acid. None of those compounds were investigated for their biological properties.

The last monomeric xanthone isolated so far from a lichen source is cladoxanthone A (=1,5-dihydroxy-2,4,6-trichloro-7-methylxanthone), obtained from *Cladonia incrassata* [115]. The occurrence of a methyl substituent on C-7 is an unprecedented structural feature among lichen xanthenes, thus questioning the underlying biogenetic schemes. A possible hypothesis to account for the structure of this xanthone is to consider ziganein as a possible anthraquinone precursor [116]. It is noteworthy that this metabolite presents a substitution pattern identical to that of cladoxanthone A and it was isolated from the endophytic fungus *Sporormiella minimoides* [116] (Figure 7). Cladoxanthone A revealed an antibacterial effect towards *Staphylococcus aureus* even though the paucity of the compound precluded the determination of a minimal inhibitory concentration [115].

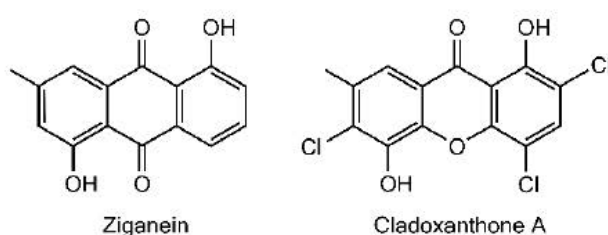


Figure 7. Compared chemical structures of ziganein and cladoxanthone A.

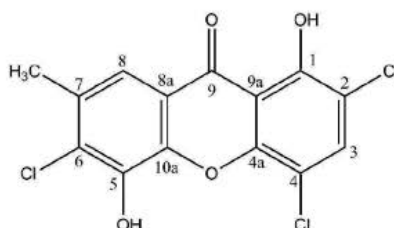
Regarding dimeric xanthenes, known metabolites of the secalononic acid series were first isolated from lichen sources in 2009, *i.e.*, secalononic acids B, D and F were purified from *Diploicia canescens* [117]. The joint occurrence of these isomers in this lichen is not surprising because of their biosynthetic relationship. Indeed, the association of the two monomeric tetrahydroxanthone blennolides A and B, respectively, yields secalononic acids B and D [47]. Secalononic acid F then represents a hybrid dimer of blennolides A and B. It is noteworthy that each of these compounds displays an identical configuration at C-10a, suggesting that the cyclization is catalyzed by a specific enzyme giving rise to a unique type of product [117]. Secalononic acid is a major environmental mycotoxin essentially known for its production by the microbial *Penicillium oxalicum*, a notorious foodstuff contaminant. Such a presence represents an alarming health issue given the acute toxicity and the teratogenic effects of secalononic acid D [118,119], warranting extended investigations of its bioactivities which highlighted its pleiotropic pharmacological activities. Secalononic acids D and F revealed antimicrobial activities against *Bacillus megaterium* while secalononic acid A displayed activity against *Bacillus subtilis* and *Piricularia oryzae* [120]. Likewise, secalononic acid B is an effective antimicrobial (*Bacillus megaterium* and *Escherichia coli*) as well as antifungal (*Microbotryum violaceum*) and antialgal agent (*Chlorella fusca*) [47]. Several reports suggested the cytotoxic activity of secalononic acid derivatives [117]. Bioassay-guided fractionation of the extracts of the marine lichen-derived *Gliocladium* sp. T 31 streamlined the isolation of secalononic acid D as the cytotoxic metabolite against four cell lines in a highly variable range of 0.03–15 μM , suggesting selective pharmacodynamic properties [121]. Further studies revealed a submicromolar IC_{50} of secalononic acid D on the carcinoma KB cells and an inhibition of human topoisomerase 1 with a promising IC_{50} of 0.16 $\mu\text{g}/\text{mL}$ [122]. More recently, secalononic acid D was shown to down-regulate the expression of efflux pump ABCG2 which is known to confer the Multidrug Resistance phenotype [123]. As a last contribution to its cytotoxic activity, secalononic acid D exhibits an anti-angiogenic activity via the Akt/mTor/P70S6K pathway [124]. Another feature of the pleiotropic activities of secalononic acid D depends on the inhibition of protein kinase C and several other Ca^{++} -dependent enzymes through competitive inhibition [125]. Subsequent disruptions of cell signaling might account for the teratogenicity of these compounds. Indeed, it was demonstrated on a murine model that secalononic acid D decreases the levels of Epidermal Growth Factor (EGF) as well as its associated signal transduction [126]. As a consequence, inhibition and alteration of transcription factors in the developing murine plate following an exposition to the toxin at normal human dietary levels were observed, resulting in the cleft palate condition [127,128].

Hirtusneanoside is a new xanthone dimer isolated from *Usnea hirta* corresponding to a rhamnoside of an unsymmetrical dimeric tetrahydroxanthone [46]. If the oxygenation pattern can be fully rationalized according to the biosynthetic pathway discussed earlier, this structure contains several additional methyl groups of unknown origin. Hirtusneanoside was proven to be active against *Staphylococcus aureus* and *Bacillus subtilis* [46]. The enzymatic hydrolysis of hirtusneanoside yielded α -L-rhamnose and the aglycone named hirtusneanin, the physico-chemical data of which were also reported by Rezanka and Sigler [46].

Available physico-chemical properties regarding the newly described lichen compounds are listed below.

Cladoxanthone A

$\text{C}_{14}\text{H}_7\text{O}_4\text{Cl}_3$ (343.94099)



Yellow powder

UV λ_{\max} (MeOH)(log ϵ): 381 (3.24), 323 (3.50), 259 (4.11) nm

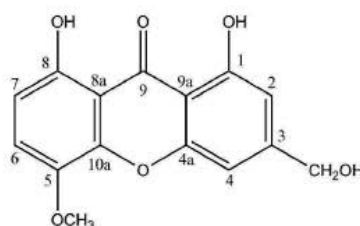
IR ν_{\max} (CHCl₃): 3353, 3056, 1642, 1597, 1450, 800 cm⁻¹

Sources: *Cladonia incrassata* [115].

Cladoxanthone A (CDCl ₃)		
Position	δ_C	δ_H (J in Hz)
1	156.2	-
-OH 1	-	13.16 (s) (1H)
2	115.2	-
3	136.6	7.80 (s) (1H)
4	111.2	-
4a	149.5	-
5	141.2	-
-OH 5	-	6.09 (s) (1H)
6	127.9	-
7	133.7	-
CH ₃ -7	20.2	2.51 (s)
8	117.0	7.73 (s)
8a	118.4	-
9a	109.7	-
10a	143.0	-

1,8-Dihydroxy-3-hydroxymethyl-5-methoxyxanthone

C₁₅H₁₂O₆ (288.06339)



Yellow needles, mp 221–222 °C

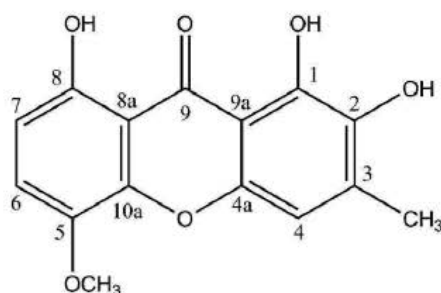
UV λ_{\max} (MeOH)(log ϵ): 387.5 (3.27), 341 (3.84), 271 (4.16), 263 (4.24), 255 (4.29), 236 (4.17)

IR ν_{\max} (KBr): 3533, 1659, 1634, 1609, 1589, 1493 cm⁻¹

Sources: Mycobiont of *Pyrenula japonica* [52].

1,8-Dihydroxy-3-hydroxymethyl-5-methoxyxanthone (DMSO- <i>d</i> ₆)		
Position	δ_C	δ_H (J in Hz)
1	160.0	-
-OH 1	-	11.10 (br s) ^a
2	107.7	6.98 (br s) (1H)
3	154.8	-
3-CH ₂ OH	62.2	4.57 (br s) (2H)
3-CH ₂ OH	-	5.58 (br s) (1H)
4	104.2	6.75 (br s) (1H)
4a	155.6	-
5	139.7	-
5-OCH ₃	56.7	3.86 (s) (3H)
6	121.1	7.45 (d, 9.0) (1H)
7	108.9	6.71 (d, 9.0) (1H)
8	152.7	-
8-OH	-	11.60 (br s) ^a
8a	107.8	-
9	184.9	-
9a	106.1	-
10a	144.8	-

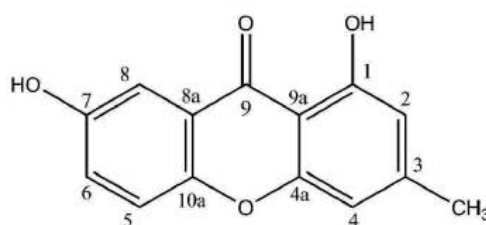
^a These signals might be switched.

1,2,8-Trihydroxy-5-methoxy-3-methylxanthoneC₁₅H₁₂O₆ (288.06339)

Yellow needles, mp 214–215 °C

UV λ_{\max} (MeOH) (log ϵ): 421 (3.42), 352 (3.58), 280 (4.27), 263 (4.18), 243 (4.17), 206 (4.23)IR ν_{\max} (KBr): 3487, 1663, 1636, 1607, 1576, 1489 cm⁻¹Sources: Mycobiont of *Pyrenula japonica* [52].

1,2,8-Trihydroxy-5-methoxy-3-methylxanthone (DMSO- <i>d</i> ₆)		
Position	δ_C	δ_H (J in Hz)
1	145.8	-
2	138.4	-
-OH 2	-	-
3	137.0	-
3-CH ₃	17.1	2.30 (s) (3H)
4	107.6	6.95 (br s) (1H)
4a	147.7	-
5	139.7	-
5-OCH ₃	56.7	3.88 (s) (3H)
6	120.5	7.45 (d, 9.0) (1H)
7	108.2	6.70 (d, 9.0) (1H)
8	152.6	-
8a	107.6	-
9	185.1	-
9a	105.9	-
10a	145.0	-

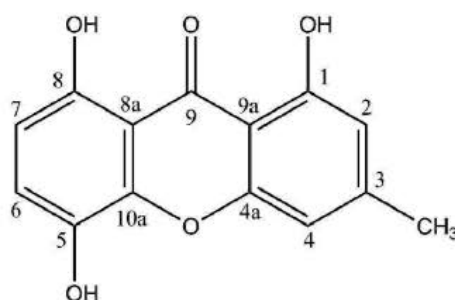
1,7-Dihydroxy-3-methylxanthoneC₁₄H₁₀O₄ (242.05791)

Yellow needles, mp 259–260 °C

UV λ_{\max} (MeOH) (log ϵ): 384 (3.84), 290 (3.98), 261 (4.58), 235 (4.45)IR ν_{\max} (KBr): 3285, 1653, 1607, 1585, 1483 cm⁻¹Sources: Mycobiont of *Pyrenula japonica* [52].

1,7-Dihydroxy-3-methylxanthone (CDCl ₃ -CD ₃ OD)		
Position	δ_C	δ_H (J in Hz)
1	161.7	-
2	111.1	6.57 (br s) (1H)
3	149.5	-
3-CH ₃	22.6	2.42 (s) (3H)
4	108.1	6.75 (br s) (1H)
4a	157.1	-
5	119.6	7.37 (d, 9.0) (1H)
6	125.5	7.29 (dd, 9.0, 2.5) (1H)
7	154.5	6.70 (d, 9.0) (1H)
8	109.0	7.52 (d, 2.5) (1H)
8a	121.6	-
9	182.5	-
9a	107.1	-
10a	150.8	-

1,5,8-Trihydroxy-3-methylxanthone

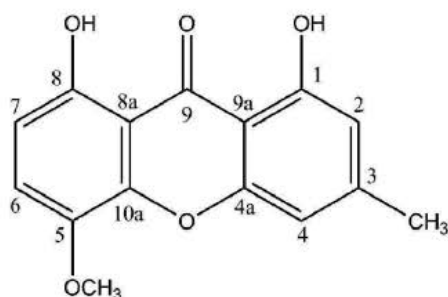
C₁₄H₁₀O₄ (258.05282)

Yellow needles, mp 277–278 °C

UV λ_{\max} (MeOH) (log ϵ): 403 (3.54), 341 (4.01), 272 (4.58), 263 (4.40), 255 (4.47), 236 (4.32)IR ν_{\max} (KBr): 3461, 1661, 1633, 1606, 1591, 1497 cm⁻¹Sources: Mycobiont of *Pyrenula japonica* and *Pyrenula pseudobufonia* [52].

1,5,8-Trihydroxy-3-methylxanthone (CDCl ₃)		
Position	δ_C	δ_H (J in Hz)
1	161.4	-
1-OH	-	11.85 (s) (1H) ^a
2	111.9	6.62 (m) (1H)
3	150.6	-
3-CH ₃	22.7	2.45 (s) (3H)
4	108.5	6.89 (m) (1H)
4a	156.9	-
5	137.8	-
6	124.6	7.24 (d, 9.0) (1H)
7	110.0	6.64 (d, 9.0) (1H)
8	153.6	-
8-OH	-	11.27 (br s) (1H) ^a
8a	108.6	-
9	186.5	-
9a	106.4	-
10a	144.7	-

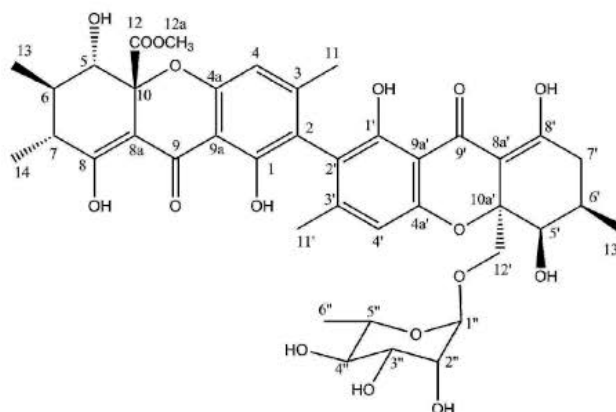
^a Signals appearing in DMSO-*d*₆ only.

1,8-Dihydroxy-5-methoxy-3-methylxanthoneC₁₅H₁₂O₅ (272.06847)

Yellow needles, mp 214–215 °C

UV λ_{max} (MeOH) (log ε): 393 (3.54), 340 (4.00), 272 (4.30), 254 (4.49), 235 (4.36)IR ν_{max} (KBr): 3445, 1661, 1631, 1609, 1585, 1489 cm⁻¹Sources: Mycobiont of *Pyrenula japonica* and *Pyrenula pseudobufonia* [52].

1,8-Dihydroxy-5-methoxy-3-methylxanthone (CDCl ₃)		
Position	δ _C	δ _H (J in Hz)
1	161.0	-
1-OH	-	11.73 (s) (1H) ^a
2	111.7	6.62 (br s) (1H)
3	149.9	-
3-CH ₃	22.6	2.42 (s) (3H)
4	108.0	6.84 (br s) (1H)
4a	156.0	-
5	140.0	-
5-OCH ₃	57.4	3.94 (s) (3H)
6	120.8	7.23 (d, 9.0) (1H)
7	109.1	6.70 (d, 9.0) (1H)
8	154.2	-
8-OH	-	11.33 (br s) (1H) ^a
8a	108.3	-
9	185.6	-
9a	105.9	-
10a	145.6	-

^a Signals appearing in DMSO-*d*₆ only.**Hirtusneanoside**C₄₀H₄₆O₁₇ (798.27350)

Faint yellow crystals, mp 231–232 °C

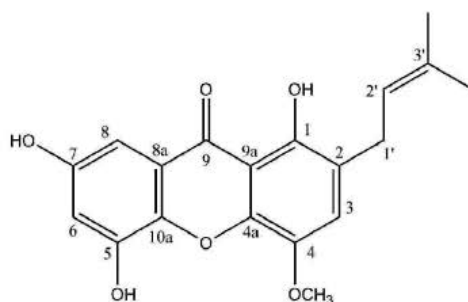
$[\alpha]_D^{20} = -251$ ($c = 0.02$ in MeOH)

UV λ_{\max} (MeOH)(log ϵ): 340 (3.24), 275 (4.01), 230 (4.52) nm

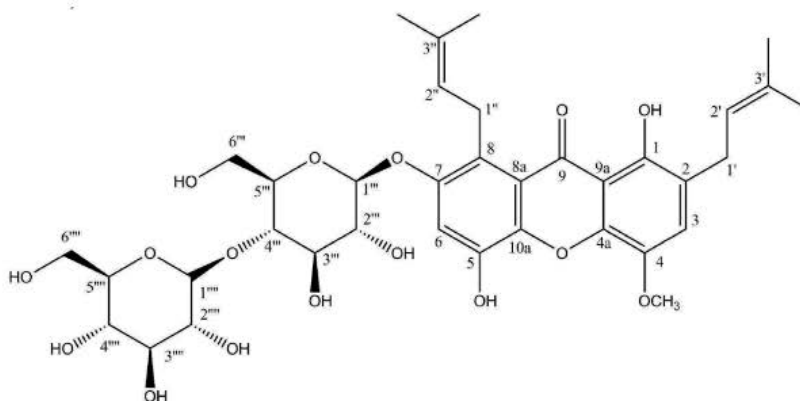
IR ν_{\max} (CHCl₃): 3290, 1735, 1620, 1590, 870 cm⁻¹

Sources: *Usnea hirta* [46].

Hirtusneanoside (DMSO- <i>d</i> ₆)		
Position	δ_C	δ_H (<i>J</i> in Hz)
1	159.2	-
-OH 1	-	11.5 (br s) (1H)
2	116.7	-
3	149.6	-
4	109.2	6.66 (s) (1H)
4a	156.8	-
5	68.8	4.02 (d, 9.5) (1H)
6	31.3	2.05 (ddq, 10.3, 9.5, 6.7) (1H)
7	36.7	2.36 (dq, 10.3, 6.4) (1H)
8	177.8	-
-OH 8	-	13.7 (br s) (1H)
8a	101.3	-
9	186.8	-
9a	105.7	-
10a	85.1	-
11	20.7	1.94 (s) (3H)
12	171.3	-
12a	54.3	3.73 (s) (3H)
13	15.6	1.09 (d, 6.7) (3H)
14	17.3	1.01 (d, 6.4) (3H)
1'	159.6	-
1'-OH	-	11.5 (br s) (1H)
2'	118.1	-
3'	150.2	-
4'	109.3	6.69 (s) (1H)
4a'	156.7	-
5'	68.9	4.07 (d, 1.3) (1H)
6'	28.5	2.28 (dddq, 11.3, 6.7, 6.5, 1.3) (1H)
7'	33.6	2.48 (dd, 19.2, 11.3) (1H) 2.35 (dd, 19.2, 6.5) (1H)
8'	177.6	-
8'-OH	-	13.7 (br s) (1H)
8a'	101.8	-
9'	186.6	-
9a'	106.3	-
10a'	84.4	-
11'	20.6	1.96 (s) (3H)
12'	64.5	3.89 (d, 13.0) (1H) 3.51 (d, 13.0) (1H)
13'	17.7	1.04 (d, 6.7) (3H)
1''	101.1	5.01 (d, 1.5) (1H)
2''	72.2	3.89 (dd, 2.5, 1.5) (1H)
3''	70.9	3.71 (dd, 9.5, 2.5) (1H)
4''	74.5	4.32 (t, 9.5) (1H)
5''	69.7	4.13 (dq, 9.5, 6.5) (1H)
6''	18.6	1.31 (d, 6.5) (3H)

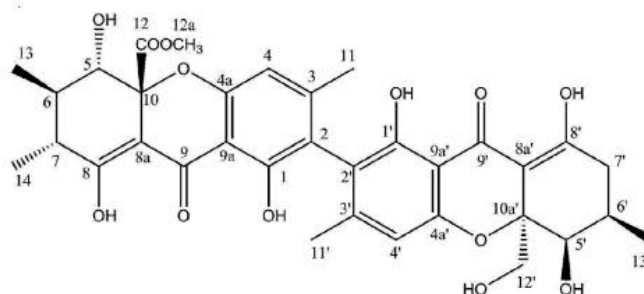
Umbilicaxanthone AC₁₉H₁₈O₆ (342.11034)Sources: *Umbilicaria proboscidea* [44].

Umbilicaxanthone A (CDCl ₃)		
Position	δ _C	δ _H (J in Hz)
1	150.9	-
1-OH	-	13.25 (s) (1H)
2	118.2	-
3	120.1	6.51 (s) (1H)
4	142.6	-
4-OCH ₃	56.4	3.75 (s) (3H)
4a	140.9	-
5	146.4	-
6	102.1	6.15 (d, 2.1) (1H)
7	156.9	-
8	106.3	a
8a	128.9	-
9	179.8	-
9a	116.1	-
10a	136.5	-
1'	22.0	3.19 (d, 6.6) (2H)
2'	123.5	5.92 (td, 6.6, 1.3) (1H)
3'	131.3	-
4'	25.9	1.64 (s) (3H)
5'	17.9	1.57 (s) (3H)

Umbilicaxanthoside BC₃₆H₄₆O₁₆ (734.27859)

Pale yellow needles, mp 133 °C

Hirtusneanine

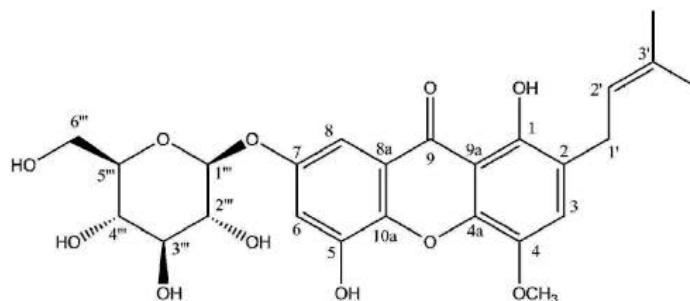
C₃₄H₃₆O₁₃ (652.21559)

Pale yellow crystals, mp 251–253 °C

 $[\alpha]_{\text{D}}^{20} = -232$ ($c = 0.01$ in MeOH)UV λ_{max} (MeOH)(log ϵ): 338 (3.97), 275 (4.04), 231 (4.43) nmIR ν_{max} (CHCl₃): 3290, 1734, 1608, 1590, 870 cm⁻¹Sources: *Usnea hirta* [46].

Hirtusneanine (DMSO- <i>d</i> ₆)		
Position	δ_{C}	δ_{H} (<i>J</i> in Hz)
1	159.2	-
-OH 1	-	11.5 (br s) (1H)
2	116.7	-
3	149.6	-
4	109.2	6.66 (s) (1H)
4a	156.8	-
5	68.8	4.02 (d, 9.5) (1H)
6	31.3	2.05 (ddq, 10.3, 9.5, 6.7) (1H)
7	36.7	2.36 (dq, 10.3, 6.4) (1H)
8	177.8	-
-OH 8	-	13.7 (br s) (1H)
8a	101.3	-
9	186.8	-
9a	105.7	-
10a	85.1	-
11	20.7	1.94 (s) (3H)
12	171.3	-
12a	54.3	3.73 (s) (3H)
13	15.6	1.09 (d, 6.7) (3H)
14	17.3	1.01 (d, 6.4) (3H)
1'	159.6	-
1'-OH	-	11.5 (br s) (1H)
2'	118.1	-
3'	150.2	-
4'	109.3	6.69 (s) (1H)
4a'	156.7	-
5'	68.7	4.07 (d, 1.3) (1H)
6'	28.5	2.28 (dddq, 11.3, 6.7, 6.5, 1.3) (1H)
7'	33.6	2.48 (dd, 19.2, 11.3) (1H)
		2.35 (dd, 19.2, 6.5) (1H)
8'	177.6	-
8'-OH	-	13.7 (br s) (1H)
8a'	102.1	-
9'	186.6	-
9a'	106.3	-
10a'	84.1	-
11'	20.6	1.96 (s) (3H)
12'	68.7	4.14 (dd, 13.0, 7.0) (1H)
		3.75 (dd, 13.0, 4.7) (1H)
12'-OH	-	3.28 (m) (1H)
13'	17.7	1.04 (d, 6.7) (3H)

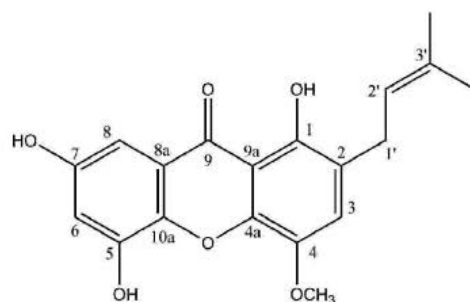
Umbilicaxanthoside A

C₂₅H₂₈O₁₁ (504.16316)

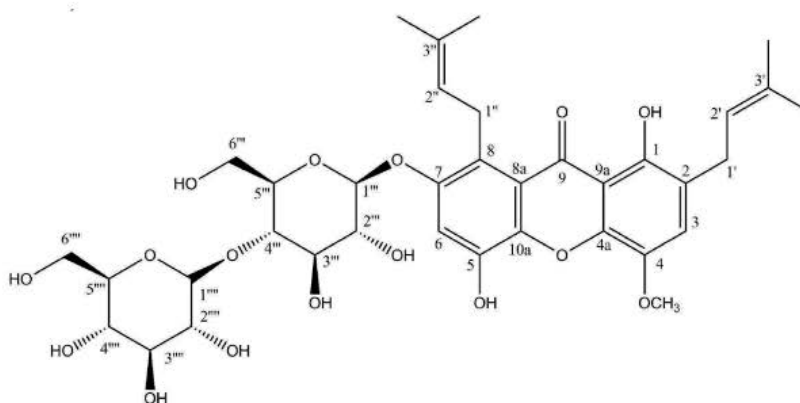
Yellow needles, mp 114 °C

 $[\alpha]_D^{23} = -35$ UV λ_{\max} (MeOH) (log ϵ): 345 (3.90), 310 (4.15), 270 (4.05), 245 (4.50).IR ν_{\max} (KBr): 3320, 2945, 2905, 1643 cm⁻¹Sources: *Umbilicaria proboscidea* [44].

Umbilicaxanthoside A (CDCl ₃)		
Position	δ_C	δ_H (J in Hz)
1	150.9	-
1-OH	-	13.25 (s) (1H)
2	118.2	-
3	120.1	6.51 (s) (1H)
4	142.6	-
4-OCH ₃	56.4	3.75 (s) (3H)
4a	140.9	-
5	146.4	-
6	104.8	6.39 (d, 2.1) (1H)
7	153.0	-
8	108.1	6.73 (d, 2.1) (1H)
8a	128.9	-
9	179.8	-
9a	116.1	-
10a	136.5	-
1'	22.0	3.19 (d, 6.6) (2H)
2'	123.5	5.92 (td, 6.6, 1.3) (1H)
3'	131.3	-
4'	25.9	1.64 (s) (3H)
5'	17.9	1.57 (s) (3H)
1''	99.8	4.80 (d, 7.3) (1H)
2''	74.7	3.52 (dd, 8.9, 7.3) (1H)
3''	77.2	3.58 (t, 8.9) (1H)
4''	71.4	3.41 (t, 8.9) (1H)
5''	78.6	3.45 (m) (1H)
6''	62.6	3.93 (dd, 11.8, 2.3) (1H) 3.72 (dd, 12.1, 5.2) (1H)

Umbilicaxanthone AC₁₉H₁₈O₆ (342.11034)Sources: *Umbilicaria proboscidea* [44].

Umbilicaxanthone A (CDCl ₃)		
Position	δ _C	δ _H (J in Hz)
1	150.9	-
1-OH	-	13.25 (s) (1H)
2	118.2	-
3	120.1	6.51 (s) (1H)
4	142.6	-
4-OCH ₃	56.4	3.75 (s) (3H)
4a	140.9	-
5	146.4	-
6	102.1	6.15 (d, 2.1) (1H)
7	156.9	-
8	106.3	a
8a	128.9	-
9	179.8	-
9a	116.1	-
10a	136.5	-
1'	22.0	3.19 (d, 6.6) (2H)
2'	123.5	5.92 (td, 6.6, 1.3) (1H)
3'	131.3	-
4'	25.9	1.64 (s) (3H)
5'	17.9	1.57 (s) (3H)

Umbilicaxanthoside BC₃₆H₄₆O₁₆ (734.27859)

Pale yellow needles, mp 133 °C

UV λ_{\max} (MeOH) ($\log \epsilon$): 355 (4.06), 319 (4.01), 271 (3.96), 244 (4.08)

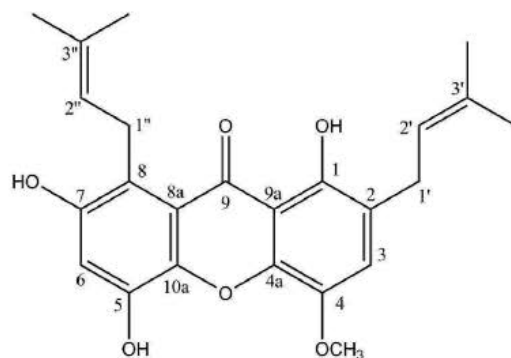
IR ν_{\max} (KBr): 3350, 2950, 2900, 1640 cm^{-1}

Sources: *Umbilicaria proboscidea* [44].

Umbilicaxanthoside B (CDCl_3)		
Position	δ_{C}	δ_{H} (J in Hz)
1	151.0	-
1-OH	-	13.30 (s) (1H)
2	117.8	-
3	119.4	6.47 (s) (1H)
4	143.2	-
4-OCH ₃	56.3	3.75 (s) (3H)
4a	141.3	-
5	147.1	-
6	103.7	6.23 (s) (1H)
7	153.2	-
8	118.4	-
8a	129.6	-
9	183.1	-
9a	114.6	-
10a	135.7	-
1'	25.4	3.38 (d, 7.2) (2H)
2'	123.8	5.39 (td, 7.2, 1.2) (1H)
3'	130.9	-
4'	26.2	1.65 (s) (3H)
5'	18.4	1.79 (s) (3H)
1''	26.1	4.19 (d, 6.8) (2H)
2''	124.8	5.37 (td, 6.8, 1.5) (1H)
3''	132.0	-
4''	25.9	1.67 (s) (3H)
5''	18.0	1.84 (s) (3H)
1'''	99.8	5.05 (d, 8.1) (1H)
2'''	74.2	3.52 (dd, 8.9, 8.1) (1H)
3'''	76.9	3.58 (t, 8.9) (1H)
4'''	78.2	3.12 (dd, 9.3, 8.9) (1H)
5'''	78.7	3.45 (m) (1H)
6'''	62.6	3.93 (dd, 12.1, 2.3) (1H)
		3.72 (dd, 12.1, 5.2) (1H)
1''''	104.1	5.15 (d, 8.0) (1H)
2''''	73.8	3.52 (dd, 9.0, 8.0) (1H)
3''''	76.5	3.58 (t, 9.0) (1H)
4''''	69.7	3.41 (t, 9.0) (1H)
5''''	76.9	3.45 (m) (1H)
6''''	62.6	3.93 (dd, 12.1, 2.2) (1H)
		3.72 (dd, 12.1, 5.2) (1H)

Umbilicaxanthone B

$\text{C}_{24}\text{H}_{26}\text{O}_6$ (410.17294)

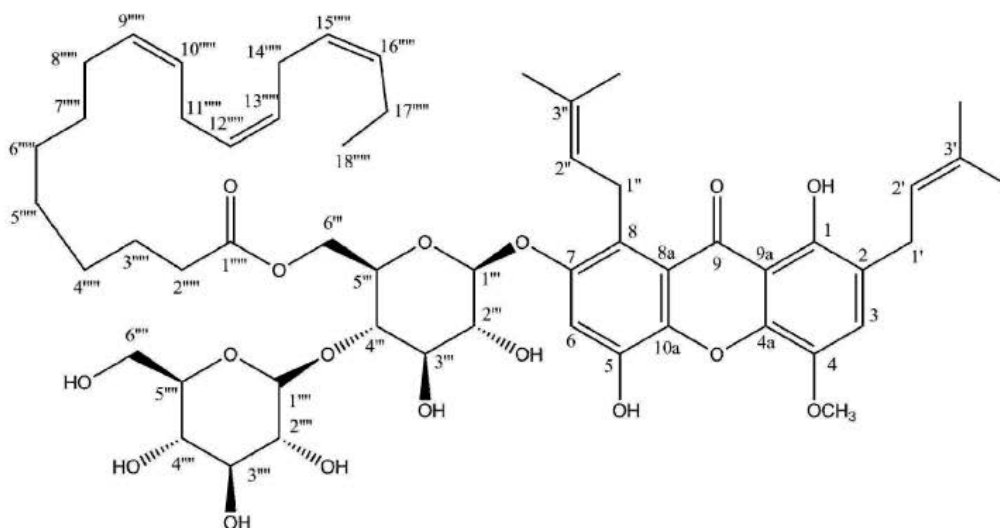


Sources: *Umbilicaria proboscidea* [44].

Umbilicaxanthone B (CDCl ₃)		
Position	δ _C	δ _H (J in Hz)
1	151.0	-
1-OH	-	13.30 (s) (1H)
2	117.8	-
3	119.4	6.49 (s) (1H)
4	143.2	-
4-OCH ₃	56.3	3.75 (s) (3H)
4a	141.3	-
5	146.2	-
6	102.4	6.27 (s) (1H)
7	157.2	-
8	117.6	-
8a	129.6	-
9	183.1	-
9a	114.6	-
10a	135.7	-
1'	25.4	3.38 (d, 7.2) (2H)
2'	123.8	5.39 (td, 7.2, 1.2) (1H)
3'	130.9	-
4'	26.2	1.65 (s) (3H)
5'	18.4	1.79 (s) (3H)
1''	26.1	4.19 (d, 6.8) (2H)
2''	124.8	5.37 (td, 6.8, 1.5) (1H)
3''	132.0	-
4''	25.9	1.67 (s) (3H)
5''	18.0	1.84 (s) (3H)

Linolenylumbilicaxanthoside B

C₅₄H₇₄O₁₇ (994.49260)



Pale yellow needles, mp 133 °C

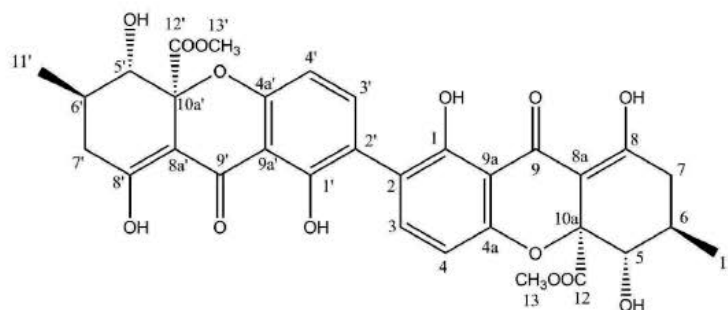
UV λ_{max} (MeOH) (log ε): 355 (4.06), 319 (4.01), 271 (3.96), 244 (4.08)

IR ν_{max} (KBr): 3350, 2950, 2900, 1640 cm⁻¹

Sources: *Umbilicaria proboscidea* [94].

Linolenylumbilicaxanthoside B (CDCl ₃)		
Position	δ_C	δ_H (J in Hz)
1	151.0	-
1-OH	-	13.30 (s) (1H)
2	117.8	-
3	119.4	6.47 (s) (1H)
4	143.2	-
4-OCH ₃	56.3	3.75 (s) (3H)
4a	141.3	-
5	147.1	-
6	103.7	6.42 (s) (1H)
7	153.2	-
8	118.4	-
8a	129.6	-
9	183.1	-
9a	114.6	-
10a	135.7	-
1'	25.4	3.38 (d, 7.2) (2H)
2'	123.8	5.39 (dd, 7.2, 1.2) (1H)
3'	130.9	-
4'	26.2	1.65 (s) (3H)
5'	18.4	1.79 (s) (3H)
1''	26.1	4.19 (d, 6.8) (2H)
2''	124.8	5.37 (dd, 6.8, 1.5) (1H)
3''	132.0	-
4''	25.9	1.67 (s) (3H)
5''	18.0	1.84 (s) (3H)
1'''	99.8	5.05 (d, 8.1) (1H)
2'''	74.2	3.50 (dd, 8.9, 8.1) (1H)
3'''	77.1	3.58 (t, 8.9) (1H)
4'''	76.7	3.05 (dd, 9.3, 8.9) (1H)
5'''	76.1	3.54 (m) (1H)
6'''	65.3	4.51 (dd, 12.1, 2.3) (1H) 4.03 (dd, 12.1, 5.2) (1H)
1''''	104.1	5.15 (d, 8.0) (1H)
2''''	73.8	3.52 (dd, 9.0, 8.0) (1H)
3''''	76.5	3.61 (t, 9.0) (1H)
4''''	69.7	3.41 (t, 9.0) (1H)
5''''	76.9	3.45 (m) (1H)
6''''	62.6	3.93 (dd, 12.1, 2.2) (1H) 3.72 (dd, 12.1, 5.2) (1H)
1'''''	172.0	-
2'''''	34.6	2.25 (m) (2H)
3'''''	25.0	1.68 (m) (2H)
4'''''	29.2	1.29 (m) (6H)
5'''''	29.3	1.29 (m) (6H)
6'''''	29.1	1.29 (m) (6H)
7'''''	30.3	1.33 (m) (2H)
8'''''	27.3	1.96 (m) (2H)
9'''''	131.8	5.37 (m) (1H)
10'''''	131.7	5.42 (m) (1H)
11'''''	25.7	2.68 (m) (2H)
12'''''	128.3	5.35 (m) (2H)
13'''''	128.4	5.35 (m) (2H)
14'''''	25.6	2.73 (m) (2H)
15'''''	127.1	5.43 (m) (1H)
16'''''	131.9	5.36 (m) (1H)
17'''''	20.6	1.93 (m) (2H)
18'''''	14.2	1.06 (t, 6.8) (3H)

Secalonic acid A

C₃₂H₃₀O₁₄ (638.16356)

Faint yellow crystals, mp 231–232 °C

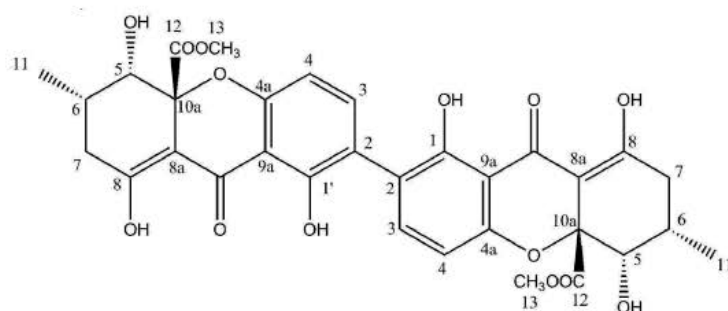
 $[\alpha]_D^{26} = -64.1$ ($c = 0.1$ in CHCl₃)UV λ_{\max} (MeOH)(log ϵ): 338 (4.52), 260 (4.12), 228 (4.32) nmIR ν_{\max} (CHCl₃): 3464, 1726, 1610, 1585, 1566, 1436, 1233, 1067 cm⁻¹Sources: *Diploicia canescens* [117].

Spectral data: [129].

Enantiomeric secalonic acid D: similar physicochemical data except $[\alpha]_D^{26} = +64.1$ ($c = 0.14$ in CHCl₃)

Secalonic Acid A (CDCl ₃)		
Position	δ_C	δ_H (J in Hz)
1, 1'	159.4	-
-OH 1,1'	-	11.75 (s) (2H)
2, 2'	118.2	-
3, 3'	140.2	7.46 (d, 8.5) (2H)
4, 4'	107.6	6.63 (d, 8.5) (2H)
4a, 4a'	158.3	-
5, 5'	76.9	3.93 (dd, 11.3, 1.6) (2H)
-OH 5,5'	-	2.81 (d, 2.2) (2H)
6, 6'	29.2	2.41 (m) (2H)
7, 7'	36.3	2.74 (dd, 19.0, 6.1) (2H)
8, 8'	177.5	-
-OH 8,8'	-	13.78 (s) (2H)
8a, 8a'	101.5	-
9, 9'	187.2	-
9a, 9a'	106.9	-
10a, 10a'	84.7	-
11, 11'	18.0	1.17 (d, 6.4) (6H)
12, 12'	170.3	-
13, 13'	53.3	3.73 (s) (6H)

Secalonic acid B

C₃₂H₃₀O₁₄ (638.16356)

Faint yellow crystals, mp 231–232 °C

$[\alpha]_D^{20} = +133.7$ ($c = 0.38$ in CHCl_3)

UV λ_{max} (MeOH)(log ϵ): 338 (4.52), 260 (4.12), 228 (4.32) nm

IR ν_{max} (CHCl_3): 3582, 3014, 1747, 1611, 1589, 1214, 1058, 796, 726 cm^{-1}

Sources: *Diploicia canescens* [117].

Spectral data: [47]

Secalonic acid B (CDCl_3)		
Position	δ_{C}	δ_{H} (J in Hz)
1, 1'	159.4	-
-OH 1,1'	-	11.85 (s) (2H)
2, 2'	118.7	-
3, 3'	139.7	7.42 (d, 8.5) (2H)
4, 4'	107.5	6.57 (d, 8.5) (2H)
4a, 4a'	157.2	-
5, 5'	71.4	4.12 (d, 1.4) (2H)
-OH 5,5'	-	2.57 (s) (2H)
6, 6'	28.5	2.12 (m) (2H)
7, 7'	32.6	7, 7' α 2.52 (dd, 19.0, 11.5) (2H)
		7, 7' β 2.41 (dd, 19.0, 6.1) (2H)
8, 8'	179.8	-
-OH 8,8'	-	13.96 (s) (2H)
8a, 8a'	99.9	-
9, 9'	187.7	-
9a, 9a'	107.0	-
10a, 10a'	84.8	-
11, 11'	17.5	1.18 (d, 6.8) (6H)
12, 12'	171.2	-
13, 13'	53.4	3.72 (s) (6H)

7. Conclusions

Even though lichens offer the widest diversity of compounds in the fungal realm, the bioactivities of their secondary metabolites remain under-investigated in regards to any other fungi [130], especially xanthenes, despite being widely considered as a promising class of compounds exerting pleiotropic pharmacological activities. Xanthenes might have originally suffered from their ubiquitous distribution compared to metabolites restricted to the lichenized condition (e.g., depsides, depsidones, depsones...). However, as end products of a distinct biosynthetic pathway to that of higher plants, lichen xanthenes display unique substitution patterns which enrich the diversity of xanthenes rather than produce cross-phyletic structures. Furthermore, recently discovered lichen xanthenes extend their diversity through unexpected structural features (e.g., prenylations, glycosylations, unprecedented substitution patterns...) and, as a consequence, less than 10% are known from non-lichen sources. In addition, their structural elucidation may be misleading for the spectroscopists, with the presence of multiple possible isomers. Innovative analytical approaches both alleviate and shorten the dereplication holdup while recent advances in spectroscopy ensure reliable structural assignments. Analytical aspects no longer hamper the study of these valuable metabolites.

Acknowledgments: The authors are grateful to David Rondeau for DART-HRMS analyses that used the mass spectrometry facilities of the DReAM platform of IETR. The authors are also indebted to Stéphane La Barre for improving the English style of this manuscript.

Author Contributions: P.L.P. performed DART experiments, P.L.P. and J.B. contributed to the writing of the paper.

Conflicts of Interest: The authors declare no conflict of interest.

References

1. Masters, K.-S.; Bräse, S. Xanthonenes from fungi, lichens, and bacteria: The natural products and their synthesis. *Chem. Rev.* **2012**, *112*, 3717–3776. [[CrossRef](#)] [[PubMed](#)]
2. Lesch, B.; Bräse, S. A Short, Atom-Economical Entry to Tetrahydroxanthenones. *Angew. Chem. Int. Ed.* **2004**, *43*, 115–118. [[CrossRef](#)] [[PubMed](#)]
3. Vieira, L.M.M.; Kijjoo, A. Naturally-occurring xanthonenes: Recent developments. *Curr. Med. Chem.* **2005**, *12*, 2413–2446. [[CrossRef](#)] [[PubMed](#)]
4. El-Seedi, H.; El-Barbary, M.; El-Ghorab, D.; Bohlin, L.; Borg-Karlson, A.-K.; Goransson, U.; Verpoorte, R. Recent insights into the biosynthesis and biological activities of natural xanthonenes. *Curr. Med. Chem.* **2010**, *17*, 854–901. [[CrossRef](#)] [[PubMed](#)]
5. Huneck, S.; Yoshimura, I. *Identification of Lichen Substances*; Springer: Berlin, Germany, 1996.
6. Elix, J.A.; Stocker-Worgotter, E. Biochemistry and secondary metabolites. In *Lichen Biology*; Cambridge University Press: Cambridge, UK, 2008; pp. 104–133.
7. Cacho, R.A.; Chooi, Y.-H.; Zhou, H.; Tang, Y. Complexity generation in fungal polyketide biosynthesis: A spirocycle-forming P450 in the concise pathway to the antifungal drug griseofulvin. *ACS Chem. Biol.* **2013**, *8*, 2322–2330. [[CrossRef](#)] [[PubMed](#)]
8. Schätzle, M.A.; Husain, S.M.; Ferlino, S.; Müller, M. Tautomers of anthrahydroquinones: Enzymatic reduction and implications for chrysophanol, monodictyphenone, and related xanthone biosyntheses. *J. Am. Chem. Soc.* **2012**, *134*, 14742–14745. [[CrossRef](#)] [[PubMed](#)]
9. Anderson, J.A.; Lin, B.K.; Williams, H.J.; Scott, A.I. Deoxygenation of phenolic natural products. Enzymic conversion of emodin to chrysophanol. *J. Am. Chem. Soc.* **1988**, *110*, 1623–1624. [[CrossRef](#)]
10. Anderson, J.A.; Lin, B.-K.; Shan, S.W. Purification and properties of emodin deoxygenase from *Pyrenochaeta terrestris*. *Phytochemistry* **1990**, *29*, 2415–2418. [[CrossRef](#)]
11. Franck, B.; Bringmann, G.; Flohr, G. Sequence analysis of ergochrome-biosynthesis by competitive incorporation. *Angew. Chem. Int. Ed.* **1980**, *19*, 460–461. [[CrossRef](#)]
12. Henry, K.M.; Townsend, C.A. Ordering the reductive and cytochrome P450 oxidative steps in demethylsterigmatocystin formation yields general insights into the biosynthesis of aflatoxin and related fungal metabolites. *J. Am. Chem. Soc.* **2005**, *127*, 3724–3733. [[CrossRef](#)] [[PubMed](#)]
13. Okorie, D.A. A new phthalide and xanthonenes from *Anthocleista djalensis* and *Anthocleista vogelli*. *Phytochemistry* **1976**, *15*, 1799–1800. [[CrossRef](#)]
14. Suárez, A.I.; Blanco, Z.; Compagnone, R.S.; Salazar-Bookaman, M.M.; Zapata, V.; Alvarado, C. Anti-inflammatory activity of *Croton cuneatus* aqueous extract. *J. Ethnopharmacol.* **2006**, *105*, 99–101. [[CrossRef](#)] [[PubMed](#)]
15. Gachet, M.S.; Kunert, O.; Kaiser, M.; Brun, R.; Zehl, M.; Keller, W.; Muñoz, R.A.; Bauer, R.; Schuehly, W. Antiparasitic compounds from *Cupania cinerea* with activities against *Plasmodium falciparum* and *Trypanosoma brucei rhodesiense*. *J. Nat. Prod.* **2011**, *74*, 559–566. [[CrossRef](#)] [[PubMed](#)]
16. Sriyatep, T.; Chakthong, S.; Leejae, S.; Voravuthikunchai, S.P. Two lignans, one alkaloid, and flavanone from the twigs of *Feroniella lucida*. *Tetrahedron* **2014**, *70*, 1773–1779. [[CrossRef](#)]
17. El-Seedi, H.R.; Hazell, A.C.; Torssell, K.B. Triterpenes, lichexanthone and an acetylenic acid from *Minuartia guianensis*. *Phytochemistry* **1994**, *35*, 1297–1299. [[CrossRef](#)]
18. Jiménez, C.; Marcos, M.; Villaverde, M.C.; Riguera, R.; Castedo, L.; Stermitz, F. A chromone from *Zanthoxylum* species. *Phytochemistry* **1989**, *28*, 1992–1993. [[CrossRef](#)]
19. Hu, L.-H.; Yip, S.-C.; Sim, K.-Y. Xanthonenes from *Hypericum ascyron*. *Phytochemistry* **1999**, *52*, 1371–1373. [[CrossRef](#)]
20. Frisvad, J.C.; Smedsgaard, J.; Larsen, T.O.; Samson, R.A. Mycotoxins, drugs and other extrolites produced by species in *Penicillium* subgenus *Penicillium*. *Stud. Mycol.* **2004**, *49*, 201–241.
21. Broadbent, D.; Mabelis, R.P.; Spencer, H. 3,6,8-Trihydroxy-1-methylxanthone—An antibacterial metabolite from *Penicillium patulum*. *Phytochemistry* **1975**, *14*, 2082–2083. [[CrossRef](#)]
22. Wang, Q.-X.; Bao, L.; Yang, X.-L.; Guo, H.; Yang, R.-N.; Ren, B.; Zhang, L.-X.; Dai, H.-Q.; Guo, L.-D.; Liu, H.-W. Polyketides with antimicrobial activity from the solid culture of an endolichenic fungus *Ullocladium* sp. *Fitoterapia* **2012**, *83*, 209–214. [[CrossRef](#)] [[PubMed](#)]

23. McMaster, W.J.; Scott, A.I.; Trippett, S. 894. Metabolic products of *Penicillium patulum*. *J. Chem. Soc.* **1960**, 4628–4631. [[CrossRef](#)]
24. Wezeman, T.; Bräse, S.; Masters, K.-S. Xanthone dimers: A compound family which is both common and privileged. *Nat. Prod. Rep.* **2015**, *32*, 6–28. [[CrossRef](#)] [[PubMed](#)]
25. Nagem, T.J.; Oliveira, F.F. Xanthones and other constituents of *Vismia parviflora*. *J. Braz. Chem. Soc.* **1997**, *8*, 505–508. [[CrossRef](#)]
26. Kato, L.; de Oliveira, C.M.A.; Vencato, I.; Lauriucci, C. Crystal structure of 1,7-dihydroxyxanthone from *Weddellina squamulosa* Tul. *J. Chem. Crystallogr.* **2005**, *35*, 23–26. [[CrossRef](#)]
27. Huang, Z.; Yang, J.; Cai, X.; She, Z.; Lin, Y. A new furanocoumarin from the mangrove endophytic fungus *Penicillium* sp. (ZH16). *Nat. Prod. Res.* **2012**, *26*, 1291–1295. [[CrossRef](#)] [[PubMed](#)]
28. Sob, S.V.T.; Wabo, H.K.; Tchinda, A.T.; Tane, P.; Ngadjui, B.T.; Ye, Y. Anthraquinones, sterols, triterpenoids and xanthones from *Cassia obtusifolia*. *Biochem. Syst. Ecol.* **2010**, *38*, 342–345. [[CrossRef](#)]
29. Kornsakulkarn, J.; Saepua, S.; Komwijit, S.; Rachtawee, P.; Thongpanchang, C. Bioactive polyketides from the fungus *Astrocystis* sp. BCC 22166. *Tetrahedron* **2014**, *70*, 2129–2133. [[CrossRef](#)]
30. Ginde, B.S.; Hosangadi, B.D.; Kudav, N.A.; Nayak, K.V.; Kulkarni, A.B. Chemical investigation on *Cassia occidentalis* Linn. Part I. Isolation and structure of cassiollin, a new xanthone. *J. Chem. Soc. C Org.* **1970**, 1285–1289. [[CrossRef](#)]
31. Yang, H.-Y.; Gao, Y.-H.; Niu, D.-Y.; Yang, L.-Y.; Gao, X.-M.; Du, G.; Hu, Q.-F. Xanthone derivatives from the fermentation products of an endophytic fungus *Phomopsis* sp. *Fitoterapia* **2013**, *91*, 189–193. [[CrossRef](#)] [[PubMed](#)]
32. Yamakazi, M.; Okuyama, E. Isolation and structures of oxaphenalenones dimers from *Talaromyces bacillosporus*. *Chem. Pharm. Bull. Tokyo* **1980**, *28*, 3649–3655.
33. Yao, Q.; Wang, J.; Zhang, X.; Nong, X.; Xu, X.; Qi, S. Cytotoxic polyketides from the deep-sea-derived fungus *Engyodontium album* DFFSCS021. *Mar. Drugs* **2014**, *12*, 5902–5915. [[CrossRef](#)] [[PubMed](#)]
34. Hay, A.-E.; Aumond, M.-C.; Mallet, S.; Dumontet, V.; Litaudon, M.; Rondeau, D.; Richomme, P. Antioxidant xanthones from *Garcinia vieillardii*. *J. Nat. Prod.* **2004**, *67*, 707–709. [[CrossRef](#)] [[PubMed](#)]
35. Baguley, B.C. Antivascular therapy of cancer: DMXAA. *Lancet Oncol.* **2003**, *4*, 141–148. [[CrossRef](#)]
36. Xiao, Z.; Morris-Natschke, S.L.; Lee, K.-H. Strategies for the optimization of natural leads to anticancer drugs or drug candidates. *Med. Res. Rev.* **2016**, *36*, 32–91. [[CrossRef](#)] [[PubMed](#)]
37. Gutierrez-Orozco, F.; Failla, M.L. Biological activities and bioavailability of mangosteen xanthones: A critical review of the current evidence. *Nutrients* **2013**, *5*, 3163–3183. [[CrossRef](#)] [[PubMed](#)]
38. Shan, T.; Ma, Q.; Guo, K.; Liu, J.; Li, W.; Wang, F.; Wu, E. Xanthones from mangosteen extracts as natural chemopreventive agents: Potential anticancer drugs. *Curr. Mol. Med.* **2011**, *11*, 666–677. [[CrossRef](#)] [[PubMed](#)]
39. Elix, J.A.; Crook, C.E. The joint occurrence of chloroxanthones in lichens, and a further thirteen new lichen xanthones. *Bryologist* **1992**, *95*, 52–64. [[CrossRef](#)]
40. Paping, K.; Boonpragob, K.; Lumbsch, H.T. A new species and new records of *Lecanora* (*Lecanoraceae*, Ascomycota) from south-east Asia. *Lichenologist* **2011**, *43*, 47–50. [[CrossRef](#)]
41. Obolskiy, D.; Pischel, I.; Siriwatanametanon, N.; Heinrich, M. *Garcinia mangostana* L.: A phytochemical and pharmacological review. *Phytother. Res.* **2009**, *23*, 1047–1065. [[CrossRef](#)] [[PubMed](#)]
42. Botta, B.; Vitali, A.; Menendez, P.; Misiti, D.; Monache, G.D. Prenylated flavonoids: Pharmacology and biotechnology. *Curr. Med. Chem.* **2005**, *12*, 713–739. [[CrossRef](#)]
43. Ishida, M.; Hamasaki, T.; Hatsuda, Y. The structure of two new metabolites, emerin and emericellin, from *Aspergillus nidulans*. *Agric. Biol. Chem.* **1975**, *39*, 2181–2184. [[CrossRef](#)]
44. Řezanka, T.; Jáchymová, J.; Dembitsky, V.M. Prenylated xanthone glucosides from Ural's lichen *Umbilicaria proboscidea*. *Phytochemistry* **2003**, *62*, 607–612. [[CrossRef](#)]
45. Sanchez, J.F.; Entwistle, R.; Hung, J.-H.; Yaegashi, J.; Jain, S.; Chiang, Y.-M.; Wang, C.C.C.; Oakley, B.R. Genome-based deletion analysis reveals the prenyl xanthone biosynthesis pathway in *Aspergillus nidulans*. *J. Am. Chem. Soc.* **2011**, *133*, 4010–4017. [[CrossRef](#)] [[PubMed](#)]
46. Řezanka, T.; Sigler, K. Hirtusneanoside, an unsymmetrical dimeric tetrahydroxanthone from the lichen *Usnea hirta*. *J. Nat. Prod.* **2007**, *70*, 1487–1491. [[CrossRef](#)] [[PubMed](#)]
47. Zhang, W.; Krohn, K.; Zia-Ullah; Flörke, U.; Pescitelli, G.; Di Bari, L.; Antus, S.; Kurtán, T.; Rheinheimer, J.; Draeger, S.; Schulz, B. New mono- and dimeric members of the secalonic acid family: Blennolides A–G isolated from the fungus *Blechnoria* sp. *Chemistry* **2008**, *14*, 4913–4923. [[CrossRef](#)] [[PubMed](#)]

48. Leuckert, C.; Ahmadjian, V.; Culberson, C.F.; Johnson, A. Xanthonones and depsidones of the lichen *Lecanora dispersa* in nature and of its mycobiont in culture. *Mycologia* **1990**, *82*, 370–378. [[CrossRef](#)]
49. Brunauer, G.; Hager, A.; Krautgartner, W.D.; Tuerk, R.; Stocker-Wörgötter, E. Experimental studies on *Lecanora rupicola* (L.) Zahlbr.: Chemical and microscopical investigations of the mycobiont and re-synthesis stages. *Lichenologist* **2006**, *38*, 577–585. [[CrossRef](#)]
50. Molina, M.C.; Crespo, A.; Vicente, C.; Elix, J.A. Differences in the composition of phenolics and fatty acids of cultured mycobiont and thallus of *Physconia distorta*. *Plant Physiol. Biochem.* **2003**, *41*, 175–180. [[CrossRef](#)]
51. Tanahashi, T.; Takenaka, Y.; Ikuta, Y.; Tani, K.; Nagakura, N.; Hamada, N. Xanthonones from the cultured lichen mycobionts of *Pyrenula japonica* and *Pyrenula pseudobufonia*. *Phytochemistry* **1999**, *52*, 401–405. [[CrossRef](#)]
52. Takenaka, Y.; Tanahashi, T.; Nagakura, N.; Hamada, N. Production of xanthonones with free radical scavenging properties, emodin and sclerotiorin by the cultured lichen mycobionts of *Pyrenula japonica*. *Z. Naturforsch. C* **2000**, *55*, 910–914. [[CrossRef](#)] [[PubMed](#)]
53. Maymo-Gatell, X.; Chien, Y.; Gossett, J.M.; Zinder, S.H. Isolation of a bacterium that reductively dechlorinates tetrachloroethene to ethene. *Science* **1997**, *276*, 1568–1571. [[CrossRef](#)] [[PubMed](#)]
54. Bedard, D.L.; Ritalahti, K.M.; Löffler, F.E. The *Dehalococcoides* population in sediment-free mixed cultures metabolically dechlorinates the commercial polychlorinated biphenyl mixture Aroclor 1260. *Appl. Environ. Microbiol.* **2007**, *73*, 2513–2521. [[CrossRef](#)] [[PubMed](#)]
55. Löffler, F.E.; Yan, J.; Ritalahti, K.M.; Adrian, L.; Edwards, E.A.; Konstantinidis, K.T.; Müller, J.A.; Fullerton, H.; Zinder, S.H.; Spormann, A.M. *Dehalococcoides mccartyi* gen. nov., sp. nov., obligately organohalide-respiring anaerobic bacteria relevant to halogen cycling and bioremediation, belong to a novel bacterial class, *Dehalococcoidia* classis nov., order *Dehalococcoidales* ord. nov. and family *Dehalococcoidaceae* fam. nov., within the phylum *Chloroflexi*. *Int. J. Syst. Evol. Microbiol.* **2013**, *63*, 625–635. [[PubMed](#)]
56. Krzmarzick, M.J.; Crary, B.B.; Harding, J.J.; Oyerinde, O.O.; Leri, A.C.; Myneni, S.C.; Novak, P.J. Natural niche for organohalide-respiring *Chloroflexi*. *Appl. Environ. Microbiol.* **2012**, *78*, 393–401. [[CrossRef](#)] [[PubMed](#)]
57. Krzmarzick, M.J.; McNamara, P.J.; Crary, B.B.; Novak, P.J. Abundance and diversity of organohalide-respiring bacteria in lake sediments across a geographical sulfur gradient. *FEMS Microbiol. Ecol.* **2013**, *84*, 248–258. [[CrossRef](#)] [[PubMed](#)]
58. McNamara, P.J.; Krzmarzick, M.J. Triclosan enriches for *Dehalococcoides*-like *Chloroflexi* in anaerobic soil at environmentally relevant concentrations. *FEMS Microbiol. Lett.* **2013**, *344*, 48–52. [[CrossRef](#)] [[PubMed](#)]
59. Krzmarzick, M.J.; Miller, H.R.; Yan, T.; Novak, P.J. Novel Firmicutes group implicated in the dechlorination of two chlorinated xanthonones, analogues of natural organochlorines. *Appl. Environ. Microbiol.* **2014**, *80*, 1210–1218. [[CrossRef](#)] [[PubMed](#)]
60. Bates, S.T.; Cropsey, G.W.G.; Caporaso, J.G.; Knight, R.; Fierer, N. Bacterial communities associated with the lichen symbiosis. *Appl. Environ. Microbiol.* **2011**, *77*, 1309–1314. [[CrossRef](#)] [[PubMed](#)]
61. Gonzalez, I.; Ayuso-Sacido, A.; Anderson, A.; Genilloud, O. Actinomycetes isolated from lichens: Evaluation of their diversity and detection of biosynthetic gene sequences. *FEMS Microbiol. Ecol.* **2005**, *54*, 401–415. [[CrossRef](#)] [[PubMed](#)]
62. Grube, M.; Cardinale, M.; de Castro, J.V.; Müller, H.; Berg, G. Species-specific structural and functional diversity of bacterial communities in lichen symbioses. *ISME J.* **2009**, *3*, 1105–1115. [[CrossRef](#)] [[PubMed](#)]
63. Krumins, V.; Park, J.-W.; Son, E.-K.; Rodenburg, L.A.; Kerkhof, L.J.; Häggblom, M.M.; Fennell, D.E. PCB dechlorination enhancement in Anacostia River sediment microcosms. *Water Res.* **2009**, *43*, 4549–4558. [[CrossRef](#)] [[PubMed](#)]
64. Lumbsch, H.T.; Feige, G.B.; Elix, J.A. The joint occurrence of chloroxanthonones in Southern Hemisphere *Lecanora* species (Ascomycotina; *Lecanoraceae*). *Bot. Acta* **1994**, *107*, 30–35. [[CrossRef](#)]
65. Feige, G.B.; Lumbsch, H.T.; Huneck, S.; Elix, J.A. Identification of lichen substances by a standardized high-performance liquid chromatographic method. *J. Chromatogr. A* **1993**, *646*, 417–427. [[CrossRef](#)]
66. Culberson, C.F.; Kristinsson, H.-D. A standardized method for the identification of lichen products. *J. Chromatogr. A* **1970**, *46*, 85–93. [[CrossRef](#)]
67. Culberson, C.F.; Culberson, W.L.; Johnson, A. A standardized TLC analysis of β -orcinol depsidones. *Bryologist* **1981**, *84*, 16–29. [[CrossRef](#)]
68. Arup, U.; Ekman, S.; Lindblom, L.; Mattsson, J.-E. High performance thin layer chromatography (HPTLC), an improved technique for screening lichen substances. *Lichenologist* **1993**, *25*, 61–71. [[CrossRef](#)]

69. Leuckert, C.; Knoph, J.-G. European taxa of saxicolous *Lecidella* containing chloroxanthones: Identification of patterns using thin layer chromatography. *Lichenologist* **1992**, *24*, 383–397.
70. Yoshimura, I.; Kinoshita, Y.; Yamamoto, Y.; Huneck, S.; Yamada, Y. Analysis of secondary metabolites from lichen by high performance liquid chromatography with a photodiode array detector. *Phytochem. Anal.* **1994**, *5*, 197–205. [[CrossRef](#)]
71. Santesson, J. Identification and isolation of lichen substances. In *The Lichens*; Academic Press: New York, NY, USA; London, UK, 1973; pp. 633–652.
72. Boluda, C.G.; Rico, V.J.; Hawksworth, D.L. Fluorescence microscopy as a tool for the visualization of lichen substances within *Bryoria* thalli. *Lichenologist* **2014**, *46*, 723–726. [[CrossRef](#)]
73. Kauppi, M.; Versegny-Patay, K. Determination of the distribution of lichen substances in the thallus by fluorescence microscopy. *Ann. Bot. Fenn.* **1990**, *27*, 189–202.
74. Sundholm, E.G. Total synthesis of lichen xanthones. Revision of structures. *Tetrahedron* **1978**, *34*, 577–586. [[CrossRef](#)]
75. Elix, J.A.; Crook, C.E.; Hui, J.; Zhu, Z.N. Synthesis of New Lichen Xanthones. *Aust. J. Chem.* **1992**, *45*, 845–855. [[CrossRef](#)]
76. Elix, J.A.; Musidlak, H.W.; Sala, T.; Sargent, M.V. Structure and synthesis of some lichen xanthones. *Aust. J. Chem.* **1978**, *31*, 145–155. [[CrossRef](#)]
77. Le Pogam, P.; Herbette, G.; Boustie, J. Analysis of Lichen Metabolites, a Variety of Approaches. In *Recent Advances in Lichenology*; Springer: New Delhi, India, 2015; pp. 229–261.
78. Nielsen, K.F.; Smedsgaard, J. Fungal metabolite screening: Database of 474 mycotoxins and fungal metabolites for dereplication by standardised liquid chromatography-UV-mass spectrometry methodology. *J. Chromatogr. A* **2003**, *1002*, 111–136. [[CrossRef](#)]
79. Le Pogam, P.; Schinkovitz, A.; Legouin, B.; le Lamer, A.-C.; Boustie, J.; Richomme, P. Matrix-free UV-laser desorption ionization mass spectrometry as a versatile approach for accelerating dereplication studies on lichens. *Anal. Chem.* **2015**, *87*, 10421–10428. [[CrossRef](#)] [[PubMed](#)]
80. Le Pogam, P.; Legouin, B.; le Lamer, A.-C.; Boustie, J.; Rondeau, D. Analysis of the cyanolichen *Lichina pygmaea* metabolites using *in situ* DART-MS: From detection to thermochemistry of mycosporine serinol. *J. Mass Spectrom.* **2015**, *50*, 454–462. [[CrossRef](#)] [[PubMed](#)]
81. Sica, V.P.; Raja, H.A.; El-Elimat, T.; Kertesz, V.; Van Berkel, G.J.; Pearce, C.J.; Oberlies, N.H. Dereplicating and spatial mapping of secondary metabolites from fungal cultures *in situ*. *J. Nat. Prod.* **2015**, *78*, 1926–1936. [[CrossRef](#)] [[PubMed](#)]
82. Molinski, T.F. NMR of natural products at the “nanomole-scale”. *Nat. Prod. Rep.* **2010**, *27*, 321–329. [[CrossRef](#)] [[PubMed](#)]
83. Wolfender, J.-L.; Marti, G.; Thomas, A.; Bertrand, S. Current approaches and challenges for the metabolite profiling of complex natural extracts. *J. Chromatogr. A* **2015**, *1382*, 136–164. [[CrossRef](#)] [[PubMed](#)]
84. Boustie, J.; Grube, M. Lichens—A promising source of bioactive secondary metabolites. *Plant Genet. Resour. Charact. Util.* **2005**, *3*, 273–287. [[CrossRef](#)]
85. Mietzsch, E.; Lumbsch, H.T.; Elix, J.A. *WINTABOLITES (Mactabolites for Windows) Users Manual*; University Essen: Essen, Germany, 1992.
86. Elix, J.A.; Kalb, K.; Rupprecht, J.; Schobert, R. Available online: <http://liaslight.lias.net/identification/Navkey/Metabolites/index.html> (accessed on 22 January 2016).
87. Rambold, G.; Elix, J.A.; Heindl-Tenhunen, B.; Köhler, T.; Nash, T.H.; Neubacher, D.; Reichert, W.; Zedda, L.; Triebel, D. LIAS light—Towards the ten thousand species milestone. *MycKeys* **2014**, *8*, 11–16. [[CrossRef](#)]
88. Brodo, I.M. The lichens and lichenicolous fungi of Haida Gwaii (Queen Charlotte Islands), British Columbia, Canada. 5. A new species of *Lecanora* from shoreline rocks. *Botany* **2010**, *88*, 352–358. [[CrossRef](#)]
89. Perez-Vargas, I.; Hernandez-Padron, C.; Etayo, J.; Pérez de Paz, P.L.; Elix, J.A. New species of *Pertusaria* (lichenized Ascomycota: *Pertusariaceae*) from the Canary Islands. *Lichenologist* **2010**, *42*, 35–41. [[CrossRef](#)]
90. Elix, J.; Øvstedal, D.O. Lichen phytochemistry II: Some species of *Calopadia*. *Australas. Lichenol.* **2009**, *65*, 7–9.
91. Elix, J.A. Five new species of *Phyllopsora* (lichenized Ascomycota) from Australia. *Australas. Lichenol.* **2006**, *59*, 23–29.
92. Sérusiaux, E.; Lücking, R.; Lumbsch, T. *Sporopodium isidiatum* (*Pilocarpaceae*), new from Papua New Guinea and Sri Lanka, with a key to the world’s *Sporopodium* species. *Mycotaxon* **2008**, *103*, 255–262.

93. Frank, M.; Niemann, H.; Böhler, P.; Stork, B.; Wesselborg, S.; Lin, W.; Proksch, P. Phomoxanthone A—From mangrove forests to anticancer therapy. *Curr. Med. Chem.* **2015**, *22*, 3523–3532. [[CrossRef](#)] [[PubMed](#)]
94. Řezanka, T.; Dembitsky, V.M. Identification of acylated xanthone glycosides by liquid chromatography-atmospheric pressure chemical ionization mass spectrometry in positive and negative modes from the lichen *Umbilicaria proboscidea*. *J. Chromatogr. A* **2003**, *995*, 109–118. [[CrossRef](#)]
95. Honda, N.K.; Pavan, F.R.; Coelho, R.G.; de Andrade Leite, S.R.; Micheletti, A.C.; Lopes, T.I.B.; Misutsu, M.Y.; Beatriz, A.; Brum, R.L.; Leite, C.Q.F. Antimycobacterial activity of lichen substances. *Phytomedicine* **2010**, *17*, 328–332. [[CrossRef](#)] [[PubMed](#)]
96. Ingólfssdóttir, K.; Chung, G.A.; Skúlason, V.G.; Gissurarson, S.R.; Vilhelmsdóttir, M. Antimycobacterial activity of lichen metabolites in vitro. *Eur. J. Pharm. Sci.* **1998**, *6*, 141–144. [[CrossRef](#)]
97. Micheletti, A.C.; Honda, N.K.; Pavan, F.R.; Leite, C.Q.; Matos Mde, F.; Perdomo, R.T.; Bogo, D.; Alcantara, G.B.; Beatriz, A. Increment of antimycobacterial activity on lichexanthone derivatives. *Med. Chem.* **2013**, *9*, 904–910. [[CrossRef](#)] [[PubMed](#)]
98. Kathirgamanathar, S.; Ratnasooriya, W.D.; Baekstrom, P.; Andersen, R.J.; Karunaratne, V. Chemistry and bioactivity of *Physciaceae* lichens *Pyxine consocians* and *Heterodermia leucomelos*. *Pharm. Biol.* **2006**, *44*, 217–220. [[CrossRef](#)]
99. Carlos, I.Z.; Carli, C.; Maia, D.C.; Benzatti, F.P.; Lopes, F.; Roese, F.M.; Watanabe, M.; Micheletti, A.C.; dos Santos, L.C.; Vilegas, W.; et al. Immunostimulatory effects of the phenolic compounds from lichens on nitric oxide and hydrogen peroxide production. *Rev. Bras. Farmacogn.* **2009**, *19*, 847–852. [[CrossRef](#)]
100. Brandao, L.F.; Alcantara, G.B.; Matos, M.; Bogo, D.; Freitas, D.; Oyama, N.M.; Honda, N.K. Cytotoxic evaluation of phenolic compounds from lichens against melanoma cells. *Chem. Pharm. Bull.* **2013**, *61*, 176–183. [[PubMed](#)]
101. Gomes, N.G.; Lefranc, F.; Kijjoo, A.; Kiss, R. Can some marine-derived fungal metabolites become actual anticancer agents? *Mar. Drugs* **2015**, *13*, 3950–3991. [[CrossRef](#)] [[PubMed](#)]
102. Abdel-Lateff, A.; Klemke, C.; König, G.M.; Wright, A.D. Two new xanthone derivatives from the algicolous marine fungus *Wardomyces anomalus*. *J. Nat. Prod.* **2003**, *66*, 706–708. [[CrossRef](#)] [[PubMed](#)]
103. Ebada, S.S.; Schulz, B.; Wray, V.; Totzke, F.; Kubbutat, M.H.; Müller, W.E.; Hamacher, A.; Kassack, M.U.; Lin, W.; Proksch, P. Arthrinins A–D: Novel diterpenoids and further constituents from the sponge derived fungus *Arthrinium* sp. *Bioorg. Med. Chem.* **2011**, *19*, 4644–4651. [[CrossRef](#)] [[PubMed](#)]
104. Ikeda, M.; Kurotobi, Y.; Namikawa, A.; Kuranuki, S.; Matsuura, N.; Sato, M.; Igarashi, Y.; Nakamura, T.; Oikawa, T. Norlichexanthone isolated from fungus P16 promotes the secretion and expression of adiponectin in cultured ST-13 adipocytes. *Med. Chem.* **2011**, *7*, 250–256. [[CrossRef](#)] [[PubMed](#)]
105. Dayan, F.E.; Romagni, J.G. Lichens as a potential source of pesticides. *Pestic. Outlook* **2001**, *12*, 229–232.
106. Huneck, S.; Schreiber, K. Wachstumsregulatorische eigenschaften von flechten-und moos-inhaltsstoffen. *Phytochemistry* **1972**, *11*, 2429–2434. [[CrossRef](#)]
107. Nguyen, K.-H.; Chollet-Krugler, M.; Gouault, N.; Tomasi, S. UV-protectant metabolites from lichens and their symbiotic partners. *Nat. Prod. Rep.* **2013**, *30*, 1490–1508. [[CrossRef](#)] [[PubMed](#)]
108. Stocker-Wörgötter, E.; Hager, A.; Elix, J.A. Intraspecific chemical variation within the crustose lichen genus *Haematomma*: Anthraquinone production in selected cultured mycobionts as a response to stress and nutrient supply. *Phytochem. Rev.* **2009**, *8*, 561–569. [[CrossRef](#)]
109. Lumbsch, H.T.; Schmitt, I.; Barker, D.; Pagel, M. Evolution of micromorphological and chemical characters in the lichen-forming fungal family *Pertusariaceae*: Character evolution in lichens. *Biol. J. Linn. Soc.* **2006**, *89*, 615–626. [[CrossRef](#)]
110. Blaha, J.; Baloch, E.; Grube, M. High photobiont diversity associated with the euryoecious lichen-forming ascomycete *Lecanora rupicola* (*Lecanoraceae*, Ascomycota). *Biol. J. Linn. Soc.* **2006**, *88*, 283–293. [[CrossRef](#)]
111. Fernandes, S.C.; Alonso-Varona, A.; Palomares, T.; Zubillaga, V.; Labidi, J.; Bulone, V. Exploiting mycosporines as natural molecular sunscreens for the fabrication of UV-absorbing green materials. *ACS Appl. Mater. Interfaces* **2015**, *7*, 16558–16564. [[CrossRef](#)] [[PubMed](#)]
112. Millot, M.; Di Meo, F.; Tomasi, S.; Boustie, J.; Trouillas, P. Photoprotective capacities of lichen metabolites: A joint theoretical and experimental study. *J. Photochem. Photobiol. B* **2012**, *111*, 17–26. [[CrossRef](#)] [[PubMed](#)]
113. Wader, G.R.; Kudav, N.A. Chemical investigation of *Cassia occidentalis* Linn. with special reference to isolation of xanthenes from *Cassia* species. *Indian J. Chem.* **2008**, *26B*, 703.

114. Fujimoto, H.; Satoh, Y.; Yamaguchi, K.; Yamazaki, M. Monoamine Oxidase Inhibitory Constituents from *Anixiella micropertusa*. *Chem. Pharm. Bull. (Tokyo)* **1998**, *46*, 1506–1510. [[CrossRef](#)]
115. Dieu, A.; Millot, M.; Champavier, Y.; Mambu, L.; Chaleix, V.; Sol, V.; Gloaguen, V. Uncommon chlorinated xanthone and other antibacterial compounds from the lichen *Cladonia incrassata*. *Planta Med.* **2014**, *80*, 931–935. [[CrossRef](#)] [[PubMed](#)]
116. Leyte-Lugo, M.; Figueroa, M.; del Carmen González, M.; Glenn, A.E.; González-Andrade, M.; Mata, R. Metabolites from the endophytic fungus *Sporormiella minimoides* isolated from *Hintonia latiflora*. *Phytochemistry* **2013**, *96*, 273–278. [[CrossRef](#)] [[PubMed](#)]
117. Millot, M.; Tomasi, S.; Studzinska, E.; Rouaud, I.; Boustie, J. Cytotoxic Constituents of the Lichen *Diploicia canescens*. *J. Nat. Prod.* **2009**, *72*, 2177–2180. [[CrossRef](#)] [[PubMed](#)]
118. Mislivec, P.B.; Tuite, J. Species of *Penicillium* occurring in freshly-harvested and in stored dent corn kernels. *Mycologia* **1970**, *62*, 67–74. [[CrossRef](#)] [[PubMed](#)]
119. Ciegler, A.; Hayes, A.W.; Vesonder, R.F. Production and biological activity of secalonic acid D. *Appl. Environ. Microbiol.* **1980**, *39*, 285–287. [[PubMed](#)]
120. Andersen, R.; Buechi, G.; Kobbe, B.; Demain, A.L. Secalonic acids D and F are toxic metabolites of *Aspergillus aculeatus*. *J. Org. Chem.* **1977**, *42*, 352–353. [[CrossRef](#)] [[PubMed](#)]
121. Ren, H.; Tian, L.; Gu, Q.; Zhu, W. Secalonic acid D; A cytotoxic constituent from marine lichen-derived fungus *Gliocladium* sp. T31. *Arch. Pharm. Res.* **2006**, *29*, 59–63. [[CrossRef](#)] [[PubMed](#)]
122. Guo, Z.; She, Z.; Shao, C.; Wen, L.; Liu, F.; Zheng, Z.; Lin, Y. ¹H and ¹³C NMR signal assignments of Paecilin A and B, two new chromone derivatives from mangrove endophytic fungus *Paecilomyces* sp. (tree 1–7). *Magn. Reson. Chem.* **2007**, *45*, 777–780. [[CrossRef](#)] [[PubMed](#)]
123. Hu, Y.; Tao, L.; Wang, F.; Zhang, J.; Liang, Y.; Fu, L. Secalonic acid D reduced the percentage of side populations by down-regulating the expression of ABCG2. *Biochem. Pharmacol.* **2013**, *85*, 1619–1625. [[CrossRef](#)] [[PubMed](#)]
124. Guru, S.K.; Pathania, A.S.; Kumar, S.; Ramesh, D.; Kumar, M.; Rana, S.; Kumar, A.; Malik, F.; Sharma, P.R.; Chandan, B.K.; et al. Secalonic acid-D represses HIF-1 α /VEGF mediated angiogenesis by regulating the Akt/mTOR/p70S6K signaling cascade. *Cancer Res.* **2015**, *75*, 2886–2896. [[CrossRef](#)] [[PubMed](#)]
125. Wang, B.H.; Polya, G.M. The fungal teratogen secalonic acid D is an inhibitor of protein kinase C and of cyclic AMP-dependent protein kinase. *Planta Med.* **1996**, *62*, 111–114. [[CrossRef](#)] [[PubMed](#)]
126. Reddy, R.V.; Bouchard, G.F.; Johnson, G.; Reddy, C.S. Disruption of Epidermal Growth Factor signaling in the mouse palate by secalonic acid D: An *in vivo* study. *Toxic Subst. Mech.* **1998**, *17*, 19–32.
127. Balasubramanian, G.; Hanumegowda, U.; Reddy, C.S. Secalonic acid D alters the nature of and inhibits the binding of the transcription factors to the phorbol 12-O-tetradecanoate-13 acetate-response element in the developing murine secondary palate. *Toxicol. Appl. Pharmacol.* **2000**, *169*, 142–150. [[CrossRef](#)] [[PubMed](#)]
128. Hanumegowda, U.M.; Dhulipala, V.C.; Reddy, C.S. Mechanism of secalonic acid D-induced inhibition of transcription factor binding to cyclic AMP response element in the developing murine palate. *Toxicol. Sci.* **2002**, *70*, 55–62. [[CrossRef](#)] [[PubMed](#)]
129. Qin, T.; Porco, J.A. Total Syntheses of Secalonic Acids A and D. *Angew. Chem. Int. Ed.* **2014**, *53*, 3107–3110. [[CrossRef](#)] [[PubMed](#)]
130. Gómez-Serranillos, M.P.; Fernández-Moriano, C.; González-Burgos, E.; Divakar, P.K.; Crespo, A. *Parmeliaceae* family: Phytochemistry, pharmacological potential and phylogenetic features. *RSC Adv.* **2014**, *4*, 59017–59047. [[CrossRef](#)]



© 2016 by the authors; licensee MDPI, Basel, Switzerland. This article is an open access article distributed under the terms and conditions of the Creative Commons by Attribution (CC-BY) license (<http://creativecommons.org/licenses/by/4.0/>).

Annexe 7 : Supporting Material Anal. Chem. 2015; 87(10):
10421-10428

**Matrix-free UV-laser desorption ionisation mass spectrometry as a versatile approach for
accelerating dereplication studies on lichens**

P. Le Pogam^a, A. Schinkovitz^b, B. Legouin^a, A.-C. Le Lamer^{a,c}, J. Boustie^{a*}, P. Richomme^{b*}

^a *Université de Rennes 1, UMR CNRS 6226 PNSCM, 2 Avenue du Professeur Léon Bernard, 35043
Rennes*

^b *Université d'Angers, EA 921 SONAS/SFR 4207 QUASAV, 16 Boulevard Daviers, 49100 Angers*

^c *Université Paul Sabatier Toulouse 3, 118 Route de Narbonne, 31062 Toulouse*

*Corresponding authors :

Pr. Joël Boustie : joel.boustie@univ-rennes1.fr

Pr. Pascal Richomme : pascal.richomme@univ-angers.fr

ABSTRACT

This supporting material contains place and date of harvest and voucher specimen number of lichens described in this study (Table S-1). Then are displayed molecular formulas associated with all molecules detected as either single compounds and/or within lichen extracts (Figure S-1). Further are depicted LDI-MS (Figures S-2 – S-42) and ESI-MS spectra (Figures S-43 – S-79) associated with all studied pure molecules and lichen acetone extracts. All spectra are acquired in negative-ion mode except for mycosporine serinol which was ionized using positive mode.

EXPERIMENTAL SECTION**Mass spectrometry and instrument settings**

LDI experiments were carried out on a Bruker Biflex III time-of-flight (TOF) mass spectrometer (bruker Daltonik, Bremen, Germany) equipped with a 337-nm pulsed nitrogen laser (model VSL-337i, Laser Sciences Inc., Boston, MA). Spectra were acquired in the linear positive and negative mode within mass range of 20 to 2000 Da. The acceleration voltage was 19 kV, pulse ion extraction was 200 ns and laser frequency was 5 ns. Experiments were performed within a laser energy range of 30-80% (46.2 μJ -103.2 μJ), depending on sample requirements. For LDI analyses, single molecules and extracts were prepared at a concentration of 10 mg.mL⁻¹ in dichloromethane (DCM) or a mixture of DCM and pyridine 9:1 (v/v), depending on sample solubility. Mycosporine serinol was dissolved in distilled water.

For direct injection, ESI-MS solutions of single compounds and lichen extracts were prepared in DCM at concentrations of 0.5 mg mL⁻¹ and 1.0 mg mL⁻¹ respectively. These samples were introduced into an expression CMS single quadrupole (Advion) using a mixture of MeOH/ water (+ 0.1% formic acid) 9:1 (v/v) at a flow rate of 200 $\mu\text{L min}^{-1}$.

Full scan mass spectra were recorded in the negative ion mode in a mass range of 100 and 1200 Da applying the following parameters: detector gain 1200, ESI voltage 3.5 kV, capillary voltage 180 V, source voltage 20 V, source voltage dynamic 20 V, nebulizer gas pressure 60 psig, desolvation gas flow rate 4L min⁻¹, capillary temperature 250°C and source gas temperature 50°C. Full scan mass spectra were recorded in the positive ion mode in a mass range of 100 and 1200 Da using the following parameters: detector gain 1200, ESI voltage 3.5 kV, capillary voltage 180 V, source voltage 40 V, source voltage dynamic 0 V, nebulizer gas pressure 60 psig, dissolution gas flow rate 4L min⁻¹, capillary temperature 250°C and source gas temperature 20°C. Data processing and evaluation for MS measurement was performed with the Data and Mass Express 2.2.29.2 software (Advion).

The LC-ESI and ESI mass spectra were all obtained from the same single quadrupole analyzer (Advion, Ithaca, USA). The MS system was coupled to a HPLC system (Prominence Shimadzu, Marne La Vallée, France) equipped with a Kinetex C18 HPLC column (100 x 4.6 mm – 2,6 μ - 6A, Phenomenex) and consisting of a quaternary pump (LC20ADSP), a surveyor autosampler (SIL-20AHT), and a diode array detector (SPD-M20A). HPLC analyses were performed by gradient elution using the following parameters: A (0.1% formic acid in water) and B (acetonitrile). T: 0 min, 20 % B; 0-25 min, 80 % B linear; 25-30 min, 100 % B linear ; 30-35 min 100% B ; 35-40 min 20% B linear. The flow rate was 0.2 mL min⁻¹.

Table S-1 : Place and date of harvest and voucher specimen number of lichens described in this study..... 292

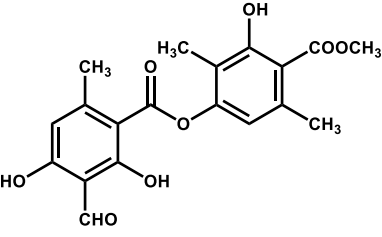
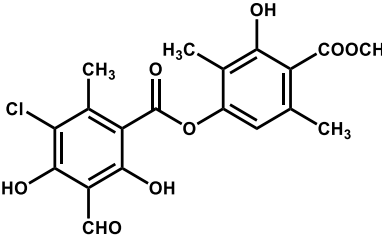
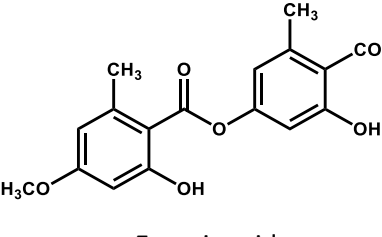
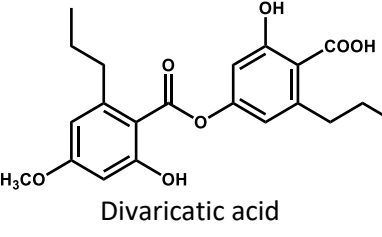
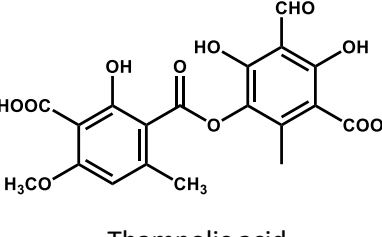
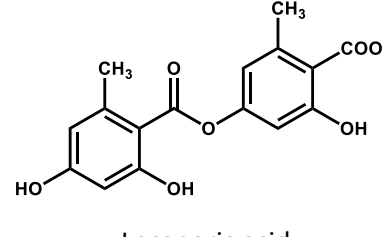
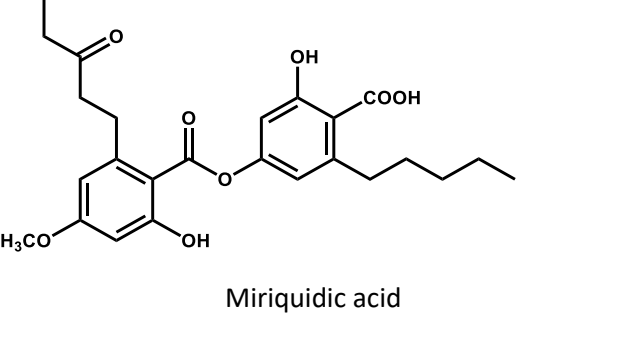
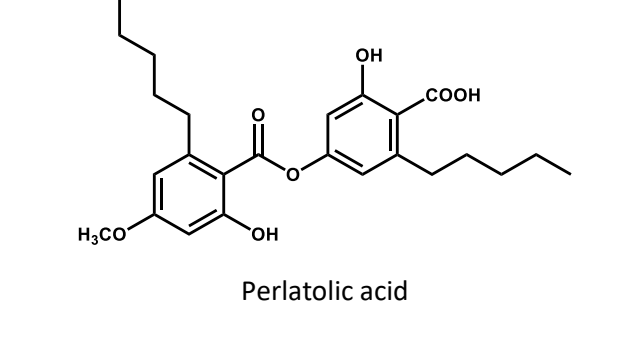
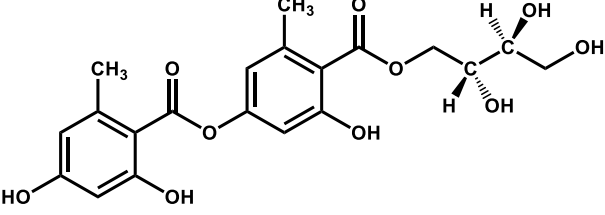
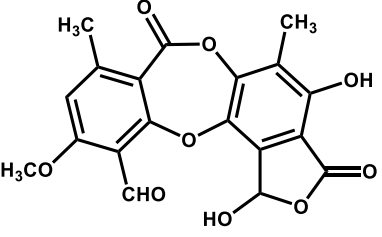
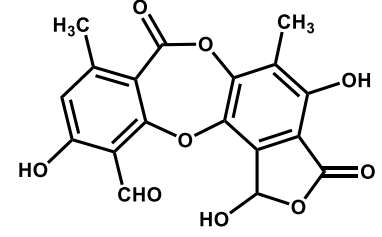
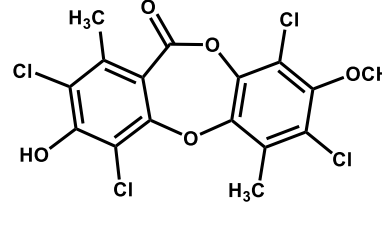
Figure S- 1: Structures of studied molecules, either as single compounds or within lichen extracts. 297

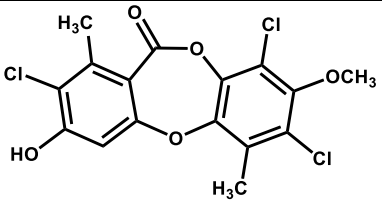
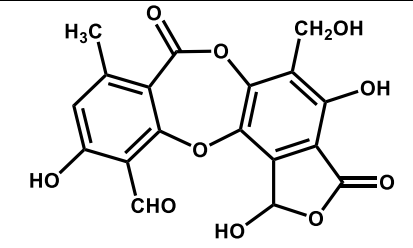
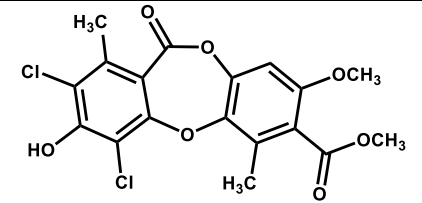
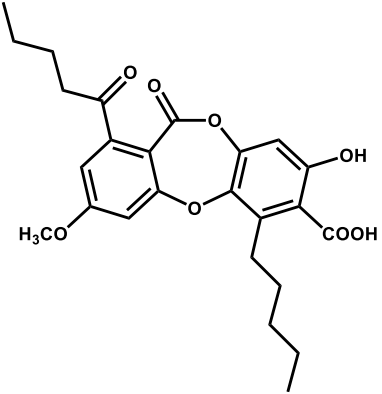
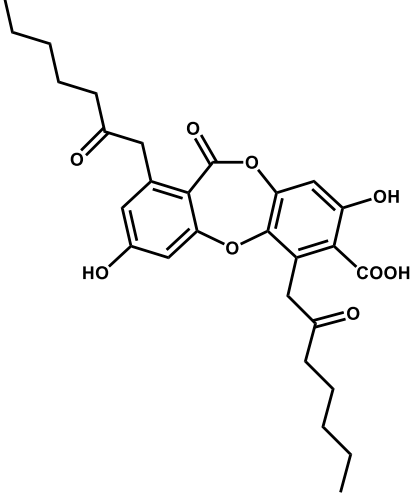
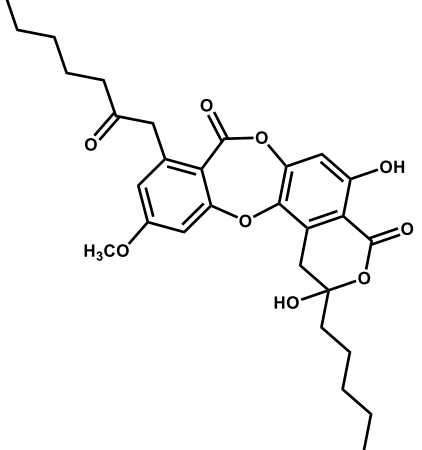
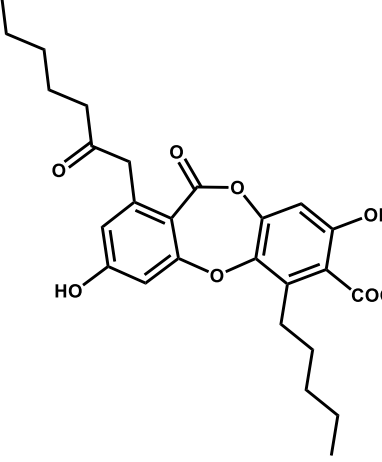
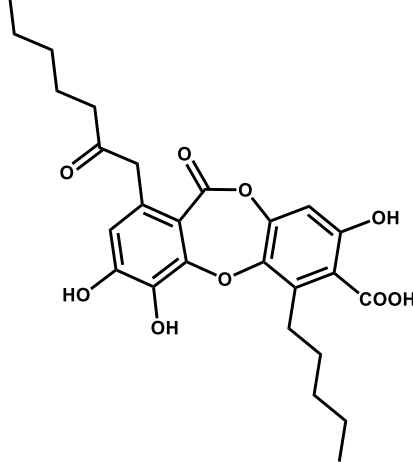
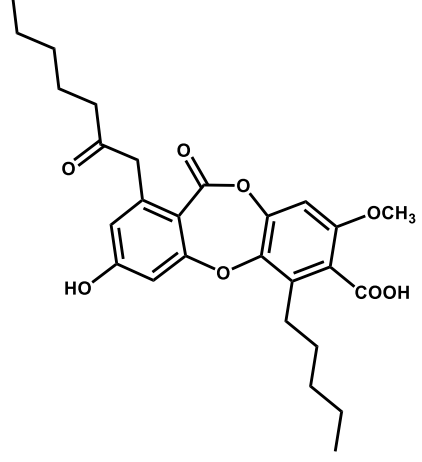
Figure S- 2: Negative LDI mass spectrum of atranorin	298
Figure S- 3: Negative LDI mass spectrum of divaricatic acid	298
Figure S- 4: Negative LDI mass spectrum of evernic acid.....	298
Figure S- 5: Negative LDI mass spectrum of thamnolic acid	299
Figure S- 6: Negative LDI mass spectrum of lobaric acid.....	299
Figure S- 7: Negative LDI mass spectrum of stictic acid	299
Figure S- 8: Negative LDI mass spectrum of variolaric acid.....	300
Figure S- 9: Negative LDI mass spectrum of pannaric acid	300
Figure S- 10: Negative LDI mass spectrum of usnic acid	300
Figure S- 11 : Positive LDI mass spectrum of usnic acid	301
Figure S- 12: Negative LDI mass spectrum of β -collatolic acid.....	301
Figure S- 13 : Negative LDI mass spectrum of lobarin.....	301
Figure S- 14: Negative LDI mass spectrum of sakisacaulon A	302
Figure S- 15: Negative LDI mass spectrum of haemoventosin	302
Figure S- 16: Negative LDI mass spectrum of chrysophanol	302
Figure S- 17: Negative LDI mass spectrum of emodin.....	303
Figure S- 18 : Negative LDI mass spectrum of parietin.....	303
Figure S- 19: Negative LDI mass spectrum of epanorin	304
Figure S- 20: Negative LDI mass spectrum of rhizocarpic acid.....	304
Figure S- 21: Negative LDI mass spectrum of vulpinic acid	304
Figure S- 22: Negative LDI mass spectrum of thiophanic acid	305
Figure S- 23: Negative LDI mass spectrum of secalonic acid D	305
Figure S- 24: Negative LDI mass spectrum of roccellic acid	306
Figure S- 25: Negative LDI mass spectrum of lichesterinic acid	306
Figure S- 26: Negative LDI mass spectrum of lepraric acid	306
Figure S- 27: Positive LDI mass spectrum of mycosporine serinol	307
Figure S- 28: Negative LDI mass spectrum of the acetone extract of <i>Cladonia portentosa</i>	307
Figure S- 29: Negative LDI mass spectrum of the acetone extract of <i>Diploicia canescens</i>	307
Figure S- 30: Negative LDI mass spectrum of the acetone extract of <i>Evernia prunastri</i>	308
Figure S- 31: Negative LDI mass spectrum of the acetone extract of <i>Flavocetraria nivalis</i>	308
Figure S- 32: Negative LDI mass spectrum of the acetone extract of <i>Lecidella asema</i>	308
Figure S- 33: Negative LDI mass spectrum of the acetone extract of <i>Ophioparma ventosa</i>	309
Figure S- 34: Negative LDI mass spectrum of the acetone extract of <i>Pertusaria amara</i>	309
Figure S- 35: Negative LDI mass spectrum of the acetone extract of <i>Pseudevernia furfuracea</i>	309
Figure S- 36: Negative LDI mass spectrum of the acetone extract of <i>Ramalina cuspidata</i> var. <i>stenoclada</i>	310
Figure S- 37: Negative LDI mass spectrum of the acetone extract of <i>Ramalina siliquosa</i> var. <i>crassa</i>	310
Figure S- 38: Negative LDI mass spectrum of the acetone extract of <i>Roccella fuciformis</i>	310
Figure S- 39: Negative LDI mass spectrum of the acetone extract of <i>Roccella phycopsis</i>	311
Figure S- 40: Negative LDI mass spectrum of the acetone extract of <i>Tephromela atra</i>	311
Figure S- 41: Negative LDI mass spectrum of the acetone extract of <i>Usnea filipendula</i>	311
Figure S- 42: Negative LDI mass spectrum of the acetone extract of <i>Vulpicida pinastri</i>	312
Figure S- 43: Negative LDI mass spectrum of the acetone extract of <i>Xanthoria parietina</i>	312
Figure S- 44: Negative ESI mass spectrum of atranorin	313
Figure S- 45 : Negative ESI mass spectrum of divaricatic acid	313
Figure S- 46 : Negative ESI mass spectrum of evernic acid	313
Figure S- 47 : Negative ESI mass spectrum of thamnolic acid.....	314
Figure S- 48: Negative ESI mass spectrum of lobaric acid	314

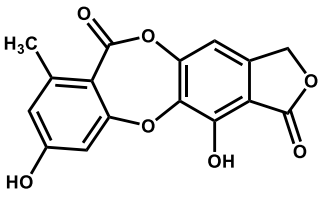
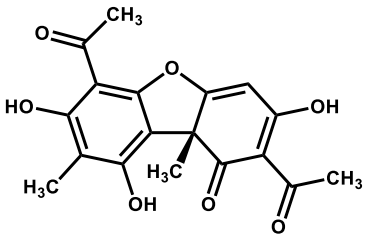
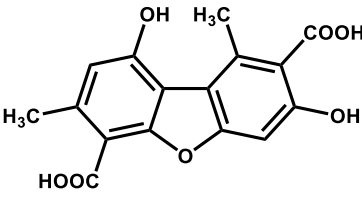
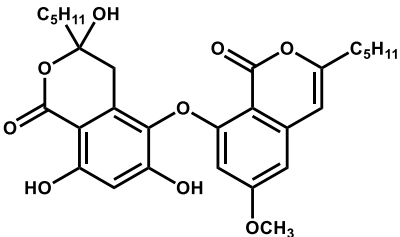
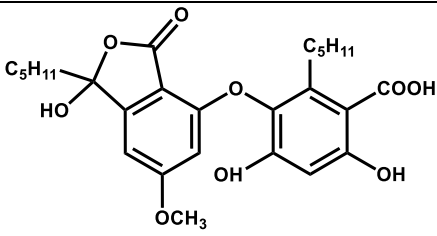
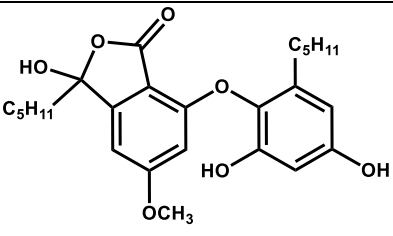
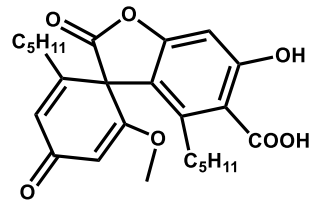
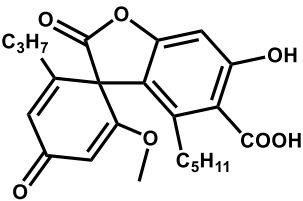
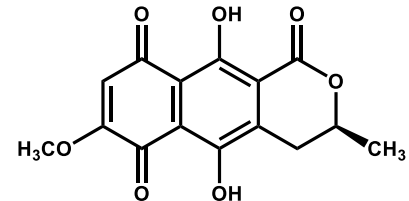
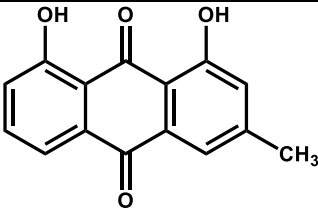
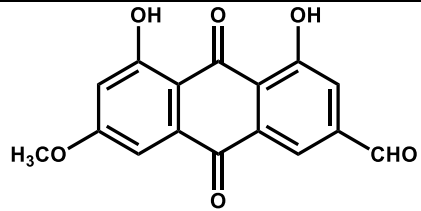
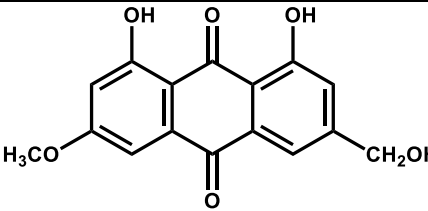
Figure S- 49 : Negative ESI mass spectrum of stictic acid.....	314
Figure S- 50 : Negative ESI mass spectrum of variolaric acid	314
Figure S- 51 : Negative ESI mass spectrum of pannaric acid.....	315
Figure S- 52 : Negative ESI mass spectrum of usnic acid.....	315
Figure S- 53 : Negative ESI mass spectrum of β -collatolic acid	315
Figure S- 54 : Negative ESI mass spectrum of lobarin	315
Figure S- 55 : Negative ESI mass spectrum of sakisacaulon A.....	316
Figure S- 56 : Negative ESI mass spectrum of emodin	316
Figure S- 57 : Negative ESI mass spectrum of epanorin	316
Figure S- 58 : Negative ESI mass spectrum of rhizocarpic acid	316
Figure S- 59 : Negative ESI mass spectrum of vulpinic acid	317
Figure S- 60 : Negative ESI mass spectrum of thiophanic acid.....	317
Figure S- 61 : Negative ESI mass spectrum of secalonic acid D.....	317
Figure S- 62 : Negative ESI mass spectrum of roccellic acid.....	318
Figure S- 63 : Negative ESI mass spectrum of lichesterinic acid.....	318
Figure S- 64 : Positive ESI mass spectrum of mycosporine serinol	318
Figure S- 65 : Negative ESI mass spectrum of the acetone extract of <i>Cladonia portentosa</i>	318
Figure S- 66 : Negative ESI mass spectrum of the acetone extract of <i>Diploicia canescens</i>	319
Figure S- 67 : Negative ESI mass spectrum of the acetone extract of <i>Evernia prunastri</i>	319
Figure S- 68 : Negative ESI mass spectrum of the acetone extract of <i>Flavocetraria nivalis</i>	319
Figure S- 69 : Negative ESI mass spectrum of the acetone extract of <i>Lecidella asema</i>	319
Figure S- 70 : Negative ESI mass spectrum of the acetone extract of <i>Ochrolechia parella</i>	319
Figure S- 71 : Negative ESI mass spectrum of the acetone extract of <i>Ophioparma ventosa</i>	320
Figure S- 72 : Negative ESI mass spectrum of the acetone extract of <i>Pertusaria amara</i>	320
Figure S- 73 : Negative ESI mass spectrum of the acetone extract of <i>Pseudevernia furfuracea</i>	320
Figure S- 74 : Negative ESI mass spectrum of the acetone extract of <i>Ramalina cuspidata</i> var. <i>stenoclada</i>	320
Figure S- 75 : Negative ESI mass spectrum of the acetone extract of <i>Ramalina siliquosa</i> var. <i>crassa</i>	321
Figure S- 76 : Negative ESI mass spectrum of the acetone extract of <i>Roccella fuciformis</i>	321
Figure S- 77 : Negative ESI mass spectrum of the acetone extract of <i>Roccella phycopsis</i>	321
Figure S- 78 : Negative ESI mass spectrum of the acetone extract of <i>Tephromela atra</i>	321
Figure S- 79 : Negative ESI mass spectrum of the acetone extract of <i>Usnea filipendula</i>	322
Figure S- 80 : Negative ESI mass spectrum of the acetone extract of <i>Vulpicida pinastri</i>	322
Figure S- 81 : Negative ESI mass spectrum of the acetone extract of <i>Xanthoria parietina</i>	322

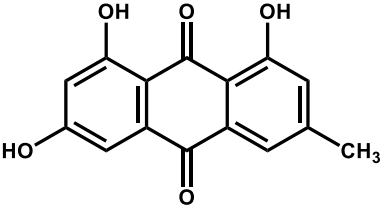
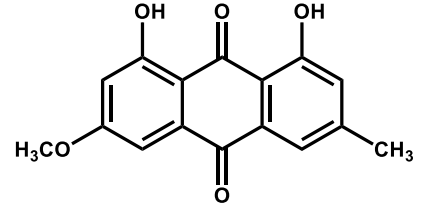
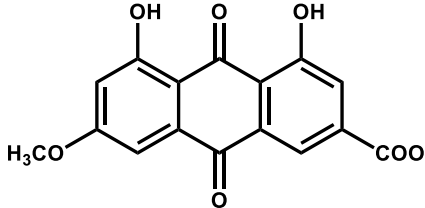
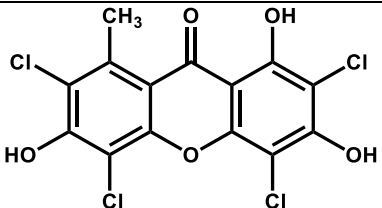
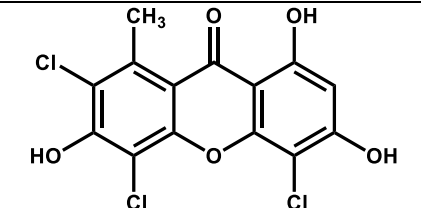
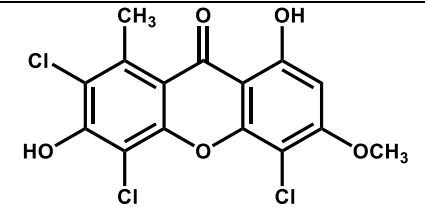
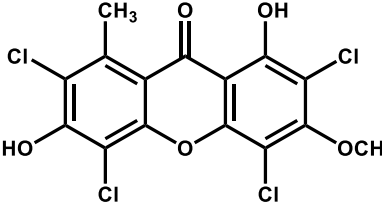
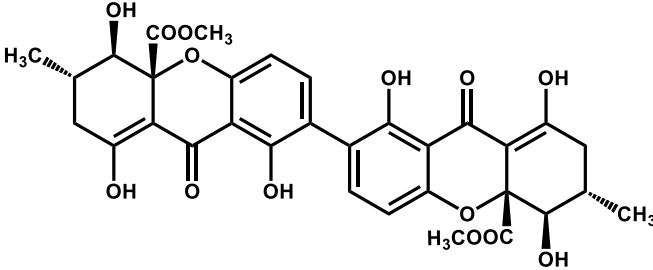
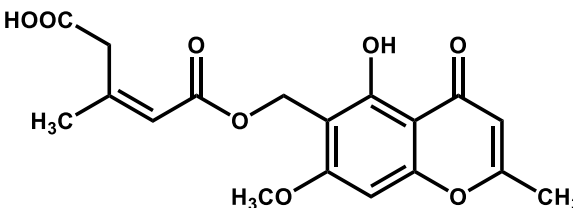
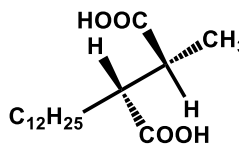
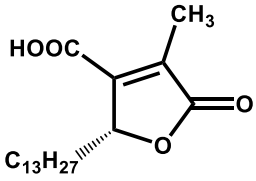
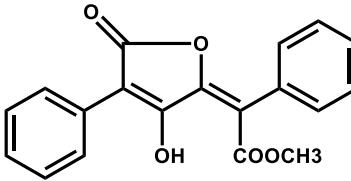
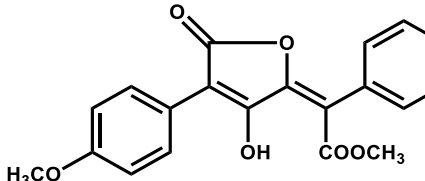
Table S-1 : Place and date of harvest and voucher specimen number of lichens described in this study.

Lichens	Voucher specimen	Place and date of harvest	Reference
<i>Cladonia portentosa</i>	JB/05/48	Cressensac (Lot) - 2005	(Chollet-Krugler et al., 2008)
<i>Diploicia canescens</i>	JB/06/10	Dinard (Ille-et-Vilaine) - 2006	(Millot et al., 2009)
<i>Evernia prunastri</i>	JB/06/51	Cressensac (Lot) -2006	
<i>Flavocetraria nivalis</i>	JB/02/37	Font-Romeu (Pyrénées Orientales) - 2002	
<i>Lecidella asema</i>	2014/JYM/04	Pointe du Raz (Finistère) - 2014	
<i>Ophioparma ventosa</i>	JB/09/58	Obergurgl (Austria) - 2009	(Le Pogam et al., 2016a)
<i>Pertusaria amara</i>	JB/07/108	Liffré (Ille-et-Vilaine) - 2007	(Bonny et al., 2011)
<i>Pseudevernia furfuracea</i>	JB/00/04	Meymac (Corrèze) - 2000	
<i>Ramalina siliquosa</i> var. <i>crassa</i>	JB/11/e496	Carantec (Finistère) - 2011	(Parrot et al., 2013)
<i>Ramalina cuspidata</i> var. <i>stenoclada</i>	JB/11/e495	Trégastel (Finistère) - 2011	(Parrot et al., 2013)
<i>Roccella fuciformis</i>	JB/05/57	Ploumanach (Côtes d'Armor) - 2005	(Parrot et al., 2015)
<i>Roccella phycopsis</i>	JB/05/46	Ile de Bréhat (Côtes d'Armor) - 2005	(Parrot et al., 2015)
<i>Tephromela atra</i>	JB/05/e56	La Guimorais (Ille-et-Vilaine) - 2006	(Millot et al., 2008)
<i>Usnea filipendula</i>	JB/00/78	Ventadour (Corrèze) - 07/2000	
<i>Vulpicida pinastri</i>	JB/14/198	Jausier (Alpes Maritimes) - 04/2014	
<i>Xanthoria parietina</i>	JB/06/59	Dinard (Ille-et-Vilaine) - 01/2006	

DEPSIDES		
 <p>Atranorin</p>	 <p>Chloroatranorin</p>	 <p>Evernic acid</p>
 <p>Divaricatic acid</p>	 <p>Thamnic acid</p>	 <p>Lecanoric acid</p>
 <p>Miriquidic acid</p>	 <p>Perlatolic acid</p>	
 <p>Erythrin</p>		
DEPSIDONES		
 <p>Stictic acid</p>	 <p>Norstictic acid</p>	 <p>Diploicin</p>

 <p>Dechlorodiploicin</p>	 <p>Salazinic acid</p>	 <p>Gangaleoidin</p>
 <p>Lobaric acid</p>	 <p>α-alectoronic acid</p>	 <p>α-collatolic acid</p>
 <p>Physodic acid</p>	 <p>3-hydroxyphysodic acid</p>	 <p>2'-O-methylphysodic acid</p>
<p>DIBENZOFURANS AND RELATED</p>		

 <p>Variolaric acid</p>	 <p>(+)-Usnic acid</p>	 <p>Pannaric acid</p>
DIPHENYLETERS		
 <p>β-collatolic acid</p>	 <p>Lobarin</p>	 <p>Sakisacaulon A</p>
DEPSONES		NAPHTHOQUINONE
 <p>Picrolichenic acid</p>	 <p>Subpicrolichenic acid</p>	 <p>Haemoventosin</p>
ANTHRAQUINONES		
 <p>Chrysophanol</p>	 <p>Fallacinal</p>	 <p>Fallacinol</p>

 <p>Emodin</p>	 <p>Parietin</p>	 <p>Parietic acid</p>
XANTHONES		
 <p>Thiophanic acid</p>	 <p>Asemone</p>	 <p>3-O-methylasemone</p>
 <p>3-O-methylthiophanic acid</p>	 <p>Secalonic acid D</p>	
CHROMONE		ALIPHATIC ACID
 <p>Lepranic acid</p>		 <p>Roccellic acid</p>
PARACONIC ACID	PULVINIC ACID DERIVATIVES	
		

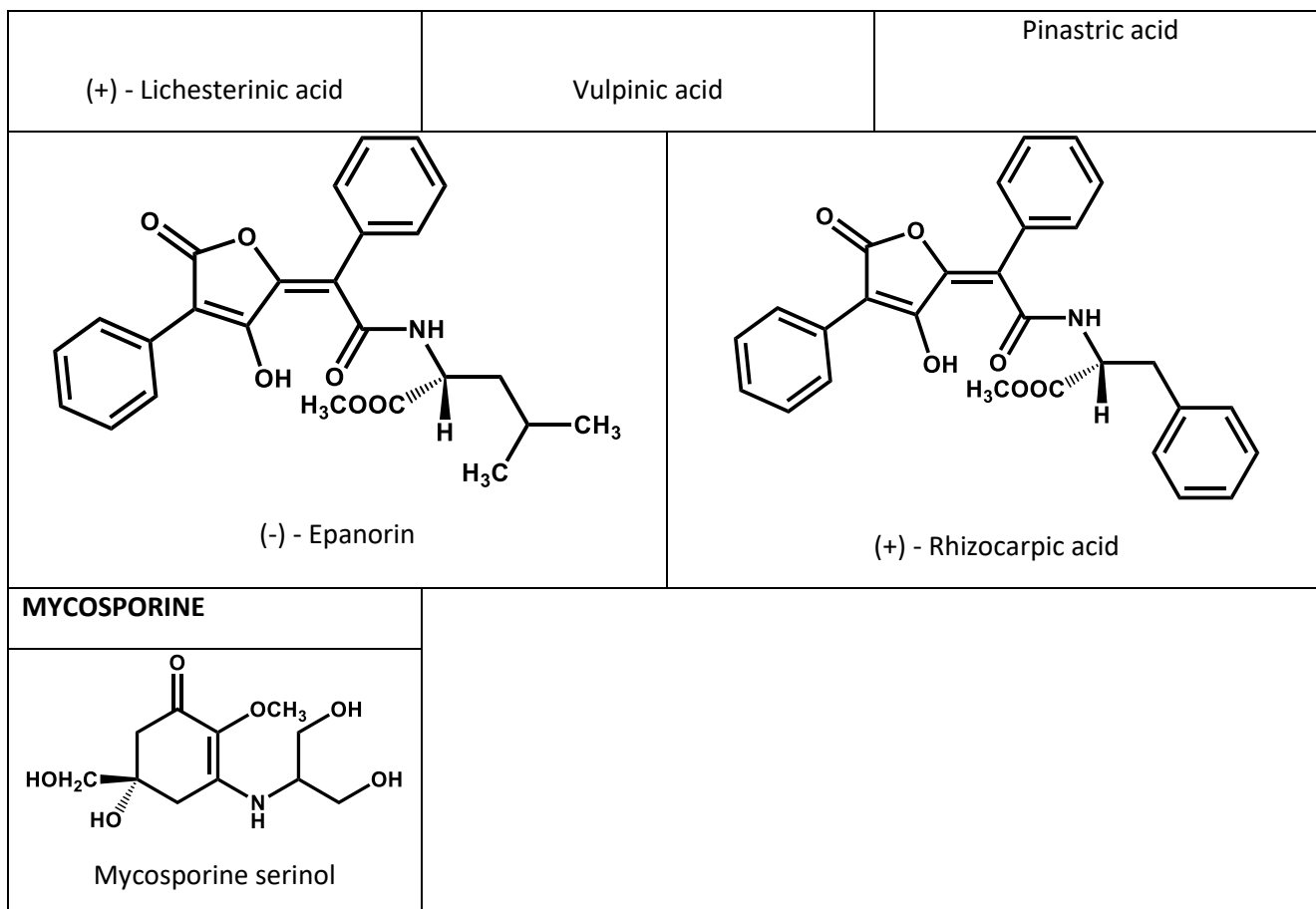


FIGURE S- 1: STRUCTURES OF STUDIED MOLECULES, EITHER AS SINGLE COMPOUNDS OR WITHIN LICHEN EXTRACTS.

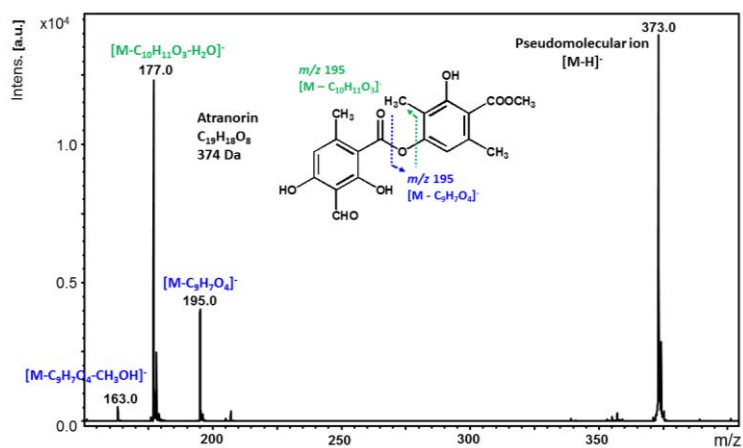
LDI-MS SPECTRA**SINGLE MOLECULES****DEPSIDES**

FIGURE S- 2: NEGATIVE LDI MASS SPECTRUM OF ATRANORIN

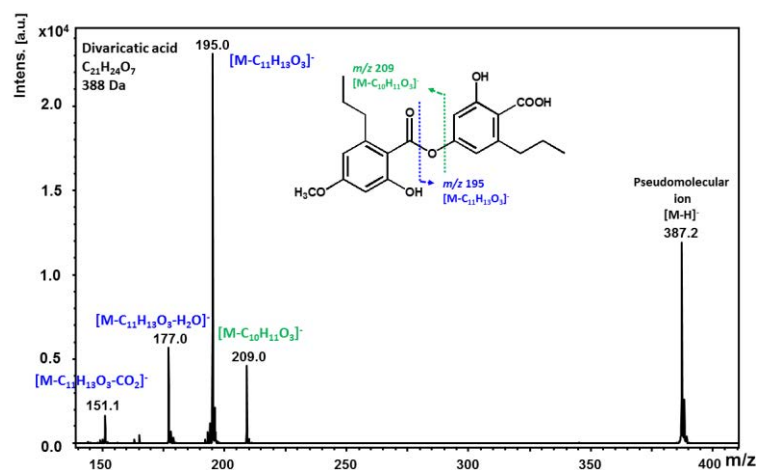


FIGURE S- 3: NEGATIVE LDI MASS SPECTRUM OF DIVARICATIC ACID

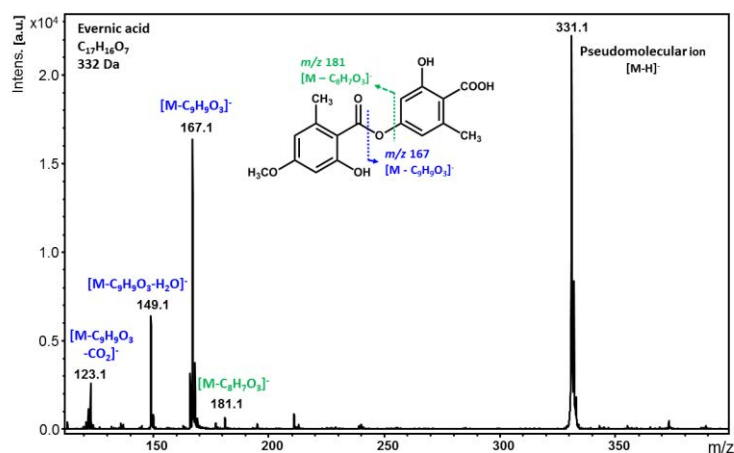


FIGURE S- 4: NEGATIVE LDI MASS SPECTRUM OF EVERNIC ACID

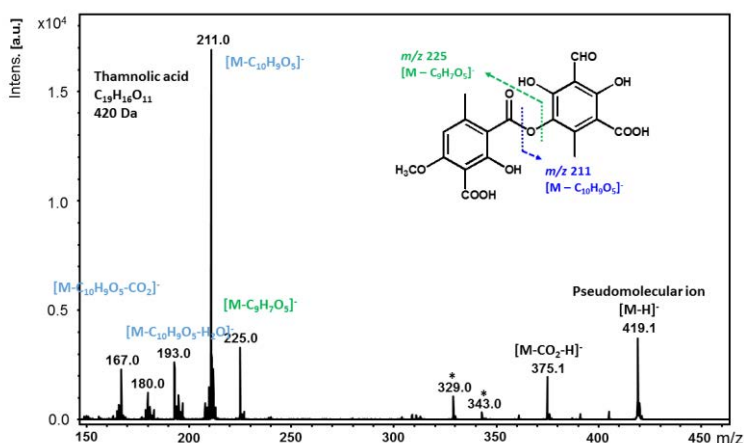


FIGURE S- 5: NEGATIVE LDI MASS SPECTRUM OF THAMNOLIC ACID

DEPSIDONES

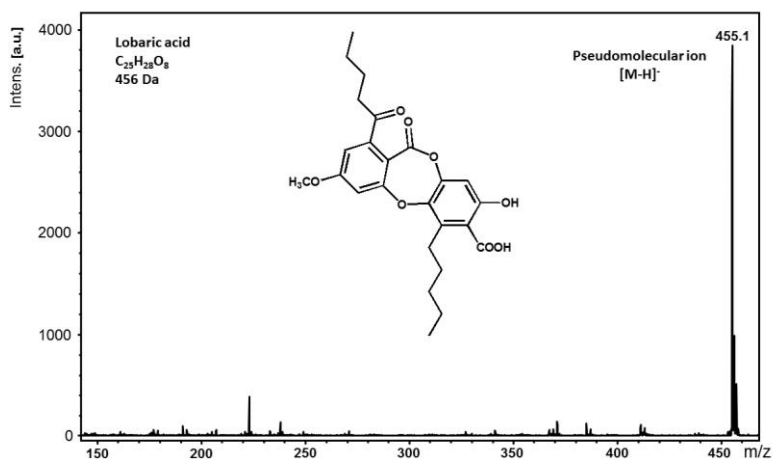


FIGURE S- 6: NEGATIVE LDI MASS SPECTRUM OF LOBARIC ACID

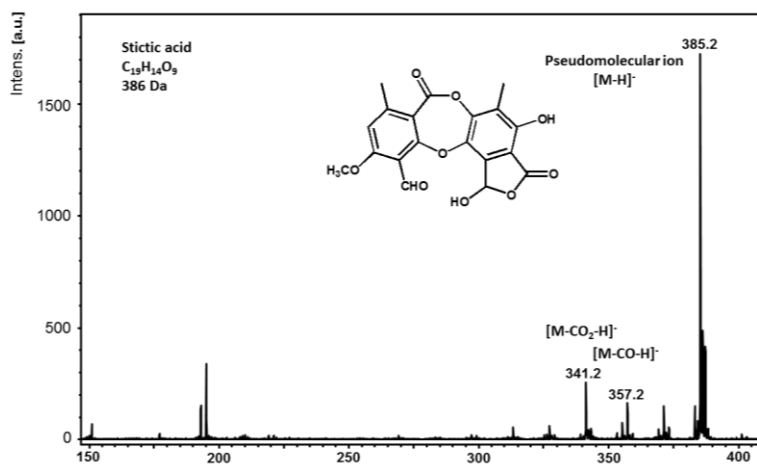


FIGURE S- 7: NEGATIVE LDI MASS SPECTRUM OF STICTIC ACID

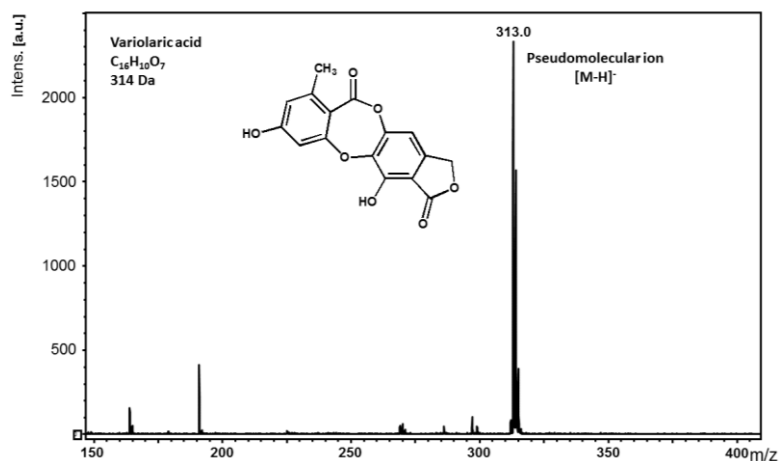


FIGURE S- 8: NEGATIVE LDI MASS SPECTRUM OF VARIOLARIC ACID

DIBENZOFURAN AND RELATED

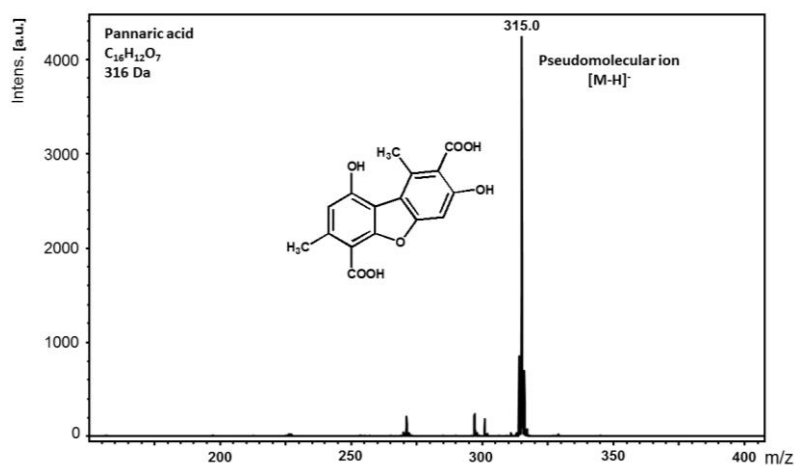


FIGURE S- 9: NEGATIVE LDI MASS SPECTRUM OF PANNARIC ACID

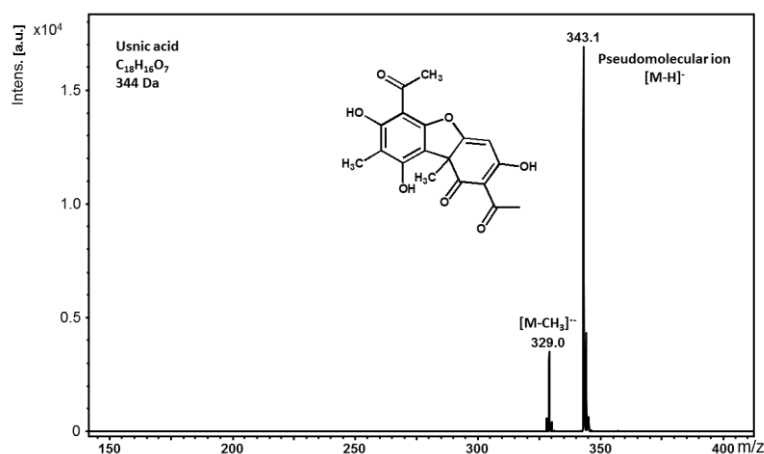


FIGURE S- 10: NEGATIVE LDI MASS SPECTRUM OF USNIC ACID

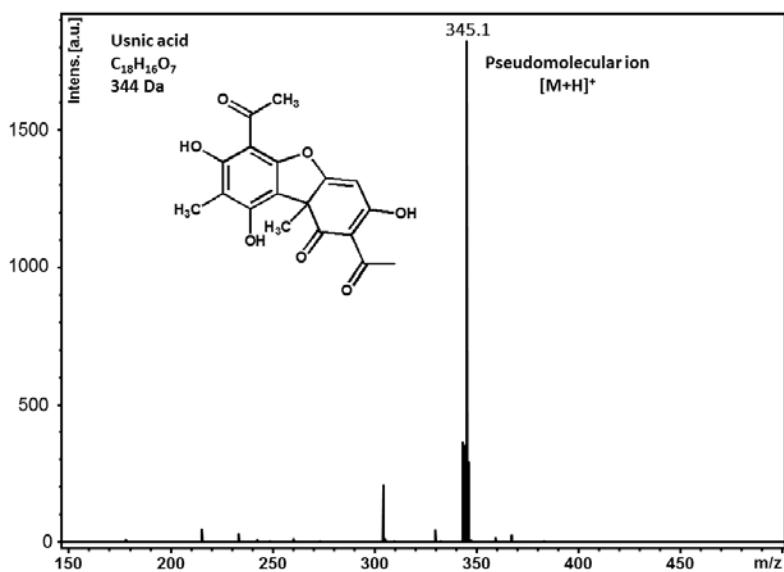


FIGURE S- 11 : POSITIVE LDI MASS SPECTRUM OF USNIC ACID

DIPHENYLEETHERS

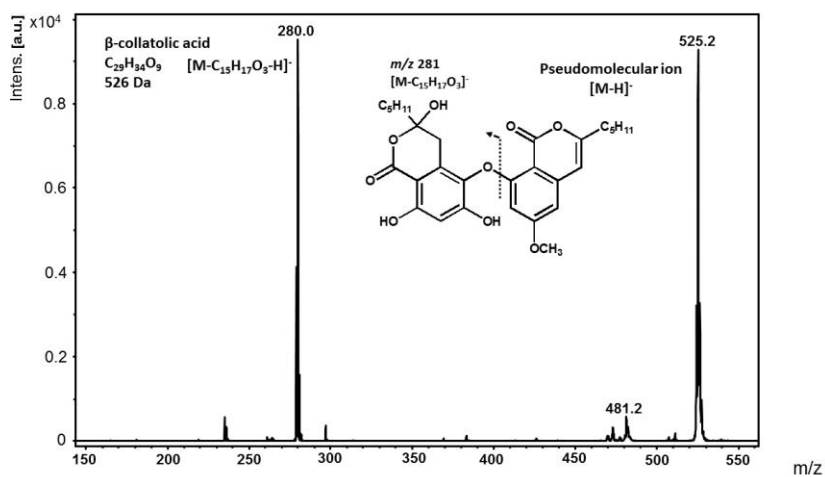


FIGURE S- 12: NEGATIVE LDI MASS SPECTRUM OF B-COLLATOLIC ACID

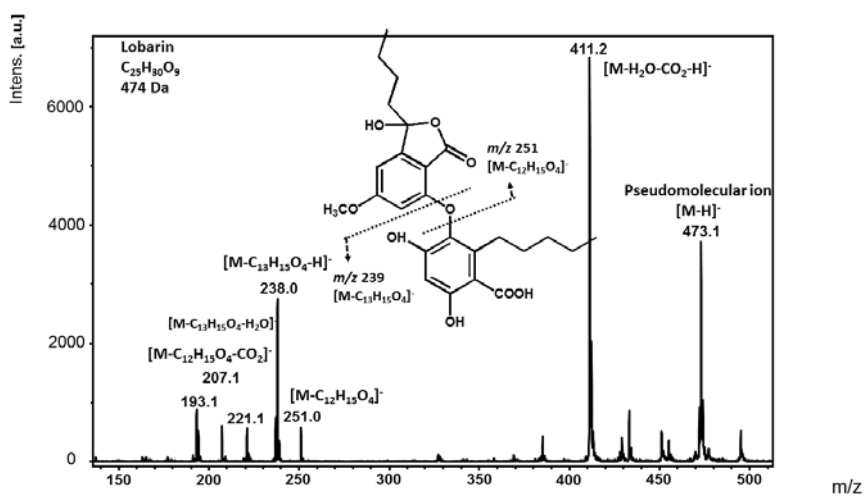


FIGURE S- 13 : NEGATIVE LDI MASS SPECTRUM OF LOBARIN

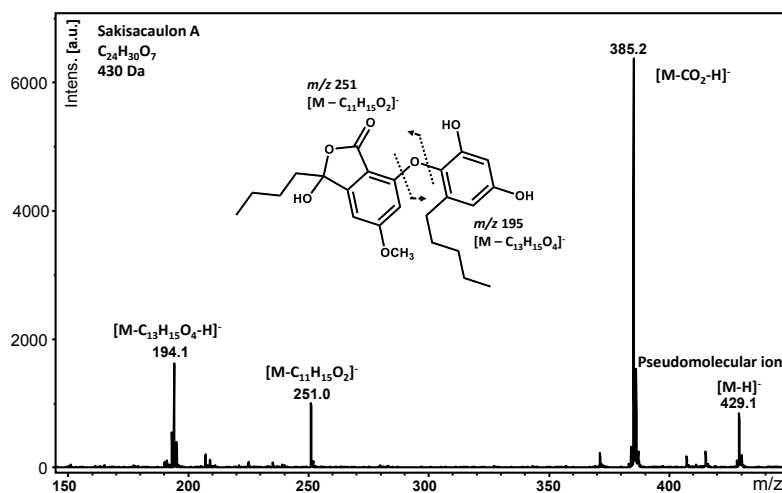


FIGURE S- 14: NEGATIVE LDI MASS SPECTRUM OF SAKISACAULON A

QUINONES

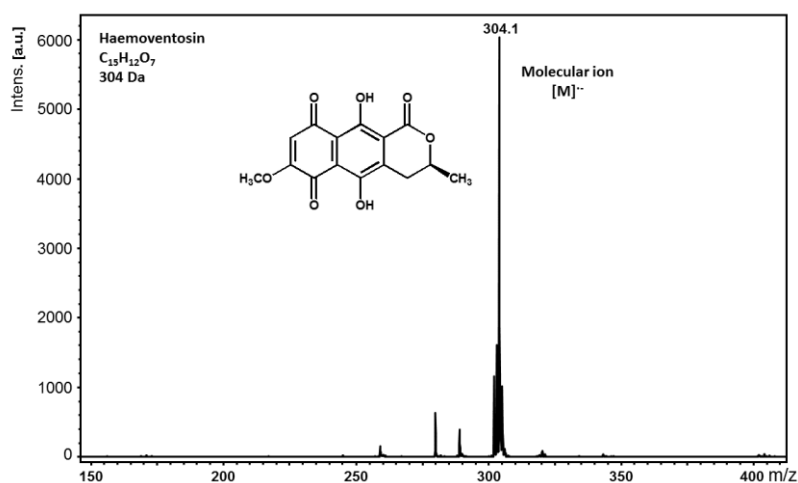


FIGURE S- 15: NEGATIVE LDI MASS SPECTRUM OF HAEMOVENTOSIN

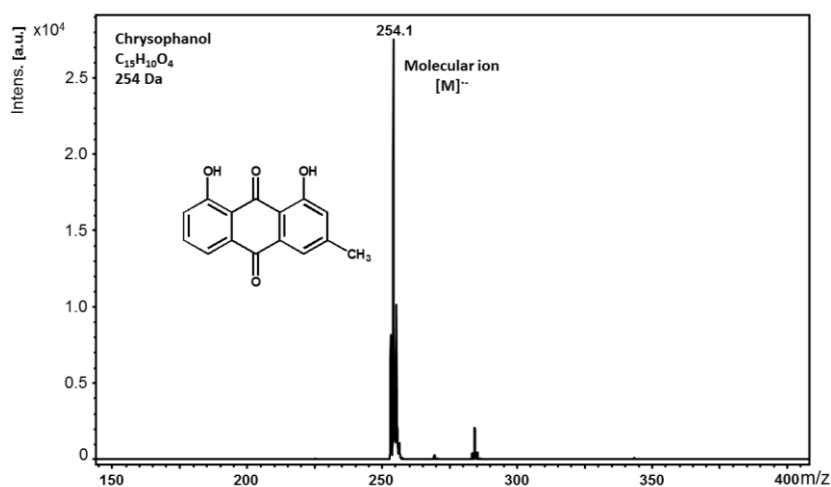


FIGURE S- 16: NEGATIVE LDI MASS SPECTRUM OF CHRYSOPHANOL

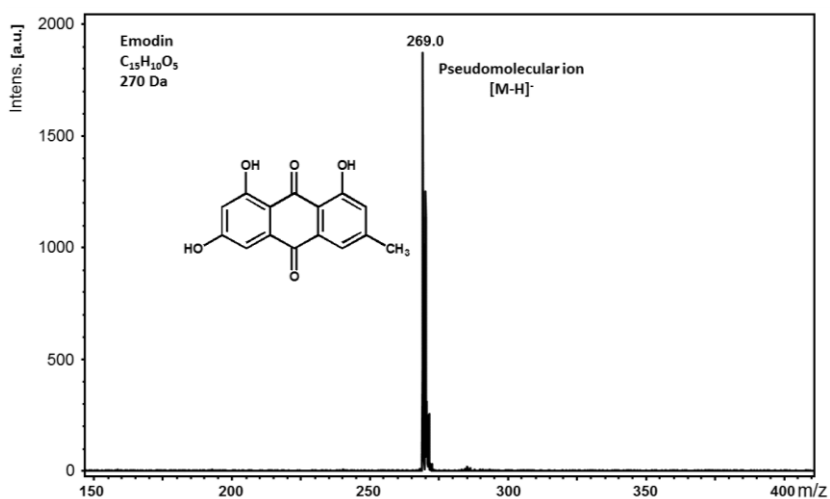


FIGURE S- 17: NEGATIVE LDI MASS SPECTRUM OF EMODIN

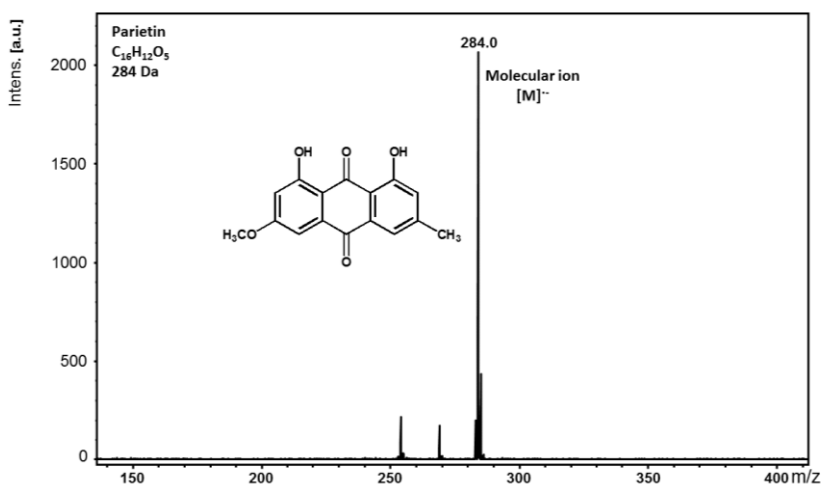


FIGURE S- 18 : NEGATIVE LDI MASS SPECTRUM OF PARIETIN

PULVINIC ACID DERIVATIVES

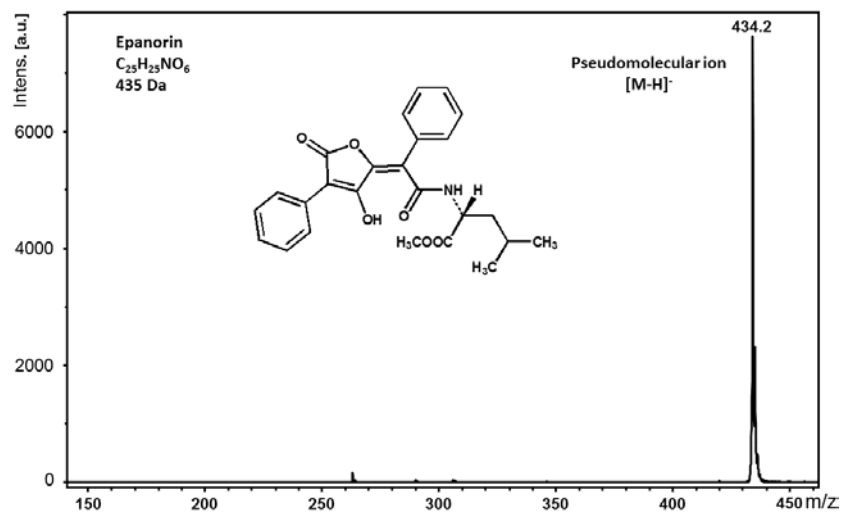


FIGURE S- 19: NEGATIVE LDI MASS SPECTRUM OF EPANORIN

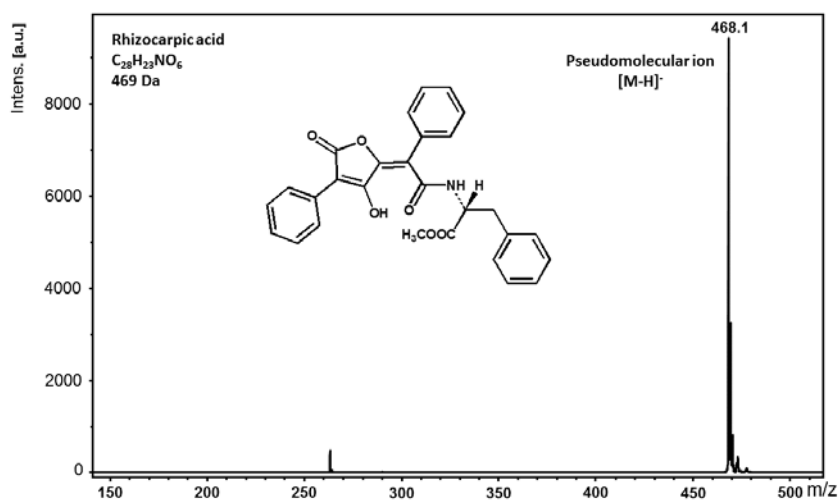


FIGURE S- 20: NEGATIVE LDI MASS SPECTRUM OF RHIZOCARPIC ACID

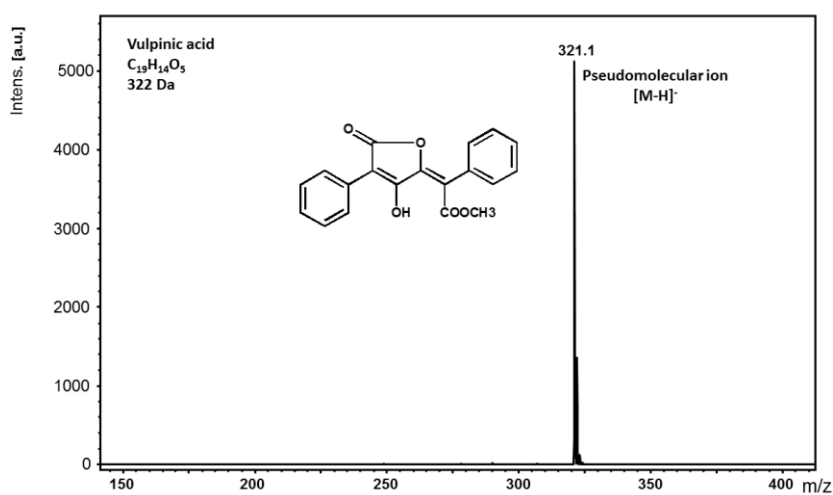


FIGURE S- 21: NEGATIVE LDI MASS SPECTRUM OF VULPINIC ACID

XANTHONES

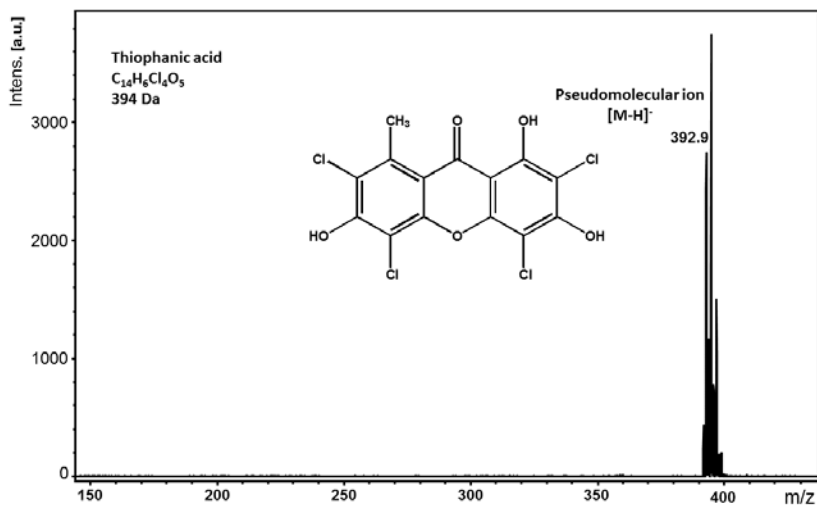


FIGURE S- 22: NEGATIVE LDI MASS SPECTRUM OF THIOPHANIC ACID

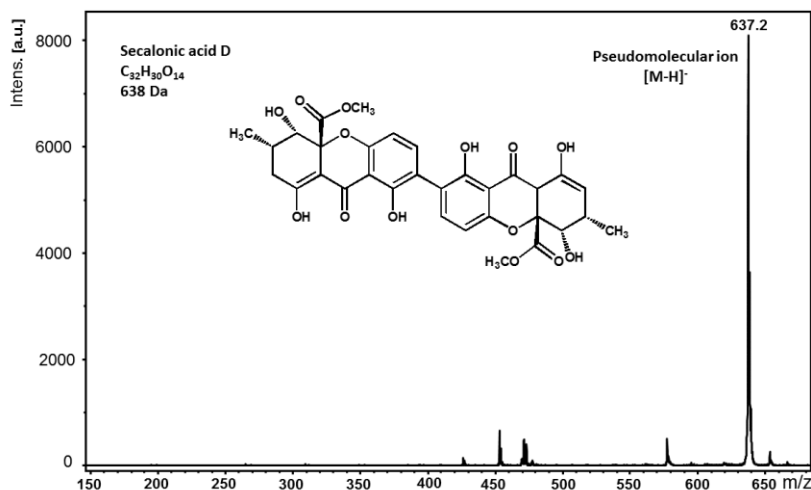


FIGURE S- 23: NEGATIVE LDI MASS SPECTRUM OF SECALONIC ACID D

ALIPHATIC AND PARACONIC ACIDS

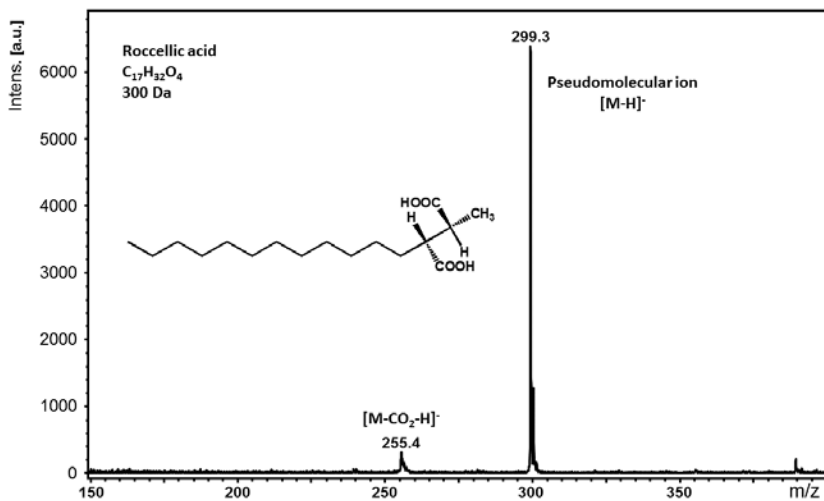


FIGURE S- 24: NEGATIVE LDI MASS SPECTRUM OF ROCCELLIC ACID

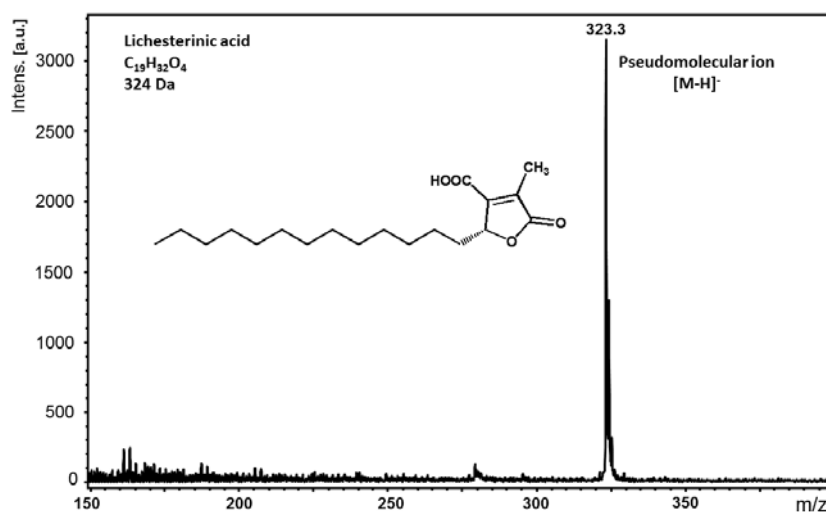


FIGURE S- 25: NEGATIVE LDI MASS SPECTRUM OF LICHESTERINIC ACID

CHROMONES

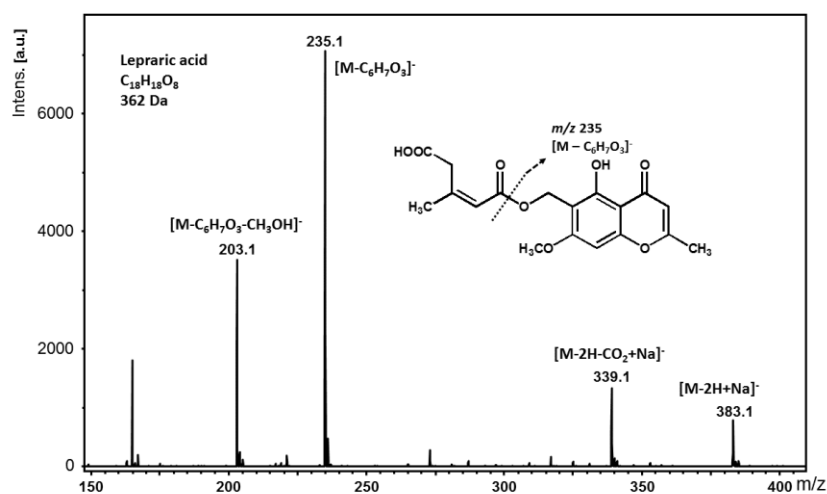


FIGURE S- 26: NEGATIVE LDI MASS SPECTRUM OF LEPRALIC ACID

MYCOSPORINE

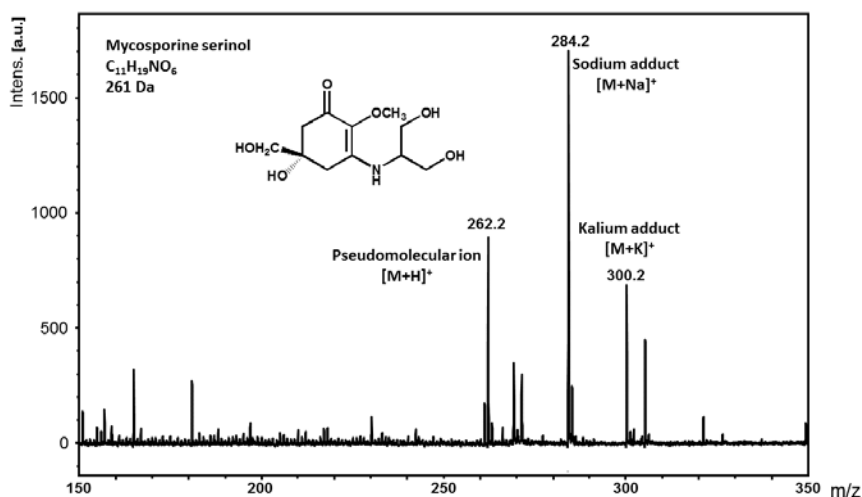
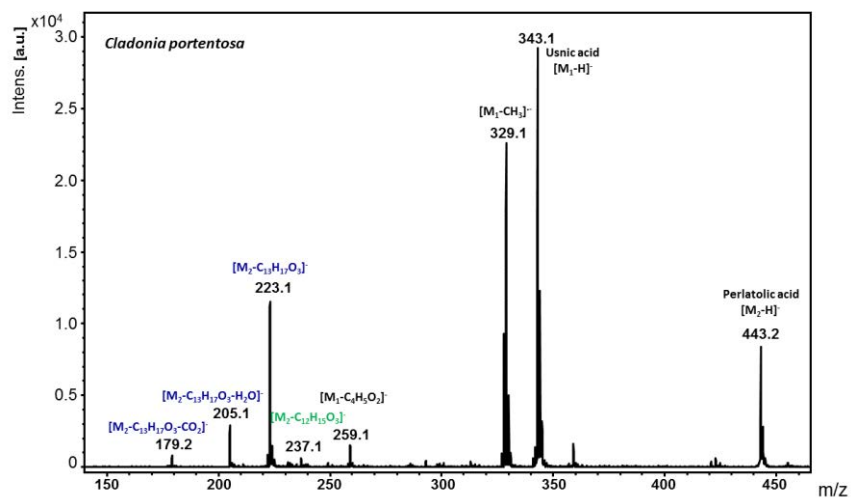
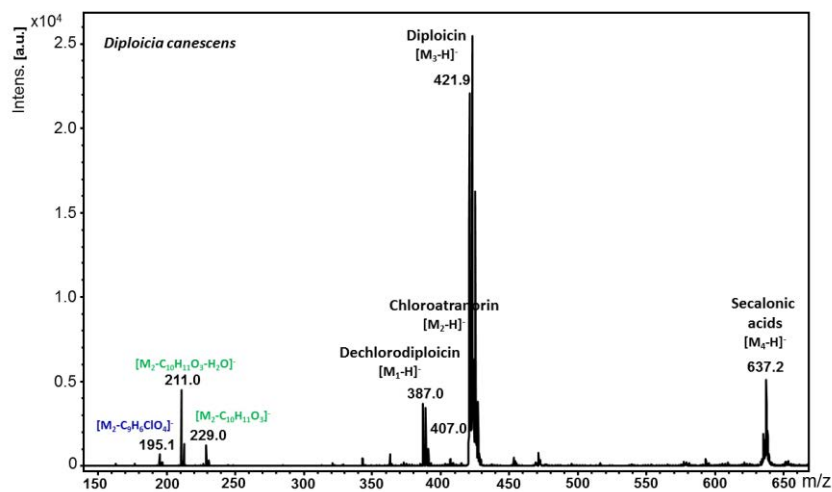
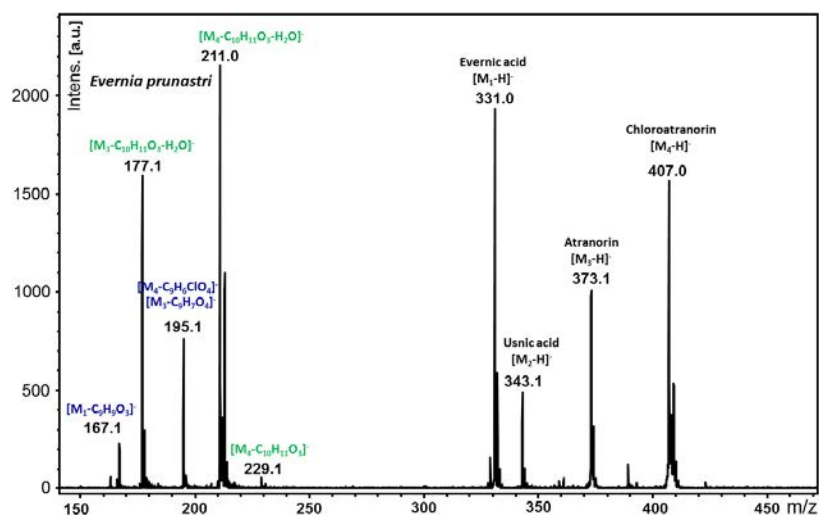
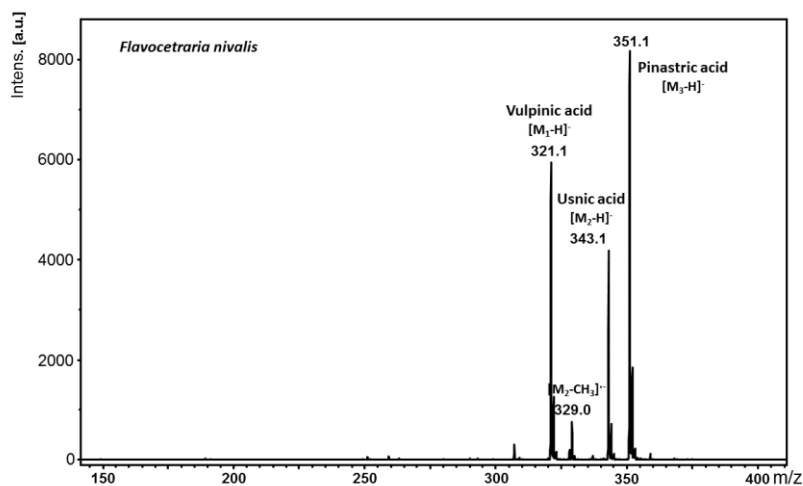
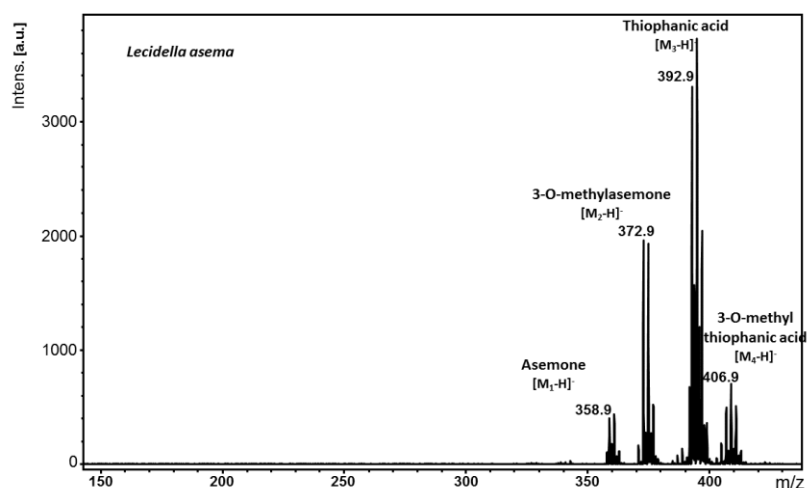
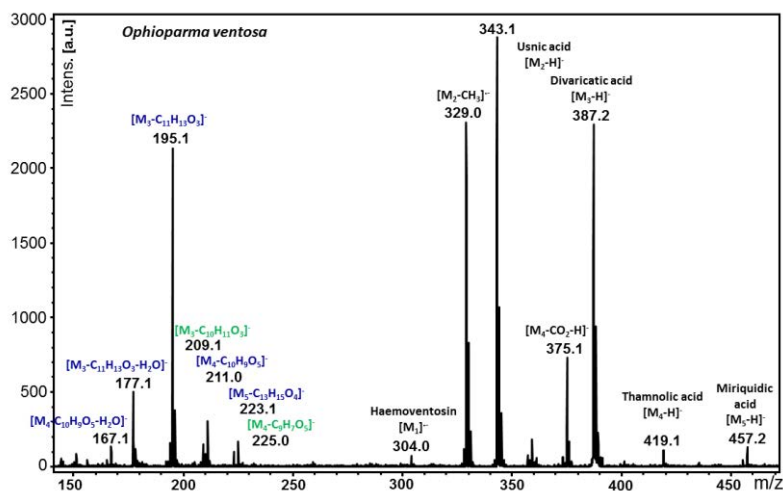
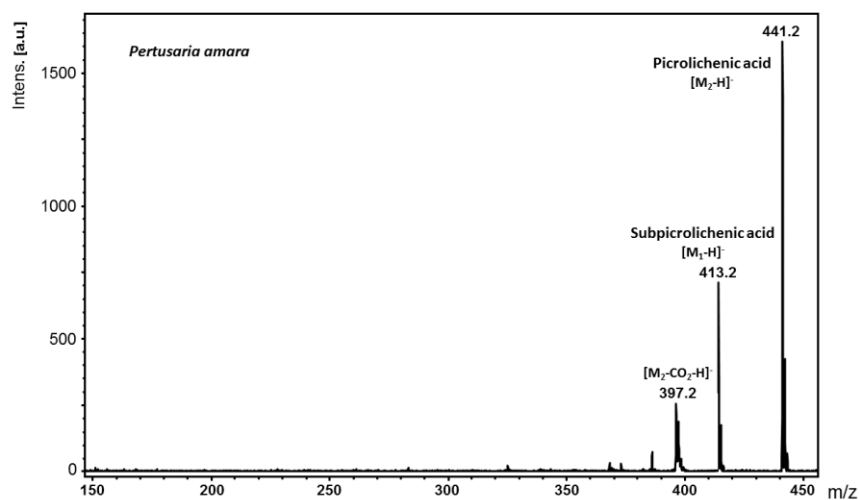
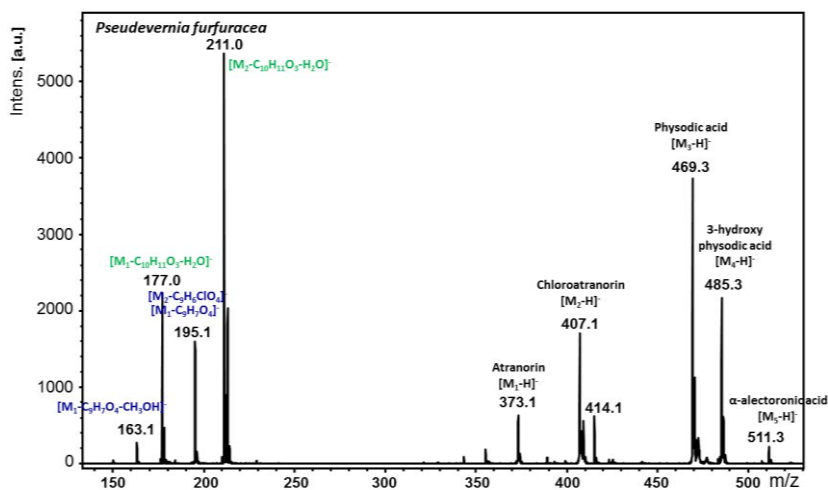


FIGURE S- 27: POSITIVE LDI MASS SPECTRUM OF MYCOSPORINE SERINOL

EXTRACTS

FIGURE S- 28: NEGATIVE LDI MASS SPECTRUM OF THE ACETONE EXTRACT OF *CLADONIA PORTENTOSA*FIGURE S- 29: NEGATIVE LDI MASS SPECTRUM OF THE ACETONE EXTRACT OF *DIPLOICIA CANESCENS*

FIGURE S- 30: NEGATIVE LDI MASS SPECTRUM OF THE ACETONE EXTRACT OF *EVERNIA PRUNASTRI*FIGURE S- 31: NEGATIVE LDI MASS SPECTRUM OF THE ACETONE EXTRACT OF *FLAVOCETRARIA NIVALIS*FIGURE S- 32: NEGATIVE LDI MASS SPECTRUM OF THE ACETONE EXTRACT OF *LECIDELLA ASEMA*

FIGURE S- 33: NEGATIVE LDI MASS SPECTRUM OF THE ACETONE EXTRACT OF *OPHIOPARMA VENTOSA*FIGURE S- 34: NEGATIVE LDI MASS SPECTRUM OF THE ACETONE EXTRACT OF *PERTUSARIA AMARA*FIGURE S- 35: NEGATIVE LDI MASS SPECTRUM OF THE ACETONE EXTRACT OF *PSEUDEVERNIA FURFURACEA*

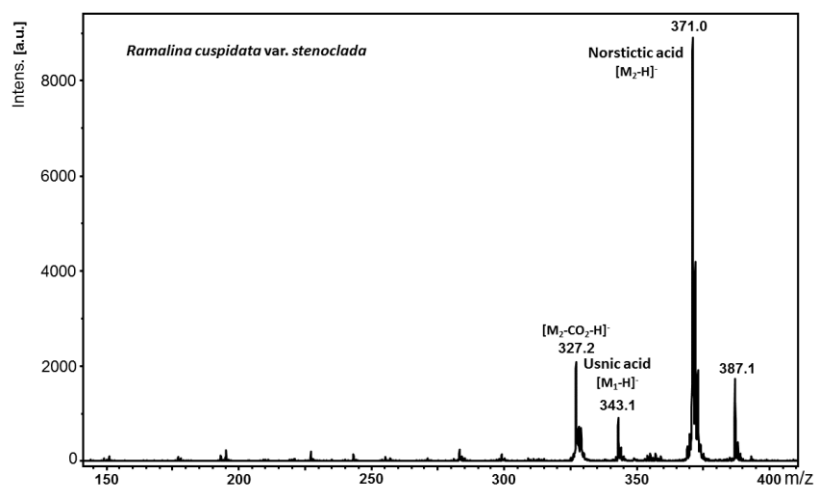


FIGURE S- 36: NEGATIVE LDI MASS SPECTRUM OF THE ACETONE EXTRACT OF *RAMALINA CUSPIDATA* VAR. *STENOCLADA*

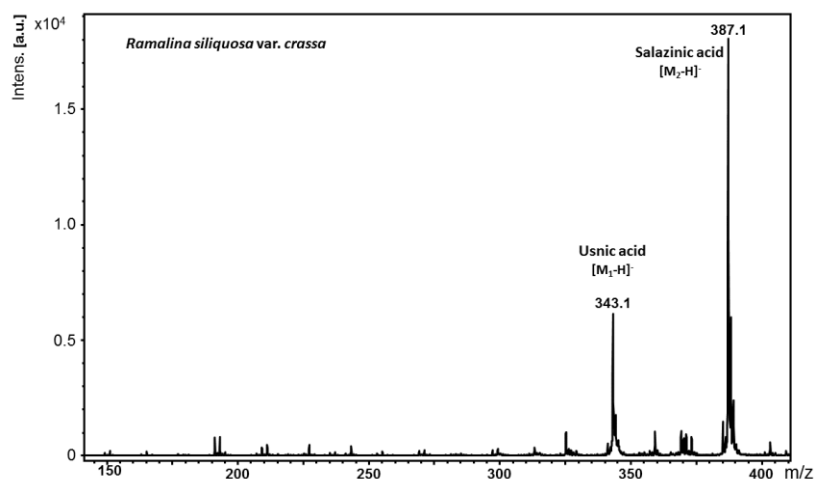


FIGURE S- 37: NEGATIVE LDI MASS SPECTRUM OF THE ACETONE EXTRACT OF *RAMALINA SILIQUOSA* VAR. *CRASSA*

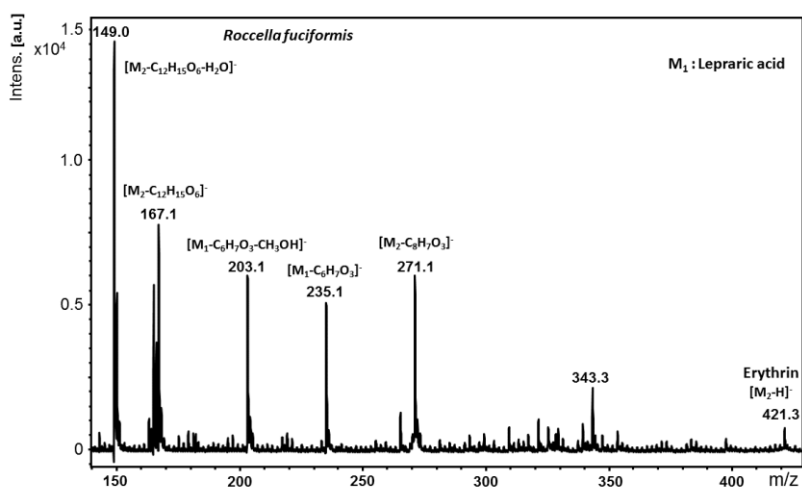
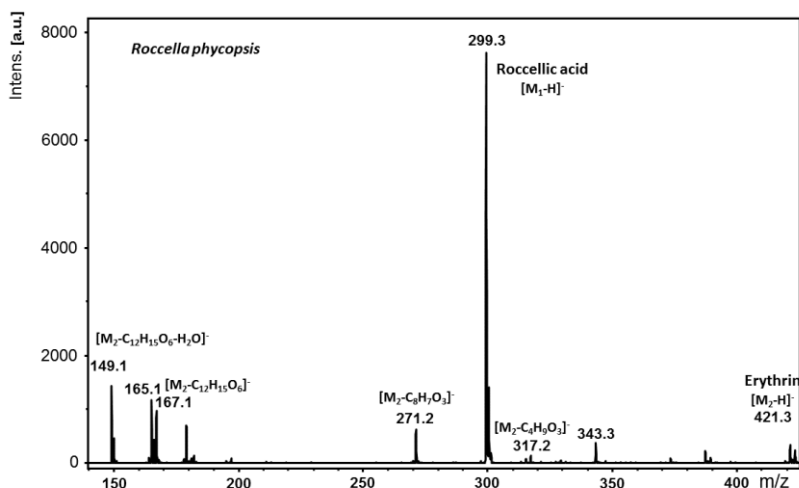
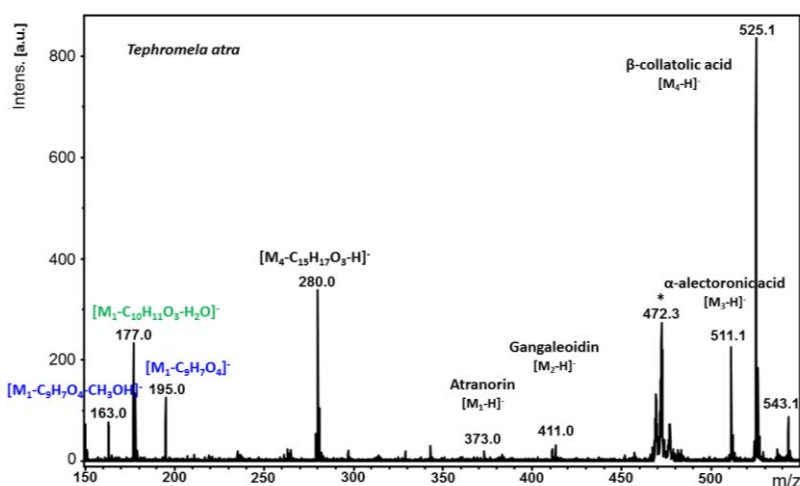
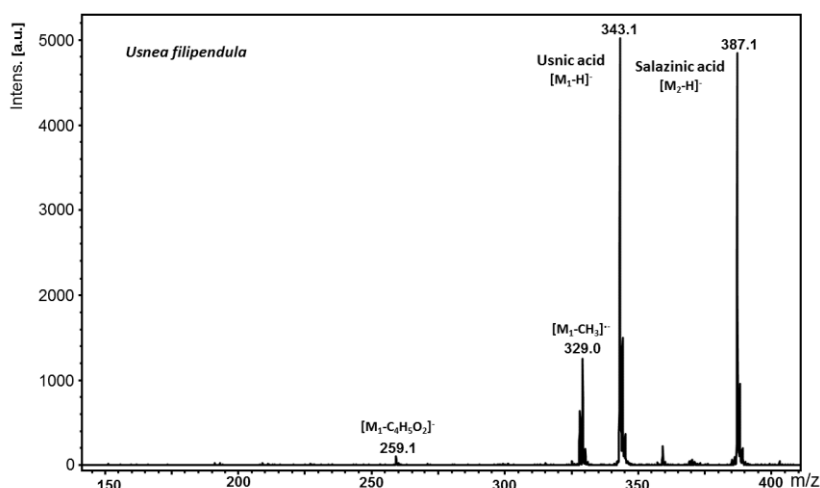
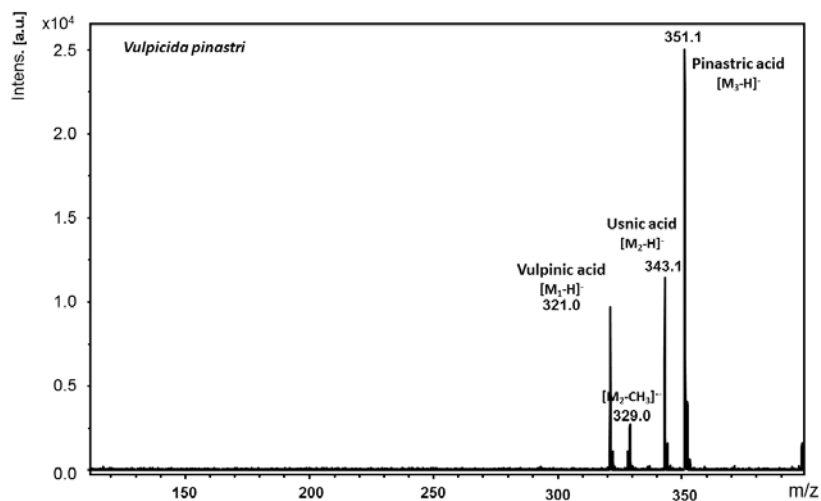
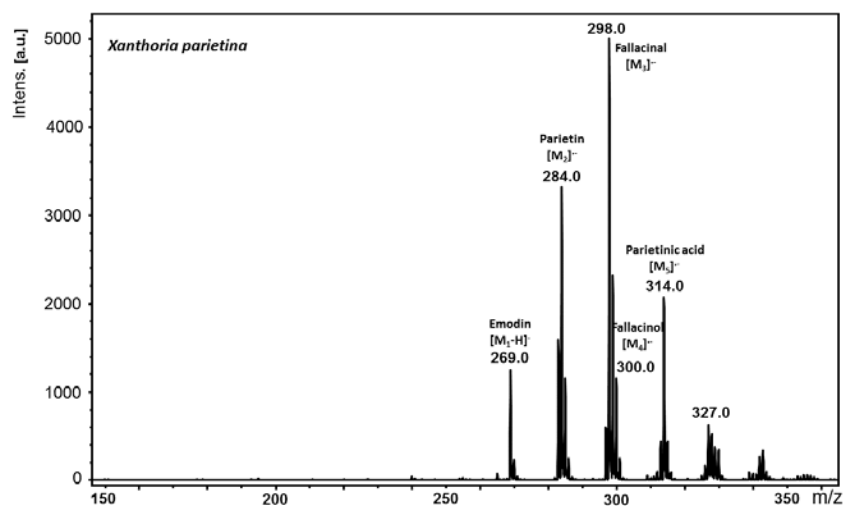


FIGURE S- 38: NEGATIVE LDI MASS SPECTRUM OF THE ACETONE EXTRACT OF *ROCCELLA FUCIFORMIS*

FIGURE S- 39: NEGATIVE LDI MASS SPECTRUM OF THE ACETONE EXTRACT OF *ROCELLELA PHYCOPSIS*FIGURE S- 40: NEGATIVE LDI MASS SPECTRUM OF THE ACETONE EXTRACT OF *TEPHROMELA ATRA*FIGURE S- 41: NEGATIVE LDI MASS SPECTRUM OF THE ACETONE EXTRACT OF *USNEA FILIPENDULA*

FIGURE S- 42: NEGATIVE LDI MASS SPECTRUM OF THE ACETONE EXTRACT OF *VULPICIDA PINASTRI*FIGURE S- 43: NEGATIVE LDI MASS SPECTRUM OF THE ACETONE EXTRACT OF *XANTHORIA PARIETINA*

ESI-MS SPECTRA

SINGLE MOLECULES

DEPSIDES

Atranorin

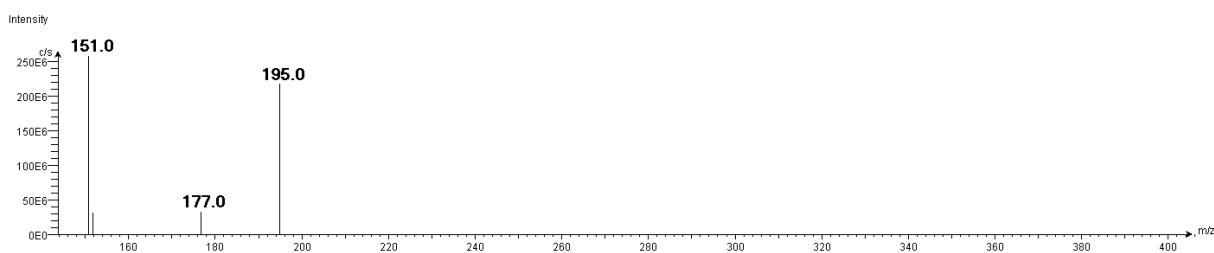


FIGURE S- 44: NEGATIVE ESI MASS SPECTRUM OF ATRANORIN

Divaricatic acid

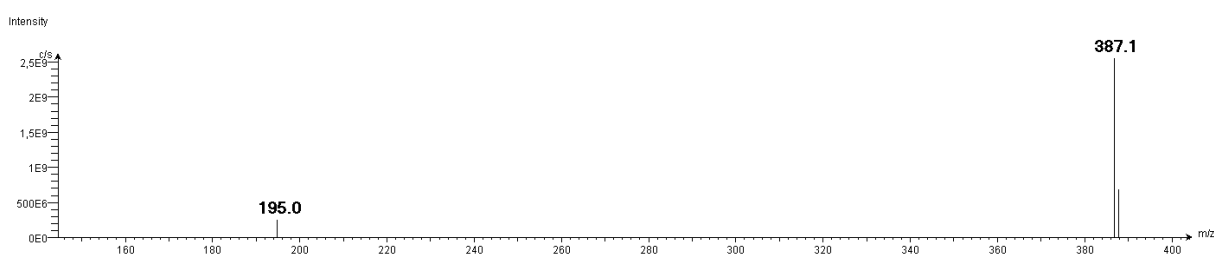


FIGURE S- 45 : NEGATIVE ESI MASS SPECTRUM OF DIVARICATIC ACID

Evernic acid

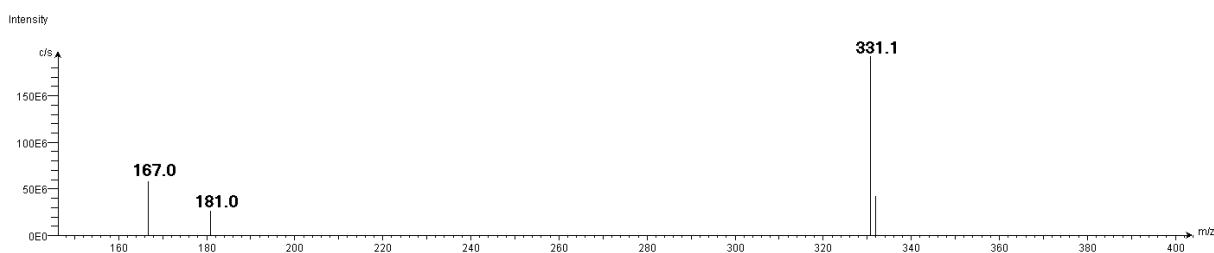


FIGURE S- 46 : NEGATIVE ESI MASS SPECTRUM OF EVERNIC ACID

Thamnolic acid

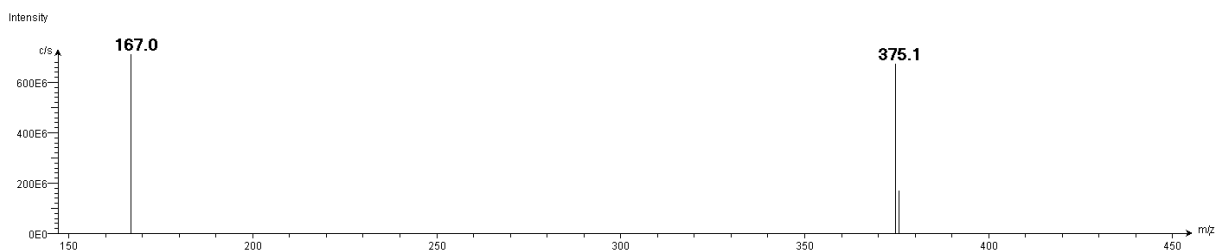


FIGURE S- 47 : NEGATIVE ESI MASS SPECTRUM OF THAMNOLIC ACID

DEPSIDONES

Lobaric acid

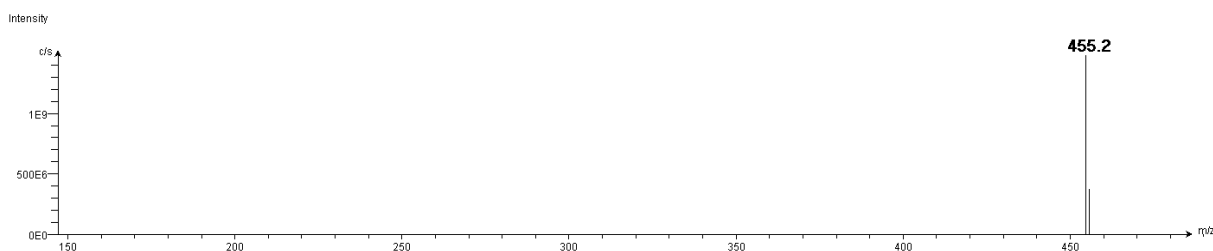


FIGURE S- 48: NEGATIVE ESI MASS SPECTRUM OF LOBARIC ACID

Stictic acid

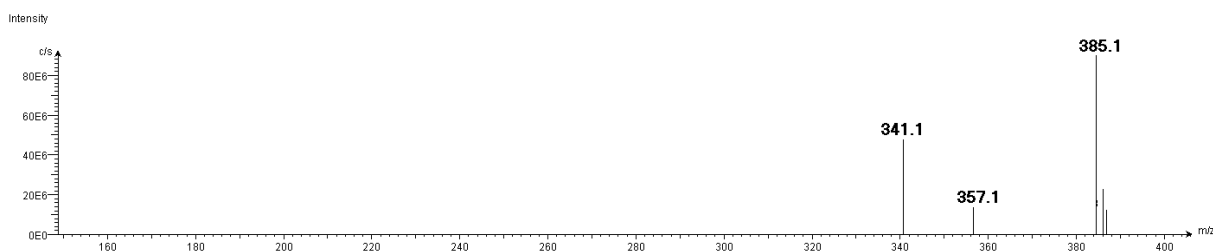


FIGURE S- 49 : NEGATIVE ESI MASS SPECTRUM OF STICTIC ACID

Variolaric acid

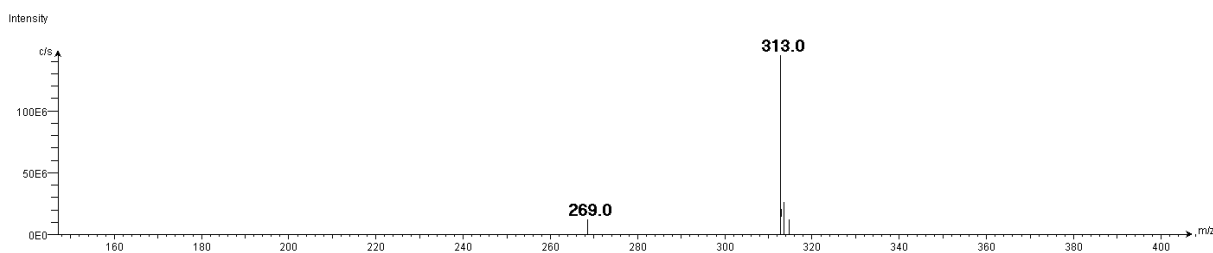


FIGURE S- 50 : NEGATIVE ESI MASS SPECTRUM OF VARIOLARIC ACID

DIBENZOFURAN AND RELATED

Pannaric acid

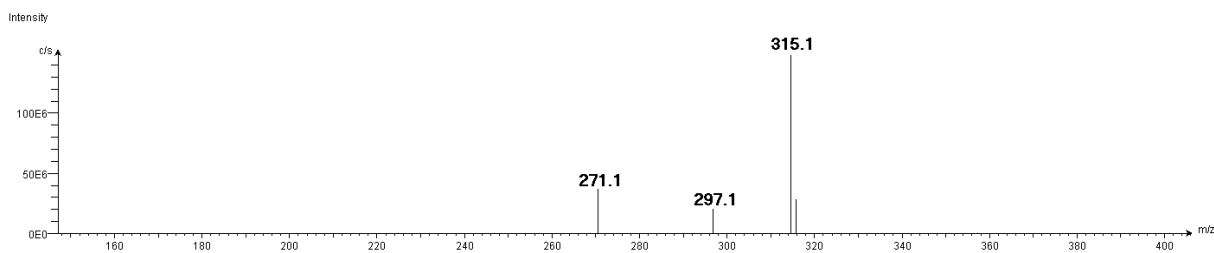


FIGURE S- 51 : NEGATIVE ESI MASS SPECTRUM OF PANNARIC ACID

Usnic acid

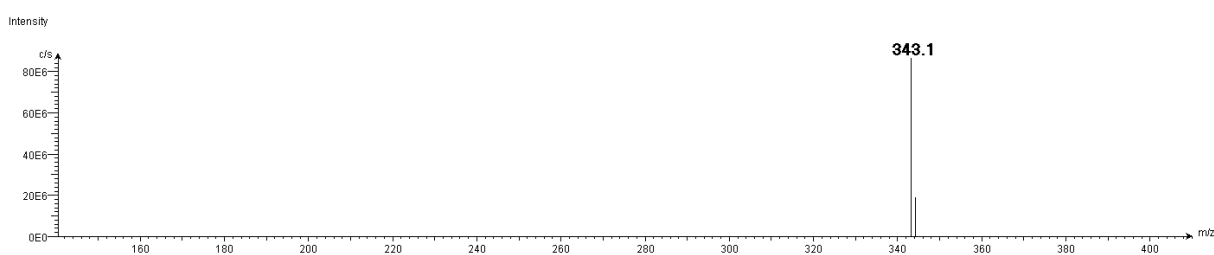


FIGURE S- 52 : NEGATIVE ESI MASS SPECTRUM OF USNIC ACID

DIPHENYLETERS

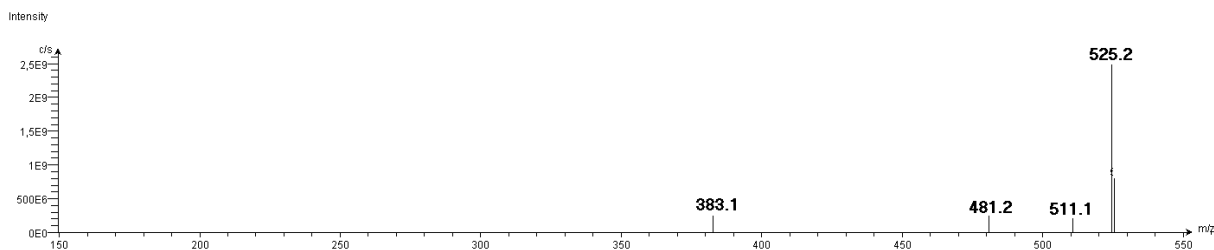
 β -collatolic acid

FIGURE S- 53 : NEGATIVE ESI MASS SPECTRUM OF B-COLLATOLIC ACID

Lobarin

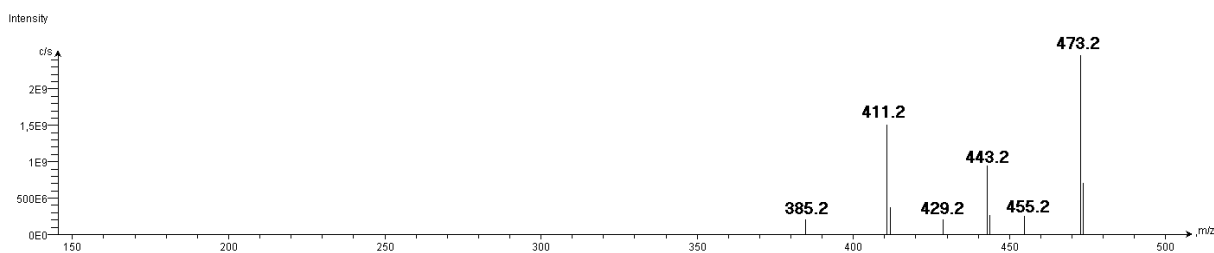


FIGURE S- 54 : NEGATIVE ESI MASS SPECTRUM OF LOBARIN

Sakisacaulon A

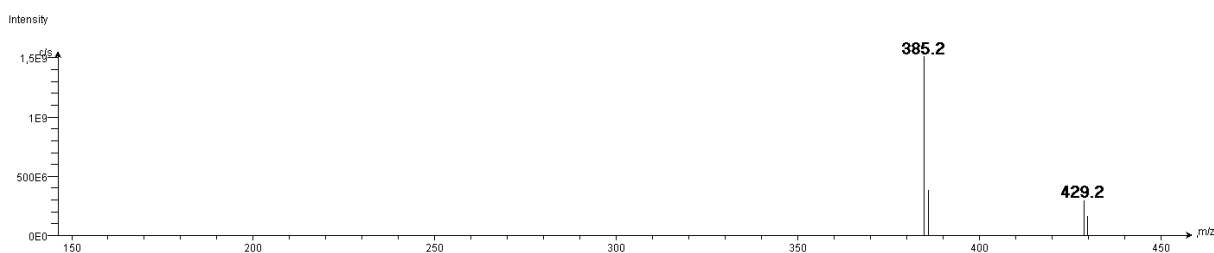


FIGURE S- 55 : NEGATIVE ESI MASS SPECTRUM OF SAKISACAULON A

QUINONES

Emodin

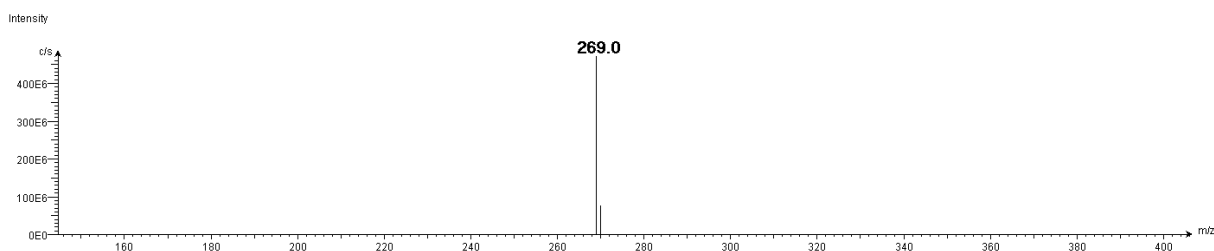


FIGURE S- 56 : NEGATIVE ESI MASS SPECTRUM OF EMODIN

PULVINIC ACID DERIVATIVES

Epanorin

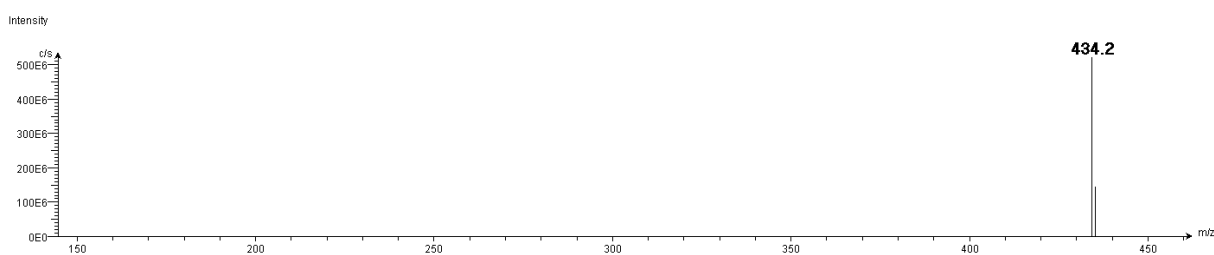


FIGURE S- 57 : NEGATIVE ESI MASS SPECTRUM OF EPANORIN

Rhizocarpic acid

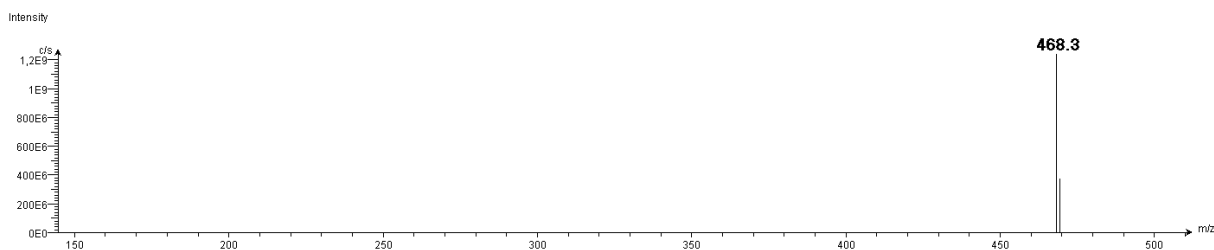


FIGURE S- 58 : NEGATIVE ESI MASS SPECTRUM OF RHIZOCARPIC ACID

Vulpinic acid

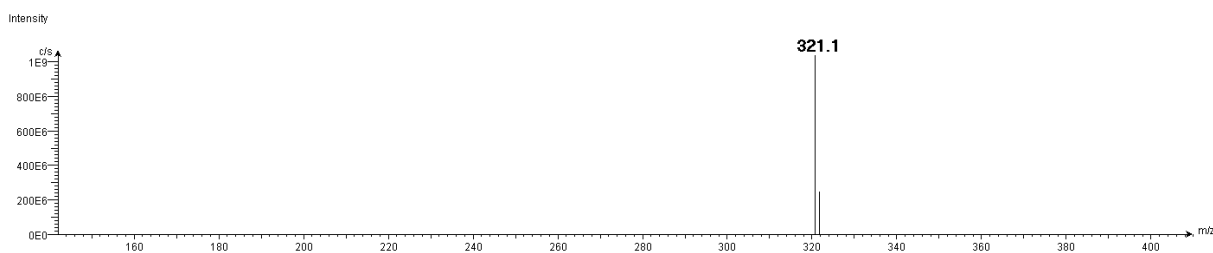


FIGURE S- 59 : NEGATIVE ESI MASS SPECTRUM OF VULPINIC ACID

XANTHONES

Thiophanic acid

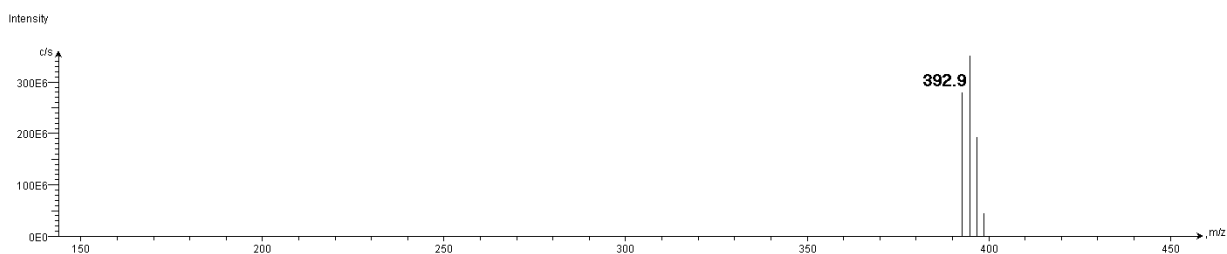


FIGURE S- 60 : NEGATIVE ESI MASS SPECTRUM OF THIOPHANIC ACID

Secalonic acid D

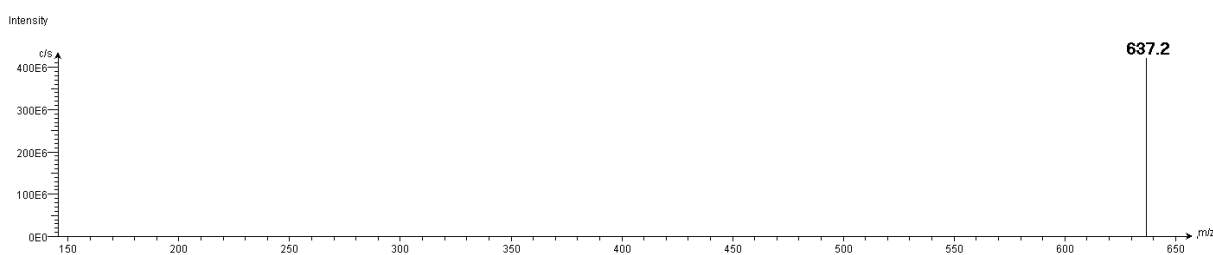


FIGURE S- 61 : NEGATIVE ESI MASS SPECTRUM OF SECALONIC ACID D

ALIPHATIC AND PARACONIC ACIDS

Roccellic acid

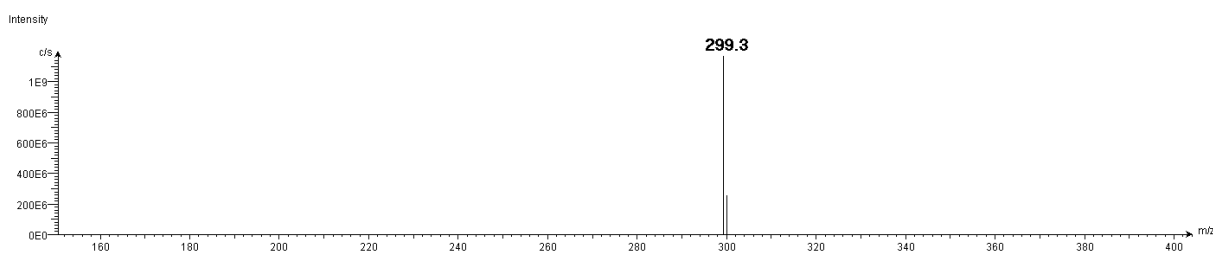


FIGURE S- 62 : NEGATIVE ESI MASS SPECTRUM OF ROCCELLIC ACID

Lichesterinic acid

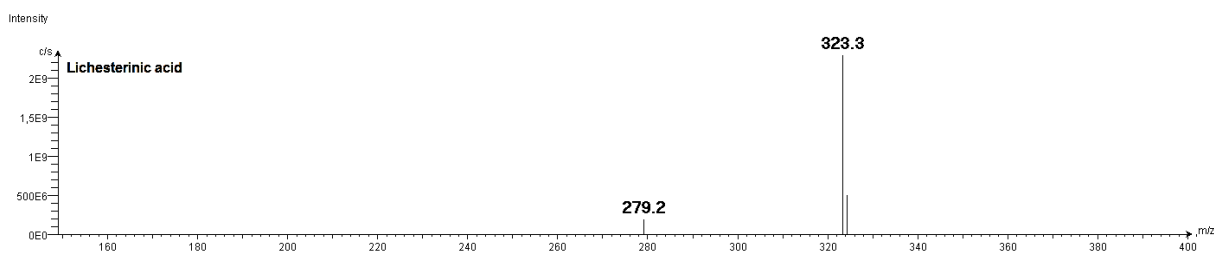


FIGURE S- 63 : NEGATIVE ESI MASS SPECTRUM OF LICHESTERINIC ACID

MYCOSPORINE

Mycosporine serinol

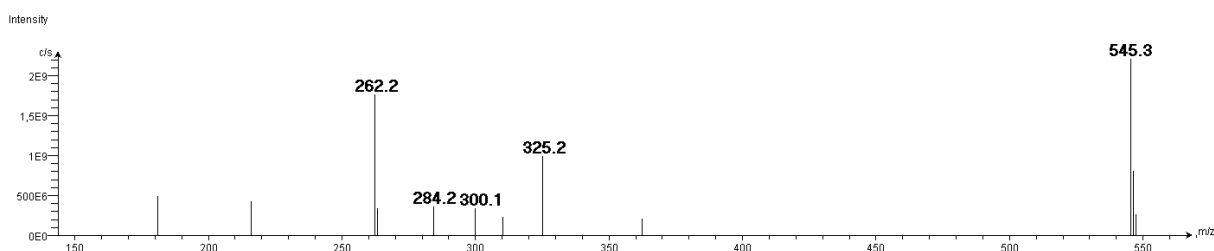


FIGURE S- 64 : POSITIVE ESI MASS SPECTRUM OF MYCOSPORINE SERINOL

EXTRACTS

Cladonia portentosa

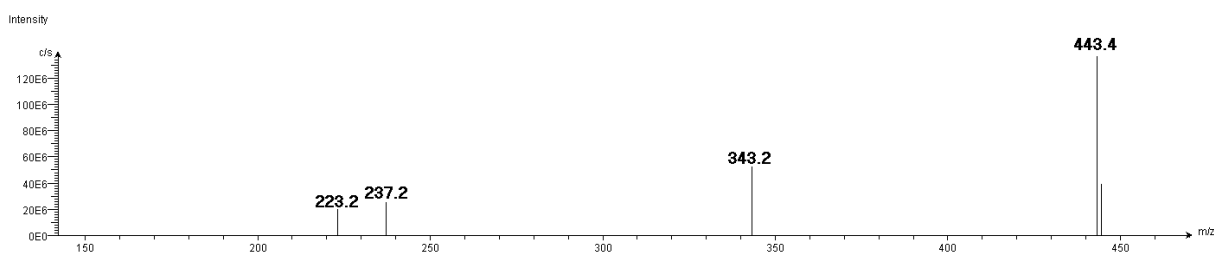


FIGURE S- 65 : NEGATIVE ESI MASS SPECTRUM OF THE ACETONE EXTRACT OF *CLADONIA PORTENTOSA*

Diploicia canescens

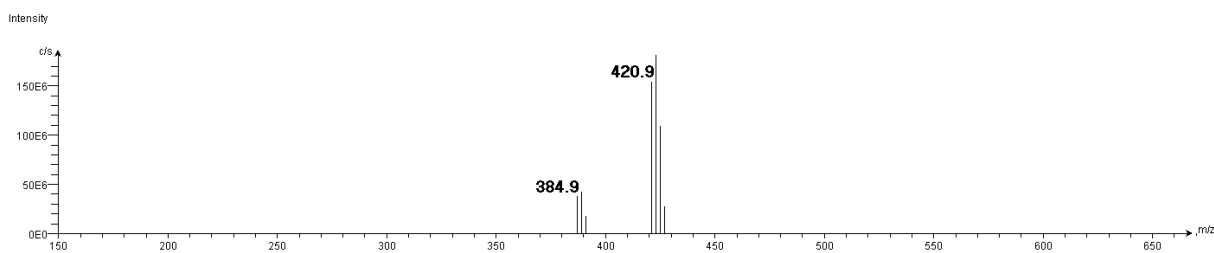
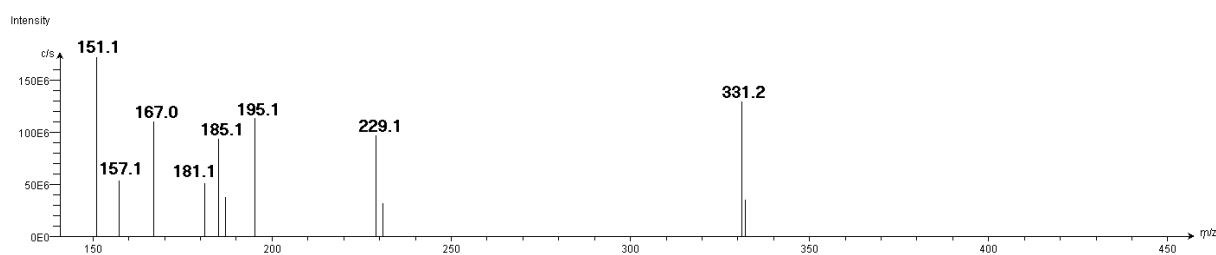
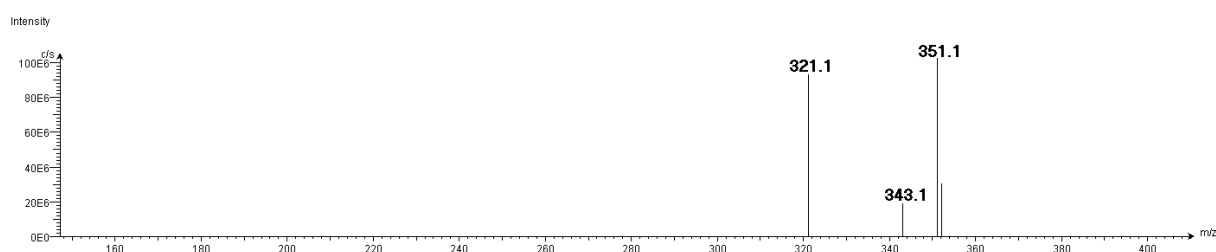
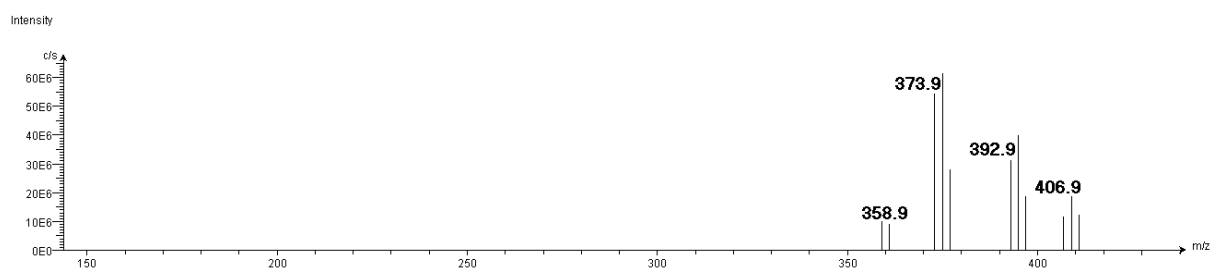
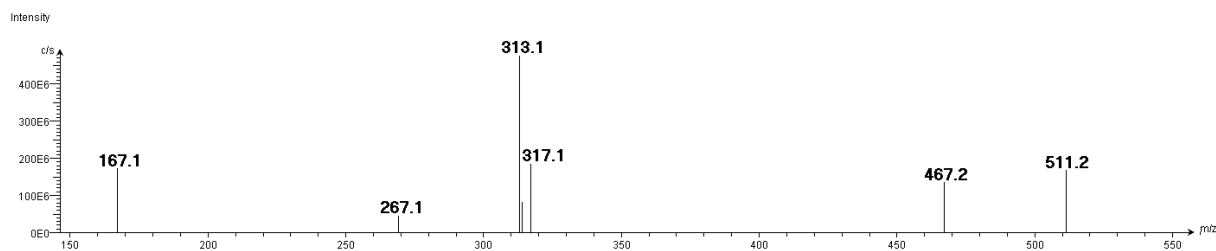
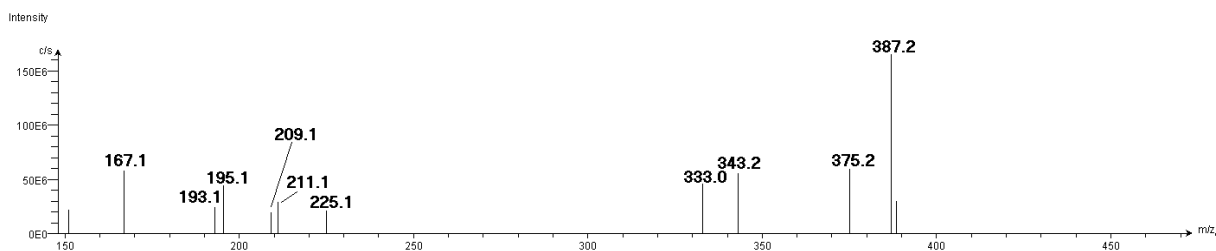
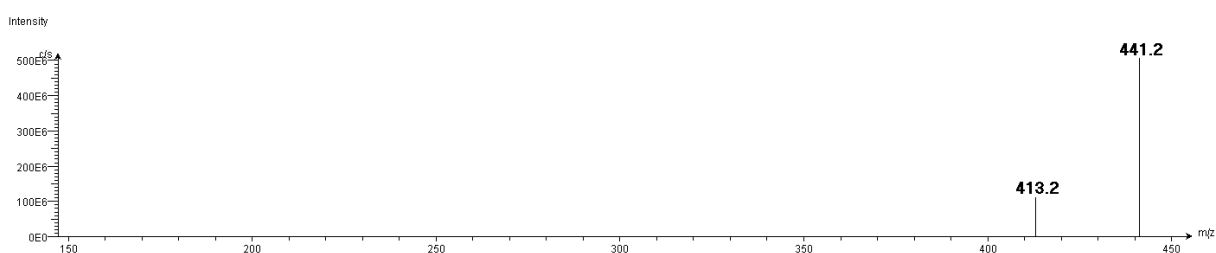
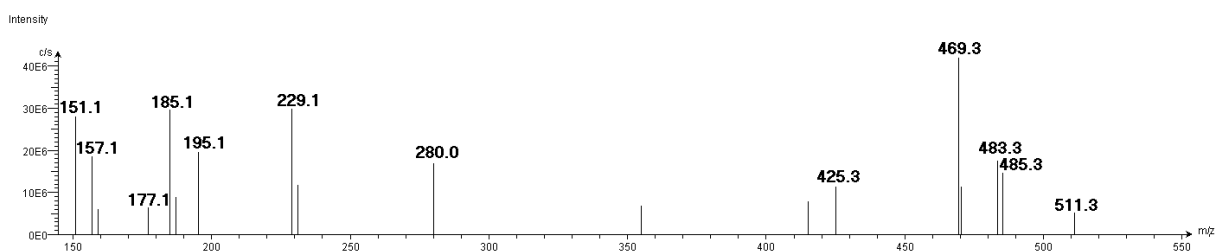
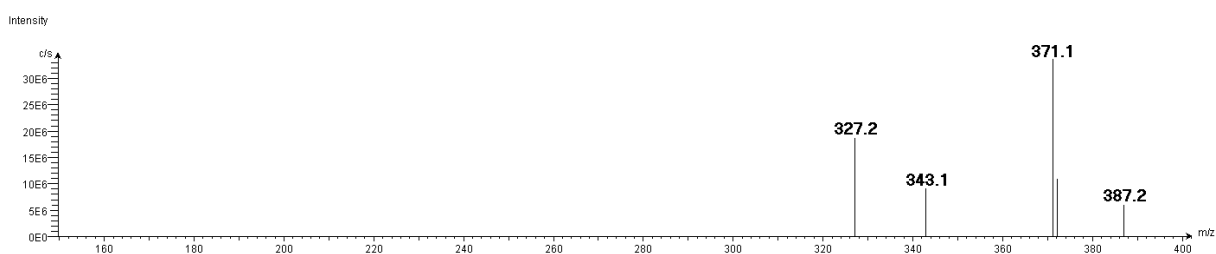
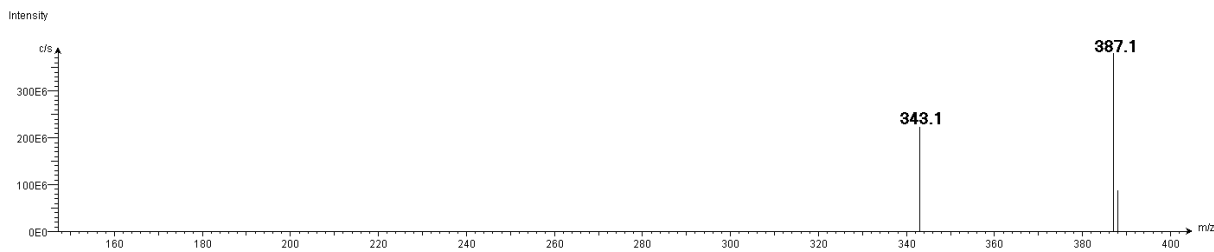
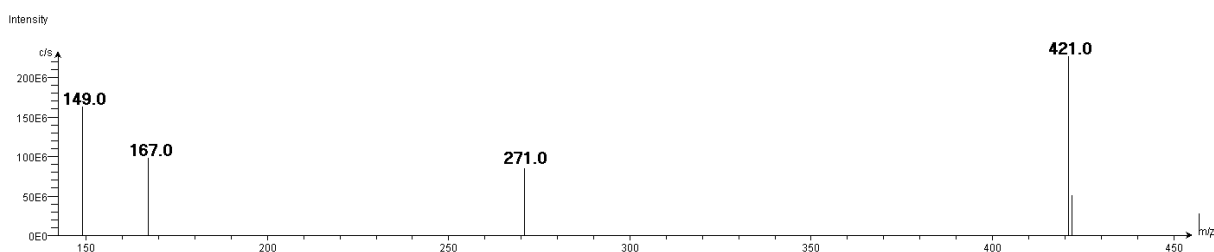
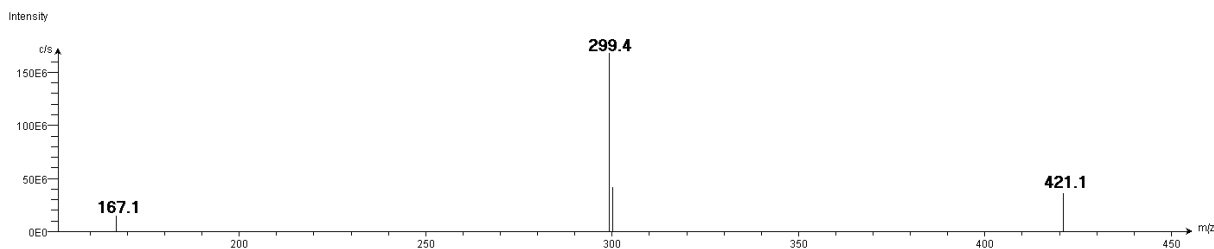
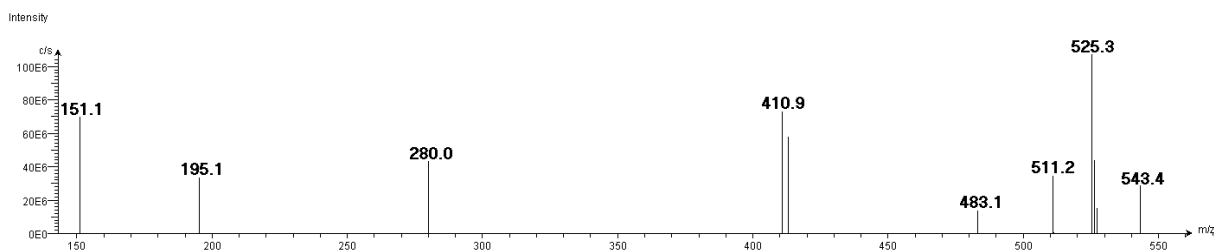


FIGURE S- 66 : NEGATIVE ESI MASS SPECTRUM OF THE ACETONE EXTRACT OF *DIPLOICIA CANESCENS**Evernia prunastri*FIGURE S- 67 : NEGATIVE ESI MASS SPECTRUM OF THE ACETONE EXTRACT OF *EVERNIA PRUNASTRI**Flavocetraria nivalis*FIGURE S- 68 : NEGATIVE ESI MASS SPECTRUM OF THE ACETONE EXTRACT OF *FLAVOCETRARIA NIVALIS**Lecidella asema*FIGURE S- 69 : NEGATIVE ESI MASS SPECTRUM OF THE ACETONE EXTRACT OF *LECIDELLA ASEMA**Ochrolechia parella*FIGURE S- 70 : NEGATIVE ESI MASS SPECTRUM OF THE ACETONE EXTRACT OF *OCHROLECHIA PARELLA*

Ophioparma ventosaFIGURE S- 71 : NEGATIVE ESI MASS SPECTRUM OF THE ACETONE EXTRACT OF *OPHIOPARMA VENTOSA**Pertusaria amara*FIGURE S- 72 : NEGATIVE ESI MASS SPECTRUM OF THE ACETONE EXTRACT OF *PERTUSARIA AMARA**Pseudevernia furfuracea*FIGURE S- 73 : NEGATIVE ESI MASS SPECTRUM OF THE ACETONE EXTRACT OF *PSEUDEVERNIA FURFURACEA**Ramalina cuspidata* var. *stenoclada*FIGURE S- 74 : NEGATIVE ESI MASS SPECTRUM OF THE ACETONE EXTRACT OF *RAMALINA CUSPIDATA* VAR. *STENOCLADA*

Ramalina siliquosa var. crassaFIGURE S- 75 : NEGATIVE ESI MASS SPECTRUM OF THE ACETONE EXTRACT OF *RAMALINA SILIQUOSA* VAR. *CRASSA**Rocella fuciformis*FIGURE S- 76 : NEGATIVE ESI MASS SPECTRUM OF THE ACETONE EXTRACT OF *ROCELLA FUCIFORMIS**Rocella phycopsis*FIGURE S- 77 : NEGATIVE ESI MASS SPECTRUM OF THE ACETONE EXTRACT OF *ROCELLA PHYCOPSIS**Tephromela atra*FIGURE S- 78 : NEGATIVE ESI MASS SPECTRUM OF THE ACETONE EXTRACT OF *TEPHROMELA ATRA*

Usnea filipendula

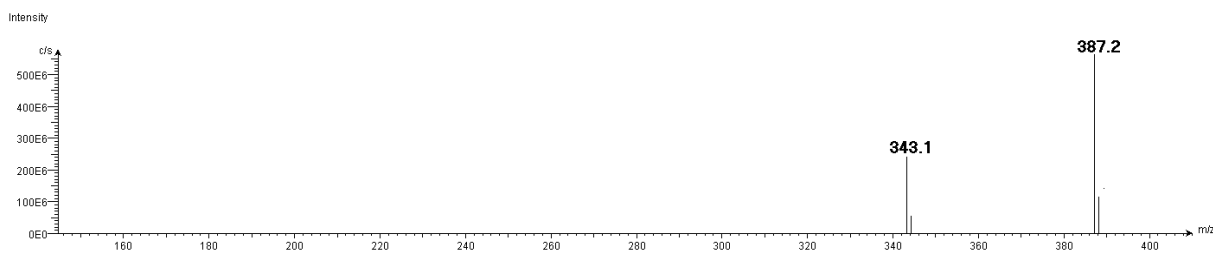


FIGURE S- 79 : NEGATIVE ESI MASS SPECTRUM OF THE ACETONE EXTRACT OF *USNEA FILIPENDULA*

Vulpicida pinastri

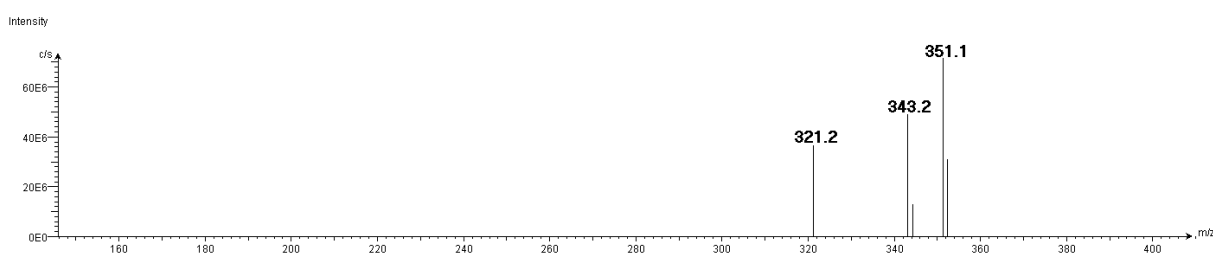


FIGURE S- 80 : NEGATIVE ESI MASS SPECTRUM OF THE ACETONE EXTRACT OF *VULPICIDA PINASTRI*

Xanthoria parietina

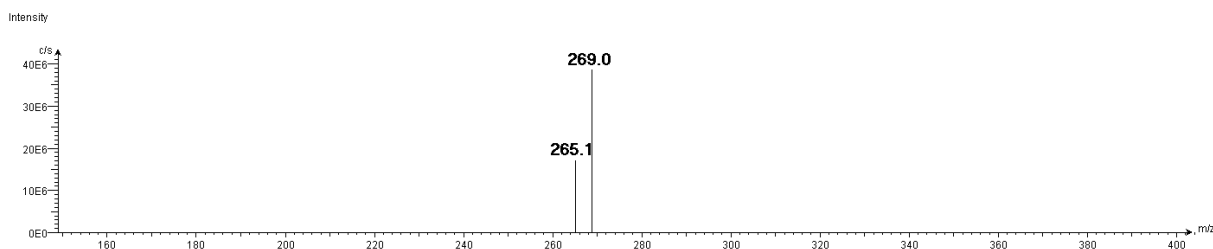


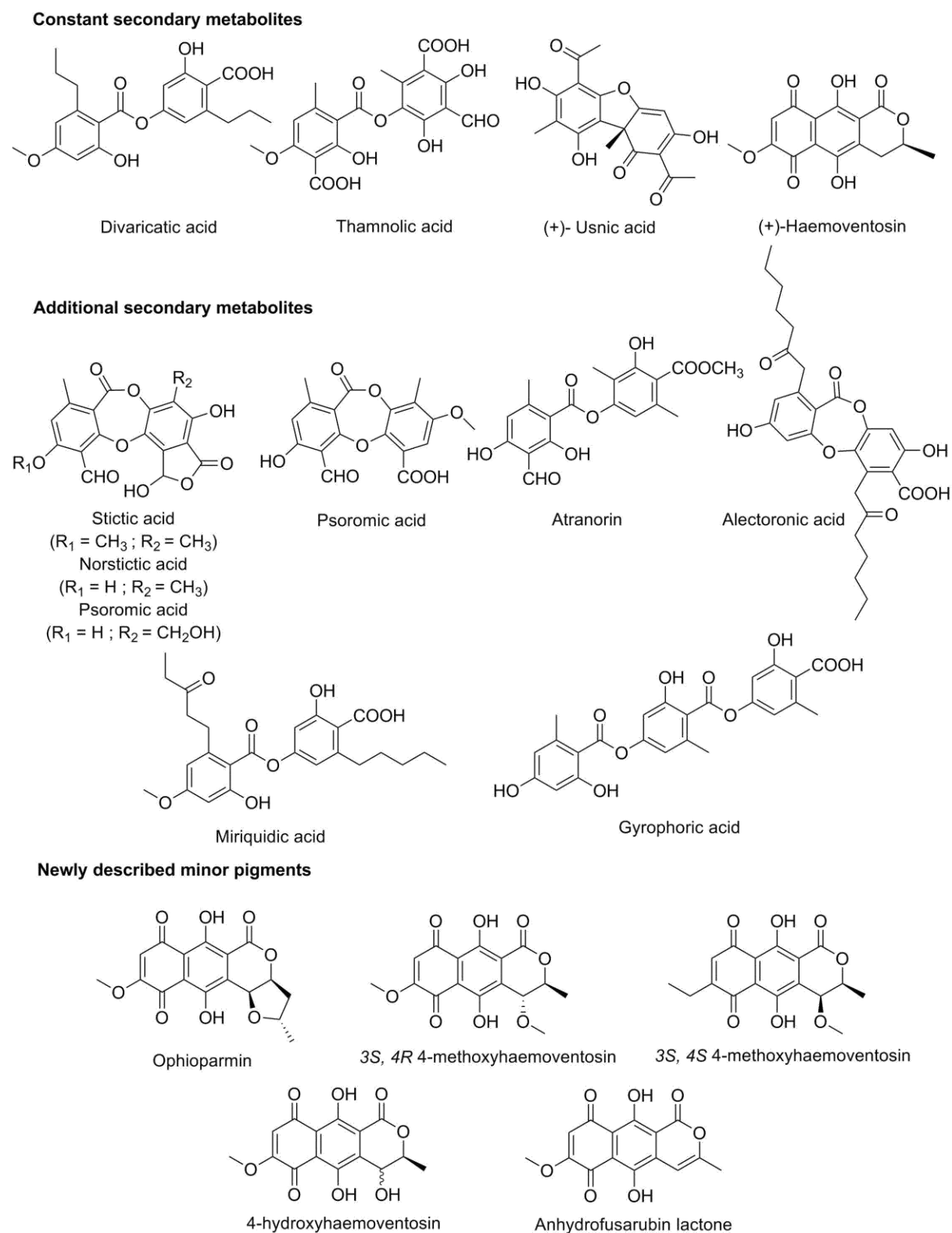
FIGURE S- 81 : NEGATIVE ESI MASS SPECTRUM OF THE ACETONE EXTRACT OF *XANTHORIA PARIETINA*

Annexe 8 : Supporting Material LDI-imaging *Ophioparma ventosa*, Sci. Rep. 2016 ; 6: 37807

Laser Desorption Ionization-Mass Spectrometry Imaging to delineate the role of lichen compounds through spatial mapping: chemical ecology of *Ophioparma ventosa*.

Pierre Le Pogam^a, Béatrice Legouin^a, Audrey Geairon^b, Hélène Rogniaux^b, Françoise Lohézic-Le Dévéhat^a, Walter Obermayer^c, Joël Boustie^a, Anne-Cécile Le Lamer^{a, d}

^a Université Rennes 1, UMR CNRS 6226 PNSCM, 2 Avenue du Pr. L. Bernard, 35043 Rennes, ^b INRA UR 1268 BIA, Plate-forme BIBS, 44300 Nantes, ^c Universität Graz, Institut Karl Franzens, Holteigasse 6, A-8010 Graz, ^d Université Toulouse 3 Paul Sabatier, UFR Pharmacie, 118 Route de Narbonne, 31062 Toulouse.

Figure S1 : Chemical structures of metabolites reported from *Ophioparma ventosa*

Chemical investigation of microsamples of *Ophioparma ventosa* thallus

Experimental data

Regarding the preparation of microsamples, random pieces or selected pieces of thallus (*ca.* 75 mg) were cut in the middle of the medulla using a razor blade prior to being crushed with mortar and pestle and subsequently extracted with 1 mL of dichloromethane for three hours. Extracts were then spotted on analytical TLC plates (Merck Silica Gel 60F254) using toluene/ethyl acetate/formic acid (70/25/5). Visualization of the plates was carried out under UV light (254 and 365 nm) and using anisaldehyde/H₂SO₄ reagent when heating.

Preliminary localization of miriquidic acid on micro-samples

The TLC monitoring of micro-samples' dichloromethane extract revealed a distribution pattern comparable to that reported during our *in situ* DART-MS investigation, with usnic acid predominantly occurring in the upper layers and divaricatic acid evidenced in deeper strata. Representative examples obtained from the Styria sample are given in Fig. S2. One should note that usnic acid sometimes substantially arises within the lower half of the thallus.

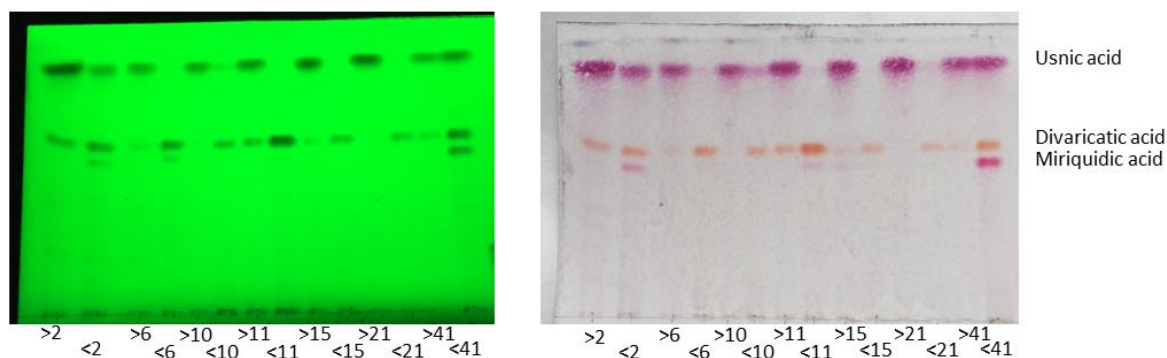


Figure S2: TLC of selected dichloromethane extract of upper and lower micro-samples of *O. ventosa* revealing the basal distribution of miriquidic acid and its uneven occurrence between different pieces of thallus. Left : UV 254 nm, right : plate sprayed using anisaldehyde

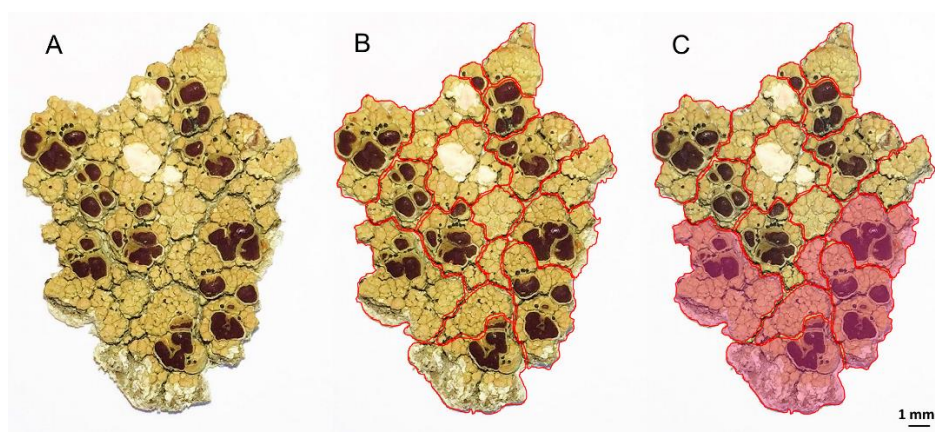


Figure S3: Longitudinal distribution of miriquidic acid in a piece of *Ophioparma ventosa* thallus (Tyrol sample). Division of a piece of thallus in small fragments (B). Rose patches refer to areas containing miriquidic acid (C)

LDI-imaging of further slices

The distribution pattern of all *Ophioparma ventosa* metabolites in slices lacking miriquidic acid is here presented on two supplementary sets of Figures.

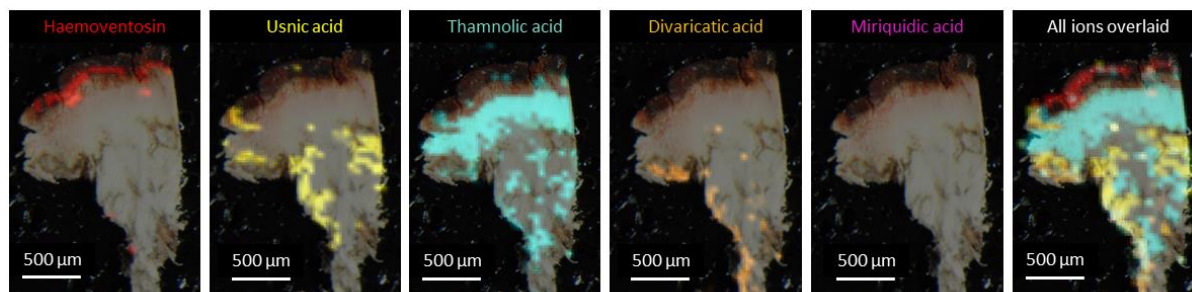


Figure S5: Spatial allocation of *O. ventosa* metabolites in a hand-cut apotheciate section obtained from the Tyrol sample.

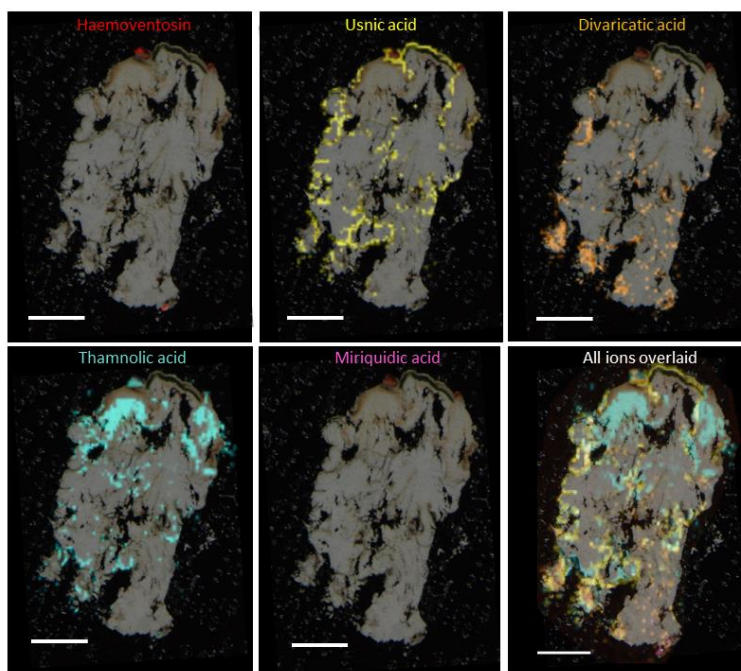


Figure S6: Distribution pattern of *O. ventosa* molecules in a cryosectioned slice from the Styria sample.

Annexe 9 : Données complémentaires de biologie moléculaire

A. Extraction de l'ADN génomique.

a. Principe

Un premier tampon (qualifié de tampon de lyse, AP1) est appliqué sur le broyat de cellules pour les lyser au moyen d'un détergent (e.g Sodium Dodecyl Sulfate). De la RNase A est ajoutée extemporanément pour dégrader l'ARN des tissus. Un second tampon (tampon de précipitation des protéines, P3) introduit de fortes concentrations de sels (e.g acétate de potassium) pour faire précipiter les polysaccharides et les protéines. Le mélange est centrifugé et le surnageant est injecté sur une première colonne pour être élué par le tampon AW, ce qui va permettre de retenir les différents débris précipités mais laisser passer l'ADN. L'éluat est alors repris par un tampon contenant de l'éthanol pour précipiter l'ADN et ainsi le retenir au sein d'une seconde colonne. Cette seconde colonne est alors éluee par un tampon de lavage (buffer AW) qui va entraîner diverses impuretés restant en solution puis par un tampon d'éluion (buffer AE) qui va désorber l'ADN de la colonne.

b. Protocole

1. 400 μ L de tampon AP1 et 4 μ L de RNase A sont ajoutés au broyat de cellules. Le tube est incubé à 65°C pendant 10 minutes et est renversé 3 fois durant cette période.
2. 130 μ L de tampon P3 sont ajoutés. Le tube est vortexé puis placé pendant 5 minutes dans la glace. Le lysat cellulaire est centrifugé 5 minutes à 14.000 rpm.
3. Le surnageant est transféré sur une colonne QIAshredder puis centrifugé 2 minutes à 20.000 g.
4. L'éluat est transféré vers un nouveau tube. 700 μ L (eq. 1,5 volume) de tampon AW1 sont rajoutés et le mélange est homogénéisé par aspiration/refoulement.
5. 650 μ L sont transférés sur une colonne DNeasy Mini Spin logé sur un tube collecteur de 2 mL. Il y a élution par centrifugation à 8.000 rpm pendant 1 minute. L'éluat est éliminé. L'étape est répétée avec l'échantillon restant.
6. La colonne est placée à la surface d'un autre tube collecteur. 500 μ L de tampon AW2 sont introduits à la surface de la colonne. L'éluion se fait par centrifugation (8.000 rpm, 1 minute). L'éluat est éliminé.
7. 500 μ L de tampon AW2 sont une nouvelle fois déposés à la surface de la colonne. Après centrifugation (14.000 rpm, 2 minutes), l'éluat est éliminé.
8. La colonne est placée sur un nouveau tube collecteur et 100 μ L de tampon AE sont déposés à sa surface. Après 5 minutes d'incubation, l'échantillon est centrifugé 1 minute à 8.000 rpm.
9. L'étape précédente est répétée.

B. Alignement de séquences pour la désignation des amorces

CLUSTAL 0(1.2.1) multiple sequence alignment

WP_019491246.1	MAQSISSLSSPSKT----HALGISASSLKTGLTLLLLLALPLNTSLVLVALLKLS---- <td>52</td>	52
WP_039715341	-----MLLPQSITPTMQIFAVFQNLGTLTLLLAIAFPFNCIIVLTALLWNLVSPQF	50
WP_015199130.1Calothrix	MTQSMSFDSTVPK-PQTGSGERISGLFKTLGTLVLLFALPVNTSIVLISLLWGLLNKPV	59
Ava_3856	MAQSLPLSSA-PATPSLPSQTKIAAIQNICTLALLLALPINATIVFISLL-----VF	53
KIJ85250.1Scytonema	MAQSLPLTSAGGATSPTAFVAQVKALFQNIATLTILLLVLPINAIVLTSLFWSRVSRF	60
WP_017743130.1	MTQSISSFSPVPATPPISVKARFIALFQNLGTLTLLLLLALPVNAVIVVISLVWNSLTRLF	60
	. :::: ** :* :*: * * :* . :* .	
WP_019491246.1	RPQNV-TTEQPKNILISGGKMTKALQLARSFHEQGHRVILLEAHKYWLTGHRFSSAVNKF	111
WP_039715341	RDRGILPVSQPKNIMLTGGKMTKALQLARSFHLVGHRRVVLVETHKYWLTGHRFSNAVDRF	110
WP_015199130.1Calothrix	GKQ-L-QTTAPQNILISGGKMTKALQLARSLHAAGHRVVLVESHKYWLTGHQFSNCVDKF	117
Ava_3856	RPQKV-KAANPQTILISGGKMTKALQLARSFHAAGHRVVLVETHKYWLTGHRFSQAVDKF	112
KIJ85250.1Scytonema	RPQTV-VAANRKNILISGGKMTKALQIARSFHAAGHRVVLVETHKYWLTGHRFSDAISRF	119
WP_017743130.1	STQQT-TVARSKNILISGGKMTKALQLARSFGAAGHRVVLVETHKYWLTGHRFSNAVSRF	119
	: * : *	
WP_019491246.1	YTVGAPEKDPGEYIQSLVDIVEKENIDVYVPCVSPVASYYDSLAKKAL-PQCEVIHCDPE	170
WP_039715341	YTVPAPEKDPGEYSQALLAIAKQENIDVYVPCVSPVASYYDSLAKSVLSGCCEVFHFDAE	170
WP_015199130.1Calothrix	YTVTAPEKHPQVYQQQLLDIVKKELDVYVPCVSPVASYYDSLAKPALSQYCEVFHCDAE	177
Ava_3856	YTVPAQDNQAIYQALVDIVKQENIDVYIPVTSVPVGSYYDSLAKPELPHYCEVFHFDAE	172
KIJ85250.1Scytonema	YTTPTPQYDPEAYIQALLDIVKKELDVYVPTSPVASYYDSLAKPALSPYCEVFHFDAE	179
WP_017743130.1	YTTPTPQYDPEAYIQTLDIVKRENIDVYVPTSPVASYYDSLAKPALSPYCEVLHFDAE	179
	** . : * : * : * * * : * : * * * * * * * * * * * * * * * * * * * : * * * : *	
WP_019491246.1	MTQMLDDKYAFAQTAQSFGLSVPKSFKITDPEQVINDFDSQEKRYILKSIYPYSVRRLD	230
WP_039715341	VTQMLDDKYDFAEKARSLGLSVPKSFKITNPEQVNFDFSDAERPYYILKSIYPYSVRRLN	230
WP_015199130.1Calothrix	VTQMLDDKHAFASEKARSFGLSVPKSFKITNPEEVINDFDSQEKRYILKSIYPYSVRRLD	237
Ava_3856	ITQMLDDKFALTKARSLGLSVPKSFKITSPEQVINDFDSGTRKYILKSIYPYSVRRLD	232
KIJ85250.1Scytonema	VTQMLDDKFAFASEKARSFGLSVPKSFKITNPEQVNFDFSGTRKYILKSIYPYSVRRLD	239
WP_017743130.1	VTQMLDDKFAFASEKARDLGLSVPKSFKITNPEQVNFDFSGTRKYILKSIYPYSVRRLD	239
	: * : * * * . : : * : * : * : * : * : * : * : * : * : * : * : * : * : * : * : * : * : *	
WP_019491246.1	LTRLPCDTPEATAAFVRSPLISSEKPWIMQEFIPGTEYCTHSTVRNGVITLHCCCESSAF	290
WP_039715341	LTKLPCATPSQTAAFVNSLPISEKPKWIMQEFIPGQYCTHSTVRNGELRMHCCCESSAF	290
WP_015199130.1Calothrix	LTKLPCETPEATAAFVRSPLISSEKPKWIMQEFIPGKEFCTHSTVRNGELRLHCCCESSAF	297
Ava_3856	LTKLPCATPEETAAFVRSPLITPEKPKWIMQEFIPGKEFCTHSTVRNGELRLHCCCESSAF	292
KIJ85250.1Scytonema	LTKLPCDTPEATAAFVRSPLISSEKPKWIMQEFIPGKEFCTHSTVRNGELRLHCCCESSAF	299
WP_017743130.1	LTKLPCDTLEETAAFVKSPLISSEKPKWIMQEFIPGKEFCTHSTVRNGELRLHCCCESSAF	299
	* *	
WP_019491246.1	QVNYENVNPKIFEWVSRFVKELGITGQVSFDFIEAEDGNIYAIECNPRTHSAITMFYNH	350
WP_039715341	QVNYENVDKPEILAWVRHFVKELGITGQVSFDFIQAEDGNIYAIECNPRTHSAITMFYNH	350
WP_015199130.1Calothrix	QVNYENVNPKIQWVKHFVKEKMGITGQVSFDFIQTVDGTVYAIECNPRTHSAITMFYNH	357
Ava_3856	QVNYENVNPKIETWVQHFVKELKLTGQISFDFIQAEDGTVYAIECNPRTHSAITTFYDH	352
KIJ85250.1Scytonema	QVNYENVNPKIQEWRHFVKELGITGQVSFDFIQAEDGTVYAIECNPRTHSAITMFYNH	359
WP_017743130.1	QVNYENVNPKIQAWVKHFVNLGFTGQVSFDFIQTDDGKYYAIECNPRTHSAITMFYNH	359
	* * * * * : * * * * * : * * * * * : * * * * * : * * * * * : * * * * * : * * * * * : * * * * * : *	
WP_019491246.1	PGVADAYLGTGNN-----LAVPIQPKSTSKPTYWYIYHEVW	385
WP_039715341	PGVADAFLESDATCNTSTSRAGLLNSSSIDNISGKPASTIYPLQPLPTSKPTYWYTHELW	410
WP_015199130.1Calothrix	PGVADAYLCKDVICHVST-----FEPLQLVSSKPTYWYLYHEFW	396
Ava_3856	PQVAEAYLSQAP-----T-----TETIQPLTTSKPTYWYLYHEVW	386
KIJ85250.1Scytonema	PDVADAYLSEEP-----F-----TEPLVPLPNSKPTYWYLYHEVW	393
WP_017743130.1	PQVSDAYLGTGP-----L-----TEPLQPLPNSKPTYWYLYHEVW	393
	* * : * * * : * * * * * : * * * * * : * * * * * : * * * * * : * * * * * : * * * * * : * * * * * : *	
WP_019491246.1	RLFNARSWDFVYRLRIITRGKDAIFSWQDPLPFLMNPWHQIFLLLIQNLRGWIRID	445
WP_039715341	RLTGIRSFQQLQTFQNIWRGQDAIFAMDDPLPFLMVHHWQIPLLLLDNLRRLKGWIRID	470
WP_015199130.1Calothrix	RLTEIRLSQFSGSLRNLRGKDAIFQLNDPLPFLMVPHWQITLLLLQNLRLHRLRGWKID	456
Ava_3856	RLTGIRSFQQLRQLGNWRGDAIYQDPLPFLMVHHWQIPLLLLNLRRLKGWTRID	446
KIJ85250.1Scytonema	RLTGIHFAQLQTVIRNLFQGTDAIYQLDDPLPFLMVHHWQIPLLLLNLRRLKGWTKID	453
WP_017743130.1	RLTGIRSFQQLQNWVRNIFRGTDAIYKLDPLPFLTVHHWQIPLLLLNLRRLKQLRGWTKID	453
	** : * : * : * * * : *	
WP_019491246.1	FNIGKLVELGGD	457
WP_039715341	FNIGKIVELGGD	482
WP_015199130.1Calothrix	FNIGKLVFEGGD	468
Ava_3856	FNIGKLVELGGD	458
KIJ85250.1Scytonema	FNIGKLVIEGGD	465
WP_017743130.1	FNIGKLVFEGGD	465
	* * * * * : *	

ANNEXE 9 : DONNÉES COMPLÉMENTAIRES DE BIOLOGIE MOLÉCULAIRE

FIGURE 74 : ALIGNEMENT DE SÉQUENCES ATP-GRASP EXTRAITES DE CYANOBACTÉRIES D'INTÉRÊT. LES SÉQUENCES CIBLÉES POUR LA DÉSIGNATION DES AMORCES DÉGÉNÉRÉES SONT SURLIGNÉES EN GRIS. AVA_3856 DE *A. VARIABILIS* ATCC 24913 ; WP_019491246.1 DE *CALOTHRIX* SP. PCC 7103 ; WP_039715341 DE *SCYTONEMA MILLEI* ; WP_015199130.1 DE *CALOTHRIX PARIETINA* ; KIJ85250.1 DE *SCYTONEMA TOLYPOTHRICHOIDES* VB-61278 ; WP_017743130.1 DE *SCYTONEMA HOFMANNI*.

CLUSTAL O(1.2.1) multiple sequence alignment

```

WP_039715343.1 MSEVQAKFTATETAFHVEGYEKIEFSLCINGAFDISNREIADQYQKYGRCLTVIDANVY 60
AFZ02505.1 MGIPQATFAATETVFHVVTGYEKIEFSLVYVNGAFDIRNTEIADSYHKFGRCLLVVDANVN 60
WP_019491244.1 MGIPHASFTATEKAFHVVTGYEKIDFSLYVNGVFDIKNTEVADSYQPFGRCLAVVDANVN 60
Ava_3858 MSIVQAKFEAKETSFHVEGYEKIEYDLVYVDGIFEIQNSALADVYQGFGRCLAIVDANVS 60
WP_026134619.1 MSTVQTKFEATESAFHVEAYEKIEYSLVYVDGVFNIKNTELAEVYRDFGRCLAVVDTNVN 60
KIJ85256.1 MSTIQAKFEATEAFHVEAYEKIEYSLIYVDGVFAIKNPQLAEVYKDFGRCLLVVDANVN 60
      *  .  .  .  *  *  .  *  *  *  *  *  *  .  .  .  .  .  *  *  *  *  *  *  *  *  *  *  *  *
      *  .  .  .  *  *  .  *  *  *  *  *  *  .  .  .  .  .  *  *  *  *  *  *  *  *  *  *  *  *

WP_039715343.1 RLYGEQIEAYFQHYNIDLTVFPITITEPNKTIATFETIIDAFAEFGLVVRKEPVLVGGGL 120
AFZ02505.1 RLYGEQIKSYFQFYDISLTVFPVTITETAKTLQTFEEIVDAFADFGLIRKEPVLVGGGL 120
WP_019491244.1 RLYGEQIRAYFRYYDIDLTVHSVTITTEPAKTLATFESVDAFADFGLIRKEPVLVGGGL 120
Ava_3858 RLYGNQIQAYFYQYYGIELRLFPITITEPKTIQTFERVIDVFADFGLVVRKEPVLVGGGL 120
WP_026134619.1 RLYGSQMQEYFYYDIDLTVFPITITAEPNKTIESFETIIDAFADFRLVVRKEPVLVGGGL 120
KIJ85256.1 KFYGSQIEQYFYYDIDLTVFPITITEPNKTIESFEKIIDAFADFGLVVRKEPVLVGGGL 120
      :  *  .  .  .  *  *  .  *  *  .  .  .  *  *  *  *  *  .  *  *  .  .  .  *  *  *  *  *  *  *  *
      :  *  .  .  .  *  *  .  *  *  .  .  .  *  *  *  *  *  .  *  *  .  .  .  *  *  *  *  *  *  *  *

WP_039715343.1 VTDVAGFACAAAYRRNSNFIRVPTTLIGLIDAGVAIKVAVNHKKLNRLGAYHAPQKVILD 180
AFZ02505.1 VTDVVGAFACASYRRSTNYIRIPTTLIGLIDAGVAIKVAVNHKKLNRLGAYHAPQKVILD 180
WP_019491244.1 VTDVVGAFACASYRRKTNIRIPTTLIGLIDAGVAIKVAVNHKKLNRLGAYHAPQKVILD 180
Ava_3858 ITDVVGFACSTYRRSSNYIRIPTTLIGLIDASVAIKVAVNHKKLNRLGAYHASKRVFLD 180
WP_026134619.1 TTDVAGFACASYRRSSNYIRIPTTLIGLIDASVAIKVAVNHKKLNRLGAYHASKRVFLD 180
KIJ85256.1 ITDVAGFACASYRRSSNYIRIPTTLIGLIDASVAIKVAVNHKKLNRLGAYHASKRVFLD 180
      *  *  .  *  *  .  .  .  .  .  .  *  *  *  *  *  *  *  *  *  *  *  *  *  *  *  *  *  *
      *  *  .  *  *  .  .  .  .  .  .  *  *  *  *  *  *  *  *  *  *  *  *  *  *  *  *  *  *

WP_039715343.1 FSFLRTLPTAQVRNGMAELVKIADVANAEEVFNLEKYGEQLLQTHFGYVDTAPELQEIA 240
AFZ02505.1 FSFLETLPVAQIRNGMAELVKIADVANSSEVFELLEYYGHELLHTHFGYVNGSEKLQEV 240
WP_019491244.1 FSFLKTLPTAQVRNGMAELVKIADVNSSEVFELLEYYGHELLHTHFGYVNGSE 240
Ava_3858 FSLLRTLPTDQVRNGMAELVKIADVVAHQEVFELLEKYGEELLRTHFGNIDATPEI 240
WP_026134619.1 FSFLGTLPPTAQVRNGMAELVKIADVANSSEVFELLEYYGHELLRTHFGYV 240
KIJ85256.1 FSLLGTLPPTAQVRNGMAELVKIADVNNKQEVFDLLEKYGEELLRTHFGNIDAT 240
      *  *  *  *  *  *  *  *  *  *  *  *  *  *  *  *  *  *  *  *  *  *  *  *  *  *
      *  *  *  *  *  *  *  *  *  *  *  *  *  *  *  *  *  *  *  *  *  *  *  *  *  *

WP_039715343.1 KVNYESIKTMIELETPLNHEIDLDRVIAYGHTWSPTLELAPNVPIFHGHAVNIDMAFSAT 300
AFZ02505.1 RLNYAAIKTMLELETPLNHEIDLDRVIAYGHTWSPTLELAPQVPLYHGHAVNIDMALSAT 300
WP_019491244.1 QVNYEAIKTMIELETPLNHEIDLDRVIAYGHTWSPTLELAPHVPLYHGHAVNIDMALSAT 300
Ava_3858 RLTYKAIHKMLELETPLNHEIDLDRVIAYGHTWSPTLELAPRIPMFHGHAVNIDMAFSAT 300
WP_026134619.1 KATYEAIKTMIELETPLNHEIDLDRVIAYGHTWSPTLELAPRIPMFHGHAVNIDMALSAT 300
KIJ85256.1 RVTYESIKSMNLEVNHEIDLDRVIAYGHTWSPTLELAPRVPIFHGHAVNIDMAFSAT 300
      :  .  *  .  .  .  *  *  .  *  *  *  *  *  *  *  *  *  *  *  *  *  *  *  *  *  *  *
      :  .  *  .  .  .  *  *  .  *  *  *  *  *  *  *  *  *  *  *  *  *  *  *  *  *  *  *

WP_039715343.1 LAARRGYISTQDRDRILGLMSRIGLALDHPDLEGLDWWQATESIMQTRDGLRAAMPKPI 360
AFZ02505.1 IAQRRGYIDVSRDRILNLSKIGLTLDPHLLDGLDWWYATQTSITQTRDGLRAAMPNPI 360
WP_019491244.1 IASQRGYISVGERDRILDLMSRIGLSDHPDLEGLDWWYATESITQTRDGLRAAMPKPI 360
Ava_3858 IAARRGYITIAERDRILGLMSRVLGSLDHPMLDIDILWRGTESITLTRDGLRAAMPKPI 360
WP_026134619.1 MAAQRGYITSEERDRILGLMSRIGLALDHPDLEGLDWWYATQTSITLTRDGLRAAMPKPI 360
KIJ85256.1 LAARRGYITQERDRILGLMSRIGLALDHPDLEGLDWWYATQTSITCTRGGLRAAMPKPI 360
      *  .  *  *  *  *  *  *  *  *  *  *  *  *  *  *  *  *  *  *  *  *  *  *  *  *  *  *
      *  .  *  *  *  *  *  *  *  *  *  *  *  *  *  *  *  *  *  *  *  *  *  *  *  *  *  *

WP_039715343.1 GTCFFVNDLTREELNAALAEHKQLCATYPRGGDGDVAVMVQEP-ELVGSV- 409
AFZ02505.1 GECFFVNDLTRQELDEALVEHRLCAELPRNGAGIDAYIGTEESELEIA-- 409
WP_019491244.1 GTCFFVNDLTREELDEAVAANKKICAKLPRSGAGIDAYIGTEEEMVGV-- 409
Ava_3858 GDCVFNLDLTREELAAALADHKLCTSYPRGGEGVDVYVPV-YQKELIGSVK 410
WP_026134619.1 GNCFFMNLDLTREELASAISEKHLKQNYPRGGEGVEMYPDSYKPELVGSEA 411
KIJ85256.1 GSCFFMNLDLTREELAEALSEKDLCKTYPRGGDGVLEPYDAYNPVLGSEA 411
      *  *  *  *  *  *  *  *  *  *  *  *  *  *  *  *  *  *  *  *  *  *  *  *  *  *
      *  *  *  *  *  *  *  *  *  *  *  *  *  *  *  *  *  *  *  *  *  *  *  *  *  *
  
```

FIGURE 75 : ALIGNEMENT DE SÉQUENCES DHQS-LIKE EXTRAITES DE CYANOBACTÉRIES D'INTÉRÊT. LES SÉQUENCES CIBLÉES POUR LA DÉSIGNATION DES AMORCES DÉGÉNÉRÉES SONT SURLIGNÉES EN GRIS. AVA_3858 DE *A. VARIABILIS* ATCC 24913 ; WP_019491244.1 DE *CALOTHRIX* SP. PCC 7103 ; WP_039715343.1 DE *SCYTONEMA MILLEI* ; AFZ02505.1 DE *CALOTHRIX* SP. PCC 6303 ; KIJ85256.1 DE *SCYTONEMA TOLYPOTHRICHOIDES* VB-61278 ; WP_026134319.1 DE *SCYTONEMA HOFMANNI*.

ANNEXE 9 : DONNÉES COMPLÉMENTAIRES DE BIOLOGIE MOLÉCULAIRE

CLUSTAL O(1.2.1) multiple sequence alignment

```
KUJ16163.1 -----MPLSGTSPTYLHVLQNASL 19
XP_007805993.1 -----MLDADSSSELLHFAQNVCL 18
XP_007681459.1 ----- 0
XP_013283808.1 -----MLQGTSPLLAHLRQNASL 18
XP_008713719.1 -----MVSSEAIKNASL 12
XP_007756893.1 -----MLDGTSSLAHLRLNAGL 18
KIW13571.1 -----MLDGTSSVLAHLRQNASL 18
KKY35075.1 -----MTVSQA---NGKSDIMAPDGIITTIPLSLAFLRVPVKEHVKIFLL 41
KUI55508.1 -----MSTR-----EPVQSSRSI--FNSTNGCLRLSLHDHIKTAFL 35
XP_003719130.1 MERVLWMPDEDVAPLLSVPNATAFFPSDPVP--ETRRYSSANSPTMAVLALGDTTKTLGI 58
KXJ90766.1 ----- 0
XP_007839533.1 -----MIRMGLYSATRSLAL 15
```

```
KUJ16163.1 ILLSICCFPLCTFIAALSSAI----SPYLKTAR--HIQHRYKWRVSSSTFRPRTILV 71
XP_007805993.1 ILLSVLLPLSTAILFLSYAV----RLFFGE----NASRQ---RSQRSPNFQPKTILV 65
XP_007681459.1 -----EAKTILV 7
XP_013283808.1 LILSLVFLPLDTFILLVSLVW---GKVFPSP---KVLNSNEAARHRDASFTRRKLVLV 68
XP_008713719.1 IILSLLFLPLDSFIATCSYLL---GWVSKP---K-----A-IRPGHQKRNVLV 53
XP_007756893.1 LFLSLAFLPLDTLILFISFLF---RTILPN----EVEHRRREAR-QDHGFHPRTILV 67
KIW13571.1 LLLSLVFLPLDTFVLISSFLV---AFIFPS---HAGGTPRQFE-SATGRNSRKILV 67
KKY35075.1 LALSIFFLPISYAIATLTAVPPSVLAYFQPFSSRTLGTALFHRTQCRAKPTFRQRTILV 101
KUI55508.1 VLLSLITLPLISYIIALALTLPPSVMTYLLPFSSSTPTGALYHRNSCRSERDFAQLTVLV 95
XP_003719130.1 IMLSIFTLPLSLTVTGLLF-LAHLIIGYFSRSAS--KSQLOQY-EANS--NSSHHQKTILV 112
KXJ90766.1 ----- 0
XP_007839533.1 VAVSVILAPWSIALALLV-----IFFRPWAS-MLGSSRYPKPKC--LSPVRSRTVLV 64
```

```
KUJ16163.1 TGVGMSKGLTLARTFYRAGHRVVGADFDYDIPV-----C-GHFSKSIETFYRLSRPSS 124
XP_007805993.1 TGVGMAKGLRIARAFYQTGHRVIGADFEPNSILV-----S-GRFSRAIDKFYRVSKPSP 118
XP_007681459.1 TGVGMTKGLALARLFYAAGHNVIADGFEPFLPT-----CSGRVSRSLTSFHKLKSKPDG 61
XP_013283808.1 TGVGMTKGLALARLFYEAGHDVIGADFEPAWAWA-----C-GRVSSALGKFYRLKPDPA 121
XP_008713719.1 TGVGMSKGLFLARAFYLAGHRVIGADFEPAWAWA-----I-GRTSKLSRFYHLRAPAG 106
XP_007756893.1 TGVGMTKGLVLRALFYEAGHDVIGADFEPAWAWA-----C-GRVSRALRKFYRLQTPGI 120
KIW13571.1 TGVGMTKGLVLRALFYEAGHDVIGADFEPAWAWA-----C-GRMSKSLRRFYTLRSPTT 120
KKY35075.1 TGVGMTKGLTLARAFWLCGYRVVAADFDVGSAAWTPWKKGRVSYSLAFDAVYSLRRPVV 161
KUI55508.1 TGVGMAKGLTLARAFWLCGHKVIADFDVGSAAWTPWHP--GWVYSRAFDKVVSLRKPVI 153
XP_003719130.1 TGVGMTKGLTLARAFHSQGHVRLGADFEPAWAWA-----SGRQSRSLSSFYSLRKPSS 165
KXJ90766.1 ---MAKGLTLARAFWLCGHVIGADVESHGIPC-----SGRFSRALSRFCKLGRPST 49
XP_007839533.1 TGVGMAKGLTIARAFYQGHVVGADFDENQAIPC-----SGRYSKGLSKFRSMKSPSS 117
*:*:*:*:* * * * * : * : * : * : * : *
```

```
KUJ16163.1 EMG-----TQ--RYMKDMIDIKKENVELWVSCSGIASGVKDGEAAEIE-----K 168
XP_007805993.1 QHG-----AA--RYVRDLVYIVEKEEVDLWVSCSGVASAAEDGQAMELLG-----R 162
XP_007681459.1 SRE-----K-QAKYITQELLNIVRKENVDIWVSCSGVASALEDGQAKEMIE-----L 106
XP_013283808.1 KAG-----AA--PYIQTLLDVVTKEKVELWVSCSGVASAVEDGMAKEVVE-----A 165
XP_008713719.1 QDA-----ST--TYVQDLLRIVLAEKIDLWVSCSGVASAVEDGQAKEIE-----Q 209
XP_007756893.1 SSA-----SSPDMYIQNLLDIVTREKVDLWVSCSGVASAVEDGMAKEVVE-----K 166
KIW13571.1 KSG-----SA--PYIQSLLDIITNEKIDLWVSCSGVSAVEDGMAKEIVE-----G 164
KKY35075.1 KDGMDREKEEVRTAYTRDICKIVEDEVVDLWVSCSGVASAVEDAMVKEALDKVSPSPRG 221
KUI55508.1 GEGMDEMEKTEVQIGYIRDICQIVKTEGVDLWVSCSGVASAVEDAMVKEALDKMPTA--N 211
XP_003719130.1 K-----TLSSSYTAQLVLDLVTRENVLDLWVSCSGVATAVEDGAAADQIE-----Q 209
KXJ90766.1 -----TSSREYIRSLVDIIEAEDVNLWVSCSGVSSAAEDAEEAKEVIE-----A 92
XP_007839533.1 S-----VQSSRSYVQQLRIVREEDVDLWVSCSGVASALEDKAKELIE-----R 162
* : : * : * : * : * : * : * : * : *
```

```
KUJ16163.1 ETCKKAIQFGLTLTETLHEKHSFIDNTRQ-LGLNVPDTHLVTSETESLAVLYPEKPR--- 224
XP_007805993.1 KTNCKSIQFDVKTETLHEKDRFIEYTKS-LGLPVPETHQVVSRTAVLNLVNEA----- 215
XP_007681459.1 VTACKCVQFDVPTTKRLHEKHSFIEYTKS-LALPVPETHVTSKAAALQVLDDA----- 159
XP_013283808.1 RTACKAVQFDVQTQTLEKHAFAHAKTDVVLTVPETHEVTSREAVLDVLRRA----- 219
XP_008713719.1 RTPCKALQFDIETTQMLHEKHTFVEHVSK-CGLTVPETYAITTRADVERILRR----- 202
XP_007756893.1 RTCKKAIQFDVHTTQILHEKHSFIQHTRD-IGLNVPETHEITSRAEVERILRE----- 218
KIW13571.1 RTGCKAIQFDVETTQTLHEKHTFIAHTRD-IGLNVPETHEIRSRAEVSVLRN----- 216
KKY35075.1 RRRCACIQFDVPTTSTLHEKSAFIRHTKA-LKLTVPETFEVTSQAQVLDALASATR--- 276
KUI55508.1 GARCACIQFDVPTTSTLHDKSTFIRHTRS-LKLCVPETYDVTSHSEVLHFLDRAAK--- 266
XP_003719130.1 STRCRCVQFNEKITARLHEKNSFIRETVR-LGLPVPETHEVAAHEDVQRVFDNR--- 261
KXJ90766.1 RTKCRCIQFDVATTMELHEKDAFMRAAKR-LGLPVPETHDVTSPQQVMEILRRSNRDDGQ 151
XP_007839533.1 ETRCKCIQFQVQETETLHEKDLFMREAGR-LGLPVPETHNLTCPPDALNILLKFKHG--- 217
* : * * * * * : * : * : * : * : *
```

```
KUJ16163.1 -----SAQGTKYVMKSVFLDDSSRADMT-LLPRPTL-----KETETHIK 262
XP_007805993.1 -----IDGKKKYIMKTIQVDDASRASTAVLPKRTL-----SPTYGHVS 254
XP_007681459.1 -----AGTGRKYIMKYIGTDDAVRGDMT-LLPLSSP-----ARTKAHIS 197
```

ANNEXE 9 : DONNÉES COMPLÉMENTAIRES DE BIOLOGIE MOLÉCULAIRE

```

XP_013283808.1 -----APHGRKYIMKTIGVDDAVRGDLT-LLPKKCE-----RETAEHLA 257
XP_008713719.1 -----APSGRHYIMKTIGVDDAVRGDMT-LLPKDTH-----DETLKHLQ 240
XP_007756893.1 -----TPSGRKYIMKTIGVDDSVRADMT-LLPKSSG-----VETSKHLA 256
KIW13571.1 -----APPGRRYIMKTIGVDDAARGDMT-LLPKSTP-----METSCHLA 254
KKY35075.1 -----ENPGRKFILKPVGMDDANRGNMT-LLPLPTA-----RETGSFVR 314
KUI55508.1 -----KHPARKFILKPVGIDANRGNMT-LLPFSAT-----HDTERHVR 304
XP_003719130.1 -----SGKGRRFIMKPVGMDDAHRGNMT-LLPLATS-----AETEAHVL 299
KXJ90766.1 QHRGGGGGGSSRGRERPFILKTVGVDDTHRANMT-LLPLLGPALGGQQDISWPDQRYVT 210
XP_007839533.1 -----MSPARKFILKTVGVDDANRGNMT-LLPLDTK-----EATKRYIS 255
:::* : * :*.. : :** * :.

KUIJ16163.1 -RLNPTPFPRFVLQKFIS-GPEYCTHSLVINGKVKAFVACPSAELLMHYVPLPTSSALSQ 320
XP_007805993.1 -KLSISKSTPWVLQQYIK-GEEYCTHSIVIDNKVKLFVACPSDDLMMHYQALPQESGLSK 312
XP_007681459.1 -RLDVSERDPWILQQYVR-GPEFCTHSLVVKGVEKAFVACPSSELLMHYEALPSDGALSM 255
XP_013283808.1 ARLNISGDAPWILQEFIQ-GREYCTHALVVAGKVKAFVACPSAELLMHYQSLPAESPLSR 316
XP_008713719.1 -HLPISSECPWILQQFVQ-GAEFCTHSLVVNGRVKAFVACPSAELLMHYQMLPPDSALS 298
XP_007756893.1 -RLKISSAQCPWILQQYIR-GKEYCTHSLVVNGEVKAFVACPSAELLMHYEALPAESPLSR 314
KIW13571.1 -KLRIESAESPWILQQFVK-GREYCTHSLVVNGQVKAFVACPSAELLMHYEALDPTSALSE 312
KKY35075.1 -RLPVSRARPWILQQFIRGGREYCTHALVVGGAVKVAACPSSELLMHYEALPADDPLTA 373
KUI55508.1 -RLPITKDKPWILQQFIRGGREYCTHSLVVVDGTVKVAACPSDELLMHYTALANDDPLCE 363
XP_003719130.1 -GLPISSACPWIVQQFIPGGREYCSHALVIRGEVRFVTFACSSSELLMHYEALPAHSQFLR 358
KXJ90766.1 -RLPISANPNWIVQQFIPGGQEYCTHALVVRNEVRCFTACPSAELLMHYEALGPESALYQ 269
XP_007839533.1 -RLSISPQRWILQEFITGGEEYCTHALVIRGEVKCFVACPSAELLMHYRALPQSALS 314
* : *:::**** : * :*:*:**** : * :*.* * :***** * *

KUIJ16163.1 AMLLYTTLYAKKT-----GPSMTGHFSIDFLVEADVAQDAERRVGVSDTEVRELSRIYP 375
XP_007805993.1 AMLHFTTEFAHRS-----GSGFTGHLSFDFMVEEKVTEGCV-----QKNIYP 354
XP_007681459.1 SMLRFTQYEAAG-----GNAFTGHLSFDFLLEMDDAERAL-----RDPSANVRLYP 302
XP_013283808.1 AMLAFTQTYAASG-----GRGFTGHLSFDFMVEDQHGKDKGRG-----NVDPRDIVLYP 366
XP_008713719.1 AMLAFTESAARG-----GEGFTGHLSFDFMVEDADL-----KSNNPTLYP 339
XP_007756893.1 AMLDFTKRYAANG-----GRGFTGHLSFDFMVEEGDE-----KAEDITLYP 355
KIW13571.1 AMLAFTRKYAANG-----GPAFTGHLSFDFMVEDDDR-----VLKAADVTLYP 355
KKY35075.1 EMLDFTTKFAAAA-----GAGFTGHLSFDFMAEEDGDG-----GARLYA 412
KUI55508.1 EMLGFTRRFAAAA-----GTGFTGHLSFDFMAEDDKNG-----GTSLYA 402
XP_003719130.1 DMLQFTKDFCARSEE---SKSMTGHLSFDFMVEDEQG-----AIHA 395
KXJ90766.1 AMLAFTREYVARNSAADGVGQMTGHLSFDFMVEDVAAS-----SDKFERRFYA 317
XP_007839533.1 AMLAFTREYIFRSPN---SEQFTGHLSFDFMVRDSDAVD-----EHTIERSLYA 359
** :* :***:*:***. :.

KUIJ16163.1 IECNPRHAHTAVVCLADESE-----DHAEAYLSILPDHEPKGISN-----G----- 415
XP_007805993.1 IECNPRHAHTAVALFSGTQG-----SVMVKAYMSVLDSSPTSGSN-----GHLDL 400
XP_007681459.1 IECNPRHTAVCLFNDTP-----EMVDAYLTLSPKAASISSSPSPTGTNSTT 350
XP_013283808.1 IECNPRHAHTAVLFGNRTSTSI---STAATAMVQAYLSIFEDVDNHH-----LN 412
XP_008713719.1 IECNPRHAHTAVLFGNTH-----RMVDAYMSLLGNAEAE----- 374
XP_007756893.1 IECNPRHAHTAVALFNGTT-----AVVDAYLSALDGAENRNGASDD-NGNGTPA 402
KIW13571.1 IECNPRHAHTAVALFNGTT-----TMADSYLSVLDKGPPT----- 389
KKY35075.1 IECNPRHAHTAVALFAQPGEQ-----MRWMVEAYASAVNAPLKLKA----- 453
KUI55508.1 IECNPRHTAVVLLGQAGGE-----VRQMVAAYLSAIESNMKLGK-----E 444
XP_003719130.1 IECNPRVHTAVVLFSPGGEV-----TRDMVRAYLWVLEHGQPDNNGSREAV---DEV 444
KXJ90766.1 IECNPRHAHTAVLFAQEGPA-----MEAMVEAYMSATSASY-ENNAGSRKTV---ANG 365
XP_007839533.1 IECNPRHAHTAVLFAQQQHGGGGAATTSAMVKAYLSALEET-PESYA---HV---L--- 410
*****.**** : .:*

KUIJ16163.1 ----HRGEALVVRPPIQGYWAGHDLVTRVLLPLLRLLRFE----- 453
XP_007805993.1 YTLSTGTS-VAYPLPTAPGYWGMGHDIVTLVHLPLRILTFR----- 441
XP_007681459.1 ATPNGLAPLPIFPNPPTKYYWLGHDLVTFVLLLLSLASLSPDG----- 395
XP_013283808.1 RTADSSIDIVRP--VAQDKYFWTGHDLVTLVLLPTLSLFPALFSGLASVPSRSGAPST 470
XP_008713719.1 -----VIFPAQTGGYKYWVGHDLATKLLSTVGLCTLS----- 408
XP_007756893.1 TTQDPTTPVIHP--AHHDKYFWIGHDLVTLVILPTSSLLFPLLP-----GRSS----- 449
KIW13571.1 ----RSSNVVRP--LCNDKYYWIGHDLVTRVFPVPTLEFLSLQ----- 425
KKY35075.1 MGNLSAAGPMVWPPADATPRYWIGHDFVTRALLPWLNLWLPKPG----- 497
KUI55508.1 PKTKNAFSRLVRPPTETTSRYWIGHDFVTLVLPVWRLLSCDLT----- 488
XP_003719130.1 NGQDH-VAEIVVPHHQIHPRYWIGHDVVLEGLLPIIKLIRGEE----- 487
KXJ90766.1 DAQSASVQVPSVSPAGSPLPRYWLADLVALVSQPLVRLILGADG----- 409
XP_007839533.1 KQNGLRREEMIVFPKSTLPRFWIAHDLFTLVLPQILNFVAGQKS----- 454
:* :*.** :

KUIJ16163.1 ----IGVMDMLELWMEFAE--HVLVWRDGTFEIWDPPWFVWLVVGYWPGMFLVS---- 501
XP_007805993.1 ----IGFWSFIHHVTFVN--HVLFWKEGTVEVWDPLPWVWLYHYVWPRQFWAC---- 489
XP_007681459.1 ----PSFREVEFESVATFGE--HVLWWDGTEWVWDPWPAPWVLYHYVWVQFAGALGGLV 448
XP_013283808.1 DSGIRASITHLTQNYTLFLH--RLLTWRDGTYEVPWDPPLPWVWLYHYVWVPRFWAC---- 523
XP_008713719.1 ----KGVSAVLSYIALVS--HLLTWRDGTFEIWDPPWVWVLYHYVWVPRFWAC---- 456
XP_007756893.1 SSASSTSVRTTLQDHAVFIRHVASPTWKDGTFPQWDPPLPWVWLYHYVWVPRFWAC---- 504
KIW13571.1 ----STVRDLMRNYIDFFT--HLLTWKDGTYEVWDPLPWVWLYHYVWVPTKFWSC---- 473

```

```

KKY35075.1      -----SGLLVDGVLGELVQ--HVLYWKDGTFFELWDPWPFVALYHHYWPRAILAS----- 544
KUI55508.1      -----VGG-ITTGVKEFAE--HVFCWKDGTFFELWDPWPFVALYHHYWPKAIVTS----- 534
XP_003719130.1 -----AKKVMKSLAELWL--HVRCWKEGSFDARDPLPTLMLYHVYWPLTTAAA----- 533
KXJ90766.1      -----AAGGQLVRGVLKFLF--HVLTKWKEGTFEIWDPMMPAVWLYHVYWPLTLLSA----- 457
XP_007839533.1 -----VHQLFCCLTEFLI--HVLTKWKEGTFEVWDPWPAVVLYHVYWPLTILSA----- 500
                :                *.:*.:*  ** *  ** **
                :                * * **** *:*

KUI16163.1      -----LWERKWWSRCNVSTQKMFGC      521
XP_007805993.1 -----LRTGKKWIRVNVSTTKIFGC      509
XP_007681459.1 GEVLGLGRGGKWSRVNVSTTKMF--      471
XP_013283808.1 -----LRDGRKWSRINVSTAKMFEC      543
XP_008713719.1 -----IRTGTGWSRVNVSTTKMFEC      476
XP_007756893.1 -----LVRGRKWSRVNVSTTKMFEC      524
KIW13571.1      -----IWTGSKWSRINVSTTKMFQC      493
KKY35075.1      -----WWKGEQWSRLNVSTTKMFIC      564
KUI55508.1      -----WWKGERWSRLNVSTTKMFSC      554
XP_003719130.1 -----WWQGRRWSRINVSTTKMFMI      553
KXJ90766.1      -----LWRGVRWSRVNVSTTKMFLC      477
XP_007839533.1 -----WWRGDDWSRVNVSTTKMFAC      520
                * * **** *:*
    
```

FIGURE 76 : ALIGNEMENT DE SÉQUENCES ATP-GRASP EXTRAITES DE CHAMPIGNONS D'INTÉRÊT. LES SÉQUENCES CIBLÉES POUR LA DÉSIGNATION DES AMORCES DÉGÉNÉRÉES SONT SURLIGNÉES EN GRIS. KUJ16163.1* DE *PHIALOCEPHALA SCOPIFORMIS* ; XP_007805993.1 D'*ENDOCARPON PUSILLUM Z07020* ; XP_007681459.1 DE *BAUDOINIA PANAMERICANA UAMH 10762* ; XP_013283808.1* DE *FONSECAEA PEDROSOI CBS 271.37* ; XP_008713719.1* DE *CYPHELLOPHORA EUROPAEA CBS 101466* ; XP_007756893.1* DE *CLADOPHIALOPHORA YEGRESII CBS 114405* ; KIW 13571.1 D'*EXOPHIALA SPINIFERA* ; KKY35075.1 DE *DIAPORTHE AMPELINA* ; KUI55508.1 DE *VALSA MALI VAR. PYRI* ; XP_003719130.1 DE *MAGNAPORTHE ORYZAE 70-15* ; KXJ90766.1 DE *MICRODOCHIUM BOLLEYI* ; XP_007839533.1 DE *PESTALOTIOPSIS FICI W106-1*.* LES PROTÉINES MARQUÉES D'UNE ÉTOILE SONT DOTÉES D'UNE RÉDUCTASE À LEUR EXTRÉMITÉ N-TERMINALE QUI N'A PAS ÉTÉ UTILISÉE POUR LES ALIGNEMENTS.

ANNEXE 9 : DONNÉES COMPLÉMENTAIRES DE BIOLOGIE MOLÉCULAIRE

CLUSTAL O(1.2.1) MULTIPLE SEQUENCE ALIGNMENT

```

XP_007681536.1      MSDMKASVQETP-----KGFHVEGYEKIEYDFSFVDGVFEKEHADLAECFSRWRRCCLAIM 55
XP_008713717.1      MSDLQATVAETP-----NGFHVQGYEKIEYDFTFIDGVFDMGNKALADCYERWGRCLAVM 55
KIW13573.1          MSDLKASVAETP-----AGFHIIEGYEKIEYDFTFIDGVFDARNRDLADCYQRWGRCLAVM 55
XP_007756891.1      MSDLKASVAETA-----AGFHVEGYEKIEYDFTFIDGVFDTSRSELADCYRRWGRCLAVM 55
XP_013283806.1      MSDLKASVAETA-----AGFHVEGYEKIEYDFTFIDGVFDTKKSDLADCYTRWGRCLAVM 55
KUJ21542.1          MSDLKATVAETKTSSGHVGFVVEGYEKIEYDFTFIDGVFDLENCNLANCYKWKRCRLAVT 60
XP_007805994.1      MSDLKATVSETK-----NGFHVEGYEKIEYDFTFIDGVFDIKNSNLADCYSRWGRVLAVT 55
XP_007839531.1      MSDLKASVSETK-----NGFHVEGYEKIEYDFTFIDGVFDVANPNLADCYRWGRVLAVT 55
KKY35074.1          MSDLKATVSETP-----KGFHVEGYEKISYDFSFVDGVFDIRNPGLAECYKPWGRVLAVT 55
KUI55509.1          MSDLKANVSETP-----QGFHVEGYEKITYDFTFVDGVFDIQNPGLASCYKPWGRVLAVT 55
XP_003719131.1      MSDLKATVSETP-----QGFHVEGYEKIEYDFTFVDGVFDVNNPGLANCYKWKGRVLAVT 55
KXJ90767.1          MSDLKANVSETA-----QGFHVEGYEKITYDFTFVDGVFDVNTQLANCYKQWGRVLAVT 55
                    **:.*.* **      **:.*:***** **:.*:*****: .  **.*: * * **:

XP_007681536.1      DLNIFNLYGKQMQEYFEHHGVLELKIHKTMIGEKAESIETFLSIVDSMNEFGIIRKEPVLV 115
XP_008713717.1      DLNIFNLYGKMQAYFDHYDIDLVDVHKTMIGEKAESMDTLLSIVDSMTKFGIFRKEPVLV 115
KIW13573.1          DSNIFDVYGEQMQRQYFDHYKIDLDIHKTMIGEKAESIDTFLSIVDSMKNKFGVFRKEPVLV 115
XP_007756891.1      DYNIFNVYGEQMQRQYFDQYKIDLDVHKTMIGEKAESIDTFLSIVDSMKNKFGIFRKEPVLV 115
XP_013283806.1      DYNIFNLYGKMQYFDHYKIDLDIHKTMIGEKAESIDTFLSIVDSMKNKFGVFRKEPVLV 115
KUJ21542.1          DLNIYNIYGGKMEKYFEHHGLELKIHKTMIGEKAESIDTFLSIVDAMNEFGIYRKEPVLV 120
XP_007805994.1      DLNIYNVYGGKMQYFDHYGLLELKIHKTMIGEKAESIDTFLSIVDSMTEFGIYRKEPVLV 115
XP_007839531.1      DKNVYVYVYGGKMEKYFRHYGLDLKIHKTMIGEKAESIDTFLSIVDSMTEFGIYRKEPVLV 115
KKY35074.1          DKNVYGLYGDKMEYFNHYGLTLKVHRTSIGEKAESIDTFLSIVDSMTEFGIYRKEPVLV 115
KUI55509.1          DKNVYVYVYGGKMEKYFRHYGLDLKIHKTMIGEKAESIDTFLSIVDSMTEFGIYRKEPVLV 115
XP_003719131.1      DKNIFGIYGRMMEKYFQHYDLDLTVKQTSIGEKAESIDTFLSIVDSMTEFGIYRKEPVLV 115
KXJ90767.1          DKNVFRMYGAKMEKYFEHHGLKFKVHQTSGEKAESIDTFLSIVDSMTEFGIYRKEPVLV 115
                    * *.: .:** :.* ** :. : : :.* *****: * *.* *.*.***: *****

XP_007681536.1      VGGGLVTDVAGFACAAYRRNTNYIRVPTTVIGLIDASVSIKVAVNYGNYKNRGLGAYHAPM 175
XP_008713717.1      IGGGLVTDVAGFACAAYRRNTNFIRIPTTVIGLIDASVSIKVAVNYGNYKNRGLGAYHAPM 175
KIW13573.1          IGGGLVTDVAGFACAAYRRNTNYIRIPTTVIGLIDASVSIKVAVNYGNYKNRGLGAYHAPM 175
XP_007756891.1      IGGGLVTDVAGFACAAYRRNTNYIRIPTTVIGLIDASVSIKVAVNYGNYKNRGLGAYHAPM 175
XP_013283806.1      IGGGLVTDVAGFACAAYRRNTNFIRIPTTVIGLIDASVSIKVAVNYGNYKNRGLGAYHAPM 175
KUJ21542.1          VGGGLVTDVAGFACAAYRRNTNFIRVPTTVIGLIDASVSIKVAVNYGEMKNRGLGAYHAPI 180
XP_007805994.1      VGGGLVTDVAGFACAAYRRNTNFIRVPTTVIGLIDASVSIKVAVNYGNYKNRGLGAYHAPI 175
XP_007839531.1      VGGGLVTDVAGFACAAYRRNTNFIRIPTTVIGLIDASVSIKVAVNYGRYKNRGLGAYHAPM 175
KKY35074.1          VGGGLVTDVAGFACAAYRRNTNFIRVPTTVIGLIDASVSIKVAVNYGNYKNRGLGAYHAPI 175
KUI55509.1          VGGGLVTDVAGFACAAYRRNTNFIRVPTTVIGLIDASVSIKVAVNYGNYKNRGLGAYHAPI 175
XP_003719131.1      VGGGLVTDVAGFACASYRRNTNFIRVPTTVIGLIDASVSIKVAVNHGRYKNRGLGAYHAPI 175
KXJ90767.1          VGGGLVTDVAGFACASYRRNTNFIRVPTTVIGLIDASVSIKVAVNYGNYKNRGLGAYHAPI 175
                    :*****.*****.*.*.***:*****:*****.*.*****:

XP_007681536.1      HTFLDFGFLRSLPVAQVRNGFAELIKISSCAHLPTFDLLDKHCEDLINTGFGRTDDAKKE 235
XP_008713717.1      KTFLDFTFLKTLPEAQIRNGFAELIKISTCAHLPTFELLEKYCTELIQTFGFRNDAPAE 235
KIW13573.1          HTFLDFGFLRSLPVAQIRNGFAELIKISTCAHLPTFDLLDKYCEQLIKTFGFRTDGAPAE 235
XP_007756891.1      HTFLDFTFRLRSLPVAQIRNGFAELIKISTCAHLPTFELLDKYCEQLIGTFGRADGAPKE 235
XP_013283806.1      RTFLDFTFRLRSLPVAQIRNGFAELIKISTCAHLPTFELLDKYCEQLIDSGFGRCDGASAE 235
KUJ21542.1          HTFLDFTFRLRSLPVAQIRNGFAELIKISTCAHLPTFELLDKYCEQLIEKSFGRADGSSKE 240
XP_007805994.1      HTFLDFTFRLRSLPVAQIRNGFAELIKISSCAHLPTFDLLDKYCEQLIETGFGFRNDAPAE 235
XP_007839531.1      HTFLDFTFRLRSLPVAQVRNGFAELIKISSCSHLQVFDLLDKYCEQLIECRFGRADGAPDE 235
KKY35074.1          HTFLDFTFRLRSLPVAQVRNGFAELIKISSCSHLQVFDLLDKYCEQLIEHKFGRDGSSEE 235
KUI55509.1          HTFLDFTFRLRSLPVAQVRNGFAELIKISSCAHLEVFNLLDKYCEQLIESKFARADGSSDE 235
XP_003719131.1      HTFLDFTFRLRSLPVAQVRNGFAELIKISSCAHLQVFDLLDKYCEQLIDSKFGRADGAPAE 235
KXJ90767.1          HTFLDFTFRLRSLPVAQVRNGFAELIKISSCAHLEVFNLLDKYCEQLIDTKFGRADHAPAE 235
                    :***** **.:** :.*:*****:*****.*.*.***:*****:*****.*.*****:

XP_007681536.1      VREAADKINRSGIYEMLKLETPNLHEIGLDRVIAYGHTWSPLHELIPSIPLRHGHASID 295
XP_008713717.1      VRKAADTINKAGIYEMLKLETPNLHEIGLDRVIAYGHTWSPLHELIPSIPLRHGHASID 295
KIW13573.1          VRKAADTINRAGIHEMLKLETPNLHEIGLDRVIAYGHTWSPLHELVPDPLRHGHASID 295
XP_007756891.1      VRDAADAINRAGIHEMLKLETPNLHEIGLDRVIAYGHTWSPLHELVPDPLRHGHASID 295
XP_013283806.1      VRNAADAINRAGIHEMLKLETPNLHEIGLDRVIAYGHTWSPLHELVPDPLRHGHASID 295
KUJ21542.1          LIDAADAINRAGIHEMLKLETPNLHEIGLDRVIAYGHTWSPLHELVPKTPLRHGHASID 300
XP_007805994.1      VRKAADTINRAGIHEMLKLETPNLHEIGLDRVIAYGHTWSPLHELVPETPLRHGHASID 295
XP_007839531.1      -----INREGIYEMLRLESPNLHEIGLDRVIAYGHTWSPLHELVPETPLRHGHASID 288
KKY35074.1          LTRAADINRAGIYEMLKLESPNLHEIGLDRVIAYGHTWSPLHELIPETPLRHGHASID 295
KUI55509.1          LRQAADINRAGIHEMLKLETPNLHEIGLDRVIAYGHTWSPLHELIPETPLRHGHASID 295
XP_003719131.1      VRSAADINRAGIYEMLKLESPNLHEIGLDRVIAYGHTWSPLHELMPETPLRHGHASID 295
KXJ90767.1          VRKAADINRAGIYEMLKLESPNLHEIGLDRVIAYGHTWSPLHELVPETPLRHGHASID 295
                    **.*.***:*****:*****.*.*.***:*****:

XP_007681536.1      MAYSATLANQRGLLSDEEHQRLKLFSTRAGLSIDHDPDFDEHVLDKGTAAILKTRDGKRLR 355
XP_008713717.1      MAYSATLANIRGLSDADHKRILDLFSTAGLSMDHHQFNIEILDKGTAKAILRTRDGLLRA 355

```


KIW13573.1	MAYSATLANLRGLSDSDHRSLLSLSFRAGLSMDHHQFDEEILDKGTKAILKTRDGLLRA 355
XP_007756891.1	MAYSATLANMRGILPDEDHKRLLNLSFRAGLSMDHHQFDEEILDKATKAILRTRDGLKRA 355
XP_013283806.1	MAYSATLANMRGILSDAEHQIRLLRFRAGLSMDHHQFDEEILDQGTKAILRTRDGLKRA 355
KUJ21542.1	MAYSATLANDRKLLITDAEHRRLNLSFRAGLSMDHHQFDEEILAKATSAILKTRDGLLRA 360
XP_007805994.1	MAYSATLANSRGLSDVEHMRLLNLSFRAGLSMDHHQFDEEILDKGTAAILKTRDGLKRA 355
XP_007839531.1	MAYSATLAMKRGLLSADEHRLLTFRAGLSIDHPQFDEVLKGTAAILKTRDGLLRL 348
KKY35074.1	MAYTATLANHRRLLSDVEHTRLLTFRAGLTIIDHPQFDEHVIDKGTAAILKTRDGLKRL 355
KUI55509.1	MAYSATLAHSRGLSDAEHTRLLTFRAGLSIDHPQFDEVLERGTAAILKTRDGLKRL 355
XP_003719131.1	MAYTATLANQGLLKDAEHKRLDLFRAGLSIDHPMFDEQVLEKGTAAILKTRDGLKRL 355
KXJ90767.1	MAYTATLANQRGLSDDEHKRLLTFRAGLSIDHPLFNDEVLAKGTEAILKTRDGLKRL 355
	: : : : * * * * * : * * * * * * : : : : : * * * * * * *
XP_007681536.1	AVPHPLGSCVFINDVEKEDLEKALRKHKEIMKSFREGAGIESFVDASDTGYTMNEAPTE 415
XP_008713717.1	AVPSPGLGSCIFLNDVSMDEMYDALKAHKLMKQYPRNGEGLEAFVDSSTGYTLNQPVE 415
KIW13573.1	AVPSPGLGCVFLNDVSMDEMYAALKKHSLMKNFPRNGEGLEAFVDSSTGYTVNNQPVE 415
XP_007756891.1	AVPAPLGKCVFLNDVSMDEMYAALKKHKSIMQNYPRNGEGLEAFVDSSTGYTVNNKPVE 415
XP_013283806.1	AVPAPLGSCVFINDVSMDEMYAALKKHKEIMKSFPRNGEGLEAFVDSSTGYTVNNVPVE 415
KUJ21542.1	AVPNPIGTCTFLNDVSAEEMNAALRRHKEIMKQFPRNGEGLEAVVDASDTGYTENAKMEE 420
XP_007805994.1	AVPRPLGSCIFINDLEPKEMHSLRRHKEIMKQFPRNGEGLEAVVDASDTGYTENHYDES 415
XP_007839531.1	AVPNPLGSCKFINDVSEHRLDALRKHKEICQTYPRQGAGIEAVVDSSTGYTENGENS -- 406
KKY35074.1	AVPNPLGSCVFINDVSEQEELLALKKHKEFAKNYPRNGEGLEAFVDSSTGYTDLASENK 415
KUI55509.1	AVPSPGLGSCVFINDVSGDEMMLVLTKHKALVNSYPRGGAGLDAYVDSSTGYADLETENM 415
XP_003719131.1	AVPNPLGSCVFINDLSAETLNDALRKHKAVCKTYPRGGEGLEAVVDSSTGYTDNAEDL 415
KXJ90767.1	AVPNPLGSCSFVNEYSTEELSQLKHKAVCKTFAREGAGLEAVVDSSTGYTDSATENS 415
	*** *:* *:* : . : : . * : * : . : : * * * : : * * * : : * * * : : * * * : : * * * : *
XP_007681536.1	QNGKHA--EEHGVTAGLKKA-VINDD-ASNGQANGGLGATNVDGFTGDPK-SAVKHAAGV 470
XP_008713717.1	-----INGVSNGLRKLNLVNDSDSTRNGV--ESNGTDV-----SKKHASRL 453
KIW13573.1	-----SSTMSNGQKLLNLVNDSDSHV-----NGHQADGKMTNGVFKASKHATTD 459
XP_007756891.1	AE-----TNGVSNGLKLLNLVNDSDTHKSGS--QTNGHSDADGKHTNGVSAAVKHASGP 466
XP_013283806.1	-----TDGVSNGLKSLTVLNDSDVQKNGI--QTNGNNGVDGKMTGHVITATKHASDP 464
KUJ21542.1	EKVL EAAAMKAGSLNG-TN--GTNGINGMNGAKTATNGANGTNGFSNGHTDTKV---KN 473
XP_007805994.1	-KAIEEAAVTAGNLNGFMN--GTNGV-----SKGV--NGHTNGHKDGPEAH-----TN 458
XP_007839531.1	--VDDAA--EEADIPPG-SK--VVNGS-----ATNGNGYGHANGNSNGDI-SLLEKAKAA 453
KKY35074.1	-SVIDTV-AENGDGLK-AK--LAAKV-----SNGT--NGHTNGHTNGHTNGHTKGF-TN 461
KUI55509.1	-SVMNTV-TGNGEGLK-RK--AAVAV-----NNGV--KKISSVHIET-----450
XP_003719131.1	-SVEAAA-KEAAVVNA-AH--TANGG-----FKGA--NGHSNKNVKNKNGILPNIGAIKTG 462
KXJ90767.1	-SVEEAA-REAGLISE-SQ--HLNDT-----SLIE--K---GKVVFDGLL-----450
XP_007681536.1	DADSAMTNGG-----AQVTDKTVNGVSNVNGKH-----498
XP_008713717.1	ERVLDGLQKSVN-----GTNGQTVNGTVNGTNGHNSNGVTNGVNGHQ-----492
KIW13573.1	EKPTGFLHGAKD-----VATNGLASGRPGLNGHTNGMHLNNGHINASRVNGVH 508
XP_007756891.1	EGVNLGN-----GTTD-----DTSNGLADGVANGINGHRNGIKVQG-----503
XP_013283806.1	EKADSLIDGIRGIGMNN---DISNGGGDGVSNELNGGSKRVEVRA-----506
KUJ21542.1	N--GVAPNGVNGNA---LKSVKVADGQ-----495
XP_007805994.1	G--ELD--GVSK-----IAQQAGFDGAEHGLMNGADGFTNGAKA-----493
XP_007839531.1	L--LSNNGHGAHKPYT-----NGVKVQA-----474
KKY35074.1	G--HSNNGVNGVHYSQVEKVMNGVH-----487
KUI55509.1	-----VRQANGVH-----458
XP_003719131.1	I--DLNGLHGLNLENS-----PLVDGVKSGL-----486
KXJ90767.1	-----NRRGIIKAQA-----459

FIGURE 77 : ALIGNEMENT DE SÉQUENCES DHQS-LIKE EXTRAITES DE CHAMPIGNONS D'INTÉRÊT. LES SÉQUENCES CIBLÉES POUR LA DÉSIGNATION DES AMORCES DÉGÉNÉRÉES SONT SURLIGNÉES EN GRIS. XP_007681536.1 DE BAUDOINIA PANAMERICANA UAMH 10762 ; XP_008713717.1 DE CYPHELLOPHORA EUROPAEA CBS 101466 ; KIW 13573.1 D'EXOPHIALA SPINIFERA ; XP_007756891.1 DE CLADOPHIALOPHORA YEGRESII CBS 114405 ; XP_013283806.1 DE FONSECAEA PEDROSOI CBS 271.37 ; KUJ21542.1 DE PHIALOCEPHALA SCOPIFORMIS ; XP_007805994.1 DE ENDOCARPON PUSILLUM Z07020 ; XP_007839531.1 DE PESTALOTIOPSIS FICI W106-1 ; KKY35074.1 DE DIAPORTHE AMPELINA ; KUI55509.1 DE VALSA MALI VAR. PYRI ; XP_003719131.1 DE MAGNAPORTHE ORYZAE 70-15; KXJ90767.1 DE MICRODOCHIUM BOLLEYI.

C. Principe du sous-clonage par Topo-cloning

L'ADN topoisomérase 1 est une enzyme à la fois dotée d'une activité d'enzyme de restriction et de ligase. L'ADN topoisomérase 1 de *Vaccinia virus* reconnaît ainsi la séquence pentamérique 5'-(C/T)CCTT-3' pour se lier de façon covalente à l'extrémité 3'-phosphate de la thymidine terminale (Shuman, 1994). La Taq polymérase employée pour la PCR a une activité transférase terminale non template dépendante qui va venir ajouter une désoxyadénosine à l'extrémité 3' des produits de PCR (Marchuk et al., 1991). Ces deux caractéristiques sont mises à profit lors de la technique dite de Topo cloning qui exploite des vecteurs conçus de telle sorte qu'ils portent la séquence 5'-(C/T)CCTT-3' à leurs deux extrémités linéaires avec des topoisomérases attachées de façon covalente à chacune d'elles (on parle de vecteurs activés) (Figure 78).

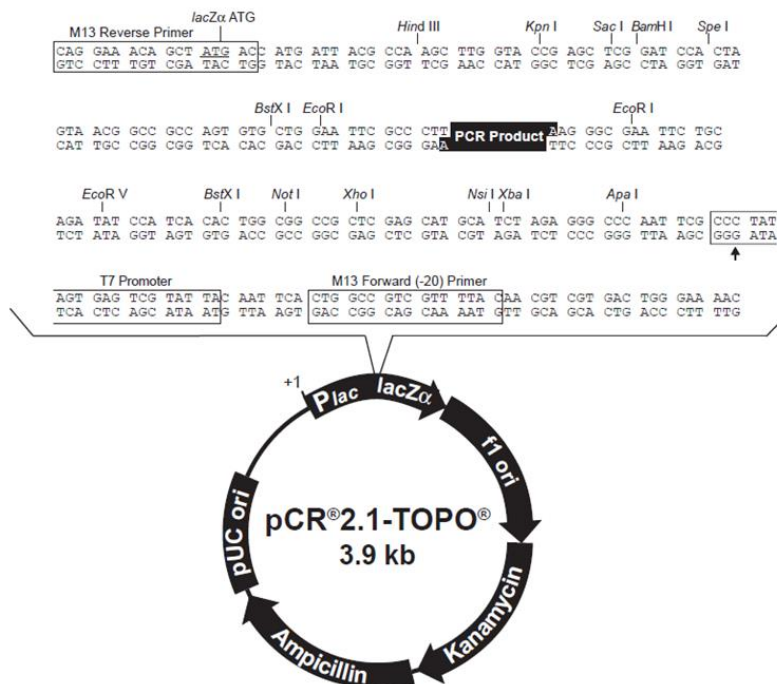


FIGURE 78 : VECTEUR PCR2.1-TOPO TA ET RÉGIONS D'INTÉRÊT

Ainsi, par simple contact avec des produits de PCR 3'-adénylés, ces derniers peuvent directement s'intégrer au sein d'un Topo vecteur en la seule présence d'une concentration en sels appropriée.

D. Transformation des cellules électro-compétentes et principe de la transformation par électroporation

Le transfert d'ADN dans les bactéries a été effectué dans le cadre de ces travaux par électroporation. Cette technique consiste à appliquer un champ électrique intense mais extrêmement bref (quelques millisecondes) en utilisant deux électrodes placées de part et d'autre des parois d'une chambre contenant une suspension mixte de cellules à transformer et d'ADN (Dower et al., 1988). Les parois cellulaires sont perméabilisées lors du choc électrique et l'ADN peut être transféré dans les cellules selon une migration polarisée (l'ADN est attiré par l'anode du fait de sa charge négative). L'exposition des cellules à ces voltages est très nocive et entraîne la mort de 50 à 75% d'entre elles (Bel-Vialar, 2002). Le protocole ayant permis d'obtenir les cellules électro-compétentes et le procédé de transformation sont décrits à la suite.

Préparation et transformation des cellules électro-compétentes

1. Des cellules d'*E. coli* DH-10b sont cultivées une nuit en milieu liquid LB-10 sous agitation à 200 rpm
2. 2 mL de pré-culture sont inoculés dans 200 mL d'un milieu de culture frais et les cellules croissent à 37°C sous agitation à 200 rpm jusqu'à atteindre une densité optique aux alentours de 0,6 à 600 nm (habituellement, durée de 2 à 2,5 heures).

À partir de cette étape, tout se déroule à 4°C :

3. La culture cellulaire est transférée dans un tube sterile préalablement refroidi. Le tube est centrifugé 10 minutes à 4.000 rpm puis le surnageant est éliminé.
4. Les cellules sont remises en suspension dans 200 mL d'une solution aqueuse stérile à 10% de glycérol. Le tube est centrifugé pendant 10 minutes à 4.000 rpm puis le surnageant est éliminé.
5. Les cellules sont remises en suspension dans 40 mL d'une solution aqueuse stérile à 10% de glycérol. Le tube est centrifugé pendant 10 minutes à 4.000 rpm puis le surnageant est éliminé.
6. L'étape 5 est répétée.
7. Le culot cellulaire est repris par 2 mL d'une solution de glycérol à 10% et est aliquoté à raison de 50 µL par tube Eppendorf. Les cellules sont directement congelées dans l'azote liquide et conservées à -80°C dans l'attente de leur transformation.

Pour la transformation :

1. Les cellules électro-compétentes sont immergées dans la glace pendant 10 minutes.
2. Le produit issu du Topo cloning est ajouté aux cellules électrocompétentes.
3. L'électroporation a lieu à un voltage de 1250 V.
4. 500 µL de milieu liquide LB-10 sont rapidement ajoutés et le tube est incubé à 37°C pendant une heure.
5. Les cellules sontensemencées à la surface d'une gélose LB-10-Carbénicilline-X-Gal-IPTG pour une incubation d'une nuit à 37°C. Composition des géloses : 20 mL LB-10+Agar, 20 µL carbenicillin (50 mg/mL), 40 µL 40 mg/mL X-Gal et 10 µL IPTG 1M.

E. Sélection des cellules recombinantes

Il reste ensuite à sélectionner les cellules ayant intégré le plasmide recombinant. Les différentes régions d'intérêt du vecteur pour réaliser ce criblage sont représentées sur sa cartographie (Figure 78).

Les cellules transformées (recombinantes ou non) sont caractérisées par leur résistance à la kanamycine et à l'ampicilline (Rüther, 1980).

Le repérage des clones d'intérêt parmi les différentes colonies peut ensuite être effectué par le système X-Gal, basé sur les propriétés d'une enzyme, la β -galactosidase, issue de l'opéron lactose (Rüther, 1980). La β -galactosidase est une enzyme codée par le gène LacZ et est constituée de deux sous-unités (LacZ- α et LacZ- ω), chacune d'entre elles étant nécessaire à l'activité catalytique de l'enzyme. La souche hôte qui sera utilisée pour le clonage est modifiée par génie génétique pour ne synthétiser que le fragment ω de l'enzyme. Lorsque cette souche modifiée est transformée par un plasmide contenant le fragment α du gène LacZ, les deux fragments vont s'associer pour livrer une β -galactosidase fonctionnelle (α -complémentation). L'activité de la β -galactosidase est évaluée en présence d'isopropyl β -D-1-ThioGalactopyranoside (IPTG) (inducteur) et de 5-bromo-4-chloro-3-indoyl β -D-galactopyranoside (abrégé X-Gal) (substrat). Sous l'effet d'une β -galactosidase fonctionnelle, X-Gal est hydrolysé en galactose et en 5-bromo-4-chloro-3-hydroxyindole (X) qui va spontanément s'oxyder et dimériser pour livrer un dérivé de l'indigo de couleur bleue (Rüther, 1980) (Figure 79).

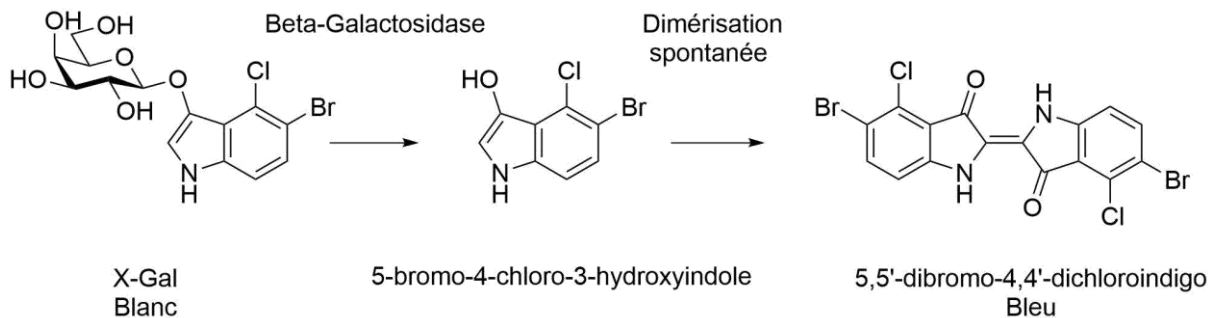


FIGURE 79 : MÉTABOLISATION DE X-GAL PAR LA B-GALACTOSIDASE

- les colonies transformées non recombinées réalisent l' α -complémentation pour permettre à la cellule de métaboliser X-Gal, à l'origine d'une couleur bleue ;
- les colonies transformées recombinées (plasmide avec insert) apparaissent blanches car LacZ- α est inactivé par l'insertion du transgène dans le plasmide. X-Gal n'est alors pas métabolisé et les colonies restent blanches (Figure 80).

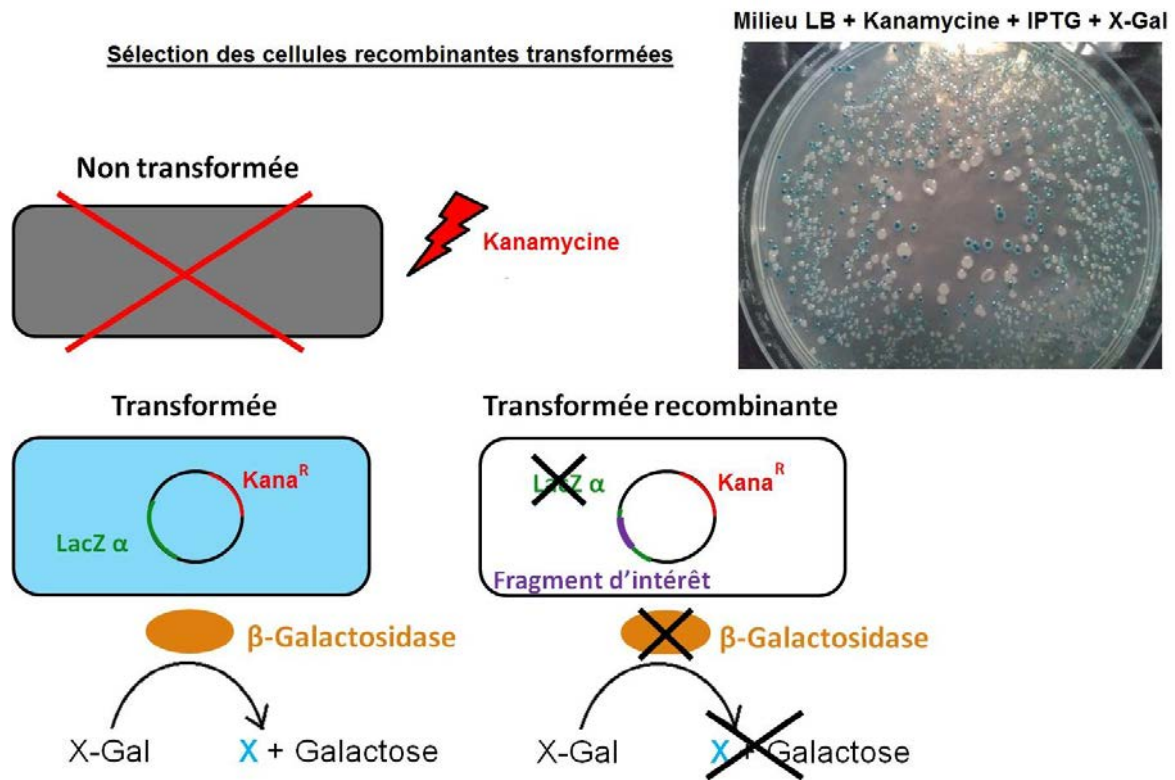


FIGURE 80: SÉLECTION DES CLONES TRANSFORMÉS RECOMBINANTS PAR LE SYSTÈME LACZ. FIGURE ADAPTÉE DE [HTTP://OL.SAULNIER.FREE.FR/ESPACE_TRAVAIL/BLANC_BLEU.HTML](http://ol.saulnier.free.fr/espace_travail/blanc_bleu.html)

F. Protocole de purification de l'ADN plasmidique par lyse alcaline

a. Principe

Dans un premier temps, le milieu de culture est éliminé par centrifugation. Le culot bactérien est alors resuspendu dans un premier milieu tampon contenant de l'EDTA pour déstabiliser les membranes bactériennes et inactiver les DNases. Les bactéries sont ensuite lysées à l'aide d'un détergent à pH 13 (NaOH 0,2 M + Sodium Dodécyl Sulfate). À un tel pH, l'ADN est dénaturé, ces deux brins se dissocient. La neutralisation rapide du milieu par l'adjonction d'une troisième solution contenant de l'acétate de potassium 3M à pH 5,5 permet à l'ADN de se renaturer mais avec des différences notables entre l'ADN chromosomique et l'ADN plasmidique :

- l'ADN chromosomique très long nécessite beaucoup de temps pour se réappairier et ne peut finalement pas aller au terme du processus car l'ADN simple brin précipite du fait d'une concentration élevée en sels ;
- l'ADN plasmidique – beaucoup plus court – parvient à se reformer et demeure en solution.

Une centrifugation permet d'éliminer les membranes, les protéines et l'ADN chromosomique qui précipitent de l'ADN plasmidique qui demeure dans le surnageant. L'ADN plasmidique est ensuite précipité par l'isopropanol.

b. Protocole

L'ADN plasmidique est purifié des cellules *d'E. coli* au moyen d'un kit QIAprep Spin Miniprep.

Tampon P1:

50 mM Tris-HCl, pH 8,0
10 mM EDTA, pH 8,0

Tampon P2:

200 mM NaOH, 1% SDS

Tampon P3:

3 M KOAc, pH 5,5 (ajusté au moyen d'acide acétique)

Tampon TE:

10 mM TrisHCl (pH 8), 1 mM EDTA.

Protocole:

1. Les colonies recombinantes sont cultivées une nuit dans 2 mL de milieu liquide LB-10 à 30°C en présence de 0,1% de kanamycine.
2. Les cellules sont centrifugées à 13.000 rpm pendant 3 minutes, le surnageant est éliminé.
3. Le culot de cellules est remis en suspension dans 250 µL de tampon P1 supplémenté par 3.5 µL de RNase A à 10mg/mL.
4. 250 µL de tampon P2 sont ajoutés et le tube Eppendorf est retourné plusieurs fois pendant 5 minutes (pas plus).
5. Lorsque la solution s'éclaircit, 300 µL de tampon P3 sont ajoutés et le tube est retourné plusieurs fois pendant 5 minutes.

6. Le tube Eppendorf est centrifugé pendant 10 minutes à 13.000 rpm et le surnageant est transféré dans un nouveau tube Eppendorf.
7. 560 µL d'isopropanol sont ajoutés au surnageant, le tube Eppendorf est retourné plusieurs fois avant d'être centrifugé à 13.000 rpm pendant 10 minutes.
8. Le surnageant est éliminé et le précipité est séché à l'air une dizaine de minutes en gardant le tube Eppendorf renversé à la surface d'un papier absorbant.
9. Le précipité est dissous dans 30 µL de tampon TE et est conservé à -20°C.
10. 4 µL de cette solution sont envoyés au séquençage.

L'insertion du fragment d'ADN peut être vérifiée par digestion avec les enzymes de restriction ou par PCR.

G. Fragments de gènes séquencés

```
CCGTGGAAAATAGGTACGCGGGGTGCTAATTCTAAAGTAGGACTCCAACATGACCATAGGCTAT
AACTCGATCTAGGTCTAATTCGTGTAAGTTGGGTACTTCATATCCAACATTTTCTTGATGGCTTTG
TAAGTCAACTTATGAGCGACTTCTTTGATTTCTCTGTAGCATCAATGTTACCGAAGTGAGTGCGA
AGTAATTCCTCACCGTATTCTTCGAGCAATTCAAATACTTCTTTGTGCCAACTACGGCAATTTTGA
CCAATTCGCCATCCCGTT
```

FIGURE 81 : SÉQUENCE DU FRAGMENT DE GÈNE AMPLIFIÉ PAR LES AMORCES DHQS-LIKE CYANOBACTÉRIENNES SUR *RIVULARIA SP.* MICRODISSÉQUÉ

>ATPCyano_pair 1_Total lichen gDNA clone 1

```
GGCTATCGGGGCATCAATTTCCCGCGCTGTCAAGGGCTTTTTACCGTTCCCGTTCCTGAAAAAGAACCAGAAGCCTATT
GTCAGGCATTAATTGCGATCGCTCAAGAAAAGCAGATCGATTTATTTGTGCCTGTTCTAGCCCGATTGCCAGCTACTACGA
TTCTTTGGCTAAAAAGGCTTTAGAACCCTATTGCGAATCGATTACCTCGATCCAAAACTACCGCCATTCTCGATGATAAAC
ATGCTTTTTGTGATCAAGCACGAGAATTTGGCTTATCCGCACCCAAGGTATTTTCGATTACCGATCCGCAGCAGATTTTGA
TTTTGACTTTGAGAGTGACGGCAGTACCTACATTGTCAAAAAGTATCCCTACGATTCTGTCTTGCGCTTAGACTTAACCAAAT
TACCTTTGCAGATATGGAAAGCTATGTTCTGATGTTTGCCTATTAGCGAAGCCAAGCC
```

>ATPCyano_pair 1_Total lichen gDNA clone 2

```
TATCAGGGAATAGATTTTCTAATGCTATTGCAGTTTCTATACTGTTCTGAGCCTAAAGAAGATTGGAATGGTTATTCTCAG
AAATTACTAGATATTATAAAAAAGAAAATATAGATGTATTATTCCAGTATCTGCTGCAACTTTAACTACTACGAATCGTTA
GTCAAACCTGTTTTAGCTGAACATTGTGAAGTCTTACATTTTGATATAGAAATTACGGAAATGTTAGACAATAAATTTACATTT
ATGAAAAAGCGAAAACTTTTGGGTTGACTGTTCTAAATCATTTCTAATTACCAATGCACAACAAATTTCTTGATTTGATTTT
GTCAAAGATGGAAGTCAGTATATTTTAAAAAGTATCCCTATGACTCAGTGCGCCGTTTAAACATGACAAAAGCTACCAATGAA
GTCAGCAGAGGATATGAGTCAATTTGTCAAAAACCTTGCCTATTAGTACAGAA
```

FIGURE 82 : SÉQUENCES DES FRAGMENTS DE GÈNE AMPLIFIÉS PAR LES AMORCES ATP-GRASP CYANOBACTÉRIENNES SUR LE LICHEN TOTAL MAIS PAS SUR *RIVULARIA SP*

Analyses de lichens par spectrométrie de masse : déréplication et histolocalisation

Les lichens, organismes symbiotiques associant un champignon et un partenaire photosynthétique (algue verte et/ou cyanobactérie), sont caractérisés par la biosynthèse de métabolites secondaires uniques dotés de bioactivités variées.

Pour valoriser au mieux cette ressource privilégiée, des méthodes innovantes de spectrométrie de masse ont été développées dans le but de minimiser la préparation de l'échantillon et la durée des analyses. Deux techniques de spectrométrie de masse ont été évaluées en ce sens : le DART-MS et le LDI-MS. L'apport de chacune de ces deux méthodes a pu être établi sur un large panel de lichens, représentant une part importante de l'espace chimique couvert par ces organismes. Il a été démontré que des profils chimiques complets pouvaient être obtenus respectivement à partir de thalles lichéniques et d'extraits acétoniques totaux. Compte tenu de la très large utilisation de la CCM pour l'analyse chimique de lichens, les possibilités offertes par le couplage de la CCM à l'ionisation electrospray ont également été explorées.

Une seconde partie de ces travaux avait pour but de cartographier la distribution des métabolites secondaires au sein du thalle lichénique. À ces fins, des analyses d'imagerie LDI ont été réalisées sur une coupe transversale d'un lichen crustacé modèle : *Ophioparma ventosa*. Ce lichen a été étudié en phytochimie pour identifier six naphthopyranones à partir des apothécies dont quatre nouvelles structures. Les principaux métabolites de ce lichen ont pu être imagés par LDI-MSI avec une résolution spatiale de 50 µm environ. Une corrélation entre la distribution des molécules et leur rôle écologique présumé permet d'avancer des hypothèses d'écologie chimique. Des approches conjointes reliant histolocalisation et étude génétique des partenaires de la symbiose ont été entreprises. La recherche des gènes de la biosynthèse de la mycosporine sérinol chez les symbiontes isolés de *Lichina pygmaea* par microdissection capture laser a été initiée en ce sens. D'autres approches innovantes comme l'analyse cristallographique par diffraction de poudre par les rayons X sont également abordées dans ce document articulé autour de six publications issues de ce travail et de deux articles en cours de soumission.

Mass spectrometric analyses of lichens: from dereplication to histolocalization

Lichens are self-sustaining symbiotic partnerships comprising a fungus associated with a green alga and/or a cyanobacteria. This consortium produces unique secondary metabolites that are endowed with various biological activities.

To harness this privileged chemodiversity, innovative mass spectrometry techniques were developed in the course of this study to accelerate the dereplicative holdup through both a minimal sample preparation and a decrease of the time of analysis. Two approaches were considered during this work: DART-MS and LDI-MS and their adequacy for lichen dereplication was assessed on a vast array of samples encompassing a wide range of metabolites. Both of them facilitated complete chemical profiles, respectively from unprocessed lichen material and crude acetone extracts. Since TLC still enjoys a wide-spread popularity among lichenologists, the advantages offered by TLC-ESI-MS hyphenation were evaluated as well.

A second part of this manuscript focused on the histolocalization of lichen metabolites. For this purpose, LDI mass spectrometry imaging studies were undertaken on the crustose lichen *Ophioparma ventosa*. The phytochemical investigation of this species afforded the isolation of six naphthopyranones from its apothecia, four of them being new molecules. LDI-MSI revealed the distribution patterns of all the main metabolites of this lichen, reaching a spatial resolution of 50 µm. Most interestingly, the distribution pattern of imaged metabolites within the thallus is highly organized and is related to their ecological relevance. Joint strategies combining histolocalization and genetic investigation of lichen symbionts separated using laser capture microdissection were also considered. As such, an investigation of the biosynthesis of mycosporine serinol within *Lichina pygmaea* dissociated symbionts was initiated. Further analytical strategies such as X-ray powder diffraction are introduced in this thesis that contains six publications and two drafts to be submitted.